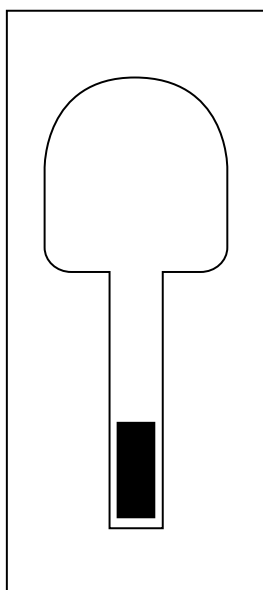


OECD/NEA
International Stripa Project
1980–1992

Overview Volume II



Natural Barriers

Paul Gnirk

January 1993

OECD/NEA INTERNATIONAL STRIPA PROJECT
OVERVIEW VOLUME II
NATURAL BARRIERS

Paul Gnirk

January 1993

FOREWORD

In 1990, the Joint Technical Committee of the International Stripa Project made a decision to commission the preparation of a set of three reports that would provide a comprehensive overview of the investigative activities and results of the three phases of the project. Two of the reports were intended to focus on the investigations dealing with the natural barriers and the engineered barriers as separate topics. The third report was expected to summarize the contents of the other two reports and to highlight the principal achievements of the project in advancing the state of technology for the siting and development of geologic repositories. Subsequently, in 1991, Dr. Malcolm Gray was selected to be the author of the overview report on the investigations of the engineered barriers, with review of the report to be provided by Dr. Ferruccio Gera. Dr. Paul Gnirk was selected to be the author of the overview report on the investigations of the natural barriers, with review of the report to be provided by Dr. Charles Fairhurst. Dr. Fairhurst and Dr. Gera were selected to be the lead authors of the summary report, with assistance provided by the authors of the other two reports and Dr. Bengt Stillborg, the Stripa Project manager. Detailed outlines of the two overview reports on the natural barriers and the engineered barriers were developed by Dr. Gnirk and Dr. Gray, respectively, in late 1991. During the first part of 1992, these authors, together with Dr. Stillborg, met with representatives of each of the seven member countries of Phase 3 for the purpose of presenting the outlines and obtaining comments and suggestions on the proposed scope and contents of the reports. During the last part of 1992, draft copies of the reports were prepared and sent to the member countries for review and comment. All comments, both oral and written, were considered and incorporated to the extent practicable.

This report is a summary of the principal results and achievements from the investigations in the Stripa Project that dealt with characterisation of the natural barriers and simulation of groundwater flow and solute transport by numerical modelling techniques. Three principal themes evolved during the course of planning and conducting the research activities in the Stripa mine over the three phases and thirteen years of the project. The first theme, which emerged at the outset of the project and continued essentially to the end, was centered around the development of techniques and strategies for characterising saturated, fractured granitic rock masses. Emphasis was placed on the development of remote sensing tools and techniques for use in boreholes, such that the natural state of the rock mass would be minimally disturbed and the data would reflect closely the true *in situ* conditions. The outcome of this research work can be described collectively in terms of the radar, seismic, and hydraulic methods for both single-borehole and crosshole testing, methods and techniques for determining the residence times and origins of groundwaters, and an understanding of the essential requirements for the design of a tracer test. The second theme, which first appeared as such in Phase 2 and later became an integral part of Phase 3, dealt with the application of the testing techniques and strategies for obtaining the data to develop a conceptual model of the geologic, hydrologic, and geochemical characteristics of a saturated, fractured granitic rock mass. The volumes of rock contained in the various conceptual models ranged from some 300 billion cubic metres for the Stripa area to about one million cubic metres for the site of the characterisation and validation programme in Phase 3. The third theme, which was a principal feature of

Phase 3, dealt with the development and application of numerical modelling approaches for simulating groundwater flow and solute transport in a rock mass that was both fractured and water saturated. These approaches involved the development of rather sophisticated fracture-network models and the use of an established equivalent-porous-media model. A process for evaluating the validity of the models for the Stripa granite was developed and implemented through a combination of field experiments, numerical calculations, and expert judgement.

Although the research work at Stripa was conducted mainly in the saturated, fractured granite, some of the achievements are applicable in a general sense to other rock types at other site areas. These include the strategy of site characterisation in progressive stages using borehole-based testing techniques, together with a systematic procedure for developing a conceptual geohydrologic model of the rock mass. The geochemical techniques for determining the residence times and origins of groundwaters, together with the basic understanding of solute transport in channels within fracture planes, provide valuable starting points when planning future tests and experiments of a similar nature. Finally, the efforts to develop and implement a formalized and focussed process for evaluating the validity of numerical models yielded a documented case history for reference and use in the future.

For the most part, the Stripa Project became a reality in 1980 because of the collective efforts of Mr. Lars-Bertil Nilsson, Dr. Rudi Beck, and Professor Paul Witherspoon, in collaboration with Mr. Jean-Pierre Olivier. Mr. Nilsson, as Chairman of the Joint Technical Committee during Phases 1 and 2, and Dr. Beck, as a Technical Subgroup Chairman in Phases 1, 2, and the early part of 3, were instrumental in organizing and focussing the research activities of the project. These individuals, together with the country representatives of the Joint Technical Committee and, in particular, their Chairman during Phase 3, Mr. Per-Eric Ahlström, are acknowledged for their foresight and cooperation on an international level in guiding the overall activities of the project to a fruitful conclusion. The author wishes to express his appreciation to the members of the Technical Subgroup and the Task Force on Fracture Flow Modelling, the Principal Investigators, the Stripa Site Manager, and the Stripa Project Manager for their collective enthusiasm and spirited efforts in conducting the investigative activities of Phase 3. The thoughtful and contributory comments provided by Dr. Charles Fairhurst during reviews of the several drafts of this report, along with those of Dr. Ferruccio Gera, Dr. Malcolm Gray, and Dr. Bengt Stillborg, were sincerely appreciated. Finally, the author thanks Ms. Peggy Schultz for her patience and care in typing the drafts and final manuscript of this report, and the U.S. Department of Energy, the Swedish SKB, and RE/SPEC Inc. for their continuous and willing support of his involvement in the International Stripa Project since 1980.

TABLE OF CONTENTS

| | Page |
|--|------|
| Foreward | i |
| 1 Introduction | 1 |
| 1.1 Purpose and Approach | 2 |
| 1.2 Evolution of the Characterization and Modelling Activities | 2 |
| 1.3 Scope of the Report | 6 |
| 2 Development of Characterization Methods | 7 |
| 2.1 Hydraulic Testing Methods | 7 |
| 2.1.1 Single-Borehole Hydraulic Testing | 8 |
| 2.1.2 Crosshole Hydraulic Testing | 23 |
| 2.1.3 Significant Achievements | 28 |
| 2.2 Seismic Testing Methods | 30 |
| 2.2.1 Detection of Fracture Zones | 30 |
| 2.2.2 Improvements in Data Processing and Instrumentation | 45 |
| 2.2.3 Significant Achievements | 53 |
| 2.3 Radar Testing Methods | 53 |
| 2.3.1 Electromagnetic Properties of Rock | 54 |
| 2.3.2 Testing System | 55 |
| 2.3.3 Single-Borehole Reflection Testing | 56 |
| 2.3.4 Crosshole Testing | 58 |
| 2.3.5 Integrated Analysis of Radar Data | 61 |
| 2.3.6 Single-Borehole Directional Radar | 63 |
| 2.3.7 Significant Achievements | 65 |
| 2.4 Hydrogeochemical Characterization Methods | 67 |
| 2.4.1 Groundwater Sampling Sites | 67 |
| 2.4.2 Hydrochemistry of the Stripa Area | 68 |
| 2.4.3 Fracture Mineralogy | 69 |
| 2.4.4 Origin of Salinity in the Stripa Groundwaters | 72 |
| 2.4.5 Isotope Geochemistry | 75 |
| 2.4.6 Aqueous Sulphates | 77 |
| 2.4.7 Radionuclide Concentrations | 79 |
| 2.4.8 Summary of the Geochemical Characteristics of Stripa | 80 |
| 2.4.9 Significant Achievements | 81 |
| 2.5 Solute Transport Experiments | 82 |
| 2.5.1 Concepts of Fracture Transport | 83 |
| 2.5.2 Diffusion in the Granitic Rock Matrix | 85 |
| 2.5.3 Migration in a Single Fracture in Granite | 89 |
| 2.5.4 Migration in a Large Fractured Granitic Mass | 93 |
| 2.5.5 Migration in Fracture Channels | 100 |
| 2.5.6 Migration in a Fracture Zone | 109 |
| 2.5.7 Significant Achievements | 110 |
| 2.6 Summary of Significant Achievements | 111 |
| 3 Application of Characterization Methods | 113 |
| 3.1 Conceptual Model of the Stripa Area | 114 |
| 3.1.1 Regional Geology | 114 |
| 3.1.2 Tectonic Features | 116 |
| 3.1.3 Stripa Mine Geology | 118 |

| | | |
|-------|--|-----|
| 3.1.4 | Fracture Zones | 118 |
| 3.1.5 | Fracture Characteristics | 121 |
| 3.1.6 | Hydrology | 125 |
| 3.1.7 | Geochemistry | 127 |
| 3.1.8 | Simulation of the Groundwater Flow System | 129 |
| 3.1.9 | Significant Achievements | 139 |
| 3.2 | Conceptual Model of the Crosshole Site | 140 |
| 3.2.1 | Site Characteristics | 141 |
| 3.2.2 | Scope of the Characterization Activities | 143 |
| 3.2.3 | Radar and Seismic Testing Results | 143 |
| 3.2.4 | Geophysical Model of the Crosshole Site | 144 |
| 3.2.5 | Hydraulic Investigations | 149 |
| 3.2.6 | Design of Future Characterization Strategies | 154 |
| 3.2.7 | Significant Achievements | 157 |
| 3.3 | Conceptual Model of the SCV Site | 158 |
| 3.3.1 | SCV Programme | 158 |
| 3.3.2 | Site Characteristics | 163 |
| 3.3.3 | Geohydrologic Model of the Site | 186 |
| 3.3.4 | Validation Experiments | 193 |
| 3.3.5 | Significant Achievements | 219 |
| 3.4 | Summary of Significant Achievements | 224 |
| 4 | Modelling of Groundwater Flow and Solute Transport | 225 |
| 4.1 | Model Validation Process and Criteria | 225 |
| 4.1.1 | Definition of Model Validation | 225 |
| 4.1.2 | Model Validation Process | 226 |
| 4.1.3 | Model Validation Criteria | 228 |
| 4.2 | Groundwater Flow and Transport Models | 229 |
| 4.2.1 | Fracflow Equivalent-Porous-Media Model | 229 |
| 4.2.2 | Harwell Fracture-Flow Model | 233 |
| 4.2.3 | Golder Fracture-Flow Model | 241 |
| 4.2.4 | LBL Fracture-Flow Model | 252 |
| 4.2.5 | Verification of Groundwater Flow and Transport Codes | 260 |
| 4.3 | Validity of the Groundwater Flow Models | 268 |
| 4.3.1 | Simulated Drift Experiment | 269 |
| 4.3.2 | Validation Drift Inflow Experiment | 273 |
| 4.3.3 | Assessment of Model Validity | 281 |
| 4.4 | Validity of the Groundwater Transport Models | 282 |
| 4.4.1 | Radar/Saline Tracer Experiment | 282 |
| 4.4.2 | Tracer Migration Experiment | 286 |
| 4.5 | Evaluation of Model Validity | 298 |
| 4.6 | Summary of Achievements | 301 |
| 5 | Concluding Remarks | 303 |
| 5.1 | Summary of Significant Achievements | 303 |
| 5.2 | Transfer of Technology | 306 |
| | References | 309 |
| | Bibliography | 323 |

1 INTRODUCTION

The Stripa Project was an international research effort that was organized in 1980 for the purpose of developing techniques and methodologies for characterizing potentially suitable sites in granite for the geologic disposal of heat-generating radioactive wastes and for enhancing the long-term safety of repository systems at such sites by means of engineered barriers. At that point in time, the member countries were collectively interested in the use of granite as a repository host rock. The need to develop technology to explore in detail large bodies of granite and to design safe underground disposal facilities was clearly recognized. The Stripa mine, located in granite in Sweden, was available for use as a research facility for the development of this technology. As such, the Stripa Project was initiated in 1980 and continued through three phases of research activities that ended in 1992.

The need to develop tools and techniques to evaluate the geohydrologic characteristics of a saturated, fractured rock mass was recognized at the very outset of the Stripa Project. An emphasis was placed on the development of tools and techniques that would minimally disturb the natural state of the rock mass during testing, such that the data would closely reflect the true *in situ* conditions. This goal suggested the use of remote sensing techniques in boreholes. Also, this approach seemed to be the most cost-effective way of exploring large volumes of rock, such as required in the search for geologic disposal sites. The data collected by remote sensing from a few strategically placed boreholes could be used both to make a preliminary assessment of the suitability of the site for long-term containment of radioactive waste, and to guide additional characterization efforts to investigate specific features and anomalies. As the Stripa Project progressed through the decade, the research efforts became more focussed on the application of the tools and techniques to characterization of site areas within the Stripa mine, together with the development and application of numerical modelling approaches for simulating groundwater flow and solute transport.

Because the Stripa mine was operated for several centuries, the general geology of the rock mass in and around the mine and the surface hydrology in the general area were already well documented when the project began. For these reasons, the Stripa Project concentrated on methods to evaluate the characteristics of the structural features and hydrology within the rock mass that contained the mine. The structural features were principally the discrete zones of intensive fracturing in the granite, and the systems of less intensive fracturing contained within the masses of rock between these discrete fracture zones. The groundwater hydrology and its associated geochemistry reflected the disturbance produced by mining activities over the many years, together with the groundwater conditions at the surface and in the surrounding rock masses. Similarly, the natural state of stress in the rock mass had been redistributed because of the mined excavations. Thus, when investigations began in 1980, the natural state of the rock mass at Stripa was one that reflected an adjustment to the disturbances induced by underground mining over a period of several centuries.

1.1 PURPOSE AND APPROACH

This report summarizes the main research results and achievements from those investigations in the Stripa Project that dealt with characterization of the natural barriers and simulation of groundwater flow and transport. Although there were many investigations conducted over the thirteen years, three central research themes emerged over the three phases of the Project. These themes dealt with the development and subsequent application of characterization methods and the modelling of groundwater flow and solute transport within a saturated, fractured granitic rock mass. The significant achievements that resulted from the investigations within each of the themes are discussed with some thought given to their potential for application to other rock types and conditions.

1.2 EVOLUTION OF THE CHARACTERIZATION AND MODELLING ACTIVITIES

The Stripa mine is located in Sweden, approximately 250 km west of Stockholm, as shown in Figure 1-1. Mining of iron ore began in the fifteenth century and ended in 1976 when the ore reserves were exhausted. In 1976, the Swedish Nuclear Fuel Company (SKBF) leased the mine and initiated *in situ* experiments in the granite rock that had hosted the iron ore. These experiments were designed to provide preliminary technical data for use in evaluating the suitability of granite for deep disposal of high-level radioactive wastes from nuclear power reactors. In 1977, the Swedish-American Cooperative (SAC) Programme was initiated and *in situ* experiments were conducted in the Stripa granite over a period of about three years. One of the principal activities of this programme involved an assessment of fracture hydrology within the rock mass at Stripa. This assessment included geophysical and geochemical studies, *in situ* stress measurements, evaluations of the fracture characteristics, and a large macropermeability test in the rock mass surrounding a newly excavated drift. As shown in the evolutionary diagram in Figure 1-2, the results from the SAC Programme directly influenced the thinking that led to the investigations during the first phase of the Stripa Project.

Phase 1 of the Stripa Project, beginning in 1980 and ending in 1985, was essentially a learning exercise for the researchers (Executive Summary of Phase 1, 1986). The tools and methods used to evaluate the hydraulic characteristics of a "large" fractured rock mass within the Stripa mine were based principally on existing technology. A large fracture zone within the site for the hydraulic investigations was discovered by accident during drilling of one of the exploration boreholes. This was indeed a fortunate discovery in that emphasis in testing shifted from an evaluation of the hydraulic characteristics of the rock mass in general to an evaluation of the hydraulic characteristics of the fracture zone. In fact, this development would chart the course of activities in Phase 2.

The hydrogeochemical investigations were undertaken by a group of experts from many countries, whose collective talent formed the basis for developing the geochemistry programme in Phases 1 and 2. The design of tracer migration experiments in a fractured rock mass was in its infancy in 1980. As such, the tests in the Stripa mine focussed on the migration of

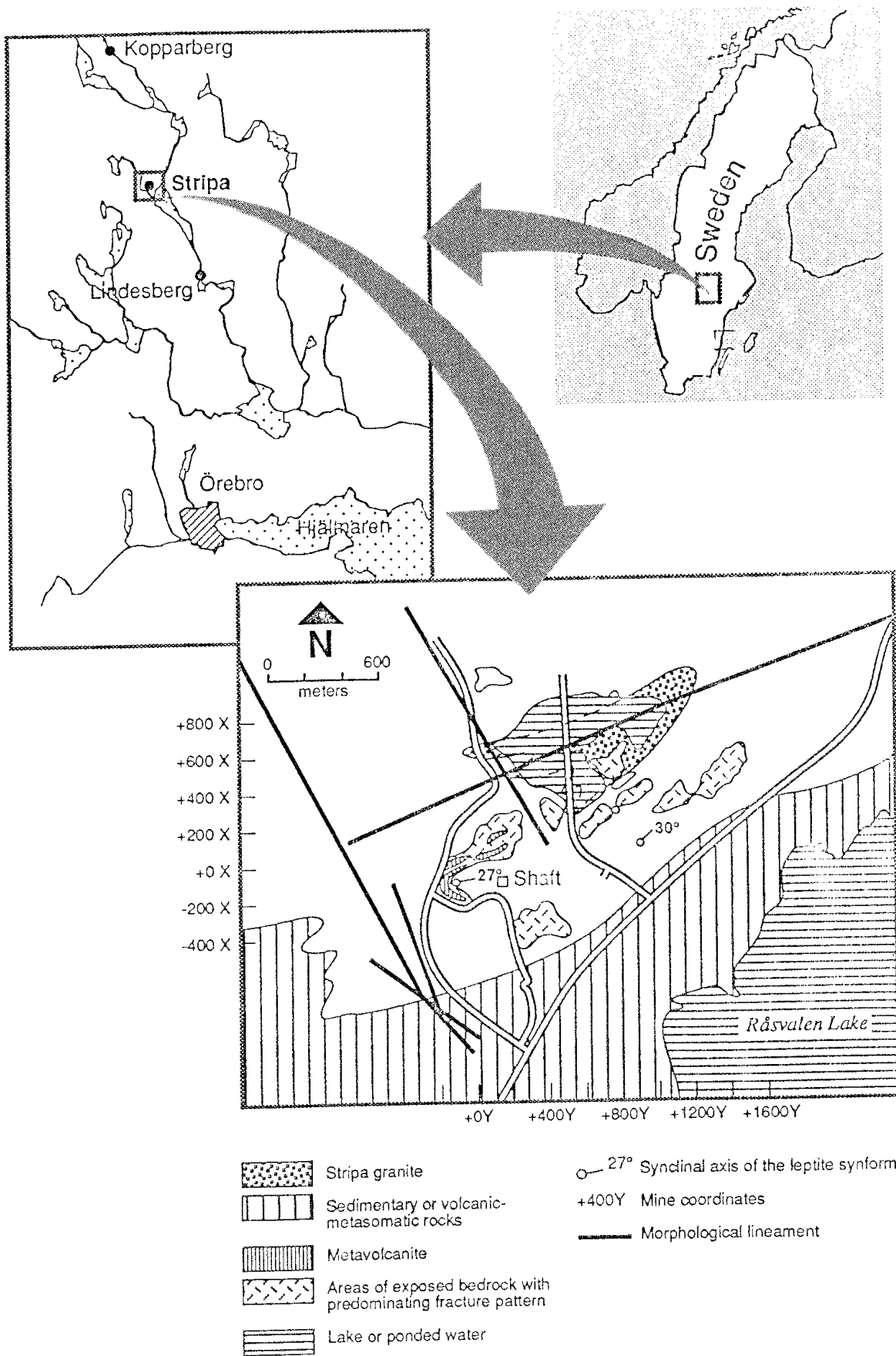


Figure 1-1 Location of the Stripa mine (Dershowitz et al, 1991 a).

tracers within single fractures that could be identified in the granitic walls of an existing drift.

Based on the knowledge and experience gained during the first three years of Phase 1, the activities of Phase 2 were designed to develop specific techniques for characterizing fracture zones in saturated, fractured granitic rock masses (Executive Summary of Phase 2, 1989). The borehole-radar testing technique was developed and existing techniques for seismic and hydraulic testing in boreholes were adapted to evaluate the structural features in the Stripa granite. Greater attention was also given to defining the hydrologic characteristics of the Stripa area and the rock mass containing the Stripa mine. The hydrogeochemical investigations focussed on determinations of the patterns of groundwater circulation from the surface to depths below the mine workings. A tracer test was conducted in a large fractured rock mass that had been characterized by core logging, borehole photography, and observations of fractures and structure in the walls of drifts.

In 1985, it became evident that the development of the improved characterization techniques was approaching a successful conclusion. It was decided that the most useful follow-up activity would be to demonstrate the applicability of the technology by characterizing a previously unexplored, or "undisturbed", site in the Stripa mine. A previously "undisturbed" volume of granite within the Stripa mine was selected as the Site Characterization and Validation (SCV) site for a programme of characterization, prediction, and validation. As such Phase 3 developed into a full-scale characterization effort of a small-scale site in the Stripa mine, together with the development and application of numerical modelling techniques for simulating groundwater flow and solute transport in a saturated, fractured rock mass.

Characterization would use techniques developed in Phase 2, together with refinements in the borehole-radar testing technique and the data interpretation schemes for the borehole-seismic testing method that took place in Phase 3. The prediction and validation exercise involved the simulation of groundwater flow and solute transport within the SCV site by means of numerical models. *In situ* experiments were conducted to evaluate the channelling aspects of solute transport in fractures, and a tracer migration experiment was performed in a well-characterized fracture zone within the site.

Thus, over a period of thirteen years, the Stripa Project progressed through sequential stages of learning, development, and application for purposes of characterizing the hydrologic, geochemical, and mechanical features of a rock mass. The end results of these efforts can be described in terms of sophisticated tools and techniques for rock mass characterization, an understanding what is required for designing a meaningful solute transport experiment in fractured granite, and effecting a process for evaluating the validity of equivalent-porous-media and fracture-flow numerical models for simulating groundwater flow and transport in a saturated, fractured rock mass.

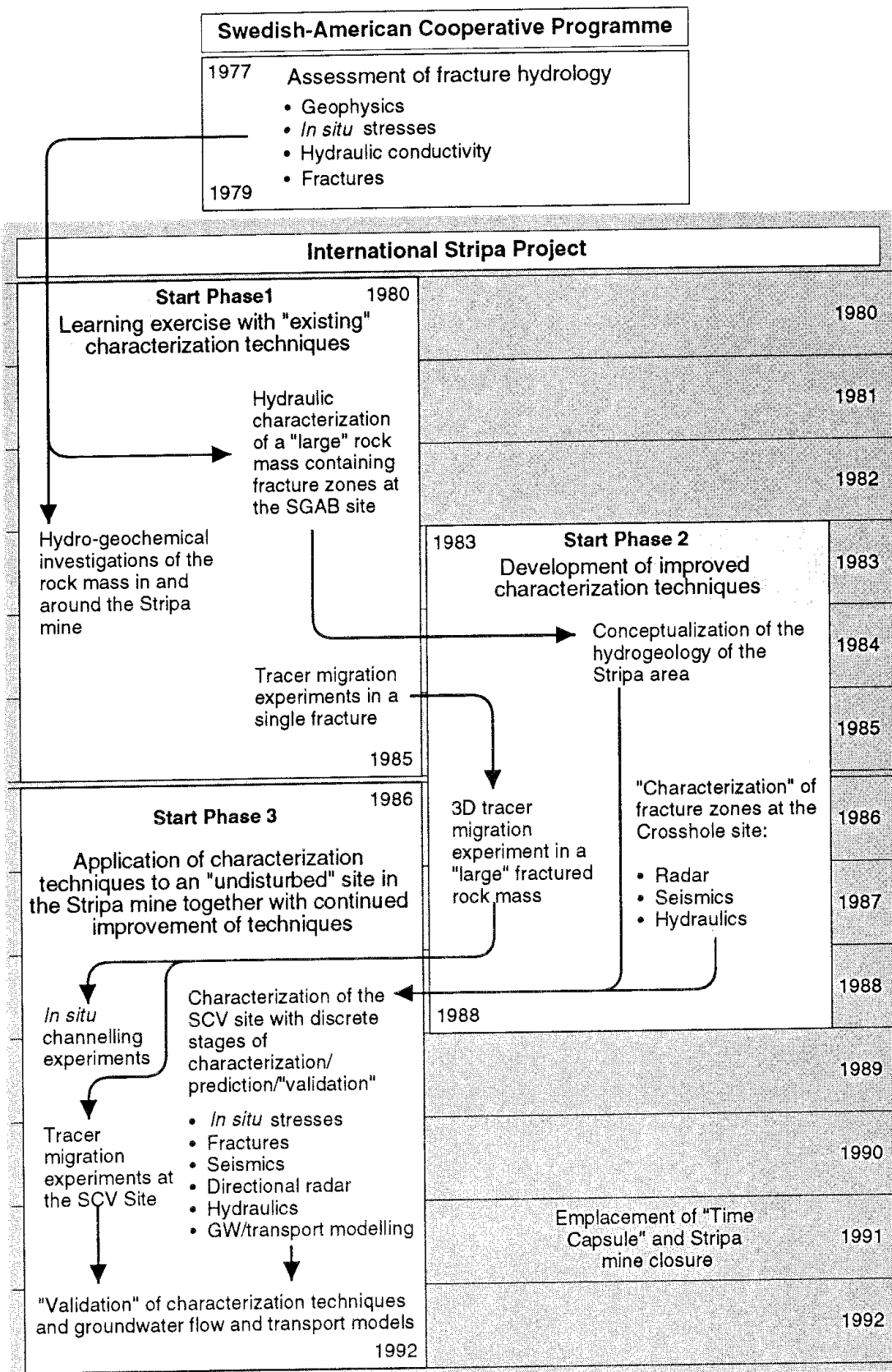


Figure 1-2 Evolution of the characterization, geochemistry, tracer migration, and modelling activities during the Stripa Project.

The development of conceptual geohydrologic models at Stripa began during Phase 2 and was continued as a significant part of Phase 3.

1.3 SCOPE OF THE REPORT

This report has been structured according to the three central themes of the Stripa Project that dealt with first the development and then the application of characterization methods and the modelling of groundwater flow and solute transport. Chapter 2 summarizes the development of the characterization methods, including the hydraulic, seismic, and radar borehole-testing methods, the hydrogeochemical characterization techniques, and the solute transport experiments. The application of these characterization methods is presented in Chapter 3 from the viewpoint of developing conceptual models of the geologic, hydrologic, and geochemical features of a rock mass. In particular, conceptualizations of the geohydrologic features of the Stripa area and the Crosshole site and SCV site within the Stripa mine are discussed in detail. Chapter 4 focusses on the modelling of groundwater flow and transport at the SCV site by means of equivalent-porous-media and fracture-flow models, including the development of such models and the evaluation of their validity for simulating groundwater flow and solute transport at the SCV site. Chapter 5 summarizes the significant achievements of the Stripa Project in terms of rock mass characterization, and discusses the potential for transfer of such technology to other sites and rock types.

2 DEVELOPMENT OF CHARACTERIZATION METHODS

The development of characterization methods in the Stripa Project began in 1980 with a focus on the measurement of hydraulic, transport, and geochemical properties of a saturated, fractured granitic rock. The identification of zones of extensive fracturing in the Stripa granite led in 1983 to the development of remote-sensing techniques, involving seismic and electromagnetic wave propagation, for quantifying the geometric characteristics of such zones. Concurrently, the hydraulic testing techniques were improved in order to evaluate the hydrologic characteristics and conditions of these zones. Later, in 1986, refinements were made in the remote-sensing techniques and the associated data interpretation schemes.

Because of the several centuries of mining, the complexity of the groundwater chemistry within the rock mass at Stripa dictated a need for improvements in techniques for obtaining "uncontaminated" groundwater samples and for evaluating the range of "ages" of the waters that existed from the surface to depths below the mine workings at Stripa. Tracer tests in single fractures in the Stripa mine in Phase 1 provided a measure of confidence for undertaking a large-scale tracer test in a substantial volume of the fractured granite in Phase 2. The results of these tests demonstrated the need for comprehensive characterization of the structural features and their hydrologic properties at a site before undertaking the tracer test itself. This approach was taken in designing and implementing the tracer test at the SCV site in Phase 3.

The emphasis in this chapter is placed on the characterization tools and techniques that were developed principally in Phases 1 and 2, including the testing equipment and procedures and typical results. The application of these tools and techniques in an integrated and comprehensive manner is discussed extensively in Chapter 3 in the context of the detailed characterization of the SCV site in the Stripa mine that took place in Phase 3.

2.1 HYDRAULIC TESTING METHODS

The hydrologic programme of research in the Stripa Project began in 1980 in Phase 1 with the intent of developing tools and techniques to quantify the hydraulic conductivity of a large volume of granitic rock by means of tests conducted in a few boreholes. During the drilling of the boreholes at the test site in the Stripa mine, a significant fracture zone was encountered in one of the vertical boreholes. Subsequently, the programme was expanded to include hydraulic testing of the fracture zone to evaluate its connectivity with the other boreholes at the site. The results of these investigations led to a focussed effort in Phase 2, beginning in 1983, to develop a method for measuring the distribution of hydrologic properties and conditions within

fracture zones, as well as for evaluating the connectivity of the zones throughout a site, by means of crosshole testing. In crosshole hydraulic testing, a hydraulic source is placed in one borehole and receivers in another borehole. Sinusoidally varying pressure and flow rates are used as sources in order to decrease the time required for the zones to regain their pre-test head conditions and to minimize the influence of a fluctuating head distribution within the rock mass around the test site. The hydraulic testing tools and techniques and data interpretation schemes, developed over a period of some six years in Phases 1 and 2, were applied extensively in the hydrologic characterization of the SCV site in Phase 3.

2.1.1 Single-Borehole Hydraulic Testing

The purpose of the geohydrologic investigations in Phase 1 was to develop borehole testing methods and instruments in order to study the geologic, geophysical, hydraulic, and hydro-geochemical characteristics of large crystalline rock masses, and to determine the hydraulic characteristics of, and interactions between, fracture zones in a crystalline rock mass (Carlsson et al, 1980; Carlsson and Olsson, 1985a,b,c). These investigations were carried out on the 360 m level of the Stripa mine at a location known as the SGAB site, and involved the use of an orthogonal array of three boreholes. Conventional well-logging tests were also conducted, including core-logging, borehole deviation, natural gamma, single-point resistance, resistivity, temperature, self potential, and borehole-fluid resistivity. Subsequently, in Phase 2, single-borehole hydraulic tests were conducted in the suite of boreholes in an area known as the Crosshole site located immediately adjacent to the south side of the SGAB site. The purpose of these tests was to measure the specific storage and hydraulic conductivity of the rock mass in support of the crosshole hydraulic testing (Black et al, 1986, 1987; Noy et al, 1988).

As mentioned previously, the groundwater system in and around the Stripa mine had been influenced by the mining activities during the past several centuries. As mining took place, new flow paths were activated in the rock and the drainage thresholds successively lowered. Because of the rather slow rate of mining, the groundwater system probably adjusted itself continuously to remain in balance with the drainage from the underground drifts. That is, the groundwater system was probably in a quasi steady-state condition. Since the mine was in effect a potential sink, it was convenient to use the natural drainage for water extraction and to measure the pressure build-up after closing the boreholes, or the pressure fall-off after opening the boreholes, in the Phase 1 tests. By this technique, no foreign water was introduced into the groundwater system, and the disturbances to the head distribution were limited. However, it was intended that water injection tests be carried out to evaluate the applicability of such techniques in an underground environment.

Test Sites

The Stripa pluton is located in a supra-crustal belt with structures striking mainly in the NE-SW direction. Because the tectonic activity has been relatively mild since the intrusion, the monzogranite of the pluton is

generally not foliated. As shown in Figure 2-1, the pluton is an elongated intrusion that parallels pre-existing bedding and foliation planes. The contact between the leptites and the monzogranite was intersected by the accessway to the SGAB site for the geohydrologic tests. The site, as shown in Figure 2-2, was located on the 360 m level of the Stripa mine, approximately 300 m south-to-southeast from the ventilation shaft. The intrusive monzogranite penetrates the metamorphic basement rock as a thin veneer. At the contact, the monzogranite occurs partly as inclusions or dikes in the leptite. On a microscopic scale, it is a fine-grained, pinkish homogeneous granitoid with an aplitic appearance of the matrix and scattered larger grains of muscovite. To the north of the ventilation shaft, the monzogranite appears at the bedrock surface in the center of a structural elevation. A few outcrops further to the north and northwest indicate that the lower part of the leptite sequence, dominated by metavolcanics, forms a nearly antiform structure that strikes to the north and is bordered to the west and southeast by stratigraphic younger mica schists. The basal limit of the metavolcanics, as well as the continuation of the Stripa monzogranite to the northwest and southwest below the leptites, are not known. The SGAB and Crosshole sites were located in a massive monzogranite in contact with the north limb of the leptite syncline. On the basis of previous boreholes drilled from the surface and the subsurface, the known vertical extent of monzogranite in the mine area is about 850 m.

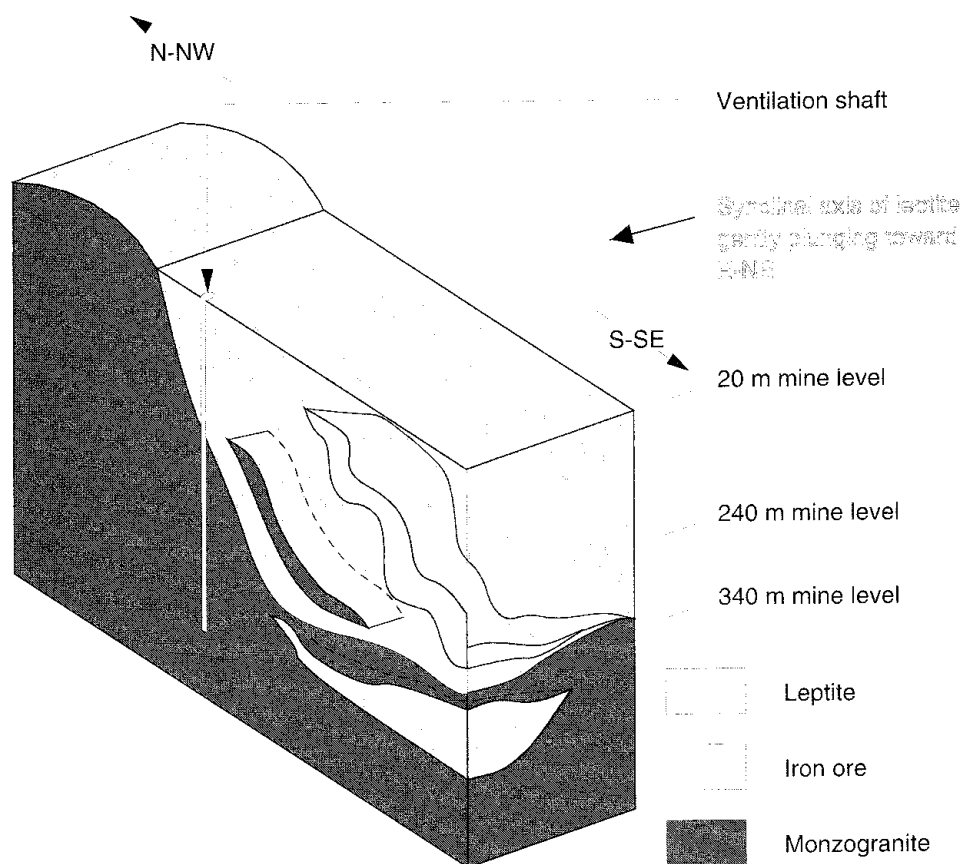


Figure 2-1 A generalized view of the Stripa pluton (Carlsson et al, 1981).

This conceptualization of the Stripa geology is based on data from surface and subsurface exposures and boreholes, and from investigations conducted during the SAC programme.

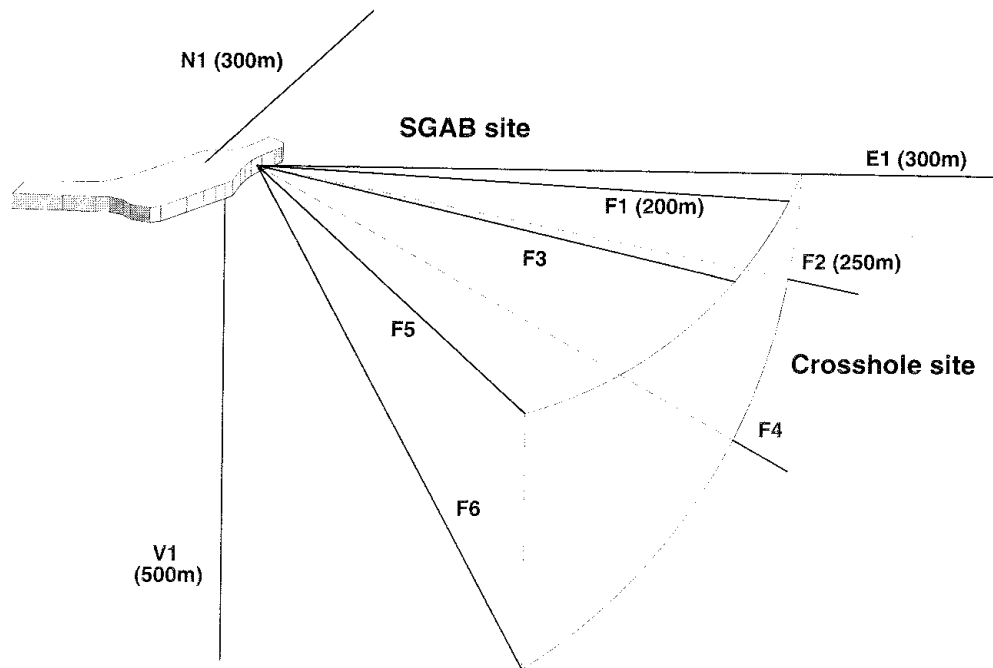
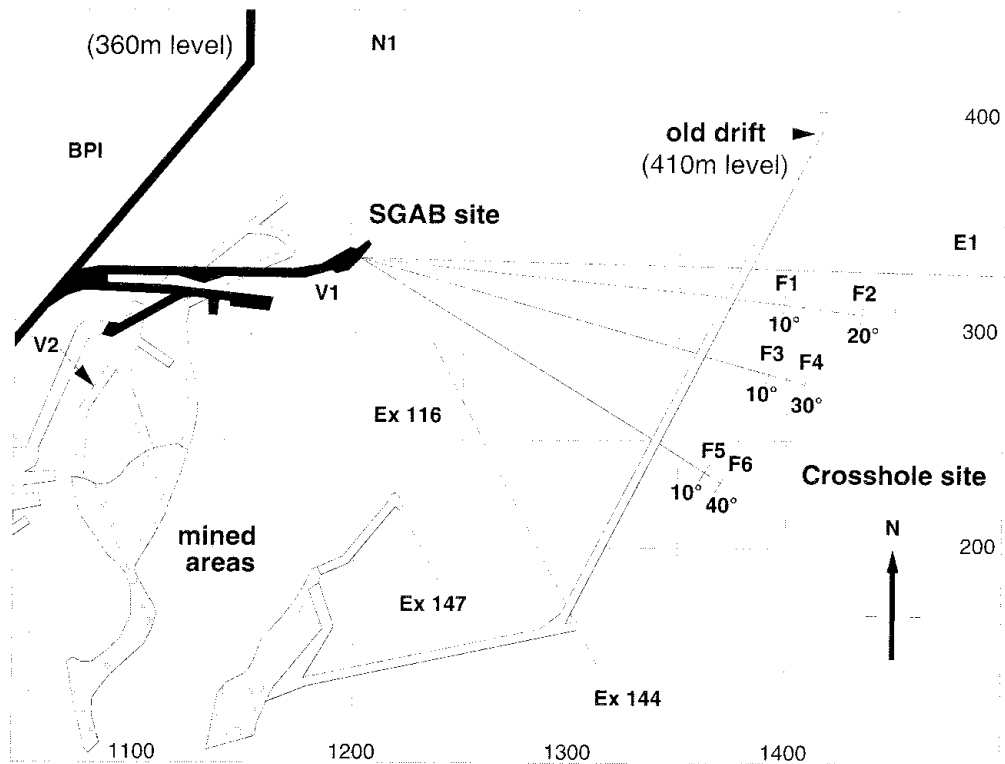


Figure 2-2 Plan and perspective views of the borehole arrays at the SGAB and Crosshole sites (Carlsten et al, 1985; Black et al, 1987).

The SGAB site was used for the hydraulic investigations in Phase 1, and the Crosshole site for the radar, seismic, and hydraulic investigations in Phase 2. All of the boreholes were drilled from the end of a drift on the 360 m level.

Three boreholes were core drilled from the end of a drift at the SGAB site on the 360 m level of the mine. The two subhorizontal boreholes, designated as N1 and E1, were drilled to distances of 300 m with dip inclinations of about 10°. The third drillhole, designated as V1, was drilled to a depth of about 506 m where a heavily fractured zone was encountered. It was not possible to continue the drilling operation without stabilization of the fracture zone. Stabilization could have introduced chemical substances into the rock mass and conceivably affected the hydrochemical investigations. Consequently, the drilling of borehole V1 was terminated, and a fourth borehole, known as V2, was drilled from a second site on the 410 m level. Borehole V2 was originally drilled to a depth of 471 m during the SAC programme and was deepened during Phase 1 to a depth of 822 m, which was 1230 m below the ground surface. The 76 mm-diameter boreholes were drilled with rotary drilling equipment using standard double-core barrels with a maximum core capacity of 6 m. Deviations of the boreholes were found to be minor, as expected because of the homogeneity of the Stripa granite.

A crosshole electrical method, known as the *Mise a la Masse* method, was used to determine the orientation of the fracture zone encountered in drillhole V1. A current electrode was positioned in the fracture zone in borehole V1 and the potential field was measured by means of electrodes positioned in boreholes E1, N1, and V2. Based on model calculations of the potential field, the strike and dip of the fracture zone were estimated to be N40E and 70SE, respectively. This orientation was comparable to a strike of N70E and a dip of 60SE inferred from geomorphologic and structural observations in the rock mass surrounding the Stripa mine.

The variation in fracture frequency as a function of depth is shown in Figure 2-3. These data were based on core logs from vertical boreholes SBH1 and SBH2 drilled from the surface and boreholes V1, V2, N1, and E1 drilled from the underground levels (Carlsson et al, 1981, 1982a,b). Apart from the rock mass at depths less than about 100 m and the fracture zone at a depth of about 820 m, the frequency was about two fractures per metre. However, vertical boreholes tend to underestimate the existence of vertical or steeply dipping fractures. With the inclusion of the data from boreholes N1 and E1, the frequency was increased to about four fractures per metre. Based on data from oriented core, three steeply dipping fracture sets, striking to the north, were identified, along with a fourth nearly horizontal fracture system. The three near-vertical fracture sets at the SGAB site are different in orientation from those observed at the SAC area located to the west. The difference in orientation was probably governed by the configuration of the leptite syncline, in that the fracturing in the rock mass located closer to the contact between the granite and the leptite would be influenced by the syncline.

The Crosshole site, shown in Figure 2-2, was located on the 360 m level of the Stripa mine and consisted of a rock mass defined by seven boreholes that outlined a tilted pyramid with a height and base of about 200 m. The site was situated immediately south of the SGAB site, with the north boundary defined by borehole E1 which was drilled in Phase 1. The top of the tilted pyramid was defined by boreholes F1, F3, and F5, which were drilled to distances of 200 m at inclinations of 10° and strikes ranging from S84E to S58E. The bottom of the pyramid was defined by boreholes F2, F4, and

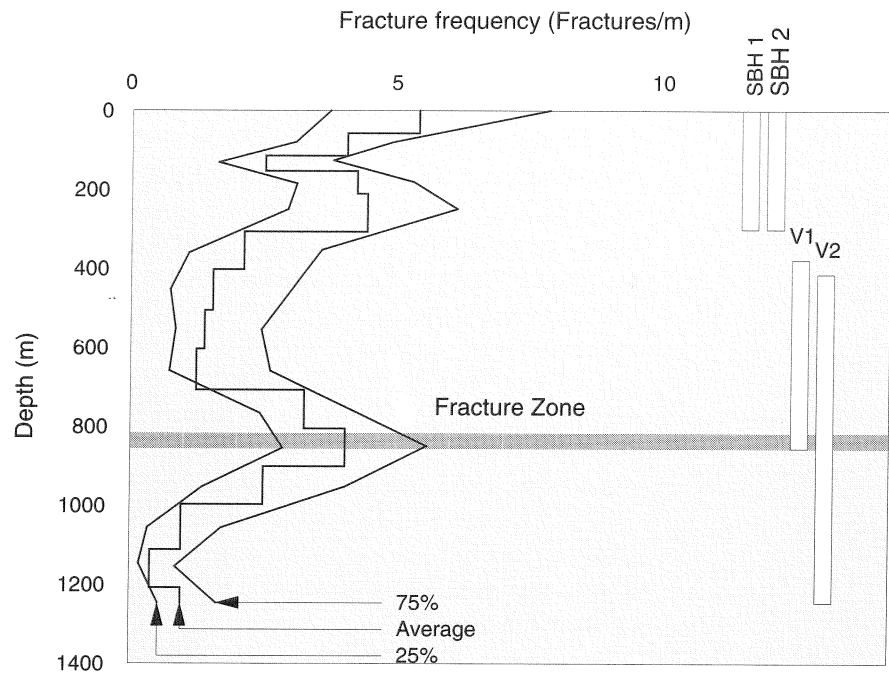


Figure 2-3 Fracture frequency as a function of depth at the SGAB site (Carlsson and Olsson, 1985c).

The frequency is assumed to be log-normally distributed.

F6, which were drilled to distances of 250 m at inclinations increasing from 20° to 40° and bearings ranging from S84E to S58E.

Standard well-logging tests were conducted in each of the F boreholes (Carlsten and Stråhle, 1985; Magnusson et al, 1987). The drill cores were mapped by visual observation to determine rock type, fractures, and fracture minerals. The orientations of the fractures were determined by means of a TV camera that photographed the wall of each borehole. These data, when analyzed, indicated that the collection of seven boreholes had intersected five major planar zones of fracturing, designated as A, C, D, E, and F, and one highly fractured zone of limited extent, designated as B. Zone B contained small, dispersed cavities and exhibited high porosity. The fracture zones struck to the NE/N-NE and dipped steeply toward E-SE or W-NW. The fractures in the "intact" rock mass between the fracture zones exhibited strikes and dips that were similar to those of the fracture zones.

Single-Borehole Hydraulic Testing Equipment

The equipment for the pressure build-up testing, shown in Figure 2-4, consisted of a double-packer system with a downhole probe containing the pressure transducers (Jacobsson and Norlander, 1981). The system was positioned either by wire or pipeline, depending on the inclination of the boreholes. The downhole probe, containing two pressure transducers and one thermal element, was connected to the double-packer system and to a surface-control valve. The packers were inflated with nitrogen gas from the surface by means of a connecting nylon tube. When inflated, the packers enclosed two test sections located between the packers and between the

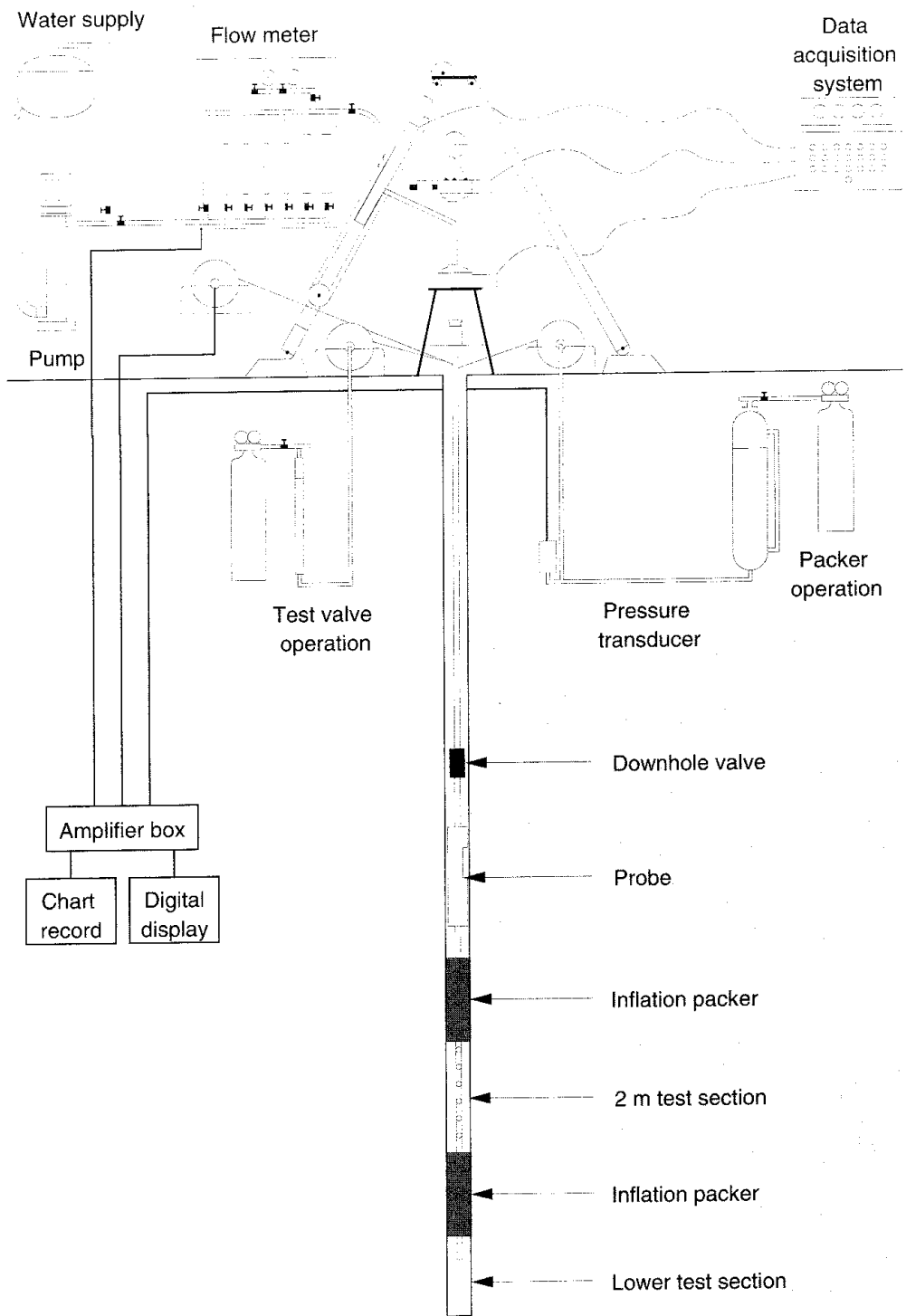


Figure 2-4 Schematic view of the equipment used for the pressure build-up tests (Jacobsson and Norlander, 1981; Carlsson and Olsson, 1985a).

bottom packer and the bottom of the hole. These two test sections were connected to the pressure transducers in the probe, as well as to the surface in order to recover water samples.

The equipment used for the injection tests, similar to that shown in Figure 2-4, consisted of a double-packer assembly with a packer spacing of 10 m, injection tubes, pressure transducer, and test valve. The surface unit included equipment to regulate the inflation of the packers, a pump, a flow meter, and an electronic system for the pressure transducer. The flow meter had the capability to make measurements over a range of about 0.000001 ℓ/s to 0.1 ℓ/s . Although laboratory tests showed that the packers would seal with an overpressure of 0.4 MPa, an overpressure of 1.5 MPa was used during the field testing.

Single-Borehole Shut-In Tests at the SGAB Site

A borehole shut-in test involved sealing off a section of a borehole and monitoring the buildup in water pressure within the packed-off section. The expected pressure response as a function of time is shown in Figure 2-5. The packer system was positioned in a borehole at the section of interest and the packers were inflated with nitrogen gas. The flow from the section between the last packer and the bottom of the borehole decreased to zero as the pressure in the section increased. The main test section, located between the packers, was allowed to produce water in a free-flow condition for a period of at least twelve hours. Then, the down-hole valve was closed and the pressure increased in the packed-off section. The pressure increase in each test section was monitored for about five days, at which time the down-hole valve was opened. The test cycle was complete when the packers were deflated and free-flow conditions resumed.

Shut-in tests were performed in selected 2 m sections in boreholes E1 and N1 and in selected 3.7 m sections in borehole V2 (Carlsson and Olsson, 1985a). The test sequence began in the section located nearest to the borehole collar and was continued along the borehole. This procedure gave

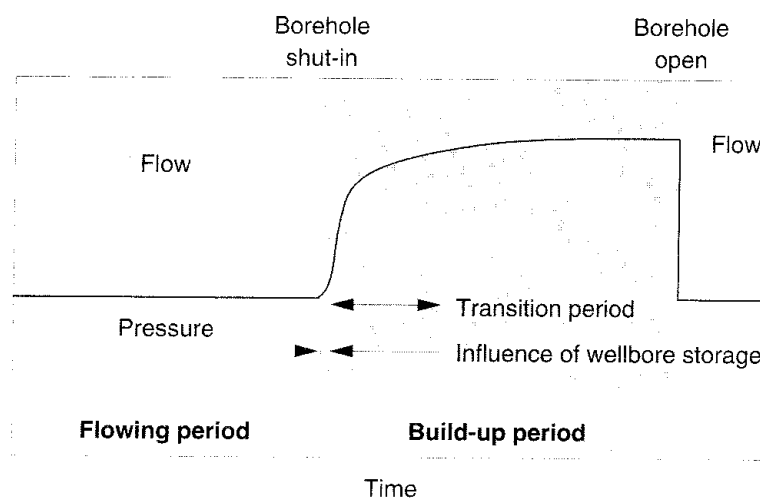


Figure 2-5 Pressure response as a function of time for a borehole shut-in test (Carlsson and Olsson, 1985c).

time for the natural pressure around the borehole to rise to its "natural undisturbed" value before the actual test in the selected section was performed. In addition, shut-in tests were performed in the lowermost part of the V1 borehole containing the highly fractured zone, and in five different sections of borehole V2 containing visible fracture zones.

The data were evaluated by first considering flow regimes (Raghavan, 1980), and secondly by considering wellbore storage and skin effects (Agarwal et al, 1970). By use of these procedures and the data from 29 pressure build-up tests, the hydraulic conductivity was found to range from about 10^{-12} m/s to 10^{-8} m/s. The tested sections, chosen on the basis of data obtained from core logs and standard well-logging evaluations, represented principally highly fractured zones that were expected to have relatively high values of hydraulic conductivity. The time-dependent head changes in boreholes N1 and E1, shown in Figure 2-6, indicated transitions from linear to radial flow over the test durations. The head changes in boreholes V1 and V2, shown in Figure 2-7, were representative of double-porosity behavior of the rock mass.

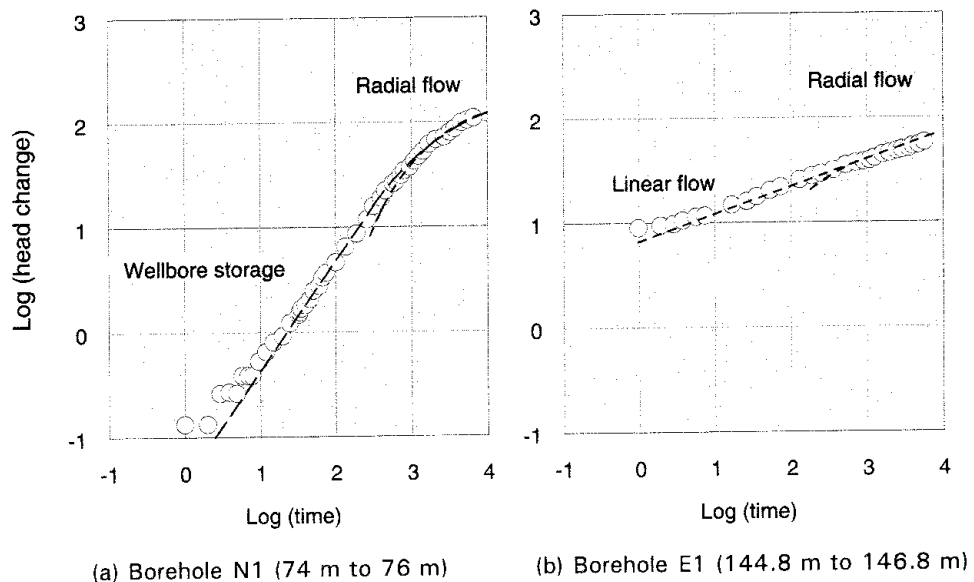


Figure 2-6 Examples of the two principal types of time-dependent head responses obtained from the borehole shut-in tests (Carlsson and Olsson, 1985c).

The curve on the left was obtained in borehole N1 and the unit slope in early time indicates wellbore storage, with a transition to radial flow in later time. This type of curve is generally representative of positive or zero skin effect. The curve on the right was obtained in borehole E1 and is indicative of linear flow behavior during the early part of the test, with a transition to radial flow in later time. This type of curve represents in general a negative skin effect, indicating that the fractures interact closely with the borehole. The units of head change and time are metres and minutes, respectively.

Single-Borehole Water-Injection Tests at the SGAB Site

Using the equipment shown in Figure 2-4, water injection tests were conducted in 10 m sections over the entire lengths of boreholes E1, N1, and

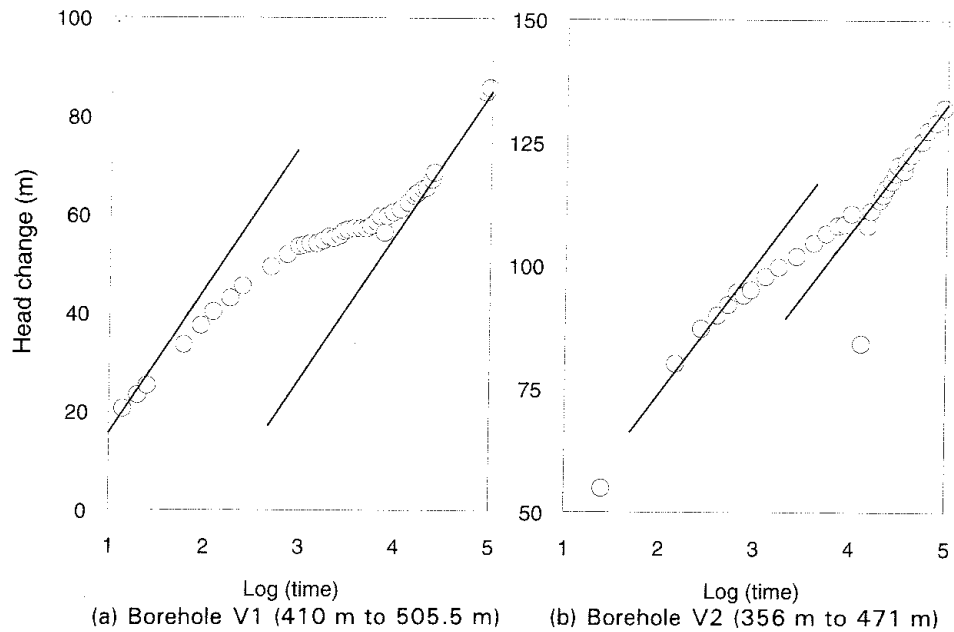


Figure 2-7 Examples of time-dependent head responses from shut-in tests in boreholes V1 and V2 that illustrate double-porosity behavior (Carlsson and Olsson, 1985a,c).

The unit of time is minutes.

V1 (Carlsson and Olsson, 1985b). As illustrated in Figure 2-8, a test began by allowing a small build-up in water pressure, followed by water injection for two hours. The injection flowrate was monitored continuously during this time. After the injection was discontinued, the pressure fall-off, or recovery, was monitored for two or more hours. On average, the total testing time for a 10 m section of borehole required one working day, including installation and testing.

When conducting an injection test, the pressure in the test section should be the same as that in the surrounding rock mass. Because of the very low hydraulic conductivity of the Stripa rock, this would have required a long time. Instead, the injection test was performed as a test superimposed on the natural change of the water pressure in the rock mass when the test section was shut-off. At the same time, testing began in the section of the borehole nearest the collar and proceeded away from the collar. It was expected that this testing sequence would allow adequate time for the pressure in the part of the borehole beyond the last packer to rise close to its natural state. However, when moving the equipment from one test section to the next, a disturbance was created in the new section. Thus, when the next test was performed, a build-up in pressure had already occurred in the new section. This condition gave a very rapid decrease in the water-injection rate, in some cases approaching zero, and an increase in head exceeding the applied excess pressure.

In addition, over the tested section, a large hydraulic gradient existed in the direction parallel to the borehole. Between the borehole collar and the first

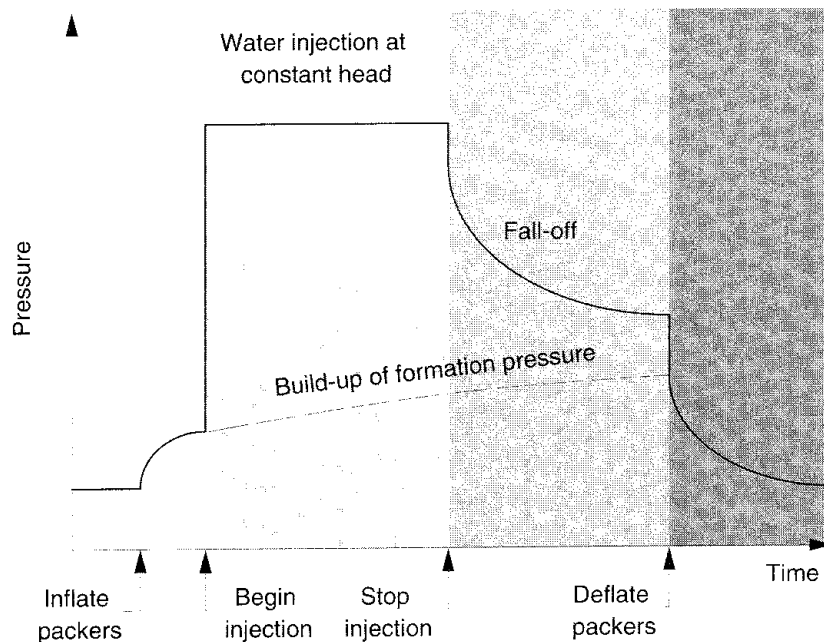


Figure 2-8 Pressure response as a function of time for a borehole water injection test (Carlsson and Olsson, 1985b).

packer, the hydraulic head in the borehole was expected to correspond to the drift level. Between the last packer and the end of the borehole, the head approximated the natural formation head. In the tested 10 m section between the packers, there existed a gradient which represented the difference between the drift level and the natural formation head along the borehole. To avoid the large gradient and thereby minimize its influence on the test data, a third packer should have been placed 10 m to 20 m in front of, or beyond, the first packer.

To achieve consistency in the data interpretation, it is advisable that certain testing requirements be met. In particular, during the recovery period after the water injection has been discontinued, other testing activities in the general area of the site should be discontinued in order to minimize any change in the formation pressure. Furthermore, the equipment used for the injection tests should be capable of creating injection heads well above the pseudo-stationary formation head. If a significant change in formation pressure occurs during the testing, then this perturbation should be taken into account when evaluating the pressure build-up response obtained in the test. In summary, it is important that a steady-state natural-formation pressure condition be established in the test section prior to any testing.

The frequency distribution of the hydraulic conductivity in 10 m sections in borehole V1 above the highly fractured zone is shown in Figure 2-9. The median value is about 10^{-13} m/s, which can be compared to a median value of about 10^{-11} m/s obtained from 6.6 metre test sections in the upper portion of borehole V2 during the period of the SAC investigations. The values calculated from the data obtained during injection were in general lower than those calculated from the data obtained during the recovery, for hydraulic conductivities below about 10^{-11} m/s.

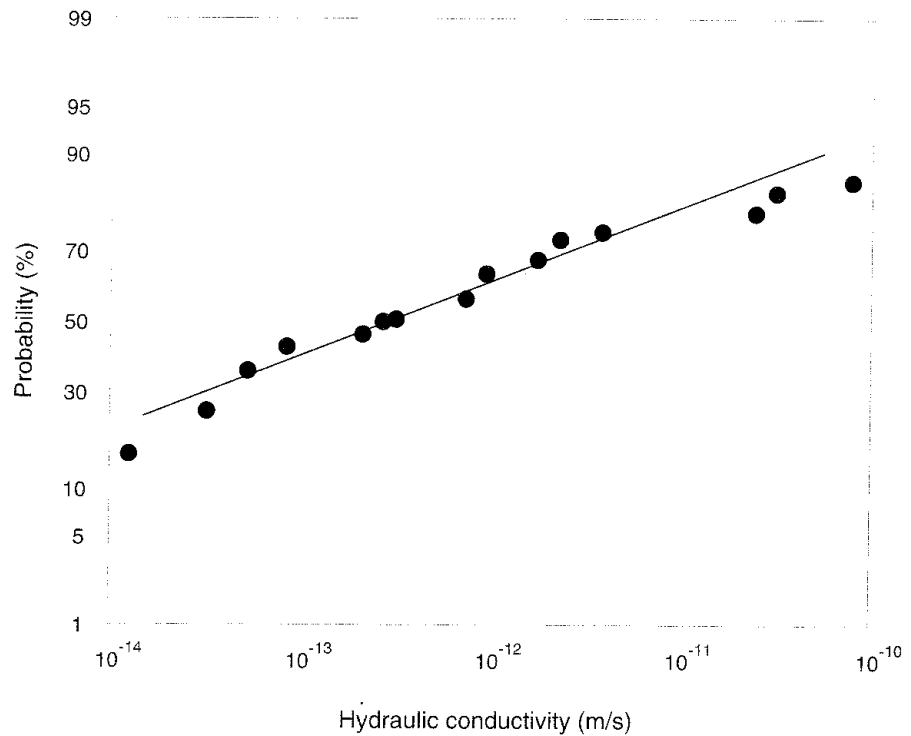


Figure 2-9 Frequency distribution of the hydraulic conductivity in 10 m sections in borehole V1 above the highly fractured zone (Carlsson and Olsson, 1985c).

Single-Borehole Hydraulic Tests at the Crosshole Site

By the use of equipment and testing procedures similar to those described previously, constant-head hydraulic tests were conducted in boreholes F1 and F2 at the Crosshole site (Black et al, 1987). In borehole F6, constant-head hydraulic tests were performed in zones of low hydraulic conductivity, and constant-flow injection tests were performed in zones with relatively high hydraulic conductivity. As shown in Figure 2-10, the form of the data obtained from the constant-head hydraulic tests in borehole F6 was similar to that obtained in boreholes F1 and F2, except that longer periods of time were allowed for the formation head to stabilize before imposition of the applied head.

Pulse and slug tests were conducted principally in boreholes F3, F4, and F5, and to a limited extent in boreholes F1, F2, F6, and E1. The form of the data is shown in Figure 2-11. The tests involved creating a sudden head change in a packed-off section of a borehole and measuring the subsequent return of the head to its original equilibrium value. In the slug test, the head was changed and observed within a tube containing an open water level. In the pulse test, the head applied to an enclosed volume of water connected to the test zone was changed and observed. The pre-test period after borehole shut-in, during which the formation pressure is allowed to attain a quasi steady-state condition, is particularly important in this form of

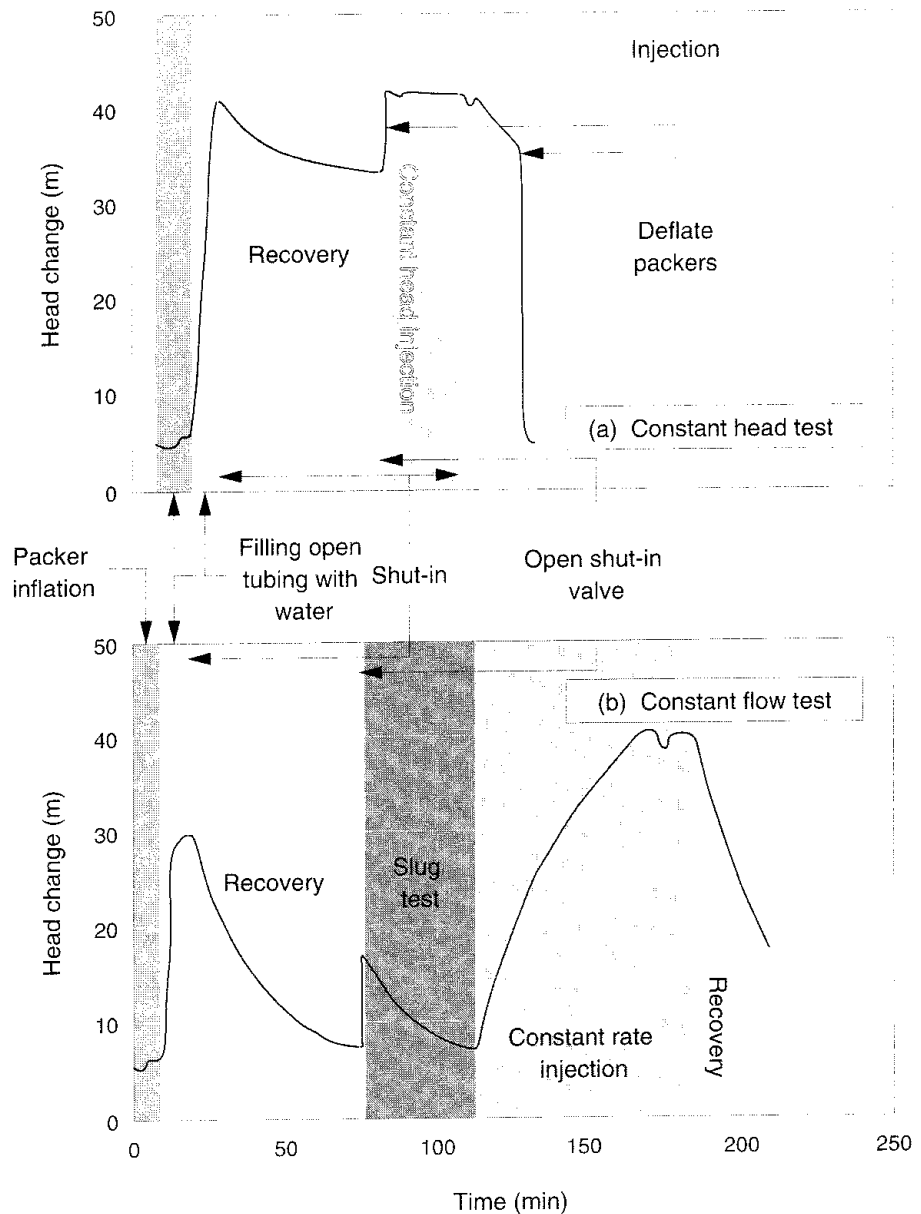


Figure 2-10 Examples of the time-dependent head responses in borehole F6 during constant-head and constant-flow injection tests (Black et al, 1987).

The constant head test was conducted over the 195 m to 205 m interval of borehole F6, and the constant flow test over the 213 m to 223 m interval.

testing. Minor changes in the formation head can cause large distortions in the calculated specific storage. In most cases, the pre-test period was continued until the rate of change of head was less than 0.01 m/min, or the time rate of change was very close to linear. Both tests were semi-automatic in that a valve had to be opened and closed manually, while the timing of the test and the data collection were both controlled by the central microcomputer.

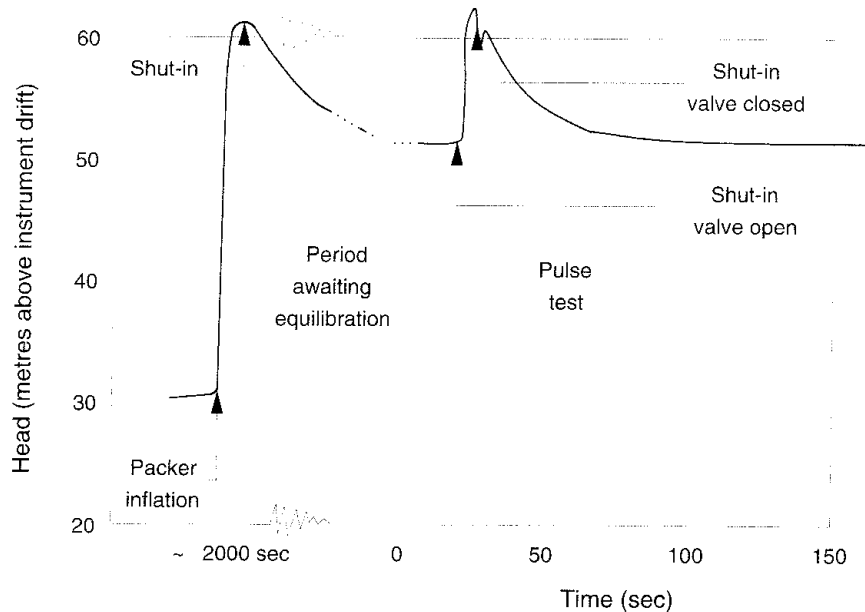


Figure 2-11 Example of the time-dependent pressure response in borehole F3 during a pulse injection test (Black et al, 1987).

After the sudden change at the beginning of a slug or pulse test, the head in the test zone returns to an equilibrium condition at a rate that is approximately proportional to the logarithm of time. The theoretical equations that describe the change in head, as given by Cooper et al (1967) and Barker and Black (1983), are difficult to apply readily in a field situation, and, for that reason, "type" curves were developed for comparison against the test data automatically by use of a computer. It should be noted that the theoretical analysis assumes cylindrical flow in a homogeneous and isotropic porous medium. The processing method used in the field included an error-minimisation approach so that the effect of various corrections on the basic data, such as change in the formation head, could be evaluated in terms of relative error. An example of the results obtained from a slug test in borehole F3 with "uncorrected" and "corrected" data is shown in Figure 2-12. Unlike specific storage, the value of the hydraulic conductivity derived by a combination of error minimisation and curve matching is not particularly sensitive to the procedure.

Pulse tests and slug tests are transient methods which yield values of specific storage as well as hydraulic conductivity. Since the value of specific storage determined from a test reflects the storage involved in the test, the results can be used to determine whether the rock appears to be responding as a "large-storage" porous medium or as a "low-storage" fissure. Granite without fissures could be expected to have a low hydraulic conductivity for the matrix and a reasonably large specific storage. The results from tests conducted in zones of reasonably sound rock yielded conductivity values as low as 10^{-12} m/s with specific storage values ranging between 10^{-6} m⁻¹ and 10^{-4} m⁻¹. When the results are considered in their entirety, certain relationships should be apparent from the derived values of hydraulic conductivity and specific storage depending on whether the rock mass is behaving as a fractured porous medium or a homogeneous porous medium.

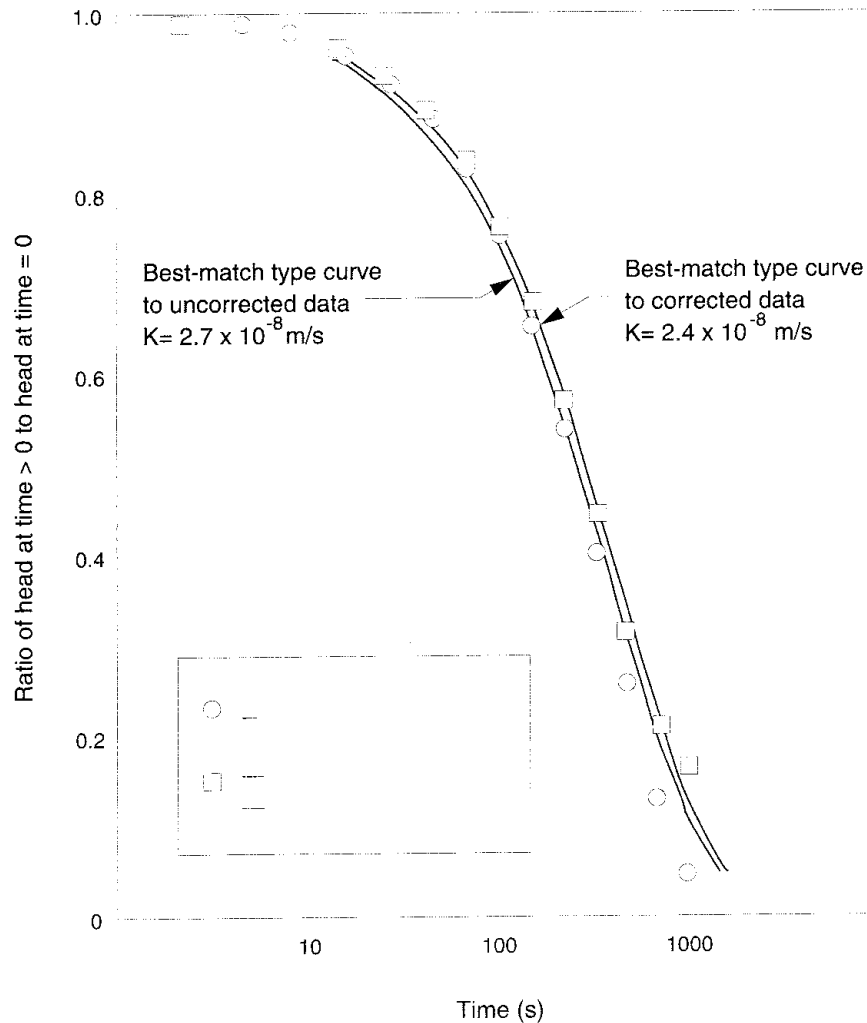


Figure 2-12 Example of the results from a slug injection test for "uncorrected" and "corrected" data sets (Black et al, 1987).

Figure 2-13 is a plot of specific storage against hydraulic conductivity for the data from the Crosshole site, along with results that could be expected from a homogeneous porous medium and from a fractured porous medium. The results appear to be roughly divided into three categories of response. The first category exhibits a specific storage in a rather constant range of 10^{-8} m^{-1} to 10^{-4} m^{-1} with hydraulic conductivities ranging between 10^{-11} m/s to 10^{-8} m/s . These values correspond to the expectations for a homogeneous porous medium. The second category of results contains values of specific storage ranging between 10^{-14} m^{-1} to 10^{-4} m^{-1} , with hydraulic conductivities between 10^{-12} m/s and 10^{-7} m/s . These values correspond to the response that would be expected from a fractured porous medium. A third category of results has values of specific storage that are less than 10^{-22} m^{-1} , which were thought to be the result of an error in the interpretation of the data. This error may be due to a positive skin effect along the borehole wall or to a change in the formation head during a test.

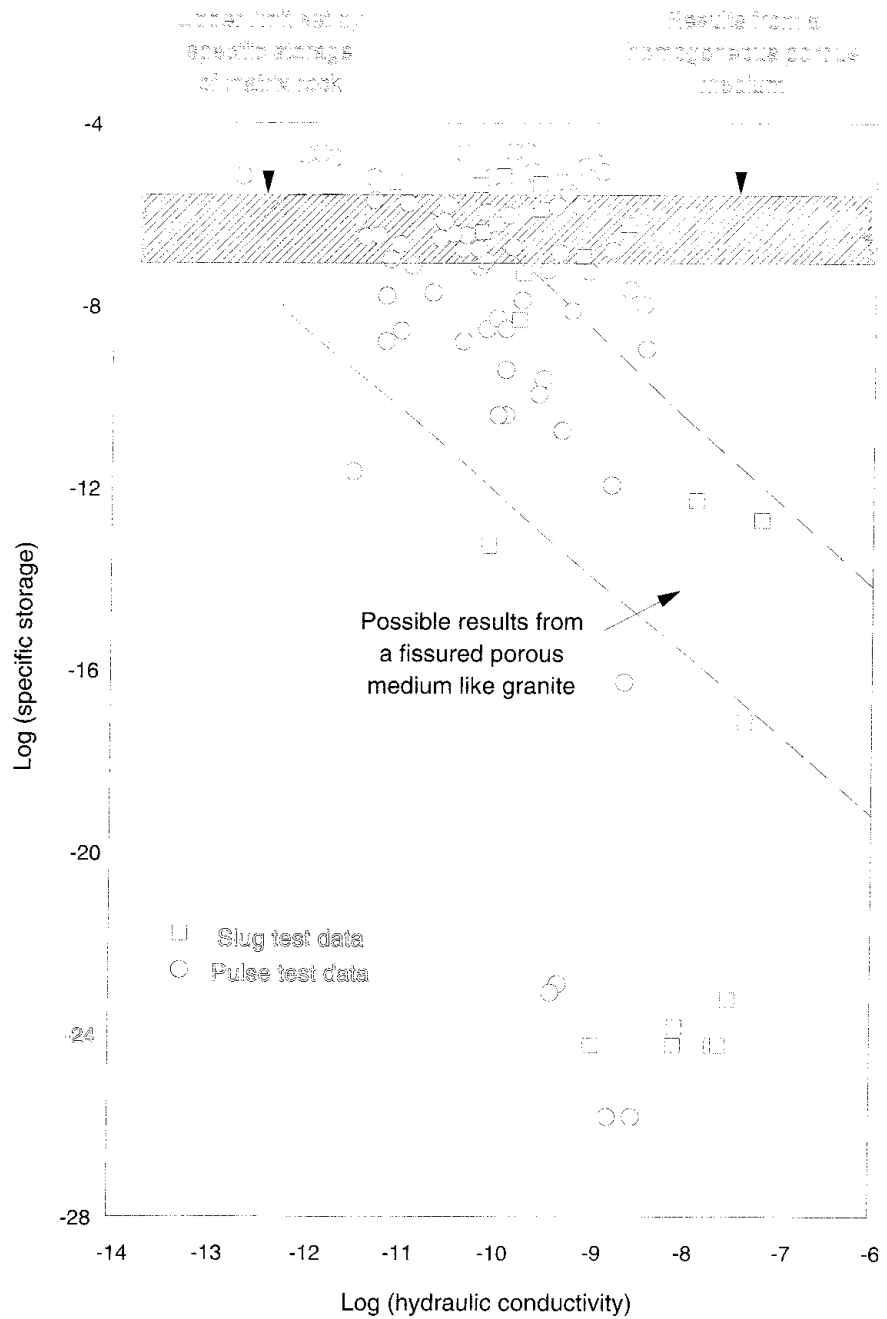


Figure 2-13 Plot of specific storage against hydraulic conductivity for slug and pulse injection-test data from boreholes F3, F4, and F5, together with expected results for differing flow concepts (Black et al, 1987).

The units of specific storage and hydraulic conductivity are m^{-1} and m/s , respectively.

2.1.2 Crosshole Hydraulic Testing

As an outgrowth of the hydraulic interference tests undertaken in Phase 1, an effort was initiated in Phase 2 to develop a method for measuring the hydraulic properties of fracture zones located between boreholes by varying the water-injection pressure and flowrate in a sinusoidal manner. At the outset, this effort required the development of a complex set of computer-controlled equipment that could operate successfully in a mine environment. The crosshole hydraulic testing took place at the Crosshole site, using both sinusoidal and constant-flow techniques.

Crosshole Interference Tests at the SGAB Site

The interference tests at the SGAB site in Phase 1 focussed on the interconnections between highly conductive zones in one borehole and parts of other boreholes (Carlsson and Olsson, 1985b). In particular, the conductive fracture zone at the bottom of borehole V1 and the deepest part of borehole N1 were used as source sections in interference tests between boreholes V1 and V2, among boreholes V1, V2, N1, and E1, and between borehole N1 and the BMT area of the Stripa mine. A schematic view of the interference-test arrangement for boreholes V1 and V2 is shown in Figure 2-14. Each test began as a pressure build-up test, but with a build-up period of the order of months. This time allowed the hydrologic conditions in the test sections to achieve a state of quasi-static equilibrium. After the build-up period, the pressure in the selected source section was released and the resulting pressure changes in the receiver sections recorded. The conditions in the source section were either free flowing, or flowing at constant rate over a long period of time comparable to the duration of the build-up period.

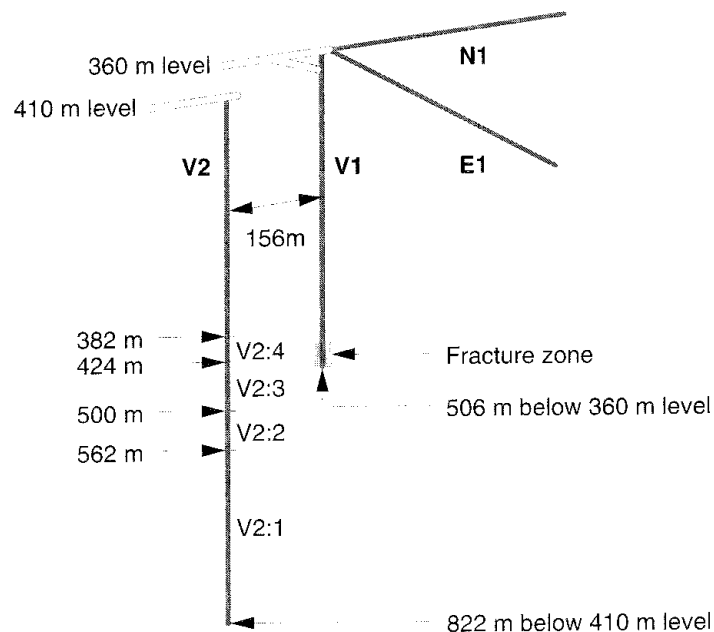


Figure 2-14 Schematic diagram of the interference test between boreholes V1 and V2 at the SGAB site (Carlsson and Olsson, 1985b).

The changes in water head in various sections of borehole V2 during injection in borehole V1 are shown in Figure 2-15. A head change of 80 m to 90 m in borehole V1 caused a 50 m change in head in borehole V2, when the length of the packed-off section in each borehole was of the order of 100 m. A 40 m increase in head in borehole V1 resulted in a 16 m change in head in borehole V2, when the length of the packed-off section in each borehole was about 50 m. These responses in the receiver sections of borehole V2 indicated a hydraulic connection to the source section in borehole V1. This connection could have been a fracture zone or zones, or a system of interconnected fractures in the rock mass between the two boreholes.

The time-dependent pressure responses in borehole V2 were evaluated on the basis of both a homogeneous, isotropic medium and a double-porosity medium, assuming radial flow into the borehole. In the double-porosity medium, the pressure response depends on the ratios of the hydraulic conductivity and the storativity of the fractured rock to those of the rock matrix. Head-response curves obtained during the interference tests were compared against curves developed by Streltsova (1983) from a theoretical model that includes the ratio of the storativities. By means of curve matching, the transmissivity and storage coefficient of the rock mass between boreholes V1 and V2 were calculated to be of the order of 10^{-7} m²/s and 10^{-8} to 10^{-7} , respectively. These values were about an order magnitude smaller than those computed for a homogeneous, isotropic medium.

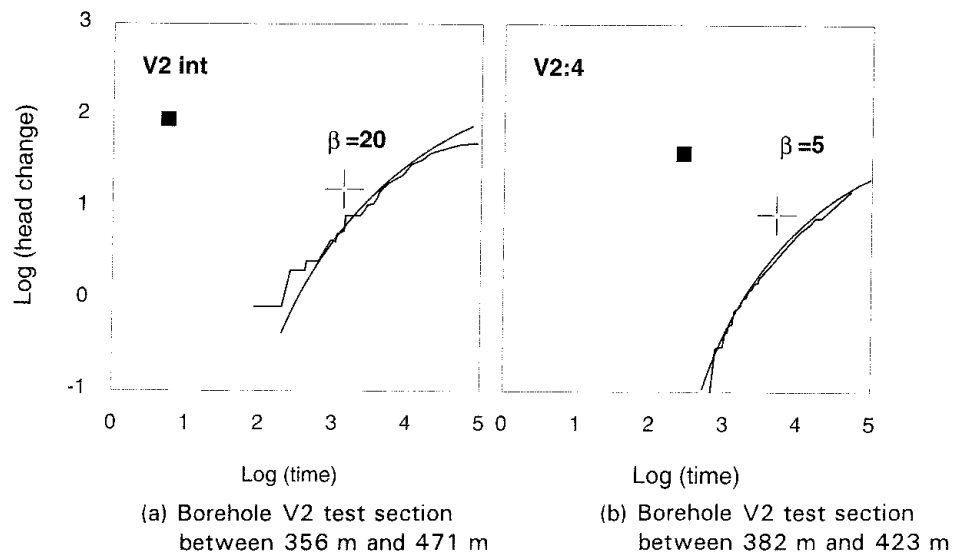
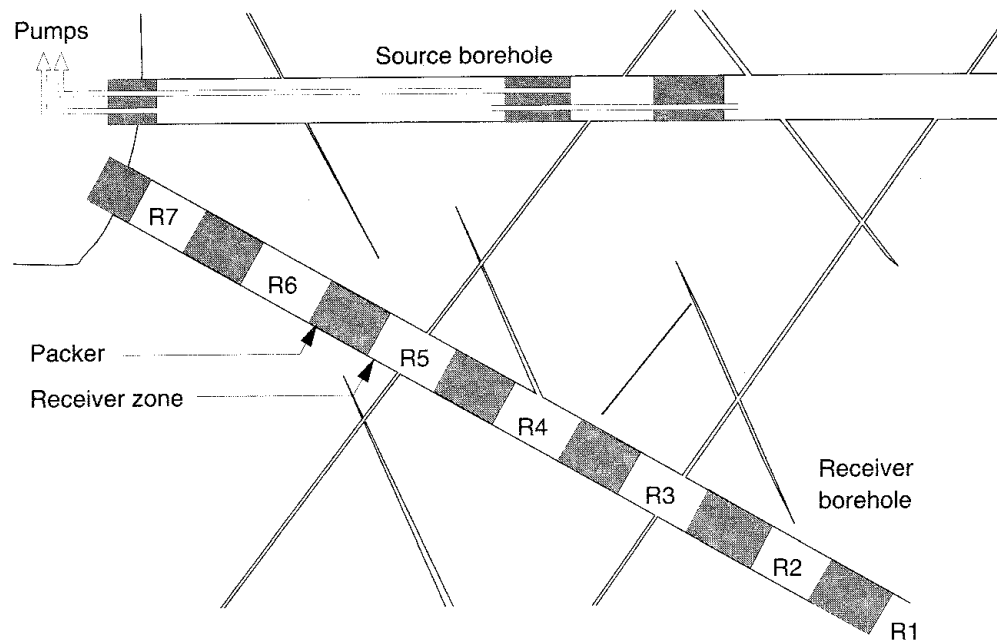


Figure 2-15 Change in hydraulic head in borehole V2 during water injection in borehole V1 (Carlsson and Olsson, 1985b).

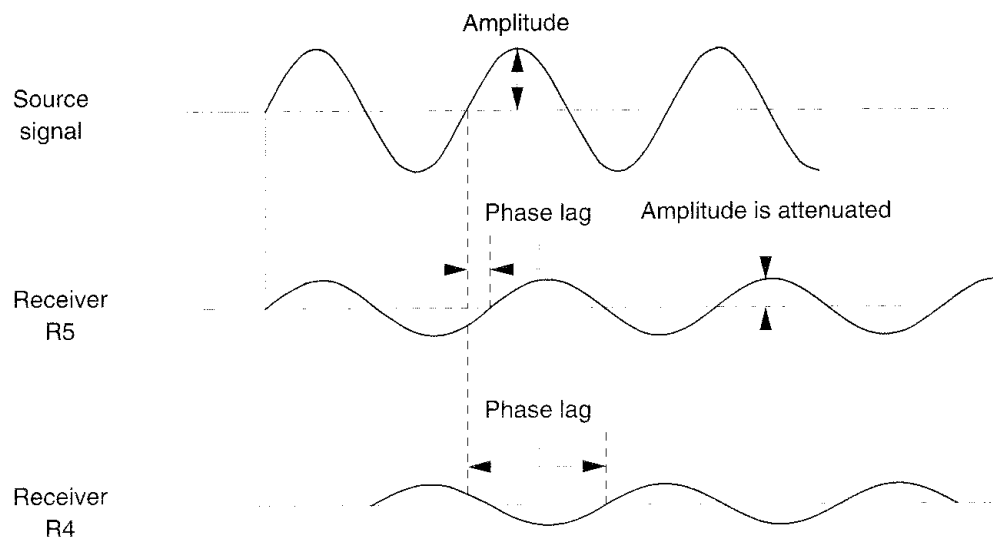
Change in head in borehole V1 during water injection is indicated by + symbol. Value of β designates best fit of data to storativity curves developed by Streltsova (1983) from double-porosity model. The units of head change and time are metres and minutes, respectively.

Crosshole Hydraulic Testing Equipment

Crosshole hydraulic testing involves the transmission of hydraulic signals through a saturated rock mass located between two or more boreholes (Black et al, 1986; Holmes and Sehlstedt, 1986). As shown in Figure 2-16, packers were positioned in one borehole to isolate a specific section of the borehole, known as the source zone, in which hydraulic signals could be generated. A rod string was used to position the packers over a borehole length of 1 m to 20 m, and to connect the source zone to pumps which injected or withdrew water to create the required variation in pressure, i.e. the hydraulic signal. A bypass tube passed through the packer assembly and connected the two sections of the borehole on either side of the packers.



(a) Source and receiver arrangement



(b) Amplitude attenuation and phase lag

Figure 2-16 Schematic view of the crosshole hydraulic-testing arrangement (Black et al, 1986).

The water pressures in the three sections of the borehole were measured by means of down-hole pressure transducers. All of the rods, tubes, and cables passed through a tapered manifold seal at the borehole collar. This seal was bolted onto a flanged pipe which was grouted into the rock at the collar.

The receiver borehole contained six hydraulically inflatable packers which isolated five short and two long zones. The packer assembly was positioned by means of a "blank rod string" using a hydraulically powered handling device. Each of the packed-off zones in the receiver borehole were connected by water-filled pressure tubes to a "pressure measuring board" in the drift. The tubes passed through a tapered manifold seal at the borehole collar, similar to that for the source borehole.

A pump, located in the drift, injected or withdrew water from the source zone, by computer command, to generate hydraulic signals. A second pump responded to pressure changes in the remaining sections of the borehole caused by water flowing around the isolating packers. Any pressure fluctuations were damped out to ensure that the hydraulic signal originated from the source zone and was not derived from the leakage of the signal to the rest of the borehole zone. Solenoid valves fastened to the entrance and exit ports of a pump were used to control the direction of flow, either into the borehole or to a storage reservoir. Each pump had an "on board" microprocessor, acting as an interface, to accept commands from the central microcomputer to increase or decrease the flow rate. These commands controlled the pump motor and solenoids to provide the required rate and direction of flow.

The "pressure measuring board" consisted of a group of solenoid-actuated valves and differential pressure transducers connected to the receiver zones by means of pressure tubes. The differential pressure transducers required a reference pressure, which was generated by a column of water in a tube installed in a nearby mine shaft. The fluctuating pressures in the receiver zones could be measured to a greater degree of accuracy with differential transducers than with absolute transducers.

The control system consisted of a microcomputer that drove a group of intelligent peripherals. The key element during a test was the ability of the control system to generate the hydraulic signal in the source zone. The central computer calculated a curve of a given shape, such as sinusoidal, square, constant rate, etc., based on information, like amplitude, frequency, etc., provided by the operator. In the control cycle, the computer compared the measured source zone pressure to that calculated from the curve and commanded the pumps to increase or decrease the injection or withdrawal rate as necessary to follow the curve. This cycle was repeated, on average, every ten seconds.

Crosshole Hydraulic Tests at the Crosshole Site

Crosshole testing at the Crosshole site was performed after completion of the single-borehole testing. Because of the fan-shaped array of boreholes, it would have been comparatively easy to perform injection tests in each one of the boreholes in turn and measure the responses in the other boreholes.

However, because of the length of the boreholes, this approach would not yield any information about the flowpaths between particular boreholes, or where the principal flowpaths intersected the boreholes. Consequently, a procedure was adopted that involved testing well-defined fracture zones previously identified by various geophysical techniques. During testing in the vicinity of these zones, the rest of the borehole and the surrounding boreholes were monitored for evidence of a signal originating from the source zone. The intent was to identify all significant crosshole connections including those selected on the basis of geophysical data.

After the operator had set the two strings of packers and measurement equipment at selected positions in the boreholes, the tests were conducted by use of a computer. A 4 m long section of a zone was packed off to separate the source from the remainder of the borehole. The receiver zone contains six packers separated by 2.4 m long straddles. The source signal was a computer-controlled sinusoidal variation in flow or pressure with a pre-selected peak amplitude and period.

Typical data, as shown in Figure 2-17(a), indicated that the signal recorded in a borehole receiver zone was imposed on a gradually changing

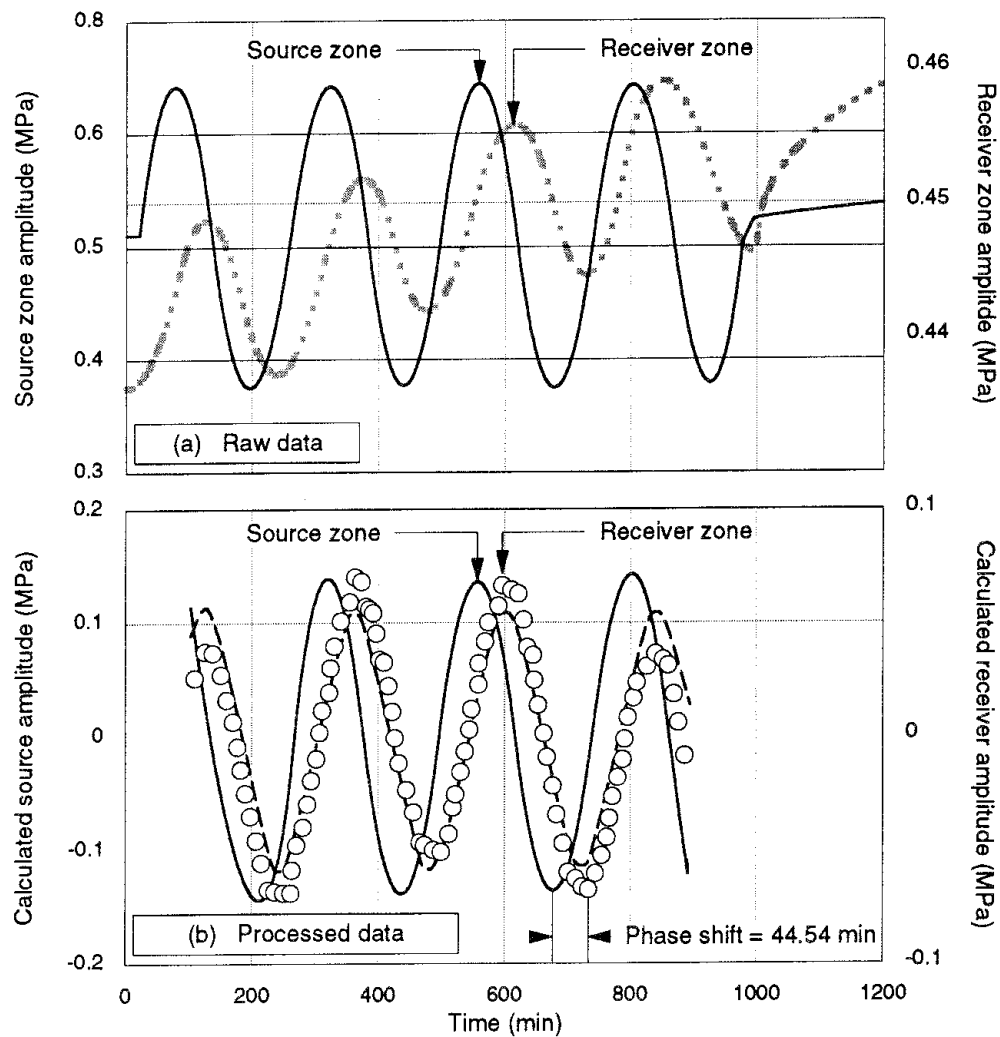


Figure 2-17 Form of the data obtained from sinusoidal hydraulic testing in the crosshole mode between boreholes F2 and F6 (Black et al, 1987).

background hydraulic head. In order to derive the amplitude attenuation and phase lag required for analysis, the raw data were corrected for the change in background head, as shown in Figure 2-17(b), by means of a microcomputer programme.

At the Crosshole site, there were no responses in boreholes E1 and F1 to the source signals. In addition, it was not possible to include borehole F6 in the sinusoidal testing because of the low heads in that particular borehole. The fracture zones defined as A and C were extensively tested in the crosshole mode. When the source was positioned in the borehole at its intersection with zone A, responses were observed in the southern part of the Crosshole site, particularly in boreholes F3, F4, and F5. On the other hand, when zone C was tested, responses were observed principally in boreholes F2, F3, and F4.

The first step in the data interpretation was to examine the data sets for consistency. There must exist a consistent relationship between the amplitude and phase shift of the received signal and the frequency of the source signal. The next step was to apply the flow concept of "fractional dimensions" in which it is hypothesized that flow occurs within a geometry that varies continuously between 1-D and 3-D. Within this conceptual framework, branching channels and fractures tend to increase the effective dimensions of the fracture flow system. Thus, as flow expands from a single channel into a fracture plane because of channel intersections, the dimension increases from 1-D to 2-D. With increasing scale, the flow dimension can be expected to approach 3-D. The derived values for the hydraulic conductivity and specific storage were checked for their appropriateness by examining the values of the head and phase lag calculated for the source zone.

The crosshole-testing results indicated that zones A and C were not simply zones of planar fractures. Rather, the zones appeared to be roughly planar systems of channels. The calculated fractional dimensions for zone A were generally greater than those for zone C, which probably indicated that the channelling in zone A was more sparse. The hydraulic diffusivity of the fracture zones ranged from 0.2 m²/s to 1 m²/s, apart from the portion of zone A that was located between boreholes F2 and F4. This was a particularly responsive zone in that, when a slug test was conducted in borehole F4, a response was observed almost instantly in borehole F2. The hydraulic diffusivity computed for this region of zone A was of the order of 100 m²/s.

2.1.3 Significant Achievements

The variety of activities of Phase 1 provided some valuable insights into the applicability, reliability, and advantages of different hydraulic testing techniques when applied to saturated, fractured crystalline rock. These included:

- To avoid the high gradients due to a potential sink caused by an underground excavation, straddle-packer systems should be used for measuring the groundwater head distribution in boreholes.

- Single-borehole pressure shut-in tests are time consuming because of the necessity to attain quasi-static hydrologic conditions, and the data interpretation requires consideration of borehole-skin and wellbore-storage effects; however, no foreign water is introduced into the borehole, no pumps are required, and the borehole is not subjected to pressures in excess of the natural background.
- Single-borehole injection-recovery tests require less time to perform than shut-in tests, but stable head conditions must exist in the packed-off borehole section before the test begins and the equipment must be capable of withstanding high pressures during the injection.
- Crosshole hydraulic-interference tests are most valuable for locating highly conductive zones in the rock mass between boreholes, and for assessing directional hydraulic conductivity over large distances when considering the "double porosity" behavior of fractured rock.

The hydraulics programme at the Crosshole site demonstrated that it was possible to design and build a complex set of computer-controlled testing equipment and to operate the equipment on a regular basis in the underground environment of the Stripa mine. An innovative aspect of the equipment was the use of the computer for the actual test operation. The hydraulic fluctuations imposed in a packed-off section of a borehole could be precisely controlled. This procedure provided good quality data with high resolution and close adherence to the theoretical assumptions underlying the test. It was shown that a sinusoidal fluctuation could be easily generated, because neither rapid changes of injection pressure or flow rate, nor long periods of steady, or "equilibrium", head conditions in the rock mass were required. The test results were effectively independent of changes in the groundwater head conditions in the rock mass due to various activities ongoing in other areas of the mine. A principal attribute of sinusoidal testing, that was unexpected, was its sensitivity to the geometry of groundwater flow in the rock mass during a test.

Interpretation of the data obtained from sinusoidal hydraulic testing required the use of the fractional dimension approach. This approach utilizes the concept that flow occurs in a pathway geometry that varies continuously between 1-D, such as pipe flow in channels, 2-D, such as radial flow in single fractures, and 3-D, such as spherical flow in a regularly fractured porous medium. The net effect of branching channels and fractures is to increase the effective dimension of the fracture flow system. The fracture zones at the Crosshole site were neither single geometrical entities nor effective equivalent porous media. The data interpretation gave results that appeared to be more consistent with what would be expected from a 1-D response than from a 2-D response.

2.2 SEISMIC TESTING METHODS

In Phase 2, an investigation was undertaken to develop a method, based on the principles of elastic wave propagation, for identifying structural features in a crystalline rock mass and for determining their geometric characteristics (Cosma et al, 1986; Cosma 1987; Pihl et al, 1986). The test procedure involved the generation of pulse signals from a source located at various depths in one borehole and detection of the signals by means of sensors placed in surrounding boreholes. The seismic technique was tested and data obtained at two sites. The Crosshole site in the Stripa mine was considered to be a "small-scale" test area where the maximum distance between boreholes was 200 m. The Gideå site in Northern Sweden was considered to be a "large-scale" test area where the maximum distance between boreholes, drilled inclined and vertical, was about 1,000 m. The data were processed by means of the tomographic inversion technique, which yielded maps of the seismic velocity distribution in the cross section between boreholes. Regions within the cross section where the seismic velocity changed appreciably were considered to be representative of structural features.

At the outset of Phase 2, there were many methods of processing seismic data in routine use for purposes of prospecting in the mining and petroleum industries. The structure of a crystalline rock mass at the scale of the Stripa mine and its surroundings, however, is usually more complex than a sedimentary formation that is explored for its potential to produce oil and natural gas. For example, boundaries of sedimentary rock formations are often distinct and nearly horizontal. In crystalline rock masses, there is often a gradation of physical properties across contacts between the different rock types because of the cooling of magmatic intrusions and related hydrothermal activity. Zones of crushed or highly fractured rock, with widths of some metres and extensions of kilometers, are generated within the rock mass in response to crustal plate movements and ice loading. These extensive fracture zones may act as primary conduits for groundwater flow. The capability of these zones to reflect seismic waves can be relatively weak, especially in relatively homogeneous rock masses such as the granite pluton in the Stripa area. These features of the rock structure can result in non-coherent backscattering in the seismic data that appears as noise. Efforts were undertaken in Phase 3 to develop multichannel filtering techniques that would allow the separation of reflection patterns that interfered strongly with each other because of the complexity of the reflector geometry, and to enhance the quality of the reflected energy by eliminating the backscattering noise (Cosma et al, 1991b). In addition, other efforts concentrated on the design of an electromechanical seismic signal transmitter, composed of stacked piezoelectric crystals, that could be used with high reliability in slim 56 mm-diameter boreholes.

2.2.1 Detection of Fracture Zones

The main objective of seismic testing for purposes of characterization is to estimate the "quality" of a rock mass. The basic physical parameters that describe the properties of the rock are the density, compressional P-wave velocity, shear S-wave velocity, and anelastic attenuation. This investigation focussed on a determination of the spatial distribution of the P-wave velocity in a rock mass, considering, in particular, the minimum travel time of the

P wave between the source and the receiver. Ideally, travel time will be the minimum value of the P-wave "slowness", i.e. the reciprocal of the compressional velocity. It should be kept in mind that a seismic pulse will be virtually unperturbed by a structural feature whose dimension is much less than the wave length.

A collection of travel-time data obtained from a distribution of sources and receivers can be processed by means of a tomographic inversion technique to determine either the distribution of the velocity or the attenuation in the medium (Ivansson, 1984). Tomography is a well known method for treating X-ray data in diagnostic radiology and in medical applications using ultrasound scans. Seismic tomography has been applied to process data obtained on a regional scale where the sources were earthquakes, and on a local scale for exploration purposes where the sources were explosive detonations. In essence, a volume of rock within the confines of a seismic array is divided into cubes which are considered to be homogeneous. An inversion procedure is used to obtain the P-wave velocity of each cube from travel-time data for the first arrivals. Both travel-time and wave-amplitude data can be treated simultaneously in the same inversion procedure to obtain the P-wave velocity and the anelastic attenuation.

Artifacts and distortions may often appear in the tomographic images because of noisy travel-time data, ray bending, misfits between cell decomposition and velocity distribution, and necessarily incomplete coverage of ray paths within the confines of a seismic array. However, the severity of the distortions is dependent on the manner in which the inversion is performed. Direct, unrestricted least-squares inversion often leads to significant artifacts. Conversely, methods that use many cells and damping generally yield much better images. However, as the number of cells is increased, direct inversion becomes computationally more difficult because of computer storage limitations. As a consequence, for a large number of cells, iterative solution methods must be used, where the rate of convergence of the solution can be improved by introducing damping and a relaxation parameter.

Test Sites

Seismic testing was conducted at the Crosshole site in the Stripa mine and at the Gideå site in Northern Sweden. The Crosshole site has been described previously in Section 2.1.1. The bedrock at the Gideå site consists of migmatized gneiss with a structural strike to the northeast and a small dip. Dolerite dikes are present in the area, usually striking E-W with widths of less than 1 m. However, two dikes in the central part of the area are 2 m to 10 m wide. Figure 2-18 is a map of the area and indicates the positions of eleven local fracture zones. Based on data obtained from a combination of core-drilled holes and percussion-drilled holes, the widths of the fracture zones were found to vary from 1 m to 24 m. Three dominating fracture zones, designated as I, II, and III, are present on the east side of the site. The widths of these zones were estimated to range between 10 m and 25 m. The crosshole seismic tests were performed in the rock volume bounded by the three core-drilled holes designated as Gi1, Gi2, Gi11. Each borehole was 56 mm in diameter and had a length of about 700 m. The distances

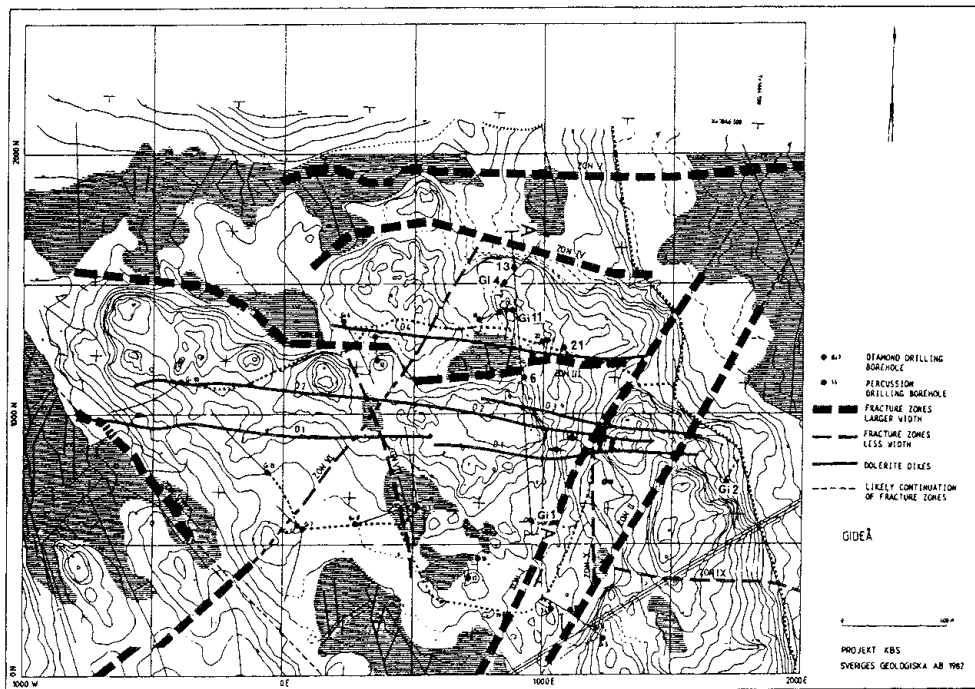


Figure 2-18 Topographic and structural map of the Gideå Site (Pihl et al, 1986).

between the collars of these boreholes in which the receivers were positioned were 750 m, 800 m, and 1050 m. The percussion-drilled holes, designated as 6, 13, and 21, had diameters of 110 mm and lengths between 90 m and 150 m, and were used as the seismic source holes.

Testing System

The basic arrangement of source and receivers for crosshole seismic testing is shown in Figure 2-19. Two boreholes are drilled at each end of the area of interest. A seismic source is placed in one borehole and receivers are placed in the other borehole and, where appropriate, on the surface of the ground or along the floor of a drift. The source applies an impulsive force to the interior of the borehole. This force generates compressional and shear waves that travel outward from the source at velocities which depend upon the density and elastic moduli of the rock. When these waves intersect the second borehole, the receivers respond by measuring continuously the amplitudes of the waves. These data are transmitted to a recording system on the surface, or in the drift, as the case may be. By varying the depths of the source and the receivers, a large amount of the area between the boreholes can be traversed by seismic waves.

The components of the testing system consist of a seismic source which generates the seismic energy, seismic receivers, amplifiers and filters, a timing system, and a data-recording system. The seismic source can be a quantity of explosive placed in the borehole and detonated, or a mechanical device containing a spring-loaded hammer assembly which, when triggered, impacts the wall of the borehole. The mechanical borehole hammer can deliver repeated impacts to the borehole wall, thereby allowing the signals measured by the receivers to be "stacked". Each borehole receiver

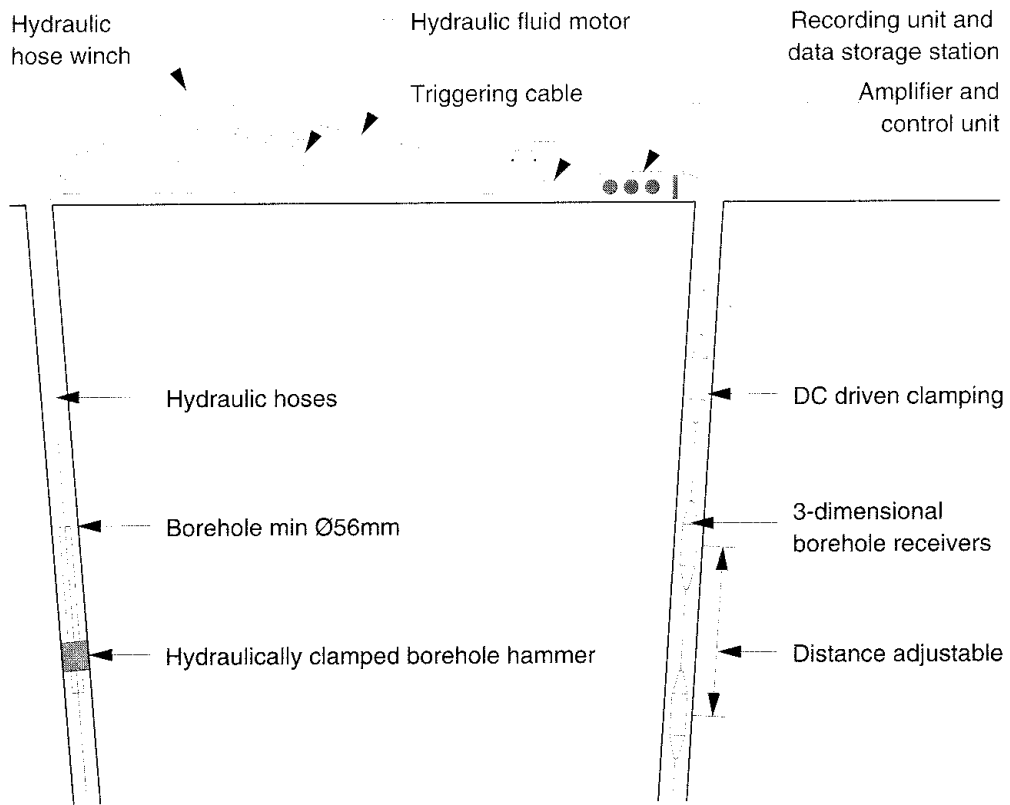


Figure 2-19 Conceptual view of crosshole seismic testing (Olsson et al, 1987a).

contained three accelerometers for measurements in the three principal directions, together with a borehole clamping mechanism to ensure good mechanical contact between the receiver and the borehole wall. The upper limit of frequency response of the accelerometers was about 8 kHz to 10 kHz. The data recording system was connected to the borehole receivers and to the borehole source by means of a timing device. This timing device sent a signal to the recording system when the explosive or mechanical source was activated. Figure 2-20 illustrates the form of the seismic signals measured by the borehole receivers and transmitted to the recording system.

Crosshole Testing at the Gideå Site

Crosshole seismic testing was conducted in three principal boreholes, known as Gi1, Gi2, and Gi11, at the Gideå site. The 56 mm diameter drillholes had lengths of about 700 m, but, because the boreholes were inclined, they penetrated to depths of 500 m to 600 m. Sources, consisting of explosive charges of penthyl-based explosive (M46), were located in shallow 1.5 m deep drillholes on the surface and in three percussion-drilled holes. In the three principal boreholes, an explosive charge consisting of "Octol" was used to prevent chemical contamination of the rock and groundwater. The three boreholes were used both for receiver measurements and as source holes, but explosive detonations and measurements were never conducted simultaneously in one hole. When a source was located deep in a principal borehole, geophones were positioned on the surface to record the seismic signals to complement the data obtained by the receivers positioned in the other principal boreholes.

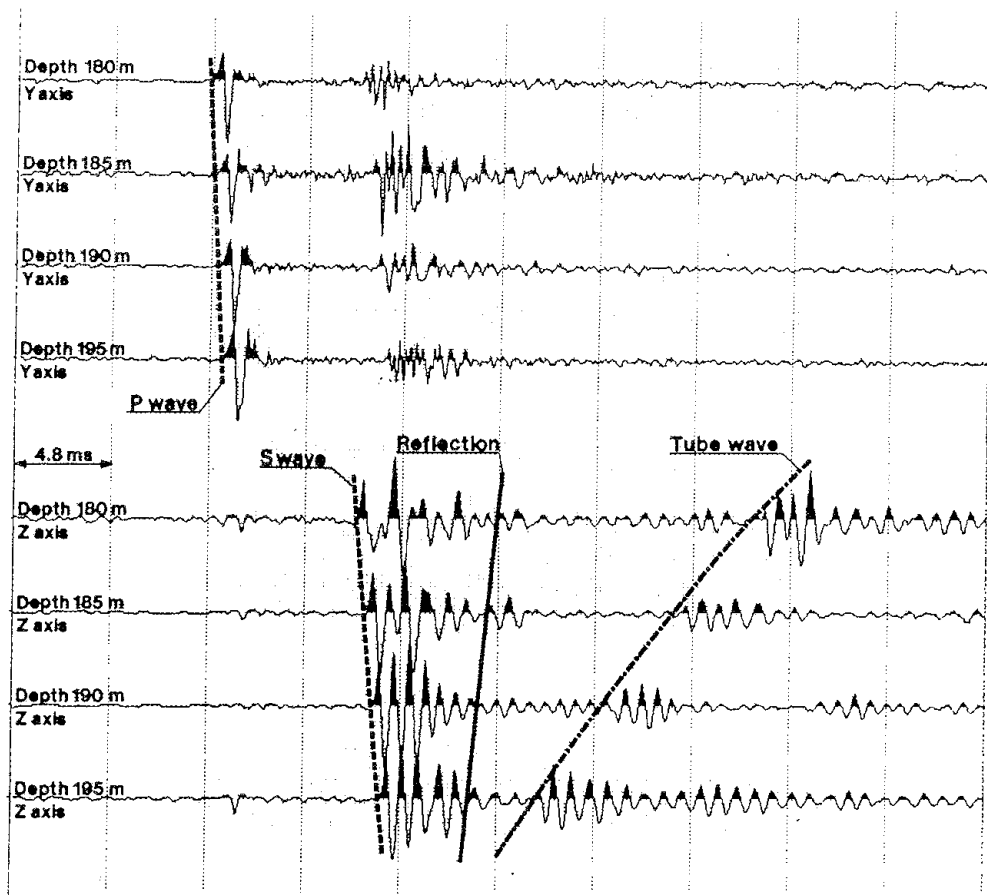


Figure 2-20 Typical seismograms showing arrivals and forms of direct and reflected waves (Cosma, 1987).

The set of four records at the top of the diagram are the radial signal components, and the set of four records at the bottom are the axial signal components, all oriented at a direction perpendicular to the source.

Figure 2-21 shows the 800 source-to-receiver ray paths in the projected cross section containing boreholes Gi1 and Gi11. The result of the tomographic inversion of all the travel times over the entire section, using a decomposition into squares of 25 m on a side, is depicted in Figure 2-22. A tomographic map with a decomposition into squares of 10 m on a side for the cross section between percussion-drilled holes 6 and 13, including borehole Gi11, is shown in Figure 2-23. Because of such factors as velocity anisotropy, ray bending, and inadequate ray coverage, the geologic structure was not uniquely determined by the experimental data set. It is important to compare the experimental results with results obtained from calculations for theoretical models of the region that contain structural features known to exist from surface mappings. In practice, it would be advisable to use results obtained from such models to determine the borehole spacings and depths required to obtain adequate ray coverage of the region of interest.

For those data sets that included measurements from both borehole and surface receivers, a 3-D tomographic inversion of the data was conducted, using a decomposition into cubes of 25 m on a side. As shown in

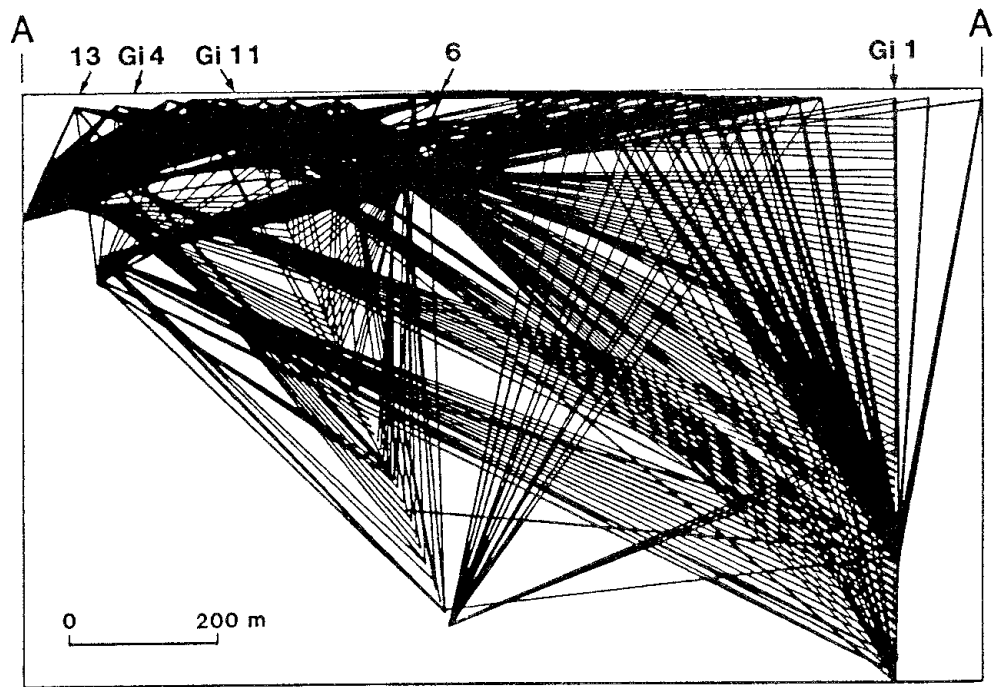


Figure 2-21 Source-to-receiver ray paths in the projected cross section at the Gideå Site containing drillholes 6 and 13 and boreholes Gi1 and Gi11 (Pihl et al, 1986).

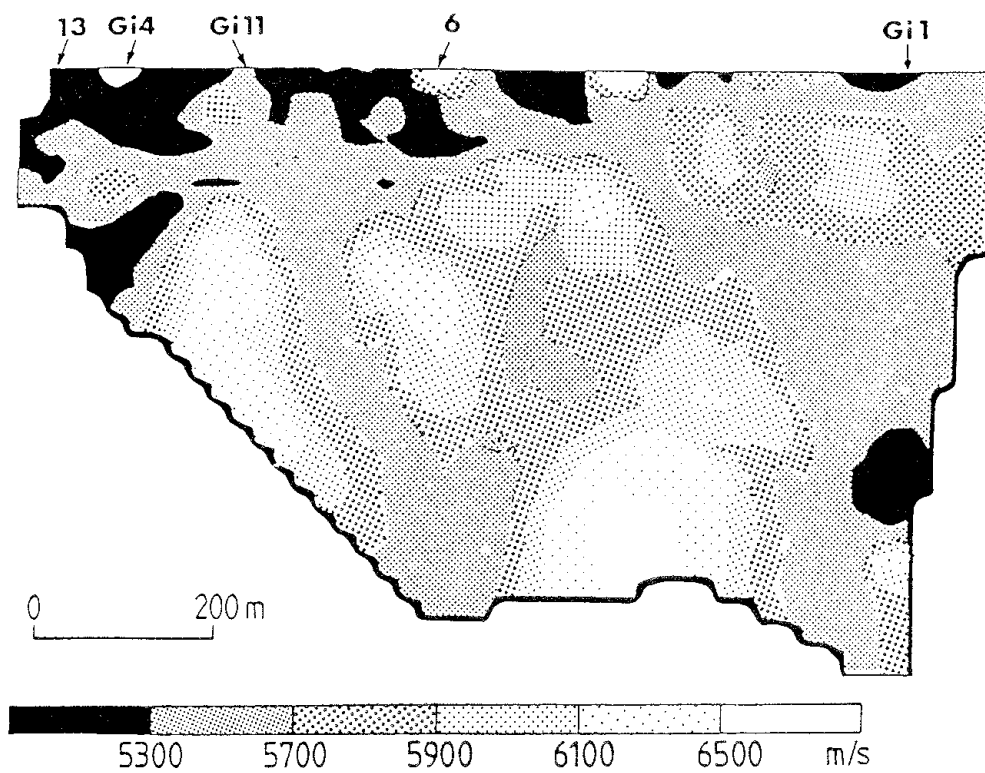


Figure 2-22 Tomographic map of the P-wave velocity distribution in the cross section at the Gideå Site between drillhole 13 and borehole Gi1 (Pihl et al, 1986).

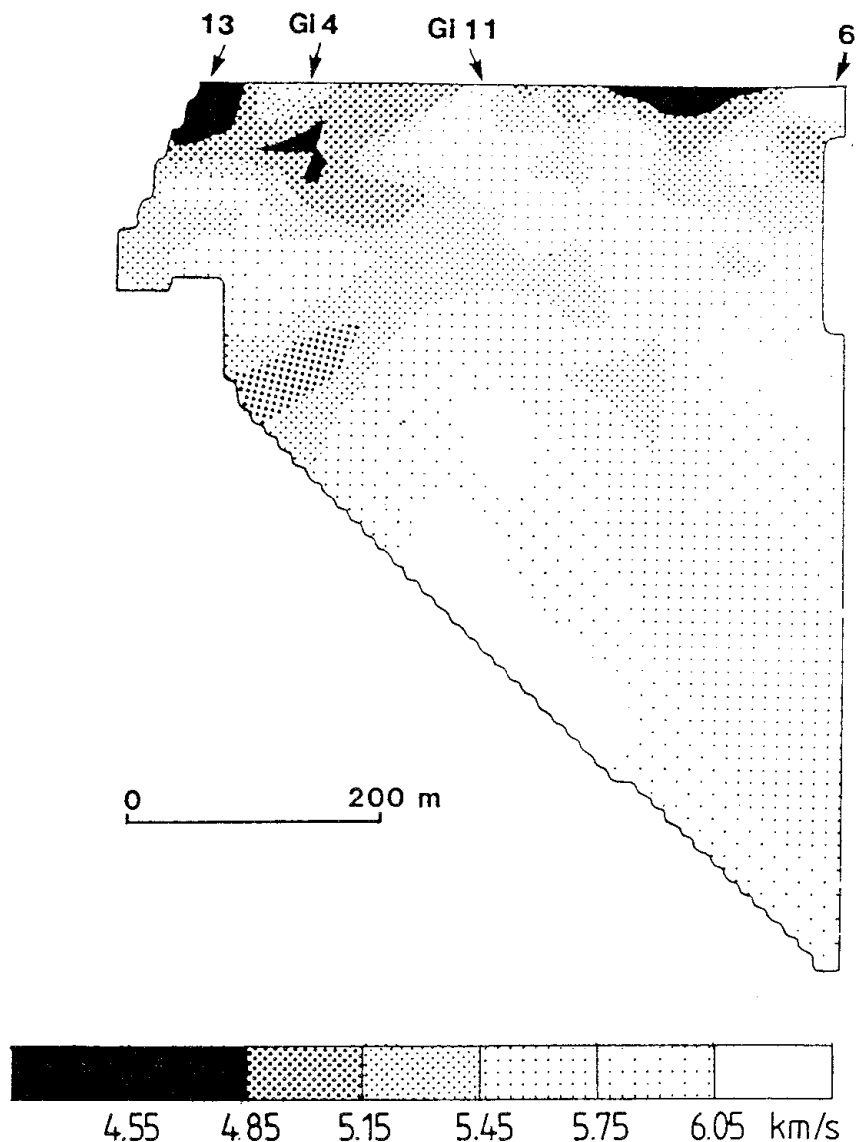


Figure 2-23 Tomographic map of the P-wave velocity distribution in the cross section at the Gideå Site between drillholes 6 and 13 (Pihl et al, 1986).

Figure 2-24, the ray coverage for the test conducted at the Gideå site was reasonably good for shallow depths of 100 m or less. Variations in the velocity distribution were observed to a depth of about 225 m. However, interpretations of geologic structure were difficult because of the large residual errors during the inversion owing to the lack of adequate ray coverage. Synthetic travel times were computed for a 3-D conceptual model which assumed increasing velocity with depth and the existence of a low-velocity fracture zone with a width of about 25 m dipping about 40° to the southeast. The tomographic inversion of the synthetic data set provided maps of the P-wave velocity distribution at 50 m intervals in the rock mass, as shown in Figure 2-25. The extension of the fracture zone was difficult to follow below about 175 m because of the low-density ray coverage. There is general agreement between the velocity distributions from the experimental data and the conceptual model. It must be kept in mind, however, that synthetic travel-time data sets for other conceptual models with differing assumptions of geologic structure could conceivably show

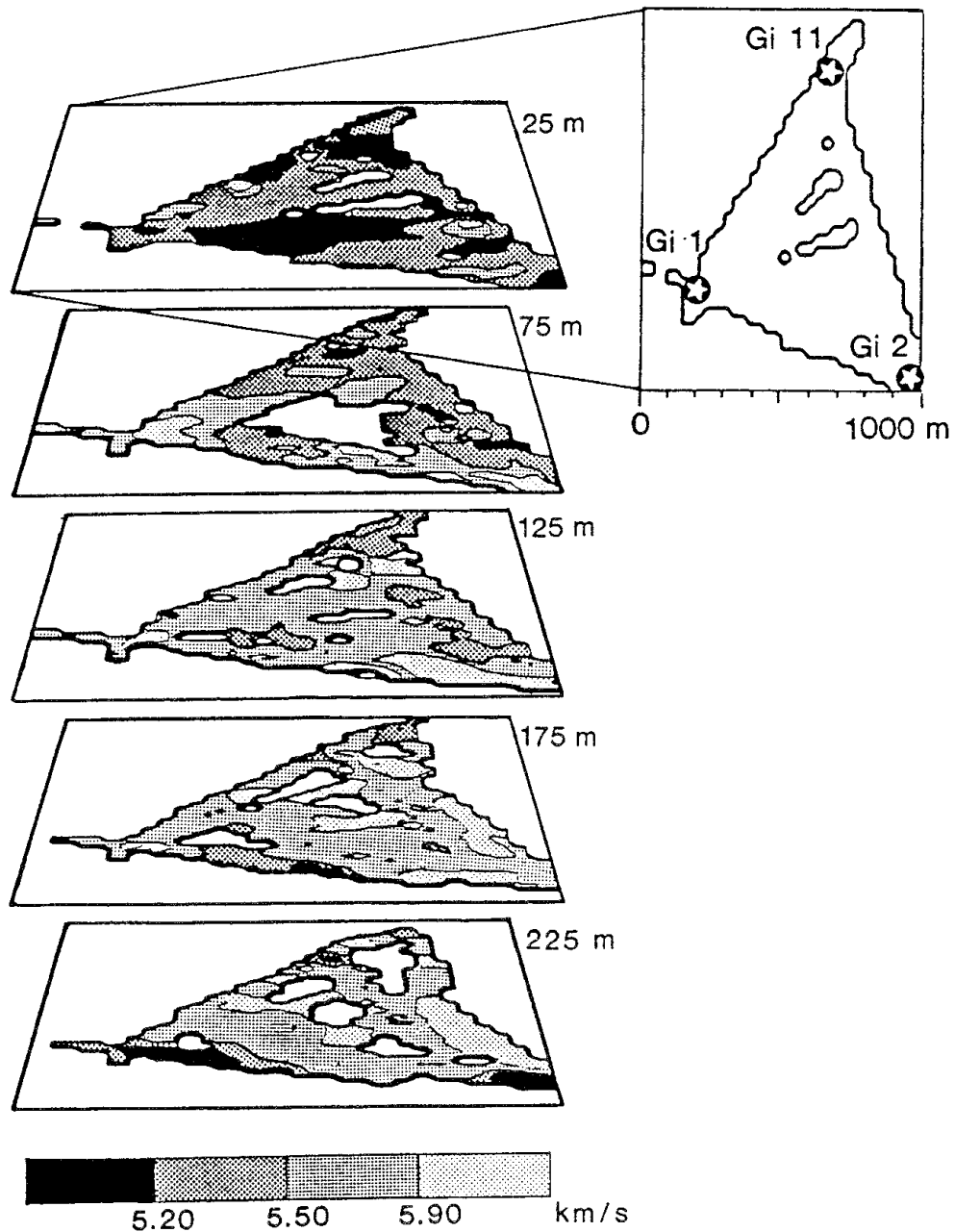


Figure 2-24 Tomographic maps of the P-wave velocity distribution at 50 m intervals in the volume of rock that was seismically tested at the Gideå Site (Pihl et al, 1986).

agreement with the tomographic maps obtained from the experimental data. To obtain an adequate level of ray coverage, receivers would have to be positioned horizontally at the bottom of the region of interest. Conceivably, this could be accomplished by means of boreholes that were deliberately deviated to curve below the region.

Tube waves, generated when a P wave passes through a discontinuity in the borehole, were observed on several recordings of the vertical component of the borehole accelerometers. As shown in Figure 2-26, tube-wave signals were detected at depths of 70 m, 150 m, and 250 m in borehole Gi11.

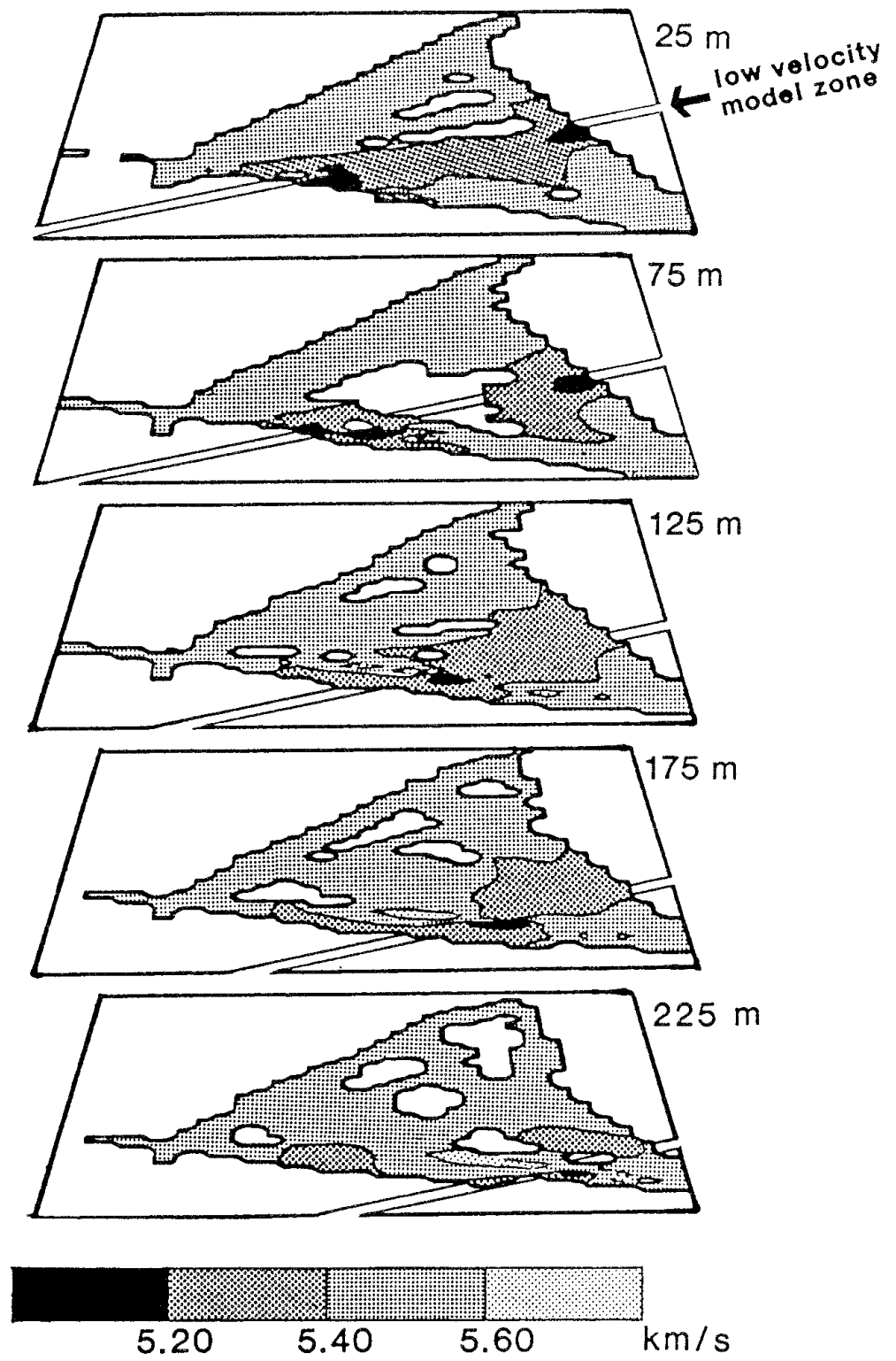


Figure 2-25 Tomographic maps of the P-wave velocity distribution at 50 m intervals in a "conceptual" model of the Gideå Site containing a dipping fracture zone (Pihl et al, 1986).

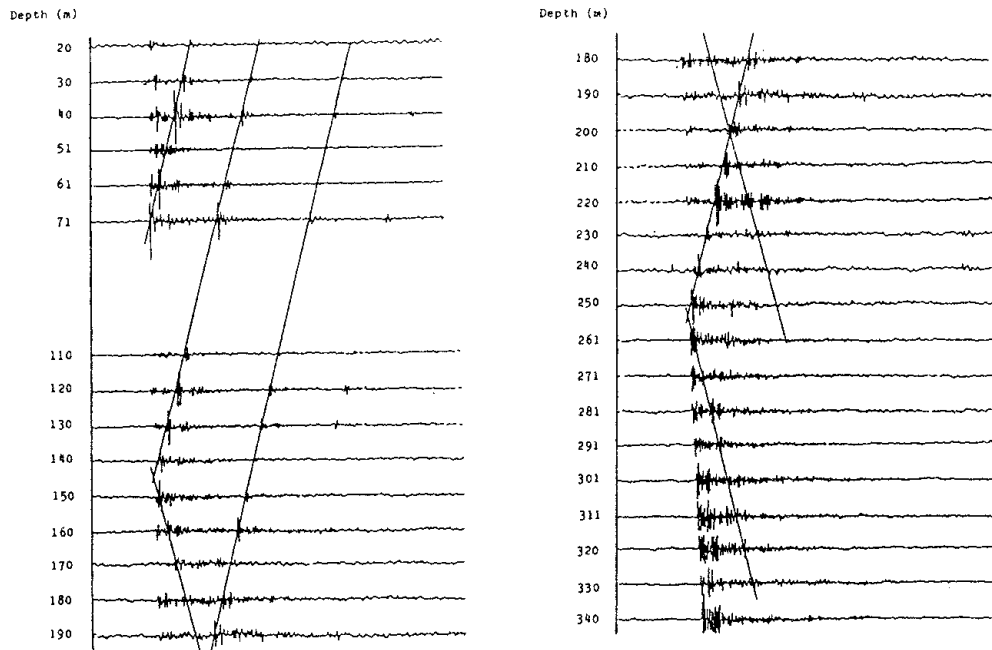


Figure 2-26 Seismogram showing the arrival of tube waves in borehole Gi11 (Pihl et al, 1986).

The sources of the tube waves are situated at depths of about 70 m, 150 m, and 250 m.

These depths were in agreement with the fracture zones identified from the core log.

Crosshole Testing in the Stripa Area

A limited amount of seismic testing was conducted in two boreholes that had been drilled from the surface into the granitic pluton at the Stripa mine. Borehole SBH4 had been drilled vertically to a depth of 372 m and borehole SBH3 to a depth of 315 m at an inclination of 50°. The purpose of this testing was to determine whether a large fracture zone, first encountered at a depth of about 865 m during the drilling of borehole V1, extended upward through the granitic pluton to the surface. An interpretation of the available geologic information suggested that the fracture zone might intersect borehole SBH4 at a depth of about 370 m, as shown in Figure 2-27 (Olsson and Jämtlid, 1984). Small amounts of explosive were detonated at fifteen different depths in borehole SBH3, and some 100 sets of signals were measured with a chain of three receivers in borehole SBH4. The tomographic map of the velocity distribution in the cross section between the boreholes, as shown in Figure 2-28, indicated a nearly horizontal, low-velocity zone intersecting the SBH4 borehole at a depth of about 140 m. In addition, there appeared to be low-velocity geologic structure at a depth of about 300 m. Tomographic maps of the velocity distribution obtained from synthetic travel-time data for various "conceptual" models of the section, containing hypothetical fracture zones, did not agree with the experimental

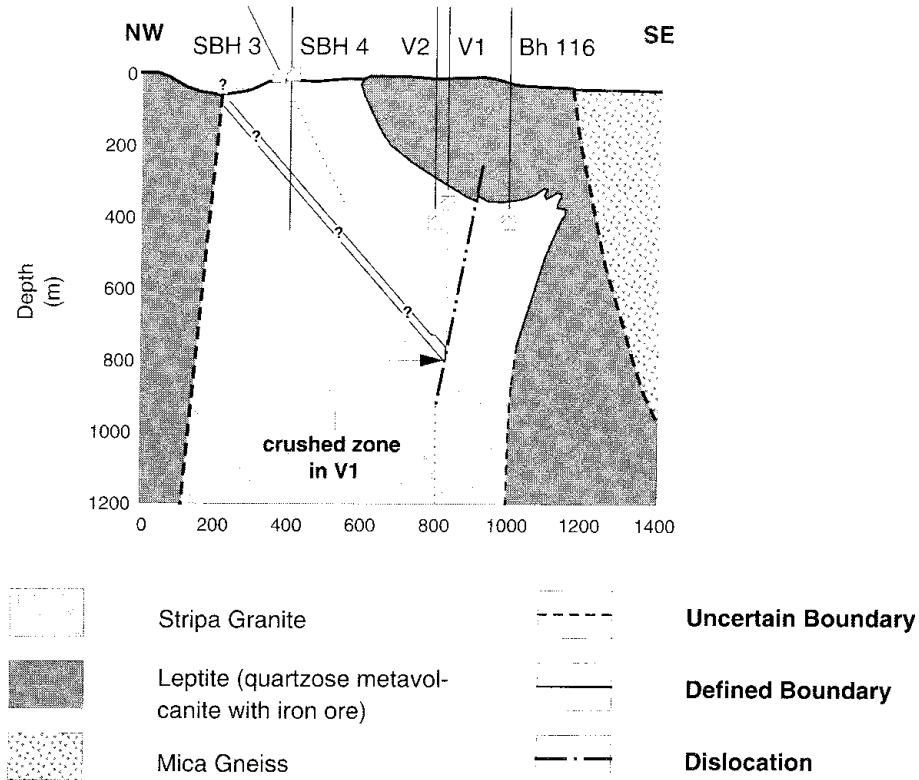


Figure 2-27 NW-SE vertical section through the Stripa granite with hypothetical projection of the fracture zone in borehole V1 to the surface (Pihl et al, 1986).

results. It was concluded that the observations in borehole SBH4 could not be related to the major fracture zone found in borehole V1.

Crosshole Testing at the Crosshole Site

Two series of seismic tests were conducted at the Crosshole site. The first test series concentrated on the cross section defined by the F5 and F6 boreholes. The source charges, consisting of small amounts of explosive, were detonated at 5 m incremental distances in borehole F5, and the seismic signals were detected by a chain of three receivers, spaced at distances of 5 m, in borehole F6. Only the travel-time data for the P-wave arrivals were inverted to obtain the tomographic map of the velocity distribution in the cross section. In the second series of seismic tests, borehole F4 was used as the source and receivers were placed in boreholes F1, F2, F3, F5, and F6. The source was a mechanical spring-loaded hammer assembly, positioned at incremental distances of 5 m in the F4 borehole. The receivers were placed at separation distances of 2.5 and 5 m in the other boreholes. Tomographic maps of the cross sections between boreholes were obtained by inversion of the travel-time data for both the P-wave and S-wave arrivals.

The source-to-receiver ray path coverage in the section between boreholes F5 and F6, along with the tomographic map of the P-wave velocity

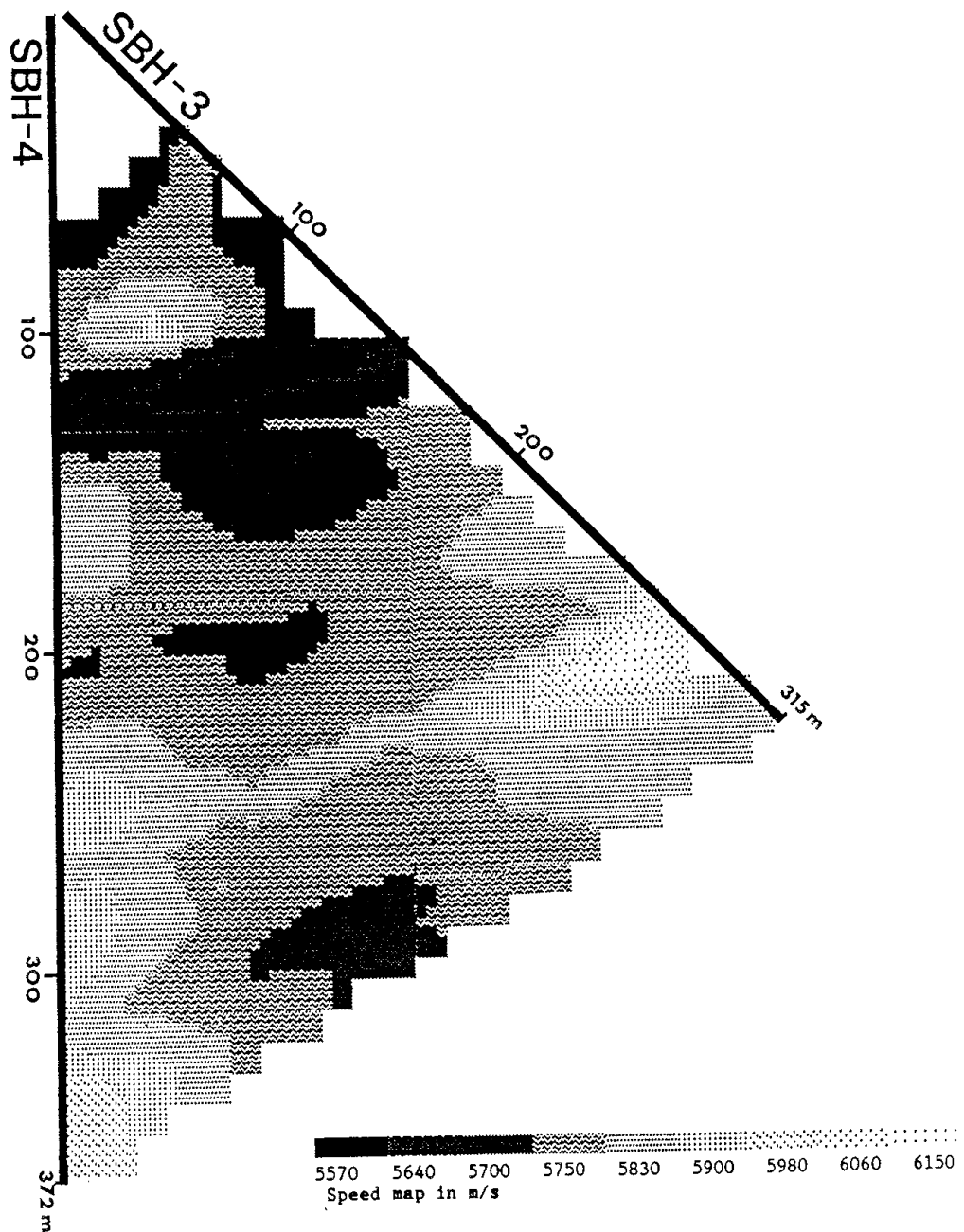
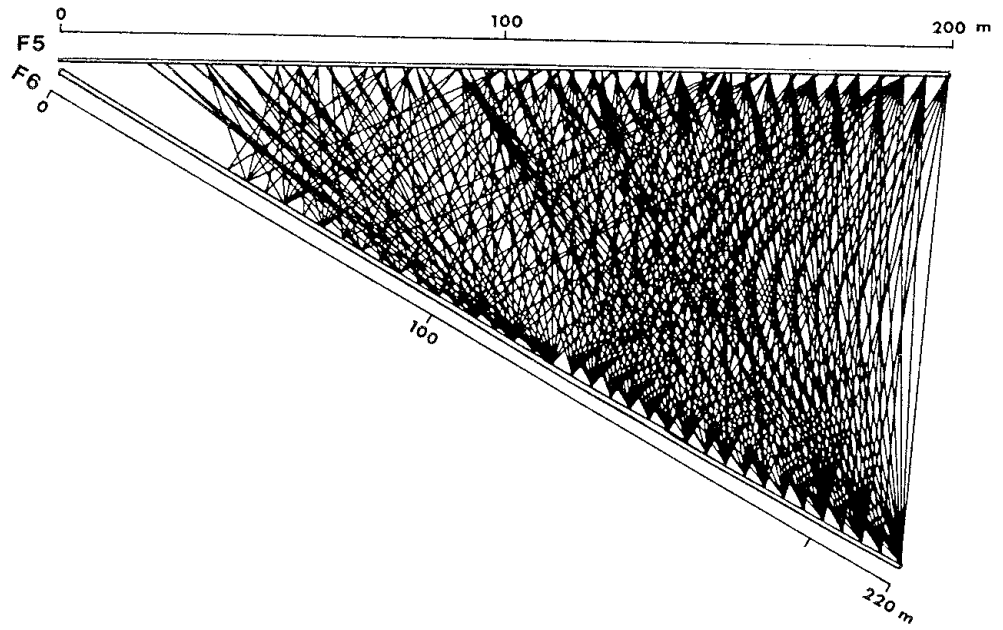
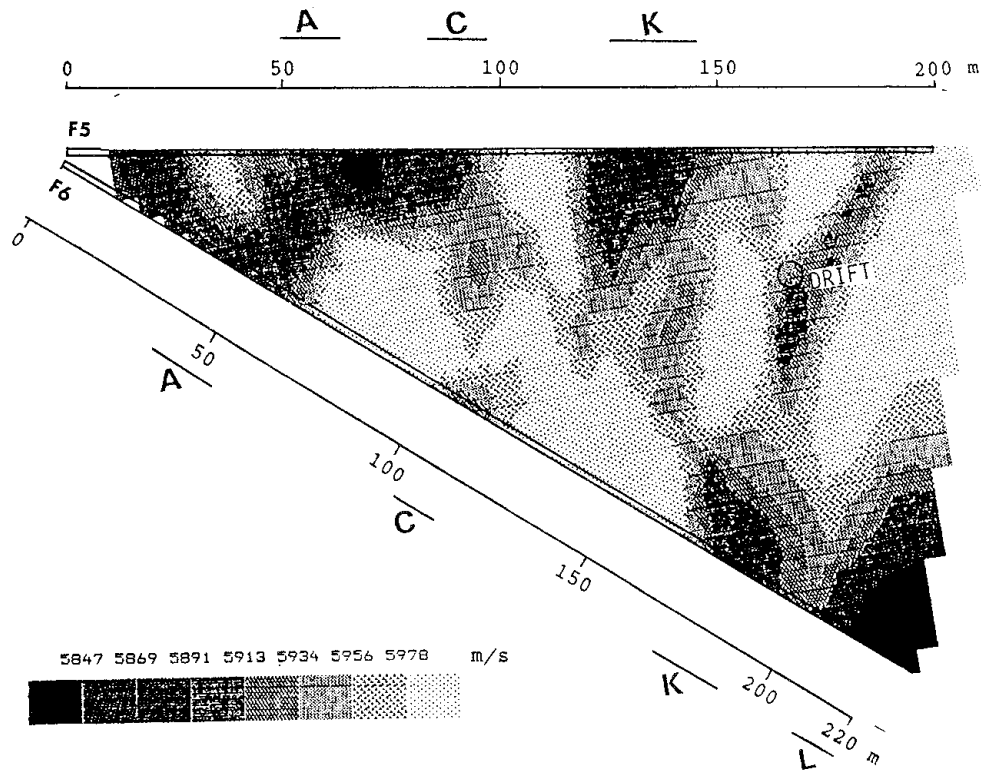


Figure 2-28 Tomographic map of P-wave velocity distribution in the cross section between boreholes SBH-3 and SBH-4 in the Stripa area (Pihl et al, 1986).

distribution from the first series of seismic tests, are shown in Figure 2-29 (Pihl et al, 1986). On the basis of core-log and other data from the boreholes at the Crosshole site, seven zones of deformed and fractured rock had been identified and correlated between the boreholes (Carlsten et al, 1985; Carlsten and Strähle, 1985). Four of these zones, namely A, C, K, and L, are indicated by the low velocity zones in Figure 2-29. The most prominent feature, zone L, intersected the F6 borehole beyond 210 m. Because of its strike to the northeast and dip towards the west, this zone did not intersect borehole F5. A strongly brecciated section of rock with high



(a) Source-to-receiver ray paths



(b) P-wave velocity distribution

Figure 2-29 Tomographic map of the P-wave velocity distribution in the cross section between boreholes F5 and F6 at the Crosshole site (Pihl et al, 1986).

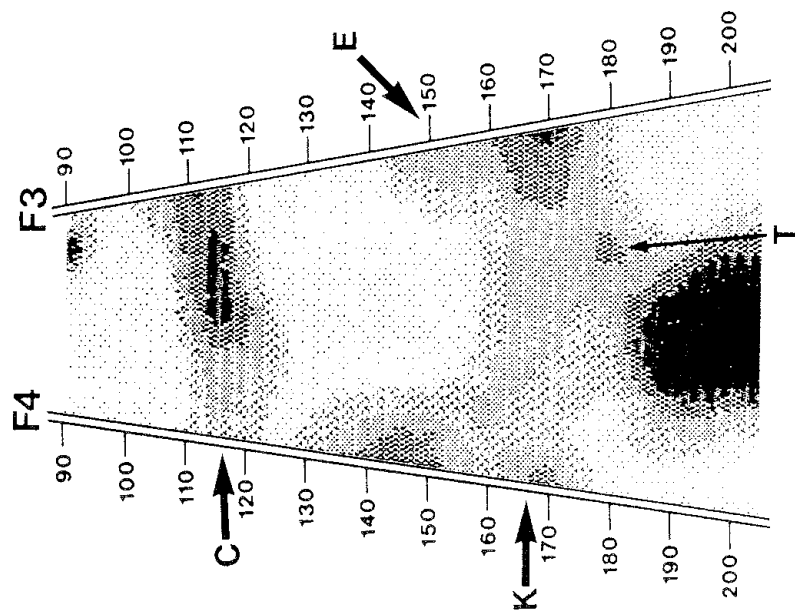
porosity was known to intersect borehole F5 between zones A and C. Because of this brecciation and the short distance between the boreholes in this part of the section, it was difficult to separate the two zones. However, the zones were more distinct due to branching near borehole F6. The low-velocity zone that intersected borehole F5 at a distance of 190 m was partly an artifact created by the intersection of a drift with the cross section about 25 m below borehole F5 and at a distance of 170 m from the location of the borehole collars.

Considerable care was taken to ensure that no systematic errors were introduced into the data analysis. A straight-line fit of the source-to-receiver travel times against distance between the source and receivers indicated that the instrumentation had not introduced a time offset into the data. Deviations from a constant average velocity for all of the rays were very small, indicating that the Stripa rock was relatively homogeneous. A few travel times, however, were conspicuously low, probably due to a geometric error as a result of the extrapolation of the curvature data for borehole F6. The effect of ray coverage on the tomographic image was assessed by conducting a series of inversions with different ray geometries. As expected, the tomographic images were more uniform when the density of rays within a section was uniform. By the use of synthetic travel-time data for "conceptual" models of the cross section, the influence of velocity anisotropy in the rock mass was found to be nonexistent.

The second series of seismic tests conducted at the Crosshole site was intended to evaluate the capability of the tomographic technique to describe the orientation, dimensions, and properties of the fracture zones (Cosma, 1987). The tomographic technique does not use *a priori* assumptions concerning the structural features to be resolved in a cross section between boreholes. Furthermore, tomography operates with areas and not with defined objects, and tends to smear out the features, whether they are linear or not, into elongated spots. It follows that the tomographic contrast plots can be interpreted in terms of position and orientation of fracture zones. However, the processing algorithm does not make any discrimination between features with clear geometry and local irregular velocity anomalies.

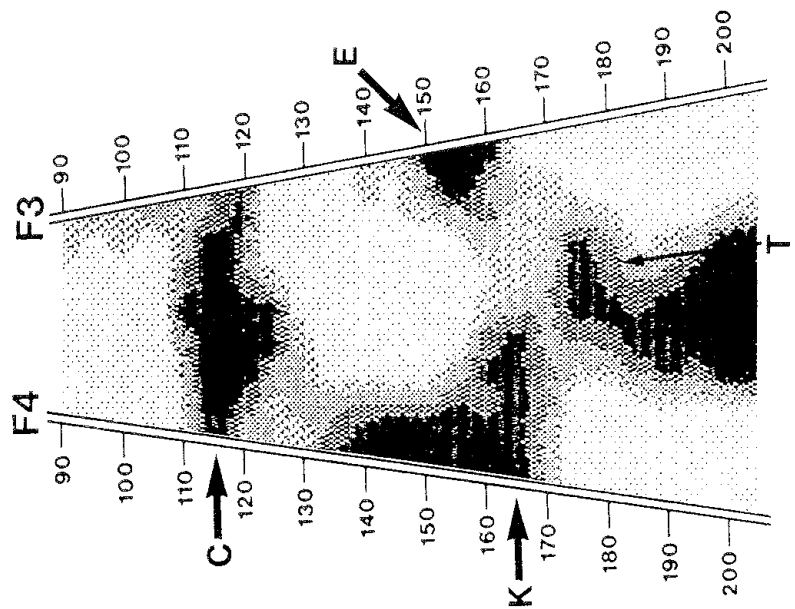
Tomographic maps of the P-wave and S-wave velocity distributions in the cross section between boreholes F3 and F4 at the Crosshole site are shown in Figure 2-30. The presence of the C, E, and K zones is clearly indicated, along with an artifact created by the intersection of a drift with the cross section about 25 metres below borehole F3. The feature that appears in borehole F4 at a distance of 130 to 140 m cannot be found unambiguously in other tomographic sections. However, the tomography is most sensitive to features that are oriented perpendicular to the bisectrix of a given section. If the same feature were to intersect the other cross sections at a steep angle, it might remain undetected. By combining the information from the cross sections between boreholes F4 and F1, F4 and F3, F4 and F5, and F4 and F6, the C and K zones were determined to be oriented subvertical and to strike to the NE-SW. The tomographic technique was found to be very sensitive to noise in the input data and, as a consequence, noisy signals containing poorly defined arrivals were not used in the tomographic inversion.

6034 6053 6071 6090 6109 6128 6146 6165 6184



(a) P-wave velocity distribution

3530 3539 3547 3556 3564 3573 3582 3590 3599



(b) S-wave velocity distribution

Figure 2-30

Tomographic maps of the P-wave and S-wave velocity distributions in the cross section between boreholes F3 and F4 at the Crosshole site (Cosma, 1987).

2.2.2 Improvements in Data Processing and Instrumentation

During Phase 3, the seismic testing method was used extensively for obtaining the orientation of the fracture zones at the SCV site (Cosma et al, 1991a). Concurrently, efforts were undertaken to refine the data processing and interpretation schemes for mapping fracture zones, and to develop a borehole seismic-signal source that could be used on a "production-line" basis in site characterization (Cosma et al, 1991b).

Seismic Reflection Data Processing

The seismic reflection testing technique allows changes in acoustic impedance within a rock mass to be detected. This is an accurate method for defining the boundaries of rock features. The position of a feature can be determined in three dimensions by this technique, but it is not possible to obtain a precise description of the rock properties within the feature. The tomographic method maps variations of the rock properties, such as wave velocity and attenuation, only in a planar section. The reflection technique gives a better image of the geometrics of the feature.

When processing seismic reflection data, it is important to separate the P-wave and S-wave fields and to eliminate tube waves. The processing concentrates on reflected events which, having traveled along longer paths, arrive later at the receivers. Furthermore, the amplitudes of these reflections are small because only a part of the energy is reflected back by discontinuities in the rock mass. For the purpose of these discussions, the testing arrangement in the field is assumed to resemble a VSP (Vertical Seismic Profile) test configuration, with a receiver array placed in a borehole and seismic sources located on a free rock surface. The data are organized in two-dimensional profiles, where the positions of the receivers along the borehole are defined by one axis and the time history of the seismic wave recorded at each receiver from the same source coincides with the other axis. The reflected signals are distributed in the profile along elongated "reflection patterns". The shape and position of the pattern are related to the position in space of the corresponding reflector, the position of the source, and the propagation velocity of the waves.

For purposes of illustrating the steps in the data-processing sequence, consideration will be given to a set of reflection data that was obtained at the SCV site in the Stripa mine. The details of the site are described in Section 3-3. The reflection data were first preconditioned, involving demodulation, bandpass filtering, amplitude compensation, tube wave suppression, suppression of direct P waves and S waves, and construction of "noise profiles".

The seismic signals used in the tests at the SCV site were 6 kHz resonant bursts of mechanical energy. These signals essentially annihilated the diffraction phenomenon and yielded tube-wave wavelengths of less than 0.25 m. To avoid aliasing in the two-dimensional filtering procedures, the spatial increment in the reflection profile had to be less than half the wavelength. This would have required that the receivers be positioned at 0.1 m increments in the borehole, which was not practicable. A demodulation routine, based on the Hilbert Transform, was applied to the

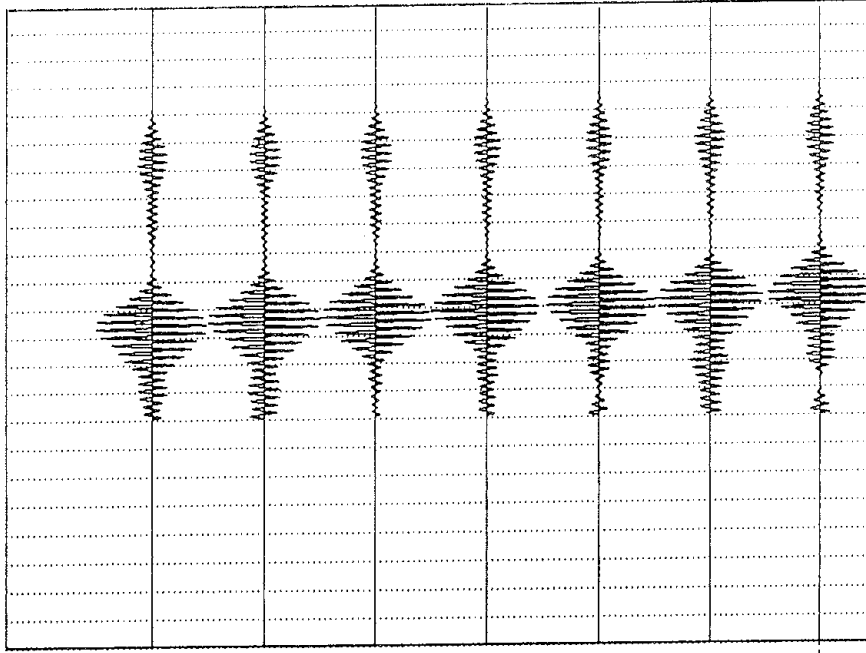
measured wave forms. The envelopes obtained by this technique for each of the three measured components were combined into a total amplitude function. Subsequently, only the slowly varying part of the phase was used to reconstruct the low frequency signals, as shown in Figure 2-31. After inspecting the spectra of the demodulated signals, a bandpass filter of 300 Hz to 1200 Hz was applied. After filtering, the signal traces were resampled in order to reduce the amount of data.

Most of the observable coherent patterns in the raw data could be associated with tube waves or S waves, as shown in Figure 2-32(a) where the P-wave arrivals have already been removed. The amplitudes of the reflected events were small due to the low reflectivity of the rock discontinuities, and cannot be seen in the profile. The tube waves were eliminated efficiently by means of a procedure that incorporates median filtering on the slant corresponding to their apparent velocity. Because tube waves were generated in, and travel along, the borehole, their apparent and real velocities were the same, resulting in straight patterns in the profile. The direct S waves were removed by a similar median filtering technique that followed the true travel-time curve. Amplitude compensation was performed to cancel the effects of geometrical spreading and attenuation and, thereby, reduced the amplitude contrast between the onsets of direct and reflected signals. This was accomplished by means of a variable gain operator that was run along the signals such that the amplitudes have, on average, the same peak values over the profile. The effect of removing the tube waves and amplitude compensation on the signal profile is shown in Figure 2-32(b).

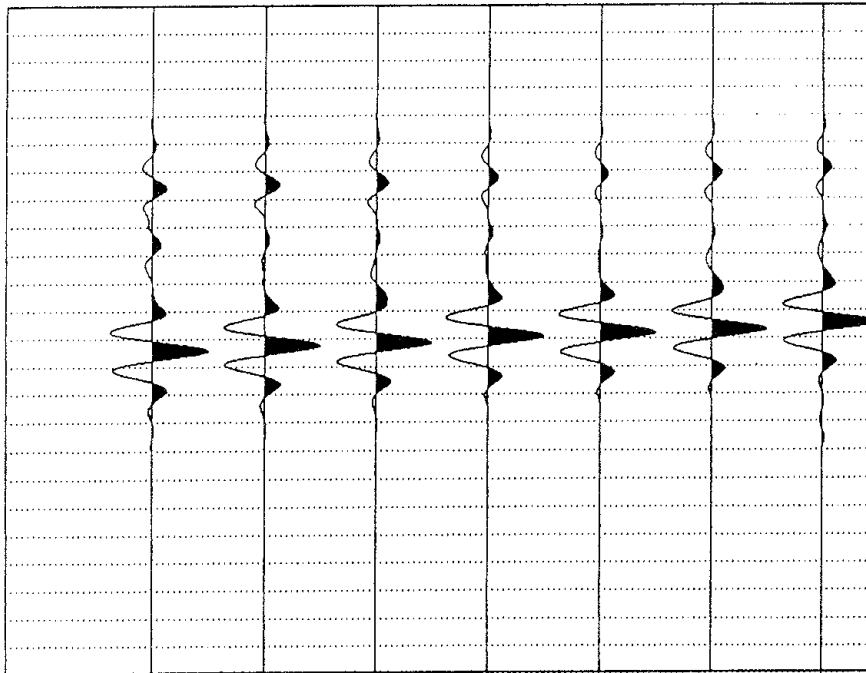
The final step in the preconditioning phase was to construct "noise profiles". The records of the real data profile from Figure 2-32 were joined together into one long seismogram in the memory of the computer. The pseudo-synthetic noise traces were constructed by taking random sequences of that seismogram. This procedure gave the same frequency spectrum and amplitude distribution as for the real data, but the phase consistency along allowed reflection paths was purely accidental.

The principal element of the data processing scheme was the application of the Image Space Transform. This processing technique was based on a Radon transform performed along a curve integrating path, which makes the method analogous to tomography. This transform and its inverse can be used as a multichannel filter to enhance the reflected signals, and as an interpretation tool to estimate the strength and position of the reflectors. The physical meaning of the procedure is that each reflection pattern can be considered as being produced by an "image source" from which the signals propagate to each detector on a direct path, much like the mirror effect in optics. The mirror on which the image source is formed is a planar reflecting feature, such as a fracture zone within a rock mass.

The Image Space Transform of the data profile in Figure 2-32 is shown in Figure 2-33(a). Apart from a few black spots, grey-shaded regions are evenly distributed in the diagram, which is an indication of the noisy nature of the data. The same procedure can be applied to the noise profile, which gives a uniform distribution of patches with roughly the same amplitude throughout the diagram. Noise is understood to be an accidental coherency. This definition allows a level of confidence to be estimated, above which coherency is not accidental and, therefore, indicative of a true reflector.

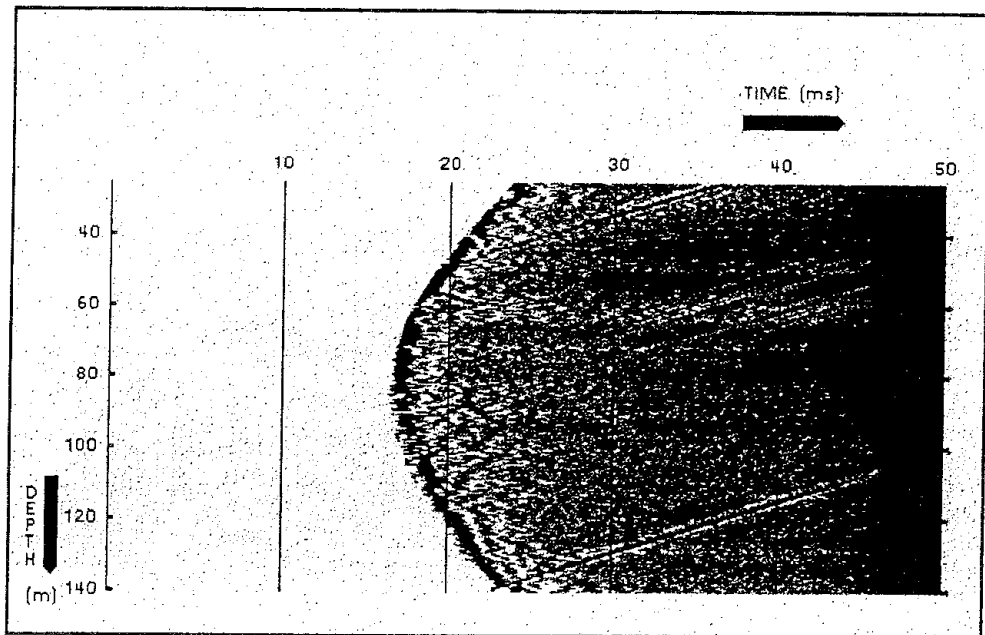


(a) Before demodulation

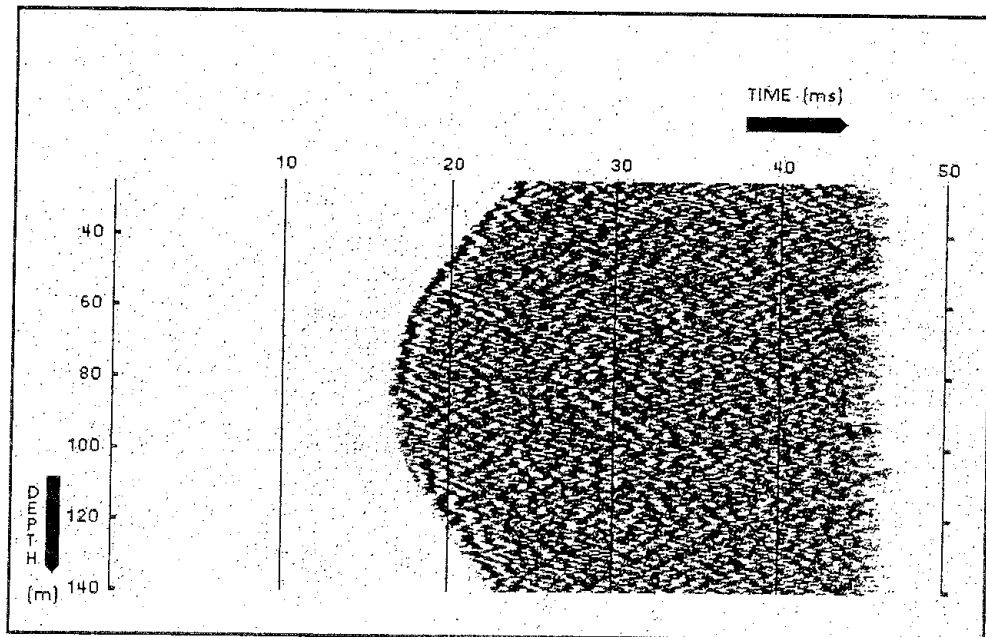


(b) After demodulation

Figure 2-31 Effect of demodulation on high-frequency seismic wave forms (Cosma et al, 1991a).



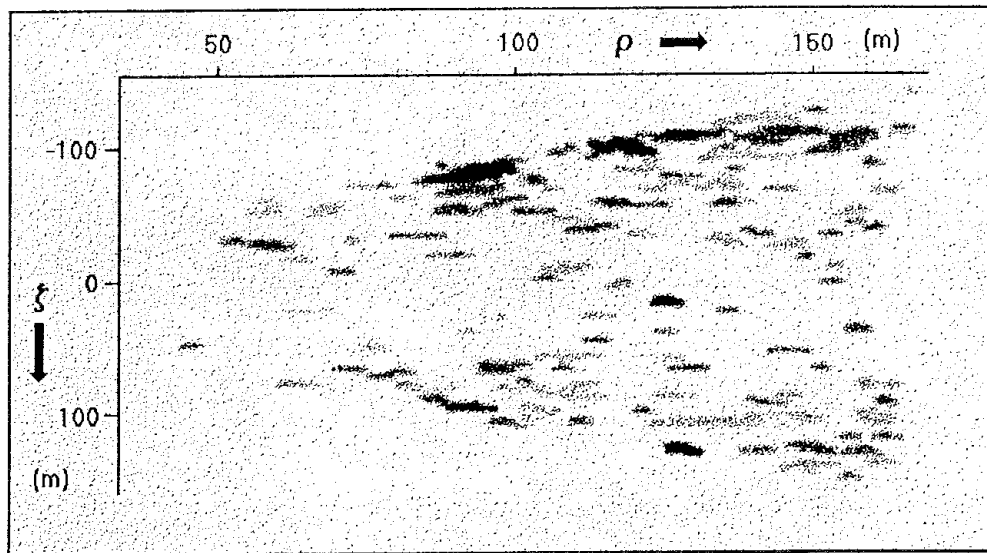
(a) Raw data, showing principally S-wave arrivals and tube waves



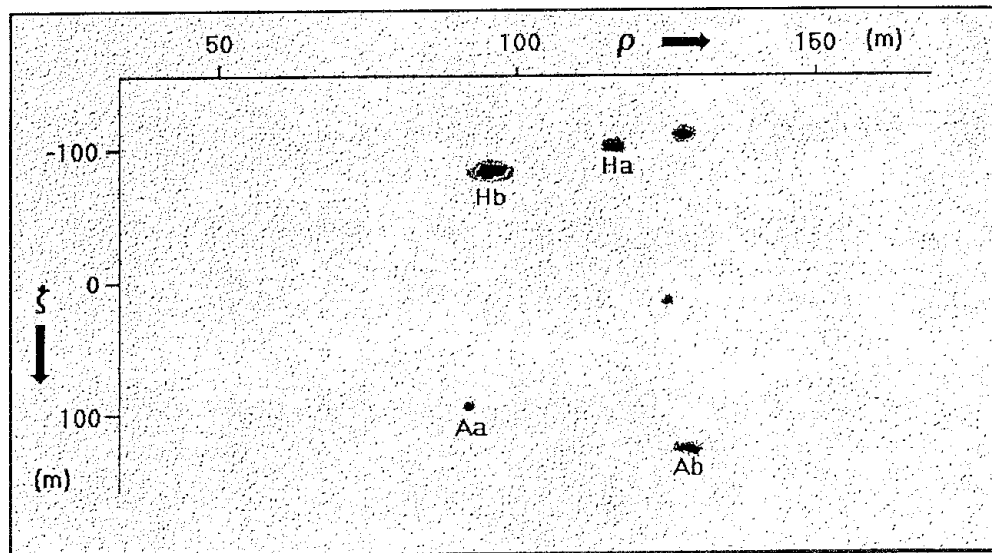
(b) After removal of tube waves and amplitude compensation

Figure 2-32 Effect of tube wave removal and amplitude compensation on a seismic data profile for the SCV Site (Cosma et al, 1991a).

The differences between the Image Space Transforms of real data and noise profiles allow real events to be isolated from the noise. This was accomplished by estimating a noise threshold level from the noise transform, and removing all values under the threshold level from the real data transform. The result of this procedure is shown in Figure 2-33(b), where the remaining events, designated as Ha, Hb, Aa, and Ab, are indicative of features within the SCV site.



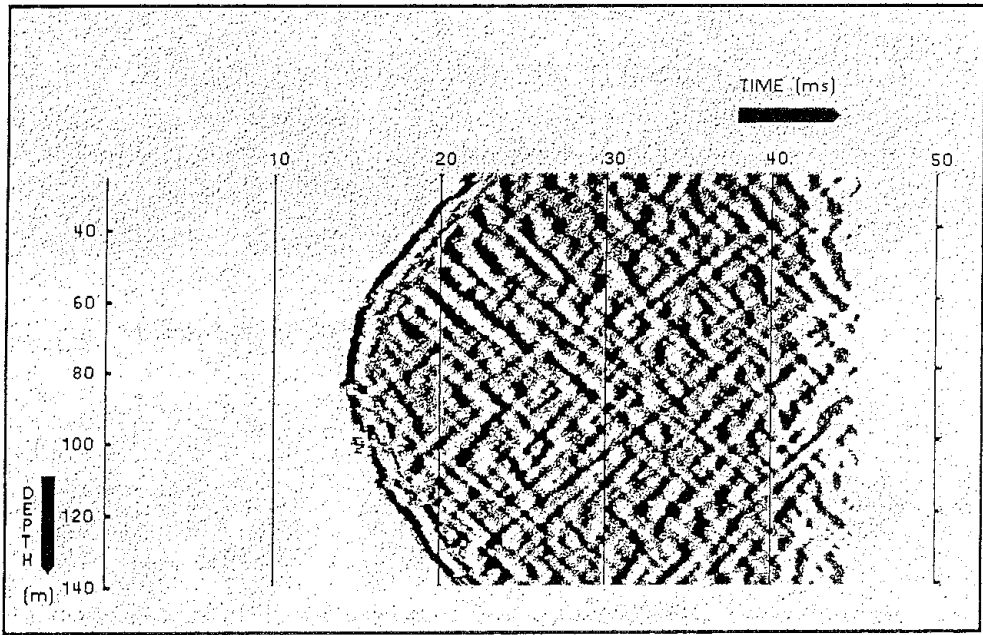
(a) Before removal of noise



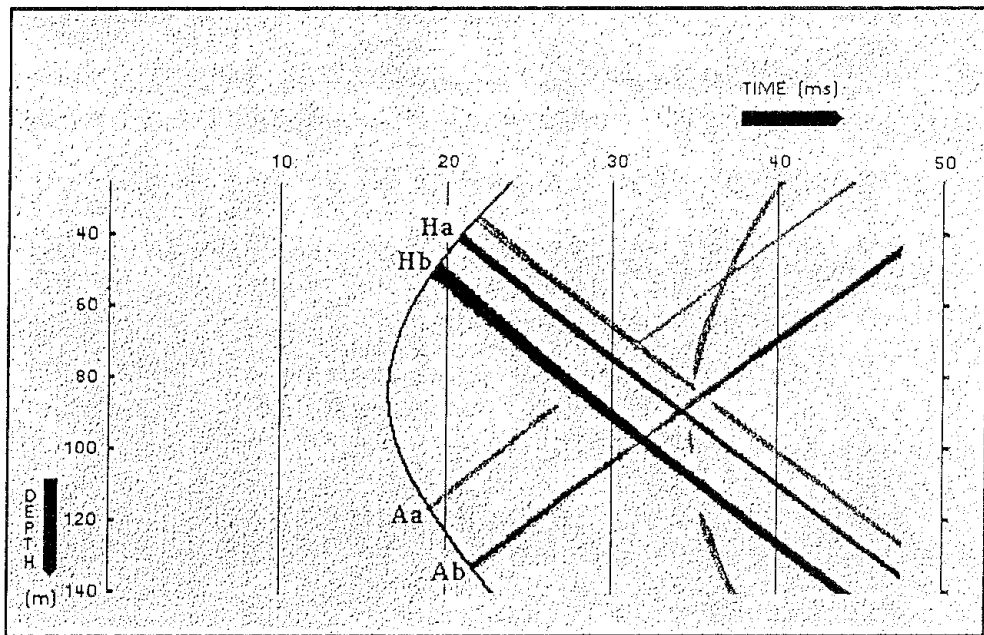
(b) After removal of noise

Figure 2-33 Effect of removing the noise from seismic data during an Image Space Transform of the profile obtained at the SCV site (Cosma et al, 1991a).

The next step is to apply an inverse transform to invert the profile into its original space. The result, shown in Figure 2-34(a) without noise filtering, was that many continuous patterns emerged, but not all of these patterns represented major features. When applying the same inverse transform to the noise profile, some patterns emerged but are much less clear than in the case for the real data. This suggested that most of the reflection events seen in Figure 2-34(a) were actually real, but very weak, indicating reflecting interfaces that were not boundaries of major features. Figure 2-34(b) shows the inverse transform to the original space of the profile when only the events over the noise threshold were retained. The structural features within the profile are now clearly indicated.



(a) Before noise filtering – continuous patterns emerge, but direct interpretation is difficult



(b) After noise filtering – only the most prominent reflectors remain

Figure 2-34 Effect of removing the noise from seismic data during retransformation into the original space of the profile (Cosma et al, 1991a).

The final step was to combine the Image Space Transforms from all profiles and then estimate the 3-D orientations of the reflectors which consistently appear in the profiles. This was accomplished by means of an interactive computer programme, which gave exact results only for features which were planar over large portions of the site. Features with strong local deviations from planarity were described by their average orientations, which may be different from those obtained by direct inspection in drifts or boreholes.

Borehole Signal Transmitter

Results obtained with low-energy piezoelectric transmitters in vibration measurements over short distances led to the notion that this type of device could be used for the generation of seismic signals in boreholes, provided that higher energy and lower frequency outputs could be developed. One of the principal difficulties in the design was the restriction imposed on the dimensions of the transmitter by the 56 mm diameter of a slim borehole which limits the energy level and frequency range of the transmitter. However, the use of a piezoelectric transmitter as a source has a number of distinct advantages. The repeatability of the shape and the level of the generated seismic signal is practically unlimited. This repeatability allows the stacking of hundreds of transmitted signals in order to improve the signal-to-noise ratio in the seismic data. In addition, the piezoelectric transmitter is extremely durable in that storage or use does not cause degradation of the instrument.

Seismic waves will propagate in solid materials which are normally inhomogeneous, fractured, fragmented, or granular. Attenuation is much higher in solid materials than in free water and several wave propagation modes are generated simultaneously by the same signal. Lower frequencies must be used in solid materials in order to reduce the attenuation. Thus, the transmitted bursts of energy can be only a few cycles long because the total duration of a single burst must be short compared to the propagation time. Additionally, the transmitter must be able to match a wide range of acoustic impedances due to the variety of rock types and the presence of cracked and uneven borehole walls. Furthermore, the instrument must be able to produce a radial strain in order to transmit energy to the rock. In principle, a cylindrical piezoelement is able to produce a radial strain when excited by an axial field.

There are many advantages in using axially polarized, relatively thin (usually 6 mm to 8 mm) circular piezoelements, such as commonly used in ultrasonic cleaning machines, surveying, and sonar systems. The elements can be stacked in a long column, which results in relatively larger displacements, and can still be connected two-by-two in parallel so that the driving voltage of the stack is the same as for a single element. The stack of piezoelements can be preloaded by a high compressive force to keep the elements pressed firmly against each other, such that the entire group behaves mechanically as a single large crystal even during the highest acceleration peaks.

One of the challenges in the instrument design was finding a method to convert the axial strain of a stack of piezoelectric elements into a radial displacement. This can be accomplished by placing two stacks of piezoelectric elements in the borehole, separated a certain distance apart, as shown in Figure 2-35. For a given frequency and corresponding distance between the stacks, a resonating cavity is formed in the borehole. It is limited by the borehole wall and the active ends of the elements that behave like pistons. It is theoretically possible to emit a frequency sweep signal without modifying the configuration of the instrument when the axial length of the cavity is proportional to the ratio of the propagation velocity in the borehole fluid and the frequency. The first stationary vibration mode is attained when a maximum pressure amplitude forms midway between the

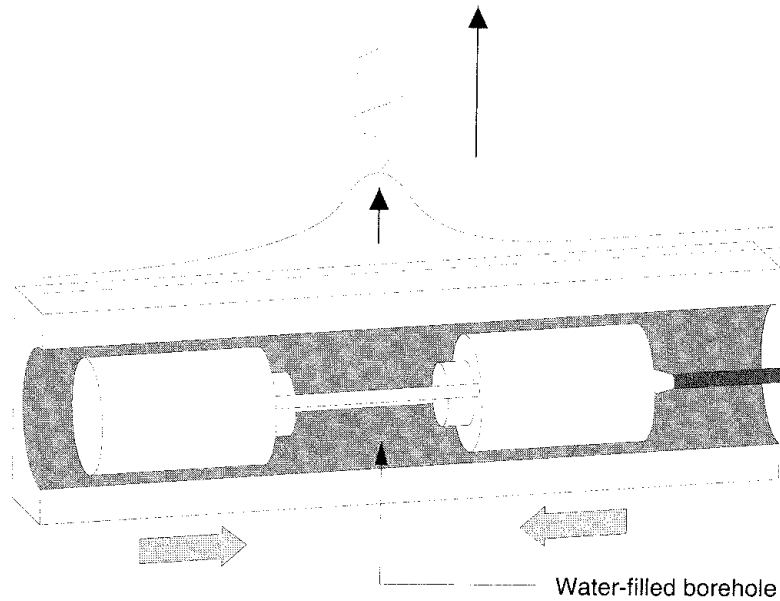


Figure 2-35 Schematic representation of the distribution of pressure amplitude along the axis of the resonant cavity for the fundamental frequency (Cosma et al, 1991b).

active heads of the stacks of piezoelements. Because higher frequencies become resonant for the same cavity length, it is therefore theoretically possible to emit a frequency sweep signal without modifying the configuration of the instrument. Other fundamental frequencies and their harmonics can be obtained by changing the distance between stacks. The principal assumption is that the pressure maxima of a standing acoustic wave in the borehole fluid produces a radial strain in the borehole wall. In the design that led to the second of two prototypes, the instrument consisted of two columns each with a metallic head piece and a stack of fifteen piezoelectric crystals. Both stacks are driven in phase by the same power supply. The distance between the stacks, or transmitter elements, can be adjusted by means of an electric motor which moves one element along its axis. Thus, the resonance condition could be attained for several fundamental frequencies after the transmitter was positioned in the borehole.

The body of the instrument consists of a thin stainless steel perforated tube with an outer diameter of 53 mm. The borehole fluid circulates freely through the perforations and fills the resonance cavity. A minimum borehole diameter in which the instrument can fit is 56 mm. In many tests in the Stripa mine, the transmitter was used in 76 mm diameter boreholes. The piezoelectric elements will function properly only within an approximate 300 Hz bandwidth around their own resonance frequency. A major resonance frequency in free air is slightly greater than 6 kHz and slightly less in water.

2.2.3 Significant Achievements

The seismic testing at the large-scale site at Gideå demonstrated that good-quality tomographic maps could be produced from travel-time data obtained for source-to-receiver distances up to 200 m in homogeneous rock. Conversely, if the rock is heterogeneous, and/or the measuring distances are large, the quality of the data diminishes and the interpretation of the tomographic maps becomes difficult. Although the calculations become time consuming, ray bending for large source-to-receiver distances can be treated by iterative ray tracing.

The borehole array at the Crosshole site in the Stripa mine was specifically designed for crosshole measurements. In particular, there were no difficulties with curved boreholes. In addition, the relatively short source-to-receiver distances, less than 200 m, and the isotropic character of the rock did not necessitate corrections for ray bending. The zones of low velocity on the tomographic maps correlated quite well with the fracture zones that had been identified on the basis of the core logs and borehole photography.

Generally speaking, high-quality travel-time data are required to obtain tomographic maps without significant "artifacts". Such data can be obtained from source-to-receiver arrays that ensure a uniform density of ray paths in the section of rock that is being tested. It is useful to produce tomographic maps from synthetic travel-time data for "conceptual" models of the rock mass, where geologic structure identified by core logging and other means is included. Such maps provide a basis for selecting the source and receiver locations to obtain an adequate and uniform density and distribution of ray paths, and, in so doing, reduce the potential for generating artifacts in the tomographic maps.

The refined seismic-data processing and interpretation techniques can be used to evaluate large amounts of data rapidly and efficiently for purposes of identifying and orienting fracture zones in a large crystalline rock mass. These techniques will certainly prove to be quite valuable in site characterization, particularly when the data represent signals generated by means of the precisely-controlled borehole transmitter containing the stacked piezoelectric elements.

2.3 RADAR TESTING METHOD

In Phase 2, an investigation was undertaken to develop a borehole radar system for identifying structural features in a crystalline rock mass and for determining their geometric characteristics (Olsson et al, 1983; Olsson and Sandberg, 1984; Olsson et al, 1987a,b). The method is based on the principles of electromagnetic wave propagation. Short pulses of energy are transmitted into the rock and reflected from inhomogeneities. The propagation time of a pulse is used to determine the distance to the reflecting object. The attenuation of electromagnetic waves in geologic media is commonly high and shows a strong frequency dependence. Geologic media are generally opaque at optical and microwave frequencies, while at low frequencies, below 1 MHz, the electromagnetic field loses its wave character

and diffusion-type processes dominate. There exists a frequency window from a few MHz to a few hundred MHz in which wave propagation effects dominate and the attenuation of the radar waves is moderate. In the radar investigations that took place at the Crosshole site, frequencies in the range of 20 MHz to 60 MHz were used. This range corresponded to wave lengths of 6 m to 2 m, respectively, in the Stripa granite which exhibited a radar-pulse velocity of about 120×10^6 m/s.

The radar investigations in Phase 2 involved the design, fabrication, and testing of a new borehole radar system. The design began in early 1983 and the first tests in the field were performed in mid 1984. The system was considered to be operational in the fall of 1984. Coincident with the development of the testing equipment, interpretation schemes and computer software for the analysis of the data were also developed. Single borehole and crosshole tests were performed initially at the Crosshole site, and, later in Phase 3, at the SCV site. The maximum depth of radar penetration in the Stripa granite ranged between approximately 100 m in the single-borehole mode and 200 m to 300 m in the crosshole mode. The absolute orientation of a fracture zone was obtained by combining single-borehole reflection data from adjacent holes. In Phase 3, a directional antenna was developed that allowed the orientation of a fracture zone to be determined from tests conducted in a single borehole.

2.3.1 Electromagnetic Properties of Rock

Measurements of the dielectric constant and conductivity were made on core samples from boreholes F1 and F2 at the Crosshole site. The measurements were made over a frequency range of 25 kHz to 70 MHz on samples in their dry condition and when soaked in water. The core samples represented "average" or intact rock, denoted as undeformed granite, and the major tectonized zones that were intercepted by the two boreholes. As shown in Figure 2-36, the average dielectric constant is approximately 5, independent

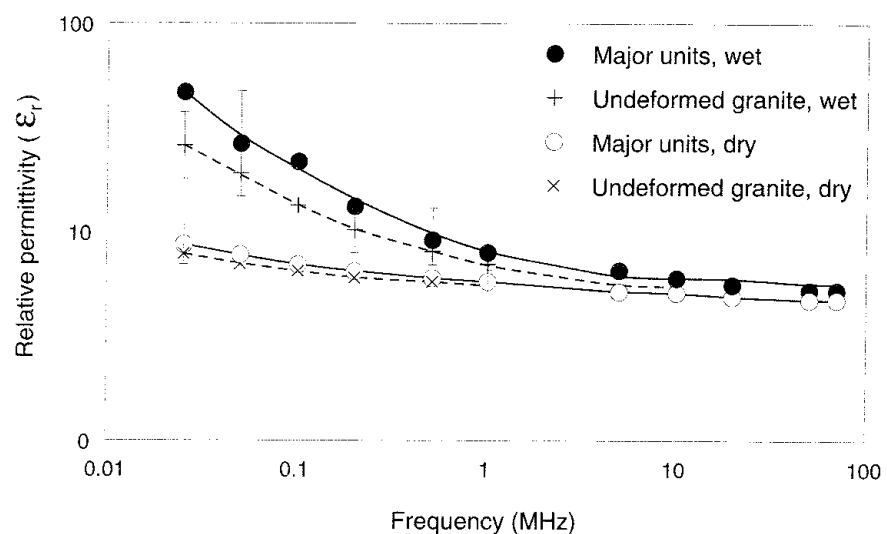


Figure 2-36 The dielectric constant as a function of frequency for different sets of core samples from the Crosshole site in the Stripa mine (Olsson et al, 1987b).

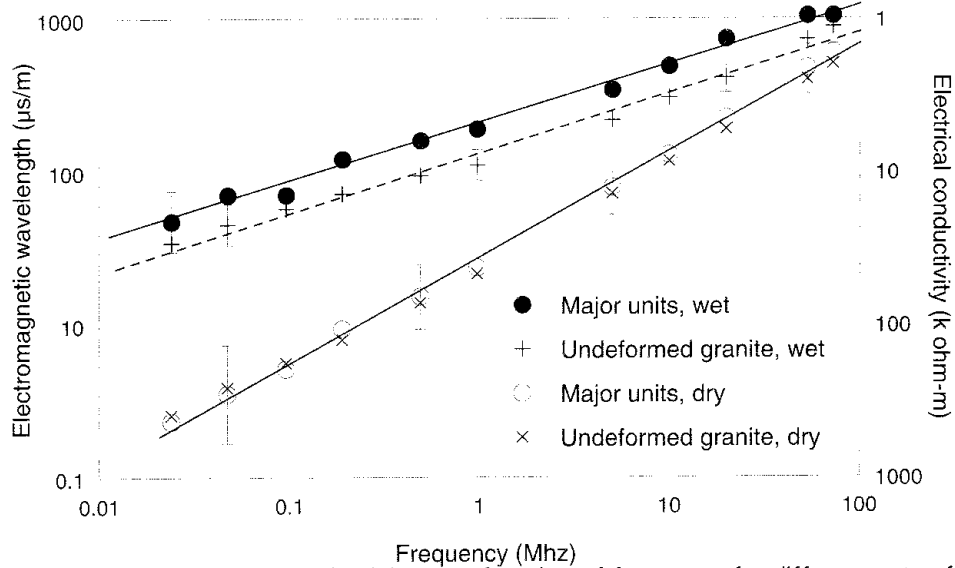


Figure 2-37 Electrical conductivity as a function of frequency for different sets of core samples from the Crosshole site at the Stripa mine (Olsson et al, 1987b).

of frequency, for dry core samples. However, as shown in Figure 2-37, the conductivity of the same samples increases in a logarithmic linear fashion with increasing frequency. The electrical properties of the dry samples of rock from both the rock mass and the fracture zones are essentially the same. The conductivity of the rock from the fracture zones is approximately twice that of the average rock for all frequencies for rock samples in a wet condition. The data from the laboratory measurements are in good agreement with those obtained from single-point resistivity measurements in the boreholes. The average resistivity values at 22 MHz and 60 MHz correspond to attenuations of 0.28 dB/m and 0.42 dB/m, respectively.

2.3.2 Testing System

The radar system consists of five different components. These include a microcomputer for control of measurements, data storage, data presentation and signal analysis, and a control unit for timing control, storage, and stacking of single radar measurements. The three borehole components of the system include a transmitter to generate short radar pulses, a receiver to detect and digitize radar pulses, and a motor-driven cable with a specially designed optical borehole cable for communication between the transmitter, receiver, and control unit. In a field test, the transmitter and receiver are positioned in the same borehole, or in adjacent boreholes. Single-borehole reflection measurements are made commonly with a separation distance of 0.5 m to 1 m between the transmitter and receiver. A pulse of electrical current is fed to the transmitter antenna, which generates a radar pulse that propagates through the rock. The pulse must be as short as possible to obtain high resolution. The borehole receiver unit contains an antenna of the same type as that in the transmitter. The pulse is received by the antenna, amplified, and recorded as a function of time. Recording the signal

is similar to what is performed by a sampling oscilloscope, in that only one sample of the received electrical signal for each pulse is taken at a specific time. A new sample is taken when the next pulse is generated, but displaced slightly in time. Thus, after about 20 to 40 samples, a replica of the entire signal is recorded. The sampling frequency and the length and position of the sampled time interval can be determined by the operator. Optical fibers are used for transmitting the trigger signals from the computer to the borehole probes and for the transfer of data from the receiver to the control unit. The optical fibers are electrical insulators and cannot support waves that propagate along the borehole. Additionally, these fibers do not pick up electrical noise and there is no deterioration of the signal along the cable as it is digitized in the borehole. Thus, the quality of the results are independent of cable length.

2.3.3 Single-Borehole Reflection Testing

The arrangement of the transmitter and receiver in a single-borehole radar reflection test is schematically shown in Figure 2-38. The transmitter and receiver are moved from location to location within the borehole with the distance between the two units remaining constant. The distance to a reflecting object in the rock mass is determined by measuring the difference in arrival time between the direct pulse and the reflected pulse. The electromagnetic wave-propagation velocity was essentially the same throughout the rock mass as verified by measurements between adjacent boreholes. The two basic patterns obtained in a radar reflection map are those due to point reflectors and those due to plane reflectors, as shown in Figure 2-38. Because the boreholes actually penetrate planar reflectors, reflections from both sides of the inhomogeneity will be observed. The radar reflection map shown in Figure 2-39 was obtained from radar

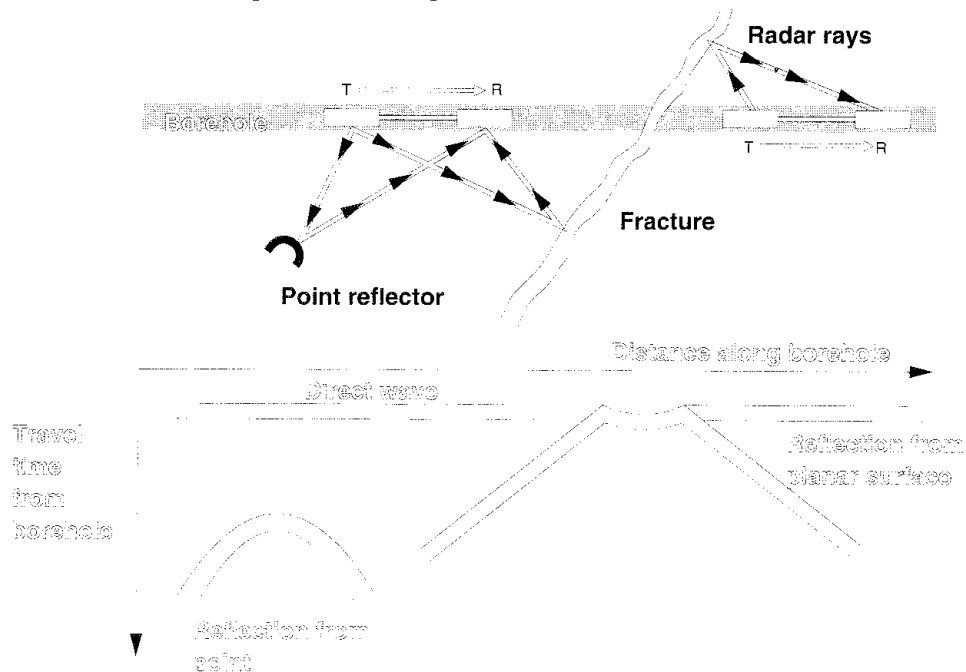


Figure 2-38 Test configuration for single-borehole radar reflection testing with the characteristic patterns generated by plane and point reflectors (Olsson et al, 1987b).

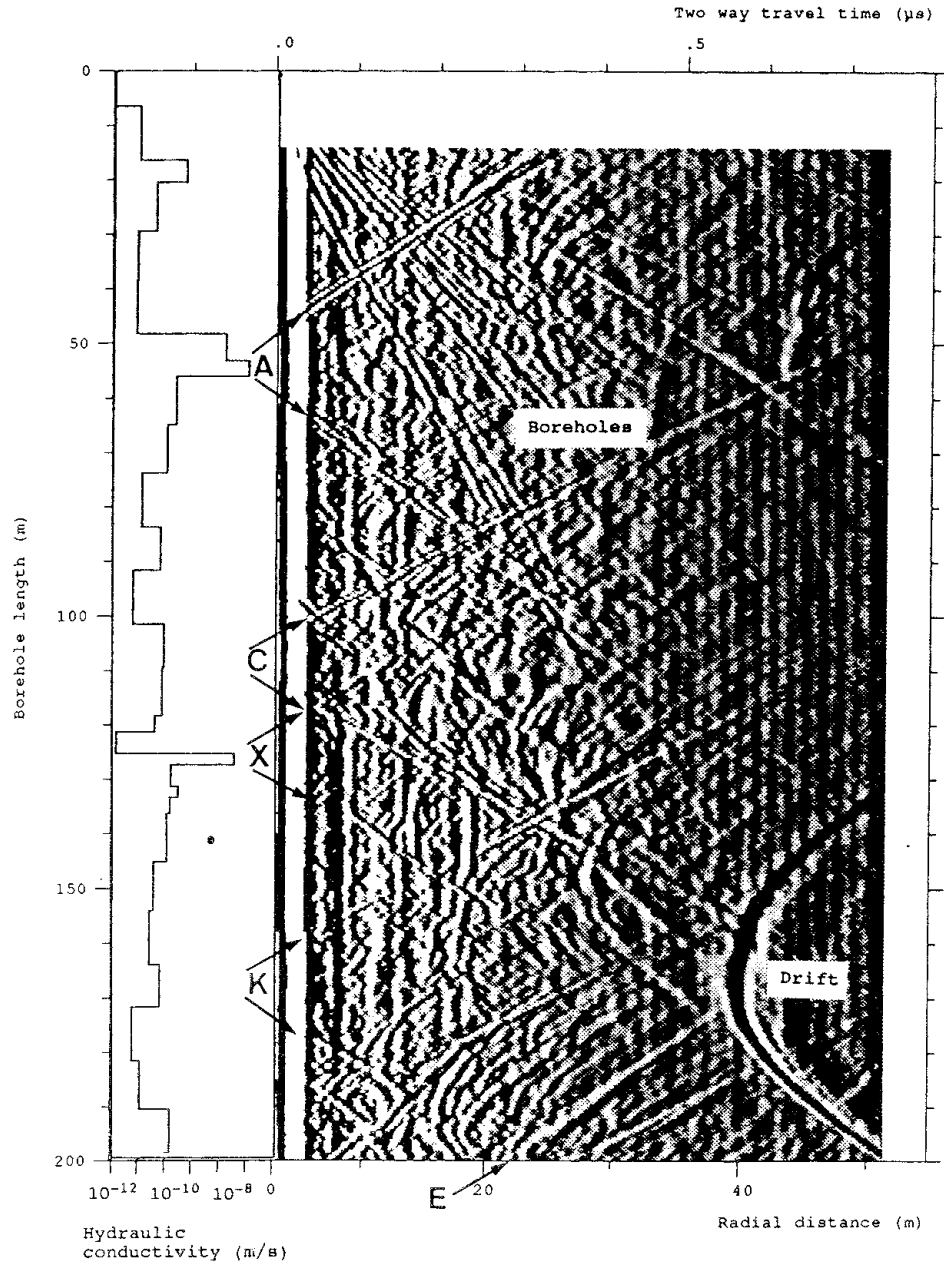


Figure 2-39 Radar reflection map obtained from tests in borehole F4 at the Crosshole site (Olsson et al, 1992).

Radar data measured with a center frequency of 60 MHz with a transmitter receiver spacing of 7.5 m. Reflections indicated by arrows are caused by fracture zones intersecting the borehole. The log of hydraulic conductivity for the borehole is shown for comparison with the fracture zone intersections.

measurements in borehole F4 at the Crosshole site. This map shows a number of plane reflectors that represent the fracture zones, and a point reflector due to a drift located about 40 m from the borehole. The fracture zones intersecting the borehole at depths of 55 m and 110 m consist of brecciated and mylonitized rock and have widths ranging from 1 m to 8 m. The reflections which appear to intersect the borehole close to its collar are

caused by other boreholes extending from the site. These boreholes were 76 mm in diameter and filled with groundwater with a resistivity of about 50 ohms. Radar maps were obtained to penetration depths of 80 m or more at the Crosshole site.

The radar image in Figure 2-39 is cylindrically symmetrical. This is because the borehole geometry requires the use of a dipole antenna. As a consequence, the spatial orientation of a fracture plane cannot be determined from measurements in a single borehole. However, the orientation can be found when measurements from several adjacent boreholes are available and combined into a Wulff stereographic projection.

2.3.4 Crosshole Testing

When the radar transmitter and receiver are placed in adjacent boreholes, both directly propagated and reflected pulses are recorded. The crosshole reflections are used to provide additional independent information about the fracture zones. The direct pulse is used in tomographic analysis to yield maps of radar velocity and attenuation in the section of rock between adjacent boreholes.

Crosshole Reflection Testing

Because of the crosshole configuration, the reflection geometry changes considerably and previously invisible zones within the rock mass between the boreholes can be detected. In principal, crosshole reflections can provide a complete determination of the orientation of a fracture zone. However, the analysis is much more complicated, together with the fact that the reflected signals are weak since the reflected pulse requires a longer propagation path than in single-borehole measurements. A radar map of the section between boreholes F1 and F6 at the Crosshole site is shown in Figure 2-40. During this measurement, the transmitter was moved along the F1 borehole while the receiver was stationed in a fixed position in the F6 borehole. As the transmitter is moved, the direct pulse registered by the receiver in the F6 borehole traces a hyperbola. Several pulses reflected from fracture zones arrive after the direct pulse. These curves will also be hyperbolae if the reflections are caused by fracture planes.

Crosshole Tomographic Analysis

The principal objective of the crosshole radar measurements at the Crosshole site was to map the extension of fracture zones between boreholes using tomographic analysis. In tomographic analysis, measurements at the boundaries of a region, as defined by boreholes, are used to obtain information about the properties of the interior of the region. Transmitter and receiver probes are located in the boundary boreholes and each ray between the transmitter and a receiver can be considered, in principle, to represent the average of a measured property of the rock along the ray path. To obtain an estimate of the properties of a localized area within the region, it is necessary that several rays pass through the area from different directions. The travel time and amplitude of the direct wave, or first

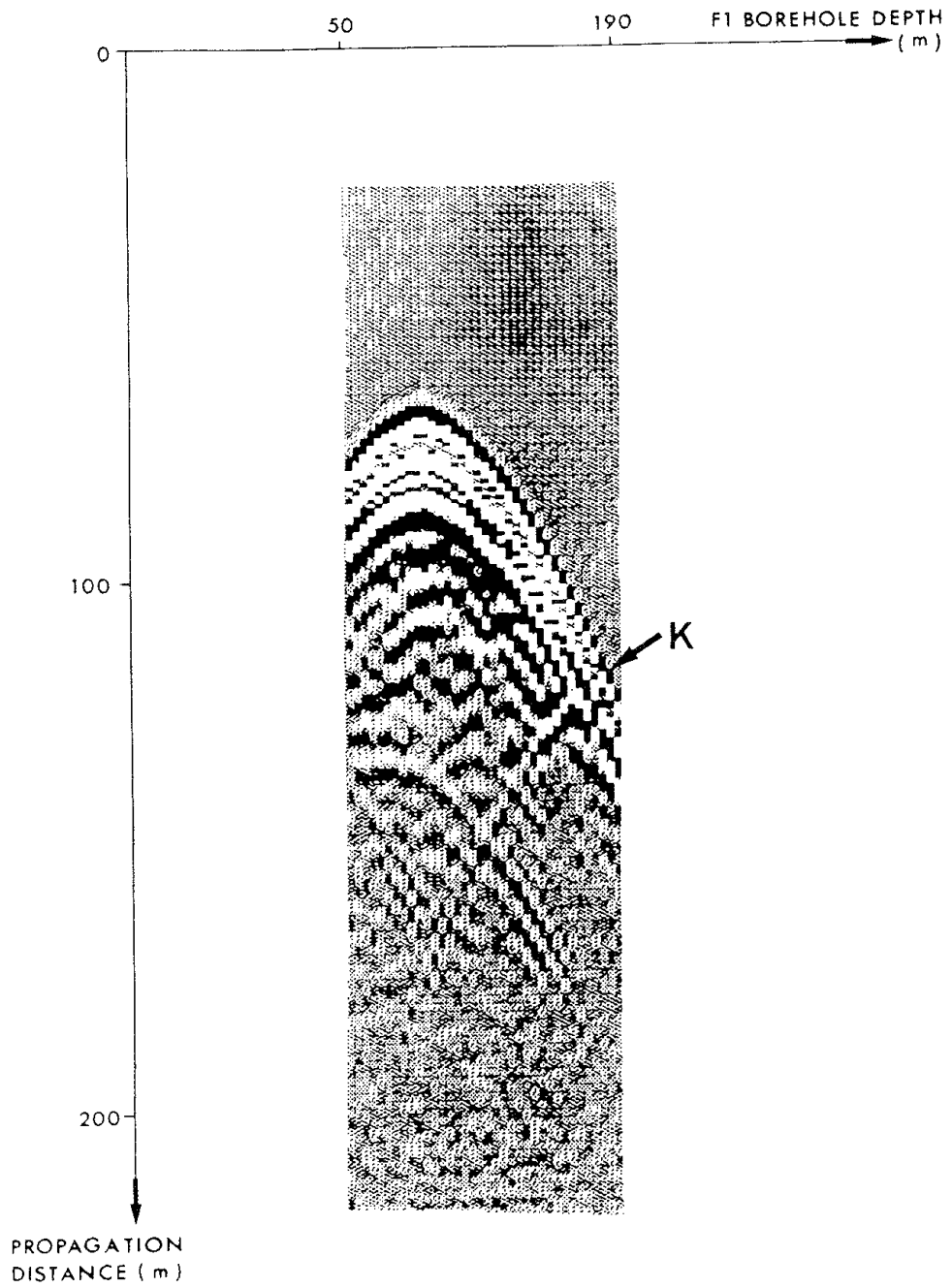


Figure 2-40 Radar reflection map for crosshole measurements between boreholes F1 and F6 at the Crosshole site (Olsson et al, 1987b).

The receiver was fixed in the F6 borehole at 112 m while the transmitter was moved in the F1 borehole. The center frequency is 22 MHz. The reflection from fracture zone K is indicated by the arrow.

arrival, between the transmitter and a receiver are extracted from the radar data. An inversion of the logarithm of the amplitude of each direct wave for an entire data set of radar scans provides an estimate of the distribution of attenuation in the region between the adjacent boreholes. The planar region between the boreholes is divided into a number of cells and, assuming straight ray paths, a system of equations are developed that interrelate the length of each ray within a cell to its attenuation within that cell. This system of equations is solved by iteration techniques to yield the spatial distributions of radar attenuation and velocity throughout the entire region between the boreholes. Commonly, a tomographic radar survey yields a large number of rays, of the order of 8,000 or more, which results in a large number of equations that must be solved simultaneously. Care must be exercised to reduce errors due to determinations of arrival time and amplitude, noise, digitization because of finite sampling frequency, and offsets in time and gain.

The generalized geometry of a crosshole tomographic section is shown in Figure 2-41, and includes an illustration of the decomposition into cells and typical ray patterns. The radar attenuation tomogram and, for purposes of comparison, the seismic velocity tomogram for the section of rock between boreholes F4 and F5 are shown in Figure 2-42. The tomograms consist of light and dark patches, where comparatively greater attenuation in radar amplitude and lower seismic velocity are shown by the dark patches. The intersections of fracture zones C and K with the plane are clearly visible. The tomograms indicate that the fracture zones undulate and vary in thickness. These particular characteristics are not readily observed from reflection data only. A drift passing between the boreholes, approximately perpendicular to the tomographic plane, gives rise to an anomaly of increased attenuation. The drift is air filled and actually has lower attenuation than the surrounding bedrock. The anomaly is caused by scattering of energy by the drift, leading to reduced amplitudes for all directly propagated pulses passing the drift.

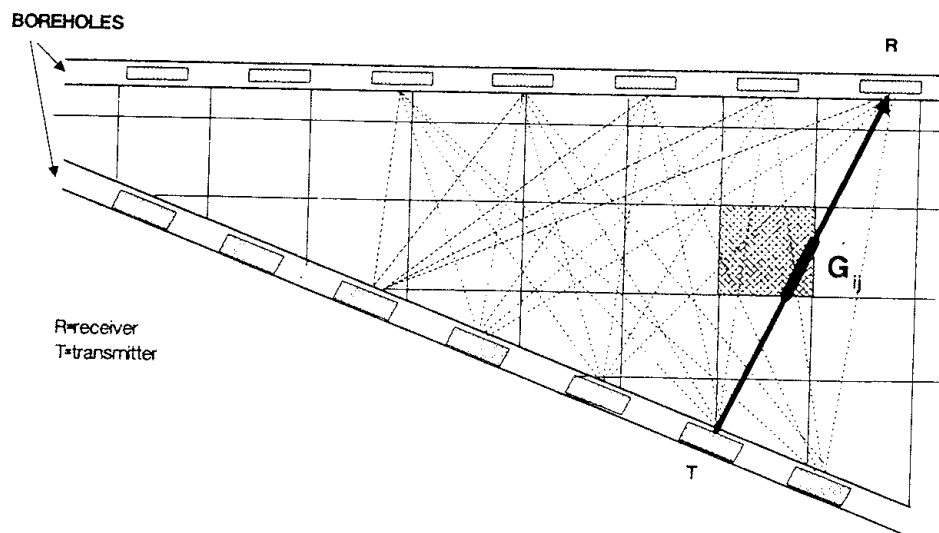


Figure 2-41 Generalized geometry of a crosshole tomographic section showing decomposition into cells and an example of ray patterns (Olsson et al, 1987b).

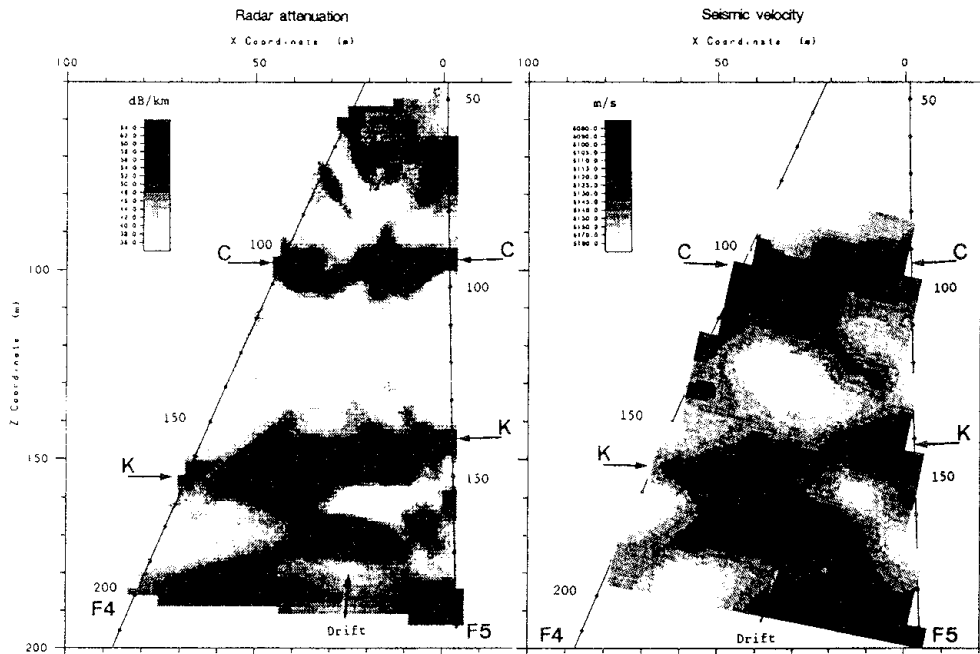


Figure 2-42 Radar attenuation and seismic velocity tomograms for a section of rock mass at the Crosshole site between boreholes F4 and F5 (Olsson et al, 1992).

2.3.5 Integrated Analysis of Radar Data

The radar data set from the Crosshole site consisted of single-borehole reflection measurements from six boreholes at two different frequencies and four crosshole tomographic sections which also included some crosshole reflection data. The single-borehole reflection measurements provided data on where the fracture planes intersected the boreholes, or their linear extensions, and the angles at which the structures intersected the boreholes. The crosshole reflection data yielded radar maps which indicated where the fracture planes intersected the boreholes, or their extensions, and a constraint on the possible orientations of the fracture planes. The tomographic maps provided a description of features in the plane between the two boreholes, including the geometric in-plane and out-of-plane variations.

The first step in the integrated analysis was to identify the major features in the three data sets and confirm that each feature was identified correctly in all data sets. Commonly, a feature was first identified in one of the tomographic maps. The possible orientations of the normal to the assumed planar feature, as obtained from the single-borehole reflection data, were plotted in a Wulff diagram, as shown by curves F5 and F4 in Figure 2-43. The intersection of the curves obtained from the tomography data and the single-borehole reflection data defined two possible orientations, as shown by the small circles A and B. This ambiguity was the result of collecting data in only one plane of the rock mass. The next step was to identify the same feature in another tomographic section through the region. For example, the single-borehole reflection data from borehole F6 was used to uniquely define the orientation of the fracture plane as being A in

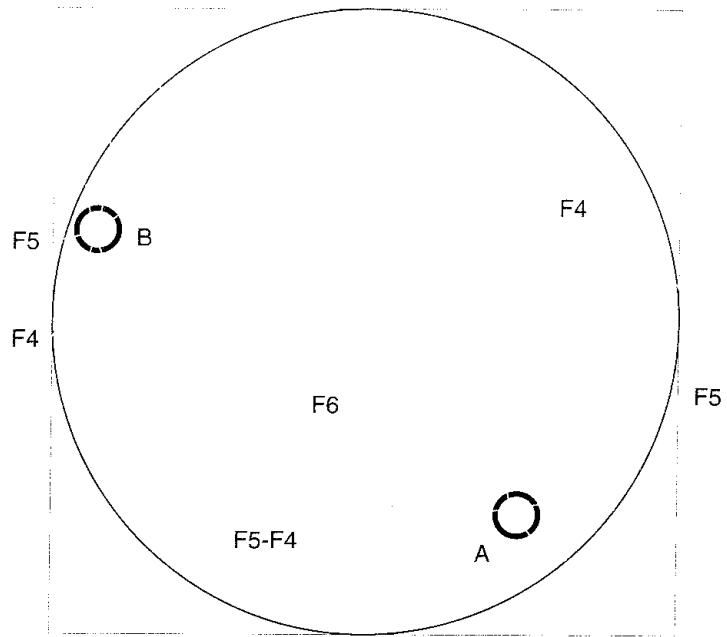


Figure 2-43 Wulff plot used to determine the orientation of a fracture zone from single-borehole reflection and crosshole tomography data (Olsson et al, 1992).

Figure 2-43. The analyses of the radar data obtained at the Crosshole site yielded a conceptual model that included four prominent structural features, as shown in Figure 2-44. These features can be categorized in two sets

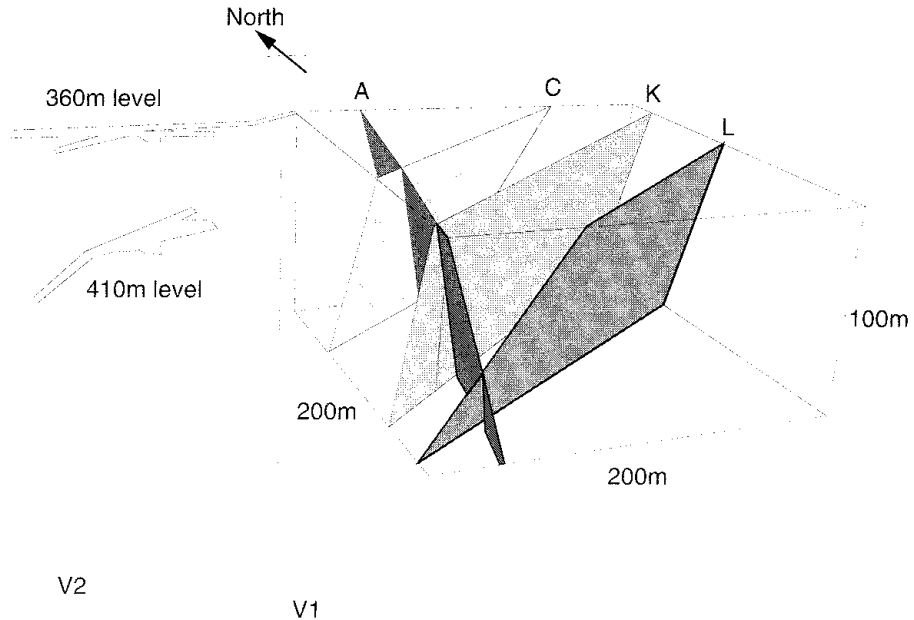


Figure 2-44 Perspective view of the four principal fracture zones identified at the Crosshole site (Olsson et al, 1987b).

characterized by different orientation. One set contained the C, K, and L zones, with a regular spacing of about 70 m. The second set, containing zone A, was oriented almost perpendicular to the first set. The analysis of the radar data assumed that the reflectors, or fracture zones, were essentially planar. In actuality, as illustrated by the tomographic maps, the zones tended to undulate to some degree and their thicknesses and contrasts to the background varied along their extensions.

The results of the hydraulic testing in borehole F4 was shown together with the radar results in Figure 2-39. A hydraulic anomaly was observed where zone A intersects the borehole, but no anomaly appeared to exist where zone C intersected the borehole. Rather, a hydraulic anomaly was observed at a borehole depth of 125 m, which is about 15 m away from zone C. A weak reflection, denoted as X in the radar reflection map, was associated with this anomaly. This feature also occurs as a localized area of increased attenuation near the borehole in the radar tomogram shown in Figure 2-42. It was concluded that this anomaly was probably a small fracture of limited lateral extent and, as such, was not included as a specific feature in the conceptual geologic model of the site. Fracture zone K did not represent a hydraulic anomaly, although it was seen clearly in both the reflection data and the tomogram. It was concluded that this particular zone was very irregular and of no hydraulic significance. The agreement between the seismic and radar results, as shown in Figure 2-42, was remarkably good considering that the two data sets reflect different physical properties of the rock mass. Fracture zones C and K were clearly seen in both tomograms, including the undulating aspects of the two zones.

Nineteen anomalies in hydraulic conductivity were identified in the six boreholes at the Crosshole site. Sixteen of these anomalies were associated with fracture zones that were included in the conceptual geologic model of the site shown in Figure 2-44, where twelve of these anomalies belonged to the four major fracture zones. Overall, the agreement between and among results from the hydraulic, radar, and seismic measurements was remarkably good.

2.3.6 Single-Borehole Directional Radar

Because of the small diameter of the boreholes, omnidirectional electric-dipole antennas were used as components of the borehole radar system. These antennas cannot provide the data that are required to determine the strike of a reflector because they are symmetrical with respect to the borehole axis. The necessary information can be obtained only by combining radar data from several boreholes which requires that the reflectors must be correctly identified in each radar reflection map. The identification of reflectors can be difficult if the fracture zones have reflection coefficients which are variable over their surfaces. In Phase 3, efforts were undertaken to develop a directional borehole antenna that could obtain the data from tests in a single borehole to determine directly the strike of a reflector (Falk et al, 1990; Falk, 1992). The outcome of this research work was a directional borehole radar system that had a maximum range of 200 m to 300 m in granite and the capability to obtain data from single-borehole tests to determine the strike of a fracture zone to an accuracy of about 3°.

Testing System

The principal components of the borehole directional-radar system are shown in Figure 2-45. The computer unit was used for control of measurements, data storage, and analysis. Timing control and stacking of the pulses was handled by the control unit. The transmitter and the directional receiver were connected to the control unit through optical fibers. The transmitter was equipped with a dipole antenna which had an omnidirectional radiation pattern relative to the borehole. The directional receiver was sensitive to the direction of the incoming radiation which made it possible to determine the location of the reflector relative to the borehole. The directional antenna consisted of an array of four loop antennas. The directional receiver also included a direction indicator which provided the

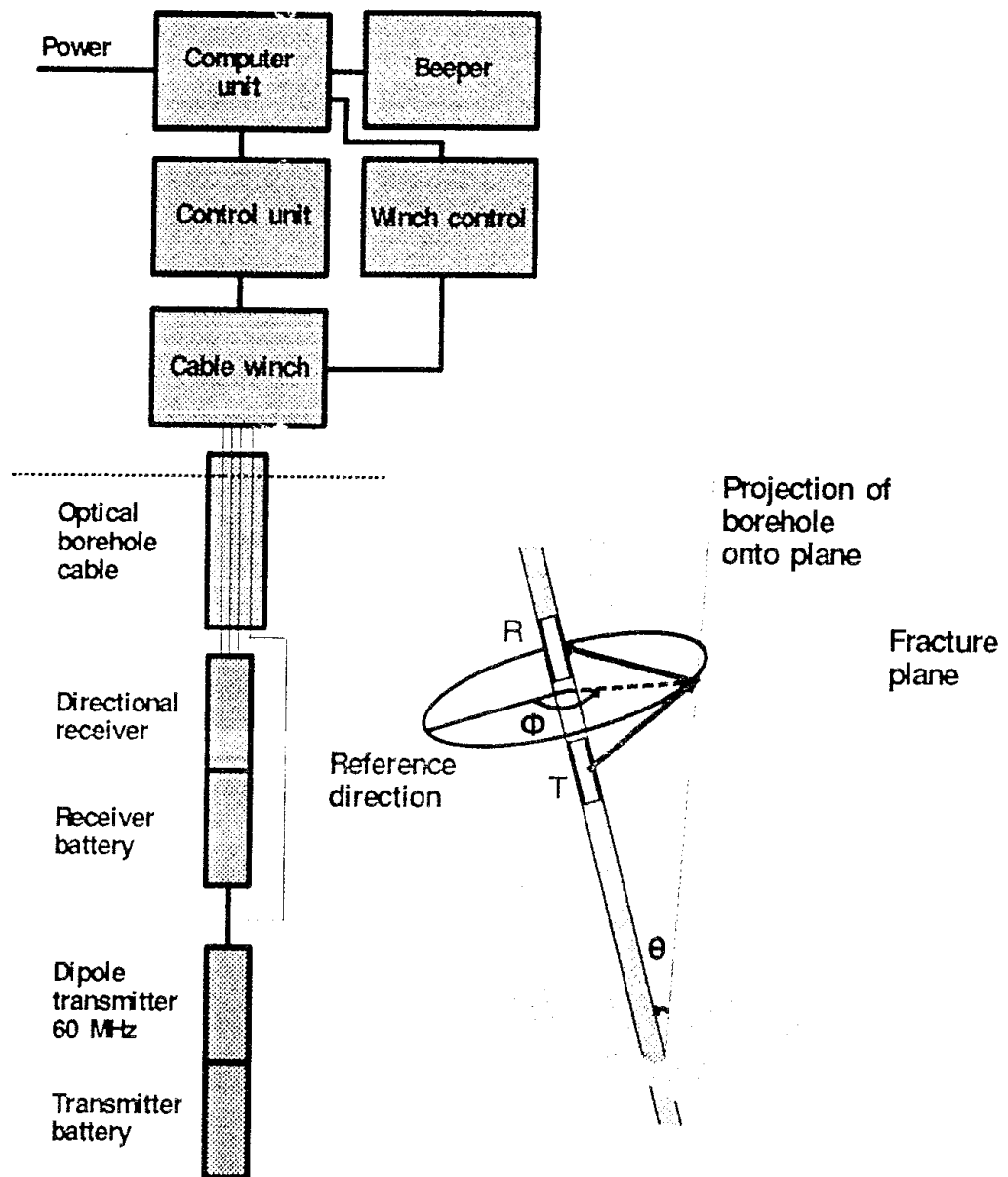


Figure 2-45 Components of the borehole directional-radar system and its principle of operation (Olsson, 1992).

means for orienting the antenna array relative to gravity or the total magnetic field vector.

Because of the dipole antenna in the transmitter, the radiated pulse was linearly polarized with the electric field in the plane spanned by the borehole and the direction of pulse propagation. Both point and plane reflectors scatter linearly polarized waves in such a manner that the reflected wave is also linearly polarized. When a single borehole measurement is performed, both of the magnetic fields of the transmitted and reflected pulses from a fracture plane will be perpendicular to the plane of the rays since the electric field is situated in that plane. If a directional antenna is used in the crosshole mode, the radiated waves reflected by a fracture zone will also appear as a linearly polarized source.

Single-Borehole Testing

Measurements with the borehole directional-radar system were made at both the Crosshole site and the SCV site in the Stripa mine. The results of the tests at the SCV site are discussed in Section 3.3. As discussed previously, the Crosshole site contained several well-defined fracture zones that varied in physical and geometric characteristics. The radar reflection map shown in Figure 2-46 was obtained with the directional radar system in borehole F4. Fracture zones K and L were two of the set of three major fracture zones at the Crosshole site with almost the same orientation. Zone E was related to a second set, containing the major fracture zone A, which was less fractured and oriented almost perpendicular to the first set. Zone C1 was a bifurcation of the major fracture zone C contained in the first set. Zone Q, which was essentially neglected during the early stages of radar and seismic testing at the Crosshole site, was found to have the same orientation as the zones in the first set, and to be located almost exactly between zones K and L.

2.3.7 Significant Achievements

The investigations at the Crosshole site have demonstrated that the borehole radar system is an efficient and accurate method for locating and characterizing fracture zones in a saturated, fractured granitic rock mass. The technique is unique in that it features an investigation range of the order of hundreds of metres into the undisturbed rock with a resolution on the order of metres. The variations in electromagnetic wave velocity and attenuation directly measured with the radar system were shown to be related to the extent of fracturing and water content of the Stripa granite. These variations can be illustrated rather clearly in tomographic maps of the sections of the rock mass between adjacent boreholes. The directional antenna developed in Phase 3 provided a means for determining the orientation of a fracture zone from test data obtained in a single borehole. Previously, a determination of such orientation was only possible when radar data from several adjacent boreholes were available. Finally, the results obtained with the borehole radar method can be correlated closely with those obtained from borehole seismic and hydraulic testing.

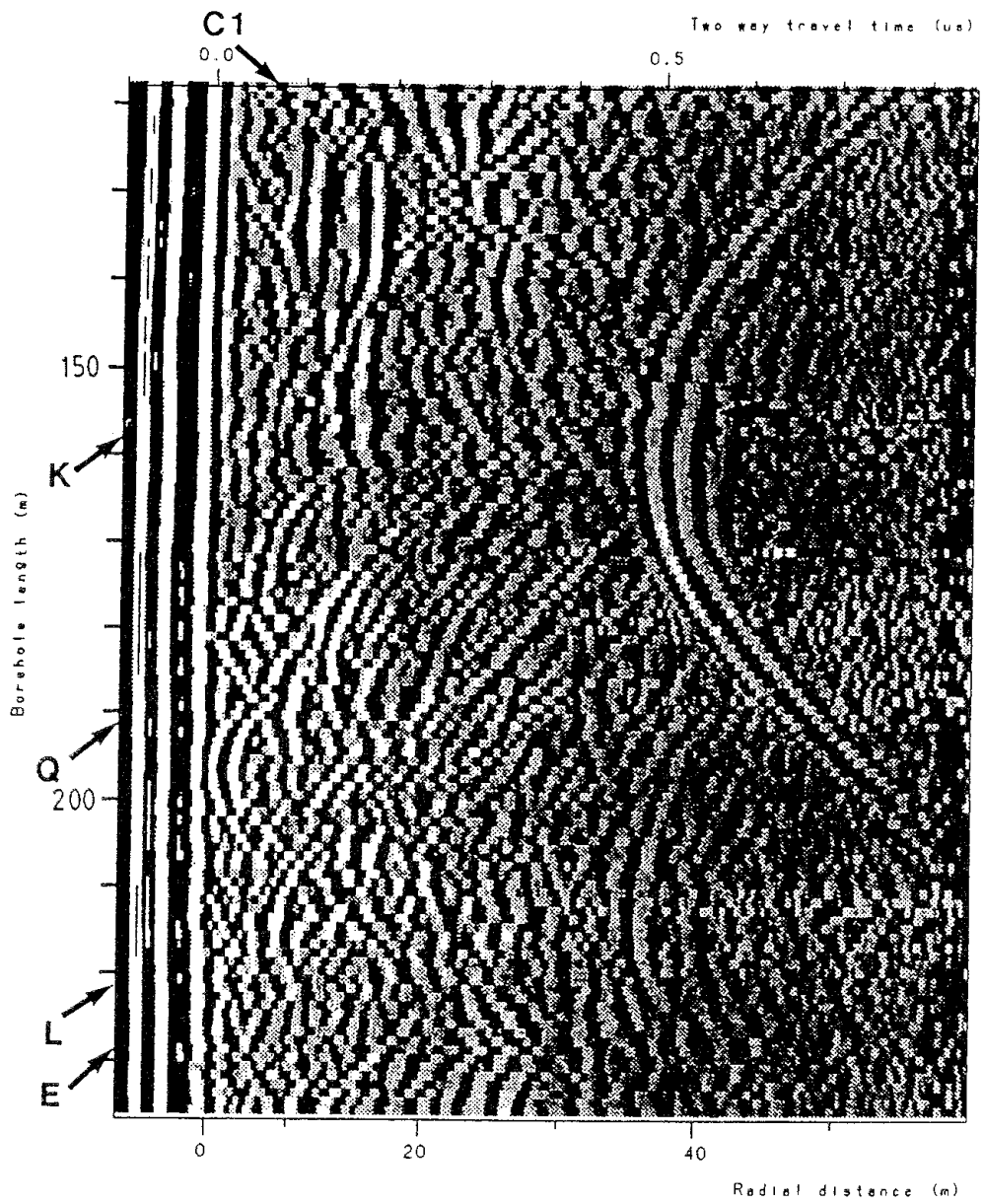


Figure 2-46 Radar reflection map obtained with the directional radar system in borehole F4 at the Crosshole site (Falk, 1992).

2.4 HYDROGEOCHEMICAL CHARACTERIZATION METHODS

Hydrogeochemical studies of the Stripa groundwaters, which began under the SAC program, were conducted for two purposes (Carlsson et al, 1983; Nordstrom et al, 1985; Davis and Nordstrom, 1992). The first was to develop sampling and analytical techniques for characterizing the geochemistry of the rock and groundwater at potential sites for geologic repositories in crystalline rock. The second purpose was to understand the origin and evolution of the groundwater in the Stripa area in order to demonstrate the manner in which the history of the groundwater could be reconstructed on the basis of chemical and isotopic analyses. In late 1980, the Hydrochemistry Advisory Group (HAG) was established, with a membership consisting of recognized experts in the field of geochemistry. During the course of the project, water samples were obtained at the surface, within the Stripa mine, and in boreholes to depths of 1200 m. The analyses of these water samples and core samples of rock from the boreholes were carried out in various laboratories in many countries by the members of the HAG.

During Phase 1, emphasis was placed on studies that dealt with the compositional control on major ions by bi-carbonate chemistry such as occurs with dissolution and precipitation of calcite in a closed system, by fluorite and barite solubility, and by feldspar hydrolysis. Additionally, the distributions of total dissolved solids and salt components within the groundwater were studied in relation to their spatial variations within the rock mass at Stripa. Investigations were initiated to examine the natural subsurface production of radioisotopes and the problems inherent to estimating groundwater age based on a single radioisotope. During Phase 2, the properties of the fluid inclusions within the minerals that filled the fractures were studied in more detail and the groundwater chemistry was monitored continuously to determine temporal changes for selected water-bearing fracture zones. The use of strontium isotope measurements in the fracture minerals and the groundwater was evaluated as an interpretive tool. Studies were undertaken to fractionate the organic compounds dissolved in the groundwaters and to determine their carbon isotope composition. Finally, the study of the subsurface production of natural radioisotopes was completed and the results were related to the age, or residence time, of the groundwater at Stripa.

2.4.1 Groundwater Sampling Sites

Groundwater samples were collected from packed-off water-bearing zones in boreholes N1, V1, and V2 at the SGAB site and from the M3 borehole in the Stripa mine. Five selected zones in borehole V2 were chosen for sampling because they exhibited sufficient groundwater discharge and a wide range of groundwater composition. Samples were collected approximately every six weeks beginning in mid 1985. In late 1986, the collection program was rescheduled to sample only three zones every three months until mid 1988. The groundwater discharge from these zones ranged between 1 ℓ/h and 18 ℓ/h , with a total dissolved solids (TDS) variation between 350 mg/ℓ and 1200 mg/ℓ . The bottom interval in borehole V1 was also monitored during the same time period. Monitoring of the groundwater

in borehole M3 was continued during Phase 2, although partway through the program the groundwater in the borehole was not allowed to flow freely.

Routine and specialized analyses were conducted on the water samples by the members of the HAG at their laboratories in many countries. Measurements of neutron flux were made in the Stripa mine to improve the estimates of subsurface production of radionuclides. Core samples from the V1 and V2 boreholes were selected for studies of fluid inclusions, strontium isotope, and additional trace elements and isotopes.

2.4.2 Hydrochemistry of the Stripa Area

During the period of 1977 through 1986, several hundred water samples were collected from boreholes at Stripa and analyzed for their chemical constituents. In general, as shown in Figure 2-47, the salinity of the groundwater increases with depth into the granite. Water from the M3 borehole, at a depth of 340 m to 341 m below the surface, had a chemistry that was similar to surface water, including, in particular, low salinity. The assumption that the water was "young" was supported by relatively higher tritium concentrations. Samples of water from borehole V2, at a depth of 797 m to 805 m below the surface, contained tritium concentrations which suggested considerable dilution of deeper water by surface water. Concentrations and ratios of concentrations for most ions were similar for water samples taken from borehole V1, at a depth of 838 m to 913 m below the surface, and borehole V2, at a depth of 810 m to 818 m. This similarity suggested that the two boreholes were connected by means of a fracture zone. The existence of a connection was substantiated by results from the crosshole hydraulic interference tests conducted in Phase 1 in these two boreholes. Water samples collected in borehole V2, at depths ranging from 898 m to 1230 m, contained concentrations which indicated "old" saline water.

Uranium concentrations in various samples of Stripa granite varied from about 26 ppm to more than 50 ppm. The uranium in the leptite was considerably less, generally about 5 ppm. Concentrations of uranium were much higher in fracture fillings than in the primary matrix of the rock, probably of the order of a few hundred to a few thousand ppm.

The pH of the deeper waters was higher than that for waters collected at the surface or in the relatively shallow borehole M3. Calcite appeared to be slightly super saturated, especially for samples with higher pH and alkalinity. Water samples from the deep sections of the boreholes contained very little magnesium, less than 0.5 mg/l, whereas water samples from the surface and in the shallow boreholes had relatively higher concentrations. All samples, including particularly those from the shallow and surface waters, were under saturated with respect to gypsum. The intermediate to deep groundwater samples were saturated or super saturated with respect to calcite, fluorite, barite, and ferric hydroxide. All of the water samples were mildly oxidizing to mildly reducing except for the groundwater at the bottom of borehole V2 which contained about 1 mg/l dissolved sulfide. The compilation of data suggested that the shallow and surface, or recent, groundwaters at Stripa had a different chemical character than waters deeper in the granite. Comparison of the data with sea water concentrations

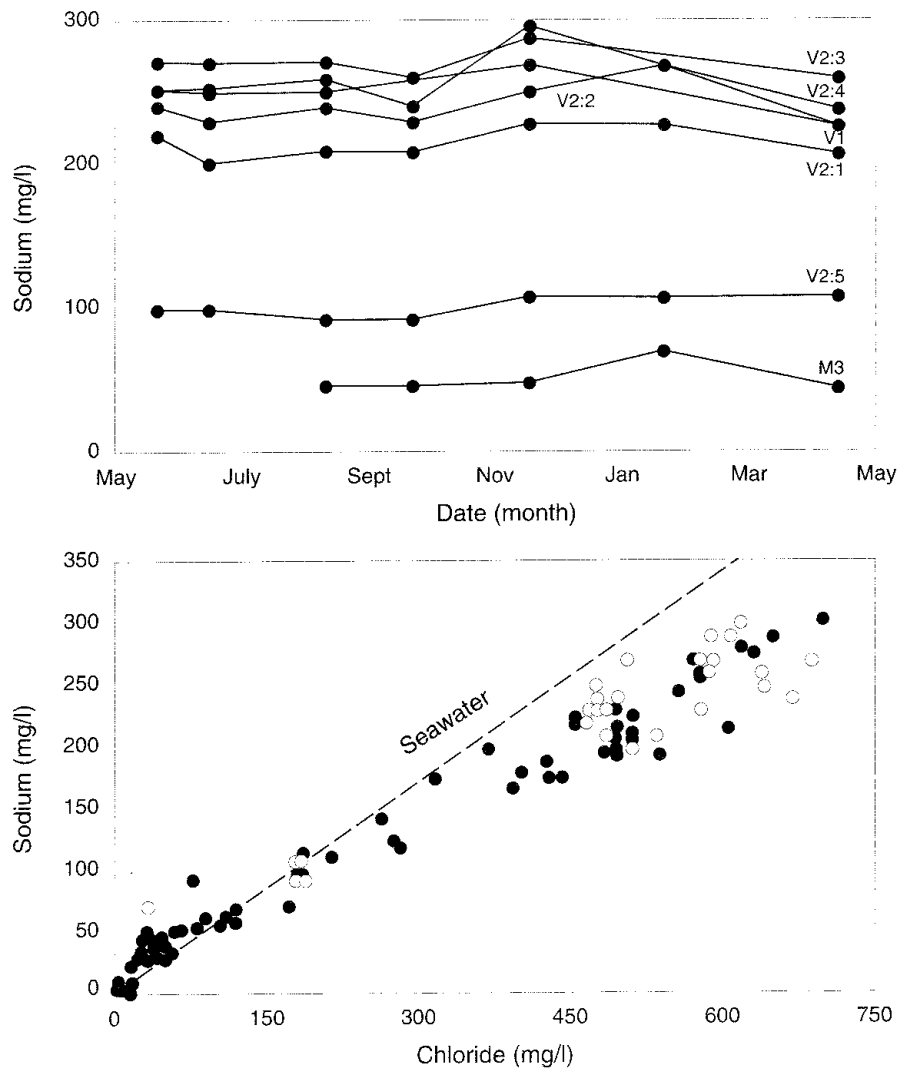


Figure 2-47 Concentration of sodium as a function of sampling date and chloride concentration (Davis and Nordstrom, 1992).

The solid circles represent Phase 1 data and the open circles represent Phase 2 data. The sampling intervals in terms of depth from the surface for boreholes M3, V1, and V2 were as follows; M3: 340-341 m; V1: 838-913 m; V2:5: 799-805 m; V2:4: 810-818 m; V2:3: 898-906 m; V2:2: 958-966 m; V2:1: 967-1230 m.

indicated that the saline Stripa waters reflected simple dilution of sea water by rain, snow melt, or other surface waters moving through the fractures in the bedrock.

2.4.3 Fracture Mineralogy

Approximately 300 fractures were sampled from rock cores from boreholes N1, V1, and V2 at the SGAB site. The fracture fillings were analyzed by a variety of methods, including thin section analysis, x-ray diffraction, mass spectrometry of ^{13}C and ^{18}O , SEM-KEBEX and microprobe analysis for all mineral phases, acid digestion of calcites by atomic absorption spectrophotometry, and instrumental neutron activation analyses for rare

earth elements. It should be noted that each fracture filling was generally not analyzed by all of these techniques.

Mineralized fractures contained smaller monomineralic veinlets, less than 1 mm in thickness, with quartz, chlorite, or calcite. Larger fractures, but less than 5 mm, contained combinations of such silicates as chlorite, mica, quartz, and feldspars, and/or calcites, and/or fluorite. Finally, large breccia or shear zones, dominated by altered feldspars, epidote, mica, and/or fluorite, and/or calcite, were observed in the core from the N1 borehole. The fractures filled with epidote usually appeared to be sealed.

The collection of petrological, mineralogical, and geochemical data indicated that the pluton in the Stripa area had undergone a very complicated history of mineral alteration in the fractures. As shown in Figure 2-48, there exists a very wide spread in the oxygen and carbon stable isotope compositions of the calcites in the fracture fillings, which indicates a wide range of fluid and thermal histories. The carbon isotope compositions in the range of -5‰ to

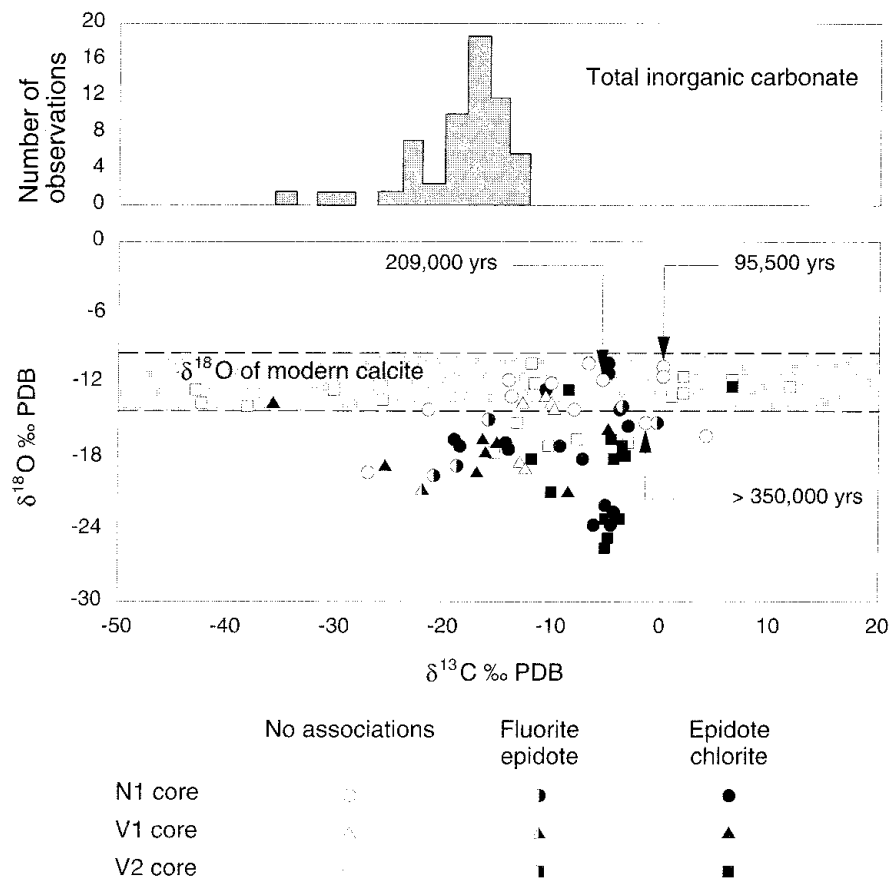


Figure 2-48 The oxygen and carbon stable isotope compositions of the calcites in the fractures of the Stripa granite (Davis and Nordstrom, 1992).

The open circles, triangles, and squares indicate calcites with no or minor mineral associations; the half-filled symbols are for hydrothermal calcites associated with fluorite; and, the filled symbols denote the earliest generation(s) of magmatic/hydrothermal origin. The range of $\delta^{18}\text{O}$ values of calcites in isotopic equilibrium with present-day groundwater is also shown. The "total inorganic carbonate" data refer to measurements of $\delta^{13}\text{C}$ in the total inorganic carbonate.

-12‰ are typical of meteoric groundwaters circulating in the pluton during later stages of cooling, where calcite is usually associated with dark chlorite and epidote (‰ is the symbol for parts per thousand). A second major group of calcites belonged to a period of "hydrothermal" generation where fluorite and epidote were the principal associated minerals, with the carbon isotope composition ranging between 0‰ and -21‰. The oxygen isotope composition varied between -14‰ and -19.5‰, which is indicative of a deposition temperature below 150°C. While the first group of calcites were represented by massive fillings found almost always in closed fractures, the second group was commonly found in veins in association with very prominent open fracture zones. The last group of calcites was almost always associated with open fractures and were represented by carbon isotope compositions above -10‰ or very negative values. These data appear to reflect calcite precipitation or recrystallization under relatively "modern" conditions.

The pluton is characterized by light rare-earth-element REE enrichment and a depletion of europium. These patterns are generally considered to have been formed under mildly oxidizing conditions. However, two other very distinctive sets of REE patterns were observed in the fracture systems of the pluton. The first pattern occurred in the first group of calcites discussed above in which the light REE pattern and Eu anomaly were similar to the host granite, but the pattern was very distinctly heavy REE enriched. This feature may be due to an extraneous heavy REE fluid that was "sweated" from a local marble or skarn and injected into the pluton subsequent to cooling, or to fractionation during initial cooling of the pluton and an early or late stage fluid concentrated in heavy REE. The second distinct pattern was similar to that for the first group of calcites, except for a distinctive Ce depletion. This appears to be a product of a hydrothermal event which emplaced the fluorite veins in the pluton, during which a thermal cooling event occurred and a different fluid, probably oxidizing and uranium rich, entered the pluton. The ⁸⁷Sr-⁸⁶Sr ratios suggest that there exists at least three major calcite groupings in the pluton, which is consistent with the conclusions drawn from the range of oxygen and carbon isotope compositions.

The presence of at least three mineralogically and geochemically distinct calcites, along with two fluorites and two to three chlorites, in the same fracture indicates a complicated, many-staged precipitation history. Each calcite group appears to have a distinct carbon-oxygen isotopic range, strontium isotopic range, and, to a limited extent, REE pattern. Based on these data, the history of the system was postulated to be one in which there was an early period of high temperature. During this time, the pluton was cooling, shrinking, and fracturing. Subsequently, two additional hydrothermal-magmatic events seem to have occurred, featuring temperatures in excess of 100°C. Finally, there appears to have been a very late cooling stage during the early pluton history, in which the temperatures were relatively lower.

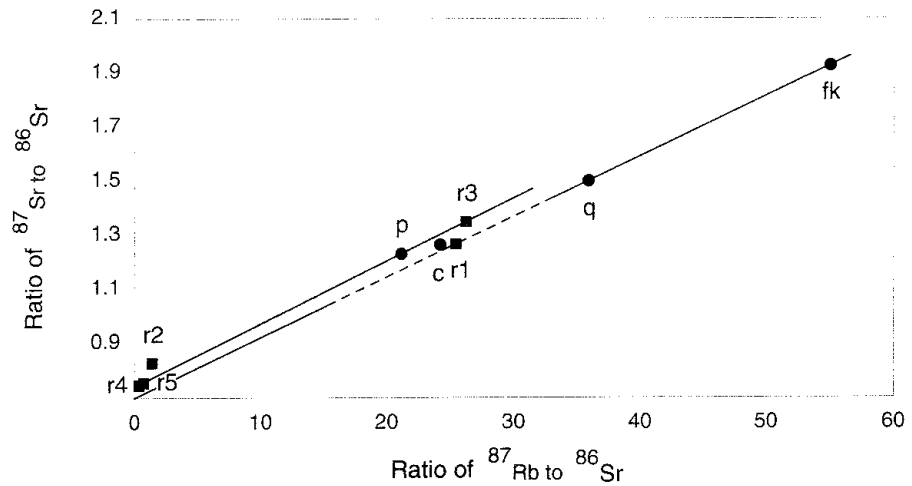
Relatively soft minerals, like calcite, may reflect the chemical characteristics of the latest fracture-healing fluids in terms of features like primary and secondary fluid inclusions. As discussed above, calcite was precipitated in at least three stages, with the last stage giving rise to many fluid inclusions, often very large, within the calcite crystals. Inclusions were unevenly

distributed and represented about 0.9% by volume of the calcite. Double-polished thin sections, 200 μm and 400 μm thick, were used in transparent and reflective microscopy to measure the volume of the inclusions. Single-phase and bi-phase aqueous fluid inclusions were measured by reducing the temperature of a piece of thin section to -90°C and recording the last melting point of ice during subsequent thawing of the inclusions. A temperature range between -25°C and $+5^{\circ}\text{C}$ was obtained, which indicated that the salinities of the inclusions ranged between 0% and 25% by weight of NaCl, with the majority of the results lying between 2% and 10%. Salinity tended to increase with increasing depth into the pluton. The fluid inclusions also contained an appreciable amount of CaCl_2 . Based on these data and the distribution of calcite precipitation with depth, it was hypothesized that the fractures at Stripa probably originated shortly after the emplacement of the pluton as a result of cooling and contraction of the intrusive body. The fracture filling was probably also deposited shortly after the emplacement, occurring as a result of mixing a hot deep-seated upward-moving brine solution with a cool calcite-saturated groundwater. Heating deposited calcite, and cooling deposited fluorite and quartz.

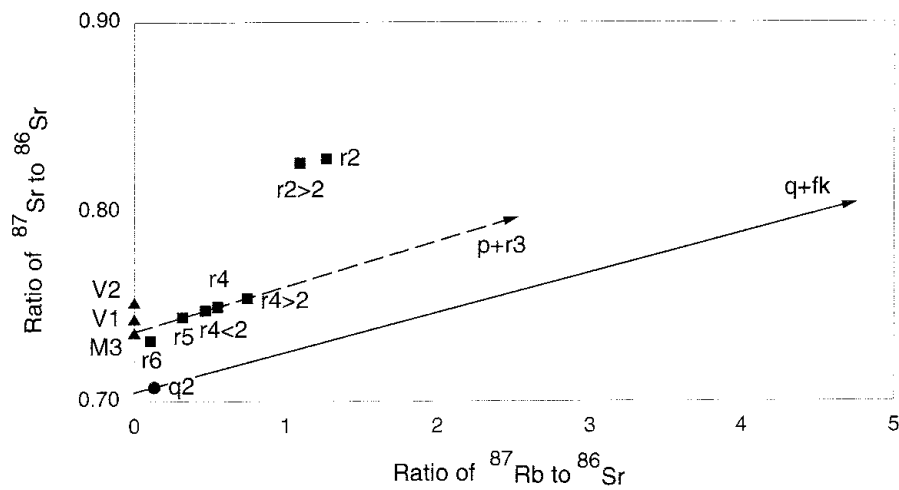
2.4.4 Origin of Salinity in the Stripa Groundwaters

The different characteristics in the chemical composition of the groundwaters of the Stripa area were based initially on considerations related to analytical data for the major trace elements, and were confirmed later by means of stable isotope geochemistry (Nordstrom et al, 1985; Fritz et al, 1987). These results indicated that the deep groundwater in the granitic body at Stripa has an abnormally high salinity, up to 700 mg/l of chloride, and a high pH which increases with depth up to values between 9 and 10 with an accompanying decrease in alkalinity. The saline water contains Na-Ca-Cl and SO_4 and differs significantly from the shallow groundwater which is generally of the Ca-Mg-Na- HCO_3 type. The Ca-Mg ratio of the deep water was exceptionally high for the relatively low temperatures of its environment, and the ratios of Br and I to Cl were much higher in the deep Stripa water than in sea water. The Rb-Sr isotopic method was applied to some minerals from the granitic body and from fracture coatings, to some solutions collected in the fractures and fissures of the main body, and to some fluid inclusions of the quartz grains separated from the granitic body. Concurrently, geochemical modelling, involving speciation calculations of the Si-Ca-Mg- HCO_3 - CO_2 values of the water with respect to some components of the rock, was undertaken to investigate the origin of the salinity in the waters. Because analytical results had excluded simple mixing of aqueous sources, such as sea water and groundwater, the origin of salinity was thought to be related to the granitic rock body itself. This meant that a long-term solution-rock interaction had occurred, wherein either leaching of fluid inclusions and/or a reaction with minerals in the fractures and fissures of the rock had occurred. This type of long-term interaction would give a specific signature to the water chemistry, specifically in regard to the Ca-Mg-pH- CO_2 system.

Plots of ratio of ^{87}Sr to ^{86}Sr as a function of the ratio of ^{87}Rb to ^{86}Sr for the granitic rock mass, the fracture coatings, and the groundwater at Stripa are shown in Figure 2-49. The scatter of the data for the granitic rock mass suggests a complex geologic history as the mineral separates do not fit on an



(a) Granitic rock mass and fracture coatings



(b) Groundwater and fracture coatings

Figure 2-49 Rb-Sr isochron diagrams for the granitic rock mass, fracture coatings, and groundwater at Stripa (Davis and Nordstrom, 1992).

M3, V1, and V2 designate boreholes. r1..., r6 are borehole depths ranging from 43 to 502 m below the 360 m level of the Stripa mine. The granitic and fracture-coating components are denoted by p: plagioclase; c: biotite-chlorite mixture; r: whole rock; fk: k-feldspar; m: muscovite.

isochron with their entire rock. The plagioclase fraction, together with its whole rock as denoted by r3, gives the highest apparent age at about 1.63 Ga with an initial $^{87}\text{Sr}-^{86}\text{Sr}$ ratio of about 0.748 Ga (1 Ga equals 10^9 years). This value is too high to represent the time of rock formation, as such values are indeed rare for Precambrian plutonic rocks which exhibit $^{87}\text{Sr}-^{86}\text{Sr}$ ratios of about 0.705. With this latter ratio, a reasonable minimum age for the granitic rock at Stripa can be assumed to be about 1.71 Ga. This estimate is close to an age determination of 1.69 Ga established on the basis of K-Ar by Wollenberg et al (1982). The Rb-Sr apparent age for the microcline and the rock mass is significantly lower at 1.39 Ga and, by combining the muscovite with the rock mass, is even lower at 0.80 Ga. These data suggest a period of very late crystallization. The fracture

coatings contain mineral paragenesis similar to that of the granite body, with quartz, microcline, plagioclase, and chlorite that is sometimes present in large amounts. The Rb-Sr data for these coatings plot on the line drawn through the granitic whole rock and its plagioclase fraction. This relationship suggests that these coatings could have formed at the same time as the plagioclases, perhaps during early hydrothermal activities in the granitic body and perhaps coincident to fracturing during cooling of the pluton. The "metabasaltic rock" has the lowest value for all of the samples from the rock mass, which confirms its mafic origin.

Samples of water from deep sections in boreholes V1 and V2 were found to be strongly depleted in Rb and Sr when compared to sea water, but their $^{87}\text{Sr}/^{86}\text{Sr}$ ratios were significantly more radiogenic. The very low $^{87}\text{Rb}/^{86}\text{Sr}$ ratio excludes the possibility of an evaporitic concentration of marine origin, by either an *in situ* enrichment of radiogenic ^{87}Sr from decay of ^{87}Rb , or by leaching of alkali-rich salts. Neither the ^{87}Rb and ^{87}Sr contents nor the $^{87}\text{Sr}/^{86}\text{Sr}$ ratio can be explained on the basis of simple dilution of sea water by groundwater. However, the ratios are very close to those of the fracture coatings, especially for the chlorite-rich small size fraction separated from the r4 sample. These coatings were assumed to have been developed closely after intrusion of the granitic body.

Even though quartz is stable in the solutions presently existing in the pluton, it was hypothesized that leaching of fluid inclusions could have occurred in the microfractures of the quartz grains. After intensive crushing of rock samples, the rock powder was leached with dilute HCl(1N) to recover the fluids from the inclusions. The ratios of $^{87}\text{Sr}/^{86}\text{Sr}$ and $^{87}\text{Rb}/^{86}\text{Sr}$ represent the low end-member of the mixture line drawn through the microcline, the quartz-microcline mixture, and the quartz fluid inclusions, as shown in Figure 2-49(a). The $^{87}\text{Sr}/^{86}\text{Sr}$ ratio for the fluid inclusions in the quartz from the granitic rock mass is probably representative of the hydrothermal environment that occurred after emplacement of the pluton. Using this ratio for the age calculations of the minerals in the rock mass, the ages of the plagioclase and the microcline would be 1.71 Ga and 1.53 Ga, respectively.

A proportion of salinity in the Stripa groundwaters is due to the Ca content. A pH of 9.27 measured in a sample of groundwater is high enough to induce chemical speciation with a very high $[\text{Ca}^{2+}]/[\text{H}^+]^2$ activity ratio. This condition favors saturation with respect to calcite even when the alkalinity is very low as was the case at Stripa, and also induces a very low equilibrium value for $f\text{CO}_2$ as shown in Figure 2-50 where the results for different waters from the Stripa mine are plotted. The high values of pH and Ca are consistent with low carbon dioxide values at saturation with respect to calcite. The high ratio of Ca to alkalinity allows this saturation to occur without the presence of abundant calcite in the fracture. The very low calculated values of carbon dioxide indicate that sampling and pH measurements were not significantly disturbed by the atmosphere, and that such values are consistent with a long-term reaction for a water-rock system close to the atmosphere without sources of inorganic carbon. The Mg concentrations, however, are too low to be involved in a carbonate phase, and the solutions are significantly under saturated with respect to magnetite and dolomite. The pH values are high enough to produce relatively large $[\text{Mg}^{2+}]/[\text{H}^+]^2$ activity ratios. The Stripa groundwaters with the highest pH values correspond to the saturation state for the Mg-chlorite or clinocllore.

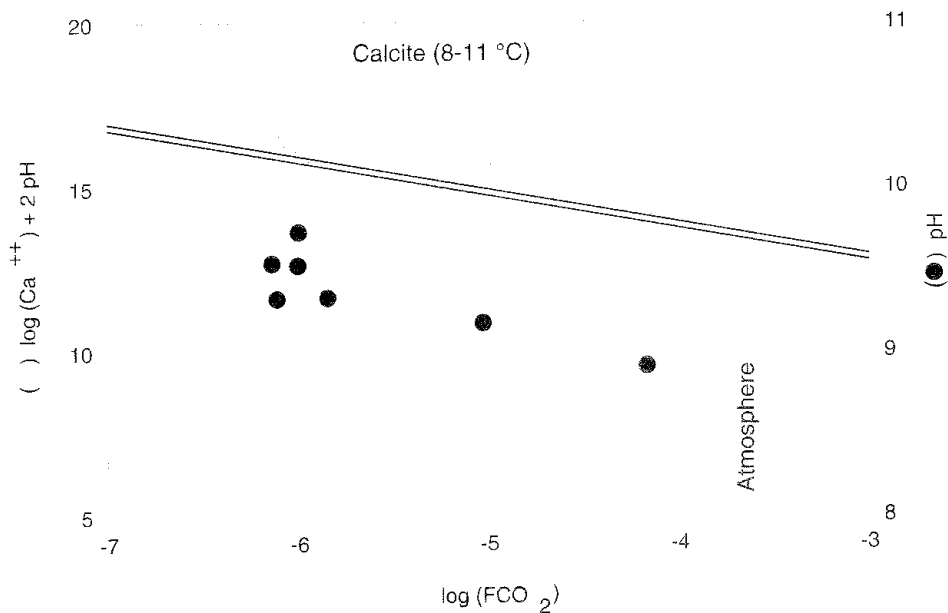


Figure 2-50 Saturation state of solution with respect to calcite and pH in a $[Ca^{++}]-[H^+]-SCO_2$ activity diagram at mine temperatures of 8 to 11 °C (Davis and Nordstrom, 1992).

The low Mg content could be related to a low temperature chlorite control of the chemistry of the solution, which is typical in hydrothermal waters with a higher silica content but lower pH values. This argument favors a relationship between the chemistry of the groundwaters and the mineral components of the fractures in the granitic rock mass at Stripa.

The Rb-Sr geochemical and geochronological study of the rocks, minerals, and groundwaters from the Stripa granite, together with thermodynamic considerations of alkalinity with Ca and Mg controls in the waters, suggests the following scenario for the origin of water salinity. The magmatic intrusion of the pluton at Stripa occurred at least 1.71 Ga ago. Fracture coatings were produced by a later hydrothermal activity which may have occurred 1.63 Ga ago and which may be related to post-emplacement cooling. These coatings are characterized by mineral paragenesis similar to that of the rock matrix. This similarity suggests that the mineral coatings of the deep fractures were due to high temperatures, while some of the coatings in the shallower zones underwent more complicated processes. Probably less than one million years ago, dilute waters entered the granitic body, predominantly along previously formed fractures. These groundwaters interacted strongly with fracture minerals, such as chlorite, as reflected by $^{87}Rb-^{86}Sr$ and $^{87}Sr-^{86}Sr$ ratios. This hypothesis suggests that the origin of salinity in the Stripa groundwaters is a consequence of a long-term rock-water interaction.

2.4.5 Isotope Geochemistry

Concentrations of the stable isotopes, deuterium (2H), and oxygen-18 (^{18}O), in groundwater are largely determined by their original concentrations in the

recharge water together with contributions by evapotranspiration and mixing which may take place in the surface soil horizon. Both deuterium and oxygen-18 display conservative geochemical behavior unless affected by isotopic exchange, which normally is important for deuterium at high subsurface temperatures and may also possibly be of importance after long contact times with various minerals. The data for these two isotopes appear to demonstrate conclusively that the bulk of the groundwater at Stripa originated as local precipitation. The isotopic data are very close to the global meteoric base, and, in fact, the isotopic composition of the groundwater is almost the same as present-day precipitation. The data from Stripa for deuterium and oxygen-18 indicate that these stable isotopes occur in lower concentrations at depth, which is thought to be a consequence of the depletion of heavier isotopes due to colder climatic conditions in the past (Moser et al, 1989; Nordstrom et al, 1985). The Pleistocene records suggest that climates colder than present day conditions prevailed many times during the past two million years. The last time, during which temperatures were low enough to account for the isotopic composition of the deep groundwater at Stripa, was about ten thousand years ago. This argument allows a lower limit of ten thousand years to be given to the age of these waters.

Tritium (^3H), which has a half-life of 12.4 years, is commonly used to distinguish between younger water recharged after 1952 and older water recharged before 1952, and to date groundwater to about 70 years old. The first large-scale testing of thermonuclear devices took place in 1952. By assuming a pre-1952 concentration of tritium of 6 TU, together with a measured concentration of 0.3 TU of water samples from borehole V2, a subsurface residence time of about 50 years can be calculated. In contrast, groundwater from shallow sources had levels far above the historical background, indicating that a large fraction of this water must be post-1952.

Removal of calcite has no measurable effect on the ^{14}C activities of the dissolved inorganic carbon. Similarly, there exists no evidence that diffusive loss of radiocarbon into micropore water in the granite or isotope exchange with calcites in the fractures contributed in a significant way. Thus, the indications are that the total inorganic carbon (TIC) of the waters entering the shallow boreholes at the 300 m level of the mine and the top of borehole V2 have a mean residence time in excess of 20,000 years.

The geochemical history of the deeper groundwater is substantially more complex, as is the interpretation of the radiocarbon data. Organic carbon has been added to some of the more saline waters at depths between 850 m and 950 m below the ground surface, possibly as a consequence of active bacterial processes. The ^{14}C concentrations of TIC in the deep groundwaters appear to be somewhat higher than the values measured at the 300 m to 400 m levels of the mine, but low enough to assume that the deep water samples contain at least a potentially old component of groundwater.

Age dating of pre-calcite samples from fractures in the rock was undertaken by means of uranium/thorium isotopes (Milton, 1987). The ^{13}C and ^{18}O analyses indicated that the carbonate was well within the range of potentially modern precipitates and corresponded to a "mean age of deposition" of about 95,000 years. The other two samples yielded ages of about $210,000 \pm$

60,000 years and greater than 35,000 years, with the latter value most probably belonging to the hydrothermal/magmatic group.

Analyses of the fractions of dissolved organic carbon in the groundwaters at Stripa demonstrated that the hydrophobic and hydrophilic acid fractions, generally the largest fractions in natural waters, were less than 0.3 mg/ℓ. However, organic bleed from the nylon tubing used in the boreholes was a significant contaminant in the hydrophobic neutral and acid fractions. The major anthropogenic contaminant in the sampling at Stripa was N-butyl benzenesulphonamide, a plasticizer used in the manufacture of nylon polymers. The ¹³C isotopes in the inorganic carbon fractions were similar in value to those for the stable carbon isotopes for the organic carbon fractions, supporting the inference of a biogenic origin of the dissolved inorganic carbon.

Groundwater samples obtained from the suite of boreholes at the SGAB site, along with leachate from crushed rock samples from those boreholes, were analyzed for their contents of Cl isotopes. When the ³⁷Cl-³⁵Cl ratios for the rock leachates were compared to the same ratios for the groundwater, it appeared that the water in the fluid inclusions and other micropores was not everywhere in equilibrium with the freely circulating groundwater.

2.4.6 Aqueous Sulphates

As discussed in the previous sections, the salinity of the groundwater at Stripa was quite variable and increased with depth. Changes in dissolved constituents were obvious for chlorite. However, other ions increased with the amount of total dissolved solids and were controlled by geochemical processes evident in the distribution of Ca²⁺, HCO₃⁻, and pH. As a consequence, the shallow waters were of the Ca-HCO₃ type and remained diluted, whereas the deep groundwaters were of the Na-Cl-Ca-SO₄ type. The sulphur geochemistry in the groundwater system at Stripa was of special interest because of large variations in sulphate content that occurred in groundwaters from different boreholes. There was a rather systematic increase of sulphate concentrations with chlorite, from less than 1 mg/ℓ to more than 100 mg/ℓ. Both reduced and oxidized forms of aqueous sulphur coexisted locally. The isotope contents of aqueous sulphur compounds can be used as indicators of the origin of dissolved sulphate and as an index of biogeochemical redox processes.

The sulphate data for the groundwaters for the Stripa area are shown graphically in Figure 2-51. It was demonstrated that, on the basis of principal component analysis of major dissolved constituents and depth, the water samples could be separated into three distinct groups. These included shallow groundwater, groundwater from depths of 300 m to 440 m, and groundwater from depths greater than 500 m. Representative points of aqueous SO₄²⁻ from shallow groundwater lie along the straight line in the lower part of the figure which includes the results of analyses of surface water and precipitation. This is considered to be a mixing line. The end number with the heaviest isotopes would be meteoric sulphate. Such values have been observed in other countries and have been attributed to a mixture of sea spray and sulphates from the oxidation of sulphur in fossil fuels.

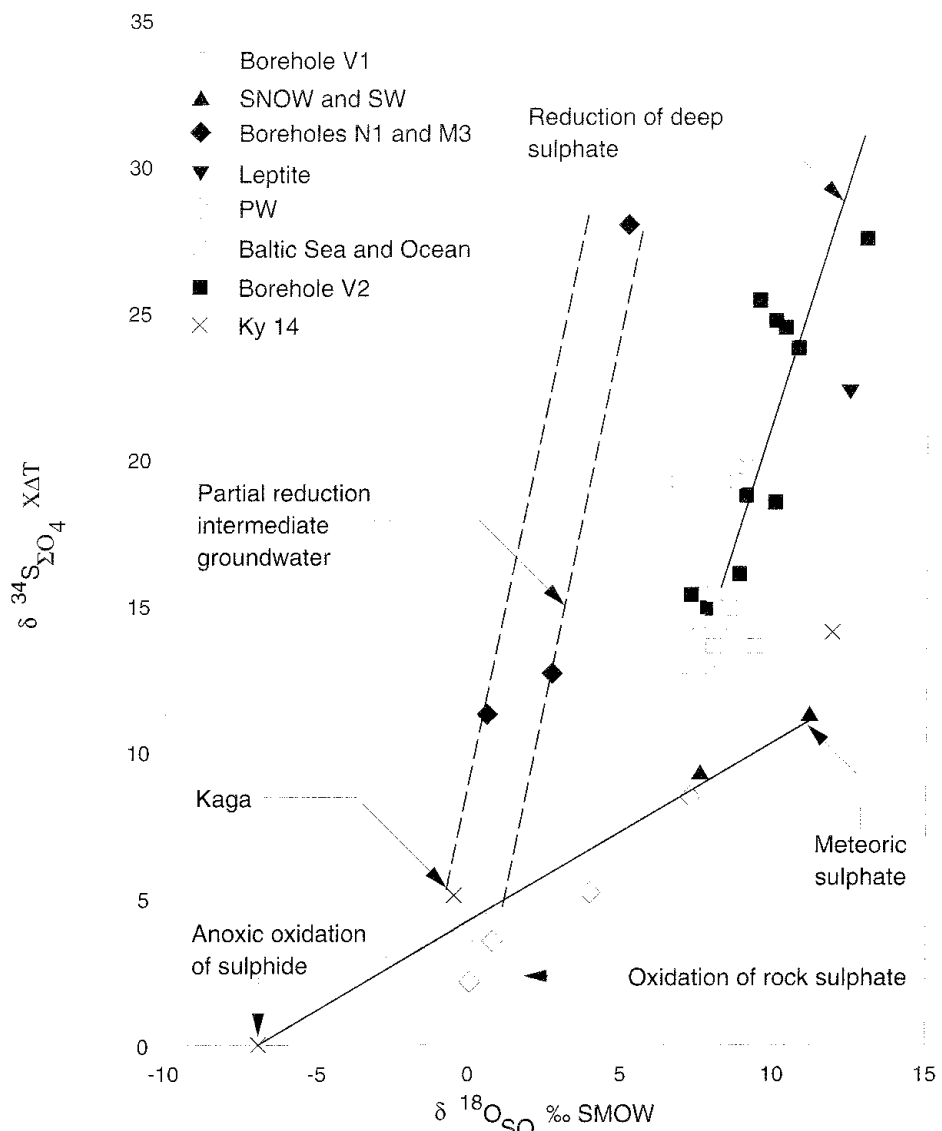


Figure 2-51 Relationship between ^{18}O and ^{34}S in the sulphate ion within various liquid and solid components of the Stripa area (Davis and Nordstrom, 1992).

Groundwater from borehole M3 and especially from borehole N1 at a depth of 340 m were depleted in sulphate. The H_2S odor of this intermediate water indicated ongoing sulphate reduction. The results for these water samples fall on the dashed trend line in Figure 2-51 with a slope that reflects the effects of bacterial reduction (Fontes et al, 1989). The low sulphate contents of these waters were attributed to the remaining fractions of partly reduced sulphate. The distribution of data points suggest that SO_4^{2-} of shallow origin was the common source of sulphate for waters in these two boreholes.

An evolutionary connection of sulphate from the shallow and intermediate zones to the deeper groundwaters could not be established on the basis of the isotopic content of sulphate from samples of water obtained from boreholes V1 and V2. The sulphates from borehole V2 appear to be a remaining

fraction of a limited sulphur reservoir after various degrees of bacterial reduction. By contrast, isotopic values for samples from borehole V1 are quite homogeneous. The water from borehole V1 had a variable sulphate content independent of isotopic ratios, which was thought to be a consequence of dilution by water of unknown origin with a low content of SO_4^{2-} .

Based on the data discussed above, the sulphate in the groundwater in the Stripa granite clearly reflected contributions from multiple sources. In the shallow groundwater, atmospheric fallout and the oxidation of reduced species of sulphur provided most of the sulphate. The chemistry of the deep groundwater indicated mixing of at least two different waters and/or sources of dissolved salts. One end member of this mixing was local fresh water of undefined age. The other end member could be a brine with an original sulphate composition similar to that of the groundwater from borehole V1. The origin of the brine was not known, except that any relation to recent or late Pleistocene sea water could be ruled out.

2.4.7 Radionuclide Concentrations

The uranium content of the Stripa granite is about an order of magnitude greater than the world average for granites. Over time, the uranium was easily accessible to the groundwater and could be readily leached from the rock matrix. Concentrations in the groundwaters ranged from 10 ppb to 90 ppb at depths of 80 m or less and in the mine waters from above the hydraulic sink produced by the deepest mining level at 410 m. The activity ratios for ^{234}U - ^{238}U for these groundwaters are characteristic of chemical leaching processes at the shallower depths. In addition, at a depth of about 350 m, the groundwaters also contain dissolved ^{234}U produced by alpha-recoil processes. At greater depths, the uranium concentrations were indicative of the changed redox conditions and were subject to activity ratio enhancement by the alpha-recoil processes. Residence times for the uranium dissolved in the deeper groundwaters, based on alpha-recoil aided ingrowth of ^{234}U , are less than 20,000 years, and less than 1,000 years for groundwaters present in some discrete fracture zones.

For more than three decades, natural radionuclides have been used to estimate the average subsurface residence time of groundwater. It is commonly assumed that the production of most of these radionuclides is a consequence of interactions of primary and secondary cosmic radiation with various elements in the atmosphere of the earth. Much of the subsurface production of radionuclides comes from the capture of neutrons which in turn will be due largely to (α, n) reactions and, to a lesser extent, directly from the spontaneous fission of ^{238}U . Because a large portion of the α particles in nature result from the decay of U and Th and their daughters, subsurface production is very sensitive to the total amount of these elements present within the host rock.

The natural neutron flux in the Stripa granite comes from (α, n) reactions on the light elements in the granite and, to a lesser extent, from spontaneous fission of ^{238}U . The neutron flux was sufficient to account for the *in situ* production of enough ^{36}Cl , ^{37}Ar , and ^{39}Ar to overwhelm the cosmogenic component in the groundwater. It was thought that most of the ^{85}Kr and ^{129}I

in the deep subsurface was probably derived directly from the natural spontaneous fission of ^{238}U . Measurable amounts of ^3H and ^{14}C in the groundwater could also be attributed to *in situ* production, but, because the quantities were so small, they could not be clearly identified against the larger cosmogenic contributions of these radionuclides to the groundwater.

2.4.8 Summary of the Geochemical Characteristics of Stripa

The study of the Rb-Sr chronology, as well as the ^{87}Sr - ^{86}Sr ratios of the rocks, minerals, and groundwaters at Stripa, indicates that the granitic pluton was intruded into the area 1.71 Ga ago and that later hydrothermal activity, about 1.63 Ga ago, produced moderately high-temperature minerals along the fractures. The low ^{87}Rb - ^{86}Sr ratios suggest that dilute water entered the granite along fractures probably less than one million years ago, and that the chemistry of the groundwater was strongly influenced by interactions between the rock and water. Comparison of the groundwater and rock compositions precludes a sea water origin of the dissolved matter, and suggests that the total saline content may not be due entirely to contributions from the fluid inclusions in the granite, at least for those constituents which were studied. Furthermore, sulphur isotopes, stable isotopes of chlorine and strontium, additional measurements of deuterium and oxygen-18, and, to some extent, studies of iodine-129 all support the conclusion that the salinity in the deeper groundwater at Stripa cannot be attributed to the direct influence of recent or late Pleistocene sea water. The origin of virtually all of the groundwater recovered from the granite during the course of the geochemical investigations was local precipitation as indicated by the concentrations of deuterium and oxygen-18 in the water. The concentrations of these elements in the deeper water was comparatively less, which suggests an origin of the water during the Pleistocene. There was no geochemical evidence that indicated the water underwent partial evaporation or geothermal alteration.

High temperature minerals dominate fracture fillings at depth, while calcite is more common near the surface. The stable carbon isotopic composition of shallow groundwater indicates that the geochemical evolution of groundwater to a depth of at least 100 m was strongly influenced by the dissolution of calcite within fractures. Below 100 m, the groundwater becomes saturated with respect to calcite, and the dissolution of silicate minerals becomes more important. Isotopic compositions of chlorine and iodine of the water in the granite do not match the isotopic compositions of the rock. This suggests a lack of equilibrium between the rock and the water, and indicates that perhaps some of the groundwater has moved laterally into the granite within the last few thousand years or less, perhaps even since subsurface mining began at Stripa.

The natural organic compounds that are dissolved in the groundwater at Stripa indicate the presence of long-chain fatty acids, including fulvic acids, and low-molecular-weight cyclic hydrocarbons. Most of the organic carbon was found to be N-butyl benzenesulphonamide which was probably leached from the nylon tubing in the water sampling system. The $\delta^{13}\text{C}$ values of the dissolved organic carbon were isotopically light and similar to those of the inorganic carbon which suggests a biogenic origin.

Significant *in situ* production of ^{36}Cl , ^{37}Ar , ^{39}Ar , ^{85}Kr , and ^{129}I occurs in the Stripa granite at rates which exceed the atmospheric production of these radionuclides. Natural fission accounts for the *in situ* production of ^{85}Kr and ^{129}I , with the production of the remaining radionuclides due to the capture of thermal neutrons. *In situ* production of ^3H and ^{14}C , if present at Stripa, is below the production level from cosmogenic sources.

The ^{14}C concentrations in dissolved organic carbon, as well as in inorganic carbon, suggests an isolation time for the deep groundwater of at least several thousand years. Even though lateral migration has taken place, most of this water has been isolated from the atmosphere for this length of time and possibly as long as a few hundred thousand years. Small amounts of ^3H in samples of groundwater from the deep boreholes suggest that surface or near-surface water has circulated at depth in the vicinity of the mine and has mixed with the deeper groundwater. However, some of this ^3H may be due to *in situ* production or to the mine ventilation system.

2.4.9 Significant Achievements

The significant achievements of the program of geochemical investigations at Stripa can be separated into three categories. The first was the development of new or rarely used field and laboratory techniques. The second category deals with new scientific insights, and the last, concerns the potential application of the results of the investigations to the characterization of potential sites for geologic repositories.

A large number of the geochemical measurements at Stripa was extremely difficult because of the low concentrations that existed in the rock and the water, the slight differences among samples from the various locations, and the fact that the constituent had never, or rarely, been measured before. Special field sampling methods were devised for the separation of dissolved gases and for the capture of trace organic fractions. Particular efforts were made to determine the composition of natural fluids in micropores within the Stripa granite by both leaching studies and direct observations of fluid inclusions. In addition to precision measurements of bromide, some of the earliest measurements of the natural nuclide ratios ^{37}Cl - ^{35}Cl , ^{36}Cl -total Cl, and ^{129}I -total I were made on both rock leachate and free-flowing groundwater. Natural levels of ^{37}Ar in the groundwater were measured for the first time. This was also the case when carbon from trace-organic fractions was separated and analyzed for ^{14}C .

A key scientific question that was addressed in the early studies at Stripa was related to the origin of dissolved solids in the groundwater from depths in excess of a few hundred metres. Consideration of the stable nuclide composition of the water, as well as the bromide-chloride ratios and concentrations of the elements in solution, eliminated the possibility of an unmodified sea water source. Although the bulk of the water probably originated as precipitation or melt water from ice, the dissolved solids in the water probably reflect a complicated history involving rock-water interaction, diffusion of ions from micropores in the larger fractures, and slow lateral movement of water carrying dissolved solids into the Stripa granite from some outside source. Consideration of dissolved solids, as well

as the ^3H content of the groundwater, demonstrated the importance of fracture flow in determining water chemistry.

For the first time, it was clearly demonstrated that a number of radionuclides, including ^{36}Cl , ^{37}Ar , ^{39}Ar , ^{85}Kr , and ^{129}I , are actually generated within a granitic rock mass in quantities which overwhelm the real cosmogenic components. These elements, along with ^3H and ^{14}C , could be the most reliable indicators of water age and, coincidentally, rates and directions of regional groundwater flow, provided that the carbonate geochemistry is well understood and the subsurface production of these elements can be quantified. The dating of groundwater is essentially a determination of the time that the water has been isolated from surface water and atmospheric portions of the hydrologic cycle. Except for ^3H dating, all dating determines the average age of the dissolved matter in the water. The age of the water itself is only determined by trying to relate the history of the dissolved matter to the complex history of the water. For the first time, a large number of techniques were used in a single study. These techniques involved isotopic disequilibrium, buildup of radiogenic gases, decay of cosmogenic radionuclides, buildup of *in situ* produced radionuclides, and matching changes in concentrations of stable nuclides with known climatic functions. Because of the natural complexity of the fracture flow system and the influence on the system by past mining operations, the results were judged to be only partially successful.

At the end of Phase 2, a subgroup of the HAG prepared a report that outlined a program for the hydrogeochemical evaluation of a crystalline rock site for geologic disposal (Andrews et al, 1988). The contents of the report were based upon experiences gained from the investigations in the Stripa area. It was the contention of the subgroup that the main purpose of geochemical characterization of a site is to identify different groundwater types and relate them to the groundwater flow patterns. In this context, the differences in the groundwater types should be evaluated within the framework of mean residence times and their relationships to various lithologies, possible mixing of groundwaters within the site, and the dominant reactions which control the chemical and isotopic compositions.

2.5 SOLUTE TRANSPORT EXPERIMENTS

Apart from human intrusion and severe tectonic activity which are commonly unexpected at a geologic repository site, the expected means for the radionuclides to migrate from the waste containers to the accessible environment is by groundwater flow in the fractures within the rock mass and by molecular diffusion. Because the waste containers will be located many hundreds of metres below the ground surface, radionuclide migration by molecular diffusion is considered to be highly unlikely. In granitic rock masses, there commonly exists fractures through which most of the water movement occurs. The rock matrix is porous and may be accessed by diffusing species. However, groundwater flow of any significance through the matrix is considered to be highly unlikely because of its low hydraulic conductivity. Knowledge of the groundwater flow rates, velocities, and pathways within the rock mass are required to evaluate the potential for transport of the radionuclides. The nuclides dissolved in the water have the

ability to diffuse into the micropores of the rock matrix which are accessed by diffusion. The rate of diffusion into the micropores will be directly influenced by the area of the fracture surfaces which are in contact with the groundwater.

As observed during the hydraulic investigations within the Stripa mine, only a small fraction of the fractures in the rock act as conduits for the bulk of the groundwater flow. These conduits, or channels, may give rise to preferential pathways and may limit the amount of rock in contact with the water. Velocity variations within the channel networks may cause both longitudinal and transverse dispersion of the migrating radionuclides. Longitudinal dispersion allows some of the nuclides to arrive earlier at a point of interest than the main concentration. Both types of dispersion may result in dilution.

During Phase 1, attention was focussed on migration of tracers within single fractures that could be identified in the granitic walls of an existing drift (Abelin and Neretnieks, 1981; Abelin and Gidlund, 1985; Abelin et al, 1985). At the same time, experiments were carried out under the SKB programme to evaluate the diffusion of tracers in undisturbed rock in the Stripa mine (Birgersson and Neretnieks, 1982, 1983). During Phase 2, the emphasis shifted to the migration of tracers over long distances, up to about 50 m, in rock that was averagely fractured (Abelin and Birgersson, 1987; Andersson and Dverstorp, 1987; Neretnieks et al, 1990). During Phase 3, experiments were conducted to evaluate the transport properties of channels within single fracture planes (Abelin et al, 1990a,b,c). In addition, a tracer migration test was performed at the SCV site in a well characterized fracture zone (Birgersson and Ågren, 1992; Birgersson et al, 1992b,c). In summary, this series of field experiments studied tracer migration in a single fracture, in a fracture network, and in a fracture zone, together with diffusion into the granitic rock mass and the transport properties of channels within a fracture plane (Birgersson et al, 1992a).

2.5.1 Concepts of Fracture Transport

The transport of solutes by water flowing through a porous or fractured rock mass is influenced by a number of geochemical, geologic, and hydraulic factors. The factors include the concentration gradient, physical features of the flow path including the mineralogy, and the hydraulic head. Generally speaking, these factors are related to a variety of so-called transport mechanisms. The mechanisms are identified as advection, hydrodynamic dispersion, diffusion into the rock matrix and adjacent pools of stagnant water, channelling within single fractures, and sorption on the fracture surface and within the rock matrix for species which diffuse into the matrix. Commonly, only advection and dispersion are considered to be important in describing solute transport within a porous media. Chemical reactions between the solute and the minerals can be included in this approach without great difficulty. This approach can also be used to describe transport in channels and between parallel walls of fractures. However, the complexity of the mathematical descriptions increases considerably for a fractured rock mass when there exists significant variability in the fracture apertures and coatings and in the porosity and diffusivity of the rock matrix.

Dispersion

In a general sense, dispersion can be thought of as an increase in the residence time distribution of a solute within water. For example, a concentration of tracer injected into water flowing within a fracture or channel will spread because of local velocity variations across the channel and, to a lesser extent, because of molecular diffusion. In a fracture network, most of the spreading is due to the mixing of waters between different pores or channels which have different residence times. In channel networks, where the flow velocities differ much more between channels and where mixing may be minimal over distances of interest, the differences in residence times between channels are the dominant cause of dispersion. Mixing "pools" at fracture intersections tend to average out the concentration differences between channels.

The mathematical formulation for transport, assuming advection and Fickian dispersion, implies that the dispersivity is constant and independent of distance. It is expected that this is a reasonable assumption over large distances when the waters in different fractures are repeatedly mixed. However, in rock masses where the main conducting fractures are relatively distinct over long distances, and channels within the fractures have relatively few intersections, these assumptions may not be very appropriate. As shown in Figure 2-52, the dispersion length for fractured rock increases with migration distance. This increase can be caused by channelling within the fractures and diffusion into the rock matrix. At depths in a granitic rock mass where both the frequency and connectivity of fracture zones decreases, mixing of waters may not be adequate over even large distances to allow dispersivity to become constant and independent of distance.

Matrix Diffusion

Most rocks have microscopically small fissures between the crystals. In a saturated rock mass, in particular, these fissures represent a somewhat interconnected pore system containing water. Molecules, smaller than the

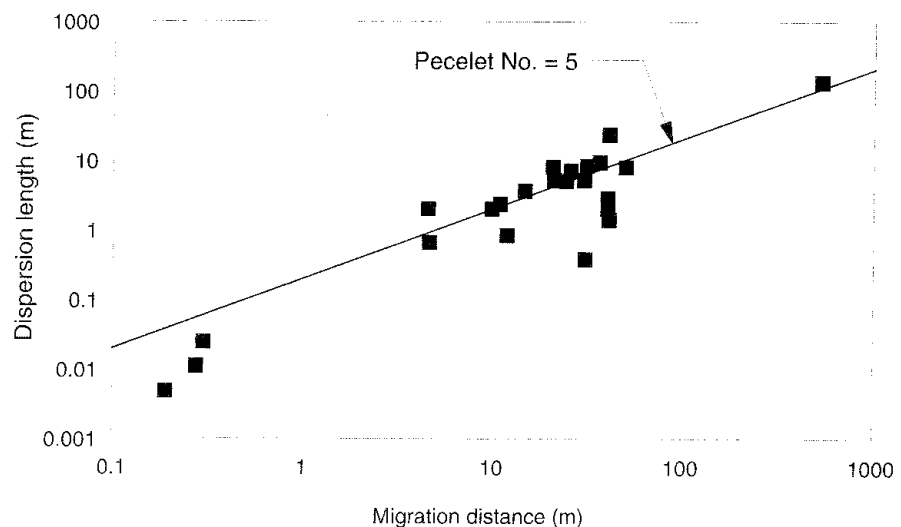


Figure 2-52 Tracer dispersion in fractured rock as a function of migration distance (Birgersson et al, 1992a; Neretnieks, 1985).

microfissures, can diffuse in and out of this pore system. The aggregate surface area of these microfissures may be orders of magnitude greater than that of the fractures containing the flowing water. Gneisses and granites in the Precambrian rock of Sweden have been found to have a continuous pore system, consisting of the microfissures between the crystals in the rock matrix and representing a porosity between 0.06% and 1% for the rock matrix (Skagius and Neretnieks, 1986a,b). Solutes within the flowing water in the fractures can diffuse into this pore system and sorb on the pore walls, as shown conceptually in Figure 2-53. The penetration depth decreases with time because of the retardation of sorbing species of solute in the water.

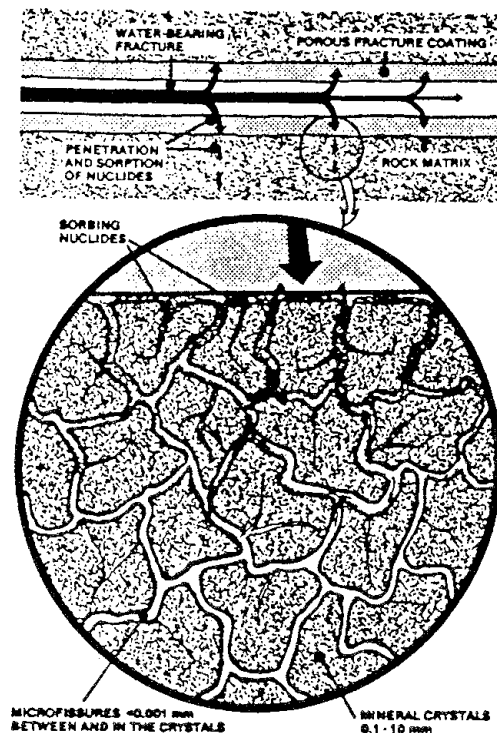


Figure 2-53 Conceptualization of the penetration and sorption of solutes in the microfissures of the rock matrix (Birgersson et al, 1992b).

Sorption

The minerals of crystalline rocks have considerable capacity for cation exchange and for forming surface complexes with anions as well as cations. The capacity to bind different ions to the surface depends on the pH, the concentration of many of the other ions, and the form of the species in solution. The solute component may be bound, i.e. adsorbed or ion exchanged, to the surface of the minerals, or it may form minerals by precipitation. Adsorption and ion exchange are commonly referred to collectively as sorption, denoting "fast" reversible reactions of the dissolved components with the surface of the rocks.

2.5.2 Diffusion in the Granitic Rock Matrix

During the early part of Phase 1, a series of laboratory and field experiments were undertaken within the SKB programme to evaluate nuclide

diffusion within the connected pore system in the matrix of granitic rock. As mentioned above, granites in Sweden have been found to have a continuous pore system consisting of microfissures between the crystals, with a porosity that varies between 0.06% and 1%.

Experimental Configuration

Three sets of *in situ* experiments were performed in the Stripa mine. In the first experiment, as shown in Figure 2-54(a), a 146 mm diameter borehole was drilled to a depth of 18 m in the floor of a drift in the Stripa mine. Subsequently, a 20 mm diameter borehole was drilled 3.5 m from the bottom of the larger borehole. A hydraulic packer was placed approximately 100 mm above the bottom of the 146 mm diameter borehole and tracer solutions were continuously injected for about three months at pressures ranging from 0.5 MPa to 0.9 MPa above the natural water pressure. This injection caused both advection and diffusion of the tracers into the rock matrix. After termination of the injection and retrieval of the packer, the small diameter borehole was over cored to a diameter of 132 mm. The 3.5 m length of core was cut into samples of 50 mm length. Subsequently, 10 mm diameter cores were obtained from the samples at different distances from the small injection hole. These cores were leached in distilled water, and the tracer concentration in the distilled water was

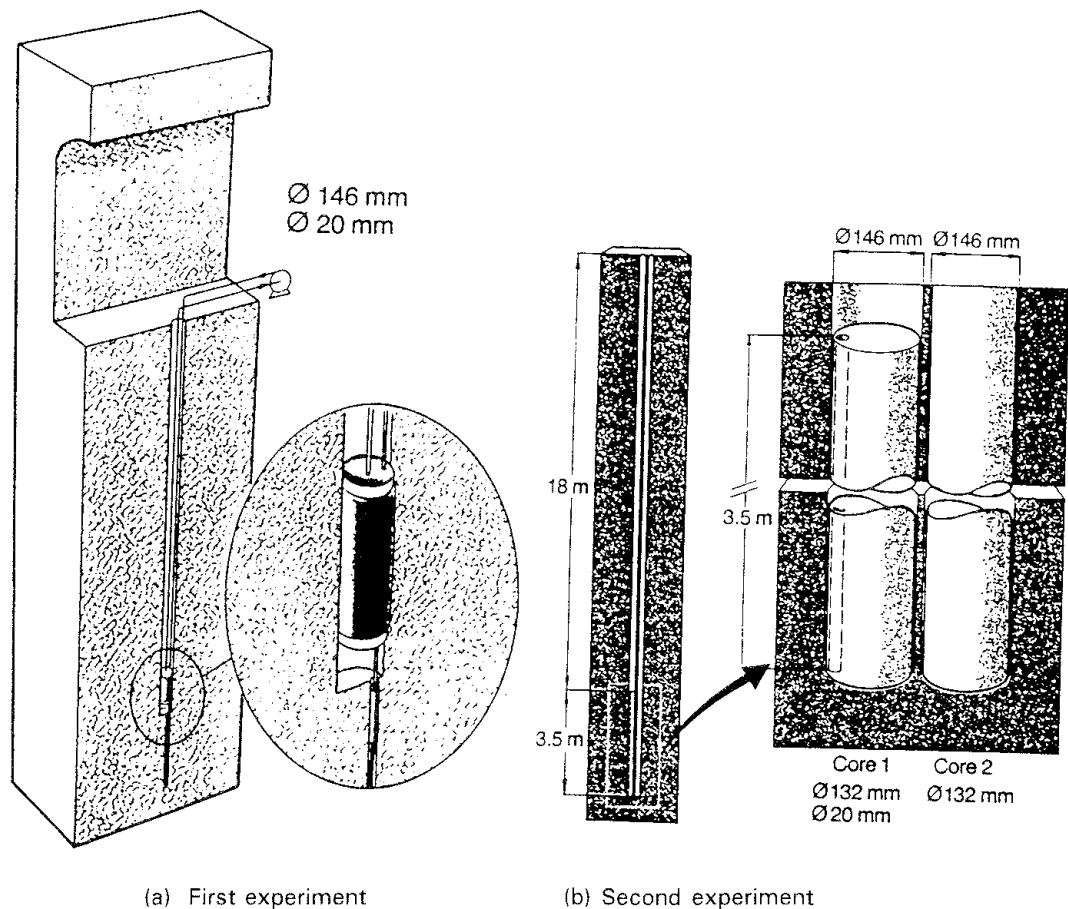


Figure 2-54 Arrangement of boreholes for the *in situ* diffusion experiments in the Stripa mine (Birgersson et al, 1992a).

determined and recalculated for the concentration in the pore water. The porosity of the small core samples was determined on the basis of the weight difference between wet and dry core.

In the second experiment, as shown in Figure 2-54(b), the injection borehole configuration was the same as that in the first experiment. However, a second 146 mm borehole was drilled next to the injection borehole. After the injection of tracers for six months, the bottoms of both boreholes were over cored to a diameter of 132 mm, and the tracer concentrations were determined in the rock matrix by the procedure described above. Thus, a tracer concentration profile was determined over a horizontal distance of about 250 mm from the injection hole.

In the third experiment, the configuration of the injection borehole was the same as in the first two experiments. However, in this instance, two 146 mm diameter boreholes were drilled next to the injection borehole, along with three 76 mm diameter boreholes located at 90° increments and at a distance of about 150 mm from the injection borehole. This experimental arrangement allowed the tracer concentration profile to be determined over a distance of about 400 mm away from the injection hole.

Mixtures of Uranin, Cr-EDTA, and I⁻ were used as tracers in all three experiments. These tracers had been tested in the laboratory and found to be stable with time and non-sorbing.

Experimental Results

The concentration profile in the rock matrix for Uranin from the third experiment is shown in Figure 2-55. The tracer concentrations were found to vary considerably with depth along the core as well as with the radial direction outward from the injection hole. The penetration depth could in

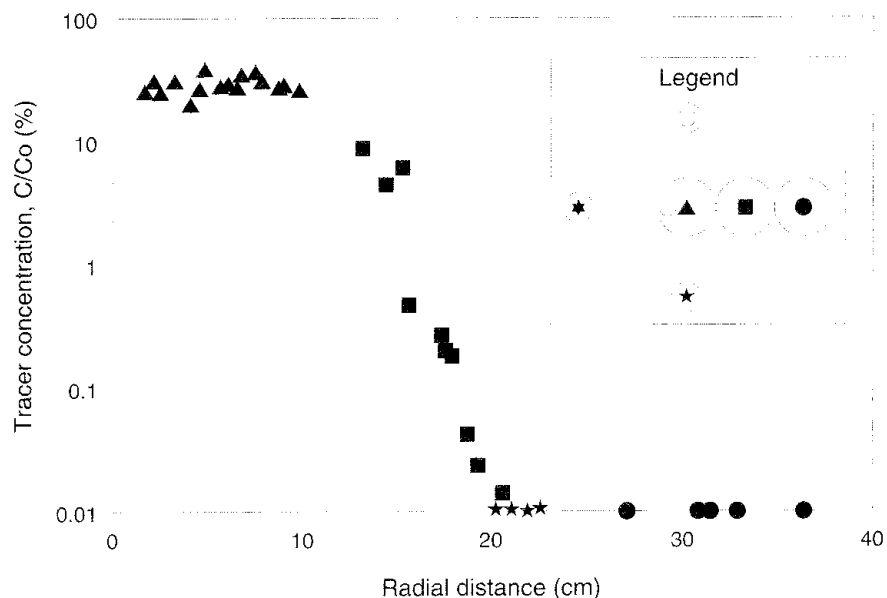


Figure 2-55 Concentration profile for Uranin in the granitic rock matrix at a depth of 1.775 m at the site of the *in situ* diffusion experiment at Stripa (Birgersson et al, 1992a).

some instances vary by a factor of two or more between sampling points separated by just a few tens of centimeters in depth, or located at the same depth but in different directions from the injection hole. The Uranin penetrated to a depth of about 200 mm into the rock matrix at a depth of 1.775 m. Data obtained at other depths indicated a penetration distance of almost 400 mm.

As mentioned previously, the porosity of every core sample was measured by comparing the weight difference between wet and dry core. These measurements did not yield any significant differences in porosities among samples. The porosity was found to vary between 0.12% and 0.51% with an average of about 0.3%. A correlation between porosity and migration distance could not be established.

The diffusivities and hydraulic conductivities of the core samples from the experimental sites were determined in the laboratory. The hydraulic conductivity was evaluated with the rock samples subjected to confining pressures of 15 to 30 MPa, corresponding to the state of stress in the rock at the experimental sites. As shown in Figure 2-56, the agreement between the laboratory and field data for both diffusivity and hydraulic conductivity was reasonably good. The *in situ* diffusivities range between about 10^{-12} m²/s to 10^{-10} m²/s, as compared to values of about 10^{-11} m²/s obtained in the laboratory. Similarly, as shown in Figure 2-56(b), the values of hydraulic conductivity from the field and laboratory were of the same order of magnitude at similar locations.

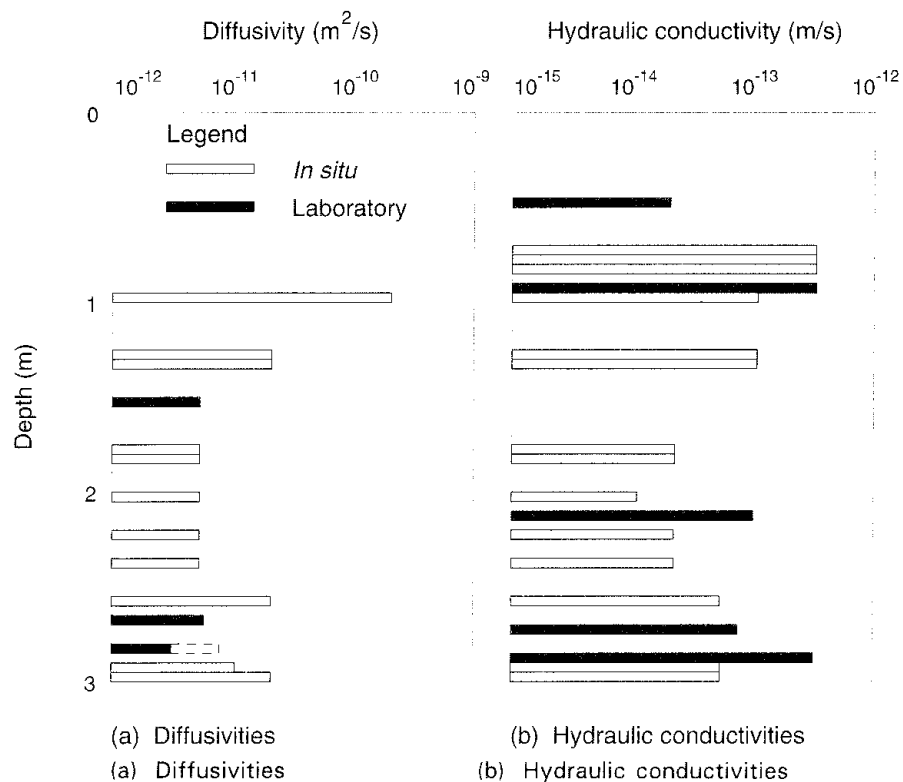


Figure 2-56 Diffusivity and hydraulic conductivity as a function of depth at the site for the *in situ* diffusion experiments at Stripa (Birgersson et al, 1992a).

The solid bars represent laboratory data and the open bars represent *in situ* data.

General Remarks

The diffusivities and hydraulic conductivities obtained from the *in situ* tracer experiments in the Stripa granite compared reasonably well with those obtained from the laboratory tests. However, the changes in the migration properties at different locations and in different directions at the test site could not be explained on the basis of the porosity and pore-size distribution data, or the direction of the microfissures, as obtained from the core samples. The tracers did migrate through the rock matrix, with, in some cases, no obvious decrease in concentration over a distance of some 400 mm.

2.5.3 Migration in a Single Fracture in Granite

During Phase 1, a tracer migration experiment was conducted in a single fracture in granite in the Stripa mine (Abelin et al, 1985; Birgersson et al, 1992a). Laboratory experiments had shown that migrating radionuclides would diffuse into the granitic rock matrix adjacent to a fracture and subsequently sorb on the walls of the micro fissures within the matrix (Allard et al, 1978; Neretnieks et al, 1982). The original purpose of the experiment was to investigate the feasibility of extending the laboratory findings to the migration of nuclides over distances up to 10 m in a natural fracture in the Stripa granite. Because of some results obtained early in the experiment, the objective was expanded to include an evaluation of the extent of channelling within single fractures.

Experimental Design

The design of the experiment began with identification of eight site locations on the 360 m level of the Stripa mine where reasonably well-defined fractures intersected a drift. Plastic sheets were glued to the rock over the fracture traces in order to monitor the water leakage from the fractures. Only four of the eight fractures produced measurable amounts of groundwater. In the preliminary investigation, a single inclined borehole was drilled from the drift through the fracture plane. A straddle packer was used to isolate the fracture zone so that tracers could be injected. Short boreholes were drilled into the fracture plane and fitted with packers close to the collars. These boreholes acted as collection points for the tracers injected into the fracture plane. Only two of the six sampling points exhibited significant water flows and, correspondingly, measurable amounts of tracer concentrations. These results indicated the distinct possibility for channelling within the fracture plane.

The drill core from the injection borehole indicated the presence of a second fracture plane in the vicinity of the fracture plane that intersected the drift. Because of this additional fracture plane and the preliminary evidence of channelling within the original fracture plane of interest, the decision was made to drill multiple boreholes into the two fracture planes for purposes of tracer injection. As shown in Figure 2-57, the configuration of the experiment involved two fracture planes that appeared to intersect in close proximity to the drift. Inclined boreholes were drilled into the fracture planes from an adjacent cross cut. The traces of the two fracture

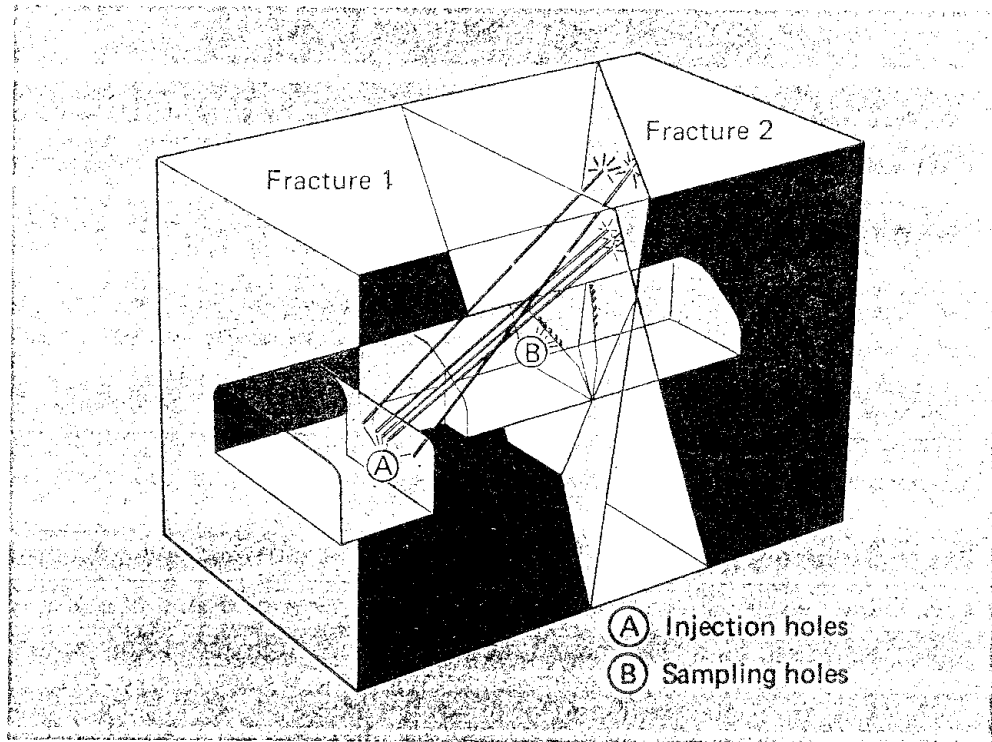


Figure 2-57 Schematic configuration of the tracer migration experiment in single fracture planes (Abelin et al, 1985; Birgersson et al, 1992a).

planes were identified in the drift and about fifteen sampling holes were installed along each trace. The most suitable injection points within the boreholes were determined on the basis of pressure pulse tests. Based on the results of these tests, four of the five borehole intersections with fracture plane 2 were used for injection purposes. The injection flow rates were generally constant, ranging from a few ml/h to about 10 ml/h. The distance between the injection sections in the fracture plane and the collection points in the drift ranged between 5 m and 10 m.

Brom Thymol Blue, Elbenyl, Eosin, Y, Iodide, and Uranin were used as nonsorbing tracers and Cs, Sr, Eu, Nd, Th, and U as sorbing tracers. Sorbing tracers were continuously injected at one injection point in fracture plane 2 over a period of eight months. Non-sorbing tracers were mixed with the sorbing tracers and injected to avoid disturbing the flow rates and the continuous injection of sorbing tracers. As mentioned above, the water and tracers were collected in short boreholes drilled into the fracture traces and the drift. Thirteen collection points were installed in fracture 1, fifteen in fracture 2, and three at locations where moisture was observed in the solid rock near the fractures.

After the injection of tracers had been discontinued, the fracture plane in the vicinity of the injection points for the sorbing tracers was core drilled. A total of sixteen cores with an average length of about 5 m were recovered. The "surface" concentration and penetration depth of the sorbing tracers in the rock matrix were subsequently determined in the laboratory.

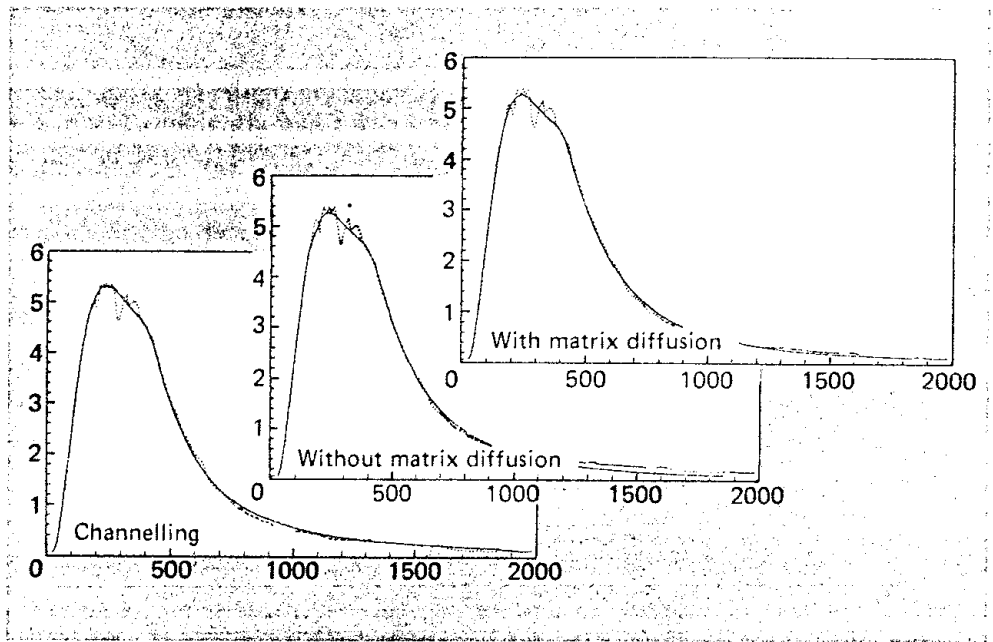


Figure 2-59 Comparison between experimental data and transport model calculations for the breakthrough of Uranin in fracture 2 (Abelin et al, 1985; Birgersson et al, 1992a).

levels of background, Th was only distinguishable on the surface of the fracture. The concentration profiles were obtained from a core sample located close to the injection hole and indicated penetration depths of about 1.4 mm into the rock matrix.

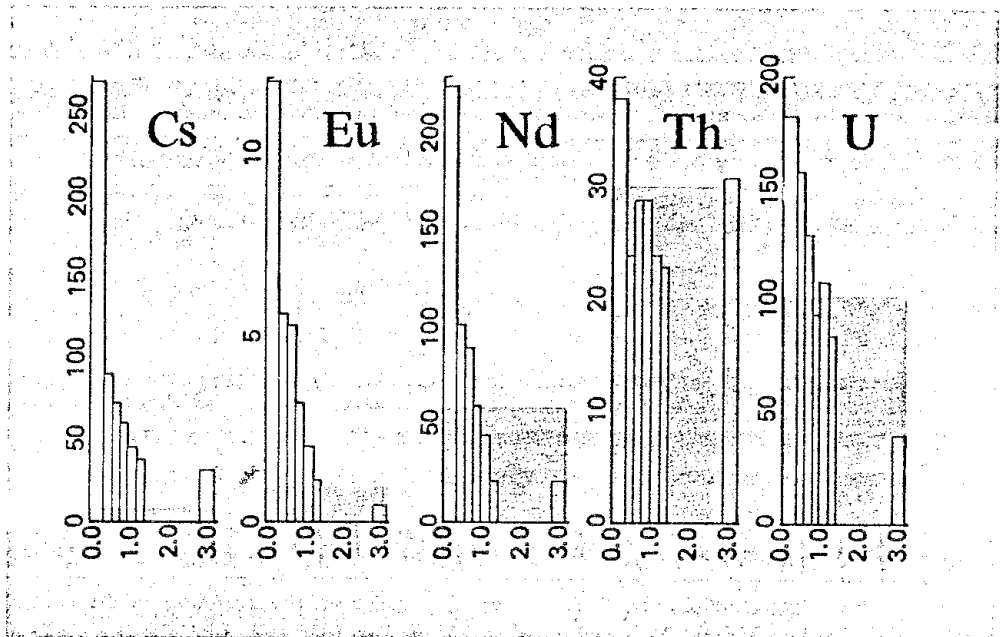


Figure 2-60 Tracer concentration profiles into the rock matrix near the injection point (Abelin et al, 1985; Birgersson et al, 1992a).

General Remarks

The irregular distribution of groundwater inflow and tracer arrival along the fracture traces, together with the multiple peaks in the tracer breakthrough curves, clearly indicated the presence of channels within the fracture planes. Based on these data, it was estimated that between 5% and 20% of the area of the fracture planes contained conductive channels. In addition, all of the mathematical models of transport considered in this investigation, involving a variety of mechanistic assumptions, fit the data equally well. Thus, it was not possible to identify specifically the key properties of fractures that controlled, or influenced strongly, tracer migration. Diffusion of tracers into the matrix was observed by direct measurement of penetration depths, and channelling was observed because of the large number of collection points in the fracture traces. The tracer breakthrough data indicated that there existed different channels which may have mixed the waters at irregular distances. Although not observed, it could be hypothesized that the channels contained zones of stagnant or near stagnant water into which the tracers diffused, as shown conceptually in Figure 2-61.

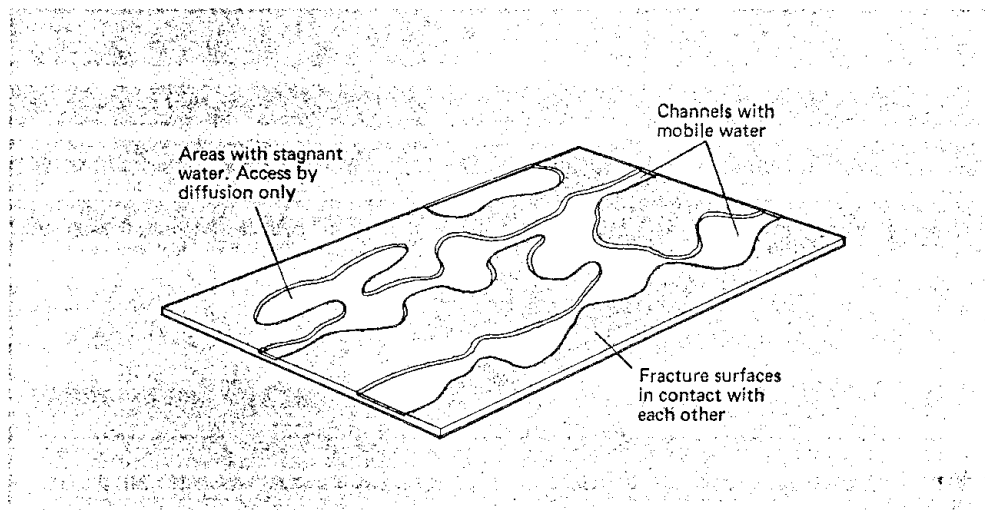


Figure 2-61 Conceptualization of water flow within channels in a fracture plane (Abelin et al, 1985; Birgersson et al, 1992a).

2.5.4 Migration in a Large Fractured Granitic Rock Mass

In Phase 2, an investigation was undertaken to study the migration of tracers in a large mass of fractured granitic rock in the Stripa mine (Abelin and Birgersson, 1987; Abelin et al, 1987a,b,c). This investigation, known as the 3-D tracer migration experiment, had multiple objectives, including, in particular, the development of techniques for conducting large-scale tracer tests in low-permeability fractured rock. The other objectives involved obtaining information on longitudinal and transverse dispersion and channelling within the rock mass, along with a determination of flow porosity and an assessment of transport model applicability. The experiment involved the construction of a drift with a length of 100 m and the injection of nine conservative tracers at various distances up to 56 m above the drift. This large number of tracers was used in order to investigate variations in the transport properties of the rock. Variations in the injection points above

the drift were chosen to ensure that at least some of the tracers would arrive during the duration of the experiment, and to obtain information on the influence of migration distance on dispersivity.

Experimental Design

At the outset of the investigation, a horizontal borehole, designated as 3D-P1 in Figure 2-62, was drilled 190 m due north into "undisturbed" granitic rock from a drift on the 360 m level of the Stripa mine. The principal purpose of this borehole was to locate a region of the rock mass in which the water circulation was relatively substantial and adequate to support a tracer migration experiment. Water inflow measurements into the pilot hole indicated a region of considerable water circulation over an interval extending from about 100 m to 185 m into the borehole. The total inflow to the pilot hole was 6.5 l/h, with the first 90 m of the hole producing about 3 l/h. At a distance of about 115 m into the pilot hole, the water inflow rate was of the order of 1.3 l/h. In this borehole section, the hydraulic conductivity approached 10^{-9} m/s as compared to values of 10^{-10} m/s or less in other portions of the pilot hole. Based on core log data, the fracture frequency was largest within the first 65 m of the borehole collar, where approximately 65% of the total number of fractures observed in the core for the entire borehole was found. In the region of relatively high water inflow, the average fracture frequency was about three fractures per metre. Based on these measurements and observations, the borehole interval of approximately 90 m to 180 m was selected as the location for the experimental site.

As shown in Figure 2-62, a drift located on the 360 m level was extended to the northeast until it intersected the pilot hole at a distance of about 100 m from the collar of the pilot hole. At this point, the drift excavation was reoriented to follow the pilot hole to a distance of about 185 m from the borehole collar. Near the end of the drift, a crosscut drift was constructed over a distance of about 25 m. In plan view, the final drift geometry resembled a cross. Three vertical boreholes were drilled upward to distances of 70 m above the drift. The drift had been located such that vertical boreholes I and II bounded the region of the granitic rock mass with

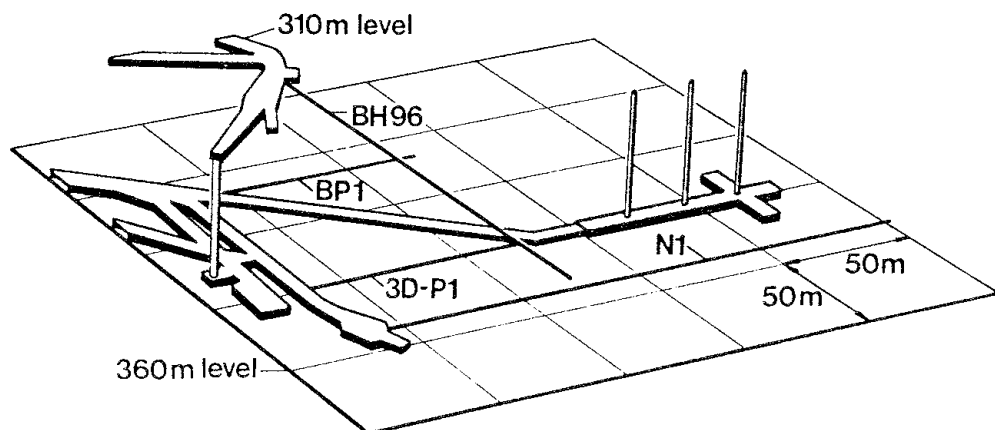


Figure 2-62 Schematic view of the layout of the 3-D tracer migration experiment in the Stripa mine (Abelin et al, 1987b; Birgersson et al, 1992a).

the high groundwater inflow rate. As shown in Figure 2-63, the drift at the experimental site was 4.5 m in width and 3 m in height, with an arched roof and 2 m high sidewalls. The roof and upper sidewalls of the drift, representing approximately 700 m² of area, were divided into about 350 sampling areas, each with an area of 2 m², and fitted with plastic sheets.

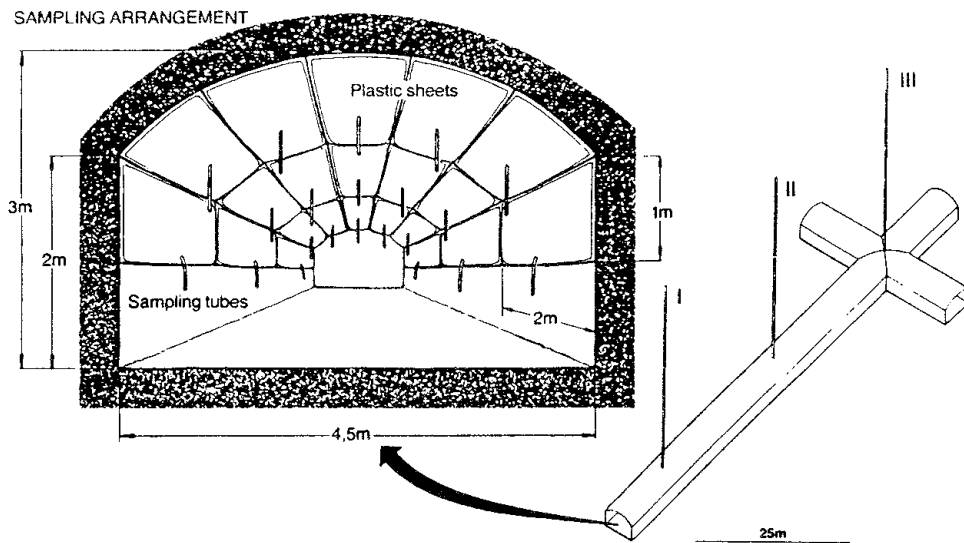


Figure 2-63 Dimensions of the drift for the 3-D tracer migration experiment (Abelin et al, 1987b; Birgersson et al, 1992a).

A total of nine tracers were injected from five different locations in the three vertical boreholes above the drift. The injection points were represented by packed-off 2.5 m long sections of the boreholes at distances of 10 m to 56 m above the test site. The locations of the injection sections were based on water inflow measurements, core loggings, TV camera inspections of the boreholes, and apparent locations of fracture zones as interpreted from the borehole radar measurements. The tracers were injected continuously for more than twenty months at "constant" water pressure, less than 10% above the natural water pressure, with variations in injection flow rate between 1 ml/h and 20 ml/h. The groundwater inflow to the drift was sampled for tracers during the duration of the injection, and for an additional six months after the end of injection.

The selection of suitable tracers for the experiment was based on a combination of considerations, including previous experience with various tracers, solubility as a function of detection limit, and distance from an injection point to the drift. In addition, consideration was given to potential interference between different tracers, diffusivity of the tracers during migration, and ease of detection in the groundwater collected in the drift. Four of the tracers, namely Elbenyl, Eosin Y, Iodide, and Uranin, had been used earlier in tracer migration experiments at the Stripa mine. The other five tracers were chosen from among 100 dyes and salts tested in the laboratory. These tracers were injected into the rock situated close to the drift or at locations in the boreholes where there was a lower possibility of the tracers reaching the drift within the timeframe of the experiment. Because of the effect of matrix diffusion on the migration of tracers, the larger molecular tracers were used at the farthest injection points. Water

samples were collected in test tubes every sixteen hours from all sampling sheets with measurable water collection. Selected test tubes were sampled for tracer content and, if any tracers were found, all the samples from that area were analyzed.

Groundwater Inflow Measurements

Groundwater inflow measurements were made in the pilot hole before excavation of the test site, in the test site for a period of 26 months, in the three 70 m long vertical injection holes, and by means of a "ventilation" test within the drift. The distribution of water inflow into the drift is shown in Figure 2-64. Maximum inflow rates of about 55 ml/h were observed in sheets located at the north end and approximately in the mid section of the long drift. In the east arm of the crosscut, a maximum inflow rate of almost 80 ml/h was observed. The total water inflow to the roof and sidewalls of the drift covered with plastic sheets was about 700 ml/h. Fifty percent of the total inflow came from approximately 3% of the covered area, although 145 of the 375 sampling sheets yielded measurable amounts of water. One sheet carried about 10% of the total inflow to the drift.

Before construction of the drift, the total inflow into the section of the pilot borehole that coincided with the excavation was 3 l/h. The distribution of

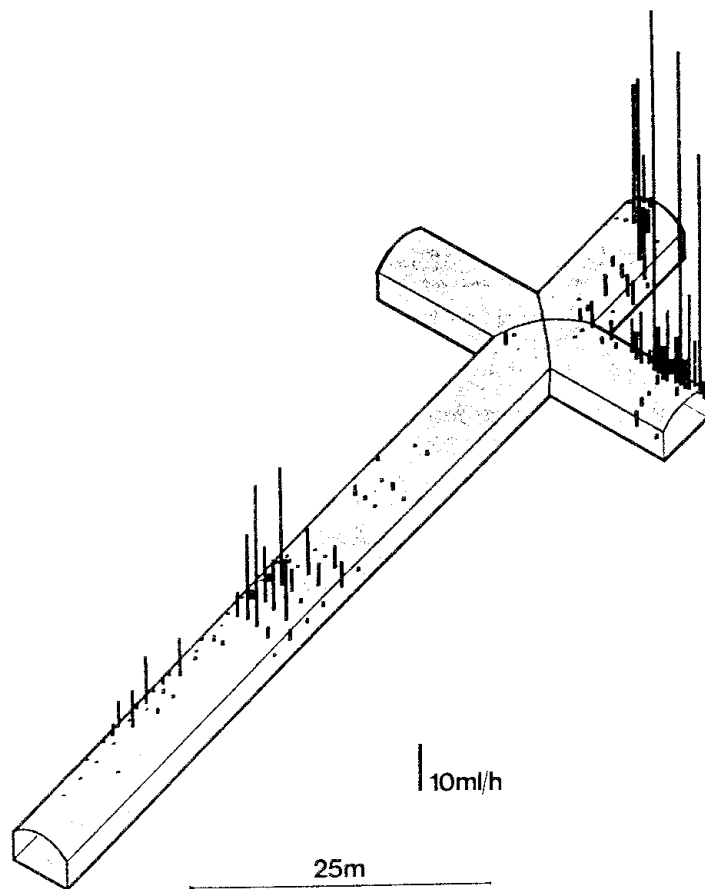


Figure 2-64 Distribution of groundwater inflow rates into the 3-D tracer migration drift before drilling the injection boreholes (Abelin et al, 1987b).

groundwater inflow to that portion of the pilot hole is compared in Figure 2-65 with that obtained for the drift. Although the distributions of high and low inflows are qualitatively similar, the total inflow into the sheets in the drift was a factor of about four smaller than that observed in the pilot hole. Because there were no collection points in the floor and lower sidewalls of the drift, a ventilation experiment was performed to determine the total groundwater inflow into the test site. For this purpose, a wall was constructed at the beginning of the access drift and the humidity difference between the inlet and outlet air to the test site was monitored over a period of about six months. Approximately 2 l/h of water inflow originated from the uncovered part of the test site. Additionally, about 400 ml/h of water originated from covered areas on the floor of the drift. When all components of the measurements were summed, the total inflow to the drift was estimated to be 3.1 l/h, which compared reasonably well with the water inflow rate that was measured into the corresponding part of the pilot hole. A comparison of water inflow rates to the drift with data from the fracture mappings indicated that areas within the drift with a larger number of fracture intersections yielded the higher groundwater inflow rates.

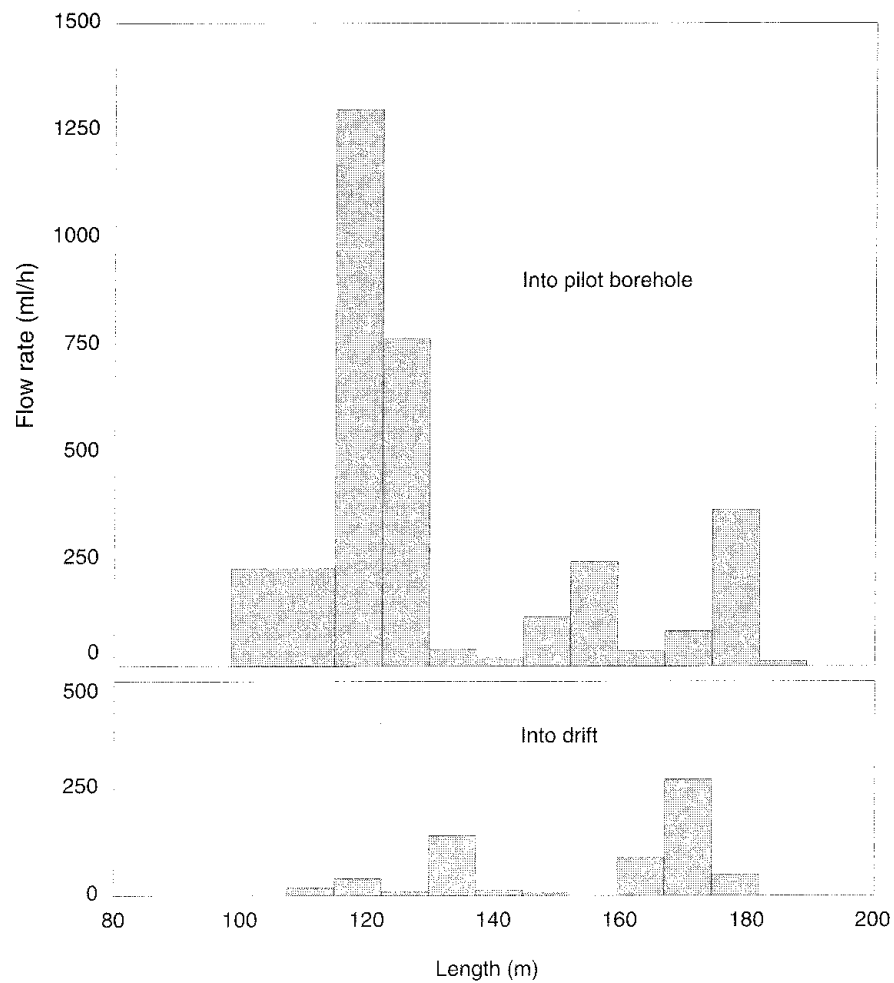


Figure 2-65 Comparison of the water inflow rates to the pilot hole before drift construction and to the drift at the test site for the 3-D tracer migration experiment (Abelin et al, 1987b).

Before excavation of the drift, the water inflow to the first 90 m of the pilot hole was approximately 3.5 ℓ/h. After construction, the water inflow to that portion of the pilot hole was negligible. However, during preparations at the SCV site in Phase 3, groundwater inflow to this 90 m section of the pilot hole resumed and reached a level of about 700 mℓ/h.

The water inflow rates to the three vertical injection holes varied considerably from borehole to borehole, ranging from 1 ℓ/h in the borehole at the south end to 17 ℓ/h in the borehole at the north end, with the center borehole producing about 4 ℓ/h. The total water inflow into these three boreholes exceeded that into the drift by a factor of about seven.

Tracer Migration

During the twenty-month injection period, six of the nine tracers appeared at collection points in the central part of the drift around injection hole II. As shown in Figures 2-66 and 2-67, the bulk of the tracer arrivals occurred in the collection panels between injection boreholes I and II. No tracers were found in the east arm of the crosscut which was the area with the highest water inflow rates. In fact, the tracers injected in borehole III appeared in the central part of the drift. During the six-month monitoring period following termination of the tracer injection, a seventh tracer, originating at the highest injection point in borehole III, appeared in panels in the central part of the drift. These arrivals occurred during preparations at the SCV site in Phase 3, including excavation of drifts and drilling of new boreholes. Elbenyl, injected at a height of 10 m in borehole II, appeared to arrive at all of the collection sheets within which it was observed within a short time period. Uranin, which was injected just below the midpoint of borehole I, appeared rather evenly in collection sheets over a longer time period. This behavior would indicate the presence of a relatively uniform pathway in the rock between the injection and collection points. The distribution of arrivals in collection panels for the other five tracers was uneven, which indicated the existence of multiple channels between the injection and collection points. The STR-7 and Fluoride tracers, with relatively large and small molecular weights respectively, were used to investigate the effects of matrix diffusion. However, these tracers never arrived at the test site in detectible concentrations. Eosin, injected in borehole I at a height of 18 m above the drift, appeared after the conclusion of the experiment in a connecting drift located approximately 150 m from the injection hole. Additionally, Uranin, injected in borehole I at a height of 32 m above the drift, was found in water from the pilot hole after the initiation of preparations at the SCV site in Phase 3.

The travel times for tracer migration between the injection and collection points varied on average between 2,000 and 7,000 hours. The recovery ranged between 2.8% and 65% for five of the tracers that appeared in the drift. The various transport models were fit to the tracer breakthrough data with varying results for the different collection points. Part of this variance could have been due to the existence of different pathways with differing transport properties between the injection and collection points. Different combinations of parameter values for the models gave fits to the data that were almost the same. The incorporation of "diffusion into the rock matrix" only produced marginal improvement in the data fits. These results

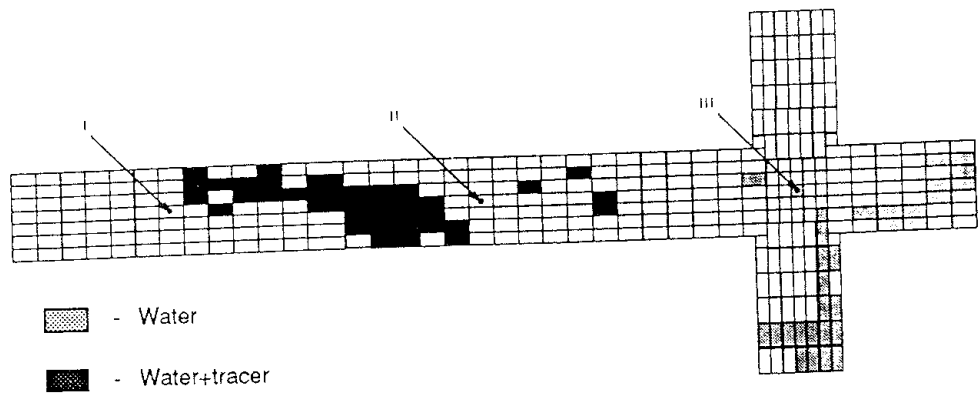


Figure 2-66 Locations of groundwater inflow and tracer arrivals in the drift for the 3-D tracer migration experiment (Abelin et al, 1987b).

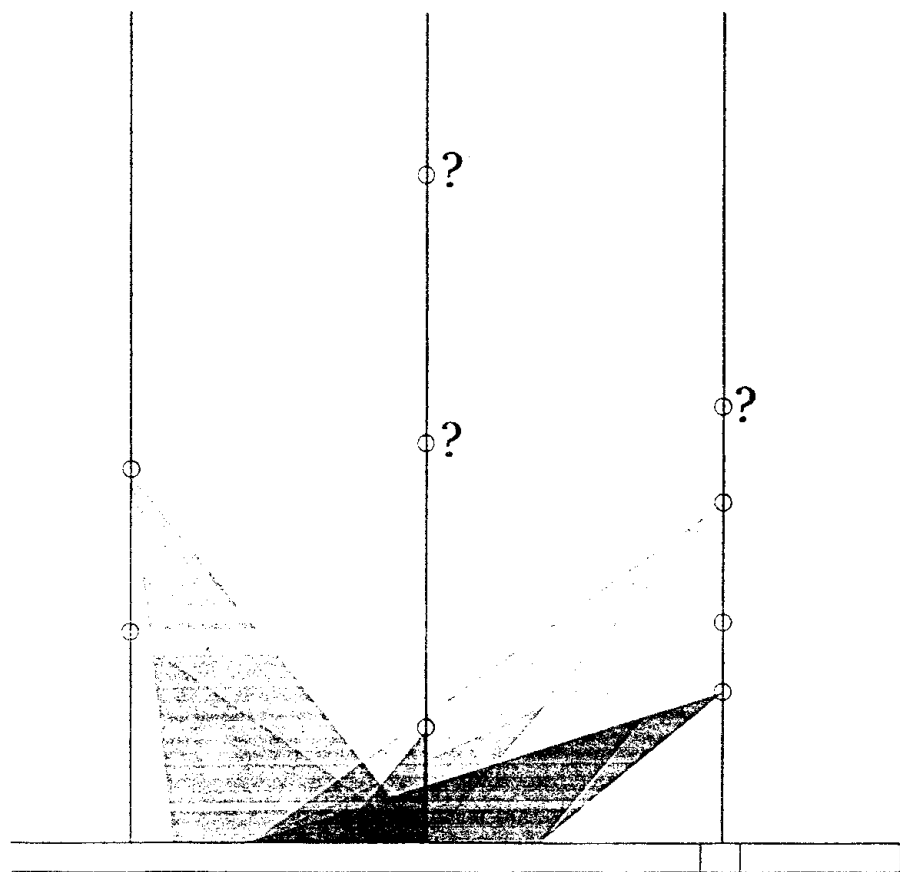


Figure 2-67 Schematic view of the migration of tracers from the injection points to the drift in the 3-D tracer migration experiment (Abelin et al, 1987b).

indicated that there existed transport mechanisms within the rock mass that were not included in the models. By assuming that the groundwater flow was radially convergent in a homogeneous porous medium where Darcy's law applied, the flow porosity was calculated to range from about 10^{-4} for the tracer injected nearest to the drift to 10^{-5} at the furthest injection points.

Summary Remarks

The outcome of the 3-D tracer migration experiment provided some interesting insights into experiment design, interactions between experiments, the effects of drift excavation, and the applicability of transport models. Considerable effort was expended before the start of tracer injection to obtain data on the rock mass characteristics around the drift and the inflow of groundwater to the drift and accessory boreholes. The drift was positioned within the region of highest groundwater inflow to the pilot hole, and suitable injection points were selected in the boreholes above the drift on the basis of borehole radar measurements, core logging, and water inflow measurements. However, this level of detail was apparently not adequate to provide a basis for explaining the tracer migration results in their entirety. The experiment clearly demonstrated the need for a greater amount of detail concerning the structure of the rock mass and the distribution of the circulating groundwater. The experiment also demonstrated that attention must be paid in the design of the water collection system to the water that flows around the drift excavation and appears in the floor of the drift.

The termination of groundwater inflow to the remaining portion of the pilot hole after construction of the drift was an interesting observation of the influence of drift construction on the groundwater flow pattern in the rock mass. The subsequent initiation of inflow to the pilot hole after the activities at the SCV site were initiated, along with the first arrivals of a tracer, was an example of how one *in situ* experiment could influence another over distances of less than 100 m.

The collection of transport models, based on various assumptions of advection, dispersion, and channelling, were not able to adequately reflect the features of the tracer breakthrough curves. This lack of agreement was probably due to uncertainties in the geometries of the flow paths within the rock mass, along with uncertainties in the geometrical features of the channels and their transport properties. This result points once again to the need for a finer level of detail in describing the structural and groundwater characteristics of the rock mass before initiating the injection of tracers.

2.5.5 Migration in Fracture Channels

The results of the two tracer migration experiments in Phases 1 and 2 indicated that channels within fractures strongly influenced the transport characteristics of a saturated, fractured granitic rock mass. In Phase 3, a series of *in situ* experiments were undertaken to study the transmissivity and aperture variations in fracture planes in granitic rock in the Stripa mine under reasonably controlled conditions (Abelin et al, 1990a,b,c). Boreholes

were drilled into the plane of a fracture and the characteristics of the fracture traces in the borehole walls were mapped. Subsequently, hydraulic tests were performed in single boreholes and between parallel boreholes in the plane of the fracture. In the double-borehole configuration, tracer tests were also conducted between the two boreholes to obtain information on fracture connectivity and residence time distributions in various channel pathways.

Experimental Design

At the outset of the investigation, more than 1 500 m of drifts on the 360 m and 410 m levels of the Stripa mine were searched for reasonably well defined fractures situated approximately perpendicular to the drift walls. On the basis of these observations, twelve fractures, all located on the 360 m level, were chosen for further evaluation. For purposes of the single-borehole experiments, a 100 mm diameter borehole was drilled along the fracture plane to a depth of about 1.5 m into the wall of the drift. This hole was drilled to obtain information on the direction and continuity of the fracture. Based on these results, the site was either abandoned or the borehole was over cored to a diameter of 200 mm with an adjustment in drilling direction. This second borehole was drilled to a depth of about 2.5 m. The location of the borehole in the fracture plane was selected such that, if desired, a second borehole could be drilled into the fracture plane at a distance of 1 m to 2 m from the first borehole. This configuration allowed tests to be conducted between the two boreholes in what was known as the double-borehole experiments.

After the 200 mm diameter borehole had been drilled, the wall of the borehole was carefully photographed. The photographs were enlarged by a factor of about three and the various properties of the fractures were measured. These properties included the total number of fractures and intersections, the trace lengths of all fractures, the apertures of open fractures, and the average thickness of the filling within fractures. Subsequently, hydraulic injection tests were performed over 200 mm sections in the boreholes using a system of straddle packers. At five of the twelve fracture sites, the injection flow rates were either minimal to nonexistent, or it was not possible to perform an injection test because the very high conductivity of the fracture. At another site, the fracture plane could not be followed with the large diameter borehole because of its undulating characteristics.

Because of the emphasis placed on evaluating the characteristics of a fracture plane, a specialized packer system was designed and fabricated. This packer system, known as the Multipede packer, consisted of two diametrically opposite rows of twenty small rubber cushions, 50 mm by 50 mm on a side, with each cushion containing a tube connected individually to the water injection system. As shown in Figure 2-68, the packer could be positioned in the borehole and the rubber cushions adjusted such that the fracture trace on each side of the borehole was covered. The small rubber cushions were pressed against the wall of the borehole by hydraulic pistons. To avoid water inflow into the borehole during testing, the water pressure within the borehole was maintained slightly above the pressure in the injection sections along the fracture traces. Because of the possibility of large flow rates for

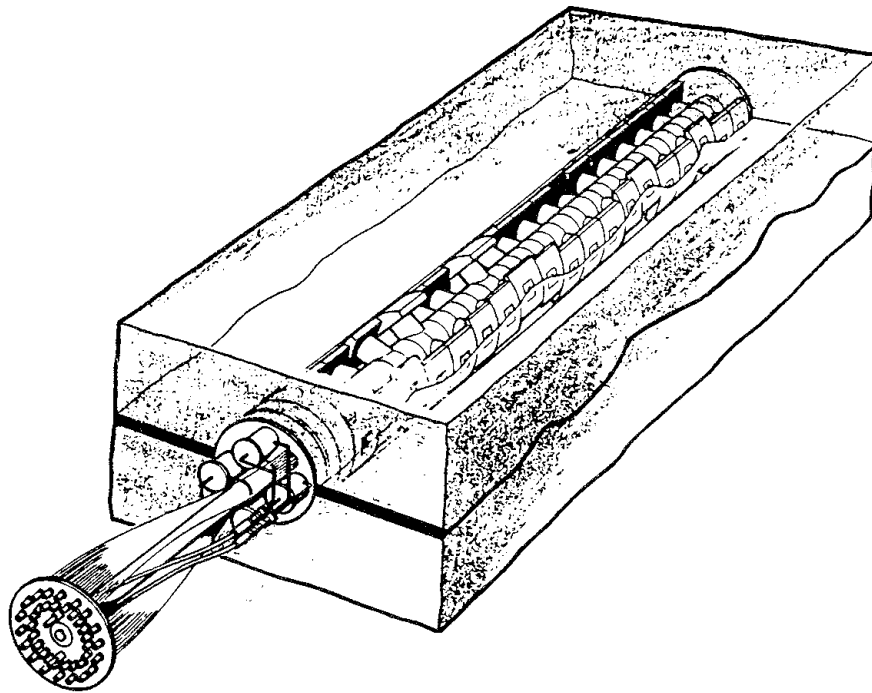


Figure 2-68 Schematic view of the Multipede packer system located in a borehole drilled parallel to a fracture plane (Birgersson et al, 1992a).

those portions of the hole not covered by the rubber cushions, the monitoring system for this portion of the device had a resolution of 1 ml/h. On the other hand, because of the relatively low flow rates for injection into the fracture planes, the monitoring system for the part of the test device with the rubber cushions had a resolution of 0.01 ml/h.

The double-borehole experiment was performed in a fracture plane where an earlier single-borehole test had indicated the existence of channels. The second borehole was drilled in the same fracture plane at a borehole-center to borehole-center distance of 1.95 m. This second borehole was also tested by means of the Multipede packer to determine the areas of the fracture traces appropriate for crosshole pressure pulse tests. Detailed pressure pulse tests were performed in both boreholes with injection over single sections, with dimensions of 50 mm by 50 mm, in one borehole and monitoring in twenty sections along the fracture trace in the second borehole.

Tracer migration experiments were performed with the double-borehole configuration. Five different nonsorbing tracers were injected from five 50 mm sections in one borehole. These sections were found to be the most conductive and to have pressure connections with the sampling borehole. The tracer solutions, consisting of Uranin, Eosin Yellowish, Elbenyl Brilliant Flavine, Duasyn Acid Green V, and Phloxine B, were continuously injected over a period of about one month. Water samples were collected at twenty different points along the fracture trace in the receptor borehole.

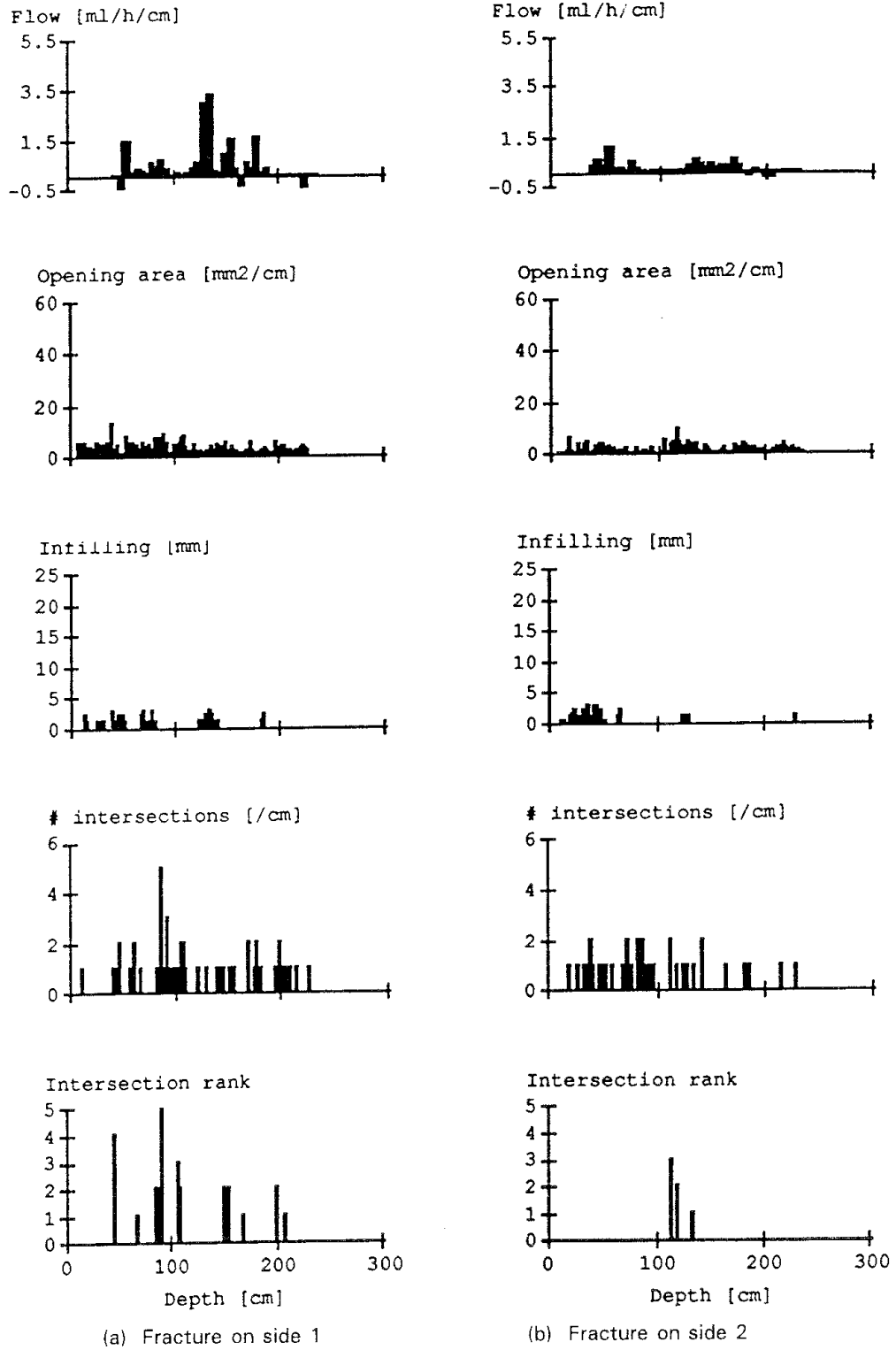


Figure 2-69 Injection flow rates and measured characteristics for the fracture intersecting borehole 7 on the 360 m level of the Stripa mine (Abelin et al, 1990c).

Water Flow Rate Measurements

An example of the results obtained from the single-borehole tests is shown in Figure 2-69. The flow rate measurements along the trace of the fracture on both sides of the borehole are shown, along with the characteristics of the fractures within the borehole as determined from measurements on the photographs. There appears to be no obvious correlation between the flow rate distributions and the characteristics of the fracture traces, except for perhaps fracture intersections. The correlation between flow rate and fracture intersections appears promising on one side of the borehole, but somewhat less so on the other side. The photographs indicated that the openings in the fracture traces resembled arrays of small holes in an otherwise nearly closed fracture. That is, the fracture planes at the borehole walls appeared to contain bundles of small tubes, or channels, rather than more or less parallel walls. Based on test data from ten fracture traces in five boreholes, the hydraulic transmissivity of the fractures was estimated to range between 10^{-10} m²/s and something less than 10^{-9} m²/s.

In the double-borehole water injection tests, one of the two boreholes in the fracture plane was completely sealed off by the inflatable packer except for a 50 mm by 50 mm section through which water was injected into the fracture. The other borehole was equipped with the Multipede packer which allowed the pressure responses to be monitored at twenty locations on the fracture trace. After completion of an injection test, the inflatable packer was moved to the next section of interest in the first borehole and another injection test was performed. This process was repeated until all points of interest had been tested. Subsequently, the Multipede packer was moved 50 mm within the second borehole and the injection process repeated in the first borehole. A compilation of all injections performed in borehole 7 and maximum pressure responses at different locations in borehole 12 in the same fracture plane are shown in Figure 2-70. The results indicate clearly a network of channels that appear to increase in density from borehole 7 to borehole 12. However, when borehole 12 was used as the injection hole and borehole 7 as the collection hole, there were only four areas of water inflow in the trace in borehole 7 at flow rates of less than 20 ml/h, and no response whatsoever in borehole 12. Under the assumptions of linear flow within the fracture plane, the data yielded transmissivities that ranged from 10^9 m²/s to 10^{-10} m²/s.

Tracer Migration

The fracture that contained boreholes 7 and 12 was chosen for the tracer tests. The tracers were injected for 750 hours at a head of 20 m and the collection hole was maintained at atmospheric pressure. Eosin Y and Phloxine B were not observed at any of the monitoring locations over the duration of the injection. Uranin was observed at seven of the monitoring locations in the collection borehole. The location of the injection and monitoring sections, along with the injection flow rates, are shown in Figure 2-71. In addition to the tracer arrivals in borehole 12, tracers in different mixtures appeared at five different locations in the drift wall away from the fracture plane. As shown in Figure 2-72, all of these locations were within about 3 m of the fracture. The first tracer arrivals in the drift wall occurred in the vicinity of the injection hole approximately ten days

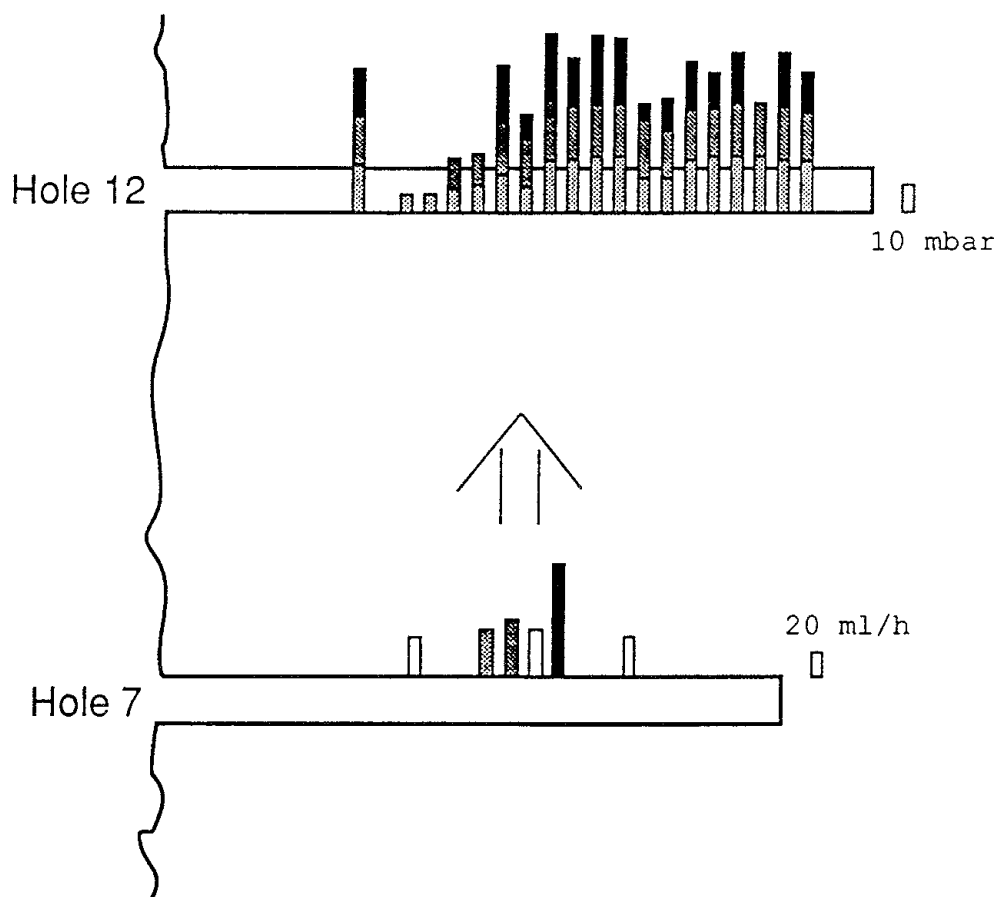


Figure 2-70 Compilation of test results from water injection tests in various sections of borehole 7 and monitoring of pressures along the fracture plane in borehole 12 (Abelin et al, 1990c).

after the start of injection. Tracers arrived at three other areas in the drift wall during the period of injection, and in an area to the left of the fracture plane approximately two weeks after the injection had ceased.

Based on the mass flow rate in the injection hole and the tracer arrival locations in the collection borehole, a conceptualization of the flow paths within the fracture plane between the two boreholes is shown in Figure 2-73. The two tracers that were injected nearest the collar of the borehole, and the tracer that was injected nearest the end of the borehole, were never observed at any detectable levels in any location in the collection borehole.

Breakthrough curves for Uranin at different locations in the collection borehole are shown in Figure 2-74. The concentration levels varied between 15% and 35% and the mean travel time was about 40 hours. At steady state conditions, the amount of tracer recovered was about 11% of that injected. This indicated that nearly 90% of the tracer migrated in pathways which were not connections between the two boreholes. The double peaks in the breakthrough curves indicated at least two pathways of transport, one of which is much shorter than the other. The water inflow rate and the collection of Uranin in the bottom section of borehole 12 is shown in Figure 2-75 as a function of time. The water inflow rate exhibited a small sinusoidal variation with a time period of about one week and a slow

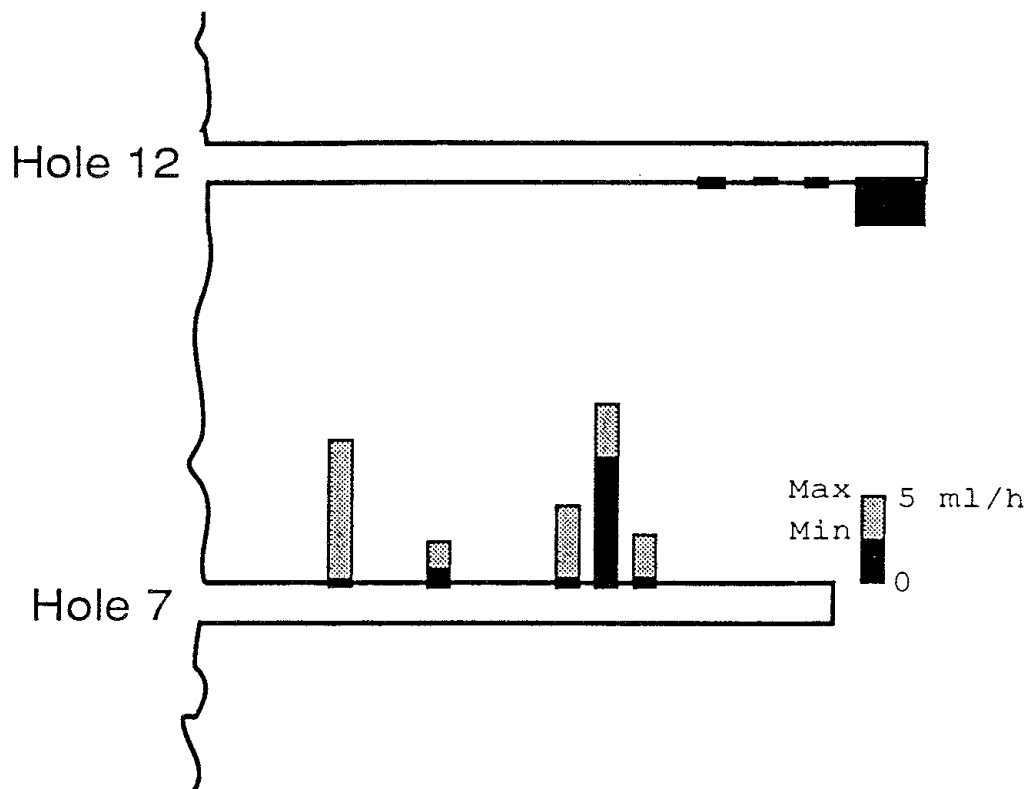


Figure 2-71 Location of the injection and monitoring sections for the tracer migration test in the fracture plane connecting borehole 7 and borehole 12 (Abelin et al, 1990c).

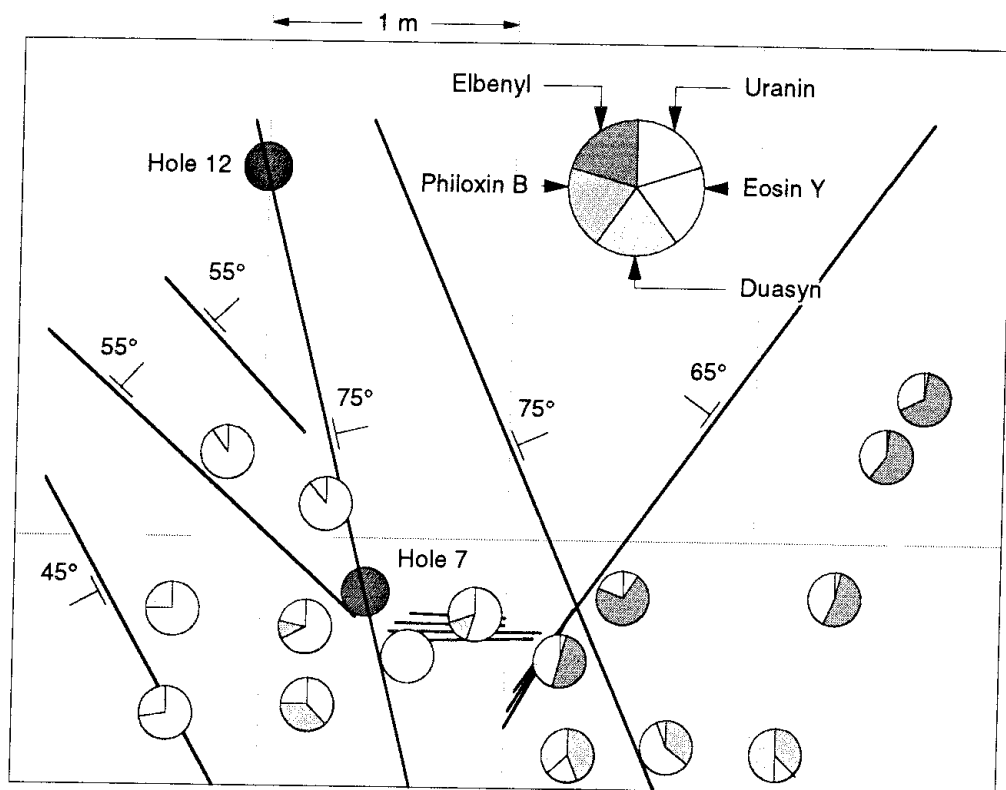


Figure 2-72 Map of the tracer arrivals in the face of the drift containing the fracture plane intersected by boreholes 7 and 12 (Abelin et al, 1990c).

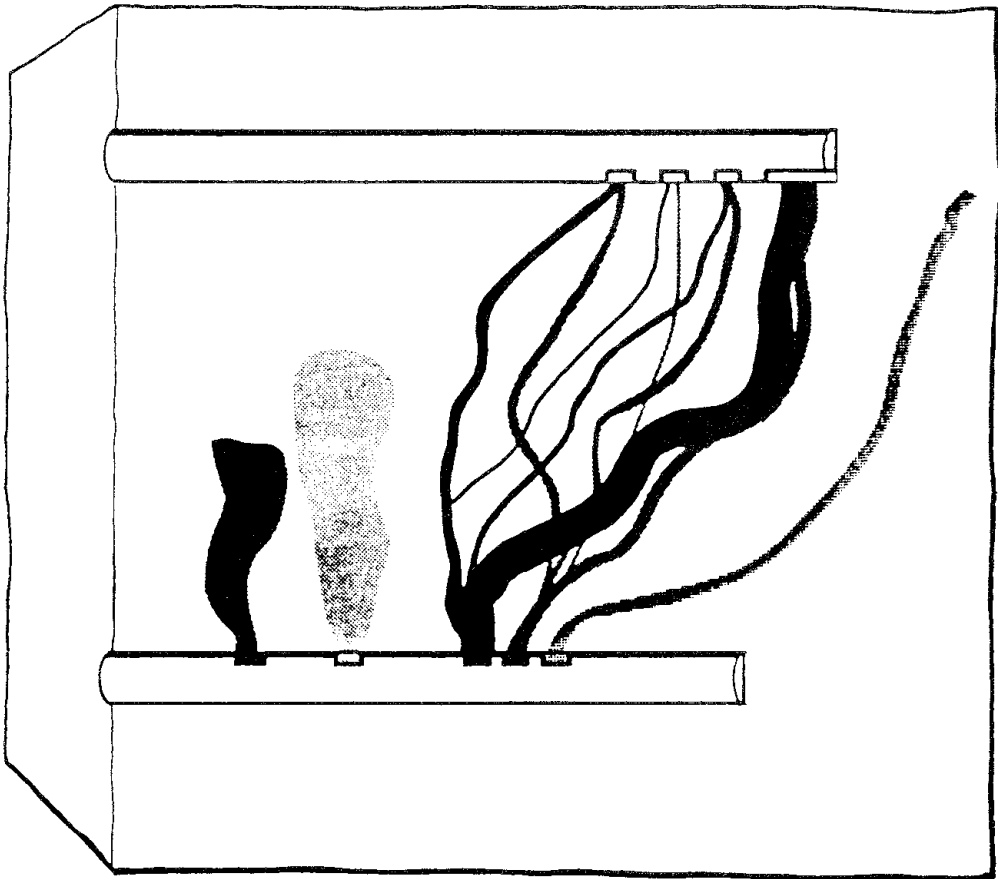


Figure 2-73 Artistic view of the flow paths along which tracers migrated between boreholes 7 and 12 (Abelin et al, 1990c).

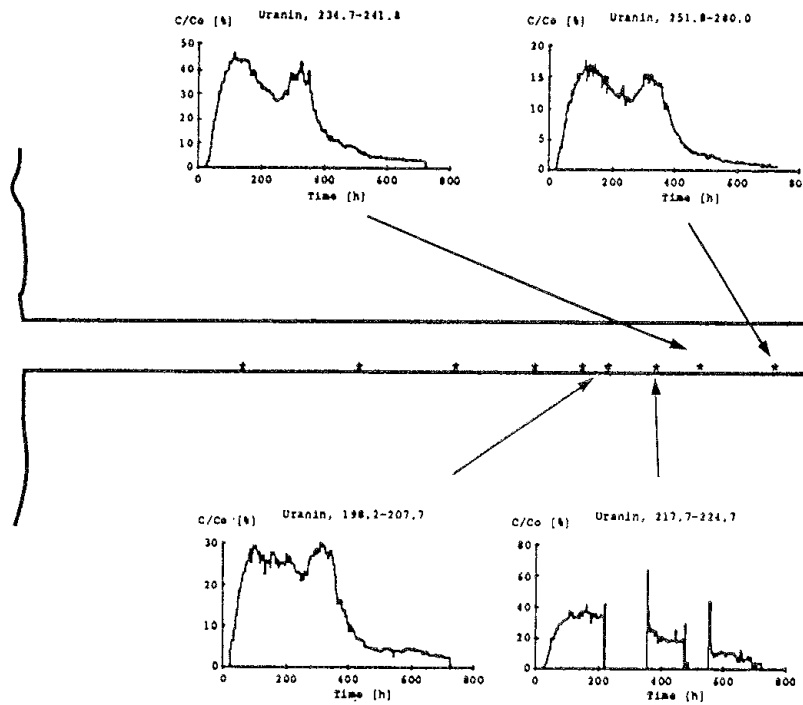
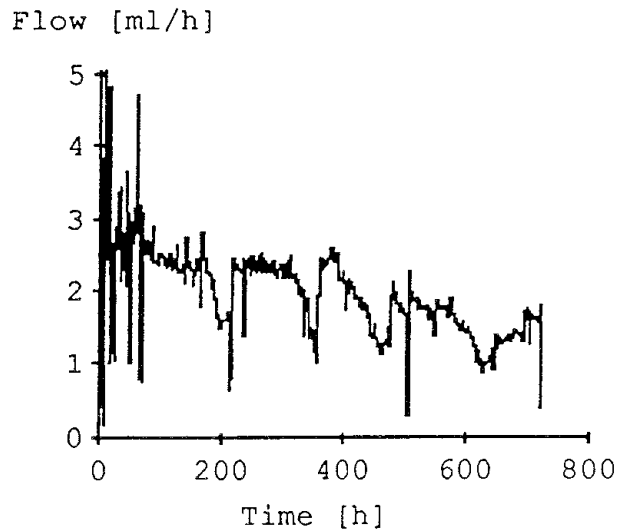


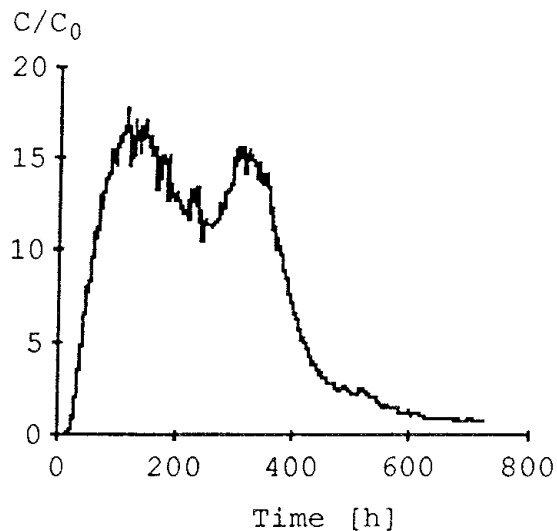
Figure 2-74 Breakthrough curves for Uranin at different locations in borehole 12 (Abelin et al, 1990c).

decrease over time. The cause of the sinusoidal variation was not known. Although the two peaks in the breakthrough curve bear some relation to the behavior of the water inflow rate, the double peaks are probably more representative of several pathways of differing length between the two boreholes.

As shown in Figure 2-75(a), the injection flow rate reaches a condition of steady state within a very short period of time, of the order of hours at most. Based on an assumption of linear flow within the fracture plane, diffusivities were calculated to range from about $10^5 \text{ m}^2/\text{s}$ to $10^4 \text{ m}^2/\text{s}$. For conditions of spherical flow, wherein the fracture geometry interconnects the rock mass with the fracture plane, the diffusivity was calculated to range from less than $10^4 \text{ m}^2/\text{s}$ to almost $10^2 \text{ m}^2/\text{s}$.



(a) Water inflow rate



(b) Uranin breakthrough curve

Figure 2-75 Water inflow rate and Uranin breakthrough as a function of time at the collection point in the bottom of borehole 12 (Abelin et al, 1990c).

Summary Remarks

The results from the experiments did not allow a correlation to be established between the flow rate of the injected water and the observed aperture distribution of the fracture traces. Results of other investigations have suggested that the pressure drop is determined by the smaller apertures along the flow path which form the pinch points for flow. The larger mechanical apertures will determine the flow aperture because those are the regions wherein the water will acquire much of its residence time. It was concluded that, for the test sites in the Stripa mine, 25% or less of the fracture plane was open to flow, with individual channel widths ranging from millimetres to a decimetre. These channels occurred in clusters with cluster widths of decimetres. The single fracture planes contained several intersecting fractures which diverted the flow from the main fracture, with some of these fractures containing dead-end channels. It can be expected that the individual fractures have properties that strongly deviate from the average.

2.5.6 Migration in a Fracture Zone

In Phase 3, a large-scale tracer test, known as the tracer migration experiment, was conducted at the SCV site as a part of the site characterization and validation programme (Birgersson and Ågren, 1992; Birgersson et al, 1992a,b,c). The objectives of this experiment were to study tracer migration in a fracture zone, as well as in the averagely fractured rock outside the fracture zone, and to obtain data to be used in evaluations of the validity of the groundwater flow and transport models applied at the SCV site. The various facets of the experiment are described in greater detail in Section 3.3.4, and the use of the data for the model validation effort is discussed in Section 4.2.5. In this section, only a brief overview of the experiment and its outcome will be given.

The tracer migration test was conducted in the rock mass that contained the SCV site, located at a depth of about 385 m below the surface. The site had a rather well-defined steeply dipping fracture zone, with a width of some 6 m, which was intersected by the so-called Validation Drift. Data obtained by radar, seismic, and hydraulic testing in boreholes clearly established the presence of this zone and the fact that it was a principal conduit for groundwater flow through the site. Crosshole radar testing was conducted in boreholes in the vicinity of the zone before and after construction of the drift with simultaneous saline injection into the zone, in order to identify the geometric and flow characteristics of the zone. The design configuration of the tracer test was based on these data and included tracer injection points principally in the fracture zone, with one injection point located in the "competent" rock. The injection points were located at distances ranging from 10 m to 25 m from the drift, and a combination of twelve different tracer substances were injected for periods of time ranging from less than a month to more than seven months. The water inflow and tracer breakthrough to the drift were monitored by a combination of plastic collection sheets on the roof and walls of the drift and sump holes in the lower walls and floor.

Approximately 150 tracer breakthrough curves were obtained and analyzed by means of an advection-dispersion transport model that included a provision for diffusion. Matrix diffusivities for the tracers were measured in laboratory tests and used in an attempt to determine values of the average amount of fracture surface in the rock in contact with the flowing water.

All of the injected tracers migrated to the Validation Drift and were collected in varying amounts. The recoveries for the metal tracers varied between 10% and 60%, although tracers were still entering the collection points in the drift when the experiment was terminated. The mean residence times were determined to vary between 1,500 and 4,000 hours on average, although considerably shorter as well as longer times were identified in some of the collection areas. The flow porosity was calculated to be slightly greater than 10^{-3} for the tracer injected closest to the drift, but decreased somewhat with increasing distance to the furthest injection point. The dispersivity of the tracers was found to be relatively very high. It was hypothesized that mechanisms other than hydrodynamic dispersion existed, such as transport of tracer in channels with different transport properties. Furthermore, it was concluded that the conventional transport models, considering advection-dispersion and advection-dispersion with diffusion, were not able without additional modification to accurately describe the details of tracer movement within the fracture zone.

2.5.7 Significant Achievements

Over a period of some twelve years in the Stripa project, tracer migration experiments were conducted in the granitic rock matrix, in single fracture planes, in a large network of fractures, and in a discrete fracture zone within the granitic rock mass in the Stripa mine. The migration distances in these experiments ranged from a few decimetres to a few metres to some tens of metres. In the 3-D migration experiments, one tracer migrated over a distance of approximately 150 m from the injection point in the borehole to a connecting drift. Two principal achievements can be identified from the collective results of this group of experiments. The first was the large amount of experience that was gained in designing a tracer migration experiment. The second was the generally qualitative understanding of how tracers migrate in saturated, fractured granitic rock.

The experiences from these experiments has demonstrated the necessity for carefully characterizing the features of the fracture and hydrologic systems in a granitic rock mass before conducting a tracer migration experiment. The complexities of the channel networks within the fractures, coupled with the interconnection of major and minor conduits of groundwater flow, can severely influence the accuracy of even the qualitative predictions of tracer movement through the rock. As demonstrated with the tracer migration experiment in the SCV programme in Phase 3, the qualitative understanding of the migration characteristics of the tracers in both the fracture zones and the "competent" rock was significantly improved because of the characterization information obtained by means of the radar/saline injection tests. Additionally, the development of the tracers in the laboratory with complementary testing of their characteristics in core samples enhances significantly the ability to design an *in situ* tracer experiment.

The transport of tracers by groundwater within a saturated, fractured granitic rock mass is strongly influenced by the geometric features of the networks of channels within both individual fractures and fracture zones. The diffusion of tracers into the matrix of the granitic rock has been demonstrated. The extent to which this mechanism will retard the transport of radionuclides depends on the area of the rock surface in contact with the flowing water and the magnitudes of the diffusivity and sorption coefficients. The analysis of data from both field and laboratory experiments has shown that the dispersion length increases proportionately with the distance between the injection and collection points. This may be due to the presence of an increasing number of distinct fractures or fracture zones with increasing volume of the rock mass, which in turn implies a potential increase in the lengths of the migration pathways such that proper averaging conditions do not exist. In the Stripa granite, 25% or less of some of the fracture planes were interpreted to be available for groundwater flow, with individual channel widths ranging from millimetres upwards to a decimetre. Channels were observed to occur in clusters with cluster widths of decimetres.

2.6 SUMMARY OF SIGNIFICANT ACHIEVEMENTS

A significant achievement of the activities spanning the three phases of the Stripa Project was the development of a suite of tools and a focussed strategy for characterizing the geohydrologic features of a saturated, fractured granitic rock mass. This suite of tools included the radar, seismic, and hydraulic methods for both single-borehole and crosshole testing, as well as borehole photography and drill core observations. For site conditions similar to those encountered at Stripa, tests in boreholes spaced as much as 200 m apart can be expected to provide data to identify the principal structural features and hydraulic anomalies. The characterization strategy begins with first identifying the distribution of major features within the rock mass by means of single-borehole radar reflection testing and tomographic inversion of crosshole radar and/or seismic data. This is followed by a combination of single-borehole and crosshole hydraulic testing in order to describe the distribution of the hydraulic properties of the structural features and the "average" rock. In particular, much of the hydraulic testing should be focussed on structural features that are expected to be the principal conduits for the transport of groundwater.

The hydrogeochemical investigations, conducted principally during Phases 1 and 2, produced a variety of techniques for quantifying the characteristics of groundwater circulation in a granitic rock mass with dimensions of kilometres. This work involved the development and implementation of methods and techniques to determine the age, or residence time, and origin of groundwater in the granitic rock mass at Stripa. One of the principal techniques involved the identification of concentrations of key radionuclides and a reliable computation of the background concentrations of these radionuclides due to subsurface equilibrium production. Much of the research by the members of the HAG was of a pioneering nature.

The tracer tests at Stripa were conducted at a variety of dimensional scales in both "competent" and fractured rock. The experiences gained in

designing and conducting these tests have demonstrated clearly the importance of understanding the groundwater flow field and the potential pathways in a rock mass prior to conducting a tracer test. There is little hope for quantifying the migration characteristics of a pathway unless the geometric aspects of the pathway and the generalized groundwater flow field within the pathway are defined before injection of the tracers into the pathway. These types of information can be obtained through the integrated use of the radar, seismic, and hydraulic borehole-testing methods. In addition, the sorbing characteristics of the tracer substances must be determined *a priori* in the laboratory.

3 APPLICATION OF CHARACTERIZATION METHODS

The development of a conceptual geohydrologic model of a site area is an essential part of an investigation in which efforts will be made to numerically simulate the groundwater flow system of the site. During the Stripa Project, characterization tools and methods were applied to obtain data to describe the geohydrology of the Stripa mine and its surroundings. In particular, conceptual geohydrologic models were developed for the general area of the Stripa mine, the Crosshole site in the vicinity of the 360 m level of the mine, and the SCV site in the vicinity of the 385 m level of the mine. These models were based on geologic, hydrologic, and geochemical data obtained by observation, laboratory tests, and field tests, as well as geologic and hydrologic information that had been obtained in pre-Stripa-Project studies. The development of the model for the SCV site was an integral part of Phase 3, while the models for the mine and the Crosshole site were developed as part of the natural evolution of the characterization activities, particularly as those activities focussed on the design and implementation of improved characterization tools and methods.

The model development exercises served three purposes. First, they were useful in demonstrating the applicability and credibility of the characterization tools, methods, and data interpretation techniques, and in providing a basis to refine such tools, methods, and techniques under realistic site conditions in an underground environment. Second, the process for development of a conceptual model was formalized into a series of distinct steps, involving the sequential application of increasingly more complex testing methods. In addition, these steps included procedures for making comparisons between data obtained from different testing methods to ensure consistency in interpretation. Finally, the models provided a basis for the development and application of numerical modelling procedures for simulating groundwater flow and solute transport in a saturated, fractured rock mass.

This chapter begins with a description of the field data and results from the numerical simulations that formed the basis for developing a three-dimensional conceptual model of the Stripa area. The particularly important features of this research work were the incorporation of the geologic and hydrologic data into a numerical model for simulating the hydrology of the area, along with the outcome of the simulations. This is followed by a discussion of the characterization activities that took place at the Crosshole site in the Stripa mine, and how the results were connected together to provide a three-dimensional conceptualization of the geohydrology of the site. An important outcome of this work was, in part, a hierarchy of characterization techniques that could be applied sequentially in the investigation of a site in a fractured, saturated granitic rock mass. This hierarchy was used in the characterization of the SCV site in the Stripa mine, as described in the later sections of this chapter. An important feature

of the work at the SCV site was a demonstration of how the borehole radar method could be used to map the migration of a tracer in a rather well-developed fracture zone within the rock mass.

3.1 CONCEPTUAL MODEL OF THE STRIPA AREA

The conceptualization of the geohydrology of the Stripa area was based on geologic, geochemical, and hydrologic information obtained from pre-Stripa-Project studies and from data collected during all three phases of the Stripa Project. These data were gathered by observation of drill core and exposed rock on the surface and in the Stripa mine, laboratory tests of the geochemical properties of the groundwaters and of the characteristics of rock fractures, and hydraulic tests in boreholes drilled from the surface and at various locations within the Stripa mine. On the basis of these data, a three-dimensional equivalent-porous-media (EPM) finite-element model of the Stripa area, including the Stripa mine, was developed and calibrated against the rate at which groundwater was pumped out of the mine and against groundwater transient times inferred from the isotope studies. This finite-element model represented a volume of rock of some 300 billion m³, with a surface expression of about 100 km². Additionally, several finite-element sub-models, representing volumes on the order of 60 billion m³, were developed to represent in greater detail the rock mass containing the mined-out cavities in the Stripa mine.

The geohydrologic model of the Stripa area and the associated data bases are documented in a series of reports and technical papers by Gale and Rouleau (1986) and Gale et al (1987, 1990b, 1990c, 1991). The regional geology of the Stripa area has been summarized in a number of Stripa Project reports that are based on the earlier work of Geijer (1938) and the more recent work by Olkiewicz et al (1979), Wollenburg et al (1982), and Lundstrom (1983).

3.1.1 Regional Geology

The bedrock of the Fennoscandian Shield in the area of the Stripa mine was deformed tectonically about 1.8 to 2 Ga ago. As shown in Figure 3-1, this bedrock consists primarily of calc-alkaline meta-volcanic and meta-sedimentary supracrustal rocks, primarily mica gneisses. The Stripa mine is completely surrounded by the meta-volcanics, known locally as leptites, which in turn are partly enclosed by the meta-sedimentary rocks to the south, southeast, and southwest. A significant thickness of metamorphosed limestone/dolomite marble is located about 4 to 5 km to the south and southeast of the mine. A relatively thin lens of marble, contained within the drainage basin for the regional flow system, is located about 4 to 5 km to the northwest.

The majority of the fold structures are thought to be due to a east-west compression that occurred during the first period of tectonic deformation in past geologic time, with the resulting fold axes, inferred from large-scale rock distribution and structural relationships, being mainly horizontal with an approximate north-south trend. Small-scale, north-south trending folds with horizontal fold axes, shown on the Stripa mine maps, support this

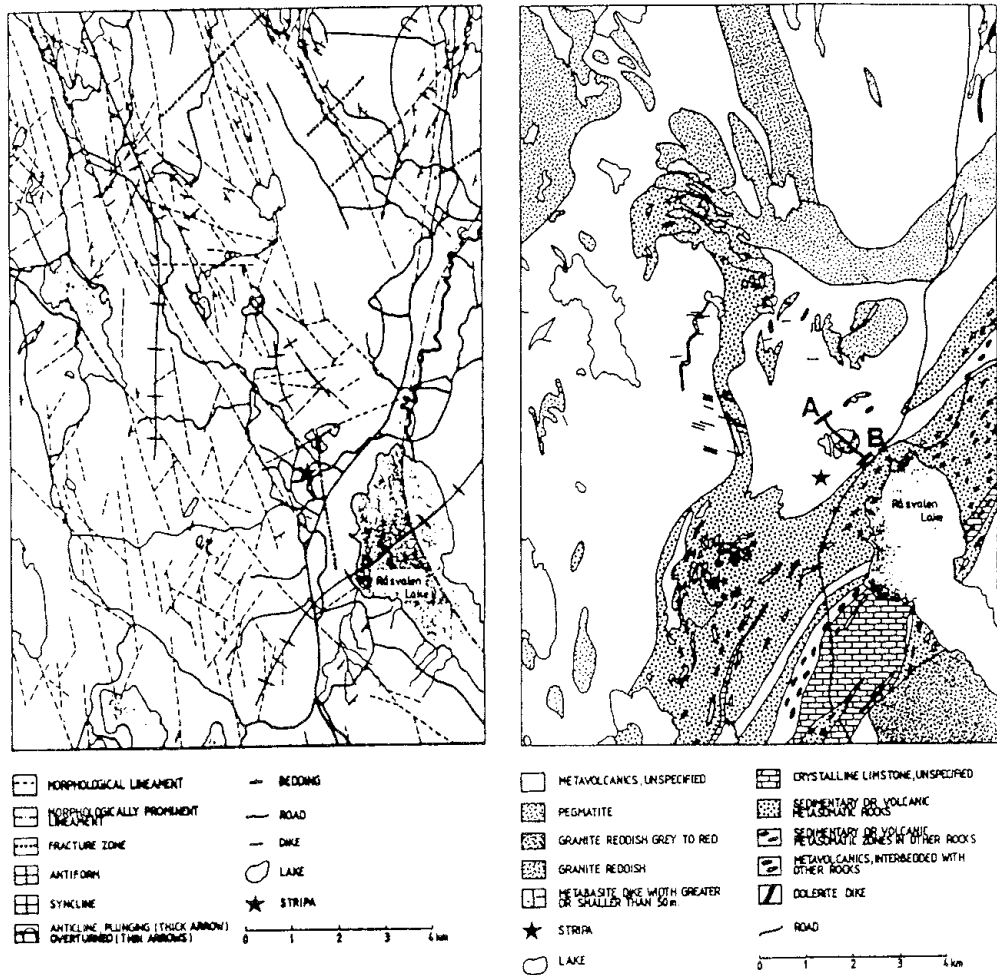


Figure 3-1 Regional geology and structures of the Stripa area (Lundstrom, 1983).

interpretation. A second period of tectonic deformation is thought to have generated a north-south compression, which gave rise to refolding, with fold axes plunging to the east and northeast, such as the truncated syncline in which the Stripa mine was developed. This local syncline, shown in Figure 3-2, is contained within the large regional, northeast trending syncline that dominates the structure of the supracrustal rocks and the preorogenic and synorogenic intrusions.

The bulk composition of selected units of the supracrustal rocks may have been altered by an initial period of intense, synvolcanic metamorphism. The second period of metamorphism gave rise to a regional facies, amphibolite to greenschist, and was followed by a third period which resulted in a lower, possibly retrograde, facies. Given the different levels of metamorphism, it is assumed that the late to post-orogenic granites, such as the Stripa granite, intruded the supracrustal rocks about 1.7 Ga ago, long after the peak of the regional metamorphism. This age date is supported by the observation that fracture zones in the post-orogenic granites show retrograde style metamorphism, consistent with the third period of metamorphism. Similarly, the 0.85 Ga to 1 Ga age of the post-orogenic dolerite dikes, such as those contained within the Stripa granite, post-date the peak of the regional metamorphism.

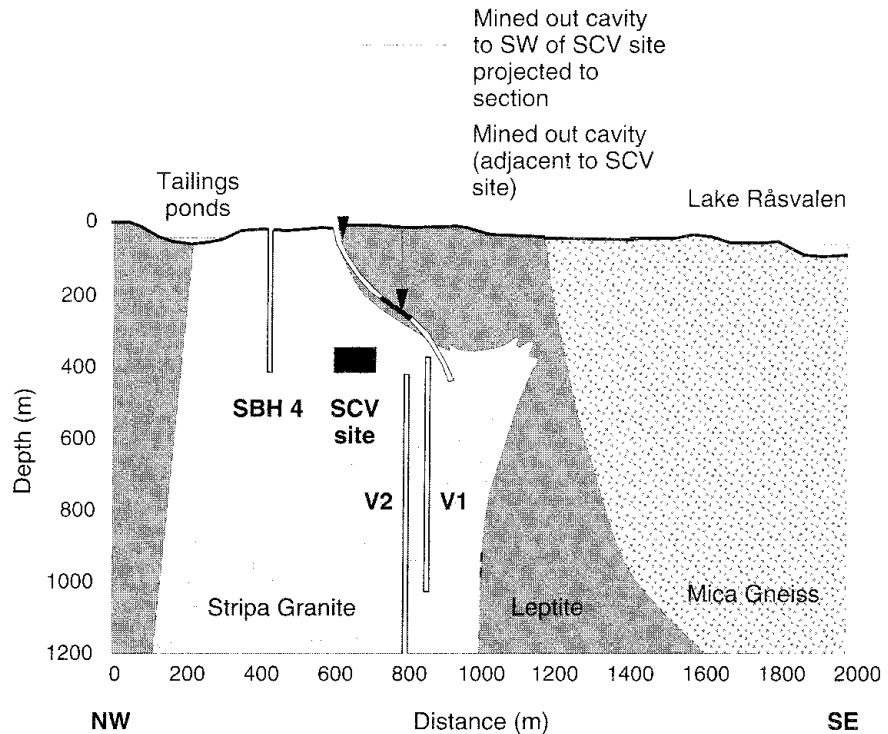


Figure 3-2 Vertical geologic section through the pluton containing the Stripa mine (Olsson et al, 1989).

The location of this profile is shown as the NW-SE line with end points A and B in the geologic map in Figure 3-1. Boreholes SBH4, V1, and V2 are shown for reference.

3.1.2 Tectonic Features

The Stripa mine is located in an uplifted part of the Precambrian crystalline basement. Northeast trending lineaments or fracture zones that exist in the Stripa area are thought to be related to the northeast trending faults that form the edge of the sub-Cambrian peneplain, located about 10 km to the east. The fault zone in this area, traceable for more than 200 km, has been activated on numerous occasions over geologic time. The last major episode took place during the Tertiary era and the fault zone is still seismically active. The northeast trending fracture zones present in the Stripa area are considered to be related to this fault zone. These fracture zones form anastomosing structures with large-scale lensoidal rock blocks, which indicates that the overall fault zone was formed as a regional shear zone.

The major features, or lineaments, in a 20 km by 20 km area, centered on the Stripa mine and shown in Figure 3-3, are based on a structural interpretation of the relief map of Bergslagen (unpublished map from the Land Survey of Sweden, LMV, 1989). The direction of "illumination" of the relief map is from the northwest with an oblique angle of 30°. Structures at right angles to this direction are pronounced. The direction of glacial striation is north-south, with zones of weakness parallel and subparallel to this direction being preferentially eroded. As shown in the Rose diagram in Figure 3-4, the bulk of the fracture zones are oriented between N10E and N20W, while a few zones exhibit northeast or east-west orientations. Within the Stripa area, the major fracture zones, as evidenced

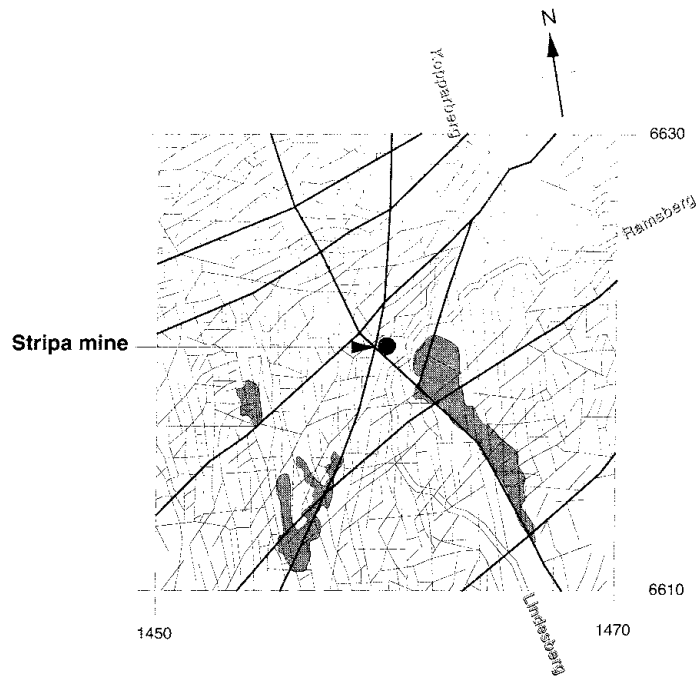


Figure 3-3 Location of major lineaments and fracture zones in the Stripa area (Gale et al, 1991).

The mapped area is 20 km on a side, and the grey areas indicate lakes. The map coordinates (RAK) are referenced to the topographical map of Sweden.

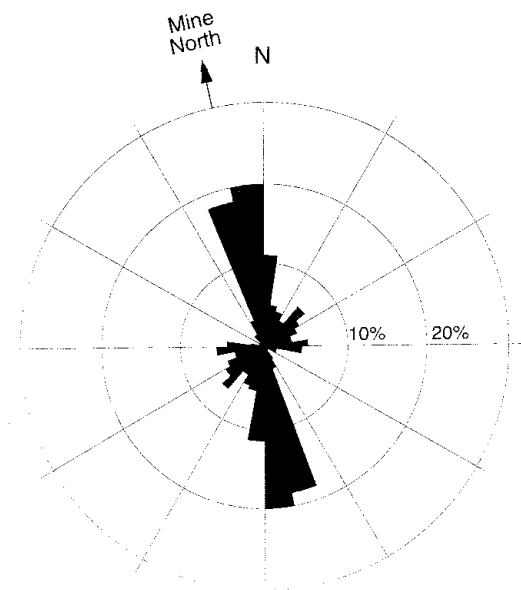


Figure 3-4 Rose diagram showing the orientation of major lineaments and fracture zones in the Stripa area (Gale et al, 1991).

by their strong topographical expressions, are oriented to the northeast, north-northeast, or northwest, and most are curved or wavy. Conversely, the east-west trending zones do not have strong topographic expressions and are more irregular and discontinuous. The abundant north-south to north-northwest trending zones are narrow and have short trace lengths compared to the other fracture zones.

3.1.3 Stripa Mine Geology

As shown in Figure 3-3, the Stripa mine is situated north of an extensive northwest trending, twisting, fracture zone, and is bordered by minor north-south fracture zones. In addition, to the north of the mine, there exists an irregular east-to-northeast trending, relatively wide, fracture zone.

In the local sense, the meta-volcanic rocks, known as leptytes, into which the Stripa granite intruded, exhibit a northeast-southwest strike. However, the local geologic structure consists of an eastward plunging syncline with an undulating pitch, that changes bearing to N60E at about the 120 m level of the mine. The syncline, which contained the iron ore zones, is asymmetric with the southern limb. The northern limb is both folded and faulted, with mapped and inferred vertical offsets along major fracture zones increasing, in a scissors-like fashion, to the east and northeast. The Stripa granite intrudes under the north limb of the syncline, where the SCV site was located as shown in Figure 3-2, and outcrops over an area of about 0.3 km² immediately north of the mine. The true size of the pluton at the surface is not known because of the extensive cover of glacial debris.

The Stripa granite is a grey, fine to medium grained, relatively uraniferous granitic rock. Several stages of fracturing are evident in the granite, including fractures that have been welded or bonded together by fracture mineralization. About 90% of the granitic matrix is composed of quartz, plagioclase, and microcline, with the remaining 10% composed principally of muscovite and chlorite.

3.1.4 Fracture Zones

The location and orientation of the major structural features in the Stripa mine, shown in Figure 3-5, are based on the old Stripa mine maps. Contoured pole diagrams for the large-scale features are shown in Figure 3-6. These figures indicate that the major structural features are oriented in the north-south to north-northwest direction, and can be divided into three clusters of large-scale features in the mine. The first cluster is a set of northwest-trending faults that intersect the northern limb of the syncline, with trace lengths generally less than 100 m and spacings of about 50 m. The second cluster contains the east to northeast trending faults, including the Ottesskolen and parallel structures located south of the Lundborgs shaft, with similar spacings but trace lengths up to approximately 500 m. A third cluster of rather abundant faults is oriented in the east to northeast direction with trace lengths as great as 500 m. The trace length distributions for these three clusters of fracture zones are shown in Figure 3-7.

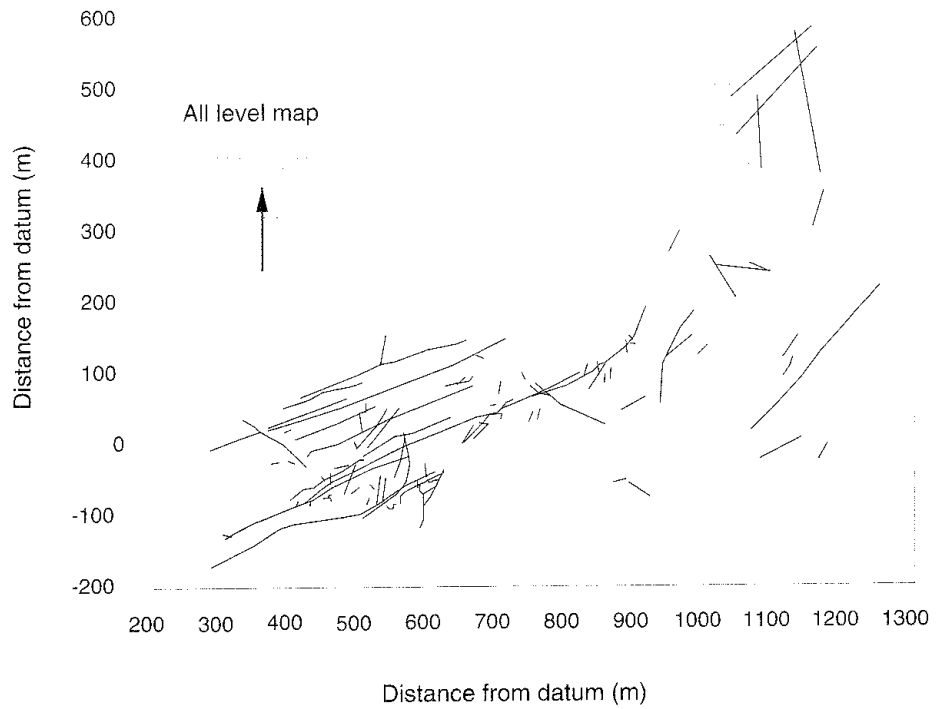


Figure 3-5 Location and orientation of the major features in the Stripa Mine (Gale et al, 1991).

The features in this diagram are based on the mine maps by Geijer (1938). The major features in the SCV site, identified during the course of the Stripa Project, are shown in the upper right hand corner of the map. The coordinates are referenced to the coordinate system of the Stripa Mine.

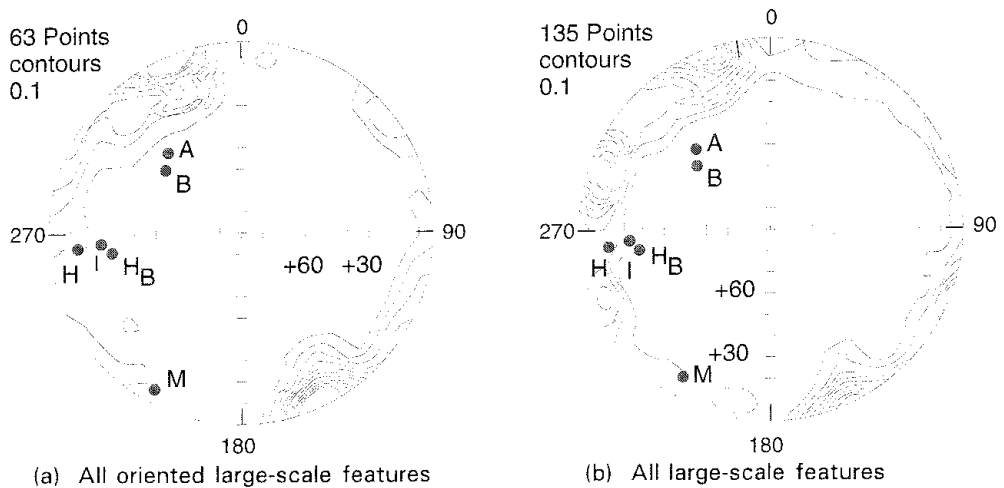


Figure 3-6 Contoured diagrams of poles to the major fracture/fault zones in the Stripa Mine (Gale et al, 1991).

The diagram on the left includes all oriented large-scale features, while the diagram on the right includes all large-scale features whether oriented or not. The points labelled A, B, H, H_B, I, and M are the poles to the planes of the major features in the SCV site.

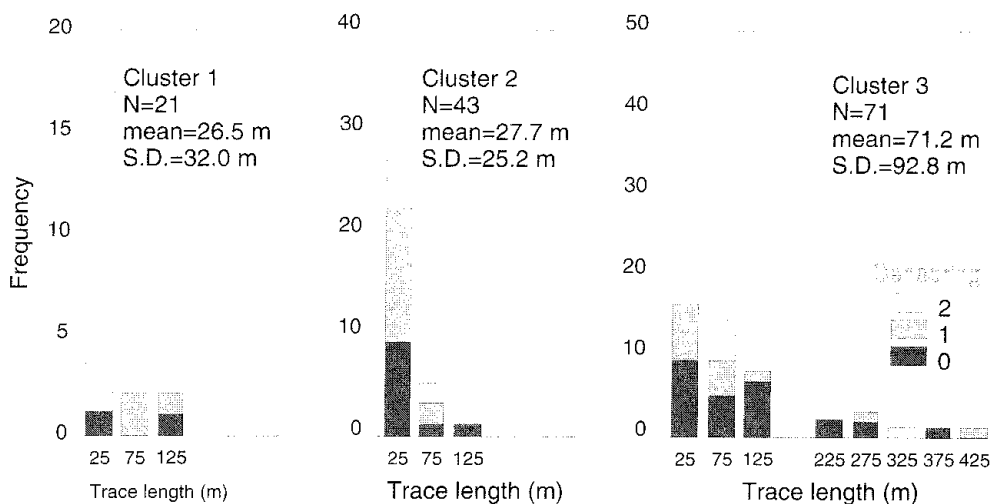


Figure 3-7 Trace-length histograms for all large-scale features in the Stripa Mine (Gale et al, 1991).

N is the number of trace-length measurements and *S.D.* is the standard deviation.

Considering the geometry of the Stripa mine and the location of the major features within the mine, the measurements of the poles to the major fracture zones indicated that the SCV site was intersected by several distinct north-trending fracture zones, denoted as H and I, a less distinct northeast-trending group, denoted as A and B, and a rather indistinct northwest-trending set represented by major feature M. All of the major features identified within the SCV site had orientations that were similar to the major fracture-zone groups identified on both the regional maps and the old mine maps. The orientation of the A and B features coincides closely with the orientation of both the sub-horizontal fracture set and the fringe of the north-south trending fracture set in the SCV site. The orientations of the H and I zones are very close to the mean orientation of the north-south fracture set, which is the most abundant set in the SCV site. It was concluded that the features in the SCV site are not inconsistent with the local and regional orientation patterns of the major features in the Stripa mine.

H Zone

Based on geophysical data, the strike of the H zone was calculated to be N10W with a dip of about 70° to 80° to the east. With this orientation, the projected intersections of the zone with the existing mine drifts were confirmed at the 310 m, 360 m, and 410 m levels. Based on drift- and borehole-mapping data, the overall geometry of the H zone was determined to be planar. However, while the zone maintained its overall dip, its southerly extension appeared to be offset or to change strike where it crossed the drifts at the 360 m level. The width of the H zone appeared to vary with both strike and dip, ranging from 2.15 m to 4.25 m across that portion of the zone which was most intensely fractured.

The H zone is characterized by a red color, or alteration, when it is exposed in the drifts and when it intersects the drill core. Selected fracture planes within the main portion of the zone are filled with breccias or mylonites, up to several cm in width, consisting of fragments of granitic rock. The fragments are generally up to several millimetres in diameter and may be angular or rounded, with the interstices between fragments filled with chlorite, sericite, epidote, carbonite, hematite, and other opaque minerals, fluorite, clay, and finely comminuted quartz and feldspar grains.

3.1.5 Fracture Characteristics

In order to develop a simulation model for the groundwater flow system at Stripa, it is necessary to know the permeability and porosity of the rock mass. These two parameters depend upon the orientation and frequency of fracturing and the state of *in situ* stress in the rock mass.

Fracture Frequency

Fractures intersecting the drill cores from the boreholes and walls of the drifts in the mine were mapped to determine their orientation, trace-length distribution, and spacing or frequency. Four main clusters or sets of fractures were identified from a combination of data from the walls and floor of the Buffer Mass Test drift and from a number of boreholes drilled from that drift. The trace lengths of the fractures in these clusters ranged upward to 4 m to 12 m, with a dominant spacing of less than 1 m to 2 m but with some maximum spacings of about 4 m to 9 m. The density of fractures within these clusters, defined as the total area of fractures per unit volume of rock, ranged from about 0.91 fractures/m to 2.64 fractures/m.

Fracture frequencies were computed for all of the core obtained from the boreholes. Although the fracture frequencies within given depth intervals exhibited log-normal distributions, there was no clear variation of fracture frequency with depth in the upper 200 m to 300 m of the rock mass at Stripa. However, as shown in Figure 3-8, the data from boreholes SBH1, SBH2, V1, and V2 show a general overall decrease in fracture frequency with depth. This trend may be related to a reduction in the number of sub-horizontal fractures with depth as observed in the V2 borehole between depths of 410 m and 1 320 m.

Permeability

In a ten-year period beginning in 1976, more than 1 000 hydraulic packer tests were performed in boreholes at Stripa. The permeabilities derived from these test data were summarized at the end of the hydrologic investigations in Phase 1, and, as shown in Figure 3-9, there exists a strong tendency for the permeability to decrease with depth (Carlsson and Olsson, 1985). The "stair-steps" in the permeability-depth plot correspond to different layers of finite elements in an EPM model developed to simulate the hydrology in and around the SGAB site in the Stripa mine. The permeabilities derived from packer injection tests in the three surface boreholes SBH1, SBH2, and SBH3 are shown in Figure 3-10. Based on the

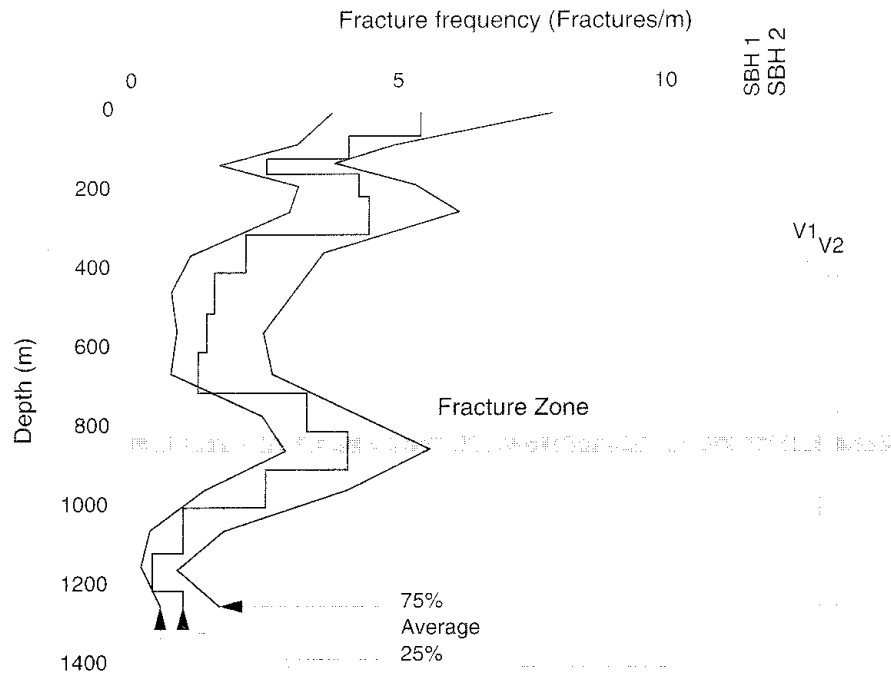


Figure 3-8 Average fracture frequency as a function of depth based on core logs from boreholes SBH1, SBH2, V1, and V2 (Carlsson and Olsson, 1985c).

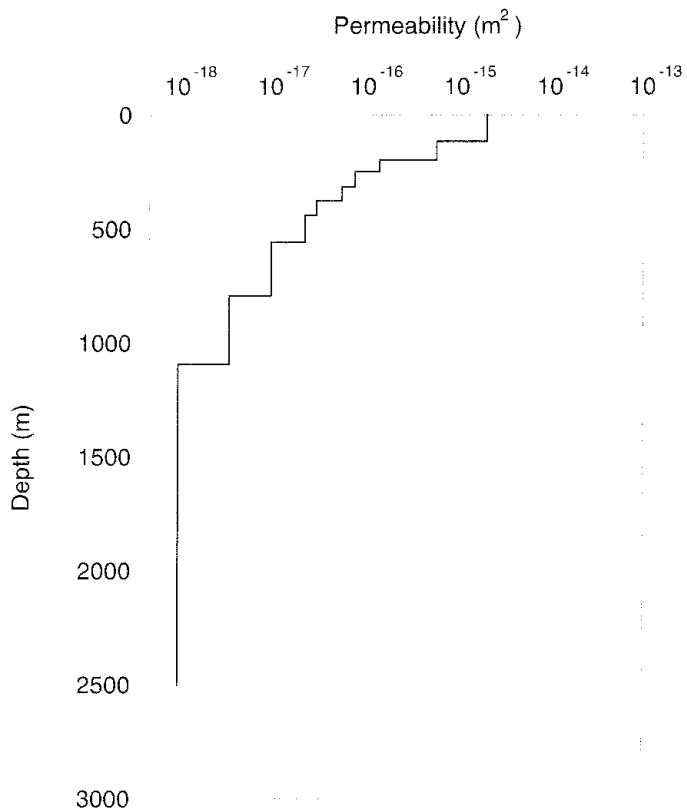


Figure 3-9 Plot of permeability as a function of depth for the Stripa area (Carlsson and Olsson, 1985c; Gale et al, 1987).

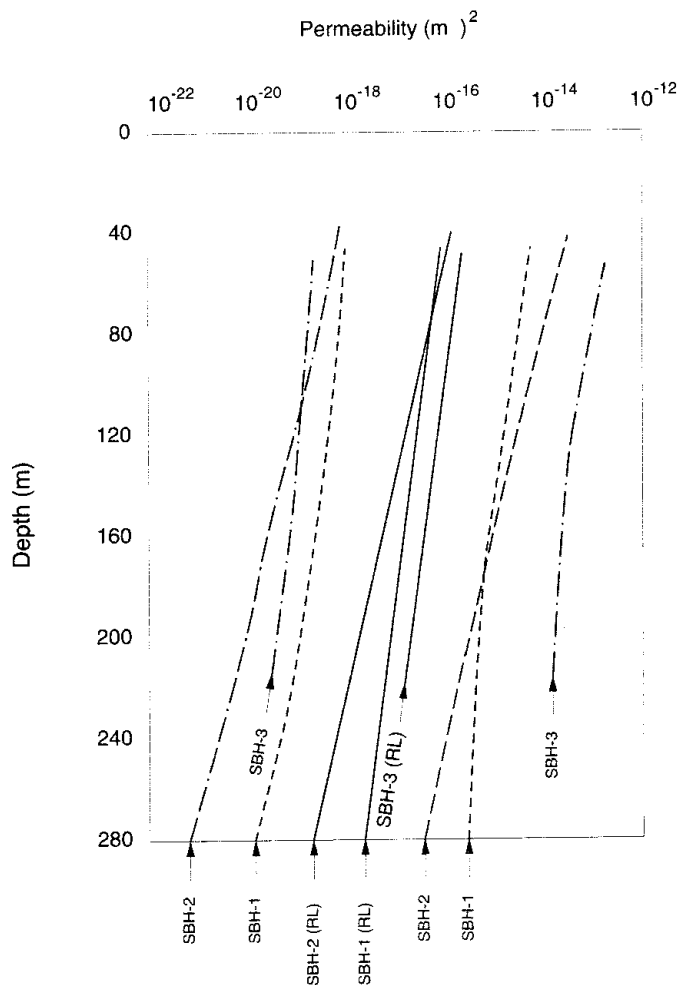


Figure 3-10 Equivalent-porous-media permeability as a function of depth for the three surface boreholes at Stripa (Gale and Rouleau, 1986; Gale et al, 1987).

The least-squares regression lines, designated by RL, are based on data from borehole hydraulic-packer tests for 2 m test intervals. The diagram also shows, for each borehole, the 95% confidence bands within which data from any given test interval will fall. These bands indicate the scatter in the data at different depths.

magnitude and orientation of the *in situ* stresses in the rock mass in which these three boreholes were located, as well as the orientation of the boreholes and the fractures intersected by the boreholes, the permeabilities of the rock surrounding borehole SBH3 should be less than those for the rock mass containing boreholes SBH1 and SBH2. This was found to be the case.

The directional permeabilities of the rock mass at Stripa were assessed by analyzing the data obtained from the packer tests in the three surface boreholes, and by generating fracture network models. The models were used to compute the relative flux rates through the networks for a full range of flow directions as a function of the geometric characteristics of the fractures in the Stripa rock. The fracture network analysis showed that the fracture geometry at Stripa would result in preferred flow rates in the north-

south direction in the horizontal plane, and in the east-west direction in the vertical plane. Fractures intersecting the east-west vertical section generally have a north-south strike, while those intersecting the north-south vertical section generally exhibit an east-west strike. However, fractures with a north-south strike are sub-perpendicular to the maximum principal stress direction. Thus, the effects of fracture geometry and *in situ* stress tend to cancel each other to some degree. The assessment of the permeability data from the three surface boreholes suggested that the maximum *in situ* permeability was oriented in the east-west direction. This implied that the effects of stress on fracture permeability tend to override the effects of fracture geometry.

Porosity

One of the significant parameters in fracture hydrology is the volume of pore space that controls groundwater movement and, in particular, how this pore space is distributed throughout the rock mass. This pore space is known as the effective, or flow, porosity. However, there can be a significant amount of dead-end pore space that does not affect water movement, but which can influence the geochemical and isotopic characteristics of the groundwater through the diffusion/mixing process. The total fracture porosity includes all fracture openings whether they contribute to the flow process or not. The effective and total porosities of the fractures at Stripa were determined in the laboratory and by evaluation of field data from the borehole packer tests and fracture mappings.

In the laboratory tests, resin was injected into a fracture in a rock core from the Stripa mine, while the fracture was subjected to the normal stress at which steady-state flow tests had been conducted. Subsequently, a number of cross-sections through each core were prepared, and the resin thickness and fracture aperture, which included the fracture pore space not filled with resin, were carefully measured. The mean resin thicknesses, which should be indicative of the effective porosity, were less than an order of magnitude greater than those calculated from the steady-state hydraulic flow test data. The size distribution of the pore structure within the fracture plane could be approximated by a log-normal distribution. In addition, the aspect ratio, defined as the ratio of the length of the pore to its width, appeared to be distributed in a log-normal fashion.

The effective and total porosities of the Stripa rock were also obtained by combining the aperture data from both the borehole packer tests and laboratory studies with the fracture statistics for trace length and spacing. The mean effective porosity of the fractures in the rock mass, as determined from the field data, was about an order of magnitude less than that computed on the basis of the hydraulic data from the laboratory tests on single fractures in the core samples. In addition, the porosity calculated from the resin-thickness data for the fractures in the core was almost two orders of magnitude greater than that computed from the field data. A probability plot of smooth and rough fracture apertures for single fractures, as computed from borehole injection test data, is given in Figure 3-11.

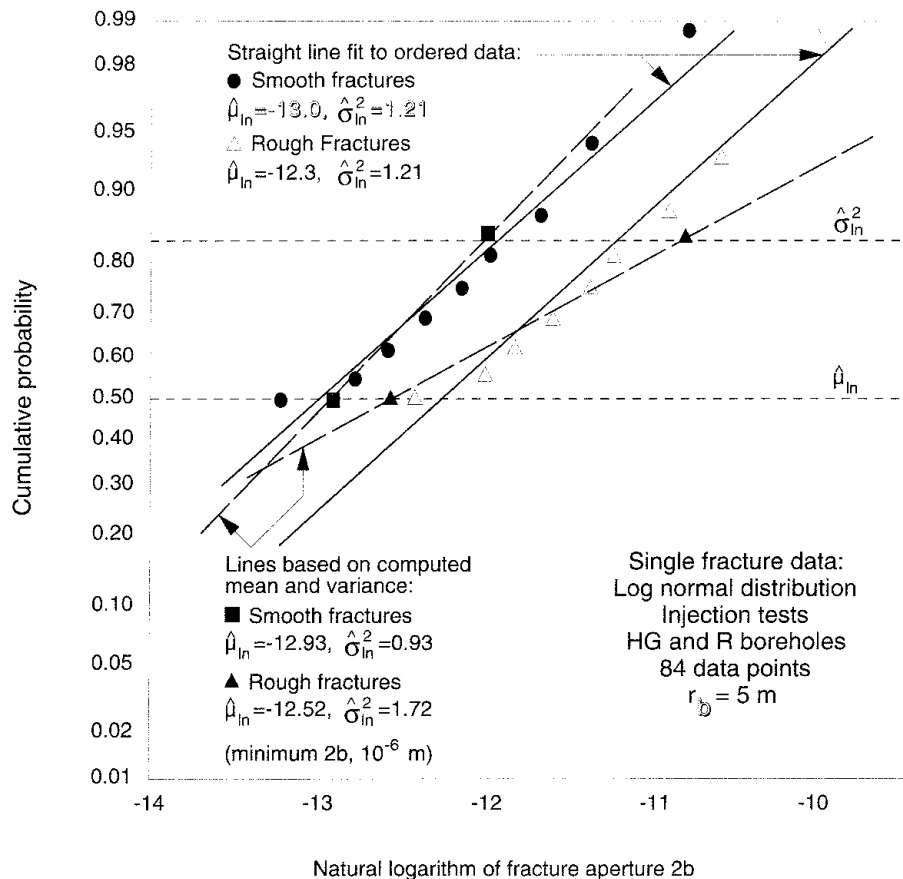


Figure 3-11 Probability plot of smooth and rough fracture apertures for single-fracture injection test data from boreholes at the Buffer Mass Test site in the Stripa Mine (Gale and Rouleau, 1986).

The fracture aperture is expressed in metres and is equal to $\exp(n)$ where n is the abscissa of the graph.

3.1.6 Hydrology

As shown in Figure 3-12, the Stripa area has a number of large and small lakes, all of which define the interface between the surface and subsurface water, and are areas of known hydraulic head. The topography is typical of preCambrian shield terrains. The surface facilities of the Stripa mine are situated at an elevation of about 140 m above sea level on the northeast side of a northwest trending valley system that rises from the 60 m level of Lake Råsvalen, located southeast of the mine, to about 250 m of elevation to the northwest. The total annual precipitation for the Stripa area is about 780 mm/yr. The annual evapotranspiration is about 480 mm/yr, with the remainder contributing to both runoff and recharge (Carlsson and Olsson, 1985c). Since recharge rates in areas of good soils are about 7 to 15%, the best estimates for the Stripa area, considering the top soil and outcrops of rock, were estimated to be about 2 to 4% of the difference between the annual precipitation and evapotranspiration.

Although very little hydrographic data were available for the streams in the area, there was considerable information on the pumping rate, or

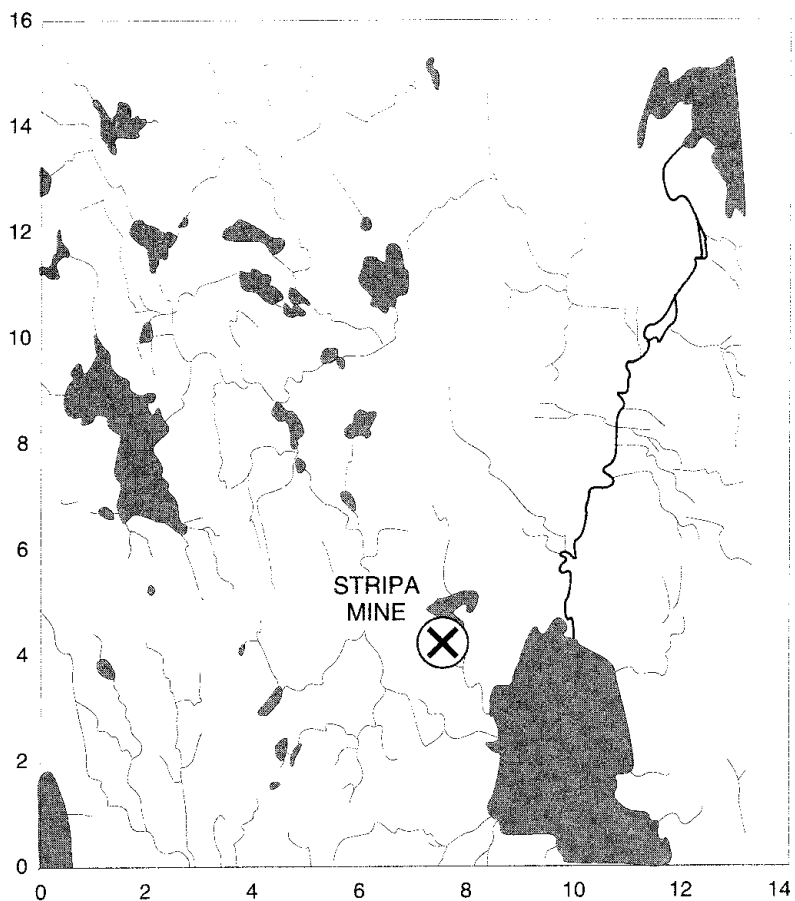


Figure 3-12 Map of the lakes and drainage systems in the Stripa area (Gale et al, 1987).

The location of the mine is marked with a X on the map. The tailings pond is located immediately north of the mine, and Lake Råsvälen to the southeast. The scales are distances in kilometres.

groundwater discharge, from the mine and on the rainfall in the immediate mine area. Based on data collected in 1985 and 1986, the average pumping rate from the mine was determined to be in the range of 480 l/min to 500 l/min.

The Stripa mine acts as a large regional groundwater sink due to the combination of the underground mine workings and the discharge of groundwater from the mine by pumping. As shown in Figure 3-13, the water pressure measurements in boreholes SBH1 and SBH3 indicated a deviation of the pressures from the hydrostatic condition, with a distinct change in hydraulic gradient beginning at a depth of about 100 m. No measurements were made below a depth of 100 m when borehole SBH2 was drilled. The data from borehole SBH3 indicated that the perturbations in the gradient began at the surface. These gradients confirmed the expected drainage effect of the old mine workings. Moreover, measurements made in a flowing borehole on the 410 m level of the mine indicated gradients directed upward, suggesting that groundwaters from a deep flow system were discharging upward into the mine (Olkiewicz et al, 1978).

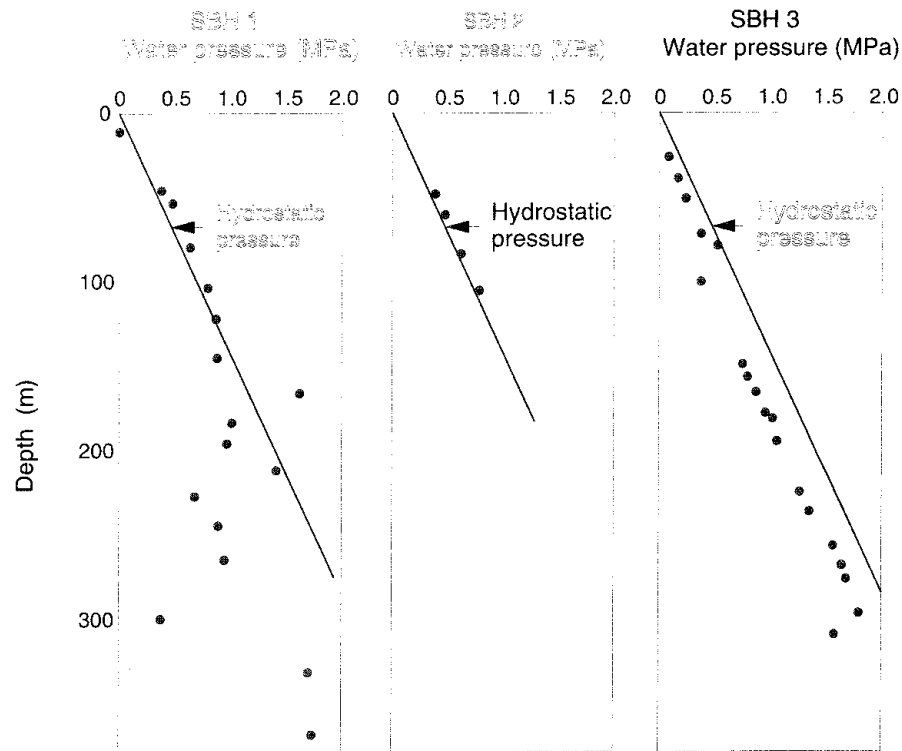


Figure 3-13 Measurements of the groundwater pressure in the three surface boreholes at Stripa (Gale, 1981).

The data points represent the pressure measurements at the midpoints of the test sections in the boreholes.

Data from hydraulic head measurements in packed-off intervals in boreholes during the macropermeability experiment in the SAC programme showed a pattern of increasing hydraulic head with increasing distance from the drift (Witherspoon et al, 1980). Figure 3-14, based on hydraulic head data from the surface boreholes and the boreholes at the SGAB site, illustrates the variation of hydraulic head in different boreholes as a function of distance from the nearest drift. Apart from borehole V2, which was thought to be influenced hydraulically by sub-vertical fracture zones encountered in the borehole, the hydraulic heads in the other four boreholes approach hydrostatic conditions at distances of about 200 m from the nearest drift. This observation suggested that the Stripa mine perturbs the flow system much more vertically than it does horizontally.

3.1.7 Geochemistry

The dating of groundwater by means of radioisotopes can be misleading because calculations of fluid residence time depend on the transfer mechanisms of solutes between rock and groundwater (Executive Summary of Phase 2, 1989). The notion that salt in fluid inclusions within the granite matrix significantly affects the salt balance in the groundwaters at Stripa imposes serious limitations on conclusions derived from Cl isotopes and salt-mixing models. It also has implications for the determination of total porosity of the rock because of the uncertainty in the degree and rate of communication of "dead end" inclusion volumes within the flow porosity.

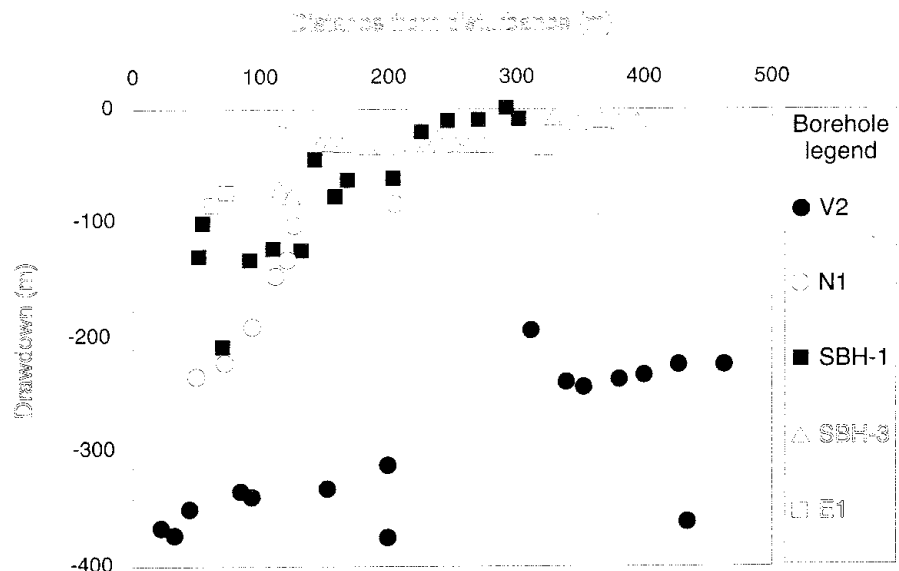


Figure 3-14 Plot of the difference in hydraulic head between an assumed hydrostatic pressure and the measured pressure in surface and underground boreholes as a function of distance from the nearest drift (Carlsson and Olsson, 1985c).

Radioisotopes

The summary of residence-time estimates for a number of isotopic systems given in Figure 3-15 confirms the presence of actively circulating modern water at shallow depths at Stripa, underlain by apparently much older, saline water (Nordstrom et al, 1985; Andrews et al, 1986; Andrews et al, 1988). The calculations of the apparent ages of the groundwaters from measurements of ^3H and ^{14}C are probably the most reliable of the radioisotope-tracer ages shown in the diagram. The "age" of the deep groundwater, based on the ^{14}C , is of the order of 25,000 yr. Tritium levels in some samples of deep groundwater indicate that shallow water is mixing down to the deeper levels, probably due to dewatering of the mine in concert with the steeply-dipping fracture zones and the resultant change in the groundwater flow pattern. Residence-time estimates based on ^{36}Cl depend on the choice of the model used to describe the source of the salt and the relative residence times in granite as compared to leptite, and strictly pertain to the solute rather than to the fluid. Residence times in excess of 100,000 years were reported for water samples from boreholes V1 and V2, although, at that time, the relative importance of Cl derived from fluid inclusions compared to that derived from leptite was not clear (Executive Summary of Phase 2, 1989).

Stable Isotopes

There exists a significant difference in the contents of heavy isotopes of oxygen and hydrogen in the shallow and deep groundwaters of the Stripa mine, with the deepest waters being approximately 2% and 10% to 15% lower in ^{18}O and ^2H , respectively, than shallow domestic well waters (Fritz et al, 1979). This difference may be due to recharge at high elevations for the deep groundwaters, or possibly because of recharge during cooler

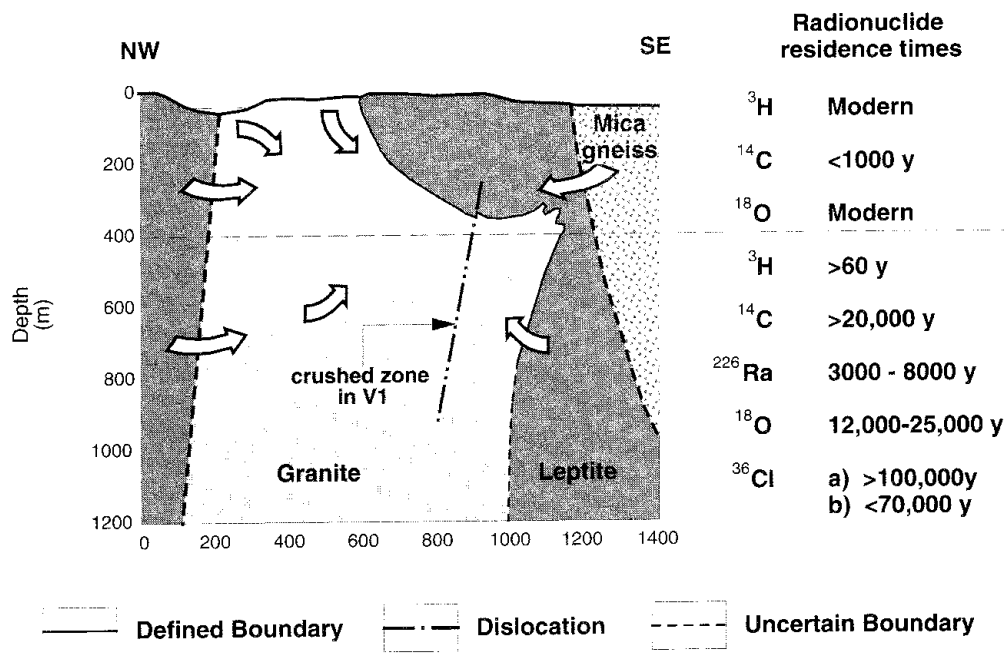


Figure 3-15 Geologic cross-section of the Stripa area illustrating the upper and lower geochemical zones and associated isotopic data for each zone (Gale et al, 1990c; Compilation based on data and conclusions of Nordstrom et al, 1985).

Shallow water and deep water are drawn into the area of the mined openings and form a mixed water.

climatic conditions in the past. Recharge at distant high elevations has been discounted, but not disproved. Because of the wide-spread occurrence in Europe of groundwaters that are depleted in the stable isotopes, along with the similarity to Stripa waters in ages and deuterium excess and the likelihood that the isotope depletions represent a period of cooler climate, the ^{18}O and ^2H depletions in the deep Stripa waters strongly suggest an age in excess of 10,000 years. This age estimate pertains directly to the water and is independent of solute and rock.

3.1.8 Simulation of the Groundwater Flow System

The purpose of developing a numerical hydrologic model of the Stripa area was to determine the configuration of the groundwater flow system in the fractured bedrock on a regional scale and in the immediate vicinity of the mine. By knowing this configuration, the regional recharge and discharge areas could be identified, along with the pathways or flow lines that the groundwater follows in moving from a recharge area to a discharge area and the associated residence times. There was also interest in determining how the configuration and residence times were affected by the presence of the mine, changes in the hydraulic properties of the bedrock, and major faults or fracture zones. This information would allow the source of the water discharging into the mine to be identified, and indicate whether the calculated residence, or travel, times were compatible with the measured chemical and isotopic signatures. To this end, finite-element models were constructed to accommodate the regional and local scales of the Stripa area

and the mine, respectively. The regional model encompassed a surface area of approximately 100 km², and the local model, centered on the mine, covered an area of approximately 20 km². The computations were performed with the computer code CFEST (Coupled Fluid, Energy, and Solute Transport), which is capable of solving three-dimensional coupled problems by the finite-element method (Gupta et al, 1986). The CFEST code, based on the concept of an equivalent porous medium, has been applied and verified on a number of test cases involving groundwater systems.

Finite-Element Model and Boundary Conditions

The plan view of the finite-element grid for the regional numerical model is shown in Figure 3-16. The distribution of the three major rock types, namely granite, leptite, and meta-sediments, represents a simplified bedrock geology which, along with the major fracture zones, was approximated from published maps of the Stripa area (Koark and Lundstrom, 1979). The grid, which extends to a depth of 3,000 m, encompasses a volume of about 300 billion m³. The finite-element grid for the local model, representing the immediate mine area shown in Figure 3-17, incorporates the bedrock geology and the major fracture zones. This model encompasses a surface area of about 20 km², extends to a depth of 3,000 m, and represents a volume of about 60 billion m³. The mined-out cavities within the mine were developed over a vertical height of 60 m or more, and plunge at a steep angle from the old surface workings on the west side of the mine to the 410 m level on the east side of the mine over a horizontal distance of about 1 km. The mined-out cavities were assigned a fixed hydraulic head, equal to the elevation head, at the nodal points at or near the mine drifts. The grid includes the 400 m deep mine shaft on the west side of the mine, the 360 m deep ventilation shaft near the experimental excavations on the northeast, and the 360 m deep Z shaft on the extreme northeast. The surface nodal point representing each shaft and each node along the depth of the shaft were assigned fixed elevation heads.

The size and shape of each element and the nodal point locations were chosen to best represent the actual topography and bedrock relationships in the area being modeled. The major fracture zones were represented by discrete elements with a width of 5 m. Two different fracture zones, trending northwest and east-northeast, were included in both finite-element grids.

Hydrologic Properties

The finite-element grid for the regional hydrologic model contained seven layers in the vertical direction, and the local model contained eleven layers, to a common depth of 3 km. The hydraulic properties were prescribed as constants within each layer. Three separate sets of properties, or three cases, were examined with the regional model. In the first case, known as the "uniform" case, all layers, including the fracture zones, were assigned a constant hydraulic conductivity of 10⁹ m/s and a constant porosity of 0.1%. In the second case, known as the "rock" case, there was no differentiation in hydraulic conductivity for the granite, leptite, and meta-sediments. On the basis of field data, logarithmic decreases in hydraulic conductivity and

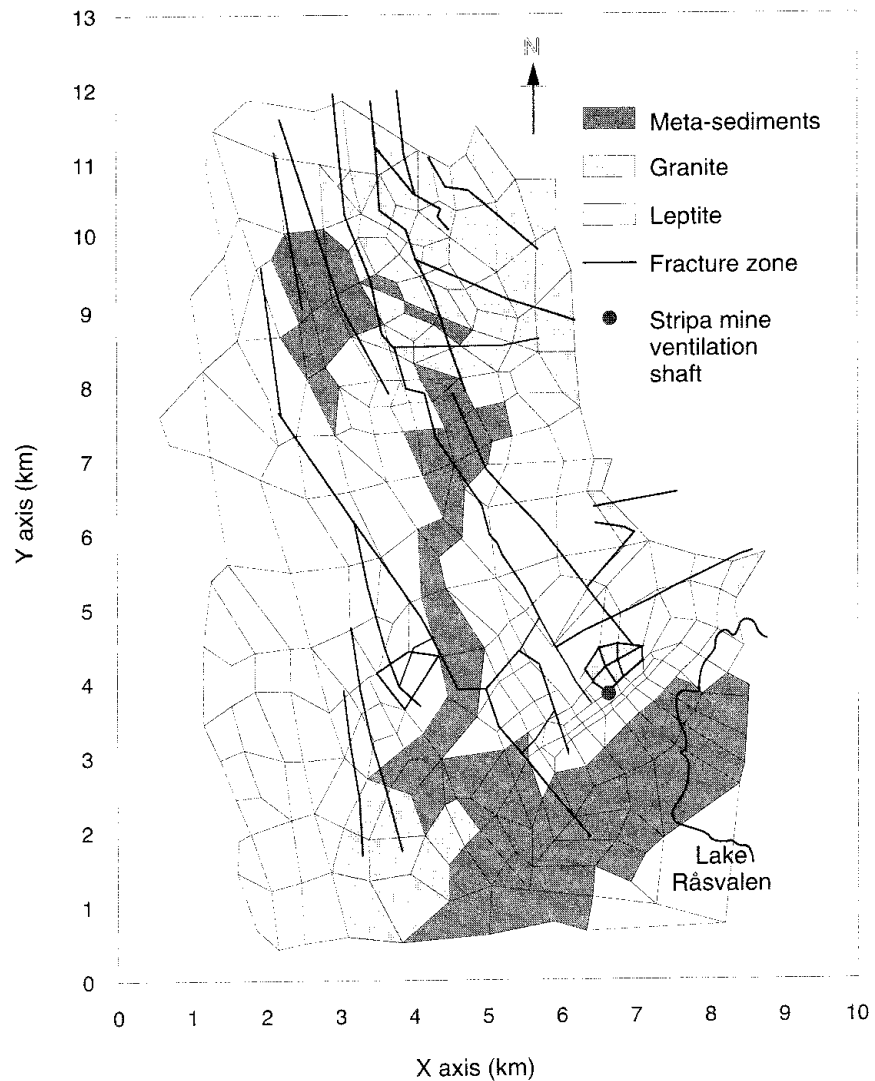


Figure 3-16 Plan view of the finite-element grid for the regional hydrologic model of the Stripa area (Gale et al, 1987).

The model is based on the simplified bedrock geology for the Stripa area, and includes the location of major lakes and fracture zones as indicated by the heavy black lines. The ends of the three referenced cross sections are indicated by E-W, NE-SW, and NW-SE. The ventilation shaft at the Stripa Mine is indicated by the black dot.

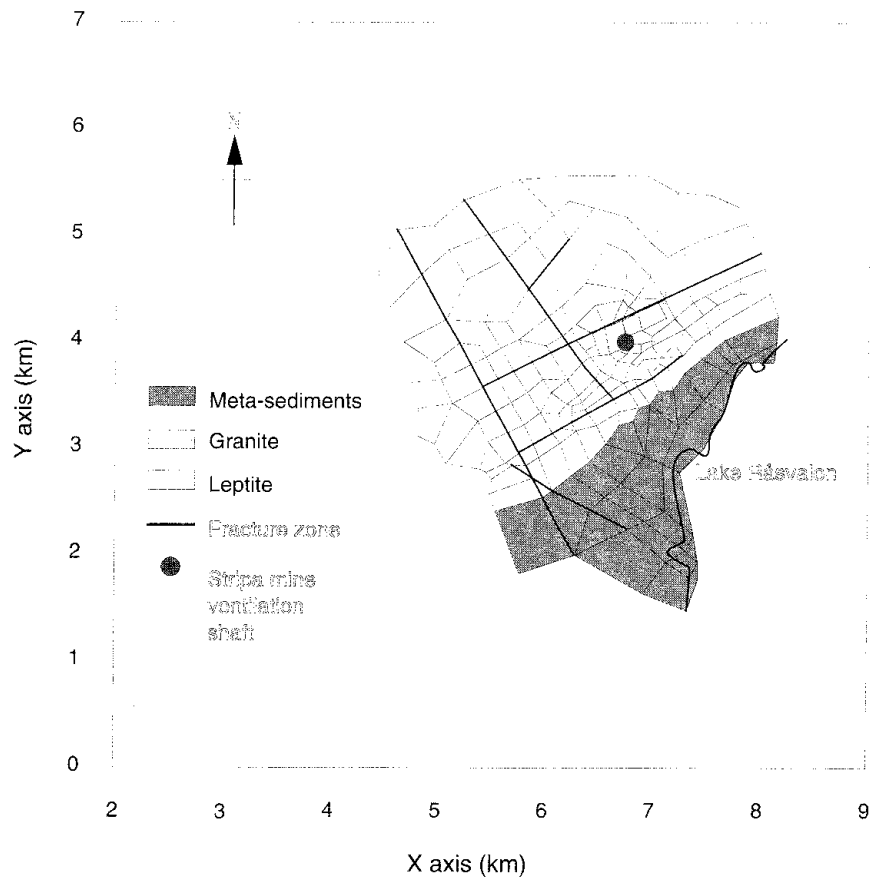


Figure 3-17 Finite-element grid for the local hydrologic model of the Stripa area (Gale et al, 1987).

The model is based on the simplified bedrock geology for the Stripa area, and includes the mine-tailings pond, Lake Råsvälen, fracture zones indicated by heavy black lines, and the ventilation shaft at the Stripa Mine indicated by the black dot.

porosity with depth were assumed and prescribed as shown in Figure 3-18 to the vertical layers of elements. The hydraulic conductivity in the vertical direction was taken to be different from that in the horizontal direction. The fracture zones were assigned values of hydraulic conductivity and porosity that were one order of magnitude greater and two orders of magnitude greater, respectively, than those for the rock mass in the same layer. For the third case, known as the "rocks" case, three different bedrock units and two different fracture zones were simulated. The values of hydraulic conductivity and porosity assigned to each layer were those shown in Figure 3-18.

Two different sets of hydraulic properties, or cases, were considered for the local model. The first case, known as the "rock" case, assumed a single rock type in which all the fracture zones had the same hydraulic properties. Based on field data, the hydraulic conductivity and porosity of the rock mass were assumed to decrease with depth in a logarithmic fashion. In the second case, known as the "rocks" case, three rock types and two fracture zones with differing properties were assumed. The variations in hydraulic conductivity and porosity with depth were similar in form to those illustrated

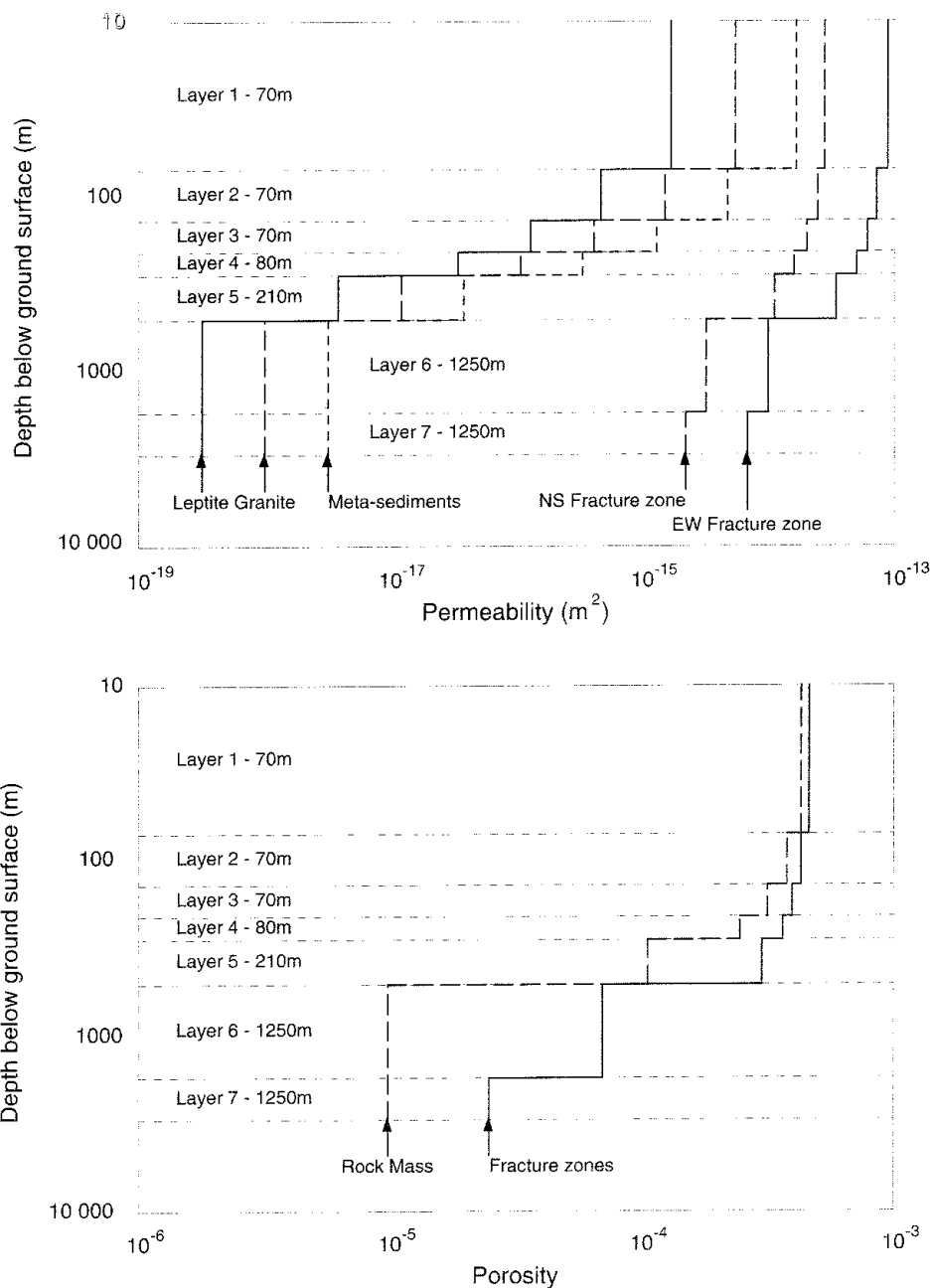


Figure 3-18 Vertical distributions of permeability and porosity used in the regional hydrologic model of the Stripa Area (Gale et al, 1987).

in Figure 3-18, except for eleven layers of finite elements as compared to seven layers for the regional model.

Model Calibration

The groundwater discharge from the Stripa mine by pumping was used as the principal calibration parameter for the two hydrologic models. The isopotentials at each nodal point in the grid located on the mine shafts and mine drifts were set equal to the elevation of that nodal point. Thus, below the water table, these nodal points represented points of groundwater

discharge into the mine. The sum of the discharges from these nodal points under steady-state conditions was assumed to give an estimate of the total groundwater discharge from the mine for the given set of hydraulic properties and boundary conditions. The "rock" case gave the best match between the measured and computed groundwater discharge rates from the mine for both the regional and local models, yielding 534 ℓ/min and 485 ℓ/min , respectively, as compared to a measured average discharge rate of 480 ℓ/min to 500 ℓ/min . The discharge rate computed with the local model should be somewhat greater than the measured discharge rate because the groundwater removed by the mine ventilation system was not taken into account.

The boundary condition at the surface for both the regional and local hydrologic models was the contour map of the water table within the region. The elevation distribution of the water table was determined by smoothing the contour elevations, which made the water table a subdued reflection of the topography. Thus, recharge calculations were avoided. Because each layer within a model had a uniform thickness, the top of the layer reflected the shape of the water table. By locating nearly all of the periphery of the surface "footprint" of the regional model along streams, rivers, lakes, and topographic/drainage divides, conditions of fixed head could be specified at these boundaries. All of the geologic boundaries, including the fracture zones, were assumed to be oriented vertically.

Isopotential Distribution of Groundwater Head

An example of the computed distribution of isopotentials of groundwater head at a depth of 290 m in the Stripa area is shown in Figure 3-19. This distribution, obtained with the regional model for the "rock" case, illustrates the rather limited influence of the mine workings on the distribution of isopotentials. In particular, the groundwater head is perturbed significantly only within about one mine "diameter" of the mine workings. This rather limited zone of influence around the mine workings is shown in more detail in Figure 3-20 at a depth of 180 m, for which the distribution of isopotentials was calculated with the local hydrologic model for the "rock" case. The distribution of isopotentials of groundwater head in cross section, shown in Figure 3-21, indicates that the mine workings influenced the groundwater system to a depth of 3,000 m or greater. The rather steep hydraulic gradients computed with the local model for the immediate vicinity of the mine were consistent with the gradients observed in boreholes drilled from the underground drifts, as shown previously in Figure 3-14.

Examples of the distribution of recharge and discharge at different depths in the Stripa area, calculated with the regional hydrologic model for the "rock" case, are shown in Figure 3-22. The outline of an area of recharge or discharge was computed by calculating the difference between the hydraulic heads of two adjoining layers of elements in the regional model. Areas in which the hydraulic heads decrease with depth were assumed to be recharge areas, and areas in which the heads increase with depth were assumed to be discharge areas. The discharge areas shown in Figure 3-22 generally correlate with the existing lakes.

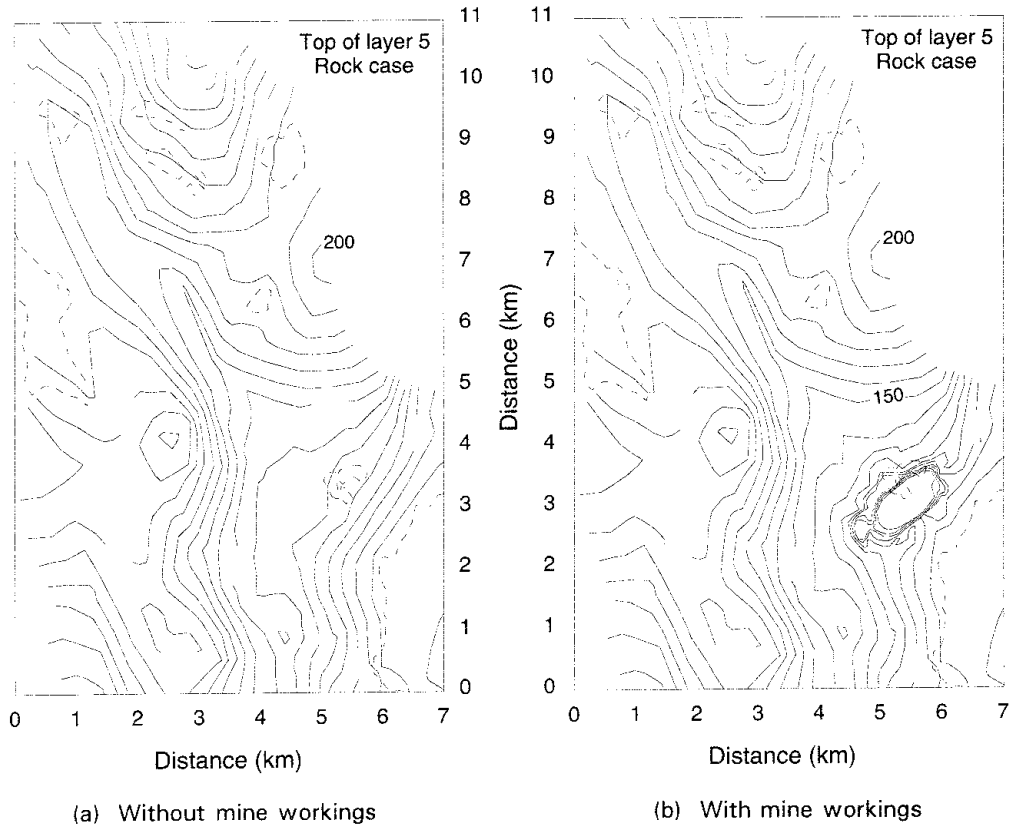
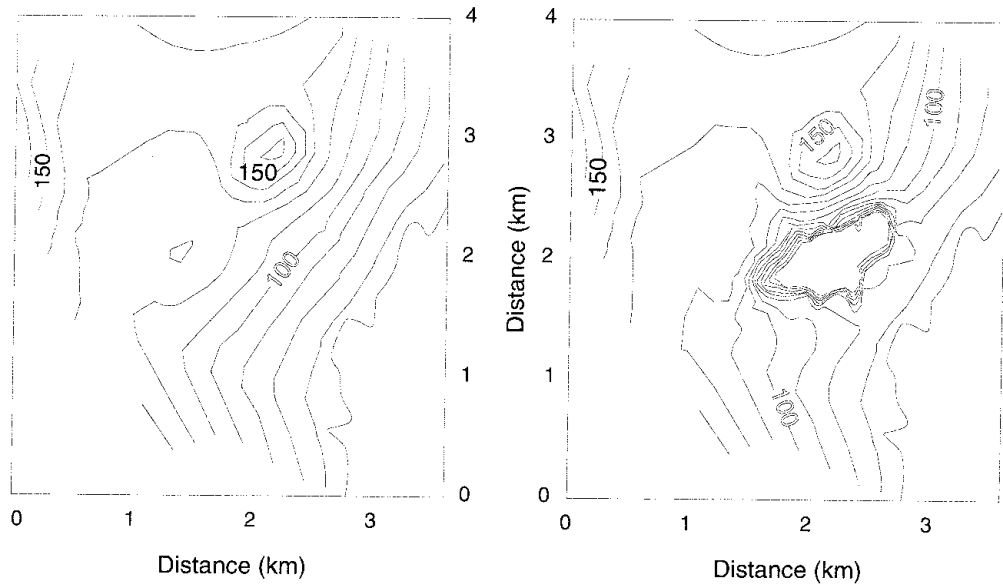


Figure 3-19 Distribution of isopotentials of groundwater head in plan view at a depth of 290 m in the Stripa area (Gale et al, 1987).

The shore lines of the lakes are shown as dashed lines. The results, in terms of metres of head, were obtained with the regional hydrologic model, assuming a single rock type and a logarithmic decrease in hydraulic conductivity with depth.

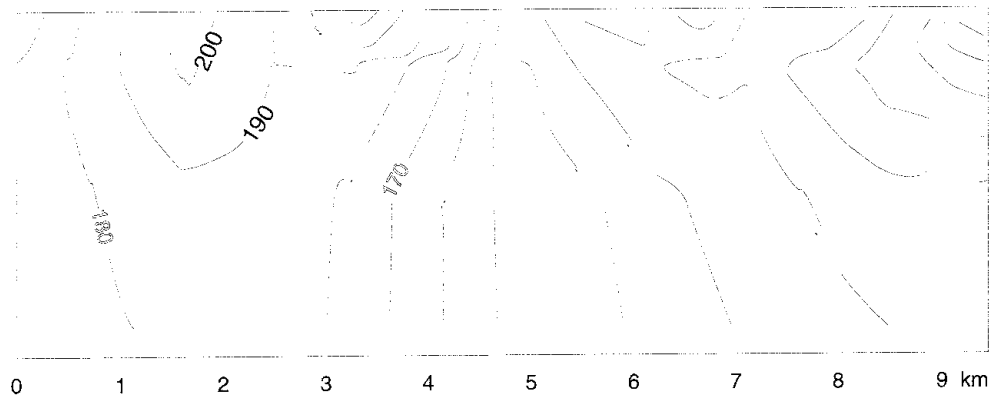


(a) Without mine workings

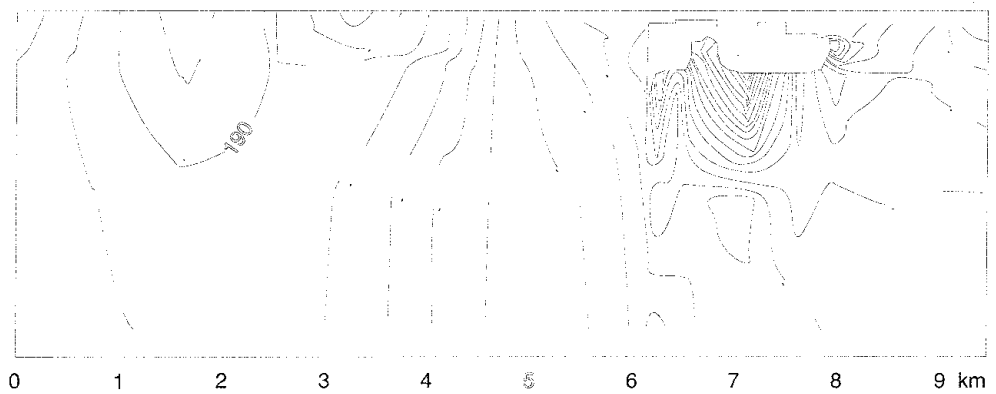
(b) With mine workings

Figure 3-20 Distribution of isopotentials of groundwater head in plan view at a depth of 180 m in the immediate vicinity of the Stripa Mine (Gale et al, 1987).

Lake Råsvalen is shown as the clear area on the lower right-hand side of each figure. The results, in terms of metres of head, were obtained with the local hydrologic model, assuming a single rock type and a logarithmic decrease in hydraulic conductivity with depth.



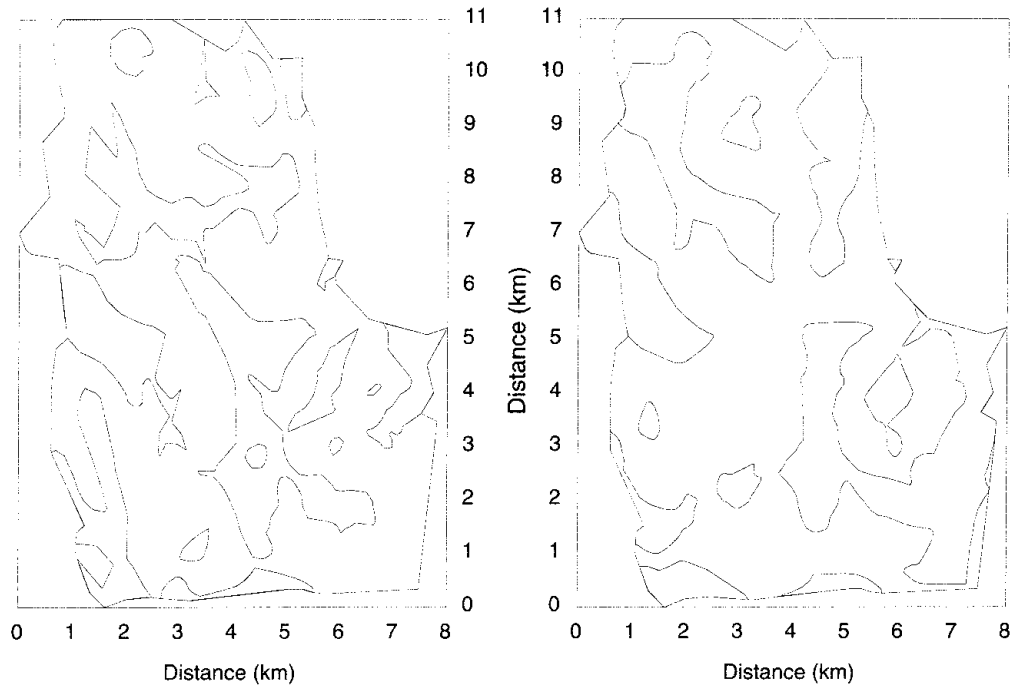
(a) Without the mine workings



(b) With the mine workings

Figure 3-21 Distribution of isopotentials of groundwater head in a NE-SW cross section through the Stripa Mine and the surrounding area (Gale et al, 1987).

The results were obtained with the regional hydrologic model, assuming a single rock type and a logarithmic decrease in hydraulic conductivity with depth.



(a) Depth interval: 0 to 56 m

(b) Depth interval: 136 m to 180 m

Figure 3-22 Distribution of areas of discharge (stippled) and recharge (clear) at several depths in the Stripa area (Gale et al, 1987).

The shore lines of lakes are shown by the dashed lines. The results were obtained with the regional hydrologic model, assuming a single type of bedrock and a logarithmic decrease in hydraulic conductivity with depth.

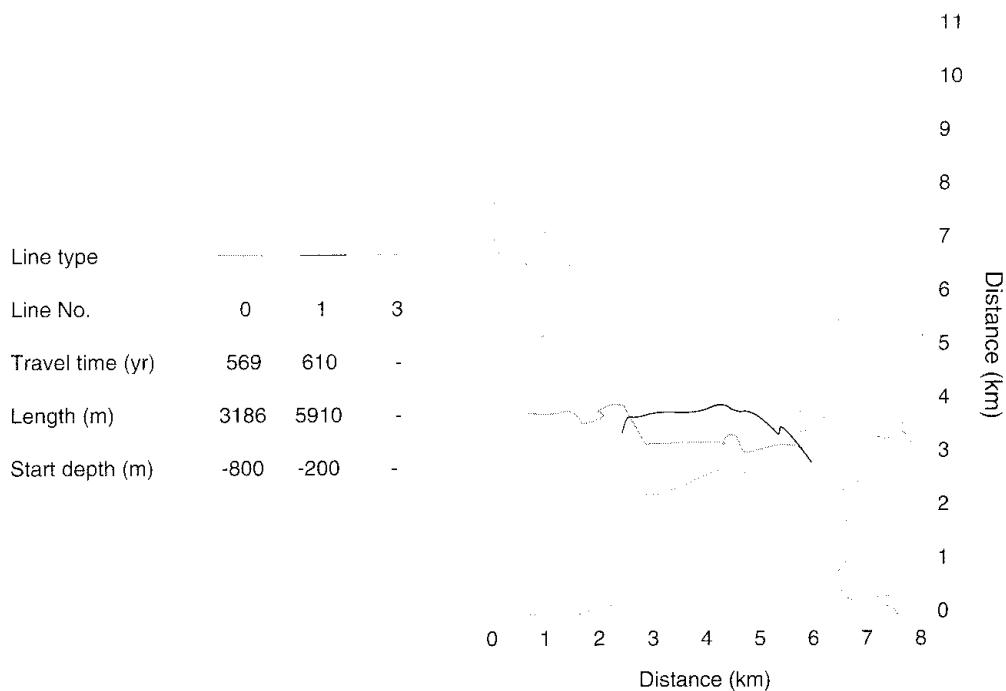


Figure 3-23 Plan view of selected stream lines for different depths and different discharge points in the Stripa Mine (Gale et al, 1987).

The results were obtained with the regional hydrologic model, assuming a single rock type and a logarithmic decrease in hydraulic conductivity with depth.

An example of the pathways followed by a limited number of stream lines in plan view is shown in Figure 3-23. All of the stream lines were initiated from points near the simulated mine workings. The stream line for "rock case 1" represents groundwater that is discharging into the bottom of the mine at a depth of 200 m below sea level. This stream line has a total length of 5 910 m and a travel time of 610 yr. Water that follows this stream line would be recharged on the west side of the regional area and would become part of a deep flow system. However, in the region of the mine acting as a sink, this water is forced upward toward the mine workings. Based on a rather limited set of simulations, the lengths of various stream lines from areas of recharge on the surface to regions of discharge within the Stripa mine ranged from about 3 200 m to 9 100 m, with corresponding travel times between 280 years and 952 years.

3.1.9 Significant Achievements

The three-dimensional hydrologic models of the Stripa area gave groundwater inflows into the Stripa mine of the order of 500 l/min, closely approximating the average pumping rate from the mine. These simulations assumed a single type of bedrock and a logarithmic decrease in hydraulic conductivity with depth. This agreement between the calculated inflow and the pumping rate is remarkably good, considering the dimensions of the area being modelled and the relative sparseness of geologic information and hydraulic data. The volumes of rock represented by the finite-element grids

ranged from 60 billion m³ to 300 billion m³, with surface "footprints" covering 20 km² to 100 km². Apart from the data collected within the mine and in boreholes in the rock above and in the immediate vicinity of the mine, the bulk of the geologic and hydrologic information for the Stripa area was based on surface observations. Notwithstanding this relatively gross level of information, the calculations of the hydraulic gradients within the vicinity of the mine were consistent with measurements made in surface boreholes, and the discharge points of groundwater flow were consistent with the location of lakes in the area. The quantification of the hydraulic conductivity of the rock mass as a function of depth, along with the inclusion of the large observable fracture zones within the model conceptualization, were clearly significant attributes of the computational model. That is, in contrast, assumptions of a uniform hydraulic conductivity within the entire rock mass and different types of bedrock produced inflow rates to the mine that were only about 20% to 50% of the pumping rate.

The computed travel times of the groundwater through the rock mass at Stripa were much shorter than those predicted on the basis of existing geochemical and isotopic data. Although this lack of agreement is disturbing, it must be kept in mind that groundwater flow models based on equivalent-porous-media assumptions traditionally predict fluxes much more accurately than travel times. This is due to the mathematical assumption of linearity of the flow equation within an individual element, coupled with the dimensions of the element as compared to those of the geologic features within the modelled region. The computed streamlines were much longer than expected and indicated that the groundwaters discharging into the mine may have been recharged at a considerable distance from the mine. The general pattern of isopotentials indicated that groundwater recharge and shallow groundwater flow within 3 km of the mine influenced the groundwater discharge into the deepest mine levels. This result supports the hypothesis based on geochemical data that mixing of shallow and deep waters occurs in at least some of the boreholes within the mine. The residence times based on porosities computed from field data were found to be too low, by an order of magnitude, when compared to time estimates based on radioisotopes. However, the higher porosities that were measured in the laboratory by means of the resin-injection technique would provide travel times more consistent with those inferred from isotope studies.

3.2 CONCEPTUAL MODEL OF THE CROSSHOLE SITE

The principal objective of the Crosshole programme in Phase 2 of the Stripa Project was to develop characterization tools and techniques that could be used to obtain information for an evaluation of the suitability of a rock mass for geologic disposal of radioactive wastes. An important criterion was that the techniques should not disturb appreciably the natural conditions within the rock mass. This required, in effect, the use of only a few boreholes. As such, the development focussed on novel remote sensing techniques, primarily borehole radar and high-resolution seismics, the use of tomographic inversion for data interpretation, and some new hydraulic testing concepts. It was intended that the testing techniques could be used in either the single-borehole or crosshole modes. The techniques were applied at the Crosshole site in the Stripa mine and the data were used to provide an

integrated evaluation of the geologic structure and associated hydraulic features of the site. As a matter of evolution in the programme, the data were assembled into a three-dimensional conceptualization of the geohydrology of the site. Comparisons between and among data obtained by the three borehole-testing techniques were used to assess the consistency of interpretation of features within the conceptual geohydrologic model, as well as to demonstrate the credibility of the data interpretation procedures.

The investigations conducted at the Crosshole site and the associated interpretations and comparisons of data have been summarized by Olsson et al (1987a), and the notion of an integrated approach to site characterization, based on the experiences with the Crosshole programme, is discussed by Black and Olsson (1990). The geologic characteristics of the Crosshole site have been summarized in reports by Carlsten et al (1985), Carlsten and Strähle (1985), and Carlsten et al (1985). The development and application of the borehole radar testing technique are described in reports and technical papers by Olsson et al (1983, 1987b, 1989), Olsson and Sandberg (1984), and Magnusson et al (1987). Similar descriptions for the borehole seismic testing method are given in reports and technical papers by Ivansson (1984), Pihl et al (1987, 1990), Cosma (1987, 1990), and Cosma et al (1986). The hydraulic testing techniques are described in reports and technical papers by Holmes (1984), Holmes and Sehlstedt (1986), Black et al (1986), Black et al (1987), Noy et al (1988), and Black and Holmes (1990).

3.2.1 Site Characteristics

The Crosshole site, shown in Figure 3-24, was located on the 360 m level of the Stripa mine and consisted of a rock mass defined by seven boreholes that outlined a tilted pyramid with a height and base of about 200 m. The site was situated immediately south of the SGAB site, with its north boundary defined by borehole E1 which was drilled during Phase 1 to a distance of 300 m at a decline of about 10°. The top of the tilted pyramid was defined by boreholes F1, F3, and F5, which were drilled to distances of 200 m with declines of 10° and strikes ranging from S84E to S58E. The bottom of the pyramid was defined by boreholes F2, F4, and F6, which were drilled to distances of 250 m with declines increasing from 20° to 40° and strikes ranging from S84E to S58E. Boreholes F2, F4, and F6 were situated directly below boreholes F1, F3, and F5, respectively. An old investigation drift, located on the 410 m level and above the pumping level of the mine, was situated immediately below and close to the ends of the "top fan" of semi-horizontal boreholes. The volume of the "tilted pyramid" of rock was about 3,000,000 m³.

The rock mass consisted of a fine to medium grained granite intersected by a few thin, less than 10 cm thick, pegmatites and quartz veins. The fracturing within the granite was concentrated in zones that exhibited high fracture intensities. The fracture zones displayed such features as brecciation, mylonitization, alteration, and red coloring. The "average" granite between the zones was massive, fine to medium grained, and grey to pale red in color.

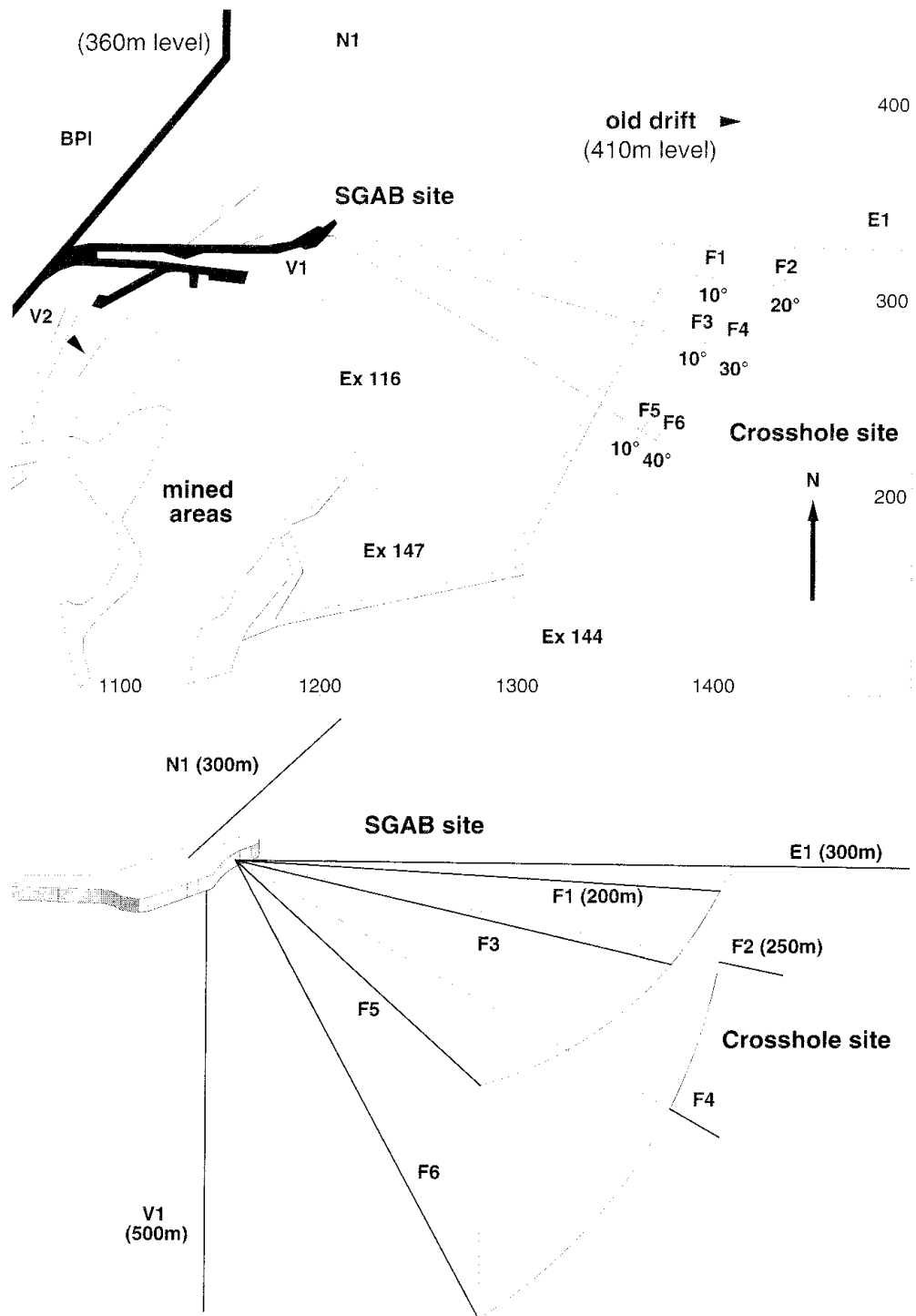


Figure 3-24 Plan and perspective views of the borehole array at the Crosshole site (Carlsten et al, 1985; Black et al, 1987).

The Crosshole site was used for the radar, seismic, and hydraulic investigations in Phase 2. All of the boreholes were drilled from the end of a drift on the 360 m level.

Standard well-logging tests were conducted in each of the F boreholes. The drill cores were mapped by visual observation for rock type, fractures, and fracture minerals. The orientations of the fractures were determined by means of a TV camera that photographed the wall of each borehole. These data indicated that the collection of seven boreholes had intersected five major planar zones of fracturing, designated as A, C, D, E, and F, and one highly fractured zone of limited extent, designated as B, containing small and dispersed cavities and exhibiting high porosity. One minor zone, designated as number 1, was also identified close to the end of the drift on the 360 m level. The strike of the fracture zones was northeast to north-northeast, with steep dips toward the east-southeast or west-northwest. The strikes and dips of the fractures in the "average" rock between the fracture zones were similar to those of the zones.

3.2.2 Scope of the Characterization Activities

Three basic types of data were obtained from the investigations conducted at the Crosshole site. These were:

- Direct observations of the geologic characteristics from rock core and on the borehole walls, and measurements of physical properties of the rock along the boreholes
- Radar and seismic measurements of the physical properties of the rock in the space between boreholes
- Measurements of the hydraulic properties of the rock immediately surrounding the boreholes and in the extensively fractured zones between boreholes.

It must be kept in mind that the derivation of the hydraulic properties of the rock from the field measurements, such as hydraulic conductivity and specific storage, is dependent on assumptions of the geometry of the groundwater flow. Because such assumptions are based on geometrical information on structural features, the intent at the outset was to construct a geometrical model of the site based essentially on the radar and seismic measurements. This "geophysical" model would describe the extent of regions with anomalous properties within the rock mass. Subsequently, the hydraulic testing would focus on these "anomalous" regions.

Radar and seismic measurements are capable of identifying the position and extent of structural features. These features are related to the fracturing of the rock. For example, increases in water content in zones of highly fractured rock will cause localized changes in the dielectric constant and electrical conductivity of the rock. These changes are the features observed by the radar. The mechanical stiffness of the rock is decreased by the presence of fractures, which, in turn, decreases the longitudinal and shear wave velocities. These decreases are observed when the rock mass is seismically tested.

3.2.3 Radar and Seismic Testing Results

Radar and seismic tests were conducted in both the single-borehole and crosshole modes. Tomographic reconstruction of crosshole data yielded

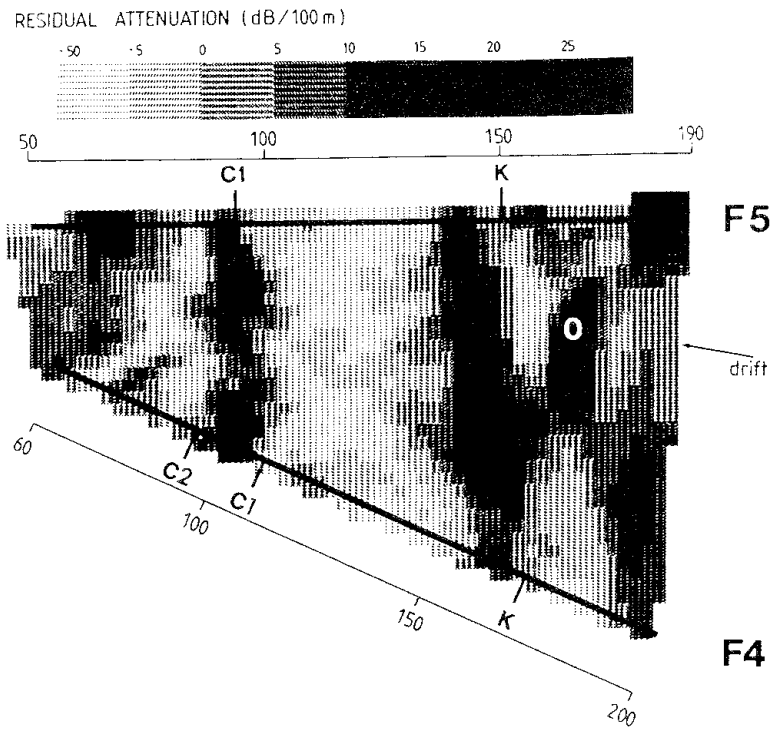
maps, such as shown in Figure 3-25, that indicated the distribution of the physical properties in the plane between two boreholes. The radar tomogram was obtained from inversion of radar attenuation data, while the seismic tomogram illustrates the distribution of seismic velocity. In these tomograms, the darker color indicates properties which are representative of increased fracturing of the rock, i.e. increased radar attenuation and reduced seismic velocity. The results shown in Figure 3-25 were obtained in the plane between the F4 and F5 boreholes, and the similarity of light and dark regions in the two patterns is quite apparent. That is, the same major features exhibiting similar forms were found in the same locations. General agreement between the radar and seismic tomography results was found over the entire Crosshole site.

Agreement between the radar and seismic results was also found to exist when identifying the locations of anomalous features that occurred at the intersections between measured sections, such as along boreholes and along lines in the region between boreholes. An example of such agreement is shown in Figure 3-26 where the F1-F4 section, tested seismically, intersects the F4-F5 section, tested with the radar, along the line of the F4 borehole. In this series of tests, the seismic measurements were spaced at 5 m along the borehole as compared to a spacing of 4 m for the radar measurements. The agreement between the light and dark regions of the patterns at the intersection along the F4 borehole is, for all practical purposes, excellent. The variation in shade within a dark region represents departures from a planar geometry in the fracture zone, as well as increases and decreases in the relative density of fractures.

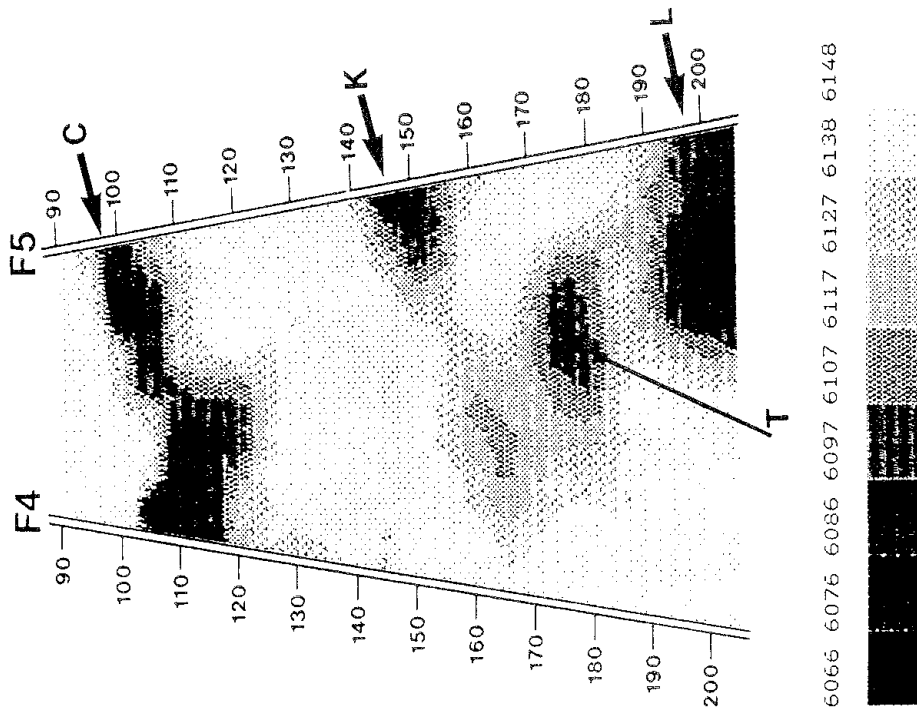
Direct comparison between radar reflection results from single-borehole tests and those obtained in the crosshole mode is not as straightforward as for the radar and seismic results. Reflection data give the position and angle of intersection of the edge of a zone with a borehole. In general, there is good agreement between both data sets with regard to the location of major zones. However, because the reflection measurements are more sensitive to changes in electrical properties than the transmission measurements, more zones are seen by reflection than by crosshole transmission.

3.2.4 Geophysical Model of the Crosshole Site

Two conceptual geologic models of the Crosshole site were developed through a combination of the information from the core logging and borehole photography and the results from the radar and seismic testing. The first model, known as the "Basic Model", contained the most significant zones identified as large anomalies in both the radar and seismic investigations. These zones also gave significant responses when testing was conducted in single boreholes. The second model, known as the "Extended Model", contained the zones included in the Basic Model as well as zones that produced relatively small anomalies and that were identified by only one of the geophysical testing methods. This latter circumstance results from different coverage of the region by different testing techniques and includes zones located outside the pyramid of boreholes as identified from the radar reflection data.



(a) Radar tomogram



(b) Seismic tomogram

Figure 3-25 Tomograms obtained from the inversion of radar amplitude data and seismic P-wave travel-time data obtained from crosshole measurements between boreholes F4 and F5 at the Crosshole site (Olsson et al, 1987a).

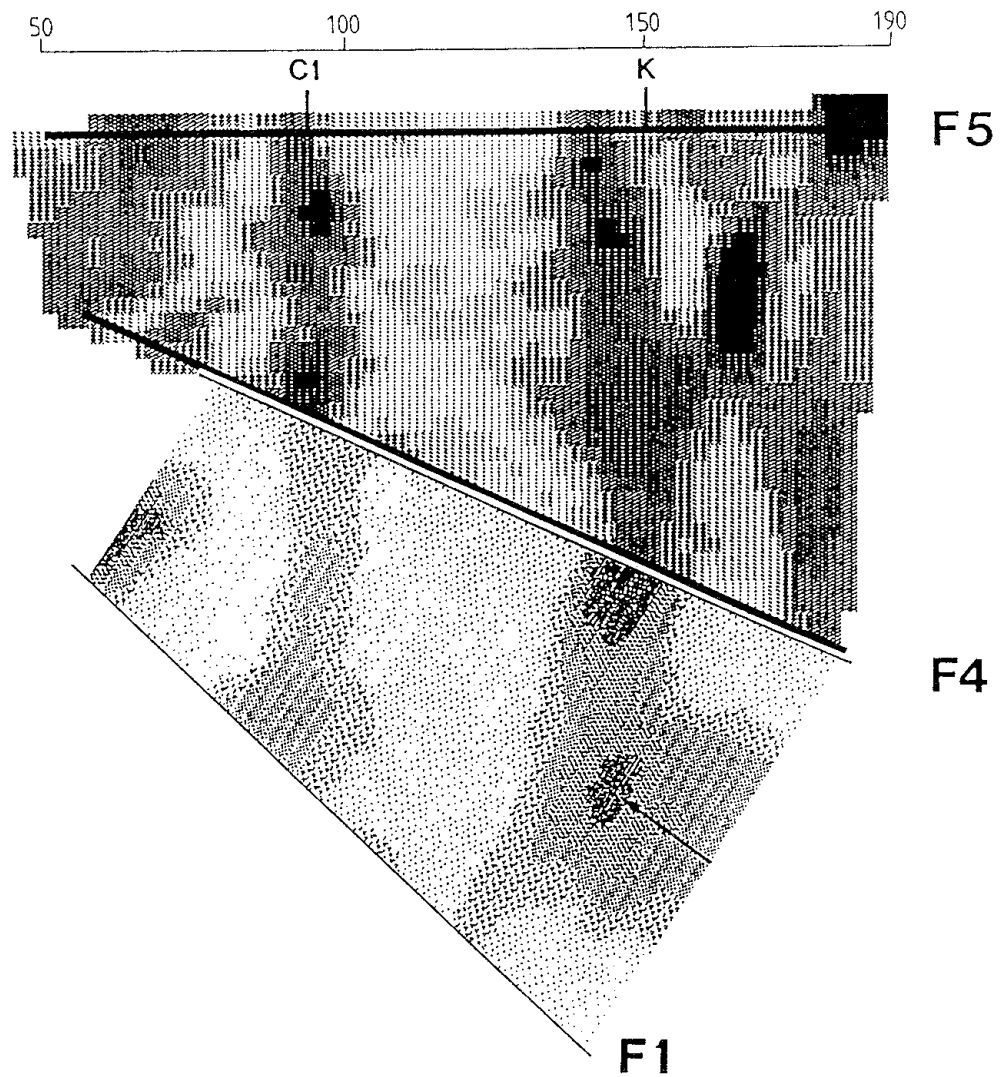


Figure 3-26 Tomograms obtained from the inversion of seismic travel-time data for the F1-F4 section and radar amplitude data for the F4-F5 section at the Crosshole site (Olsson et al, 1987a).

The density of data varied within the Crosshole site. The highest density of data occurred between all of the boreholes in the depth interval of 80 m to 200 m. In this region, a complete set of geophysical data was obtained, including results from both single-borehole and crosshole testing with the radar and seismic techniques. Radar reflection data were obtained over the entire lengths of all the boreholes, providing information outside the borehole-to-borehole sections that defined the tilted pyramid at the Crosshole site.

The Basic Model

As shown in Figure 3-27, the Basic Model includes the fracture zones designated as A, C, K, and L which were observed as prominent features by all geophysical methods. These fracture zones, as well as those identified from the core logs and borehole photographs, formed two sets, as shown in the Wulff plot in Figure 3-28. The C, K, and L zones are essentially

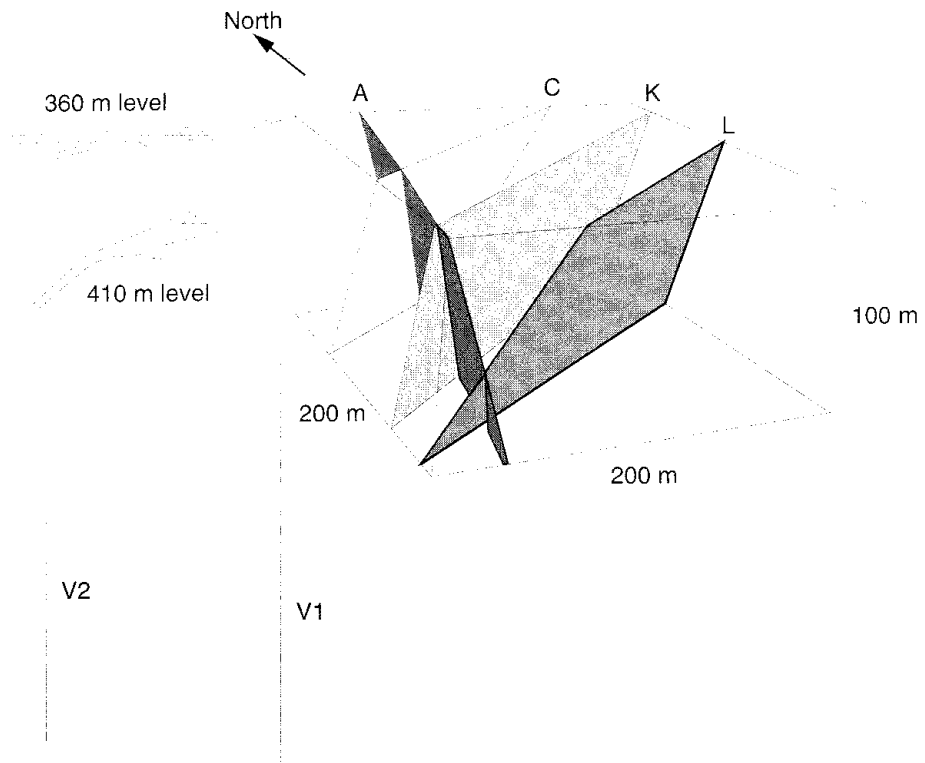


Figure 3-27 Perspective view of the fracture zones contained in the Basic Model of the Crosshole site (Olsson et al, 1987a).

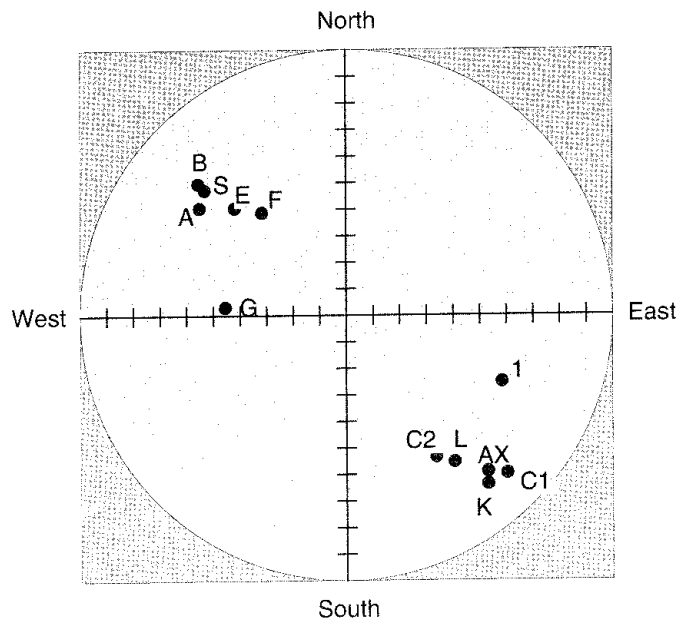


Figure 3-28 Wulff plot of normals to all fracture zones contained in both the Basic and the Extended Models of the Crosshole site (Olsson et al, 1987a).

parallel, with a strike to the northeast and a steep dip towards the northwest. On the other hand, zone A strikes to the north-northeast and exhibits a steep dip towards the southeast.

Based on radar reflection data, the orientation of zone A was found to be variable, indicating that it may be undulating. The pattern of reflections obtained from tests in boreholes F5 and F6 suggested that this zone might be intersected by another zone, or that it might be bifurcated into a few minor zones. The zone was estimated to be about 10 m thick, and, based on the core logs, contained breccia that was healed with a coarse calcite-fluorite as well as with a dense epidote-chlorite.

The C zone was clearly seen by radar reflections from all boreholes, with reflections of similar strength occurring on both sides of the fracture plane. The results from the seismic tests indicated that the zone bifurcated into at least two nearly parallel subunits. The apparent thickness of the zone was about 10 m, which compared well with the data obtained from the resistivity log. Zone C was one of the most strongly tectonized and brecciated zones encountered in the boreholes, where the breccia was healed by a complex matrix of quartzitic material, ferrogeneous material, calcite-fluorite, epidote, and chlorite.

The K zone was not described as a separate unit on the basis of the core logs, probably because of its irregular character. Within the site, this zone appeared as a series of low velocity features which connected some of the borehole intersections with the E and F zones detected by radar reflections. Based on the seismic data, it was hypothesized that this feature consisted of a series of elongated patches, with length dimensions ranging from 20 m to 60 m. Based on the core logs, the zone had a red color and was brecciated, with the density of fracturing varying from borehole to borehole.

The L zone was more than 20 m in width and was located at the very bottom of the site area. Radar reflections were strong and indicated an intensely fractured zone nearly parallel to the C and K zones. This feature exhibited the highest seismic-velocity contrasts of all anomalies detected at the Crosshole site. The zone had a red color and was brecciated, but comparatively less than the other zones, and contained a high density of fractures at its intersections with the boreholes.

The Extended Model

Crosshole seismic and radar testing can determine the existence of fracture zones quite efficiently in the plane containing the two boreholes within which the measurements were made. However, structures that lie outside this plane, or that are oriented parallel to it, cannot be detected. Such zones can only be found by means of radar reflection measurements. By this technique, five additional fracture zones were identified at the Crosshole site.

The Site zone passed through the drift from which the F boreholes were drilled into the Crosshole site. The width of the zone in the drift was 10 to 20 cm, and its orientation was essentially the same as that of the A zone. A zone, denoted as Unit 1, was identified close to the borehole collars in the

drift and determined to have an orientation similar to that of the C, K, and L zones. In addition, zones E and G were identified, with orientations similar to that for the A zone. The F zone was located by radar reflection measurements near the E zone and was determined to have approximately the same orientation.

The old drift, located on the 410 m level of the mine, was a very good reflector of radar pulses. Because the drift was oriented almost perpendicular to most boreholes, it behaved almost like a point reflector. The drift was most clearly seen in the seismic-velocity and radar-amplitude tomograms. However, it was difficult to identify in the radar-velocity tomograms because the air contained within the drift is a high-velocity medium.

3.2.5 Hydraulic Investigations

The primary purpose of the hydraulic investigations was to provide a basis for calibrating the geophysical properties measured by the radar and seismic techniques against the hydraulic properties of the rock mass. Both single-borehole injection tests and crosshole "sinusoidal" tests were conducted in sections of the boreholes that were isolated by means of straddle packers. The single-borehole tests involved constant-head injection, slug, and pulse techniques. The data from these tests were used to determine the hydraulic conductivities and transmissivities of the "average" rock and the fracture zones. The crosshole hydraulic testing concentrated on measuring the distribution of hydraulic properties within the extensively fractured zones identified by geophysics.

Hydrologic Characteristics of the Crosshole Site

The Basic Model of the geologic structure of the Crosshole site contained the four fracture zones A, C, K, and L which, based on their geophysically determined orientations, should have intersected the boreholes at twenty different locations. The Extended Model included an additional four fracture zones, denoted as E, F, G, and Unit 1, which intersected the boreholes at 33 locations. The thicknesses of the zones at these intersections were variable, depending on the technique that was used to make the observation, but did not exceed 15 m and were seldom greater than 5 m.

The most straightforward approach for comparing the hydraulic data with the structural features of the geologic model was to plot the position of transmissivity "anomalies" against the position of the fracture zones in the boreholes, as shown in Figure 3-29. The transmissivity is the product of the hydraulic conductivity and the zone length in the borehole, and the transmissivity anomalies are the fractions, in excess of 2%, of the total borehole transmissivity contributed by each zone. The A, C, and L zones accounted for about 63% of the total of nineteen anomalies identified in the suite of six boreholes, with the Unit 1 zone accounting for about 16%. Of the four major zones, zone A was consistently associated with regions of high transmissivity since it intersected every borehole within a short distance of a hydraulic anomaly. On the basis of the single-borehole hydraulic data, zone L was identified as the most significant of the four major zones, and

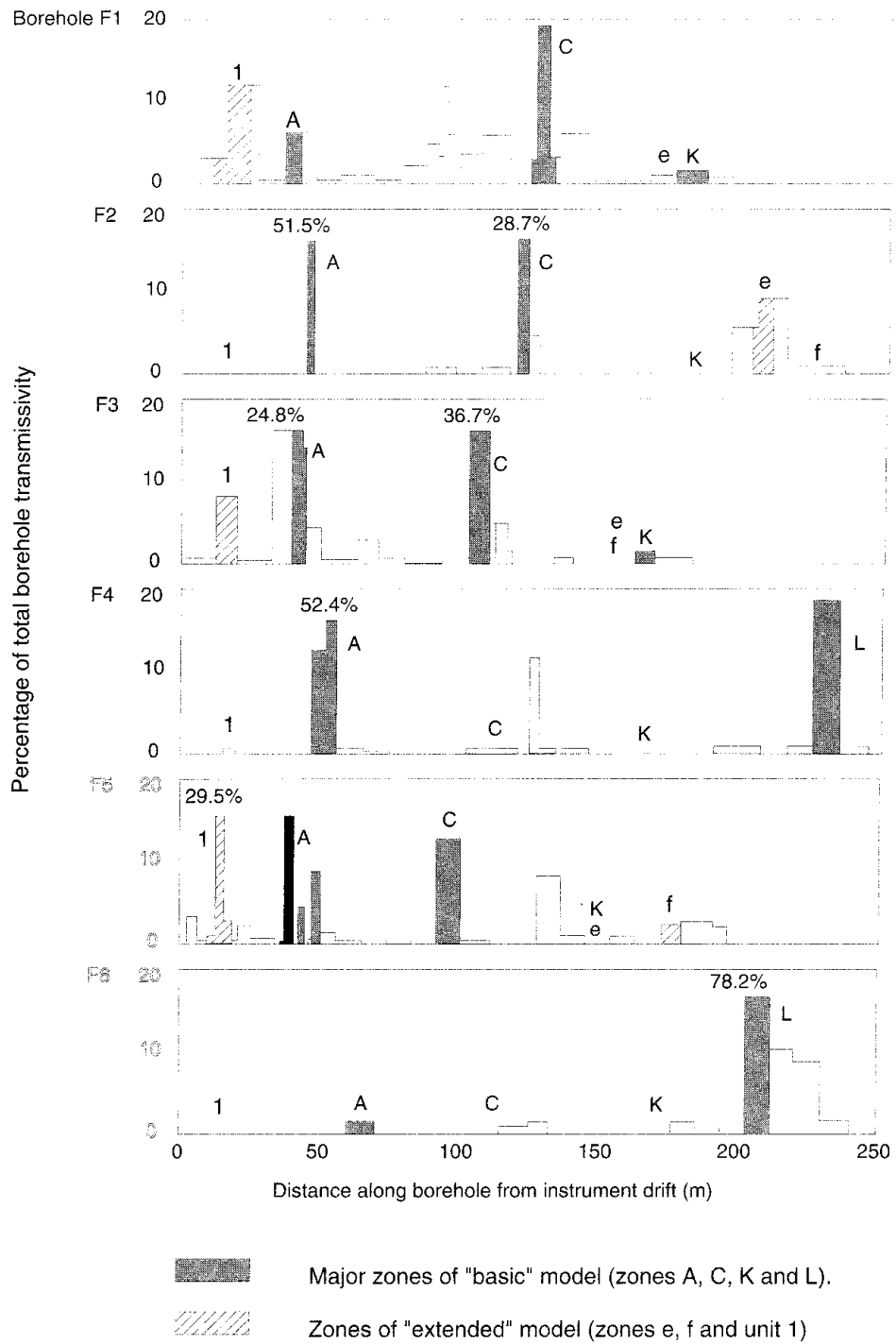


Figure 3-29 Comparison of the position of transmissivity anomalies with the position of major fracture zones in the suite of boreholes at the Crosshole site (Olsson et al, 1987a).

was associated with an anomaly at both of its expected intersections in boreholes F4 and F6. In contrast, zone K, which intersected all six boreholes, could be associated with only very small anomalies in boreholes F1 and F3. From the viewpoint of the relative significance of anomalies, borehole F6 penetrated rock which was, on average, a factor of 200 more permeable than the rock penetrated by borehole F1. However, for clarification, this statistic incorporates the transmissivity of the 8 m of rock located between 205 m and 213 m in borehole F6 which contributed 53% of the total transmissivity of the 1 300 m length of tested boreholes.

Additional information on the hydrologic characteristics of the fracture zones can be obtained by plotting the positions of "head anomalies" and "flow anomalies" against the positions of the fracture zones within the boreholes. A hydraulic head anomaly is defined as the difference between a measured head and a calculated head, assuming that the rock is a homogeneous porous medium, where the difference must persist over a finite interval of a borehole. In contrast to its lack of transmissivity anomalies, zone K accounted for about 40% of the head anomalies identified in the suite of six boreholes. A flow anomaly is defined as the product of the transmissivity and the head difference, which is a measure of the amount of water that would flow into or out of the borehole at a particular location. Zones A, C, K, and L accounted for 75% of the flow anomalies identified in the suite of six boreholes.

Clearly, a correlation exists between the hydrologic anomalies identified by single-borehole hydraulic testing and the structural features identified by single-borehole and crosshole geophysical testing. However, the hydraulic data lead to a smaller group of features than obtained from the geophysical data. Features identified by flow anomalies correlate best with features identified by geophysics.

Only zones A and C were effectively investigated by crosshole hydraulic testing. Zone A was found to be well interconnected in the center of the rock mass defined by the suite of six boreholes. As shown in Figure 3-30, the zone appears to bifurcate and increase in width in the southerly direction, as evidenced by an increasing number of responses in boreholes F3, F4, and F5. From a hydraulic viewpoint, the data indicated that the dimension of flow increased from north to south in the site, while the hydraulic diffusivity appeared to decrease from north to south. Thus, it would appear that zone A branched into more numerous but, in total, less transmissive fractures in the south part of the site. The data from the crosshole tests of zone C indicated a similar condition of increasing bifurcation and decreasing hydraulic diffusivity, but, as shown in Figure 3-30, in the northerly direction. In general, the transmissivity of the two zones was found to range between about 10^{-7} m²/s and 10^{-9} m²/s. The average hydraulic conductivity of the fracture zones was slightly greater than 10^{-8} m/s, while the average hydraulic conductivity of the rock between the fracture zones was about 10^{-10} m/s.

Comparison Between Hydraulic and Geophysical Data

A fracture zone is not a single fracture, but a zone in which the density of fractures is greater than the average for the rock mass and the fractures are

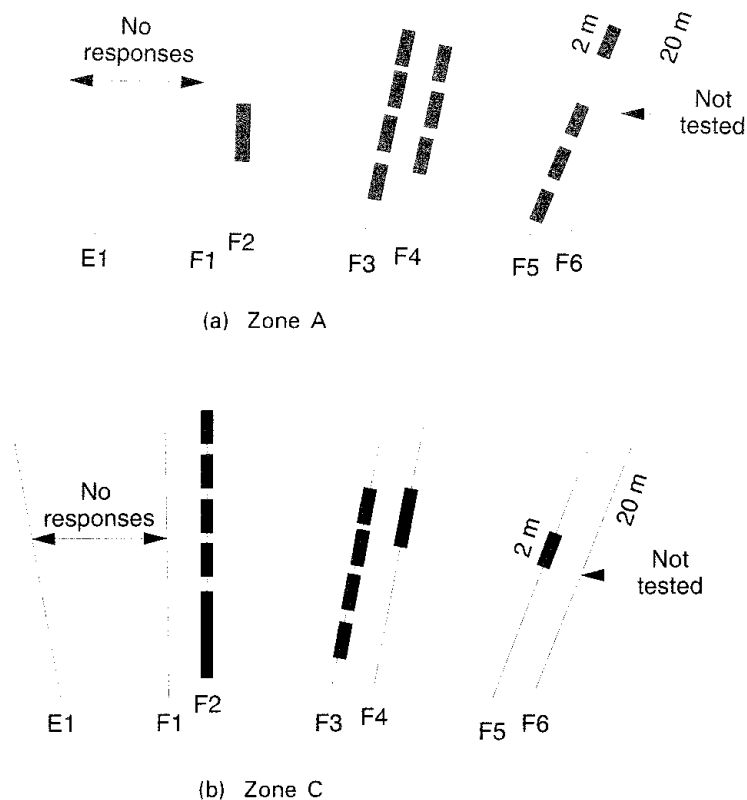


Figure 3-30 Pseudo-perspective plan view of the borehole intervals at the Crosshole site where responses were measured during crosshole hydraulic testing (Olsson et al, 1987a).

more systematically interconnected. When such zones are observed by crosshole geophysical testing and interpreted by tomographic analysis, they appear less like planes and more like interconnected patches. As described above, some forms of hydraulic anomaly, such as the flow anomaly, correlate better than others with the features identified in a "planar" geophysical model. When the hydraulic anomalies are compared directly to the tomograms, the correlation hierarchy is less distinct.

Seismic and radar tomograms for the plane sections defined by boreholes F3-F4 and F2-F5, respectively, are shown in Figure 3-31 together with the patterns of hydraulic anomalies that were identified along the boreholes. In Figure 3-31(a), the distribution of head anomalies along borehole F4 most closely match the tomogram, while the distribution of flow anomalies along borehole F3 is probably the best match. Zone K passes almost vertically across the center of the section with an apparent bifurcation in the region of borehole F4. Zone C is indicated as a clearly planar zone, but with varying strength within the section. The absence of any hydraulic anomaly associated with the intersection of zone C with borehole F4 could not be explained.

The hydraulic anomalies along boreholes F2 and F5 are compared with the radar tomogram for this section in Figure 3-31(b). Zone C is the prominent patch to the left of center, while zone K occupies the right-hand side of the

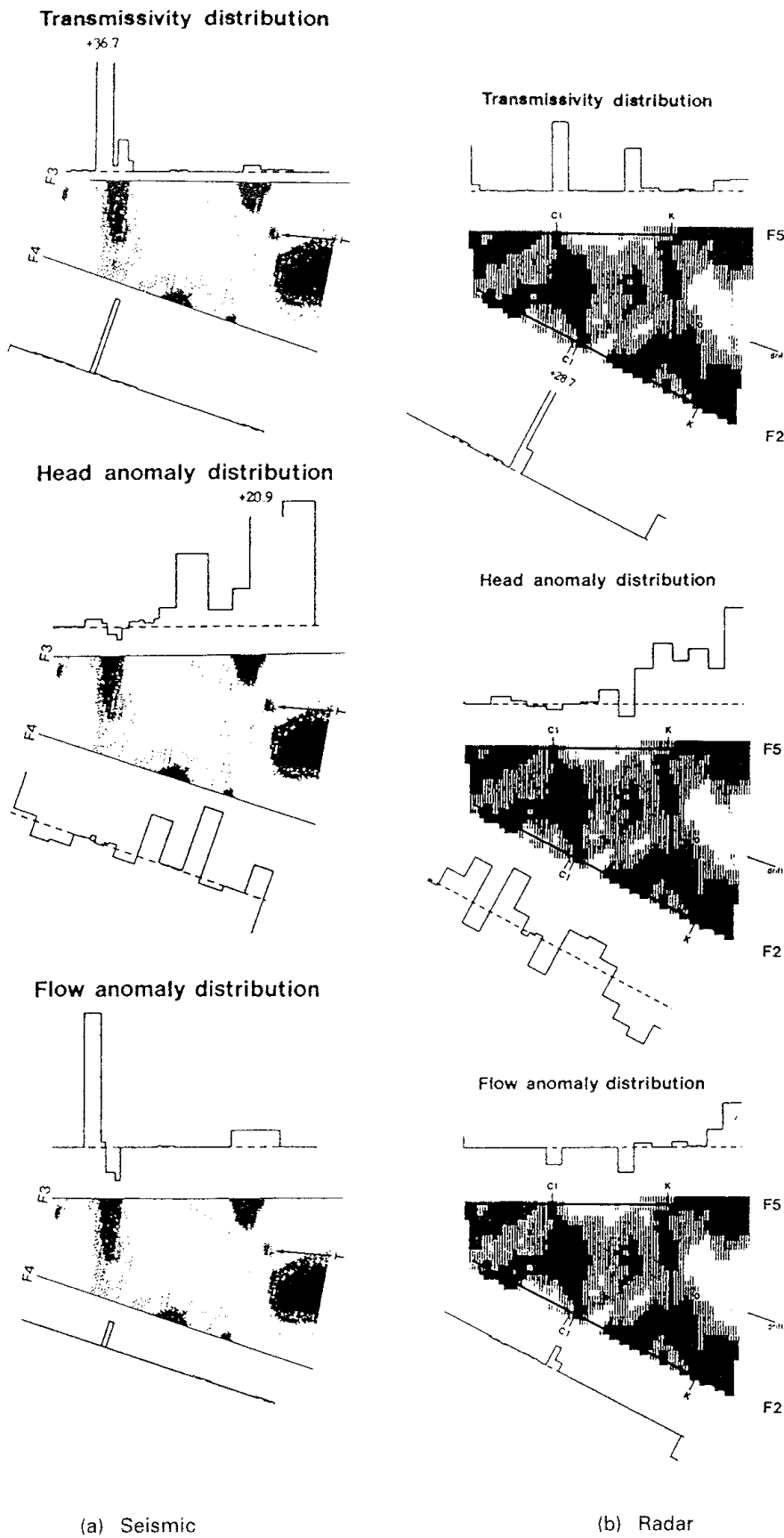


Figure 3-31 Comparison of seismic and radar tomograms with hydraulic anomalies measured in boreholes at the Crosshole site (Olsson et al, 1987a).

tomogram. The distributions of flow anomalies in the two boreholes appear to provide the best match with the pattern of the tomogram. However, zone K does not seem to yield any perceptible anomalies in any of the hydraulic profiles.

Single-borehole radar reflection testing was found to identify more structural features of interest than single-borehole hydraulic testing. This result was probably as much a consequence of a relatively coarse borehole-packer spacing, of the order of 4 m to 13 m with overlaps, as it was a real feature of the rock and the fractures.

3.2.6 Design of Future Characterization Strategies

The ultimate objective of characterization of a geologic repository site is to predict with confidence the likely velocity and direction of migration of leached radionuclides through the site and into the accessible environment. The basis for this prediction requires a conceptual model of the spatial distribution of all relevant characteristics and properties of the site. The Crosshole programme was concerned with an evaluation of characterization techniques that could be used to obtain the data necessary to construct a conceptual hydrologic model of a rock mass. The information required to develop such a model is less complex than what would be required to develop a nuclide transport model in the same rock mass. Characterization techniques tend to provide information concerning the geologic structure, such as the geometric aspects of fault zones, or properties within predetermined features, such as the hydraulic conductivity of fractures that intersect boreholes. There is some overlap between and among techniques in the types of information obtained. For example, seismic techniques provide data for determination of the location and orientation of fracture zones, and the measured wave velocities within the fracture zones are indicative of the qualitative degree of fracturing. On the other hand, hydraulic testing techniques provide information on the hydraulic conductivity and diffusivity of a fracture zone, together with limited information on the geometric distribution of those properties.

Natural Dimension of Measurements

Essentially, all of the characterization measurements at the Crosshole site were made in boreholes, and, as such, the arrangement of source and receiver inadvertently dictated a "dimension" to the results. In some instances, the measurement responded to a region around a borehole, or in the plane of a fracture zone, that was quite small as compared to the scale of the total volume being investigated. In other instances, a measurement implied some particular three-dimensional arrangement of properties, denoted as "pseudo-3D", but did not uniquely specify their position or size.

The applicability and effective "dimension" of the characterization methods that were used at the Crosshole site are given in Table 3-1. The first four techniques in the table are restricted, for all practical purposes, to obtaining data in a single dimension. To obtain the information that is required to develop a conceptual model of the geohydrology of a rock mass over distances of 100 m or more, techniques that provide geometric

characteristics over a reasonable scale and in three dimensions must be used. As indicated in the table, the crosshole radar and seismic techniques, as well as the single-borehole radar technique, have the capabilities to obtain geometric information, along with a limited amount of information on the transport characteristics of the rock mass. Conversely, the single-borehole and crosshole hydraulic tests provide primary information on the hydraulic properties of the rock mass, and a limited amount of information on the geometric characteristics of structural features.

Table 3-1 Applicability and Effective "Dimension" of the Characterization Methods used at the Crosshole Site (Olsson et al, 1987a).

| Characterization Technique | Primary Information | Secondary Information | Dimension of Measurement |
|-------------------------------------|--|--|--------------------------|
| logging of rock core | geometrical features of rock mass | fracture characteristics | 1D |
| laboratory tests on rock core | physical properties of rock matrix | fracture properties | 1D |
| single-borehole geophysical logging | electrical properties of rock matrix/mass | borehole deviation | 1D |
| single-borehole hydraulic test | hydraulic properties of rock mass/fracture zones | geometrical features of fracture zones | 1D (minor 3D) |
| single-borehole radar tests | geometrical features of fracture zones | transport properties | pseudo 3D |
| crosshole radar and seismic tests | geometrical features of rock structure | transport properties | 2D - 3D |
| crosshole hydraulic tests | hydraulic properties | geometrical features of fracture zones | pseudo 3D |

Scale of Measurements

The "scale" of a measurement technique can be thought of as having a minimum resolution size and a normal sample size. The characterization techniques that were used in the Crosshole programme featured a wide range of minimum resolutions. At the smallest scale, core logging resolved features to fractions of a millimetre. At the largest scale, the crosshole seismic and radar tests provided resolutions on the order of half a wave length, i.e. a few metres. In practice, positive identification of a structural feature would normally require that the feature have at least one dimension which is several times the minimum resolution of the testing technique.

For measurements which are primarily used for determining properties rather than geometrics, the maximum resolution is effectively determined by the maximum dimension of the region being sampled. In situations where the sample region can be subdivided, the resolution may be improved. However, as is the circumstance for all hydraulic techniques, homogeneity is usually assumed within a simple cylindrical geometry and the maximum depth dimension determines the minimum resolution. In most of the single-borehole hydraulic testing, the region around the borehole which affected the

result did not exceed a fraction of a metre. Thus, the minimum resolution of the single-borehole hydraulic testing was determined by the minimum straddle-packer interval of 2 m. In essence, the data were effectively representative of one-dimensional samples. The maximum dimension of the crosshole hydraulic testing was the distance between the source and receiver points that would result in extremely poor spatial resolution. However, the interpretation of these data was influenced by geometric characteristics of the site that were determined by geophysical testing. Thus, the resolution that can be achieved in crosshole hydraulic testing is, in reality, a function of the complexity of the geometry of the conceptual model that is being used in the interpretation of the data.

Conceptual Model of the Crosshole Site

The conceptual model of the Crosshole site, described in the preceding sections, was developed with the restrictions in scale described above. Thus, no feature included within the model could have a thickness less than a few metres. In addition, the separation between identifiable features could not be smaller than the smallest detectable size of feature. That is, if the separation was smaller, then the two features would be perceived as a single feature. The conceptual model contained features with sizes on the order of a few metres, close to the detection limit, while the average separation distance of the identified fracture zones was approximately 70 m for the two different sets of zones. The distance between zones was thus much larger than the resolution, and the model can be expected to be correct in describing a rock mass that is intersected by a number of zones which occupy a minor part of the volume.

The fracture zones of the "Basic Model" and "Extended Model" have been identified on the basis of their "extensiveness" and "strength" as determined by the geophysical testing techniques. Based on comparisons of the results from hydraulic testing, features which are "extensive" are usually "strong" geophysically and are also important from a hydrologic viewpoint. However, some of the features within the site appeared to have geophysical characteristics which could not be correlated with the hydraulic characteristics. For example, zones A, C, and L of the "Basic Model" are all more-or-less continuous fracture zones of enhanced hydraulic conductivity. On the other hand, zone K was described as a system of patches on the basis of the data from geophysical testing. The hydraulic testing indicated that this zone contained a reasonable share of the hydraulic anomalies observed in the boreholes.

Based on the data obtained from the collection of characterization techniques, the main structural features contained within the conceptual "Basic" and "Extended" models of the Crosshole site were thought to have the following characteristics:

- broadly planar
- channelled
- a branching and interconnected network of fractures
- regions of high and low hydraulic conductivity
- decreasing transmissivity associated with bifurcations.

The planar features are essentially networks of channels arranged within a broad region with a planar dimension that is much greater than its thickness.

There was no evidence to conclude that the characterization testing failed to identify the existence of features within the site that had dimensions greater than the resolution of the testing techniques. The confidence that the conceptual model accurately reflected the geometrics of the structural features was considered high. This confidence was based on the fact that both the radar and seismic testing techniques yielded descriptions of the site which agreed very well with each other. The tomographic anomalies were found in the same locations, even though the tomographs were based on the measurements of different physical properties. This was a strong indication that the features identified in the tomograms were real and not artifacts of the characterization technique. The hydraulic investigations showed that groundwater flow was concentrated within the fracture zones, and probably confined to channels within the zones. The general direction of water movement through the site could be obtained from the head distribution. The conceptual model does not, however, make it possible to predict migration pathways and transport times because of the lack of detailed knowledge of the channels within the fracture zones. Such data were not possible to obtain with the characterization techniques used at the Crosshole site.

3.2.7 Significant Achievements

The Crosshole programme demonstrated that there is an optimum structure in a programme of site characterization. One of the first objectives of a characterization programme should be to define the geometric characteristics of the major structural features. In the investigations at the Crosshole site, which was a saturated, fractured granitic rock, the distribution of major features was identified best by a combination of data from single-borehole radar reflection testing and tomographic inversion of crosshole radar and/or seismic data. The second objective would be to describe the distribution of the hydraulic properties of the structural features and the "average" rock. This can be achieved best by a combination of single-borehole and crosshole hydraulic testing, even though the latter type of testing is extremely time consuming. The detail of the site investigation can be increased considerably by using the data from high-frequency single-borehole radar in the reflection mode. In general, however, the investigations at the Crosshole site indicated that the features identified by radar reflection testing were more abundant than those identified by means of single-borehole hydraulic testing.

In summary, the hierarchy of characterization techniques that could be applied sequentially in a site investigation can be arranged as follows:

- single-borehole radar reflection testing
- single-borehole hydraulic testing
- crosshole radar testing
- crosshole seismic testing
- crosshole hydraulic testing
- tracer migration test.

In general, the techniques listed at the top of the hierarchy can be conducted relatively faster than those listed at the bottom. It should be noted that a site containing highly concentrated flow paths is the type of site which could benefit most from this form of "structured" investigation.

The Crosshole programme demonstrated that it was possible to characterize saturated, fractured crystalline rock and to develop a conceptualization of the geohydrology of the rock mass to a level of reliability and realism not previously obtainable. The programme demonstrated the advantages and importance of using geophysical methods to focus subsequent hydrologic characterization efforts on regions of the rock mass of most interest. The outcome of the investigations provided a sensible hierarchy of test methods that could be applied sequentially to characterize a site that is suspected to contain highly concentrated flow paths.

3.3 CONCEPTUAL MODEL OF THE SCV SITE

The Site Characterization and Validation (SCV) programme, proposed in 1985 and implemented in 1986, was one of the principal components of Phase 3 of the Stripa Project (Carlsson et al, 1987). The central theme of the programme dealt with characterization of a previously undisturbed block of saturated, fractured granite in the Stripa mine by means of tools and techniques developed in Phases 1 and 2. Specific experiments were designed and conducted to provide a basis for testing the validity of numerical models developed for simulation of groundwater flow and solute transport within the rock mass. Two complete cycles of characterization/experimentation, model prediction, and evaluations of model validity were completed over a period of five years, in support of the underlying notion that the model predictions should be checked against the experimental results on an iterative basis.

Characterization activities of the SCV programme, including the sequential application of various tools and techniques and the associated development of a conceptual geohydrologic model of the SCV site, were based principally on the experience gained in the Phase 2 investigations. In particular, tools and techniques developed at the Crosshole site, along with the conceptual geohydrologic models of the Crosshole site, the Stripa mine, and the Stripa area, formed the basis for the planning and implementation of the activities. The results, in terms of the site characteristics, the conceptual geohydrologic model, and the validation experiments, are described here. The details are given in reports and technical papers by Black and Olsson (1990), Black et al (1991), Olsson (1992), and Olsson et al (1989, 1990a), as well as in the many other reports and technical papers by the principal investigators and their associates as referenced throughout this section. The development of the groundwater flow and transport models, as well as the evaluations of the validity of those models in conjunction with the results of the validation experiments in the SCV programme, are described in Chapter 4.

3.3.1 SCV Programme

The SCV site was located between the 360 m and 410 m levels of the Stripa mine, about 100 m north of the old mine workings. The site encompassed a block of previously unexplored granite with a volume of some 1,000,000 m³ and dimensions of approximately 125 m to 150 m on a side and 50 m to 60 m high. As shown in Figure 3-32, this location allowed the rock mass to be explored by means of boreholes drilled from existing drifts. The east side of the site was bounded by the drift in which the 3-D tracer migration experiment was conducted during Phase 2.

The SCV programme was discretized into five stages, as shown in Figure 3-33, such that the data from the validation experiments could be compared iteratively with the model predictions (Carlsson et al, 1987; Olsson et al, 1989; Black et al, 1991). The first cycle of characterization, prediction, and validation involved Stages I, II, and III, and the second cycle consisted of Stages III, IV, and V. Refinement of the borehole seismic and radar testing techniques and development of the fracture network models occurred mainly during the early stages of the programme.

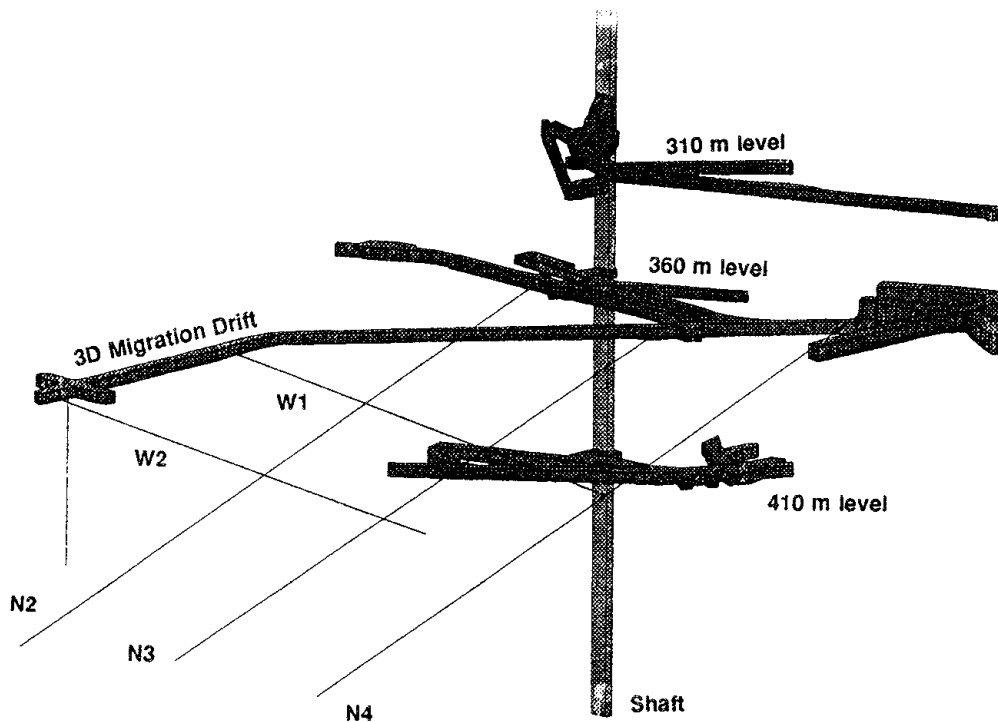


Figure 3-32 Perspective view of the SCV site in relation to the existing mine workings (Olsson, 1992).

The site was outlined by the array of N and W boreholes drilled from the 360 m level during Stage I.

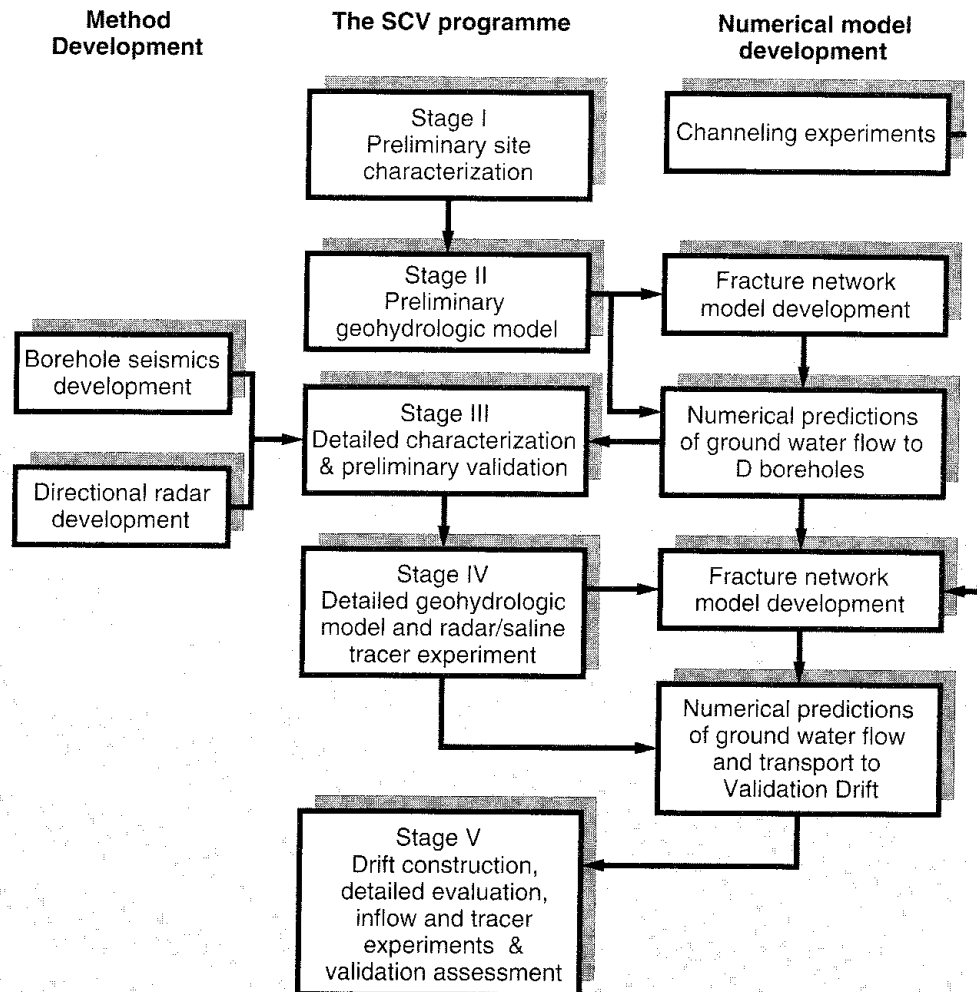


Figure 3-33 Structure of the SCV programme (Olsson, 1992).

Stage I: Preliminary Site Characterization

During Stage I, five boreholes were drilled into the site from existing drifts on the 360 m level. Three boreholes, designated as N2, N3, and N4 and spaced 60 m apart, were drilled to a distance of 200 m to the north at a dip of 19°. Two boreholes, designated as W1 and W2 and spaced 70 m apart, were drilled to a distance of 150 m to the west at a dip of 5°. Based on core logs and borehole photographs, the fracture characteristics of the rock mass in the vicinity of the boreholes were analyzed and the fracture zones were identified. Subsequently, groundwater samples were obtained from the boreholes for purposes of geochemical evaluations, and seismic, radar, and hydraulic tests were conducted in the boreholes.

Stage II: Preliminary Prediction

During Stage II, the characterization data were analyzed and a preliminary conceptual geohydrologic model of the site was developed. This model formed the basis for the numerical predictions of groundwater flow into the

D boreholes that were drilled into the site area in Stage III for the Simulated Drift Experiment.

Stage III: Detailed Characterization and Preliminary Validation

In Stage III, the access drift shown in Figure 3-34 was constructed from the 410 m level to the east side of the SCV site at the 385 m level, and a shaft was constructed from the end of the access drift to the 360 m level. Six 100 m long D boreholes were drilled from the end of the access drift in a westerly direction into the center of the SCV site. As shown in Figure 3-35, five of these boreholes, denoted as D2 through D6, formed the outline of a simulated cylindrical drift with a diameter of 2.4 m. In what was known as the Simulated Drift Experiment, the groundwater inflow to this suite of boreholes was measured and compared to modelling predictions, as described in Section 4.3.1. In addition, the three C-boreholes were drilled from the 360 m level near the entrance of the 3-D migration drift toward the central portion of the site. These boreholes were used for seismic, radar, and hydraulic testing to obtain data to refine the conceptual geohydrologic model of the site, in preparation for detailed numerical predictions of groundwater inflow to the Validation Drift which would be constructed in Stage V. During this stage, detailed data on the structural features within the site were obtained with the newly developed directional radar and high-resolution borehole seismic techniques.

Stage IV: Detailed Predictions

During Stage IV, the conceptual geohydrologic model of the site was refined on the basis of the characterization data obtained in Stage III. This model was used as the basis for modelling predictions of the fracture distribution on the walls of the Validation Drift, groundwater inflow into the Validation Drift, and tracer transport to the Validation Drift. Near the end of this stage, the first radar/saline tracer experiment was conducted at the site. Saline tracer was injected in borehole C2 at its intersection with the H fracture zone and collected in the D boreholes, concurrent with crosshole radar testing.

Stage V: Detailed Evaluation and Validation

At the beginning of Stage V, the Validation Drift was excavated along the first 50 m of the hypothetical cylinder outlined by the D boreholes. This was followed by fracture mapping of the drift walls and the second radar/saline tracer experiment. Saline tracer was injected into borehole C2 at its intersection with the H fracture zone and collected in the Validation Drift, concurrent with crosshole radar testing. In addition, the groundwater inflows to the Validation Drift and to the remaining portions of the D boreholes were measured, in what was known as the Validation Drift Experiment. Finally, boreholes T1 and T2 were drilled from the entrance of the Validation Drift upwards into the site to intersect the H zone. Subsequently, tracers, consisting of dyes and metal complexes, were injected in the T1, T2, C2, and C3 boreholes and collected in the Validation Drift, in what was known as the Tracer Migration Experiment. The results of the

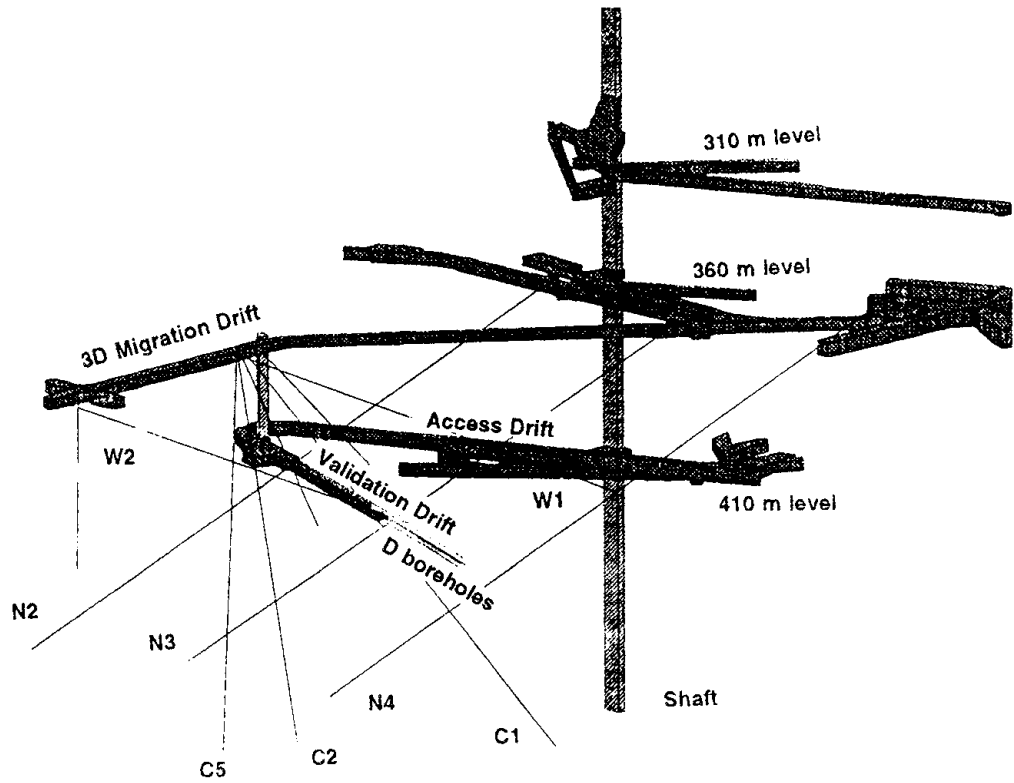


Figure 3-34 Location of the access drift, the D boreholes, the C boreholes, and the Validation Drift at the SCV site (Olsson, 1992).

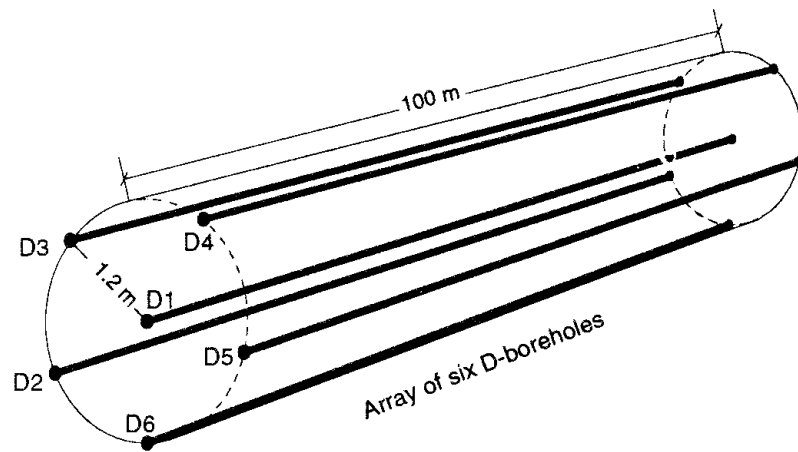


Figure 3-35 The simulated drift at the SCV site as outlined by the D boreholes (Olsson, 1992).

Validation Drift Experiment and the Tracer Migration Experiment were compared to the modelling predictions, as described in Sections 4.3.2 and 4.4.2.

3.3.2 Site Characteristics

During the course of the SCV programme, a binary description of the rock mass was adopted in order to distinguish between "fracture zones" and "averagely fractured rock". In this terminology, "fracture zones" referred to reasonably defined zones of relatively intense fracturing, such as fault zones, and "averagely fractured rock" denoted that portion of the rock mass containing a relatively uniform distribution of fracturing of low intensity. A principal objective of the characterization efforts was first to identify the fracture zones at the scale of the SCV site, and subsequently to determine their geometric and hydraulic characteristics. These zones were expected to act as major conduits for groundwater flow through the site. The zones were identified first on the basis of the core logs, borehole photography, and single-borehole geophysical measurements. Subsequently, radar and seismic tests were conducted in the boreholes to determine the geometric characteristics of the zones and to identify any other structural features that had not been intercepted by the boreholes. The hydraulic properties of the fracture zones were obtained by means of crosshole hydraulic tests. Single-borehole hydraulic tests were conducted to measure the transmissivity of the individual zones.

Groundwater flow and solute transport through the "averagely fractured rock", as well as within "fracture zones", are controlled by the geometry and properties of the individual fractures. The characteristics of the fractures within the averagely fractured rock and the fracture zones were described separately because of differences in intensity and geometry. Because the transmissivity of fractures depends in part on the effective stress across the fracture plane, the *in situ* stresses within the site were determined through a series of measurements and the stress redistribution caused by excavation of the Validation Drift was numerically modelled. The stress-permeability relationships were obtained by means of a series of laboratory and *in situ* tests on single fractures.

General Geology

The regional geology of the Stripa area, including the tectonic features, and the local geology of the Stripa mine have been previously described in Sections 2.1 and 3.1. In addition, the hydrologic features of the Stripa area and the Stripa mine were discussed in Section 3.1, along with the conceptual geohydrologic models. Generally speaking, an analysis of the distribution of the regional fracture zones or lineaments indicated that there existed a strong likelihood that the largest fracture zones in the SCV site would have a north-south trend with a smaller likelihood that any major east-west to northeast trending fracture zones would be encountered. However, because of the long trace lengths and high density of the east-northeast trending faults or fracture zones identified on mine maps, as discussed in Section 3.1, it was expected that these structures would be more abundant in the SCV site than the northerly trending features.

Fracture Zones

Based on the geologic information for the local geology of the Stripa mine, there was reason to believe that significant fracture zones could exist within and around the SCV site. The core logs from the N and W boreholes did indeed indicate the existence of such zones. The next step was to determine the geometric characteristics of these zones, as well as to locate any other zones that might have been missed by the boreholes and correspondingly determine their geometric characteristics. The investigations for such purposes included crosshole radar and seismic testing, single-borehole radar testing, and single-borehole geophysical testing (Andersson, 1989; Black et al, 1991; Cosma et al, 1988, 1991a; Fridh, 1987; Olsson et al, 1988, 1989; Sandberg et al, 1989).

As described in Section 2.3, the borehole radar technique uses electromagnetic waves concentrated in a short pulse with a wave length of 2 m to 10 m to obtain information about the structure of the rock. The technique will detect fracture zones, clusters of fractures, and tectonized zones with thicknesses in excess of about 10 cm. During a radar reflection measurement in a borehole, the reflection point traces a line on the plane of the fracture zone. Based on measurements in boreholes C1, C2, C3, D1-D6, and W1, the reflectors identified within the SCV site were plotted as planes, as shown in Figure 3-36. The reflectors are represented by circular disks, instead of just a line, to emphasize that the orientation of a reflector was actually determined. A number of reflectors with similar alignments describe a structural feature, such as zone B which dips approximately 40° to the southeast. A number of steeply dipping reflectors, grouped together in the north-south direction, were denoted as the H zone. Because the plane of the H zone was oriented almost perpendicular to the D boreholes in which the measurements were made, the sizes of these reflectors were small. The spatial distribution of 31 radar reflectors identified in boreholes C1, C2, C3, D1, and W1 are plotted in the pole plot shown in Figure 3-37. About 40% of these reflectors were attributed to major features that extended across the site, with the remaining reflectors considered to be due to minor fracture zones of limited extent. The largest pole clusters correspond to the approximate orientation of the major features identified by an integrated analysis of all data collected at the SCV site. These features are the H zone with a dip of 60° to 70° to the east and a north-south strike, and the A and B zones with a dip of 30° to 50° to the southeast and a northeast strike. The location of these features, as well as others identified during the course of the characterization activities, are included in the plan view of the conceptualization of the SCV site shown in Figure 3-38.

Radar measurements for tomographic purposes were made between boreholes W1-W2, N2-N3, N3-N4, and N2-N4 during Stage I and between boreholes W1-C1, C1-C2, and W1-C2 during Stage III. The H zone appeared consistently in all radar tomograms as a connected feature. As shown in Figure 3-39, the orientation of the zone changed somewhat and the width varied along the extent of the zone. Zones A and B generally appeared as disconnected patches of slowness or attenuation anomalies. Zone A was commonly located towards the edge of the tomograms and could not be well constructed because of the relatively poor ray coverage in the corresponding parts of the tomograms. The minor features I and K were difficult to identify in the tomograms because of their relatively weak

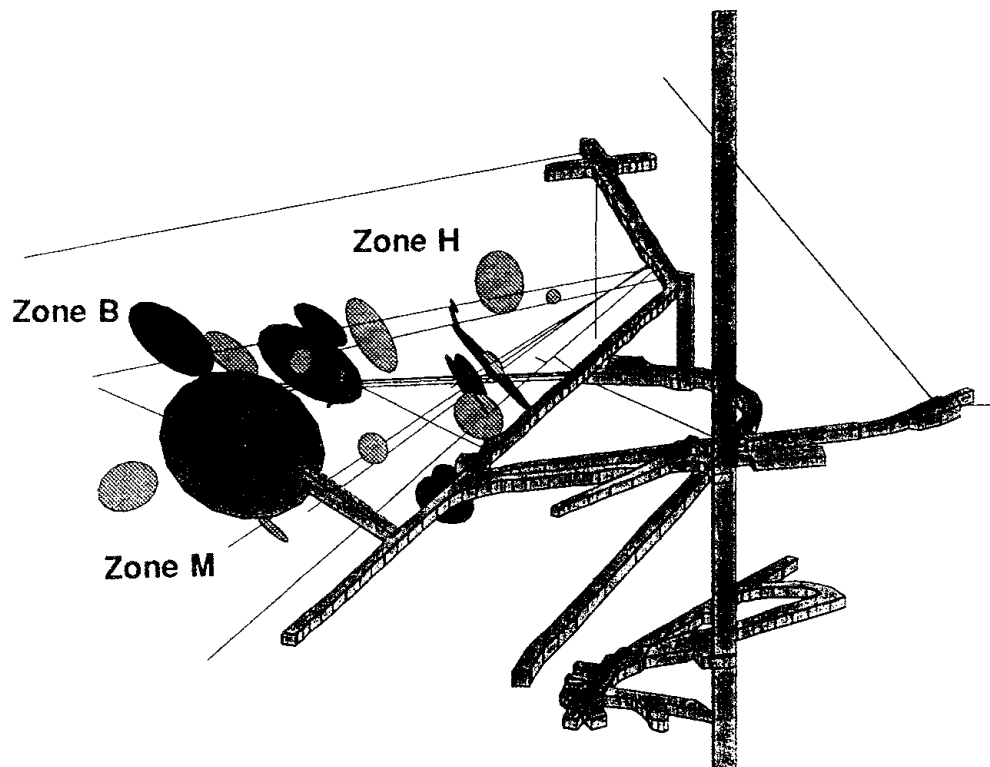


Figure 3-36 The location and orientation of radar reflectors derived from single-borehole directional radar data (Olsson, 1992).

The size of a disk is proportional to the dimension of the reflector actually observed.

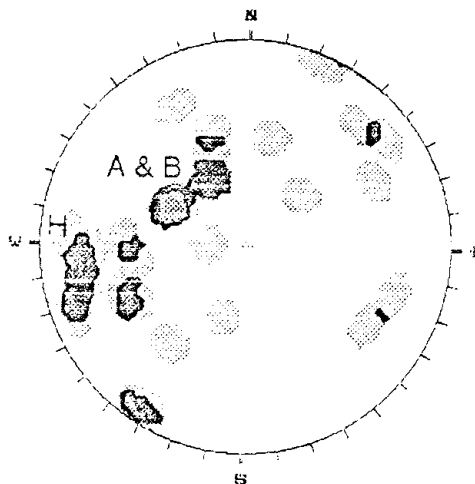


Figure 3-37 Pole plot from the lower hemisphere of a Schmidt projection for radar reflectors identified and oriented by directional radar in boreholes C1, C2, C3, D1, and W1 (Olsson, 1992).

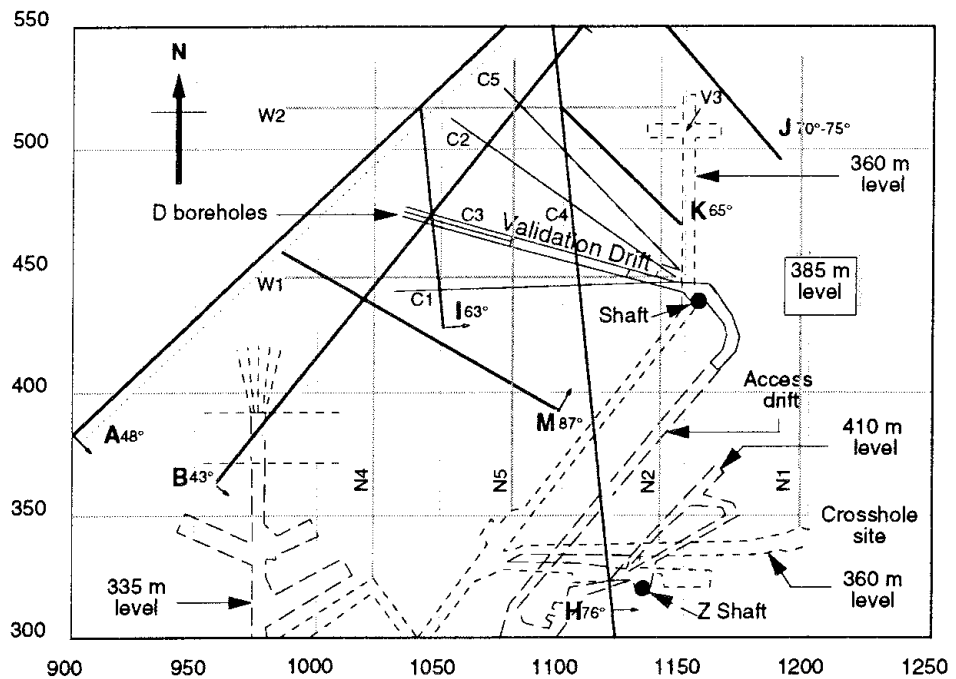


Figure 3-38 Plan view of features contained in the conceptual model of the SCV site at the 385 m level (Olsson, 1992).

response. The small displacements between anomalies in the slowness and attenuation tomograms were thought to be due to open fractures, or increased porosity, and to the presence of alteration minerals, respectively.

The data from the borehole radar testing in Stage I was obtained in semi-horizontal planes defined by boreholes N2-N3-N4 and W1-W2. This geometry and the lack of crosshole data between the N and W boreholes made it difficult to identify the same features in both planes to a reasonable high level of certainty. However, the availability of directional radar data in Stage III removed this uncertainty in interpretation. In general, the relatively large range in the reflection mode of the single-borehole radar tests, about 60 m in the Stripa granite, allowed the characterization of relatively large volumes of rock from only a few boreholes.

In Stage I, crosshole seismic tests were performed in borehole sections W1-W2, N2-N3, and N3-N4 for the purposes of tomography, while crosshole reflection measurements were made only between boreholes W1 and W2. In Stage III, crosshole tomography and reflection measurements were conducted in the C and D boreholes. As described in Section 2.2, the seismic method is a remote sensing technique that is based on the propagation of elastic waves through the rock. In the investigations at the SCV site, the wave lengths were of the order of a few metres, approximately the same as those used for borehole radar testing. Thus, the resolution of the results from the two methods was comparable. The propagation of seismic waves is sensitive to changes in density and elastic properties which are related to the fracture intensity. The velocity and attenuation of the direct P-wave arrivals were used for purposes of two-dimensional crosshole tomography, while a new three-dimensional reflection imaging technique concentrated on the S waves.

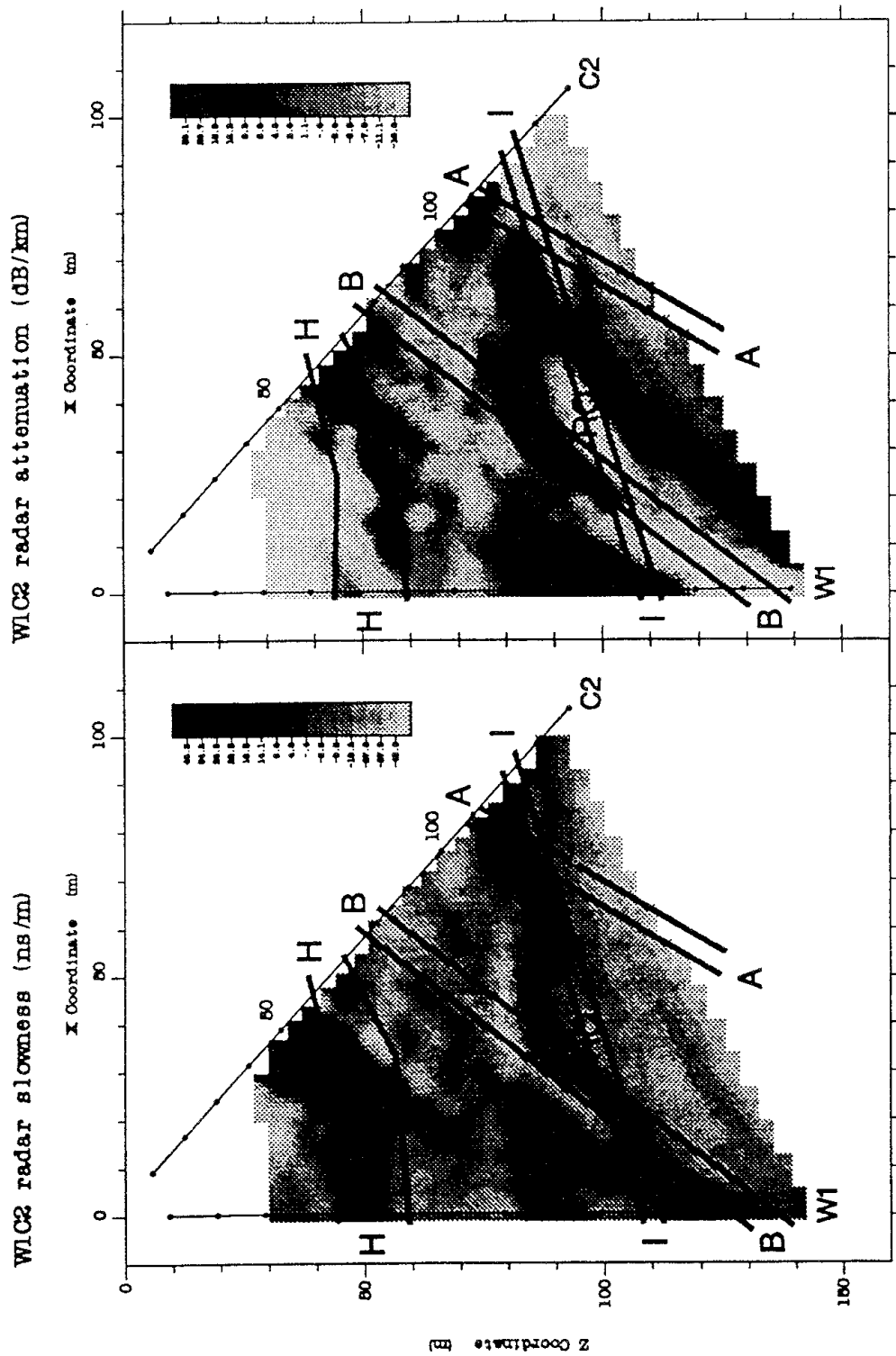


Figure 3-39 Slowness and attenuation tomograms for the section of the SCV site outlined by boreholes W1 and C2 (Olsson, 1992).

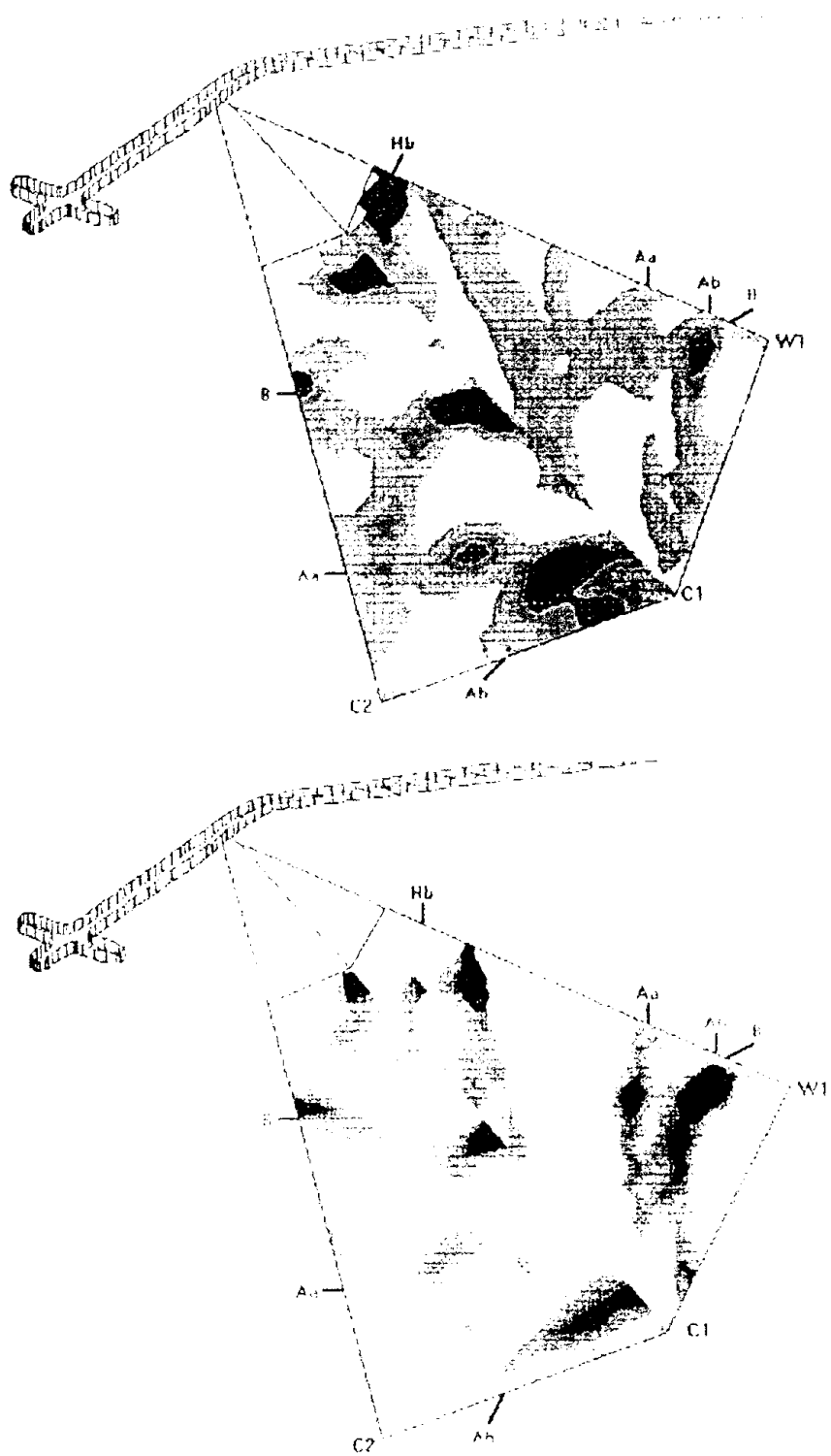


Figure 3-40 Seismic tomographic results for velocities and Q-factors in the planes defined by the W1, C1, and C2 boreholes at the SCV site (Olsson, 1992).

Sections C1-W1 and C2-C1 are shown in perspective. The projections of the features detected by the reflection measurements are marked.

The tomograms for velocity and attenuation for the same crosshole section were generally similar, as shown in Figure 3-40. Both lower velocities and higher attenuation depict generally zones of "poorer" rock, i.e. rock with a relatively high density of fracturing. However, when the contrast is very low, such as shown in Figure 3-40, variations of velocity and attenuation may appear without being connected with fracture zones. The results from the seismic testing provided a basis to identify four reflectors, denoted as Ha, Hb, Aa, and Ab, with reasonable certainty, and, zone B, with less certainty. Most likely, Ha and Hb depict zone H and Aa and Ab depict zone A. It was hypothesized that zone B could actually be a fold of zone A. The strikes and dips for these zones were found to be comparable to those determined on the basis of the borehole radar data for the A, B, and H zones.

Conventional geophysical logging was conducted in all boreholes. Borehole deviation measurements were made to map the orientation of the boreholes with an accuracy sufficient for crosshole tomography surveys, i.e. better than 0.5 m. The sonic velocity, single-point resistance, normal resistivity, and caliper logs were used for fracture identification. The caliper log did not have enough sensitivity to indicate more than a few fractures. The correlation among the other three logs was generally good, and anomalies occurred in locations where increased fracturing and/or alteration was observed in the core.

The borehole temperature and groundwater salinity logs were used to obtain data on groundwater flow. Locations of major inflow or outflow to the boreholes were identified and correlated with the sections of high hydraulic transmissivity observed during hydraulic testing. The natural gamma radiation log was used to map changes in lithology. However, this logging technique provided only limited data of usefulness due to the presence of high radon concentrations in the Stripa granite as a consequence of its high uranium and thorium contents. Because of the relatively low porosity of the granite, the neutron-logging technique was mostly sensitive to variations in lithology rather than to providing an absolute measure of water content.

Geometric Characteristics of the H zone

Based on hydraulic testing in the N and W boreholes in Stage I, the H zone was thought to be a principal pathway for groundwater flow through the SCV site. This hypothesis was confirmed essentially by the hydraulic testing in the D boreholes in Stage III. Based on the geophysical data, the strike of the H zone was determined to be 5° to the northwest with a dip of about 70° to 80° to the east. With this orientation, the projected intersections of the zone with existing mine drifts were confirmed at the 310 m, 360 m, and 410 m levels. The zone was also projected to intersect the access drift between the 385 m and 410 m levels and the Validation Drift at the 385 m level.

The overall geometry of the H zone was determined to be essentially planar, based on observations of the zone at the drift and borehole intersections. However, as shown in Figure 3-41, the southward extension of the zone appeared to be offset or to change strike where it crossed the drifts at the 360 m level. Based on the data from observations and geophysical crosshole

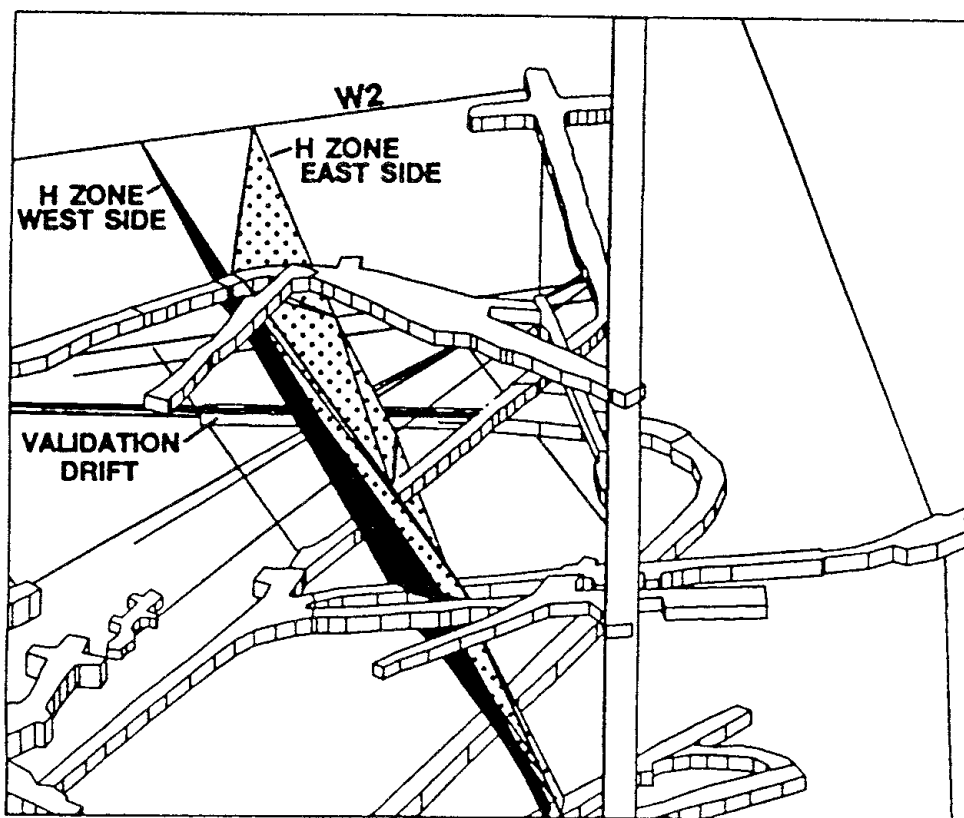


Figure 3-41 Perspective view of the SCV site showing the location of the east and west sides of the H zone (Olsson, 1992).

testing, the width of the zone appeared to vary along both the strike and the dip, with the apparent width of the most intense fracturing in the zone ranging from 2.15 m to 4.25 m. Based on the hydrologic significance of the zone in the SCV site, and its strong definition on the 310 m level, it was hypothesized that the zone extended to the surface as a structural feature and probably was represented as a well-defined surface lineament at the local scale of the mine.

Based on detailed mappings in the drifts, the fracture intensity appeared to decrease with increasing depth, apart from small lenses of intense deformation (Gale et al, 1991). The pattern of lineation orientations, showing evidence of shear displacement, suggested an oblique dip-slip fault movement, which was consistent with what appeared to be an abrupt change in the strike or offset of the H zone at the 360 m level. Based on drift mappings, the fracture pattern was found to extend at least 10 m into the rock adjacent to the fracture zone. This observation and others gave the impression that the small-scale fractures within the SCV site reflected the orientation of the large-scale features.

Characteristics of Small-Scale Fractures

Considerable effort was devoted to characterizing the geometry of the fracture system within the SCV site. The drift walls were photographed and mapped using a scan line approach to provide basic data on fracture

orientations, trace lengths, and surface characteristics (Gale and Strähle, 1988; Gale et al, 1990b; Burse et al, 1991). These data were augmented by similar information obtained from core logging and TV camera photography of the boreholes. Cluster analyses were performed on the data from each stage of the SCV programme, as well as on different combinations of borehole and scan line data.

The analysis of the fracture data from Stage I, based on six boreholes and seven scan lines, indicated the existence of at least two well-defined sub-vertical fracture sets at the SCV site, as well as potential for the existence of a sub-horizontal fracture system. At the end of Stage III, eleven scan lines and areal maps of the H zone had been completed.

A total of twelve clusters were initially defined by the cluster analysis. Later, small clusters exhibiting similar orientations were grouped together to optimize the use of the data in modelling efforts and to be more consistent with the geologic model. The mean orientations of these six statistically significant clusters are shown in Figure 3-42. The mean spacing between fractures in these clusters ranged from 0.45 m to 2.95 m, while the mean trace lengths varied from 1.67 m to 2.78 m. Clusters 1, 2, and 3, which were relatively steeply dipping, exhibited similar trace lengths ranging between 1.67 m and 1.83 m. The more gently dipping fractures in clusters 4, 5, and 6 have longer trace lengths ranging between 2.06 m and 2.78 m. Frequency histograms of raw trace length data are shown in Figure 3-43 and illustrate the degree of censoring. In addition to the censoring bias in the trace length measurements, these data also included truncation and shape biases. Truncation bias existed because only fractures having trace lengths greater than 0.5 m were mapped. When the data were corrected for censoring and truncation biases, the trace length statistics differed considerably for all clusters when compared with the initial raw data values. Values of the means and standard deviations were higher by approximately 1 m and 3 m, respectively, for the corrected data set. However, when the shape bias of fractures was taken into account, the mean fracture length decreased and ranged between 0.47 m and 0.84 m.

The intersections of the fracture zones with the boreholes were determined from the core logs, based generally on the red color associated with the fracture zones and the increased fracture frequency. Complimentary information from single-borehole and crosshole radar, seismic, and hydraulic measurements was also taken into consideration (Olsson et al, 1989; Black et al, 1991). The fracture data from the sections of the drill core were analyzed to determine the orientations and spacing of the fractures within the zones. Borehole fracture data in itself, however, does not provide a complete sample of the geometry of the fracture system in a fracture zone, especially when the boreholes have an orientation bias. To provide more detail on the geometry of the fractures adjacent to and within the H zone, the fractures in the walls of the drifts at the intersections of the zone were mapped (Gale et al, 1991). The fracture intensity within the zone was much greater than that in the average rock, with two strong sub-vertical fracture sets and a weaker sub-horizontal fracture set being present. As shown in Figure 3-44, five main clusters of fractures existed within the H zone where it intersected a drift on the same level as the Validation Drift. Nearly all the fractures terminated against other fractures, thus producing a large number of three-way fracture intersections within the network. In

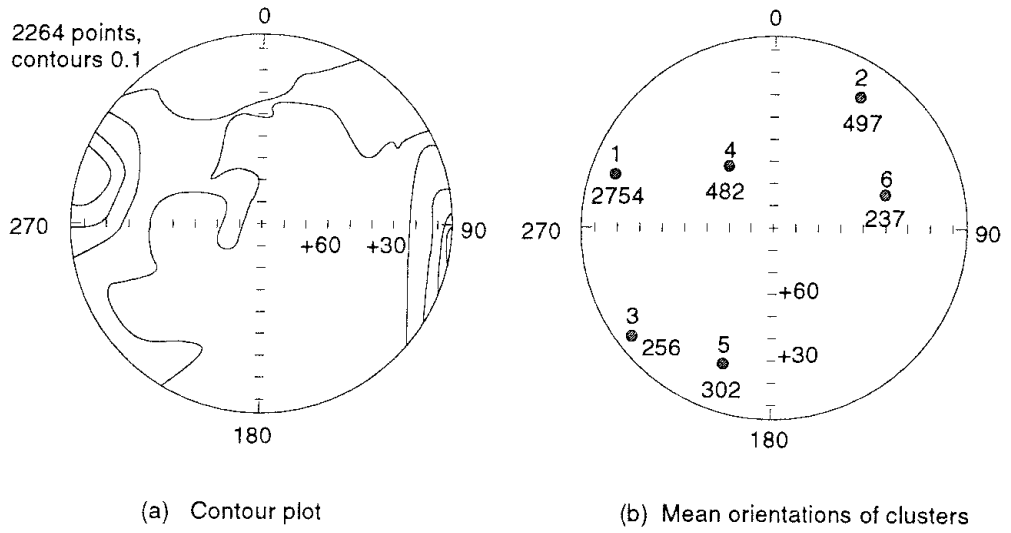


Figure 3-42 Lower hemisphere plots of the normals to the fracture planes for boreholes and scan lines at the SCV site (Olsson, 1992).

These data were obtained in Stages I and III and exclude fracture zone data.

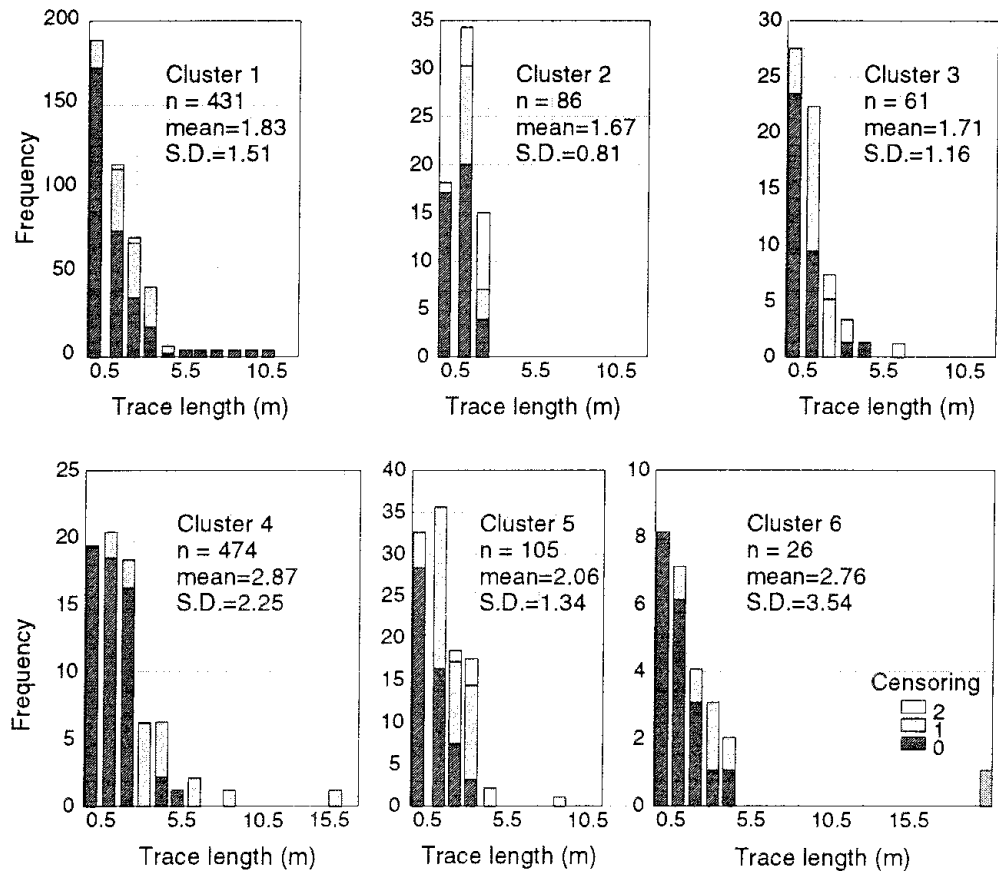


Figure 3-43 Trace length histograms for each cluster of fractures in the "averagely fractured rock" at the SCV site by degree of censoring (Olsson, 1992).

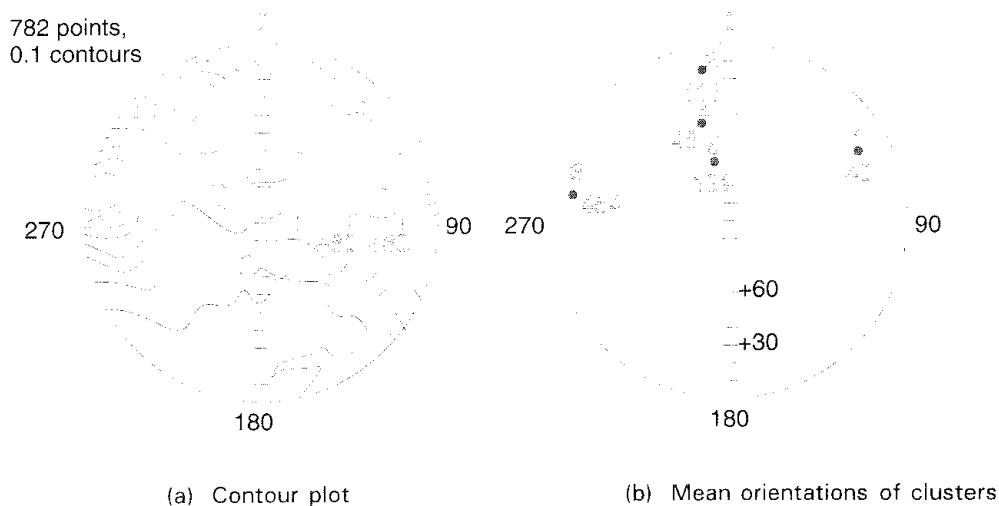


Figure 3-44 Plots of the contour of poles to fracture planes and mean cluster orientations for fractures in the H zone (Gale et al, 1991).

contrast to the variability in fracture orientations with depth within the H zone, the fractures in the "good rock" or "average rock" adjacent to the zone showed a much more consistent pattern from level to level in the mine. When all of the fracture data from the west side of the fracture zone were plotted and compared to the data from the east side of the fracture zone, a nearly identical pattern of orientations was obtained. The combined east and west data sets were dominated by two strong fracture sets, trending north-northeast to south-southwest and northwest-southeast.

Index tests, conducted on a large sample of fracture planes from the two main sub-vertical fracture sets present in the core from boreholes N3, W1, and W2, indicated that these fracture sets were characterized by low residual friction angles and low overall shear strengths (Vik and Barton, 1988). Laboratory tests on 200 mm diameter cores demonstrated that fracture transmissibility was inversely proportional to the normal stress acting on the plane raised to a power (Gale et al, 1990a; Makurat et al, 1990a,b). That is, as the normal stress was increased, the transmissibility decreased approximately in proportion to the stress raised to a power of "n". For a single cycle of loading and unloading of the fracture plane, the value of n ranged from about 0.2 for highly mineralized joints under linear flow conditions to about 1.2 for shear type fractures under radial flow conditions. The wide range in these values for the different fracture types was consistent with the wide range of permeability values measured at the SCV site.

An *in situ* block test was performed in the 3D migration drift (Barton et al, 1992). A schematic of the test arrangement is shown in Figure 3-45. The block had a volume of 2 m³ and contained a 1.4 m-long diagonal fracture coated with chlorite. Water was injected into one of the 50 mm-diameter drillholes along the fracture plane and collected in the second 50 mm-diameter drillhole, while the plane was subjected to normal stress loadings induced by the flat jacks in the slot at the edge of the block. The results indicated that, for the type of smooth, mineralized fracture plane in the block, there existed a threshold value of normal stress. Above this threshold

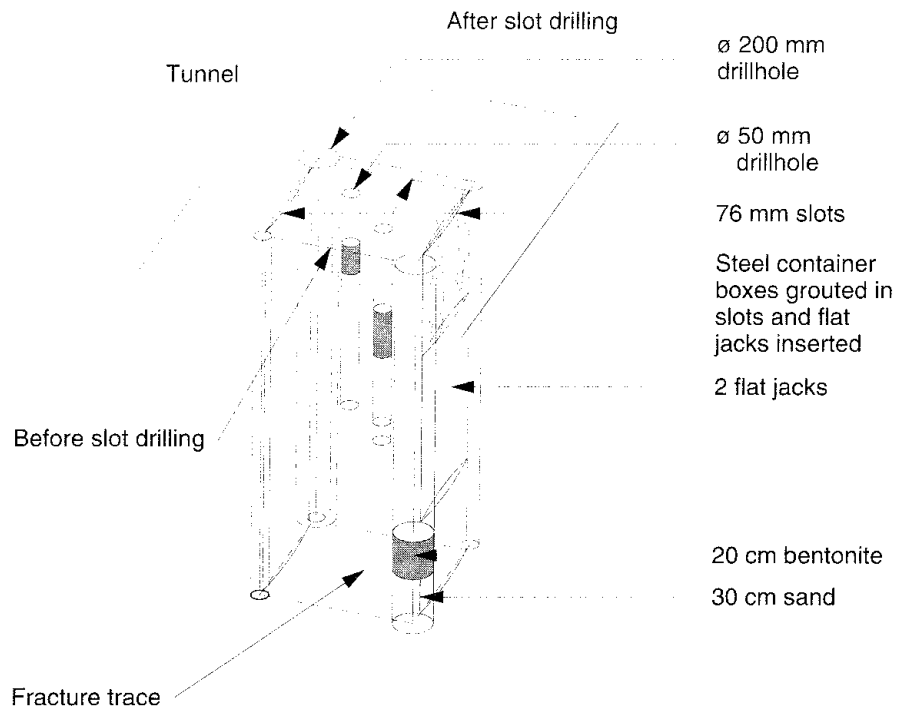


Figure 3-45 Schematic of the large-block stress-flow test performed in the 3-D migration drift (Makurat et al, 1990).

value, the hydraulic properties of the fracture were mostly governed by properties of the mineralization and to a lesser degree by the fracture roughness and aperture.

Stress Conditions

In situ stress measurements were made in nine boreholes in three locations at the approximate level of the SCV site during the early phases of the Stripa Project and during Stage I of Phase 3 (Strindell and Andersson, 1981; Bjarnason and Raillard, 1987; McKinnon and Carr, 1990). The results of these measurements, summarized in Figure 3-46, showed that in the vicinity of the drifts the major secondary principal stress was oriented approximately west-southwest to east-northeast and the minor secondary principal stress was oriented in the direction of assumed stress relief as represented by the old mine workings. The stress measurements that were made in boreholes DBH-1, DBH-2, and DBH-3 during Stage III were generally consistent with the orientation of stresses observed from the measurements made during the early phases of the Stripa Project. Based on the complete decay of stress perturbations because of the mine excavations from borehole DBH-2 to borehole DBH-1, it was concluded that the location of the Validation Drift within the SCV site was in a virgin stress field. Based on the total set of measurements, the maximum principal stress at the 385 level of the SCV site was estimated to have a magnitude of 24.4 MPa and to be oriented N75W. The minimum principal stress, assumed to be vertical, was estimated to be 10 MPa and the intermediate principal stress to be 16 MPa.

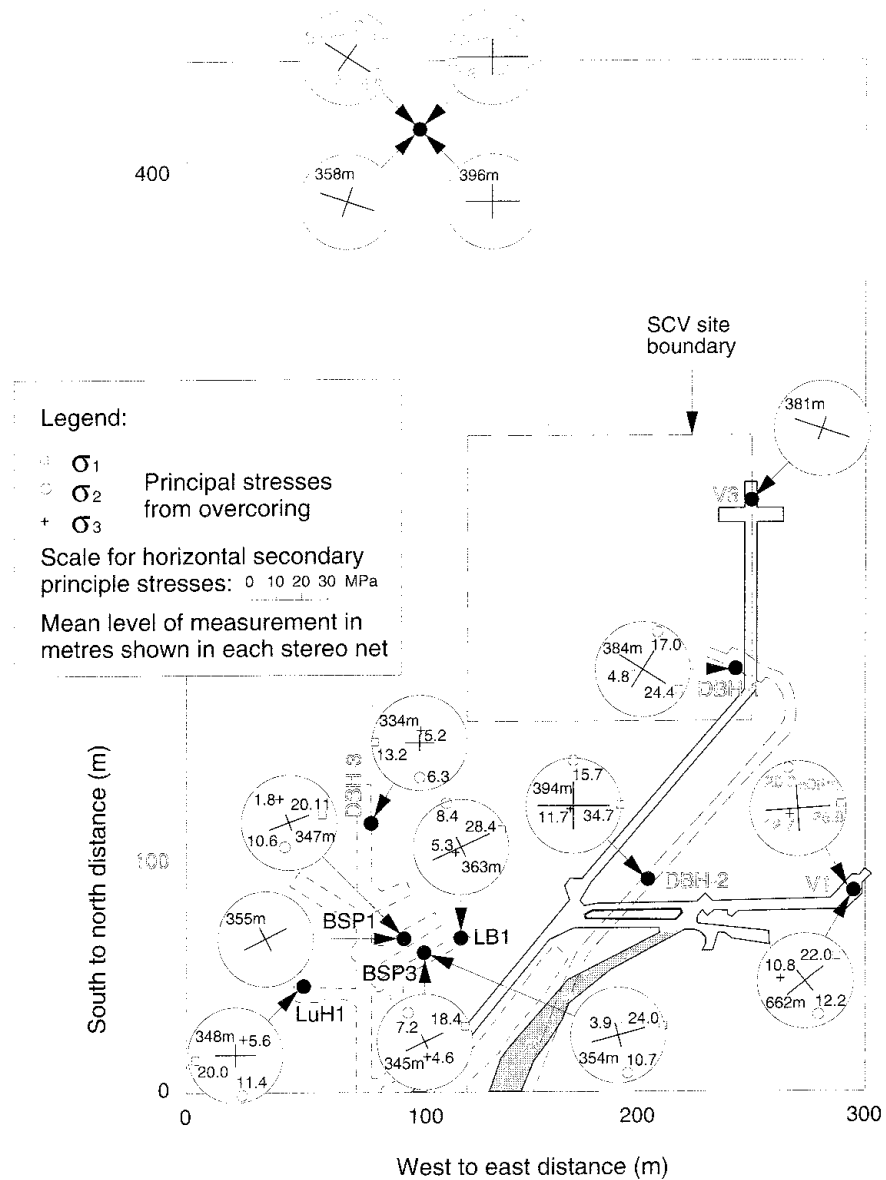


Figure 3-46 Plan view of the *in situ* stress measurements conducted in the Stripa Mine since 1977 (McKinnon and Carr, 1990).

Since the old mine workings appeared to have no effect on the state of stress in the rock mass in the SCV site into which the Validation Drift would be excavated, efforts were focussed on understanding the changes that would be induced in the stress state because of excavation of the drift. Three different modelling approaches were used to examine such changes in the stress state:

- a 3-D hybrid boundary-element/finite-element model, known as BEFE, that assumed the rock to be homogeneous, isotropic, and linearly elastic, with the fracture zones modelled as artificial planes in a continuum (McKinnon and Carr, 1990).
- a 2-D discrete fracture model, known as UDEC-BB, that simulated the strongly non-linear and scale-dependent behavior of the jointed-rock mass surrounding the underground excavation, assuming a condition of

plane strain and a two-dimensional representation of discontinuities (Monsen et al, 1991, 1992; Barton et al, 1992).

- A 3-D discrete fracture model, known as 3-DEC, which is a three-dimensional version of UDEC (Tinucci and Israelsson, 1991).

The BEFE continuum model was used to examine in detail the stress state around the Validation Drift, particularly at the locations of the fracture zones and in selected planes oriented perpendicular and parallel to the drift. Contours of shear stress are shown in Figure 3-47 for a plane oriented perpendicular to the drift and located 25 m from the western end of the drift. As expected on the basis of the magnitudes and orientations of the *in situ* stresses, the shear stresses in the roof and floor of the drift are quite high, as compared to the significantly lower stresses in the springline of the drift. The small difference between the orientation of the drift and the direction of the maximum *in situ* stress produces an asymmetry in the stress distribution, but this asymmetry disappears at a distance of a few drift diameters into the rock mass.

Fracture statistics were used in the 3-D NAPSAC code to generate stochastically the fracture geometry within two cubes with 8 m side lengths (Herbert et al, 1991). The four faces of these two cubes oriented perpendicular to the Validation Drift were used to define the discrete two-dimensional fracture geometries for the UDEC-BB models. Fracture input data were organized in the form of histograms to account for the variability in the joint roughness coefficient, joint wall compressive strength, and

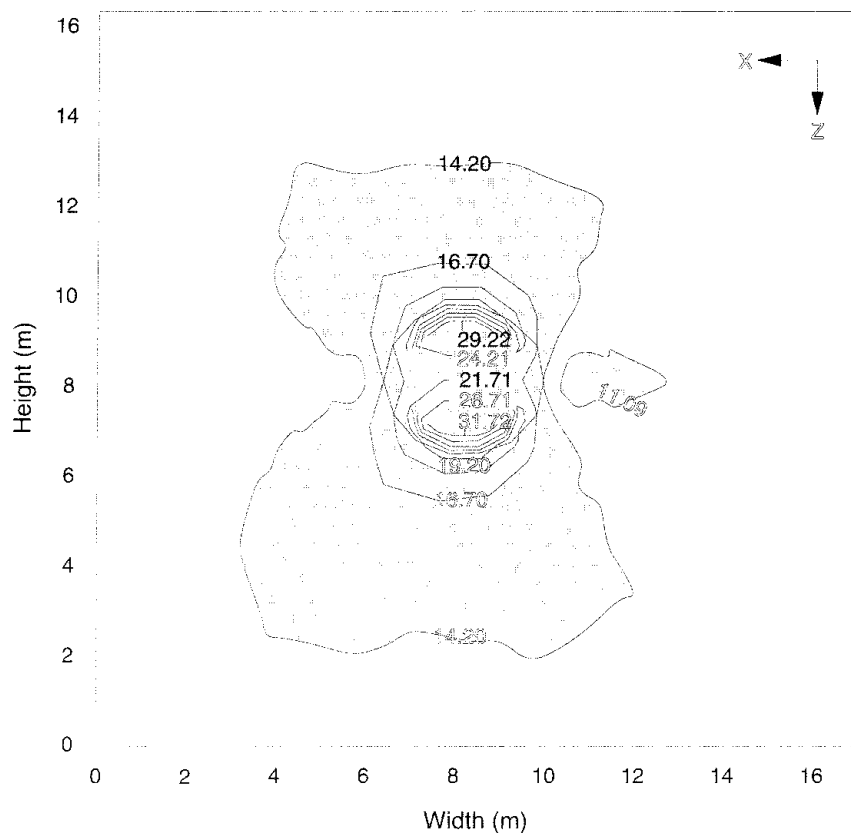
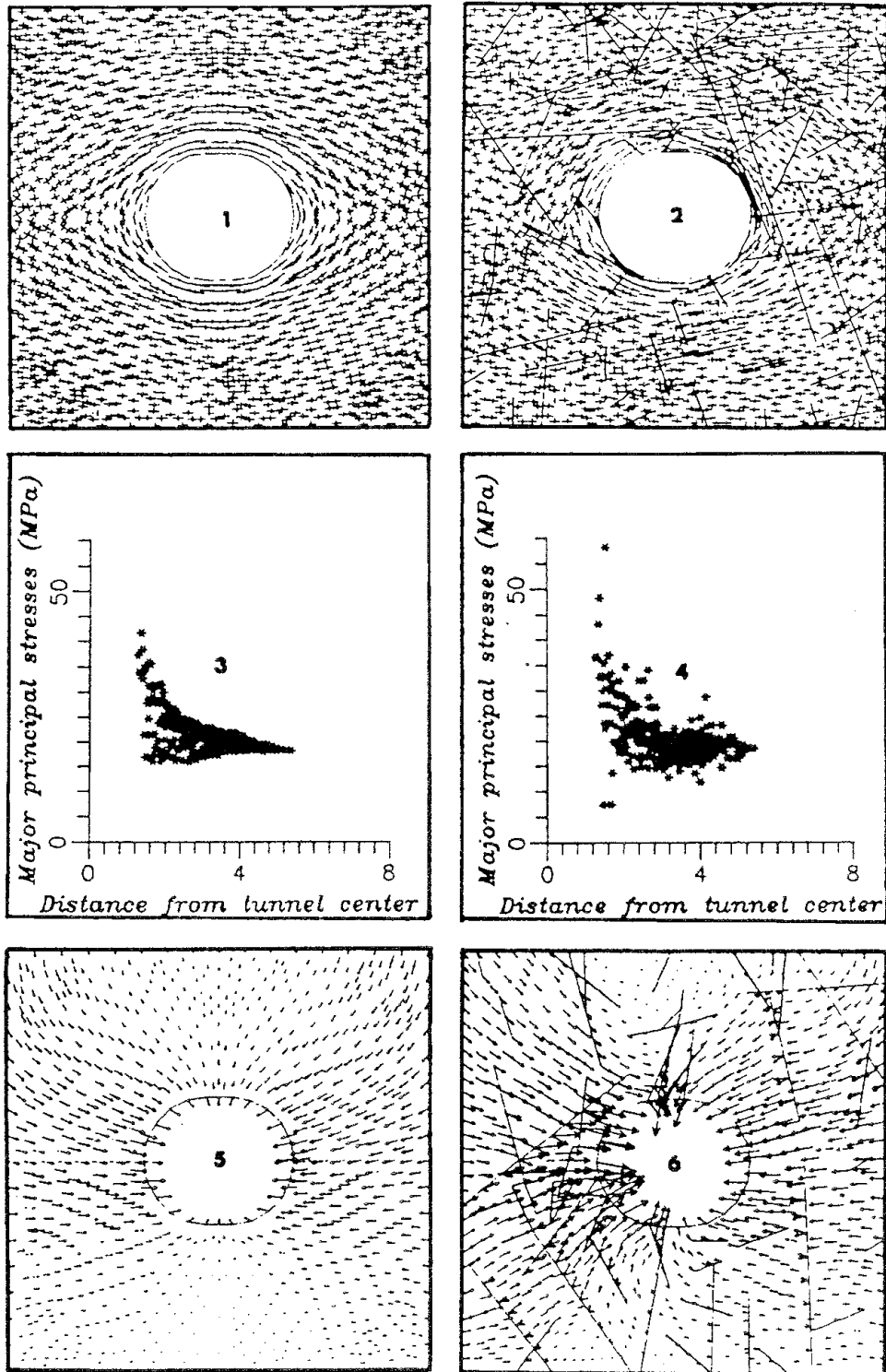


Figure 3-47 Distribution of shear stresses in a plane perpendicular to the Validation Drift as computed with the BEFE continuum model (Black et al, 1991; McKinnon and Carr, 1990).

residual friction angle. The model calculations showed that the bulk of the changes in fracture aperture occurred within a distance of 0.5 m of the drift wall. The results indicated that the shearing of fracture planes was more effective in generating channels of fracture intersections than channels generated by dilation, partly reflecting the orientation and the two-dimensional nature of the fracture system in the model. These intersection channels provided for potentially increased permeability perpendicular to the plane of the two-dimensional model, generally at radial distances of 0.5 m to 1.5 m from the drift wall. As shown in Figure 3-48, the continuum model yielded smoother stress gradients and less radial variability in the principal stresses than the discontinuum model. However, the differences in magnitude and pattern of the displacements between the two models were more significant.

In general, the 3-DEC results corresponded to those obtained by the UDEC-BB analysis for the stress redistribution, and including locally strong stress concentrations in the rock mass as a consequence of the drift excavation. The most important difference between the continuum and discontinuum models is that the fracture behavior results in a nonuniform distribution of stresses around the excavation. The excavation stress effect is most significant on features oriented obliquely to the drift. The normal stresses are relatively high immediately around the drift after the face passes by the point of observation. However, the 3-DEC model calculated normal stresses that were lower than the *in situ* stresses at a distance of 1 m to 1.5 m into the wall of the drift.

With the 3-DEC model, the most noticeable changes in normal and shear stresses occurred along planes oriented parallel to the drift. Fractures in the major fracture sets generally tended to close immediately around the drift, while further into the wall rock the fractures tended to open slightly as a result of the excavation. The computed results suggested that the shear stresses were not high enough to induce extensive slip of fractures in the rock mass around the drift. However, the difference in stiffness of fractures as compared to that of the rock mass was sufficient to give a nonuniform stress distribution around the excavation. The results also indicated that fractures most influenced by the advancing drift were oriented sub-parallel to the drift, but not intersecting it. These included two major fracture sets exhibiting sub-horizontal and sub-vertical dips along the length of the drift. Such fractures could conceivably give rise to a significant reduction in normal stress as compared to other fractures because they are oriented normal to the low radial stresses. Steeply dipping fractures oriented perpendicular to the drift did not appear to be greatly influenced by the presence of the advancing drift because the normal stresses did not change appreciably from *in situ* conditions. The direction of the normal stress to these fractures was oriented nearly the same as the major principal stress prior to excavation. However, changes in the shear stresses in the periphery of the advancing drift face might be significant. The 3-DEC analysis assumed a uniform stress field before excavation and a constant linear fracture stiffness. A nonuniform stress field might actually exist in the region around the H zone because of the differences in stiffness of the fractures within the zone and in the rock outside the zone. These variations in fracture stiffness would have significant influence on changes in fracture aperture but less so on the changes in stresses.



(a) Continuum stress analysis

(b) Discontinuum stress analysis

Figure 3-48 Comparison of the stresses and displacements in a plane perpendicular to the Validation Drift as computed with the BEFE continuum model and the UDEC-BB discontinuum model (Vik and Barton, 1988; McKinnon and Carr, 1990; Olsson, 1992).

Hydrologic Characteristics

The hydrologic characteristics of the SCV site were investigated by means of single-borehole testing, small-scale crosshole testing, and large-scale crosshole testing (Ball et al, 1991; Black et al, 1991; Doe et al, 1990a,b; Holmes, 1989; Holmes and Sehlsedt, 1991; Holmes et al, 1990; Olsson, 1992). Apart from the single-borehole testing, the hydraulic tests had to be conducted within restricted time schedules because of other experiments being conducted at the SCV site. As a consequence, the tests were often performed against varying head conditions as time was not available for full equilibration of the groundwater pressure in the rock mass within the mine. The testing focussed on the most permeable parts of each borehole, and straddle packers were used to isolate intervals of variable length containing, when possible, single fractures.

The single-borehole tests in the C, N, and W boreholes yielded average values of hydraulic conductivity ranging from about 10^8 m/s to 10^{10} m/s. However, there was no apparent correlation between average hydraulic conductivity and fracture frequency. In essence, the testing indicated that there were a few highly transmissive fractures, about 1% of the total, that carried the bulk of the water flow. The measurements of groundwater head in the boreholes indicated a pattern of high heads to the northeast of the SCV site, about 200 m of head above the 360 m level in the mine, with a decrease in heads to the south and west. This pattern reflected the likely movement of groundwater draining into the mine excavations. Analysis of the transient responses from the single-borehole tests indicated that the fracture system within the SCV site behaved as a well-interconnected network, and that tests within sections of the fracture zones generally exhibited a dimension of spherical flow.

The purpose of the small-scale crosshole testing was to determine the variability of hydraulic parameters, such as transmissivity and storativity, of fracture zones over a distance of a few metres between the D boreholes within the central interior of the SCV site. The testing programme involved isolating the B and H zones by means of packers in each of the D boreholes, and then pumping one of the boreholes and observing the response in the other boreholes. As shown in Figure 3-49, large variations in the flow rates were observed within each fracture zone over very small distances. The transmissivity of the conductive rock within the fracture zones was, on average, about 10^{-7} m²/s.

The purpose of the large-scale crosshole tests was to identify the hydraulic connections across the SCV site and determine their hydraulic properties, and, in so doing, provide data to test the conceptual models of the fracture zones. The term "large scale" implied measurements over the entire head-monitoring array that encompassed the SCV site and adjacent regions in the Buffer Mass Test area and Crosshole site. In addition to identifying the interconnections of networks of hydraulic conduits across the site, the hydraulic properties of these conduits were evaluated over scales of tens to hundreds of metres. Although some sinusoidal testing was performed, the principal test method involved constant-rate pumping from an isolated section of a borehole. During pumping, the head changes were monitored in packed-off sections of the other boreholes and throughout the general site

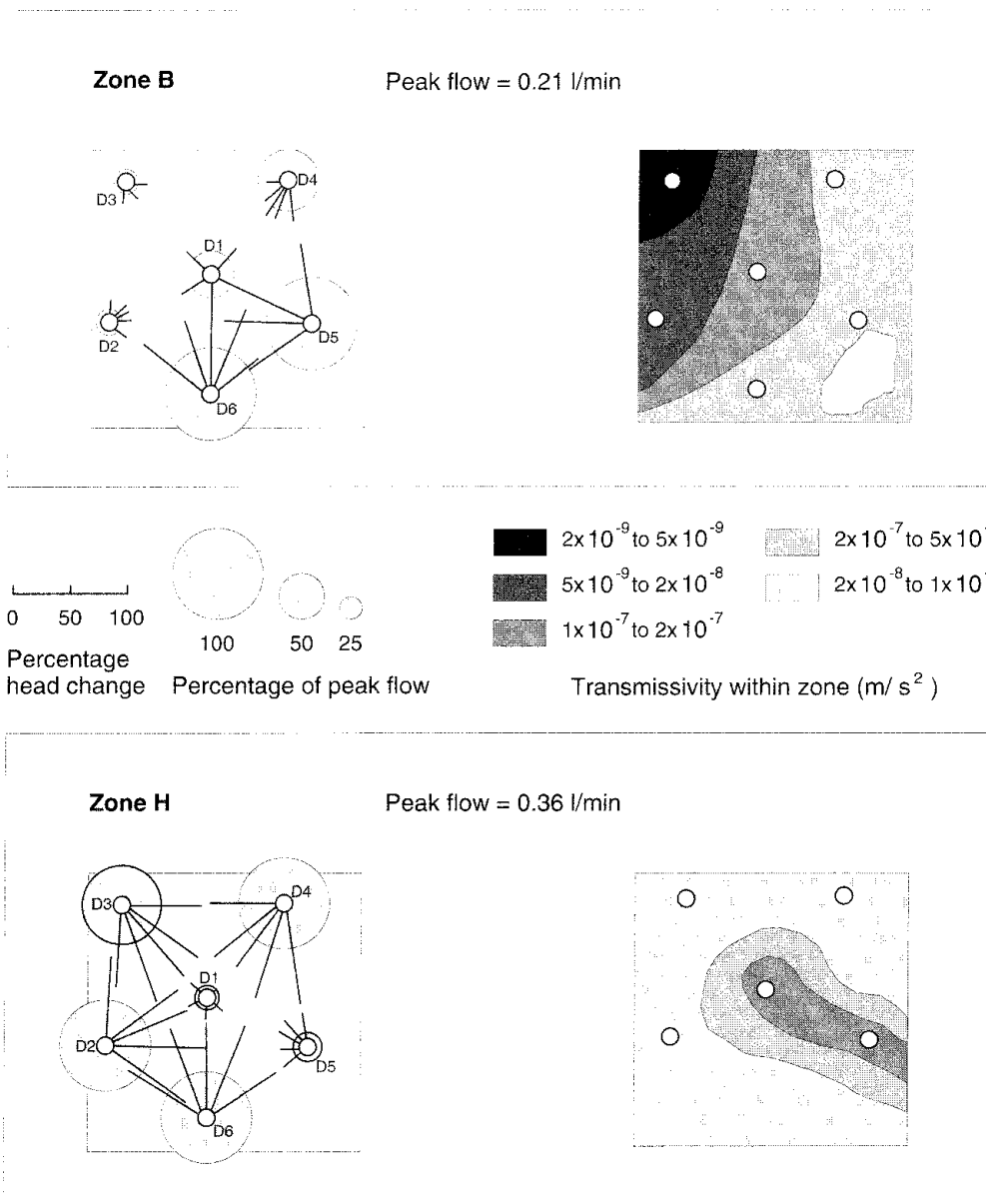


Figure 3-49 Variation in the hydraulic transmissivities of the B and H zones as determined by small-scale crosshole testing (Holmes et al, 1990; Olsson, 1992).

The units of transmissivity are m^2/s .

area by means of the Piezomac long-term head monitoring system. The Piezomac system was installed in existing boreholes during the early part of Phase 3 and was programmed to complete a cycle of measurements every thirty minutes.

The hydraulic connections were identified by tabulating the monitoring points that responded to a disturbance created by pumping at a "source interval" in a borehole. The diffusivity and dimension of the flow path were then determined by matching a type-curve to the pressure response at the observation point. Subsequently, the draw-downs were plotted as a function of distance from the source at a particular time during the testing, as shown

in Figure 3-50. In a homogeneous material or an aquifer, the drawdown points will lie along a type-curve of an appropriate dimension. The quality and consistency of the type-curve match reflects the homogeneity of the flow system. The deviation of individual points from the match indicates either an over-connection or under-connection of the particular source interval to the conduit. The value of the flow dimension derived from a fit of the data to a type-curve can be considered representative of a fracture zone over a scale of about 100 m.

The bulk of the large-scale crosshole testing focussed on the hydraulic connections to the H and B zones. These zones appeared to behave as consistent hydraulic conduits with a flow dimension between cylindrical and spherical. The consistency of the relationships between drawdown and

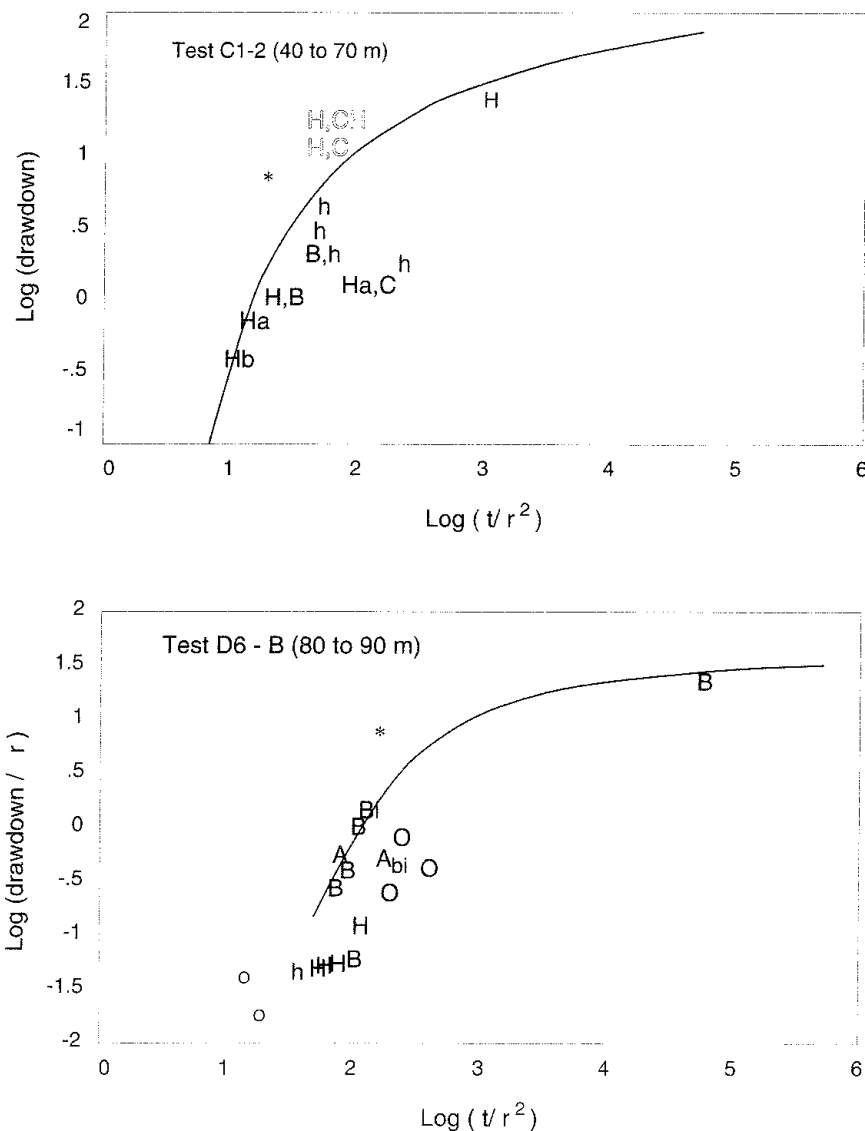


Figure 3-50 Distance-drawdown plots for large-scale crosshole hydraulic tests C1-2 and D6-B (Ball et al, 1991; Olsson, 1992).

Drawdown in a borehole is expressed in the unit of metres. The distance from the measurement point in the borehole to the source zone is designated as r in metres. The unit of time t is seconds.

distance, as shown in Figure 3-50, suggested a large-scale homogeneity of hydraulic properties within these fracture zones. The fracture zones were connected to the R, I, and N1 boreholes located outside the boundary of the SCV site. The transmissivities of the fracture zones were within the range of 10^{-7} m²/s to 10^{-8} m²/s, and the storativities ranged from 10^{-5} m⁻¹ to 10^{-6} m⁻¹.

Geochemical Characteristics of the Groundwater

The purpose of the geochemical investigations was to distinguish between different groundwater types and, based on their spatial distribution, to describe the flow paths within the fracture system at the SCV site. Although isotope analyses were made during Stage I, the geochemical studies focussed on the major constituents of the groundwater, as described by Wikberg et al (1988) and Laaksoharju (1990). Water samples were obtained from the N and W boreholes in Stage I and from the C and D boreholes in Stage III. The groundwater samples were collected from 44 packed-off fracture intervals in sections of the boreholes where the hydraulic conductivity was in excess of 10^{-8} m/s.

Multivariate statistical analysis showed that Cl⁻ and HCO₃⁻ were suitable variables for categorizing the groundwater at Stripa. The three groundwater types were shallow type-A, mixed type-B, and deep type-C, all of which contained total-dissolved-solids of less than 560 mg/ℓ. Type-A groundwater had a low concentration of Cl⁻, less than 70 mg/ℓ, and low concentrations of most other ions, with the exception of HCO₃⁻ which was greater than 50 mg/ℓ. Type-C groundwater had a high concentration of Cl⁻, greater than 150 mg/ℓ, and high concentrations of most other ions, but less than 30 mg/ℓ of HCO₃⁻. Type-B groundwater was the result of mixing between type-A and type-C groundwaters.

The chemistry of the groundwater in and around the SCV site reflected a system that was generally closed with respect to oxygen and CO₂. A reducing environment was evident from the presence of ferrous iron and sulfides. Isolation of this groundwater from sources of dissolved CO₂ was indicated by an increasing pH with depth. The vertical distribution of groundwater types within the SCV site is shown in Figure 3-51, wherein Cl⁻ is plotted as a function of depth and the approximate divisions between type A, B, and C groundwaters are indicated. The three main groundwater types were observed over a broad range of depths, reflecting the heterogeneity of the fracture system with respect to permeability. A weak trend of increasing Cl⁻ concentration with depth indicated mixing between the shallow and deep groundwaters at the SCV site. Shallow (W1 borehole) and deep (N2 borehole) groundwaters from the H zone were mixed in different proportions to simulate the mixed water composition in the D boreholes. Saturation indices for calcite were computed for the simulated waters and compared with indices computed for actual water samples from the D boreholes. The calculated and measured positive values confirmed that calcite precipitated during mixing, which correlated with the presence of calcite as a fracture mineral in the Stripa mine and with the results from other studies (Runnells, 1969; Puigdoménech and Nordstrom, 1987).

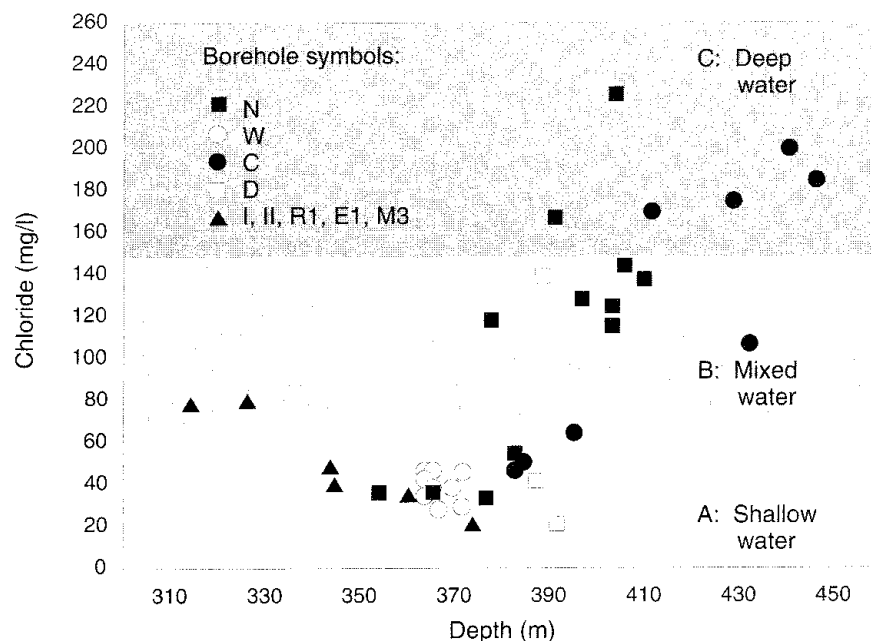


Figure 3-51 Chloride concentration of the groundwater as a function of depth within the SCV site (Olsson, 1992).

The geochemical data base indicated that there existed strong mixing of shallow and deep groundwater systems at Stripa. This conclusion was supported by the tritium data, which indicated a component of very young water in the groundwater system, and the deuterium ^{18}O data, which showed increasing age with increasing salinity. In addition, the large spread in uranium concentrations indicated that mixing between oxidizing and reducing waters had taken place at the SCV site.

Regional groundwater mixing at Stripa was indicated in Stage I on the basis of plots of chloride against sodium, where the data was obtained from analyses of samples of mixed waters collected from multiple fracture intervals and unmixed waters collected from discrete fractures, (Nordstrom et al, 1985). These flow paths were confirmed during the Stage III investigation. The flow paths within the B and H zones at the SCV site are shown in Figure 3-52. The draining of groundwater from the D boreholes over a long period of time reduced the hydraulic pressure in the B and H fracture zones. As a consequence, mixed water was formed by the drawdown of shallow water and the upwelling of deep water.

The groundwaters at Stripa contained dissolved gases which were released when the pressure was reduced, such as was observed during several experiments in the D boreholes. The total volume of dissolved gases in the groundwater from the D boreholes was approximately 3%, and was composed principally of nitrogen and carbon dioxide.

Configuration of the Groundwater Flow System

In order to simulate the groundwater flow and transport within the SCV site by means of numerical models, flow or head conditions on the boundaries of

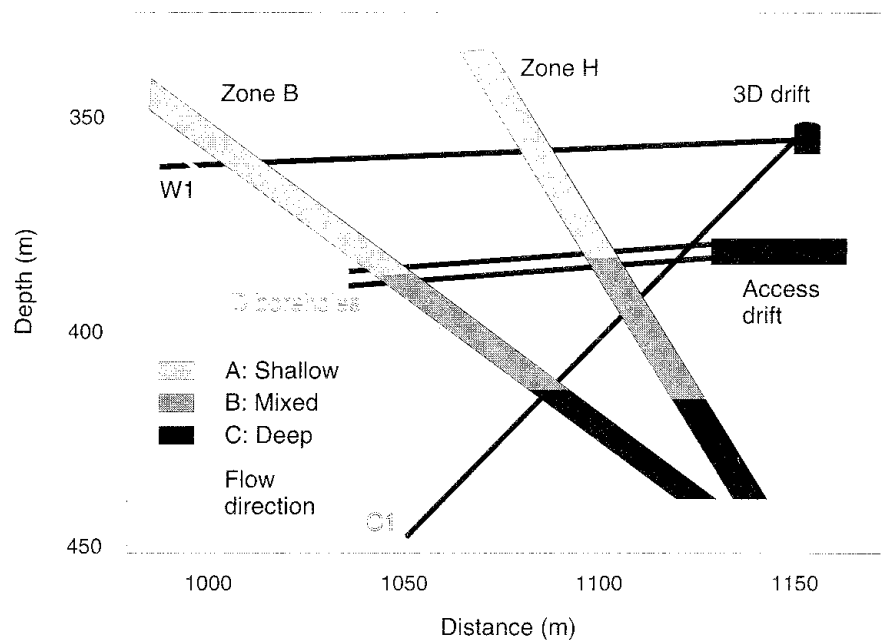
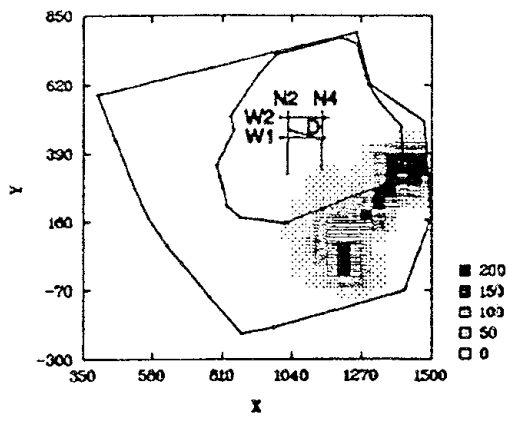


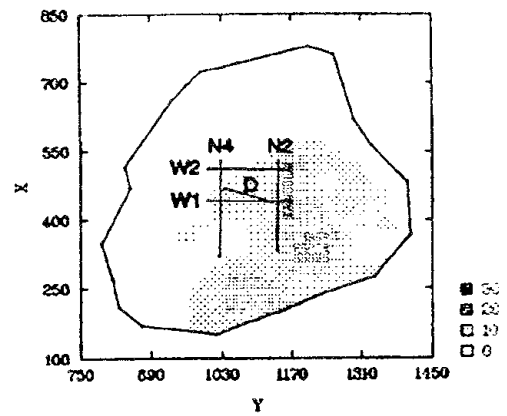
Figure 3-52 The local hydrochemical model for the SCV site illustrating the shallow (A), mixed (B), and deep (C) groundwater types and the inferred flow directions (Olsson, 1992).

the site were required. In addition, such conditions were required to map the configuration of the groundwater flow system and determine the directions of groundwater movement, thereby constraining the interpretation of the geochemical data for the groundwater. As described in Section 3.1, the three-dimensional steady-state distribution of hydraulic heads for the regional flow system was calculated by means of an equivalent-porous-media model (Gale et al, 1987). The boundary conditions for hydraulic head for a smaller local, or "sub-region", model were extracted from the computational results for the regional model. The results from both the regional and the local models indicated that the sink created by the mine excavations perturbed the groundwater flow system to depths of at least several thousands of metres. The three-dimensional distribution of hydraulic heads computed from the local model was used to provide the hydraulic-head boundary conditions for a model of a smaller region within the mine (Herbert et al, 1991). This model, known as MINE2, provided the hydraulic heads on the boundaries of the site. Finally, an equivalent-porous-media model of the SCV site was developed to provide the boundary conditions for flow and transport simulations within the immediate confines of the site. The three-dimensional MINE2 and SCV finite-element grids encompassed volumes of the order of 370 million m³ and 50 million m³, respectively.

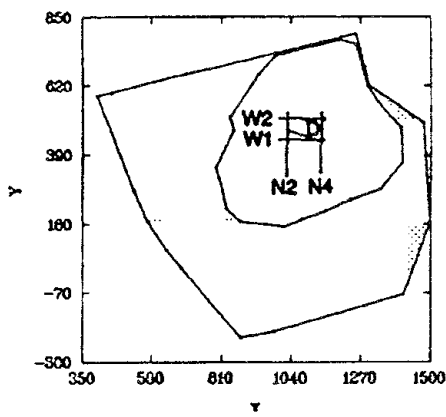
The distribution of downward and upward flowing groundwater within the SCV site, as shown in Figure 3-53, was obtained from the MINE2 and SCV models. The results from the local model indicated that the MINE2 and SCV models were situated in a zone of upward groundwater flow between the 600 m and 1250 m levels. Downward groundwater flow occurred to the north and west of the boundaries of these two models. The MINE2 model was dominated by upward groundwater flow between the 410 m and 600 m



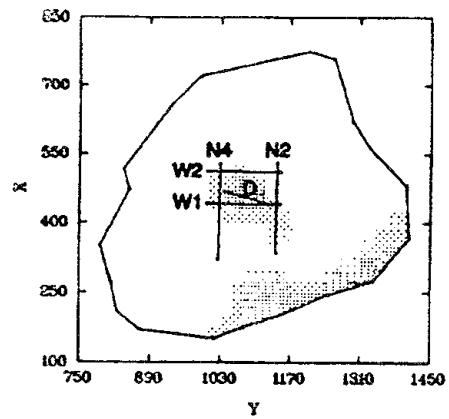
Mine 2 Model: 385 m-410 m Level



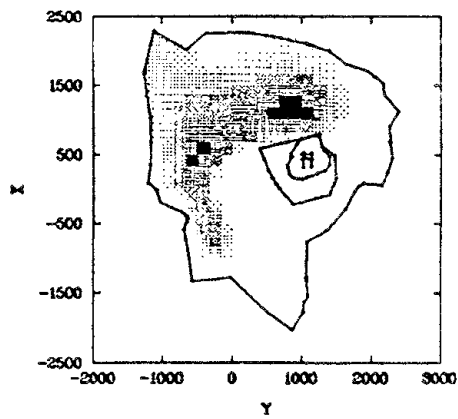
SCV Model: 310 m-360 m Level



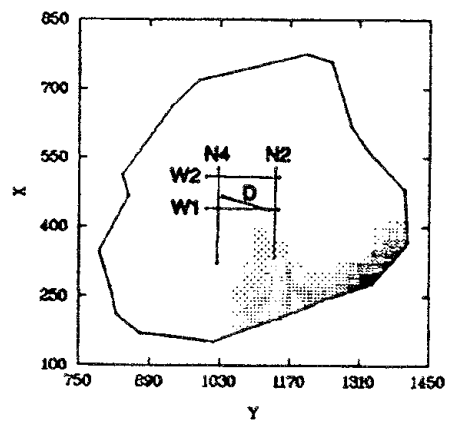
Mine 2 Model: 410 m-600 m Level



SCV Model: 360 m-385 m Level



Sub-Region Model: 600 m-1,250 m Level



SCV Model: 385 m-410 m Level

Figure 3-53 Regions of upward and downward groundwater flow within and around the SCV site as predicted by a combination of the local, MINE2, and SCV EPM groundwater flow models for different depth ranges (Olsson, 1992).

Regions of upward flow are clear and regions of downward flow are stippled.

levels, with downward flow only evident between the 385 m and 410 m levels. The SCV model yielded downward groundwater movement in the southeast portion of the model between the 385 m and 410 m levels. Between the 360 m and 385 m levels, the SCV model identified downward groundwater flow within the site, while a much larger zone was shown to encompass the central and southeast portions of the model between the 310 m and 360 m levels.

3.3.3 Geohydrologic Model of the Site

A geohydrologic model of a site is commonly a generalized description of the main geologic features in terms of lithological units and fracture zones, together with their geometries and properties, and the hydrologic features in terms of the principal hydraulic conduits and the head distribution. The development of the model of the SCV site involved identification of the major structural features and assignment of average properties to these features, along with a determination of which features were important in terms of groundwater flow and where they were located. The large-scale features were incorporated and described, while the smaller scale components, such as the flow distribution within fractures, were not included.

Based on observations and the results from borehole testing, the model development process began with the reasonable supposition that groundwater flow takes place in fractures within the rock mass, and that the rock surrounding the fractures could be characterized as having relatively low permeability. The fractures were assumed to be irregularly distributed throughout the rock mass and concentrated within fracture zones. Thus, the description of the rock mass was divided into two categories known as "fracture zones" and "averagely fractured rock". It was further assumed that these fracture zones, or "major features", were the pathways for the major portion of the groundwater flow through the SCV site. The major features were described deterministically in terms of geometry on the basis of results from borehole radar and seismic testing. Because of the relatively sparse nature of the information density on the properties of the fracture zones, such as hydraulic transmissivity, the hydraulic properties were assumed to be spatially homogeneous and represented by some average of values obtained at sampling points or by a stochastic description. Fractures in the "averagely fractured rock" were observed in drifts, in core, and by means of single-borehole geophysical tests. However, these observations were not capable of defining the lateral extent of the fractures or their properties outside the immediate region of observation. The presence of fractures, together with their size and hydraulic characteristics, in the "averagely fractured rock" between boreholes had to be inferred by means of stochastic methods from data collected in the boreholes and drifts.

Binary Model of the Rock Structure

As discussed above, a binary division of the rock mass at the SCV site was adopted in terms of "fracture zones" and "averagely fractured rock". The procedure for dividing the rock mass into these categories was based on principal component analysis of the results from single-borehole tests (Black et al, 1991). These results included normal resistivity, sonic velocity, and

hydraulic conductivity, together with observations of coated (open) fractures and data from single-borehole radar reflection tests. The procedure required that, first, the logarithm of the normal resistivity, sonic velocity, and hydraulic conductivity data be taken and, second, the data normalized by subtracting the mean value and dividing by the standard deviation for each parameter. The results obtained by this procedure for the data from all boreholes at the SCV site are given in Table 3-2. A matrix of correlation coefficients was formed and the eigenvectors were obtained for that matrix. Each eigenvector represented a weighting of the data, and new parameters, or principal components, were produced by multiplying an eigenvector by the normalized data values. The parameter obtained for the eigenvector corresponding to the largest eigenvalue represented the most important characteristic of the rock, namely the fracturing of the rock. This parameter was called the "fracture zone index".

Table 3-2 Mean values and standard deviation for data from all boreholes (Olsson, 1992). The means for the first three parameters are geometric, while the means for the last two are arithmetic.

| Parameter | Mean | Standard Deviation |
|-------------------------------|---------------------------|--------------------|
| Normal resistivity | 135 kohm | 0.1462 (log10) |
| Sonic velocity | 6.11 km/s | 0.0110 (log10) |
| Hydraulic conductivity | 2.0 10 ⁻¹¹ m/s | 1.2585 (log10) |
| Coated (open) fractures | 3.69 per metre | 4.0778 |
| Radar reflector intersections | 0.18 per metre | 0.3859 |

The information content in the principal components was related to the relative magnitude of the corresponding eigenvalue. For the first eigenvector, i.e. the "fracture zone index", almost equal weight was given to normal resistivity, hydraulic conductivity, and fracture frequency, with lesser weight given to sonic velocity and radar reflectors. The second eigenvector was dominated by information on radar reflectors. The three smallest eigenvectors were found to represent essentially noise in the data.

The frequency distribution of the "fracture zone index" values for all boreholes was skewed, as shown in Figure 3-54. The distribution was not bi-modal, but was considered to consist of two parts. One part was the more or less normal distribution centered around a mean value of slightly less than zero, and the second part was the tail of higher values. The division between the tail and the normal distribution occurred approximately at a value of two for the "fracture zone index". Thus, the binary classification of the rock mass was based on a fracture zone index of less than two for the "average rock" and a fracture zone index greater than two for the major features. Examples of the locations of "fracture zones" based on the fracture zone index, as identified in boreholes W1 and W2, are shown in Figure 3-55.

The "fracture zone index" was considered to provide a better definition of the hydraulically significant features than the single-borehole hydraulic

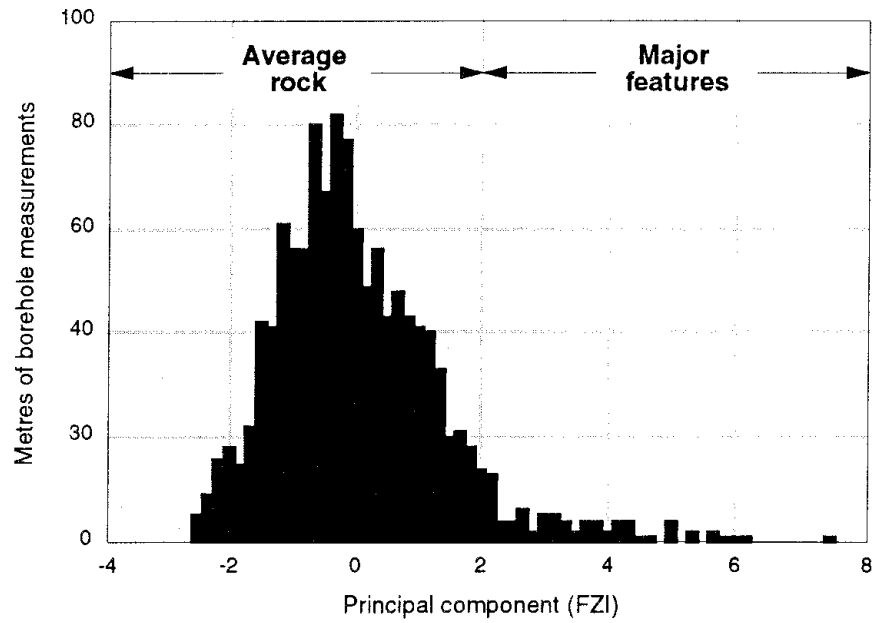
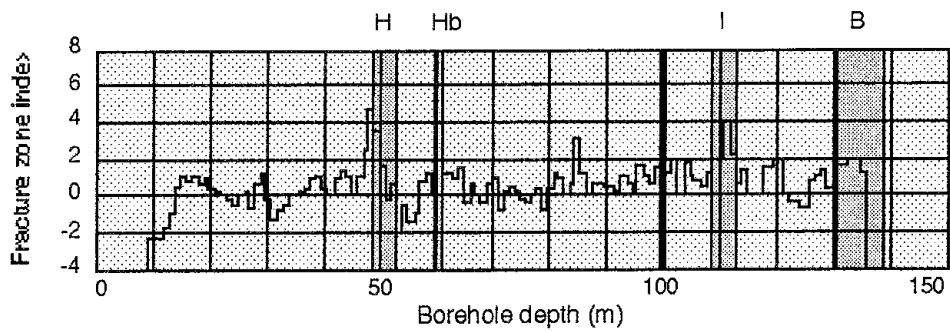
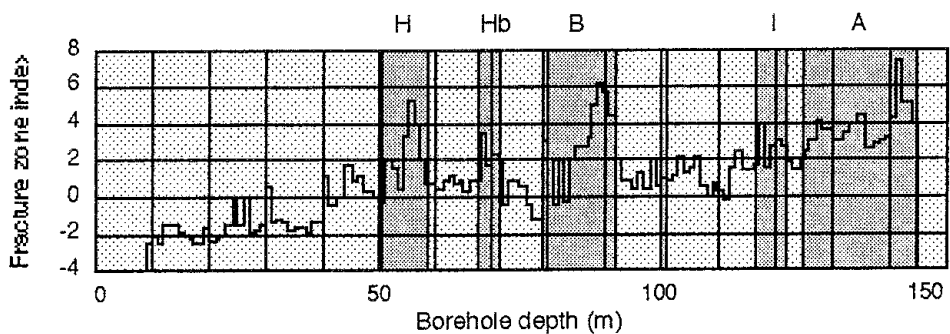


Figure 3-54 Frequency distribution of the "fracture zone index" (Olsson, 1992).

Values in the tail of the distribution for a fracture zone index greater than two are designated as "fracture zones", while values less than two are designated as "average rock".



(a) Fracture zone index for borehole W1



(b) Fracture zone index for borehole W2

Figure 3-55 "Fracture zone index" as a function of borehole depth for boreholes W1 and W2 (Olsson, 1992).

conductivity data by itself. Single-borehole hydraulic tests give results appropriate to a very small volume of rock surrounding the borehole, and, in the fractured rock at Stripa, the hydraulic properties were found to vary by more than an order of magnitude over small distances. Thus, a weighted parameter that included several types of data was considered to be preferable for defining the hydraulically important features. Approximately 7% of the total length of boreholes were found to have a "fracture zone index" greater than two, and, correspondingly, these locations accounted for 76% of the measured transmissivity. Thus, the "major features" defined on the basis of the "fracture zone index" accounted for the bulk of the groundwater flow within the SCV site.

Model Development Process

The integration of the test data for purposes of producing a geometric model of the site proved to be a formidable and complex task. The procedural steps required for the development of the model of the SCV site are shown in Figure 3-56. The first step in the process dealt with identification of the anomalous sections of the boreholes on the basis of the "fracture zone index". These anomalies were expected to be associated with specific major structural features. The geometric extent and orientation of the features were determined from radar and seismic testing data. In the next step, radar and seismic-reflection data, together with directional radar and tomographic data, were combined with the distribution of anomalies to develop a conceptual configuration of major features within the site. Projections of the expected intersections of the features with boreholes were made and checked against the borehole data. By means of this process, a geometric model of the major features within the site was developed.

The next step was to check the compatibility of the geometric model with the crosshole hydraulic responses and the head monitoring data, along with the geochemical data. If consistency could not be reasonably achieved, then additional data would be required through additional testing in the existing boreholes or testing in new boreholes.

During Stage II, a model of the structural features within the SCV site was constructed on the basis of an integrated interpretation of all data collected during Stage I. The C and D boreholes were drilled to evaluate the accuracy of the geometric predictions of the major features. Generally, the agreement between the predicted and actual locations of the fracture zones was quite good. The intersections of the B and H zones with the boreholes were accurately predicted, while there was a relatively large error, of the order of 26 m, in the predicted intersection of the A zone with borehole C1 because of an error in the predicted dip. The information base obtained by the Stage I testing was deficient because of the lack of data from the directional radar system and inclined boreholes. In addition, the lack of crosshole hydraulic measurements in Stage I did not allow a determination of the large-scale hydraulic properties and connections.

Based on the test data collected in Stage III, the conceptual model of the structural features within the SCV site was updated, although only minor modifications were necessary. No additional major features were discovered in the Stage III boreholes, and the orientations of the major features were

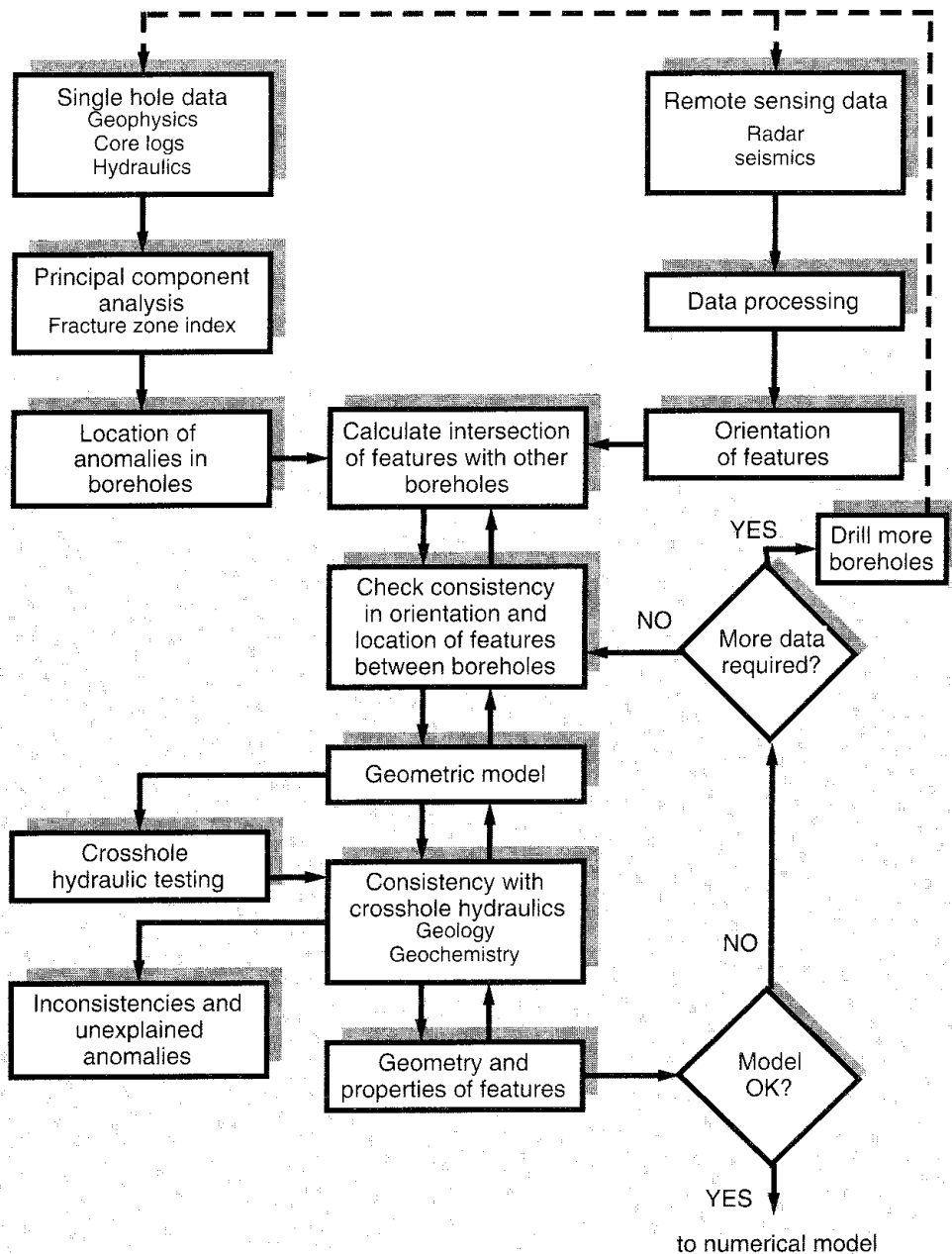
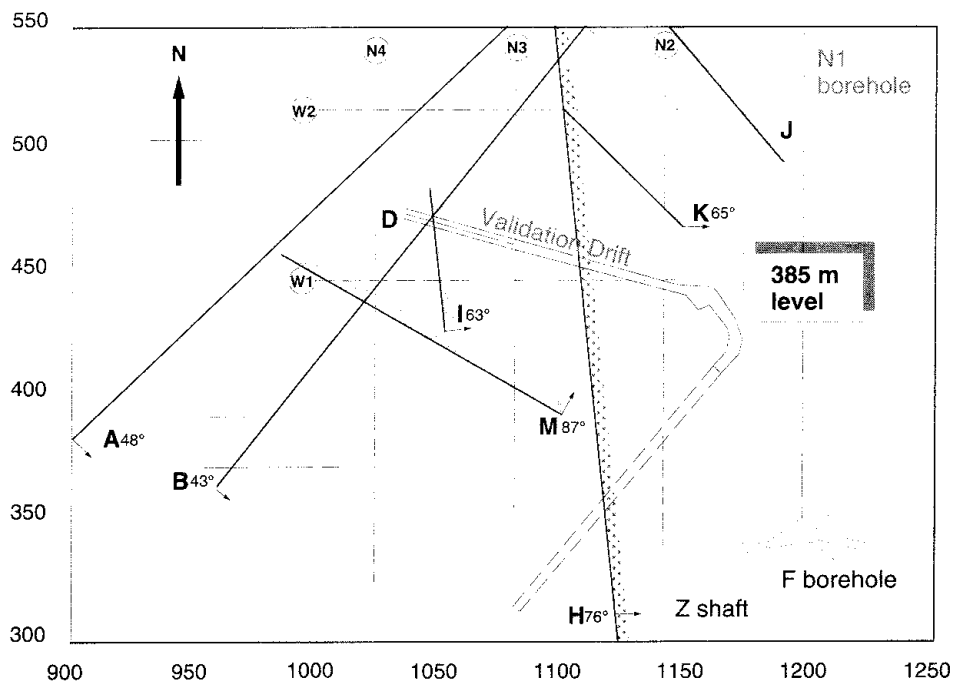


Figure 3-56 Procedural steps for construction of the conceptual model of the SCV site (Olsson, 1992).

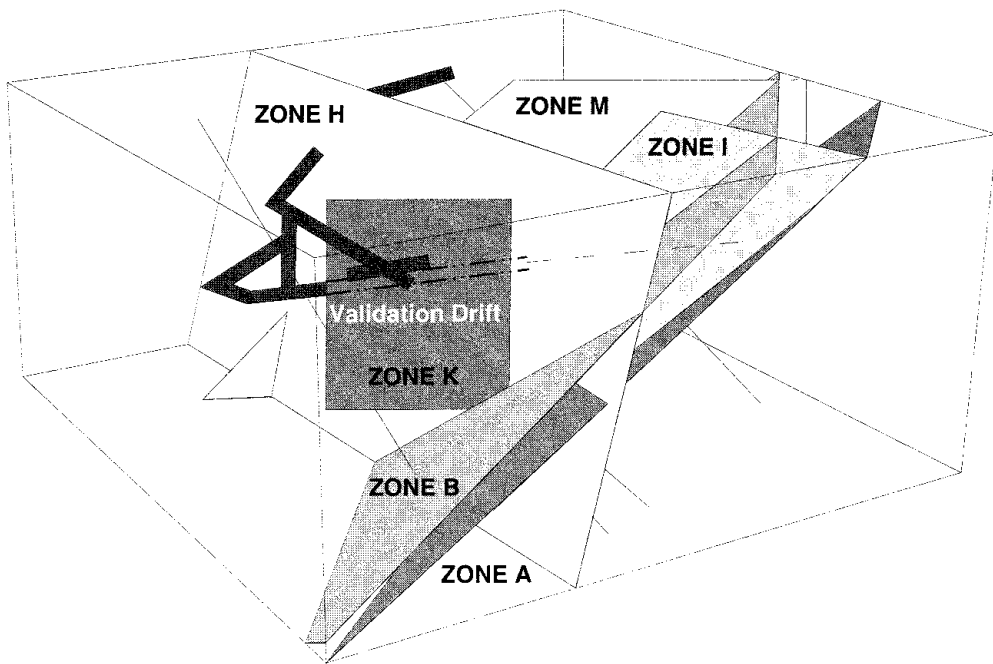
found to be approximately correct despite the deficiencies in the data set from Stage I.

Major Structural Features within the Site

The conceptual model of the SCV site, shown in Figure 3-57, contained three major features, or fracture zones, denoted as A, B, and H, and three minor features, denoted as I, K, and M. An additional feature, denoted as J, was inferred, but no additional data were collected to verify its existence,



(a) Plan view



(b) Perspective view

Figure 3-57 Perspective view of the deterministic fracture zones contained within the conceptual model of the SCV site (Olsson, 1992).

geometry, and properties. The geometric and hydraulic properties of these fracture zones are given in Table 3-3.

Table 3-3 Summary of the characteristics of the fracture zones contained in the conceptual model of the SCV site (Olsson et al, 1992).

| Zone | Dip (deg) | Strike (deg) | Real width ¹ (m) | FZI ¹ | Transmissivity (m ² /s) | | | Extent |
|------|--------------|-----------------|-----------------------------------|------------------|---------------------------------------|---------------------------------|----------------------|---------|
| | | | | | Fraction ³ % | Single Borehole ² | Cross- hole | |
| A | 48 | 47 | 6.2 | 2.72 | 18.3 | 9.9 10 ⁻¹⁰ | 5.7 10 ⁻⁸ | ≈ 3 km |
| B | 43 | 40 | 5.0 | 2.37 | 22.9 | 1.1 10 ⁻⁸ | 2.5 10 ⁻⁸ | ≈ 3 km |
| H | 76 | 355 | 5.8 | 2.39 | 33.5 | 3.8 10 ⁻⁸ | 3.3 10 ⁻⁸ | ≈ 1 km |
| I | 63 | 356 | 3.7 | 1.99 | 1.0 | 9.8 10 ⁻¹⁰ | - | ≈ 100 m |
| M | 87 | 300 | 1.5 | 1.69 | 0 | 4.6 10 ⁻¹⁰ | - | ≈ 100 m |
| K | 65 | 305 | 3 | 2.27 | 2.6 | 9.1 10 ⁻⁸ | - | ≈ 30 m |

Notes:
¹ Arithmetic mean
² Geometric mean
³ Fraction of total transmissivity measured in single hole tests contributed by zone.

The thicknesses of the fracture zones varied from 2 m to 12 m, with an average of approximately 6 m at their intersections with the boreholes. The fracture-zone-index anomalies were generally smaller in the southern part of the site and larger towards the north. Borehole W2 exhibited the largest number of fracture-zone-index anomalies, probably because of its proximity to the intersections of the A, B, and H zones. These three zones accounted for about 75% of the hydraulic transmissivity as measured by single-borehole hydraulic tests. The A, B, and H zones were considered to extend beyond the boundaries of the SCV site perhaps to the surface, which might have been the reason for the high hydraulic heads observed within the SCV site. The H zone was the most dominant feature at the site, exhibiting an approximate north-south strike, a dip of about 75° to the east, and a bifurcation into two zones, denoted as Ha and Hb, towards the north boundary of the site and beyond. This zone was consistently associated with large anomalies in the single-borehole data and contributed 33% of the total measured transmissivity in all boreholes. The zone was projected to intersect the Z shaft at a depth of approximately 460 m, which could be the reason for the decrease in head with depth and towards the south along the extent of the zone. The three minor features, denoted as I, K, and M, extended some 50 m to 100 m within the site, and provided hydraulic connections between the major features A, B, and H. The I zone connected the A and B zones with each other and with borehole W1. The K zone connected borehole N2 with the H zone. These minor features accounted for about 4% of the hydraulic transmissivity measured in the boreholes.

Model Consistency with Geohydrologic Evidence

Based on topographic expression on a regional scale, the dominant orientation of regional lineaments is north-south, with an accompanying observed orientation to the northeast. The orientations of the A, B, and H zones within the SCV site coincided with the directions of these large-scale lineaments. Furthermore, these zones could be extrapolated to the surface to coincide with the regional lineaments. Fracture mapping within the confines of the Stripa mine revealed numerous fracture zones with long trace lengths striking east-northeast, similar to the strike of the A and B zones. The H and I zones had orientations that resembled the mean orientation of the north-south fracture set, which was the most abundant fracture set within the site. The orientation of the K and M zones coincided with the orientation of the northwest-southeast trending fracture set. Thus, there existed general agreement between the projected extension of the zones within the SCV site and the regional fracture system, as well as with the fracturing in the small scale.

Large-scale crosshole hydraulic tests were conducted to evaluate the connectivity of the postulated fracture zones within the site. The results of these tests were presented as the head response in each hydraulic source section, in terms of the maximum observed drawdown multiplied by the logarithm of the separation distance between the source and the observation point. In general, as shown in Figure 3-58, the hydraulic responses were observed at expected locations consistent with the various positions of the hydraulic source within the conceptual model. A few observation points, located in fracture-zone intersections where very low permeability was observed in single-borehole tests, exhibited no responses. A number of responses were observed at locations outside the regions containing the defined fracture zones, particularly in the W1 and W2 boreholes. The response in the W2 borehole was considered to be due to its proximity with the intersections of zones A, B and H.

The anomalies that were identified but could not be explained were few and appeared to be insignificant relative to the major features contained in the conceptual model. It was concluded that the model gave a realistic representation of the flow system at the SCV site and was consistent with geologic, hydrologic, and geochemical evidence. The major fracture zones that were identified provided the principal pathways for groundwater flow, and acted as "leaky aquifers" linked to the background rock by minor zones and fracture planes.

3.3.4 Validation Experiments

Two categories of experiments were conducted at the SCV site for purposes of assessing the validity of (1) predictions of the geohydrologic characteristics of the SCV site, and (2) predictions of groundwater flow and solute transport within the site by means of numerical models. Predictions of the geometries of the fracture zones and the principal pathways of groundwater flow were made in Stage II on the basis of data collected in Stage I. General agreement was found to exist between these predictions and the actual conditions as determined by the field investigations conducted in Stage III. In Stage IV, the conceptual model of the SCV site was updated

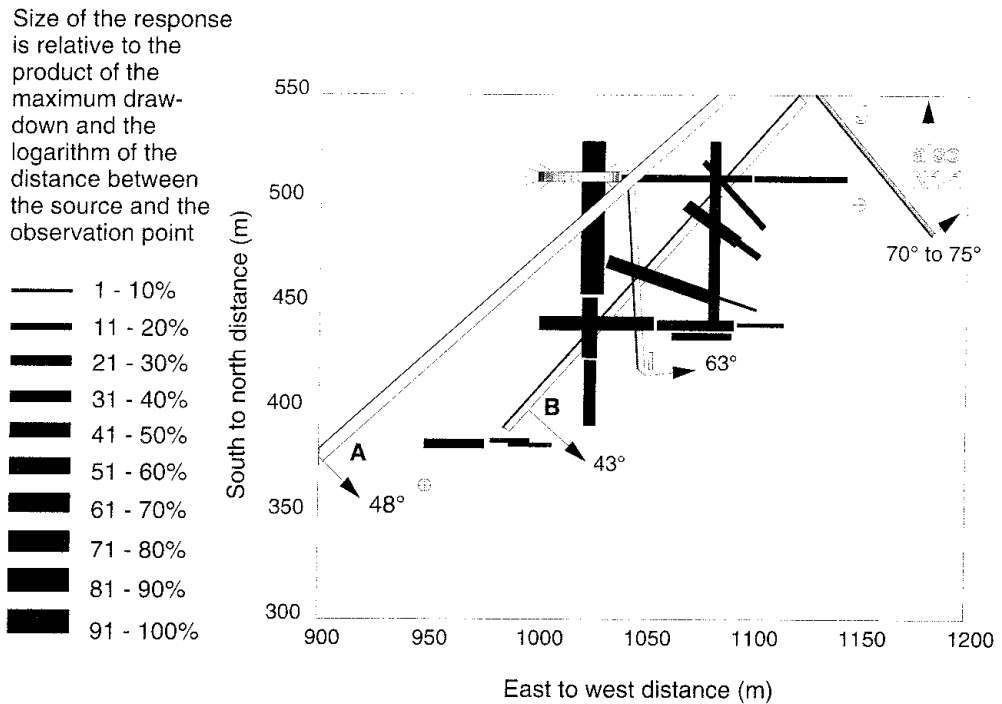


Figure 3-58 Geometrical distribution of head responses within the SCV site due to the draining of groundwater from a section of borehole W2 (Olsson, 1992).

on the basis of these data. However, apart from the construction of the Validation Drift, measurements of groundwater flow into the drift, and fracture mappings of the drift walls, no additional boreholes were drilled in Stage V for purposes of validating the final conceptual model of the geohydrology .

The experiments conducted for purposes of assessing the validity of the groundwater flow and transport models were related to fracture patterns, groundwater flow and head distribution, and tracer transport. These experiments were defined on the basis of deliberations between the principal investigators for the characterization and modelling activities and the Task Force on Fracture Flow Modelling, and can be identified as follows:

- Simulated Drift Experiment (SDE): This experiment involved the measurement of groundwater inflow to the D boreholes which outlined the periphery of the Validation Drift prior to its construction (Danielson et al, 1991). After the Validation Drift was constructed, additional measurements of groundwater inflow to the remaining sections of the D boreholes were made (Harding and Black, 1992).
- Fractures in the Validation Drift: In this investigation, the fractures in the roof, floor, and walls of the Validation Drift were carefully mapped for purposes of comparison with stochastic predictions of the patterns of such fractures by the fracture-network models (Bursey et al, 1991; Gale et al, 1991; Olsson, 1992).

- Validation Drift Experiment (VDE): This experiment involved detailed measurements of the distribution of groundwater inflow to the Validation Drift (Harding and Black, 1992; Watanabe and Osada, 1991; Watanabe, 1991a,b).
- Radar/Saline Tracer Experiment (RSTE): This effort actually involved two experiments, one before construction of the Validation Drift and one after construction (Olsson et al, 1991). In the first experiment, saline tracer was injected into the C2 borehole at its intersection with the H zone and collected in the D boreholes. In the second experiment, saline tracer was injected into the same location in the same borehole and collected in the Validation Drift.
- Tracer Migration Experiment (TME): In this experiment, tracers, consisting of dyes and metal complexes, were injected into boreholes above and below the Validation Drift and collected within the Validation Drift, as well as within one of the boreholes (Birgersson and Ågren, 1992; Birgersson et al, 1992a,b,c).
- Head Monitoring: This experiment was conducted, in effect, over the course of the preceding five experiments (Haigh et al, 1992). The groundwater heads were monitored within and around the SCV site during the experiments and during the construction of the Validation Drift. In addition, the groundwater inflow to the Validation Drift and the head responses within the SCV site were measured as a consequence of allowing borehole T1 to drain freely (Harding and Black, 1992).

The predictions that were made by the groundwater flow and transport models, and the comparisons of the calculated results with the measurements from these experiments, are discussed in detail in Chapter 4.

Simulated Drift Experiment

The Simulated Drift Experiment (SDE) involved the measurement of groundwater inflow to six D boreholes that were drilled sub-horizontally to a distance of 100 m into the central portion of the SCV site. As shown in Figure 3-59, the borehole pattern consisted of a central borehole surrounded by five parallel boreholes on a radial separation of 1.2 m, which in effect simulated a tunnel with a diameter of 2.4 m. Groundwater inflow measurements were made over the entire length of boreholes prior to construction of the Validation Drift, and over the 50 m length of boreholes that remained after construction of the Validation Drift. The first set of measurements was expected to provide data that was representative of groundwater flow through an undisturbed rock mass. The second set of measurements was expected to provide data representative of groundwater flow through a rock mass that was disturbed only by the presence of the Validation Drift. The first set of measurements were concentrated in the more transmissive sections of rock, rather than within the "averagely fractured rock", and a lower measurement limit of 3 ml/min was used. In the second set of measurements, the emphasis was placed on the distribution of inflows to the "averagely fractured rock" and a measurement limit of 0.1 ml/min was chosen.

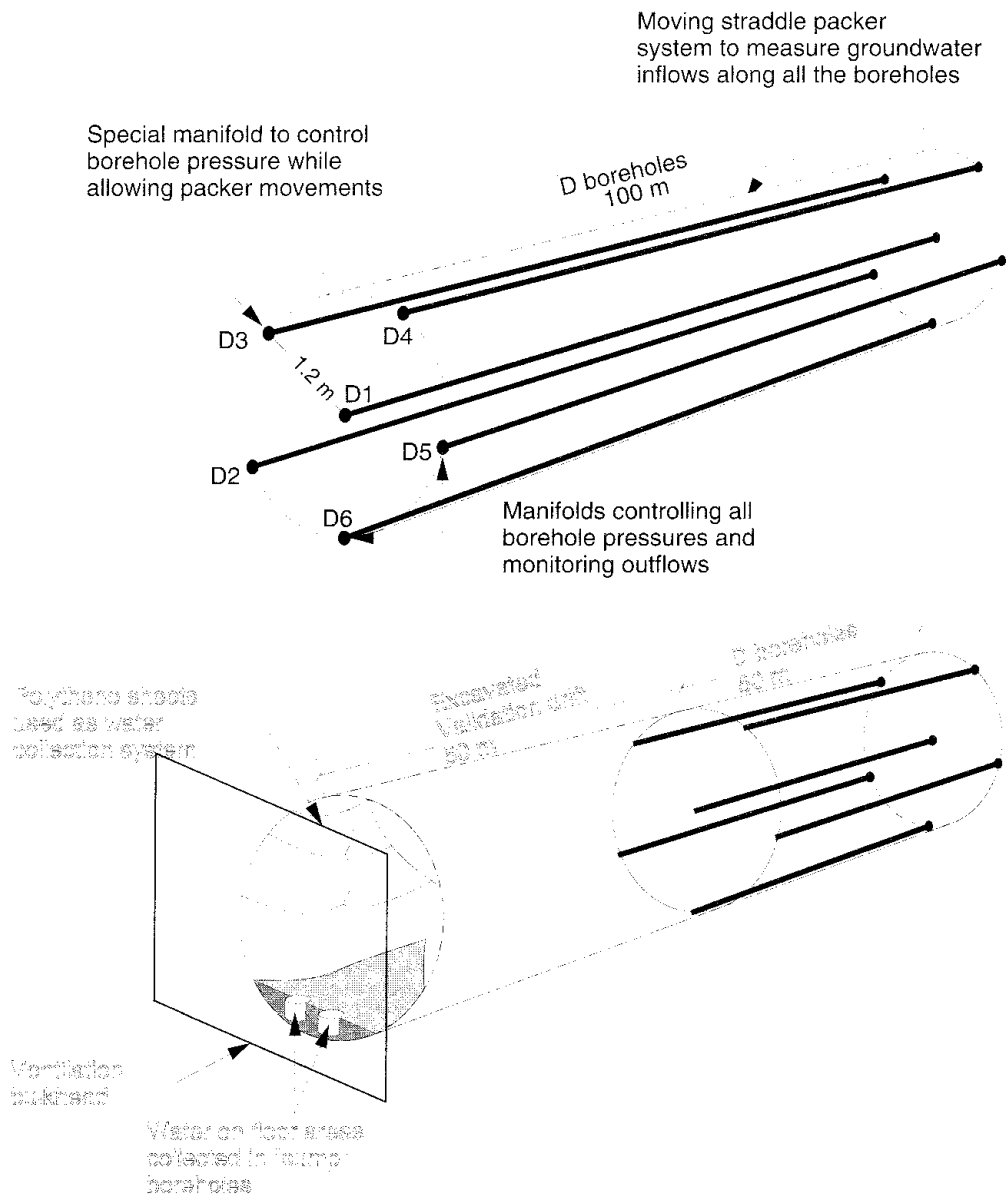


Figure 3-59 Array of D boreholes in the Simulated Drift Experiment (Olsson, 1992).

In the Simulated Drift Experiment, the distribution of groundwater inflow to the six 100 m-long boreholes was measured when the pressure within all boreholes was maintained at the same hydraulic head. In Stage V, the Validation Drift was excavated along the first 50 m of the D borehole array.

The experiment was designed such that the inflows could be measured in small isolated packed-off sections of each borehole at selected pressure steps to investigate the linearity of flow rates against pressure. As shown in Figure 3-60, the pressure in the boreholes was decreased in a sequence of three steps from 227 m of hydraulic head to 17 m of hydraulic head over a period of 68 days. Before the pressure decrease was initiated, but after installation of the hydraulic packer system, the mine pressure field was allowed to stabilize. During each step, water was abstracted from the boreholes over periods of time ranging from 17 days to 33 days, during

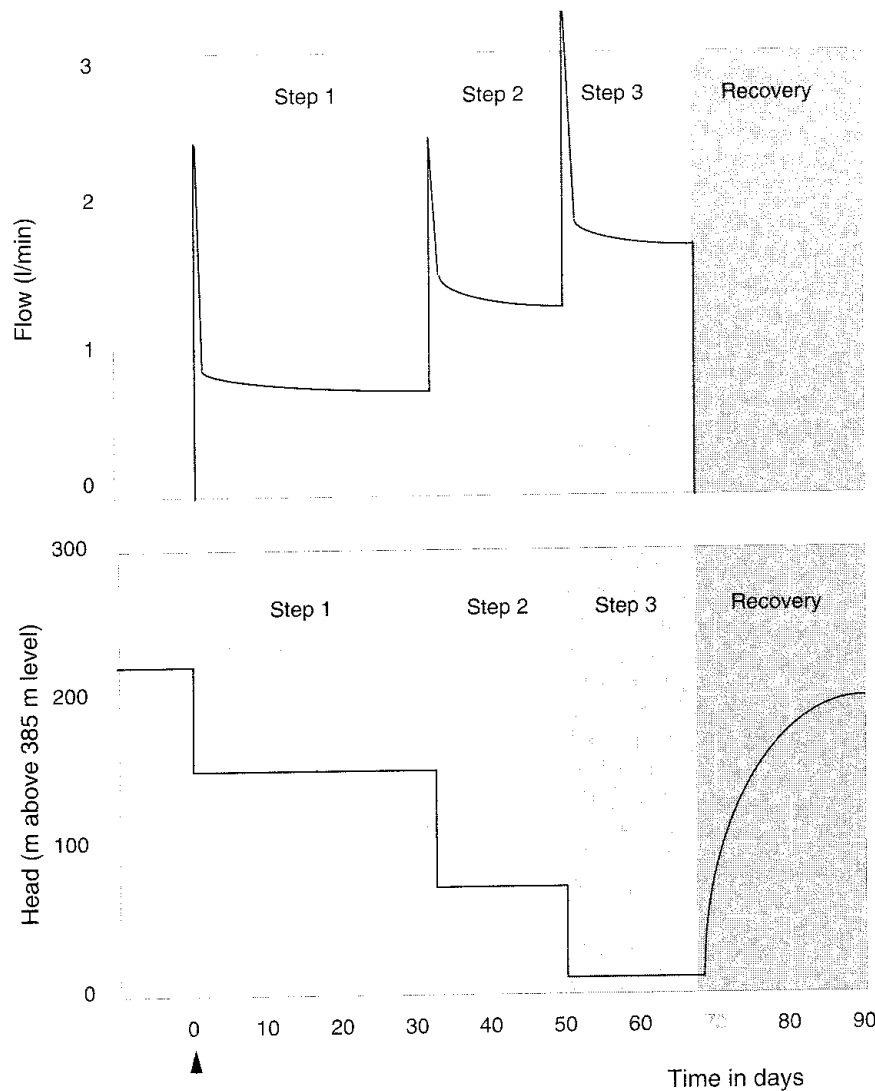


Figure 3-60 Test start
Time history of groundwater abstraction from the D boreholes during the Simulated Drift Experiment (Olsson, 1992).

which times the mine pressure field reached a condition of pseudo-stabilization. During each period of water abstraction, the pressures in all six boreholes were equalized in order to simulate the existence of the Validation Drift.

The distributions of groundwater inflow to the six D boreholes, normalized to an environmental hydraulic head of 250 m, are shown in Figure 3-61. Two zones of major inflow to each borehole, one at 25 m and the other at about 90 m, were clearly indicated by the measurements, and corresponded to the fracture zones known as H and B, respectively. In borehole D2, the inflow from the H zone occurred at two locations that were 2 m apart, while in all other boreholes the inflows from that zone were concentrated within a single 0.5 m interval. Inflows from the B zone were similar and occurred at a single location in all boreholes except D5 and D6 where there were two locations of inflow separated by a distance of 5 m. The borehole logs for

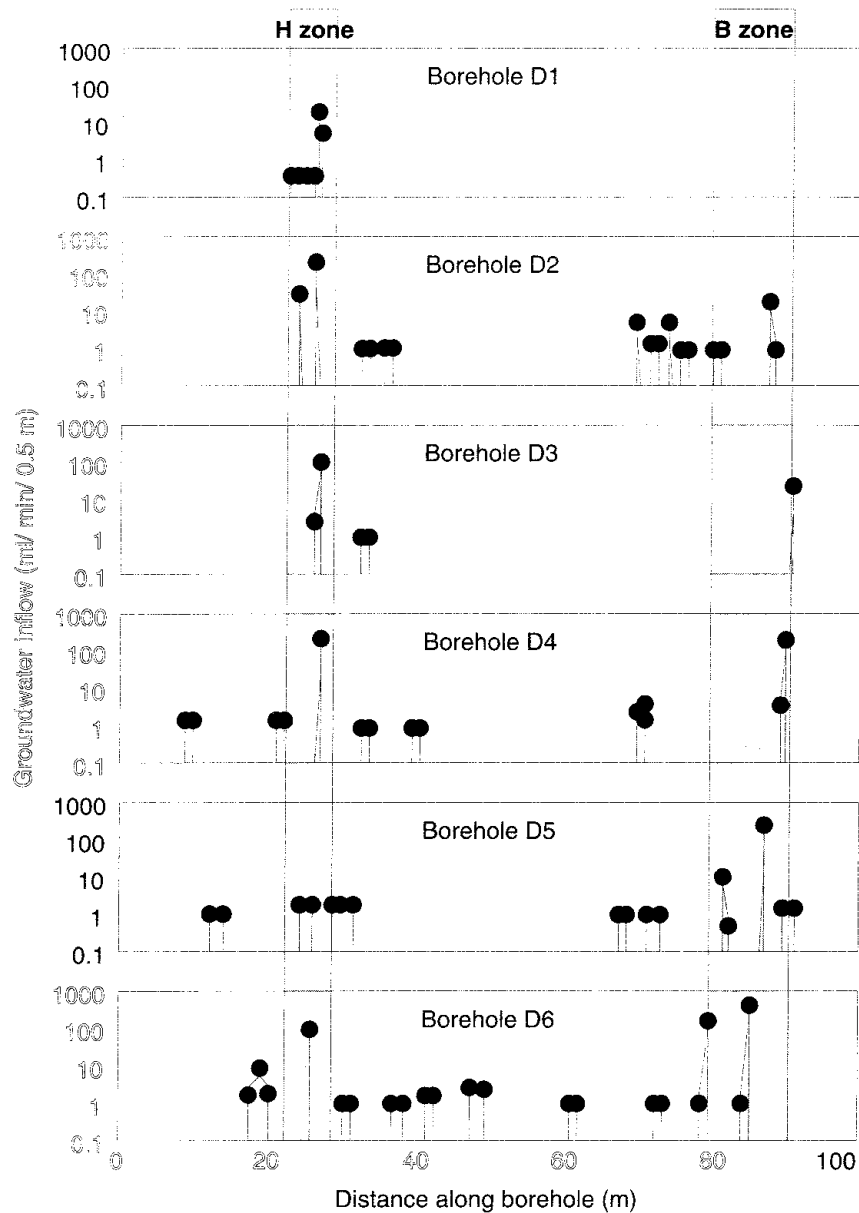


Figure 3-61 Rates of groundwater inflow to the D boreholes during the Simulated Drift Experiment normalized to an environmental head of 250 m (Danielson et al, 1991; Olsson, 1992).

the D boreholes indicated that there were between three and seven fractures associated with each well-defined inflow location. These two zones accounted for about 86% of the total measured flow from the boreholes, with the inflow from the B zone being about 50% greater than that from the H zone. The cumulative inflow rate to the six boreholes ranged from 0.734 ℓ /min to 1.71 ℓ /min over the course of steps 1, 2, and 3 of the measurement process, with about 0.065 ℓ /min of groundwater produced by the "averagely fractured rock" during step 1.

During the second set of measurements in those portions of the D boreholes remaining after construction of the Validation Drift, a packer was placed at the collar of each borehole and the pressure in each borehole was maintained at zero relative to the 385 m level of the mine. By comparison, 17 m of

head was used in step 3 of the first set of measurements. The packer assembly consisted of an array of six equally spaced packers, each 0.5 m in length and separated by a distance of 0.5 m. Depending on the magnitude of the flow rate into the boreholes, the inflow was measured in 0.5 m or 4.5 m sections of the boreholes.

The inflow distributions to all boreholes are shown in Figure 3-62, along with the inflows that were obtained during the first set of measurements. All large inflows were related to the B zone, over the interval of 81 m to 91 m, with the contribution from the "average" rock total being less than 1%. The inflows from the B zone were generally somewhat smaller during

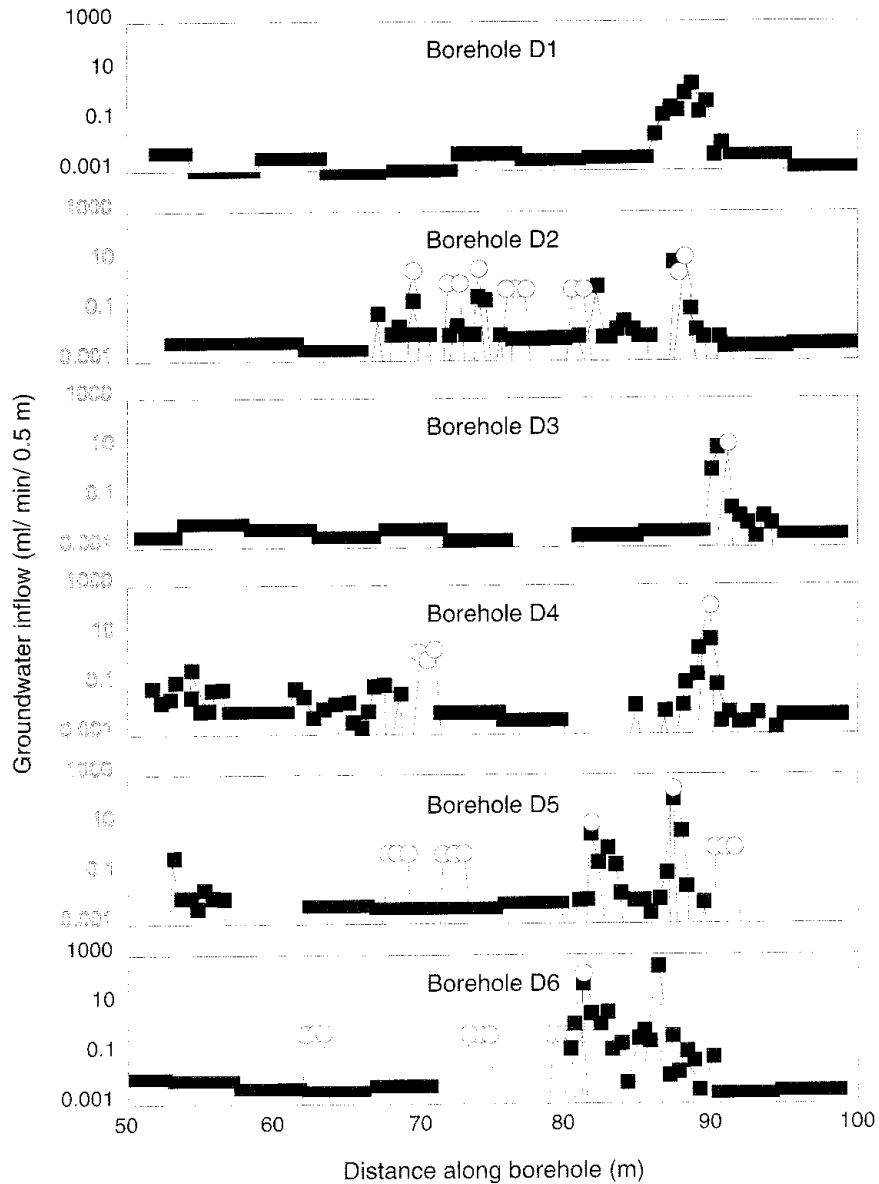


Figure 3-62 Distribution of groundwater inflow to the remaining 50 m of D boreholes after construction of the Validation Drift (Harding and Black, 1992; Olsson, 1992).

- denotes inflow during measurement after drift construction.
- inflow during measurement before drift construction (normalized to an environmental head of 250 m).

the second set of measurements than the normalized inflows obtained during the first set of measurements, while the inflows to the boreholes from the "averagely fractured rock" decreased significantly. As shown in Figure 3-63, the total inflow rate of 562 m³/min to the remaining portions of D boreholes is about half of the estimated inflow to the corresponding portions of the boreholes during the first set of measurements.

Fracture Patterns in the Validation Drift

During Stage V, the Validation Drift was excavated by means of a pilot-and-slash/drill-and-blast technique within the confines of the first 50 m of the D borehole array, to a height of 2.4 m and a width of 3 m. Subsequently, a grid system with a grid-cell size of 1 m² was painted on the drift walls, as schematically indicated in Figure 3-64. Based on a circumference of approximately 9 m and a length of 50 m, the periphery of the drift contained 450 grid cells.

The mapping of the periphery of the Validation Drift confirmed the presence of a dominant vertical, north-south trending fracture set, containing calcite as the primary mineral coating, and a weaker northwest-southeast trending set that dipped steeply to the northeast and contained no mineral coatings. Further analysis of the fracture data identified two weak fracture sets, one striking north-northeast and dipping to the east-southeast, and the other striking east-northeast and dipping to the north-northwest. The sorting of fracture orientations by termination demonstrated the progressive growth of originally free-ended, sub-horizontal fractures into T and later H junction types. Statistical analyses of the two data sets, in which the fractures were separated into those for the "averagely fractured rock" and those for the H zone, identified seven and four clusters, respectively. Two of the clusters in the average rock formed a unique and approximate conjugate pair of steeply dipping, north-northwest trending fractures. Two of the other clusters were also distinct but close to the mean orientation of one of the clusters in the data set for the H zone. The trace map for the drift and the contoured pole plots for each section of the drift are shown in Figure 3-65, and it is apparent that the mean trace lengths and apparent densities of the fractures were variable over the length of the Validation Drift (Burse et al, 1991).

There were significant variations in the area-corrected fracture densities for clusters in each of the data sets for the average rock and the H zone, as well as distinct differences between these two groups of data. As shown in Figure 3-66, the pattern of high and low values for mean trace lengths was approximately mirrored by the pattern of high and low fracture densities for clusters in both the average rock and the H zone. These data suggest that variations in fracture density may be proportional to changes in mean trace length for individual fracture clusters. After correction of the data sets for truncation and censoring biases, the calculated mean fracture lengths ranged between 0.47 m and 0.84 m for clusters in the average rock, and between 0.58 m and 0.93 m for clusters in the H zone.

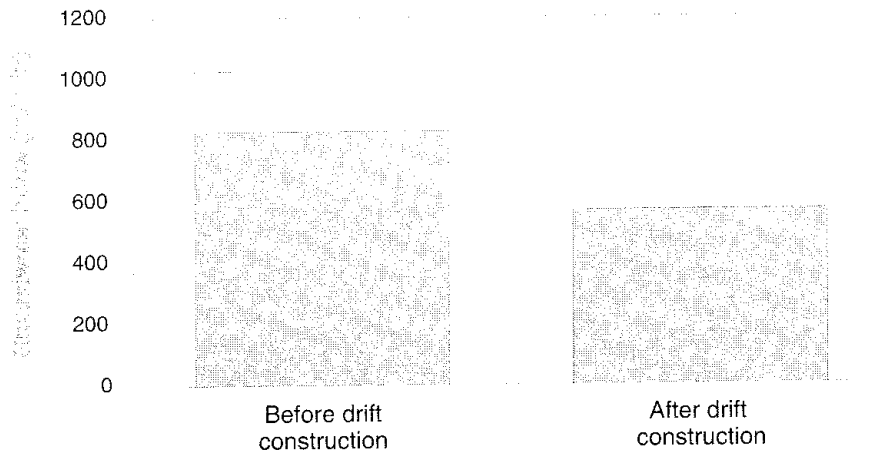


Figure 3-63 Groundwater inflow to the remaining 50 m of the D boreholes before and after construction of the Validation Drift (Harding and Black, 1992; Olsson, 1992).

The unfilled portion of the bar represents the contribution from the "averagely fractured rock" in the measurement before drift construction.

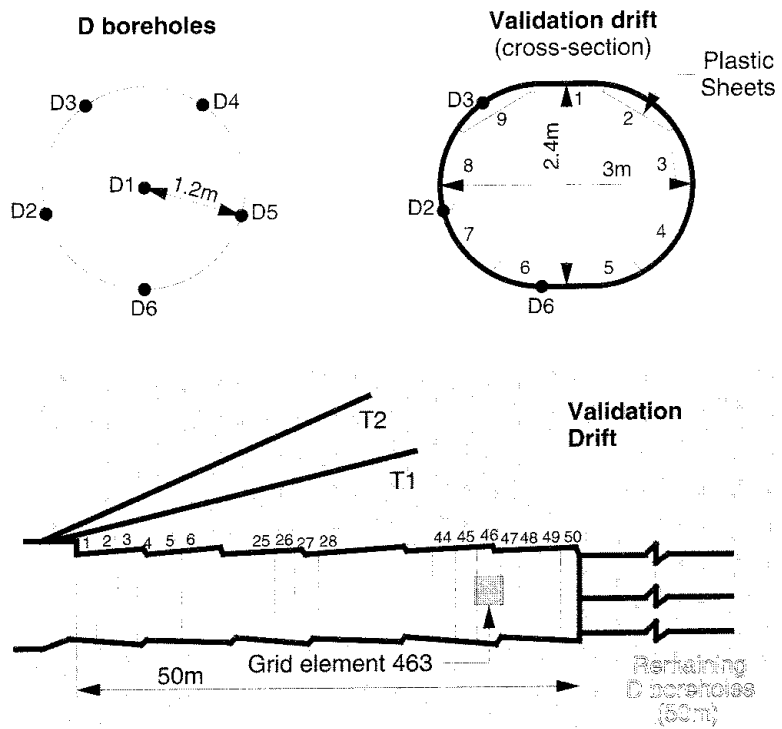


Figure 3-64 Relative position of the D boreholes and approximate shape of the Validation Drift after excavation (Olsson, 1992).

The division of the drift wall into grid cells is indicated. Cells numbered 1, 2, 3, 8, and 9 in cross section were covered with plastic sheets.

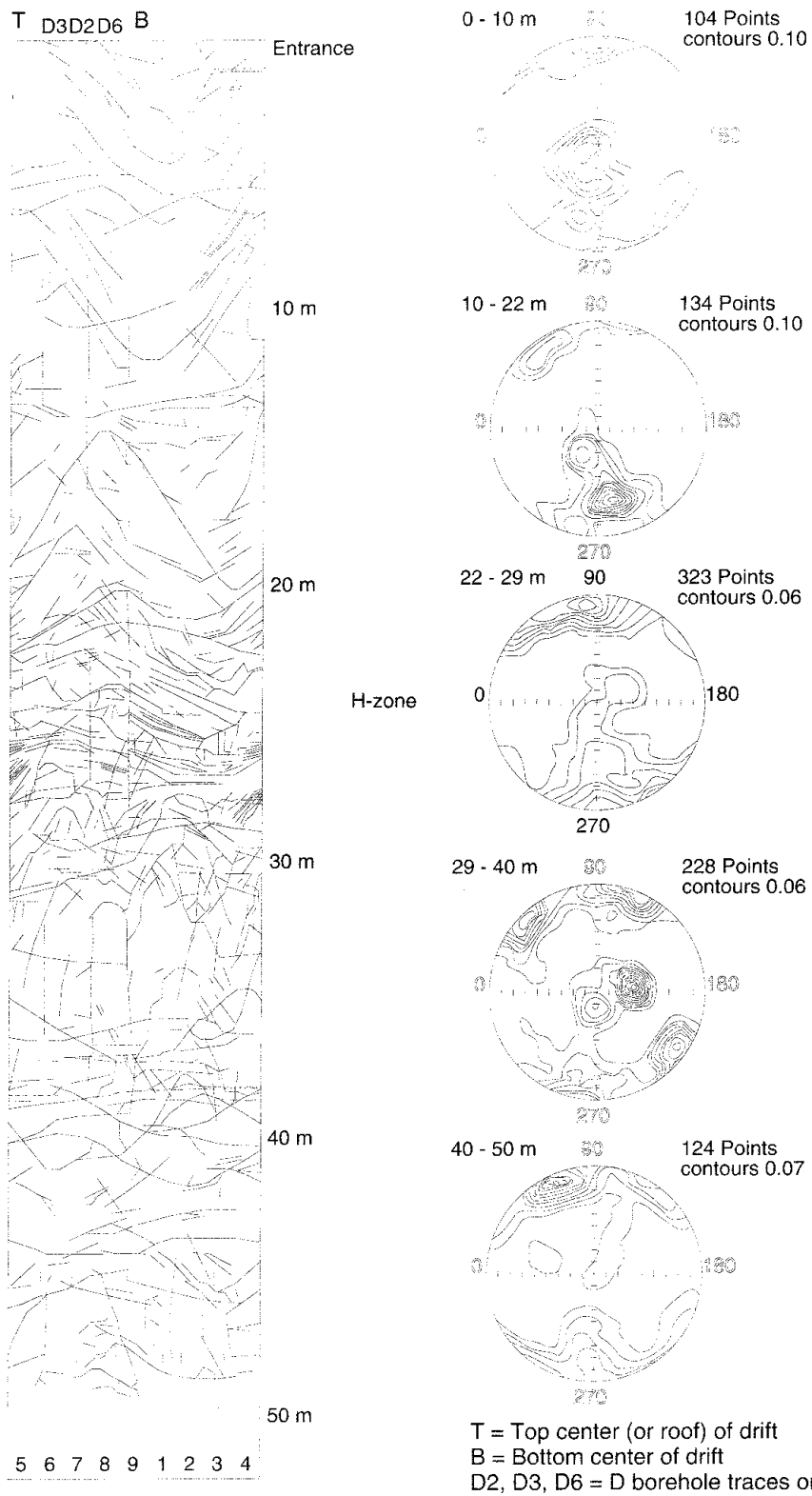


Figure 3-65 Fracture map of the Validation Drift as viewed from outside the drift (Burse et al, 1991; Olsson, 1992).

The lower hemisphere stereoplots show fracture orientations in sections along the drift.

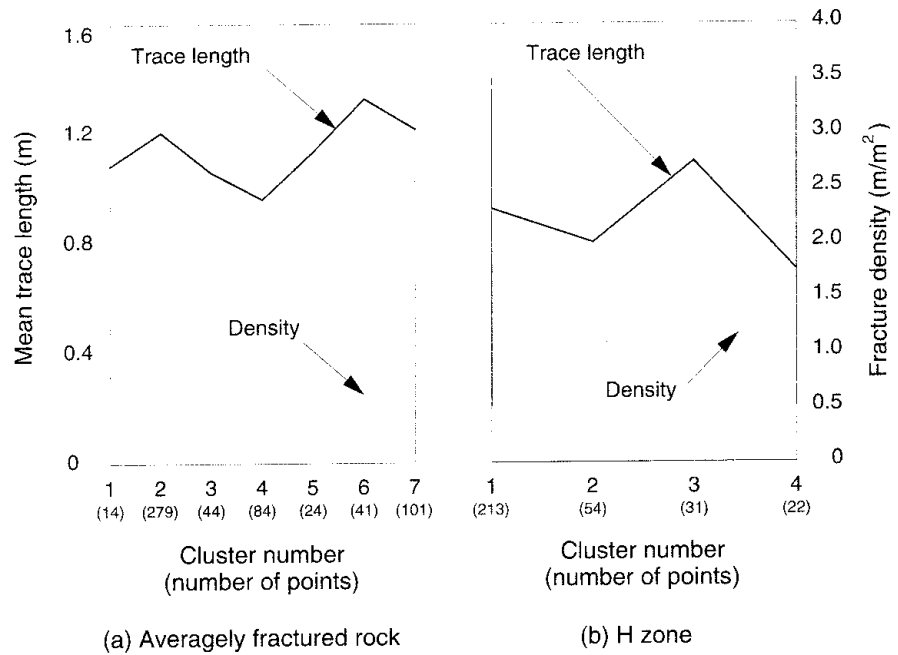


Figure 3-66 Variations in mean trace length and area-corrected density of fractures for clusters in both the average rock and the H zone of the Validation Drift (Burse et al, 1991; Gale et al, 1991; Olsson, 1992).

Groundwater Inflow to the Validation Drift

Following the excavation of the Validation Drift, the distribution of groundwater inflow to the drift was measured. The flow from the roof and upper regions of the walls was collected in a system of plastic grid sheets attached to the rock. The size of a grid sheet was 1 m by 2 m, except in the region of the H zone where the size was 1 m by 1 m. In those localities where sheets collected water from flowing fractures, the edges of the sheets were enhanced by metal plates that were cemented into slots, 5 cm to 25 cm deep, cut into the rock. The flows into the floor and lower regions of the walls were collected in "sumps" drilled into the "wet" fractures at their intersections with the grid lines. The entrance to the drift was sealed by means of a bulkhead, and measurements of the inflow and outflow air volumes, together with their humidity and temperature, formed the basis for computing the water that evaporated from the unsheeted areas of the drift.

The bulk of the groundwater inflow originated from the H zone, as shown in the distribution diagram in Figure 3-67. The total water inflow to all sampling areas in the drift was about 102 ml/min, of which 99% of the water originated from the 6 m long intersection of the drift with the H zone. One single sampling area within the zone generated 50% of the total water inflow, with the remaining 50% distributed equally between the upper and lower sections of the drift. Although there were many hundreds of fractures observed in the walls of the drift, two major fractures within the H zone were the dominant sources for water inflow to the drift. As shown in Figure 3-68, the total groundwater inflow and its distribution between the H zone and the average rock remained fairly constant throughout the monitoring period. The sudden increase in inflow after about 9 000 hours of monitoring occurred when the packers in boreholes C1 and W1 were removed and the boreholes allowed to drain, which lowered the hydraulic heads around the Validation Drift. When the packers were reinstalled after

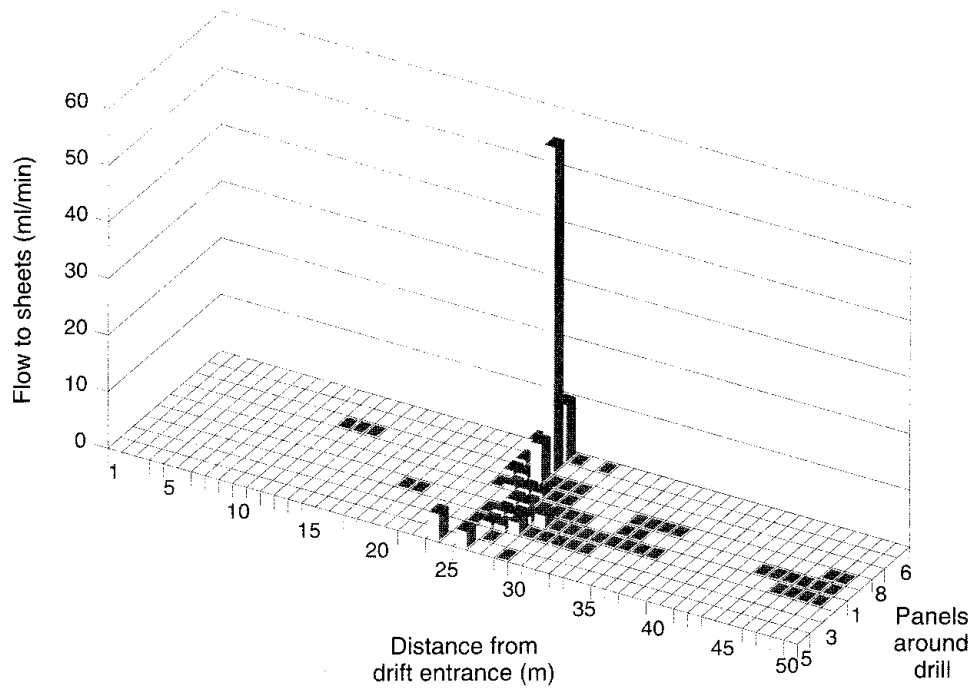


Figure 3-67 Distribution of groundwater inflow rates to the Validation Drift in January 1991 (Harding and Black, 1992; Olsson, 1992).

No inflow was recorded in the unmarked grid elements.

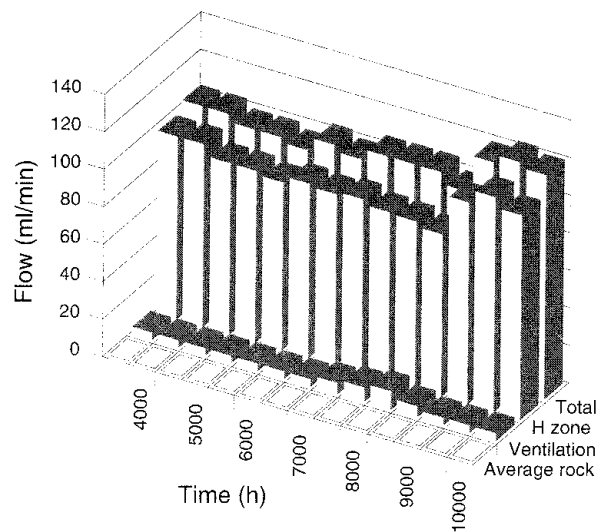


Figure 3-68 Variation in groundwater inflow to the Validation Drift as a function of time for the measurement period of September 1990 through June 1991 (Harding and Black, 1992; Olsson, 1992).

about two weeks, the pressures returned to the previous level but the inflows to the drift stabilized at a higher rate.

A comparison of the measurements of groundwater inflow to the Validation Drift and to the corresponding section of the D boreholes is given in Table 3-4. The flow to the Validation Drift was only 12% of the flow to the D boreholes, with a greater reduction in flow from the "average rock" as compared to the H zone. The observed reduction in the fraction of flow through the "averagely fractured rock" was consistent with the reduction observed when the flow to the remaining 50 m of the D boreholes was measured at a lower pressure.

Table 3-4 Groundwater inflow measurements to Validation Drift (Olsson, 1992).

| | Validation Drift | | SDE-1 | | Fraction of Validation Drift to SDE-1 inflow |
|--------------------------|------------------|---------------------|---------------|---------------------|--|
| | Inflow ml/min | Percentage of total | Inflow ml/min | Percentage of total | |
| Zone H | 101 | 99 | 745 | 85 | 13% |
| Averagely fractured rock | 1 | 1 | 131 | 15 | 1% |
| Total | 102 | | 876 | | 12% |

Measurements of evaporation were made to study the small-scale variations in inflow from the "averagely fractured rock". These measurements assumed that, for low rates of groundwater inflow, the rate of water evaporation from the rock surface was equal to the inflow. The absolute humidity was measured at two points within the layer of laminar air flow close to the drift wall. The evaporation rate was then derived by assuming that the humidity increased linearly towards the rock surface (Watanabe, 1991a). Measurements of the evaporation rate from the drift walls were made approximately one month and fourteen months after the excavation of the Validation Drift had been completed. The evaporation rate decreased from 0.38 mg/m²/s to 0.09 mg/m²/s over the period of about twelve months. To some extent, this difference can be attributed to the difference in air temperature between the two measurements. At the time of the second measurement, the air temperature had stabilized to the rock temperature and was homogeneous within the confines of the drift, which was not the case during the first measurement. The average wall evaporation rates that were obtained along the length of the drift during the first measurement are shown in Figure 3-69. The evaporation rate from the rock between the entrance to the Validation Drift and the H zone was lower than that between the zone and the end of the drift, which is in agreement with inflows to the plastic sheets.

Radar/Saline Tracer Experiment

The purpose of this experiment was to determine the transport characteristics of the H zone and the surrounding rock before and after excavation of the

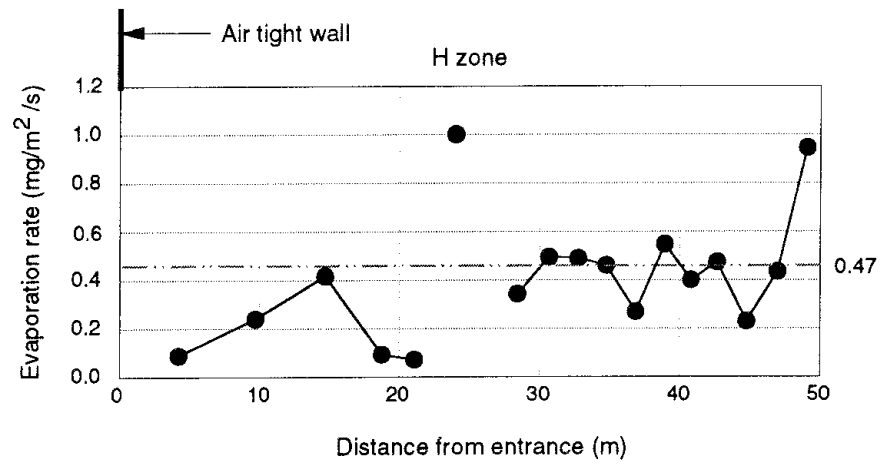


Figure 3-69 Variation in average evaporation rate along the Validation Drift during the first measurement (Olsson, 1992; Watanabe, 1991a).

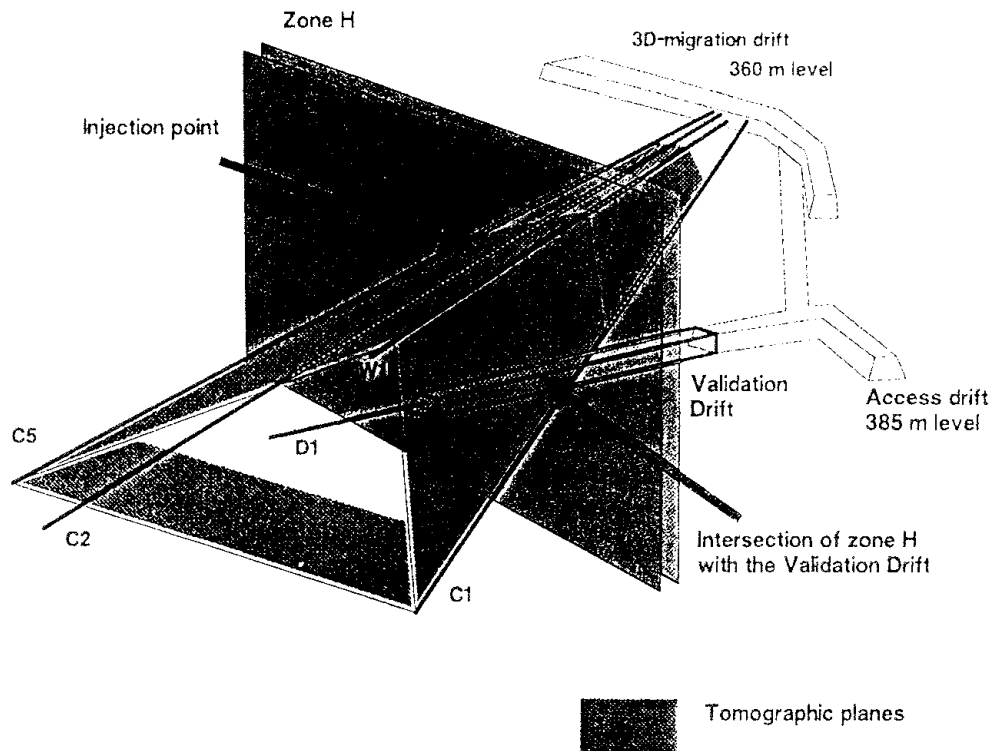


Figure 3-70 Generalized geometry of the radar/saline tracer experiment (Olsson et al, 1991a,b; Olsson, 1992).

Saline tracer was injected in borehole C2 where it intersects the H zone. Radar tomography was conducted in the planes defined by the W1-C5, C5-C1, and W1-C1 boreholes.

Validation Drift. As shown in Figure 3-70, the strike of the H zone was nearly parallel to the 3D migration drift, which was oriented in a north-south direction. The W1, C1, and C5 boreholes, all originating from a common location in the 3D migration drift, outlined the sides of a tilted pyramid which intersected the H zone. The tracer was injected in the C2 borehole at its intersection with the H zone. In the first experiment, denoted as R/STE-1, the D boreholes were used as a sink, and in the second experiment, denoted as R/STE-2, the Validation Drift was the sink. In addition, in R/STE-2, the saline tracer concentration was monitored in the T1 and T2 boreholes which penetrated the H zone above the Validation Drift. Radar tomography measurements were made across the sections defined by boreholes C1-C5, W1-C1, and W1-C5, before and during injection of the tracer. For both R/STE-1 and R/STE-2, the distance between the injection point in the C2 borehole and the collection points was approximately 28 m, and the injection flow rate and salinity of the injected fluid was 200 ml/min and 2%, respectively. During the first 362 h of tracer injection in R/STE-1, the hydraulic head in the D boreholes was maintained at 165 m, relative to the 385 m level, and then was reduced to zero (Olsson et al, 1991a). In R/STE-2, the Validation Drift served as a sink at atmospheric pressure, but the injection flow rate was reduced in two steps due to a high pressure build up in the injection interval (Olsson et al, 1991b).

The first arrival of tracer in R/STE-1 was observed in the D4 borehole approximately 10 h after the start of injection, followed shortly by arrivals in the D3 and D6 boreholes. The instantaneous recovery rate of the tracer increased from 50% to 85% after the hydraulic head in the D boreholes was reduced to zero at 362 h.

The results of radar tomography, shown in Figure 3-71, indicated that most of the tracer was confined within the plane of the H zone. Smaller amounts of tracer appeared to spread into two minor fractures or fracture zones that intersected the zone and into the "average rock" between the zone and the 3D migration drift. A conceptualization of the flow pattern within the rock mass is shown in Figure 3-72. Zone H provided the fastest pathway from the point of injection in borehole C2 to the D boreholes, and accounted for approximately 50% of the total flow. Part of the tracer flowing toward the D boreholes was diverted by the S zone both upward to the plane formed by the W1-C5 boreholes and downward to the plane formed by the C1-C5 boreholes. Some of the tracer that passed through the plane defined by the C1-C5 boreholes close to borehole C5 returned to the D boreholes through a flow path that passed through the C1-C5 plane at its intersection with the T zone.

In R/STE-2, the tracer breakthrough into the Validation Drift was concentrated in a 5 m section of the H zone in the vicinity of two semi-parallel fractures. In general, the tracer breakthrough times ranged between 20 h and 100 h for most of the grid elements, with the tracer arriving somewhat faster and less diluted in the grid panels in the roof of the drift. Only a few of the faster flow paths monitored in the roof of the drift reached steady state during the 630 h duration of the experiment.

The spatial distribution of breakthrough times and tracer concentrations are shown in Figure 3-73. The highest tracer concentrations were observed in

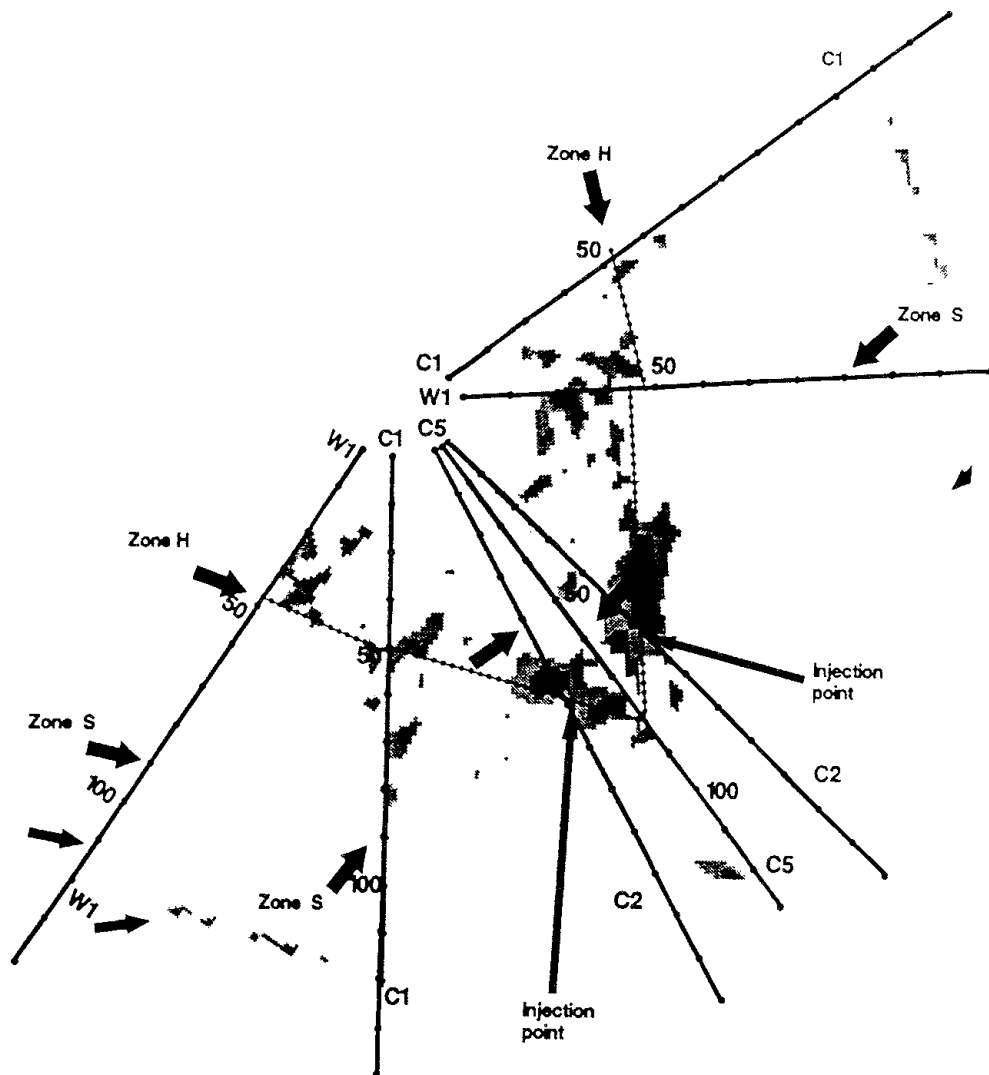


Figure 3-71 Composite of radar-difference tomograms showing the distribution of tracer in the first radar/saline tracer experiment approximately 290 hours after start of injection (Olsson et al, 1991a; Olsson, 1992).

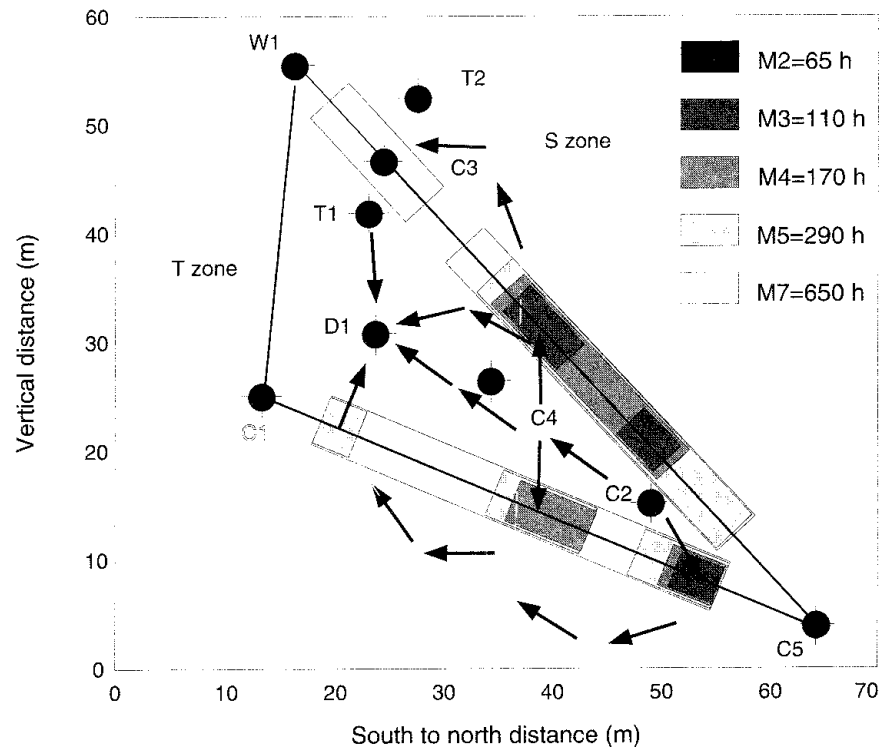


Figure 3-72 Conceptualization of saline-tracer transport within the H zone during the first radar/saline tracer experiment (Olsson et al, 1991a; Olsson, 1992).

The shading indicates when and where tracer was first observed in significant amounts.

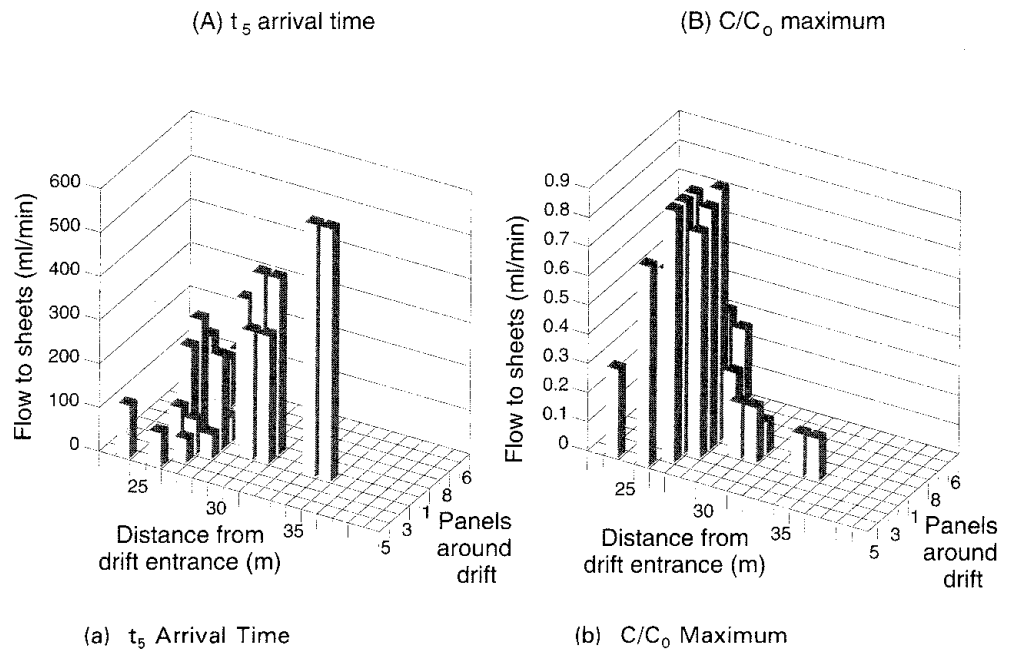


Figure 3-73 Distribution of tracer arrival times and concentrations in the Validation Drift for the second radar/saline tracer experiment (Olsson et al, 1991b; Olsson, 1992).

The arrival time data are presented as the time t_5 when the concentration had reached 5% of the maximum concentration for each grid element. The maximum concentration C/C_0 is given for each grid element.

the roof of the drift, while lower concentrations were measured in the high-flow grid elements in the floor. Tracer arrivals in six of the grid elements in the H zone were due to transport through a sub-horizontal fracture that intersected the zone a few metres above the drift. Tracer breakthrough was also observed in boreholes T1 and T2 after 180 h and 400 h, respectively. The instantaneous recovery of tracer in the Validation Drift was 21%, of which nearly 70% of that total recovered mass was found in three grid elements coincident with the location of the old boreholes D2 and D3.

Based on tomographic measurements with the radar system, the presence of tracer in significant amounts was observed close to the injection point in borehole C2, as shown in Figure 3-74, as well as along the lines of intersection between the H zone and the planes of tomographic measurement. After approximately 330 h, significant amounts of tracer were observed essentially along the entire length of the intersection with the W1-C5 plane. The observation of tracer in the radar tomograms close to the W1 borehole was consistent with the observed breakthroughs in the T1

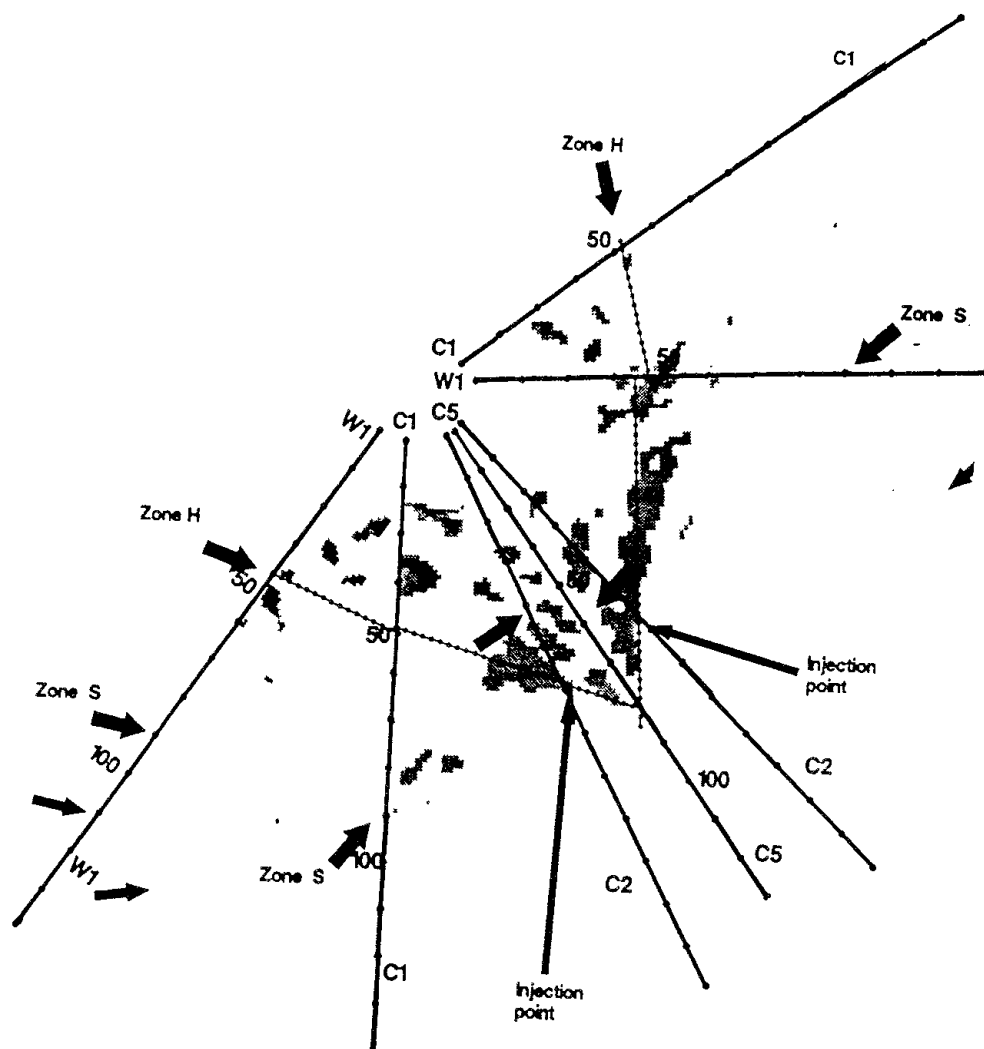


Figure 3-74 Composite of radar-difference tomograms showing the distribution of tracer in the second radar/saline tracer experiment approximately 330 h after start of injection (Olsson et al, 1991b; Olsson, 1992).

borehole after 180 h and in the T2 borehole after 400 h. The tomograms also indicated transport at points where the S zone intersected the W1-C5 and C1-C5 planes, and that this zone provided a preferred flow path for transport of the tracer away from the H zone.

The essential characteristics of the conceptualization of the flow system during R/STE-2, as illustrated in Figure 3-75, feature a flow path to the crown of the drift, along which the travel time was small and the concentration was high although only a minor portion of the total mass was transported to the drift. In addition, there existed a major flow path along which nearly 70% of the mass was transported to the floor of the drift, but over relatively longer travel times and at relatively lower concentrations. Also, there existed a preferred direction of transport from the injection borehole up and towards the W1, T1, and T2 boreholes. About 78% of the tracer was not recovered in the Validation Drift, and the bulk of that mass remained in the H zone and drained towards the Z shaft.

The collection of results indicated that there existed a significant difference between the outcomes of R/STE-1 and R/STE-2. In R/STE-1, a large portion of the tracer mass traveled along a relatively fast transport path with a mean travel time of 33 h, and along a much slower path with a mean travel time of about 220 h. Comparatively, the tracer breakthrough in R/STE-2 was much slower, exhibiting a mean travel time of about 430 h, and there existed only a very small portion of a fast flow path with a mean

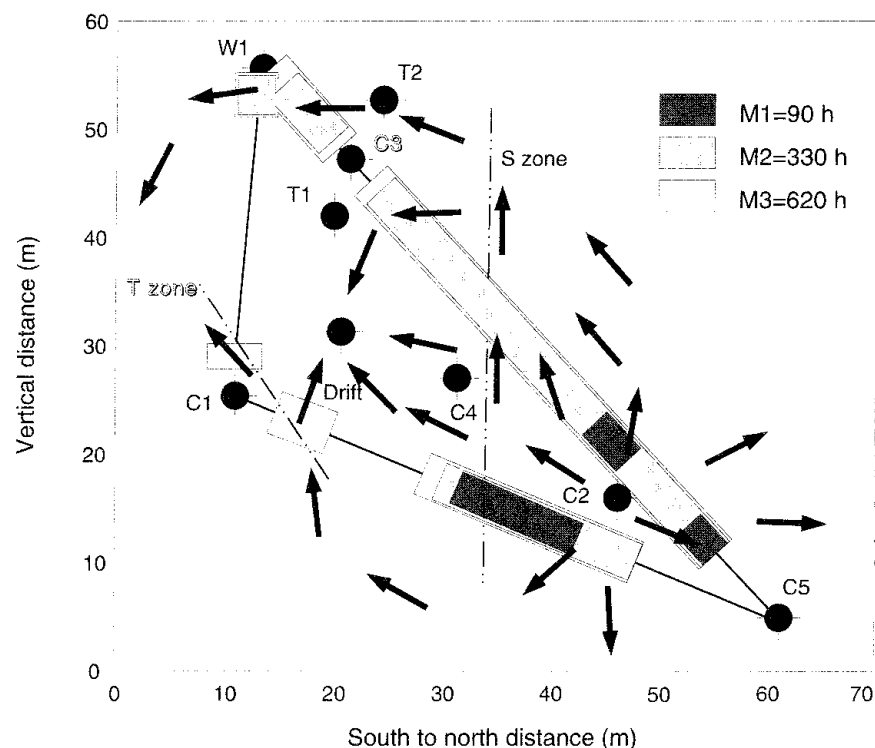


Figure 3-75 Conceptualization of saline-tracer transport within the H zone during the second radar/saline tracer experiment (Olsson et al, 1991b; Olsson, 1992).

The shading indicates when and where tracer was first observed in significant amounts.

travel time of 65 h. That is, the fastest travel time in R/STE-1 was approximately twice the fastest travel time in R/STE-2. In addition, as shown in Figure 3-76, the instantaneous recovery of the tracer mass in R/STE-2 was only about 50% to 60% of that recovered in R/STE-1. These observations are consistent with the tomogram patterns that indicate a more significant spreading of the tracer in the planes during R/STE-2 than during R/STE-1. In effect, the sink was stronger in the first experiment than in the second, even though the source strength was the same in both experiments. The measured head difference between the source and the sink in R/STE-1 was approximately 65 m, compared to 340 m in the second experiment. Thus, there existed significant "skin" effects around the Validation Drift and probably in the vicinity of the injection point. The flow porosity was estimated to be of the order of 10^{-4} , as based independently on the tracer breakthrough data and the radar-difference tomograms.

Tracer Migration Experiments

The purpose of the tracer migration experiments (TME) was to evaluate the transport of tracers under "natural" flow conditions. Tracers were injected into the H zone, as well as into the low-permeability rock near the H zone. The injection rates were quite low in order to minimize the disturbance to the groundwater flow field, in contrast to the radar/saline tracer experiments in which high injection rates were used.

A total of nine sections, eight in the H zone and one in low-permeability rock adjacent to the H zone, were chosen as injection points in boreholes C2, C3, T1, and T2, as shown in Figure 3-77. The tracers were collected in the plastic sheets and sump holes in the Validation Drift. The distances from the injection points to the drift varied between 10 m and 25 m. The tracer substances consisted of six dyes and six metal complexes. A mixture

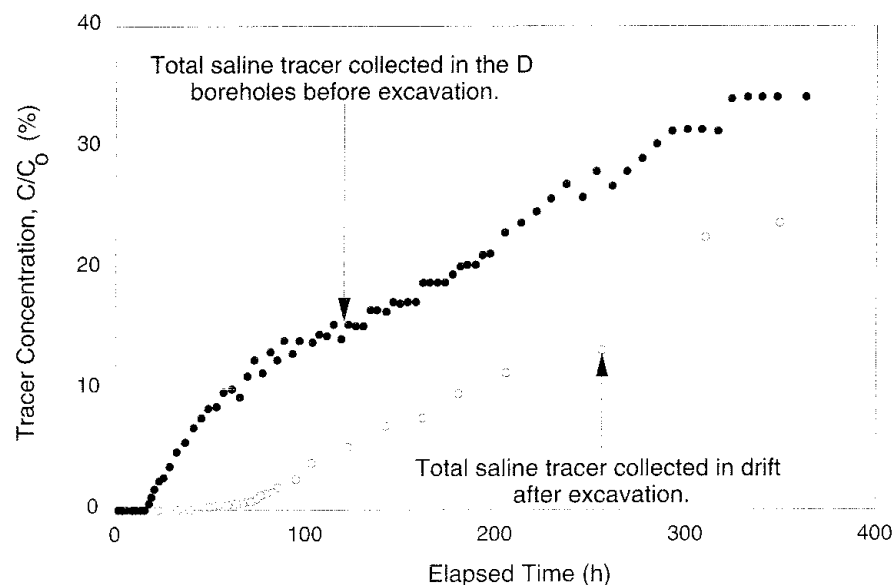


Figure 3-76 Comparison of the total breakthrough curves for the two radar/saline tracer experiments (Olsson et al, 1991b; Olsson, 1992).

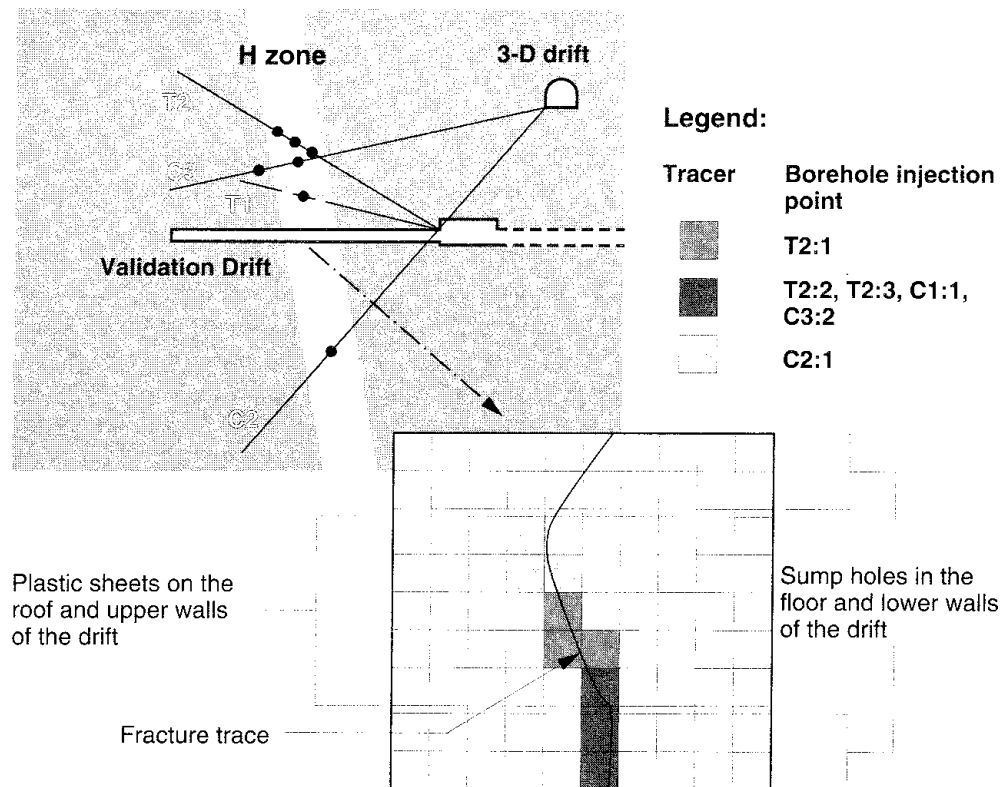


Figure 3-77 Schematic view of the configuration of the Tracer Migration Experiment and sampling areas where the major mass flow rates for the tracers were observed (Birgersson et al, 1992a,b; Olsson, 1992).

of one dye and one metal complex was injected at each injection point because the metal tracers could not be detected visually. The dyes were analyzed by means of a UV-BIS spectrophotometer, with a resolution of 0.1 ppm, and the metal tracers by means of a ICP-MS, with detection limits of 0.02 ppb. To minimize the influence of the disturbed zone around the Validation Drift, tracers were injected in borehole T2 and collected at three intervals in borehole T1.

A total of more than 200 tracer breakthrough curves were obtained in the experiment. The instantaneous recoveries in the Validation Drift for tracers injected in two sections, spaced 5 m apart, in borehole T2 in the H zone are shown in Figure 3-78. Although the distance from the injection points to the drift were approximately the same, about 20 m, the distribution of recovered tracer varied between the two injections, illustrating the difference in transport properties of the fracture zone over a relatively small region of the rock mass. The six tracer injections collected in the Validation Drift exhibited different concentration patterns at the collection points and could be grouped into three different patterns as shown in Figure 3-77. The patterns have their major mass flow rates restricted to different sections along the fracture in the H zone with the largest water inflow. Between 20% and 75% of the total mass of a tracer recovered in the drift was collected in one sampling area. Three sampling areas accounted for approximately 75% of the total recovery for one particular tracer. Tracer recovery is illustrated in Figure 3-79, where all sampling areas that received measurable concentrations of a metal-complex tracer were summed to yield

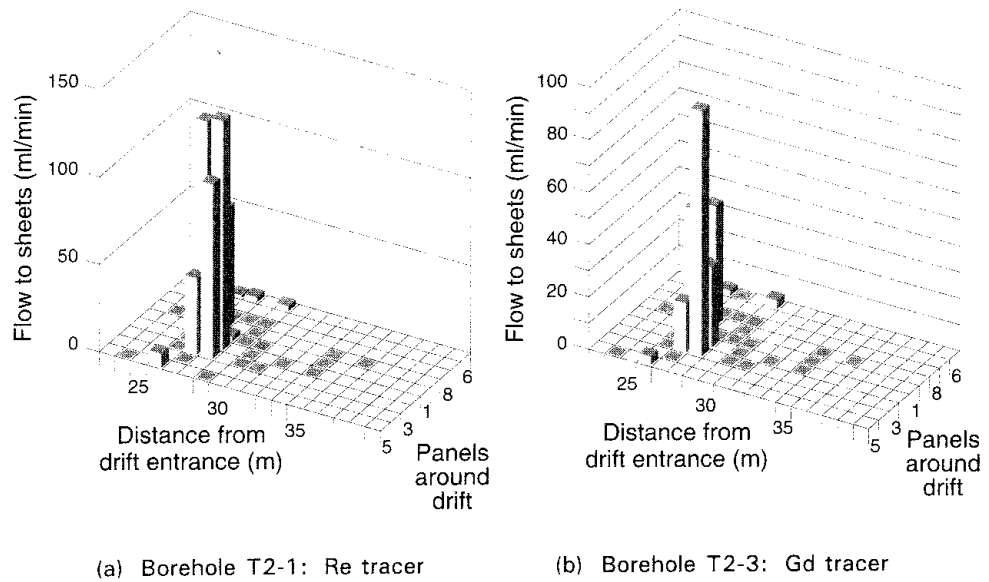


Figure 3-78 Instantaneous recovery (in parts per thousand) in the Validation Drift of tracers injected in two different sections of borehole T2 in the Tracer Migration Experiment (Birgersson et al, 1992b; Olsson, 1992).

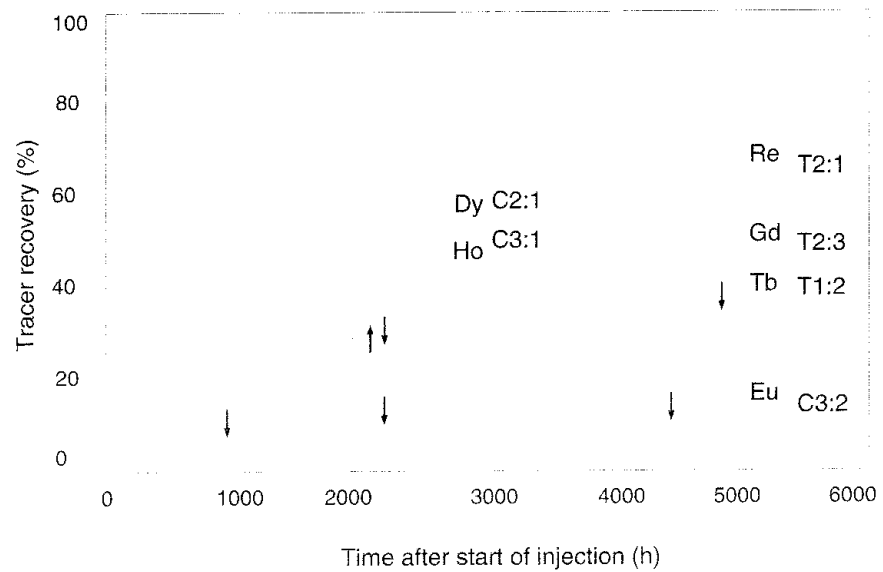


Figure 3-79 Recovery of metal-complex tracers as a function of time in the Tracer Migration Experiment (Birgersson et al, 1992b; Olsson, 1992).

The arrows indicate the time at which the tracer injection was terminated.

the total recovery in the drift. Differences in mean residence times and first arrivals can be observed. Because the recoveries were lower for the dyes than for the metal complexes and the breakthrough curves were correspondingly different, sorption and rock matrix diffusion experiments were conducted in the laboratory. The matrix diffusivity was found to be almost the same for all tracers, although some of the dyes could have been slightly sorbing or tended to degrade with time.

Based on fitting the breakthrough curves with an advection-dispersion (AD) model, mean residence times were calculated to range from 1,200 h upwards to 5,000 h for most of the breakthrough curves. The dilution factors varied from 50 to 1000 for the different tracers. The mean travel times for the tracers that were injected in borehole T2 and collected in borehole T1 varied between 300 h and 500 h. The distance between these boreholes ranged from 9.5 m to 12 m, which is comparable to the distances between some of the injection sections and the Validation Drift. Based on radially converging flow in a homogeneous porous medium where Darcy's law applies, the flow porosity was calculated to be of the order of 10^{-3} for the borehole-to-Validation Drift tests, and of the order of 10^{-4} for the T2-to-T1 borehole test.

Based on the results of the experiment, it was concluded that transport of tracers in the fracture zone, as well as in the low-permeability rock, was dominated by a few pathways. The large variation in mean travel time for tracers injected at different locations was thought to be an effect of the initial migration of the tracer from the injection section to the flow path that was connected to the Validation Drift. The uniform mean travel times for a tracer independent of sampling area indicated that most of the transport from the injection section towards the drift probably occurred in one or a few major channels. Close to the drift, however, the tracers appeared to spread over a large area, indicative of the effect of the disturbed zone around the drift due to excavation.

Hydraulic Head Monitoring

At the beginning of the SCV programme in Phase 3, a system for monitoring the hydraulic head, known as the Piezomac system, was installed in existing boreholes in the Stripa mine. During the course of the programme, additional instrumentation was installed in new boreholes that were drilled as a part of the programme and included in the monitoring system. A principal objective of the Piezomac system was to monitor the changes in hydraulic head across the SCV site as a consequence of the measurements of groundwater inflow to the D boreholes and the excavation of the Validation Drift (Carlsten et al 1988, 1990, 1991a, 1991b; Haigh et al, 1992; Persson et al, 1989). In addition, changes in hydraulic head were measured routinely during the radar/saline tracer experiments, the groundwater inflow measurements in the Validation Drift, and the tracer migration experiment, and, near the end of the SCV programme, the groundwater inflow measurement to borehole T1 when it was opened to atmospheric pressure.

The response in hydraulic head in the N and W boreholes to the first measurements of groundwater inflow to the D boreholes in the simulated

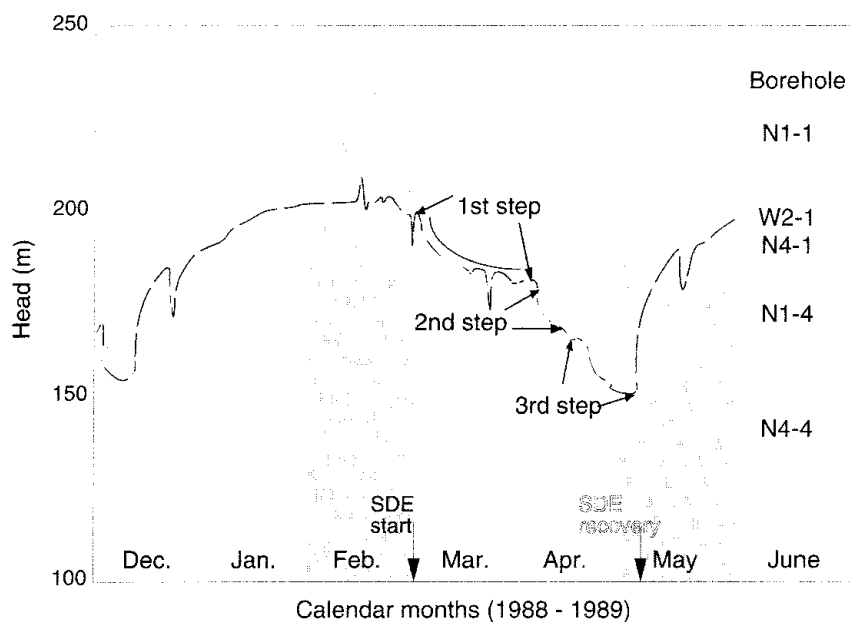
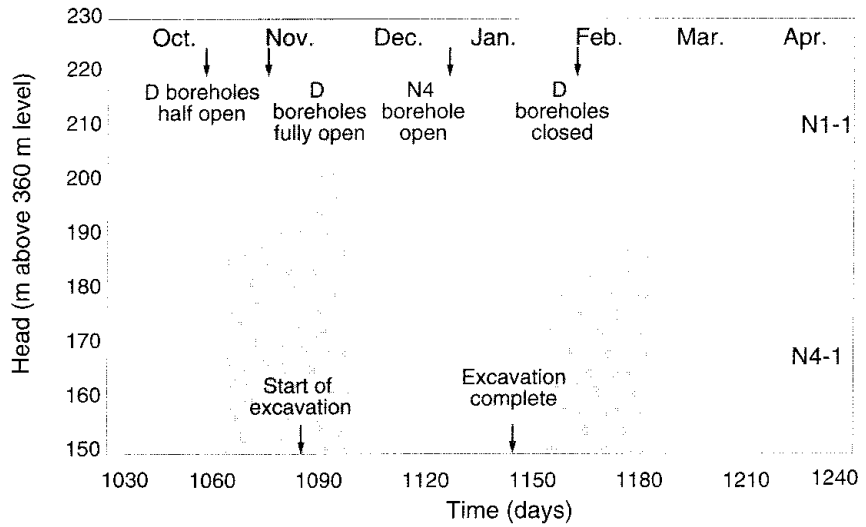


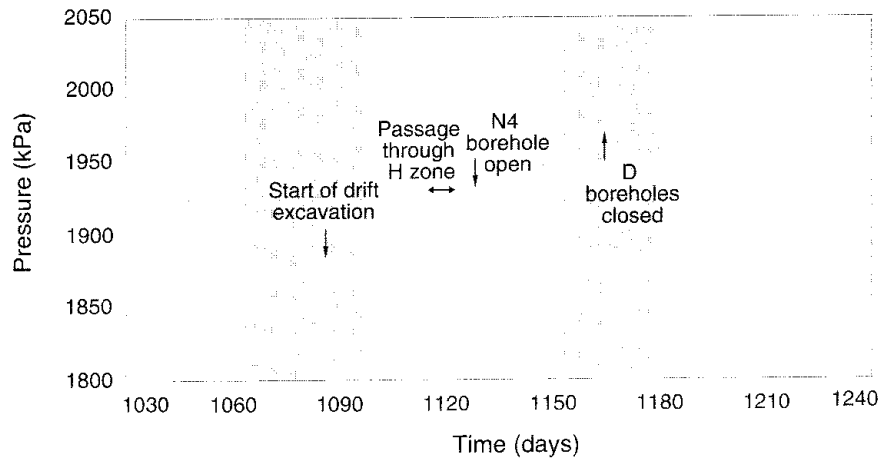
Figure 3-80 Hydraulic responses within boreholes in the SCV site during the first measurements of groundwater flow in the Simulated Drift Experiment (Olsson, 1992).

drift experiment is shown in Figure 3-80. The response to the experiment is quite clearly apparent in all borehole intervals, particularly in the two near-field N4-1 and W2-1 borehole intervals which exhibited the largest draw-downs and reflected the three steps of the experiment most clearly. The drawdown in the near-field borehole intervals was about 50 m. Steady-state conditions were not achieved during the duration of the experiment in the majority of the borehole sections monitored by the Piezomac system, although the head conditions within the site recovered rapidly after the D boreholes were closed. The connectivity across the SCV site was considered to be good because almost all of the monitoring points in the Piezomac system registered a response to the Simulated Drift Experiment.

Just before the start of the excavation of the Validation Drift in late November of 1989, the D boreholes were opened. The drift was excavated over a distance of 50 m in two months, using a drill-and-blast cycle of two to three days. The sections of the D boreholes that remained after the excavation had been completed were closed in early February of 1990. As shown in Figure 3-81, the hydraulic heads in the boreholes within the site decreased after the D boreholes were opened and decreased again at the start of drift excavation. Subsequently, during the duration of the excavation process, the hydraulic heads began to increase in most of the monitoring intervals. At the time when the remaining sections of the D boreholes were closed after the completion of excavation, the heads had attained levels that were approximately the same as those existing at the time the D boreholes were opened before excavation. This recovery in head occurred simultaneously with the drawdown provided by the drift while the excavation was in progress. Clearly, as the excavation progressed, the rock mass surrounding the drift and in front of the advancing face became less permeable because of the disturbance created by the existence of the drift. However, it was concluded that the gradual increase of head during



(a) Borehole intervals N1-1 and N4-1



(b) Borehole interval W2-5

Figure 3-81 Hydraulic responses in boreholes within the SCV site during excavation of the Validation Drift (Olsson, 1992).

excavation, together with the lack of response to excavation through the H zone, indicated that the reduction in groundwater inflow to the drift was not associated directly with stress changes in the rock mass at the advancing drift face.

On three occasions in 1990 and 1991, the groundwater inflows to three sections of the T1 borehole located in the H zone were measured. The borehole had been drilled on an incline from the access drift to above the Validation Drift for the purpose of the Tracer Migration Experiment. The final measurement was conducted for the purpose of providing data for

evaluation of the mathematical models of groundwater flow. However, the inflow to the borehole was much less than expected and, consequently, the observed head responses were few and small as shown in Figure 3-82. The responses to opening the T1 borehole to atmospheric pressure occurred relatively rapidly, but in the presence of a changing background of hydraulic head due to the closing of boreholes W1 and C1 after re-instrumentation.

In general, analysis of the Piezomac data during the course of the SCV programme indicated that activities causing prolonged draw-downs in either the B or H zone generated responses throughout the entire SCV site, and that the construction of the Validation Drift resulted in a recovery of the hydraulic heads throughout the SCV site. Furthermore, the responses in hydraulic head as a consequence of the first set of measurements in the Simulated Drift Experiment suggested that the site as a whole was very well connected. The steady recovery in hydraulic heads during construction of the Validation Drift was consistent with the reduced groundwater inflow to the drift as compared to inflow to the D boreholes during the first measurement in the Simulated Drift Experiment. Finally, because of the continuous and sometimes overlapping sequence of experimental activities within the SCV programme, the background hydraulic head within and around the site never achieved a truly steady-state condition.

3.3.5 Significant Achievements

The SCV programme was designed to sequentially characterize a previously "undisturbed" rock mass with a volume of some 1,000,000 m³ in the Stripa

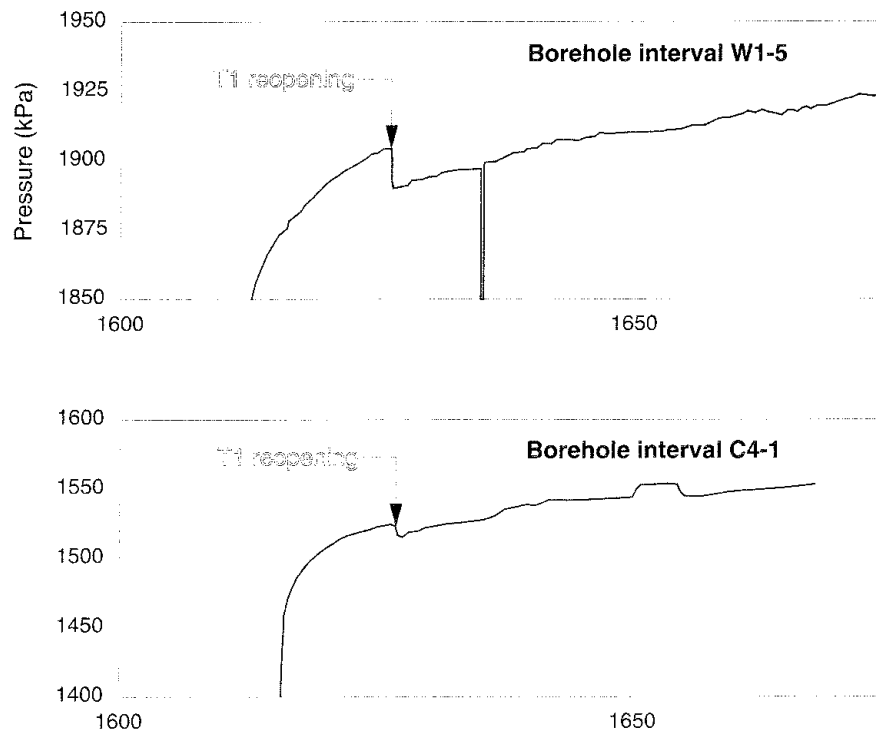


Figure 3-82 Pressure responses in borehole sections during the final inflow measurements to borehole T1 (Olsson, 1992).

mine, over the course of two cycles of data collection, interpretation, prediction and validation activities, all within a period of five years. A principal feature of the characterization effort was the progressive interfacing of increasingly more complex techniques for acquiring data and, subsequently, integrating the results into a consistent model of the geohydrology of the SCV site. Although the dimensional scale of characterization would probably only correspond to a small portion of a future repository site, the development and application of the characterization techniques and methodology should provide a framework of reference for the design of a characterization programme for a rock mass of repository proportions.

Characterization Techniques

The core and drift fracture mapping programmes were designed to provide a realistic description of the fracture geometry within the SCV site, and to determine if measurements on the periphery of the site could yield a reasonable description of the fracture characteristics within the site. For all intents and purposes, the programmes were successful at the dimensional scale of the SCV site. The fracture mapping programme demonstrated that, in any future site characterization exercise, an assessment of the general fracture geometry of a crystalline rock should be made before selecting the orientations of the test boreholes to ensure adequate and balanced sampling of all fracture sets at the site. A programme of borehole mapping, combined with scan-line and areal mapping in drifts, is required to obtain a trustworthy data base which can be used to obtain such parameters as fracture locations, heterogeneity, size, and orientation as required for network modelling. The Validation Drift Experiment demonstrated that an improved understanding of disturbed zone phenomena must be a key objective of a rock mechanics testing and modelling programme. Data must be obtained to describe the stress-transmissivity relationships for single fractures in the particular crystalline rock of interest in order to more realistically simulate the groundwater flow into and around an excavation.

The directional borehole-radar system developed within the SCV programme was a truly significant step forward for characterization of a saturated, fractured rock mass. The system provides a technique for the unique determination of the orientation of fracture zones from measurements in single boreholes, which, in effect, markedly improves reliability in defining the location and extent of fracture zones within a rock mass. Because of a high resistivity of the rock mass and the relatively simple geometric features of the fracture zones with low contrast in electric properties relative to the background, the borehole radar was found to work extremely well in the Stripa granite over ranges of the order of 60 m in the single-borehole reflection mode. For more conductive rock, however, shorter probing ranges would be expected and, correspondingly, the technique would be of less practical interest. When applied in the crosshole mode, the borehole radar can be used to produce tomographic images of the rock, displaying porosity variations in planar sections and the transport of saline tracer in the rock and fractures between boreholes.

The further development of the seismic testing technique led to a new, efficient borehole seismic source which reduced the time required to perform

a survey. The energy output of the source is relatively small which can cause problems if attenuation of the seismic waves is high. In the saturated, fractured granite at Stripa, the attenuation was low and the piezoelectric source provided probing ranges of several hundred metres and, for seismic waves of a few metres wave length, allowed the detection of fracture zones with a minimum thickness of less than a metre. New imaging techniques, developed to enhance reflections from crosshole seismic reflection measurements, were shown to be very efficient in treating the often very weak reflections from fracture zones and crystalline rock. However, to determine the orientation of a fracture zone, seismic data from at least three borehole surveys is required.

The single-borehole geophysical logging programme demonstrated that resistivity and sonic velocity data were instrumental in defining the width and location of fracture zones that intersected boreholes in the SCV site, particularly when such data were combined with data obtained from fracture mapping of borehole core and borehole hydraulic tests. The high-resolution fracture imaging tool, or borehole Televiewer, proved to be a useful technique for identifying and orienting a few fractures within a borehole, and then using these data to orient longer sections of the core.

At the outset of the characterization programme for the SCV site, it was recognized that the most transmissive fractures and their connectivity would have a major impact on the behavior of the fracture network system within the site. Consequently, a computer-controlled focussed borehole-hydraulic testing system was developed to obtain single fracture transmissivity data in a cost effective manner. The system concentrated on measurements of the most permeable single fractures to a high level of reliability, with less attention paid to the "averagely fractured rock". The use of a manifold at the collar to maintain borehole pressure, combined with the ability to test several sections of the borehole without moving the packers, allowed measurements of hydraulic conductivity and head in a relatively rapid manner. The single-borehole testing programme included constant-pressure tests for evaluation of the hydraulic geometries of individual fractures, as well as boundary effects within the rock mass. The introduction of the fractional dimension approach for characterizing the groundwater flow dimensions in a hydraulic test was a significant contribution to the data interpretation in both single-borehole and crosshole tests. The crosshole testing provided information on the "connectivity" of fracture zones across the SCV site and was used to verify the geometric model developed on the basis of results from the remote-sensing techniques. The monitoring intervals within boreholes for the large-scale crosshole testing were comparatively long, some in excess of 50 m, which, in effect, prevented evaluations of the interconnectivity between smaller fractures and the fracture zones. Small-scale crosshole tests were undertaken for the purpose of characterizing the heterogeneity of the fracture zones. However, the use of a constant-head drawdown in the source borehole did not provide a set of reciprocal data and responses from the different source boreholes that could be compared. To obtain data for comparison, the source must be a condition of constant flow rather than constant head.

The Piezomac head-monitoring system allowed the continuous measurement of heads at up to 55 observation points, and proved to be a very versatile design. Both sampling frequency and measurement points could be changed

easily by altering software settings. Because of the limited number of packers used to isolate conductive sections within a borehole, relatively long monitoring sections were used. As such, this did not permit good definition of the differing responses between the fracture zones and the hydraulic connections to the "average rock". The early installation of a head-monitoring system was considered to be essential during the characterization of a site in order to facilitate identification of hydraulic connections as quickly as possible.

The entire suite of tracer migration tests, involving saline, dye, and metal-complex tracers, was based, initially, on rather precise characterization by remote sensing techniques of a principal pathway for groundwater transport, namely the H zone. This was followed by a sequence of migration experiments with saline tracers, involving source points within the zone and in the nearby "average rock" and collection in the Validation Drift and in intervals within a borehole. Radar-difference tomography was used to determine the distribution of saline tracer within the H zone, before and after excavation of the Validation Drift, and to follow its migration in three planes surrounding the injection point. This technique also provided an independent means of estimating flow porosity for comparison with that calculated on the basis of the tracer breakthrough curves. Tracer concentrations were measured successfully in borehole intervals at ambient pressure by means of circulating water within the packed-off sections. Tracer testing between arrays of boreholes has the potential for providing data on dispersivities that are difficult to obtain otherwise, and to avoid difficulties associated with the disturbed zone around a drift. A new technique was developed for continuous injection of tracers at a relatively low constant-injection flow rate over time periods of several months, thereby minimizing the potential for disturbing the groundwater pressure and flow fields close to the collection points.

The considerable effort expended to characterize non-sorbing tracers for use in field applications resulted in a set of lanthanide-organic complexes, or simply metal complexes, which exhibited low detection limits in terms of ppb concentration and the absence of interaction between different elements. When a metal complex is used together with a dye, in the form of a mixture, the arrival of the tracer mixture at an observation point can be detected visually because of the dye, but yet allows definition of the concentration of the metal complex rather accurately. Because the dyes are slightly sorbing, they could potentially be used in combination with non-sorbing metal complexes to estimate the active, or wetted, surface available for sorption.

Characterization Methodology

The characterization of the SCV site featured an integrated effort where different scientific disciplines and testing techniques were combined to obtain the data to develop a comprehensive description of the site. The characterization programme was based initially on a combination of technology developed in Phase 2 of the Stripa Project and previous experience from characterization activities within the national radioactive waste programmes of the participating countries. For purposes of the SCV site, the investigation programme included a balanced mix of single-borehole and crosshole testing techniques. This approach provided an adequate

description of the site in terms of location and extent of fracture zones along with the data required to develop the stochastic fracture-network models.

The SCV programme demonstrated the practicability of implementing the characterization tasks within a mine environment with the intent of collecting high quality data rather than minimizing the time for data collection. It should be kept in mind that a number of the characterization tools were, for all practical purposes, used for the first time and testing procedures had to be finalized before the start of the actual data collection. Generally speaking, it was felt that the time required for single-borehole measurements by means of radar and seismic testing methods could be reduced in future characterization work. However, within the SCV programme, the time allotted for the hydraulic testing was generally too short to allow full equilibration of hydraulic heads between experiments and, consequently, adversely affected the interpretation of results.

Because 80% to 90% of the groundwater flow occurred in the fracture zones at the SCV site, the assumption was made that a binary description of the rock mass in terms of "fracture zones" and "averagely fractured rock" was appropriate. A "Fracture Zone Index" was developed on the basis of principal component analysis of single-borehole data and used to identify locations where "fracture zones" intersected the boreholes. The geometry of the fracture zones was then obtained from the radar and seismic testing data, and the reliability of the interpretations was checked by evaluating the consistency of data collected from different boreholes. Finally, the hydrologic significance of the conceptual geologic model was verified by means of crosshole hydraulic testing.

A systematic procedure was developed for constructing a model of the geohydrology of the site, and was based on:

- a set of single-borehole measurements, involving geophysical logging, core logging, and hydraulic testing, which characterized the competency of the rock mass in terms of "fracture zones" and "averagely fractured rock"
- remote-sensing radar and seismic techniques which defined the geometry of anomalous features, such as the fracture zones
- crosshole hydraulic tests which verified the hydraulic significance of the identified features and quantified their hydraulic properties.

The distance between boreholes at the SCV site was of the order of 50 m to 70 m, which was comparable to the probing range of the remote-sensing techniques that were used. During characterization of a repository site in the future, distances between boreholes can be expected to be as great as several hundred metres. Although these distances are beyond the present capability of the borehole-radar-reflection method, the directional radar could still be useful for determining the orientation of large-scale features and verifying their extent over substantial distances from the boreholes, particularly in a rock mass that exhibits low resistivity. A combination of the crosshole seismic technique with the single-borehole directional radar technique would probably be the most cost effective means to characterize the geometry of features. On a smaller scale, in terms of dimensions of tens of metres, remote sensing techniques with better resolution than used at the

SCV site are required to define the geometric aspects of structural features. In particular, the wave lengths used in the investigations at the SCV site were of the order of a few metres, which was comparable to the resolution achieved.

3.4 SUMMARY OF SIGNIFICANT ACHIEVEMENTS

The characterization tools and techniques were applied to a saturated mass of fractured granitic rock within and around the confines of the Stripa mine. The consequences of these applications, however, have significance from both rock-specific and rock-generic viewpoints. The outcome of the evolution of the development of a strategy of sequential and focussed characterization, together with the demonstration of an ordered and consistent process for developing conceptual geohydrologic models, are significant achievements for rock types and sites in general. On the other hand, the development of specific characterization tools, such as the borehole radar, and the design and implementation of a tracer migration experiment in a fracture zone are specific in most respects to saturated, fractured granitic rock. The observations of the influence of the disturbed zone around a drift on groundwater inflow and solute transport were of course specific to the granite rock in the SCV site. However, from a qualitative viewpoint, these observations may be of significance in the design of experiments to evaluate the influence of the disturbed zone in other rock types and environments.

The conceptualizations of the structural and hydrologic characteristics of rock masses in the Stripa Project encompassed volumes ranging from several hundred billion m^3 in the regional sense to about one million m^3 in the very focussed sense at the SCV site. The conceptual models at the regional and local scales were based principally on observations and interpretations of surface geologic and hydrologic features, as well as on the body of geologic observations that had accumulated during the mining of the ore body at the Stripa mine. These models, ranging over some 100 km^2 of surface area and 3 km of depth, appeared to be reasonably accurate portrayals of the geology and hydrology of the area as evidenced by the close correlation between calculated inflows of groundwater to the mine and the observed pumping rates. The conceptualizations within the confines of the mine itself ranged in volume from about 400 million m^3 to about 1 million m^3 for the SCV site. The information used to develop these models was based on a combination of observations and borehole hydraulic tests at the larger scale, and detailed borehole testing with the radar, seismic, and hydraulic techniques at the smaller scale. The fundamentally significant aspect of this wide-ranging effort for developing conceptual models was the consistency in interpretations of structural, hydrologic, and geochemical features over dimensions ranging from a few tens of metres to thousands of metres.

The notion of a sequential programme of progressive site characterization began initially with the design of the SCV programme as an iterative process of characterization, prediction, and evaluation. The sequencing aspect became more important in the closing stages of the SCV programme when experiments were being designed to test the validity of the models for simulating groundwater flow and transport.

4 MODELLING OF GROUNDWATER FLOW AND SOLUTE TRANSPORT

One of the principal objectives of Phase 3 was "to integrate different tools and methods in order to predict and validate the groundwater flow and transport in a specific volume of the Stripa granite". The intent was to conduct field experiments under strictly controlled research conditions, and to link the characterization techniques to the mathematical models so that predictions of groundwater flow and transport could be compared with field measurements. The Site Characterization and Validation (SCV) programme, as described in Section 3.3, was organized according to this objective. The Task Force on Fracture Flow Modelling was established by the Joint Technical Committee to guide the development of the numerical models for groundwater flow and transport and to develop criteria for verification and validation of the models.

A model validation process was developed, together with the criteria against which validity of the models could be evaluated. At the same time, the elements of the fracture-flow modelling approaches were developed and the computational aspects verified by using problems with known solutions. The fracture-flow models and the equivalent-porous-media modelling approach were tested initially against data obtained from the Simulated Drift Experiment and the Radar/Saline Tracer Experiments. Subsequently, the validity of each modelling approach was assessed against data obtained in the Validation Drift Experiment and the Tracer Migration Experiment.

4.1 MODEL VALIDATION PROCESS AND CRITERIA

The process for evaluating the validity of the groundwater flow and transport models, as well as the criteria against which the models would be assessed, were developed by the Task Force on Fracture Flow Modelling during the early part of Phase 3. The task force consisted of one technical expert from each of the member countries, the project manager, and the senior chairman of the Technical Subgroup. These and subsequent activities required close cooperation with the principal investigators for the characterization and modelling investigations, and included reviews by the TSG and JTC. Although the process was rather general, the application was specific to evaluations of the numerical models used to simulate groundwater flow and solute transport within the SCV site.

4.1.1 Definition of Model Validation

There have been several definitions of "model validation" proposed for use in an evaluation of the expected performance of a geologic repository. For

example, the International Atomic Energy Agency has defined validation as (IAEA, 1982):

A conceptual model and the computer code derived from it are "validated" when it is confirmed that the conceptual model and the derived computer code provide a good representation of the actual processes occurring in the real system. Validation is thus carried out by comparison of calculations with field observations and experimental measurements.

From a practical viewpoint, the validity of a model used to assess the long-term performance of a geologic repository will be based probably on reasoned judgement and expert opinion in light of the available evidence. For the very specific SCV programme of the Stripa Project, model validation was defined as (Gnirk, 1991):

A model is considered to be validated for use in a given application when the model has been determined by appropriate measures to provide a representation of the process or system which is acceptable to an assembled group of knowledgeable experts for purposes of the application.

The "appropriate measures" will be determined by the geometric and time scales of the application, the phenomenological process or features of the natural system, and the level of acceptable uncertainty for purposes of the application. The measures will involve comparison of model calculations against field observations and/or experimental measurements, considering the extent and nature of the uncertainties in the calculations, observations, and measurements in relation to those allowable for purposes of the application. The phrase "*for use in a given application*" is a key element of the definition. For purposes of the SCV programme, the given application was "*the groundwater flow and transport in a specific volume of the Stripa granite*". This is decidedly different from assessments of post-waste-emplacement groundwater flow and radionuclide transport through a geologic repository over many thousands of years into the future.

4.1.2 Model Validation Process

Four different groups were involved in the model validation process in the SCV programme. As shown in Figure 4-1, the groups were the Principal Investigators for the characterization and modelling activities in the SCV programme, the Task Force on Fracture Flow Modelling, the Technical Subgroup (TSG), and the Joint Technical Committee (JTC). The field experiments and model predictions were performed by the first group, and the validation assessments by the second group. The JTC and TSG reviewed the work plans and results, and provided general direction on the conduct of the activities.

The process consisted of four separate activities. The first activity involved principally the JTC which decided that a principal objective of Phase 3 would be "*to integrate different tools and methods in order to predict and validate the groundwater flow and transport in a specific volume of the Stripa granite*". It was further decided that both fracture-flow models and equivalent-porous-media (EPM) models would be used for making the predictions of flow and transport. The JTC formed a panel of technical

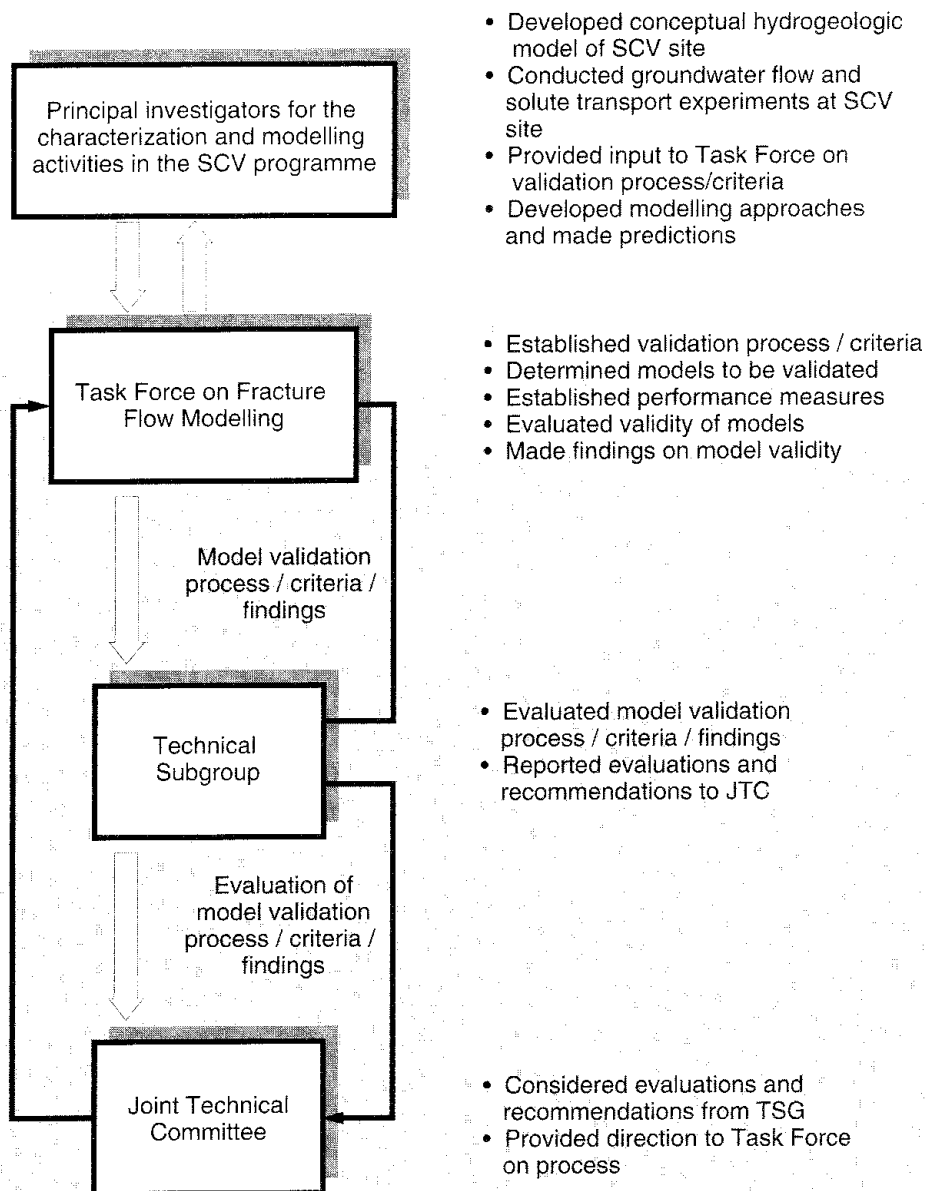


Figure 4-1 Process for evaluating the validity of the groundwater flow and transport models at the SCV site (Gnirk, 1992).

experts, known as the Task Force on Fracture Flow Modelling, and chartered this group to "guide and review the development of numerical modelling of fracture flow within the Stripa Project" and "to recommend criteria for the verification and validation of the numerical models". The task force was directed to define and implement a model validation process (Hodgkinson, 1992).

The second activity required that the task force and the principal investigators work closely together to define the specific steps in the validation process, and to identify the models to be considered. Commonly, a computer code for groundwater flow in a fractured rock medium has a

number of sub-system models or components containing the instructions for treating discrete-fracture flow, the statistical treatment of data for the hydraulic conductivity of a representative volume element, and the like. The entire collection of models and components in the computer code can be considered to be the modelling procedure. As such, consideration was given to fracture-flow modelling approaches developed by research groups at AEA Harwell in the UK and Lawrence Berkeley Laboratory and Golder Associates Inc. in the USA, and to an established equivalent-porous-media model, known as CFEST (Coupled Fluid, Energy, and Solute Transport), used by Fracflow Consultants in Canada.

The third activity, involving the combined efforts of the task force and the principal investigators, required the selection of experiments to be conducted at the SCV site to obtain data to compare against the model predictions. At the same time, it was necessary to establish the performance measures and criteria to be used in assessing the validity of a modelling procedure. Two sets of two experiments each for groundwater flow and transport at the SCV site were agreed upon. The first experiment in each set was used as a "training exercise", so that experience in modelling full-scale field situations could be obtained and the capabilities and accuracies of the sub-system models and components tested. The second experiment, known as the "validation exercise", was designed to provide a basis for judging the validity of a modelling procedure for simulating groundwater flow or solute transport in the SCV site. The criteria against which the validity of the models were judged were both quantitative, involving deterministic and/or stochastic aspects, and qualitative, in the sense of principal observable results of an experiment. It was also decided that judgements of validity should include consideration of the potential usefulness of the modelling procedure in other applications, and the feasibility of acquiring the data to support the modelling procedure.

Collectively, the fourth activity involved conducting the field experiments, performing the model predictions, assessing the validity of the modelling procedures, and reporting the results to the TSG and the JTC for review and comment. The review and comment aspects of the validation process were quite important in this multi-national effort. In essence, the views of the technical and managerial representatives from the various countries were incorporated, on balance, into the considerations and efforts of the task force and the principal investigators.

4.1.3 Model Validation Criteria

The validity of a given modelling approach for simulating groundwater flow and transport within the SCV site was evaluated on the basis of the following criteria (Gnirk, 1990):

- **Quantitative:** Do the predictive calculations adequately reflect the measured values? That is, are the predictions of the correct order of magnitude as compared to the measurements?
- **Qualitative:** Are the predicted distribution patterns of phenomena sufficiently accurate as compared to the observations? That is, are the

predictions of the patterns reasonable when compared to the observations?

The applicability of a given modelling approach for simulating groundwater flow and transport in a fractured rock mass was considered on the basis of the following criteria:

- **Usefulness:** From the viewpoint of assessing the expected performance of a geologic repository, is the modelling approach useful for representing groundwater flow and transport in a geohydrologic environment similar to that at the SCV site in the Stripa mine?
- **Feasibility:** Can the characterization data required to fully support the modelling approach be collected in a feasible and timely manner?

4.2 GROUNDWATER FLOW AND TRANSPORT MODELS

At the beginning of Phase 3, the fracture-flow models were in the early stages of development. Many of the development activities that took place subsequently dealt with the treatment and use of fracture data. The three fracture-flow modelling approaches implemented separately by AEA Harwell (Harwell), Lawrence Berkeley Laboratory (LBL), and Golder Associates (Golder) all exhibited significant differences in terms of treatment of fracture data, representation of the size and characteristics of the SCV site, and fundamental assumptions concerning the manner in which water flowed through the rock mass. The modelling approach used by Fracflow Consultants (Fracflow) made use of an existing computer code, known as CFEST, that was based on the assumptions appropriate to groundwater flow in an equivalent porous medium.

4.2.1 Fracflow Equivalent-Porous-Media Model

The equivalent-porous-media (EPM) modelling was accomplished by use of the established computer code CFEST (Gupta et al, 1982). CFEST is a three-dimensional finite-element code that is applicable to the analysis of coupled fluid, energy, and solute transport in an equivalent porous medium. This code has been applied and verified on a number of test cases and groundwater systems outside the Stripa Project, and was used to develop the hydrologic model of the Stripa area as described in Section 3.1. This modelling approach was used to predict the observed pattern of hydraulic heads in the SCV site, the groundwater flux into the D boreholes in the Simulated Drift experiment, and the groundwater flux into the Validation Drift. It also provided the hydraulic-head boundary conditions for the three-dimensional discrete fracture network modelling of the groundwater flux into the D boreholes and the Validation Drift performed by Harwell (Herbert et al, 1991). This approach also provided a means for incorporating the EPM properties generated by the Harwell fracture-flow model, as based on the measured fracture geometry and the borehole hydraulic test data, into a larger scale model that included a reasonable approximation of the far-field boundary conditions for hydraulic head. Finally, the CFEST code was used

to simulate the Radar/Saline Tracer Experiments and the Tracer Migration Experiment (MacLeod et al, 1992).

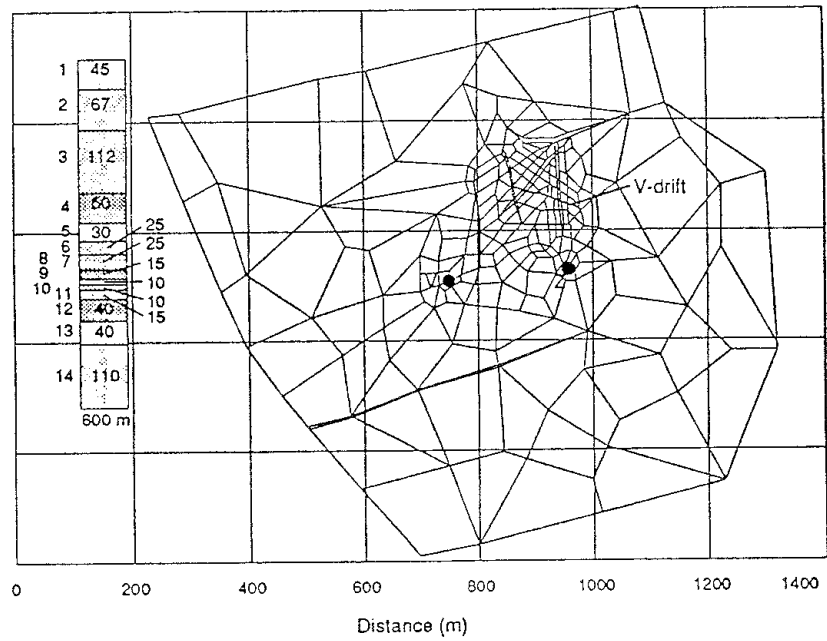
Conceptual Model of the Stripa Area

On a regional scale, the groundwater flow system depends on the topography, the distribution of surface water, and the distribution of permeability within the rock mass. As discussed in Section 3.1, the three-dimensional distribution of hydraulic heads in the Stripa area were calculated for both the regional and local-mine groundwater flow systems, under steady-state conditions, over a range of hydraulic properties, with and without the mine workings, and with and without the major fracture zones. This distribution of hydraulic heads provided the basis for defining the boundary conditions for modelling flow within the immediate area of the SCV site and for simulating inflow to the Validation Drift.

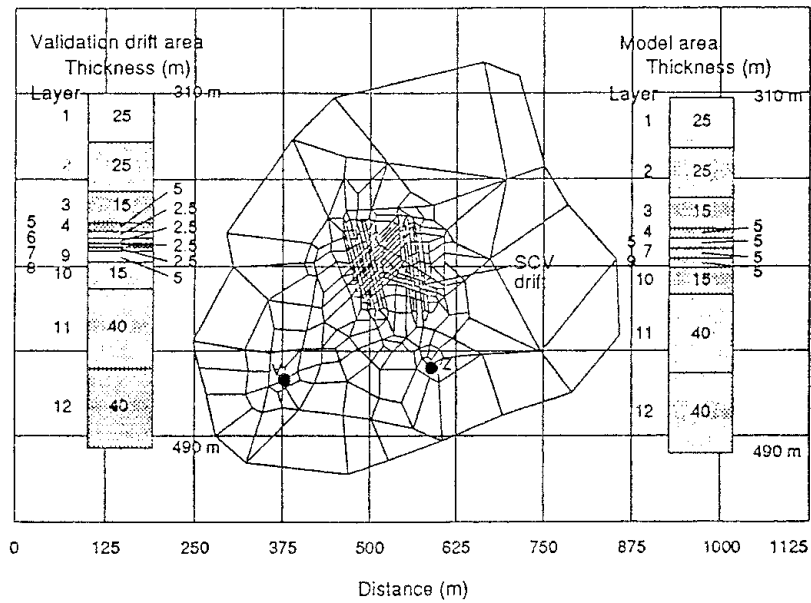
Conceptual Model of the Stripa Mine

Three finite-element meshes, known as MINE, MINE2, and SCV, were developed for purposes of the EPM modelling effort. The MINE and MINE2 models extended from the surface to a depth of about 600 m, and the surface outlines, or footprints, encompassed areas of approximately 1 km². The finite-element mesh for the MINE model was basically the same as that for the MINE2 model shown in Figure 4-2(a). The two meshes were developed to accommodate changes in the location and orientation of major fracture zones as the SCV programme progressed through the various stages of characterization activities. The hydraulic head boundary conditions for these two large-scale models were extracted from the heads that were computed from the even larger, local model, discussed in Section 3.1, that included the mined excavations in the Stripa mine. The SCV mesh, shown in Figure 4-2(b), was constructed to provide a better approximation of the inclined nature of the major fracture zones in the SCV site. This mesh contained elements with dimensions that were consistent with the size of the fracture-flow network model used by Harwell for generation of the EPM properties of the rock mass when a large percentage of the fractures were included in the network.

The MINE model, centered over the east side of the mine, consisted of fourteen layers of elements of varying thicknesses extending to a depth of 600 m. Three fracture zones, each with a uniform thickness of 5 m, a 90° dip, and a hydraulic conductivity adjusted to give the required transmissivity, were included in the mesh. These zones included the H zone trending in the north-south direction, the B zone trending in the northwest-southeast direction, and an east-west oriented zone located to the southwest of the mine workings. The hydrologic boundary conditions were interpolated from the hydraulic heads calculated from the local model that simulated the effect of the Stripa mine workings on the regional flow system. Internal nodes within the mesh, located on the mine openings and on the old mine workings, were assigned hydraulic heads equal to the elevation heads. The permeabilities of the elements in the various layers were determined from the permeability-depth relationship for granite used in the local model. In some of the numerical simulations with the MINE



(a) MINE2 Hydrologic Model



(b) SCV Hydrologic Model

Figure 4-2 Finite-element meshes for equivalent-porous-media models of the Stripa Mine and the SCV site (Herbert et al, 1991; MacLeod et al, 1992).

These models were used to predict the groundwater inflow into the D boreholes and the Validation Drift, and the tracer migration into the Validation Drift.

model, the hydraulic properties obtained from hydraulic tests in the N and W boreholes were assigned to the H zone and B zone.

The MINE2 model was used to simulate the hydraulic heads in the immediate region of the SCV site and to predict the groundwater flow into the D boreholes and the Validation Drift. The MINE2 mesh was similar to the MINE mesh, except that small changes in the surface expression were made to incorporate changes in the geometry and location of the fracture zones and to permit the addition of the fracture zone known as I. Also, significant changes in the thicknesses of the fourteen layers in the model were made to accommodate the geophysical and hydraulic features determined from the characterization activities, and to provide more detail at the level of the SCV site. The B zone was combined with the A zone and moved toward the southeast such that the combined zone would be intersected by the D boreholes. The hydraulic boundary conditions for the model and the hydraulic conductivities of the layers were selected on the same bases as for the MINE model, including an adjustment of the hydraulic conductivities of the fracture zones to reflect the measured transmissivities. The hydraulic properties of selected "average rock" and "fracture zone" elements within the SCV site were modified on the basis of field measurements.

Conceptual Model of the SCV Site

The SCV model represented the mass of rock located between the 310 m and 490 m levels of the Stripa mine. As shown in Figure 4-2(b), it consisted of ten layers of elements with the four middle layers each having a thickness of 5 m. The nodes located on the top surface of layer five represented the traces of the D boreholes and the Validation Drift. The small element size used in the mesh allowed simulation of the inclined orientation of the fracture zones and the variability in hydraulic properties along the fracture zones, and provided for both horizontal and vertical interconnection of the fracture zones. The dimensions of the elements were consistent with the size of the rock mass that could be used in the Harwell modelling effort when a large percentage of the fractures were included in the network model used to generate the EPM properties. Finally, the detail provided by the small elements was required in order to achieve grid-convergence of the flow path and tracer simulations.

Application of the Conceptual Models

The three finite-element meshes exhibited increasing detail and precision in terms of the location of major fracture zones. The initial input parameters assigned to the MINE model were taken from the data set compiled in Phase 2 for the entire mine area for purposes of modelling the regional flow. Input parameters for later simulations, using the three meshes, included the additional measurements made during the SCV programme. The MINE model was used to estimate the groundwater flow into the D boreholes on the basis of very little specific data for the SCV site. Later predictions for the groundwater flow into the D boreholes and the Validation Drift were made with the MINE2 model. This model incorporated the most recent hydraulic and geometric data for the fracture zones in the SCV site and the

best estimates of the hydraulic properties from the field measurements for the average rock. A number of MINE2 model simulations were performed to examine the different concepts for the distribution and interconnection of high-permeability zones within and adjacent to the SCV site. The SCV model was used to confirm the predictions of groundwater inflow into the D boreholes and the Validation Drift made initially with the MINE2 model. The SCV model had more detailed meshes of elements adjacent to the D boreholes and the Validation Drift. Finally, the transport predictions for the Radar/Saline Tracer and Tracer Migration experiments were made with the SCV model.

4.2.2 Harwell Fracture-Flow Model

The model for groundwater flow and transport through a connected network of discrete fractures, as developed by the group at AEA Harwell, was contained in the computer code NAPSAC (Grindrod et al, 1991; Herbert et al, 1991; Herbert and Lanyon, 1992). NAPSAC was designed to handle large fracture networks with thousands of fracture intersections, and, as such, is not particularly well suited for simple networks having only a few fractures. The model is defined within a domain formed from the union of a number of, possibly irregular, hexahedrons, forming the flow region. Pressure boundary conditions may be imposed on any fracture intersecting the overall domain boundaries, and the groundwater pressure or flux may be specified in simulated boreholes.

Generation of Fracture Networks

The fracture network for a given region is constructed by generating fractures, one at a time, where each fracture is a rectangle defined by its own orientation (dip and strike) and dimensions (specified half-side lengths and directions). The fracture centers are uniformly distributed within a cuboidal generation region, and the lengths and directions of the sides are generated independently from user-specified probability distributions, which may be constant, uniform, normal, exponential, or log-normal in distribution. It is possible to specify separate fracture sets, each comprising a sublist of fractures having certain constraint characteristics. For example, a set of fractures can be generated with a particular orientation, or with centers clustered together in a certain subdomain, to model a fracture zone or a highly permeable subregion. In this manner, fracture data from a rock mass can be incorporated into the simulation, rather than simply generating a uniformly fractured realization. Each fracture set may be constrained by a variety of characteristics so as to reflect the underlying spatial heterogeneity. Additionally, known fractures can be included explicitly within a modelled region.

Each fracture is discretized using a uniform finite-element mesh of triangles grouped together into elemental rectangles with a specified fracture aperture. The aperture can be varied over individual fractures since each element is assigned its own aperture. Spatially correlated random apertures may be generated for each rectangular fracture, with such apertures sampled from a log-normal distribution. After the fracture network is generated, all fracture intersections must be located and described prior to initiating any

computations. The intersections with the flow domain boundaries and boreholes must also be located. Each fracture is checked and terminated for intersections, and any fracture that does not intersect another fracture is deleted.

Computational Features

Each fracture is discretized so that the hydrodynamic equations can be solved numerically. The flow calculation involves determination of the pressures and fluxes at all nodes on each of the discretized fracture intersections. Groundwater is modelled as an incompressible fluid. The flow field is calculated as a steady-state condition that reflects the pressure distribution specified on the permeable boundaries of the domain. Within each fracture, the groundwater flux is calculated as a function of the fracture aperture, the fluid viscosity, and the gradient in the non-hydrostatic pressure. Given the pressure distribution or net water flux in, or out, along each fracture intersection, a detailed flow field within a single fracture can be computed. Thus, the flow field through the entire fracture network is determined by the non-hydrostatic pressure at all of the fracture intersections.

The tracer transport option in NAPSAC is designed to calculate the migration and dispersal of a tracer through a discrete fracture network for which the flow regime has been determined previously. Within the groundwater, it is assumed that transport is dominated by advection, whereby molecular diffusion may be ignored. The major cause of dispersion will be the geometry of the fracture network itself and the channelling effect of the various flow paths as defined by interconnections between and among fractures. The flow field is in effect described in the two-dimensional plane of each fracture, where the fracture apertures are assumed to be sufficiently small to allow the tracer to diffuse quickly over the cross section. At relatively low flow rates, hydrodynamic dispersion due to differential flow profiles at fracture intersections is negligible as compared to the dispersion due to the effect of preferential pathways through the fracture sets.

The transport calculations are based on a particle-tracking algorithm. The advantage of this technique for saturated fractured rock is that dominant flow paths are given primary consideration, as compared to paths through relatively stationary water. The flow paths are calculated individually for each fracture. A swarm of representative tracer particles are tracked, beginning from an initial distribution and ending at the outflowing fracture intersections with the boundaries of the flow domain. The distribution of particles may be calculated as a function of time.

Conceptualization of the Fractures within the SCV Site

As described in Section 3.3, the SCV site contained structural features that ranged in scale from small tight fractures of the order of centimetres, to large-scale fracture zones that spanned the site and dominated the flow system by acting as conduits for groundwater movement. At the smaller scale where there are very many discrete fractures in the rock, NAPSAC was used to generate numerical models which exhibited the same fracture

statistics as those based on measurements at the site. On a sufficiently large scale for some representative volume of rock, the simulation of groundwater flow was effectively independent of the precise details of the individual fractures that made up the network. On a scale smaller than this representative volume, many realizations of the fracture network statistics were performed to quantify the uncertainty in the prediction of groundwater flow.

The rock mass at the SCV site can be conceptually separated into zones of intense fracturing and the regions between such zones where rock is averagely fractured. As described in Section 3.3, the boundary between a fracture zone and the averagely fractured rock was defined on the basis of a Fracture Zone Index. The inclusion of all fractures that were mapped as being coated, and thus deemed natural, resulted in a very dense fracture network. Some of these fractures, however, probably transmitted relatively little water. Thus, the proportion of fractures that could be neglected in the development of the network model had to be determined. Because it was not possible to determine any meaningful correlation between fracture transmissivity and fracture orientation or length, a single transmissivity distribution for all fractures was assumed.

The distribution of fracture trace lengths was assumed to be log-normal, since the distribution based on field measurements was always positive and skewed, as is common for distributions of many geologic properties. The truncation and censoring biases were corrected statistically in order to obtain estimates of the parameters of the trace-length distribution. The primary input to NAPSAC, however, is the fracture length distribution rather than the trace length distribution. It has been shown that the distribution of fracture lengths can be completely determined by the full set of moments of the trace-length distribution (Herbert and Splawski, 1990). A log-normal form for the fracture-length distribution was chosen, and the moments of the trace-length distribution were related to the moments of the fracture-length distribution. Subsequently, the parameters of the fracture-length distribution were determined in terms of the fitted parameters of the trace-length distribution. Finally, the fracture spacing data collected by field measurements were used, together with the fracture-length distribution, to obtain a fracture density.

Fracture Transmissivity

The hydraulic packer-test intervals were separated into those located in the H zone and those in the average rock. Subsequently, separate statistical data sets were developed for measurements within the average rock and within the H zone. However, because the H zone was relatively narrow and the number of test intervals completely within the zone was small, data from all intervals that were located more than 50% within the H zone were included in the second data set. The assumption was then made that the hydraulic properties of each fracture could be characterized by a single effective transmissivity value, randomly sampled from a probability distribution that was independent of other fracture properties. This transmissivity was considered to correspond to Darcy flow through the fracture and any filling material, and to represent an effective "parallel plate" aperture. Where several fractures intersected the hydraulic packer-test interval, it was

assumed that the transmissivity of the test interval was simply the sum of the transmissivities of the fractures intersecting that interval. This, in effect, assumed that the flows through the separate fractures were independent, which was reasonably valid as long as the hydraulic response to the test was dominated by that part of the fracture nearest the borehole. Farther from the borehole, the fractures would intersect and the flows would interact.

The form of the distribution of fracture transmissivities was selected to be log-normal. For a given set of parameters of the distribution, the probability density for the sum of several independent random variables drawn from the distribution was numerically evaluated. From these density functions, a likelihood for the measurements in each test interval was calculated. Thus, it was possible to compute the maximum likelihood estimators for the parameters of a distribution of single fracture transmissivities. Care was taken to ensure that the numerical estimation procedure was robust, and any approximations to the frequency of measured coated fractures were chosen carefully to avoid any dominant influence of extreme data. For data at the low end of the distribution, the density function was approximated by a linear variation between the lowest calculated probability value and zero probability of zero transmissivity. For data at the high end of the distribution, use was made of a log-normal random variable with the same mean and standard deviation as the summed random variable. Thus, the algorithm was forced to obtain reasonable fits to the high transmissivity values, and, in so doing, relatively little importance was attached to improbable low transmissivity measurements.

Local Aperture Variation

The approach described above was based on the assumption that the hydraulic response of a fracture can be characterized by a single effective aperture, and that the variation in response between test intervals was due to the differences in aperture between different fractures. An alternative conceptual model assumed that the effective hydraulic aperture varied over each fracture, and that the range of responses between test intervals was due to the borehole interval intersecting different parts of the fractures. In this case, it was assumed that all fractures had the same statistical hydraulic properties, which implied a distribution of local aperture values that must be generated over all of the fracture surfaces. These two different approaches represented two extremes, where the network of fractures in the rock mass would likely be somewhere in between.

Adopting the approach of Stratford et al (1990), the distribution of the local aperture field was assumed to be log-normal, and was characterized by the mean and standard deviation of the underlying normal distribution. A spatial correlation of the local aperture was allowed, wherein a spherical correlation function characterized by a correlation length δ was specified. It was assumed that the borehole tests measured the response of a region larger than the scale of the local variation, typically of the order of 10 cm, where the main effective hydraulic aperture was given by the geometric mean local aperture (Dagan, 1979). The variation between different borehole tests depended strongly on the correlation length of the local aperture field, and the extent of channelling depended strongly on the standard deviation of the local aperture. Although the data set was sparse, the results from the

channelling experiments and the single borehole-packer tests provided enough information to fit the three parameters of the local aperture distribution, as shown in Figure 4-3.

Representative Elementary Volume of Rock

A representative elementary volume (REV) of rock can be defined as that volume of a fracture network above which no significant change in permeability occurs. In essence, an REV is the smallest volume that is statistically representative of an infinite network of fractures. The computational process involved imposing linear pressure boundaries on the faces of a cubic volume of a fracture network and calculating the fluxes through the cube for given pressure gradients. This technique allowed the transverse components of the permeability tensor to be calculated, thus making it possible to estimate the entire tensor by computing flow solutions for pressure gradients in three orthogonal directions. One drawback with this technique was that highly transmissive fractures that cross the corners of the network can cause anomalously large flows, particularly for sparsely

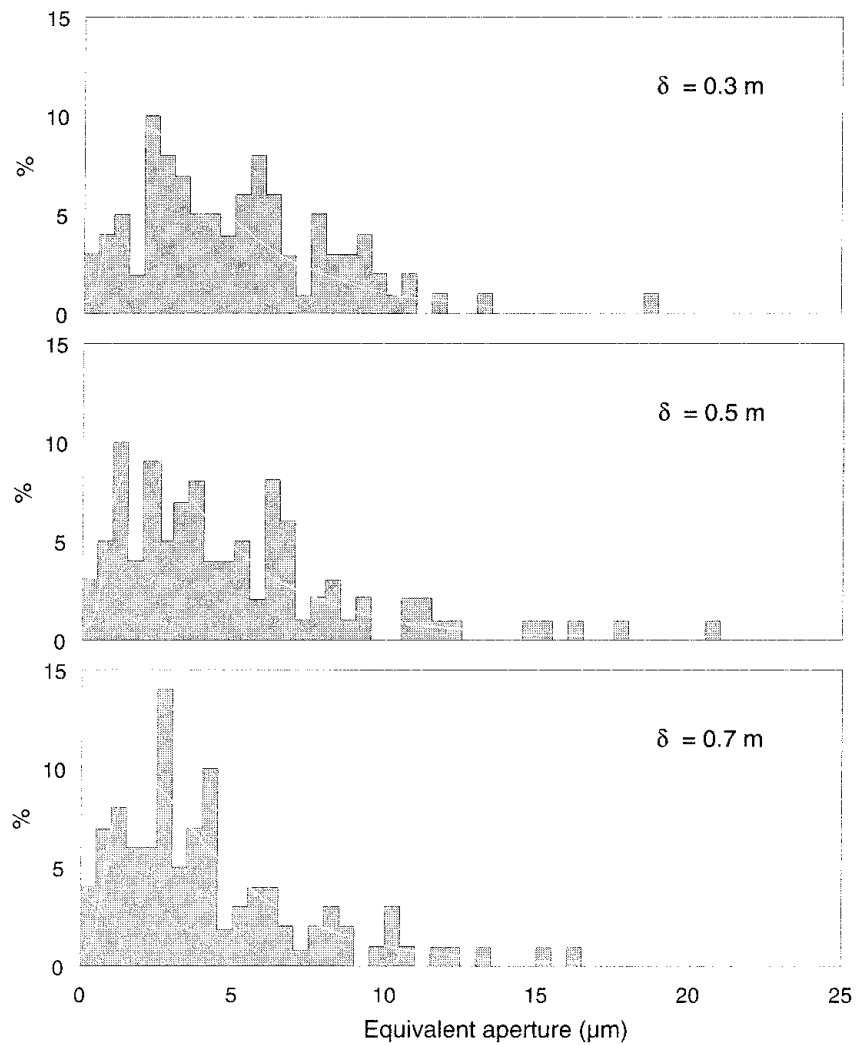


Figure 4-3 Equivalent fracture aperture frequencies as derived from simulated borehole-packer tests for different local aperture distributions (Herbert et al, 1991).

connected networks or networks with highly skewed transmissivity distributions. Once the detailed flow field had been calculated, a data base was generated with the net flux between each pair of intersections of each fracture. This data base was used to calculate the flux that passed across any arbitrary test surface within the network by summing the fluxes for all pairs of intersections lying on opposite sides of the test plane. By considering test planes on a variety of scales and moving them through the network, more information could be obtained for the variation in the permeability of a REV than obtained from surface fluxes alone.

To estimate the size of the REV for the averagely fractured rock at the SCV site, NAPSAC was used to calculate flows through cubes with sides of 10 m and 12.5 m, using the fracture statistics for the average rock at the SCV site. A realization for the cube with a side dimension of 12.5 m is shown in Figure 4-4. The flow within these cubes was analyzed by use of test planes with sizes varying from 8 m to 12 m in linear dimension. The pattern of flux crossing these test planes was calculated and the diagonal components of the permeability tensor estimated. Estimates of permeability from the 10 m cubes were found to be highly variable, while the results from 12 m planes within the 12.5 m cubes gave reasonably consistent estimates. Each realization for the cube of averagely fractured rock contained approximately 8 500 fractures and 30 000 fracture intersections. The permeability of the average rock was greatest in the vertical and north-south directions, as might be expected from the orientation of the major fracture set.

A network truncation study was conducted to determine the percentage of fractures that could be removed from the network without significantly reducing the permeability. A threshold of 90% of the permeability of the full network was specified. NAPSAC automatically removed unconnected fractures from a network, and used fracture aperture as the truncation parameter. The data base for the net flux between each pair of intersections on each fracture was interrogated, neglecting fractures with apertures below a specified threshold, to identify what portion of the least transmissive fractures might be neglected before significantly affecting the permeability. The calculation overestimated the flux through the truncated network because the flows in each fracture were assumed to be independent. That is, the decrease in connectivity due to the removal of low aperture fractures was ignored. As shown in Figure 4-5, by choosing a minimum aperture of $2.5 \mu\text{m}$, 30% of the fractures could be discarded with only 10% reduction in network permeability.

A similar set of calculations was undertaken to estimate the REV for the H zone network. Because of the greater fracture density and small fracture size within the H zone, the cubes were considerably smaller than those for the average rock. Based on the calculated results for various cube dimensions, reasonable permeability estimates were obtained with 6 m planes within a cube with a side dimension of 7 m. These cubes contained approximately 11 000 fractures and 40 000 intersections. The greatest permeability was determined to be oriented in the north-south direction, coincident with the alignment of the H zone structure. However, the variability in the component values of the permeability tensor were found to be greater than those for the average rock. The truncation study indicated that a 30% reduction in fracture density would give a 10% reduction in the overall permeability, with a minimum truncation aperture of $4 \mu\text{m}$. An

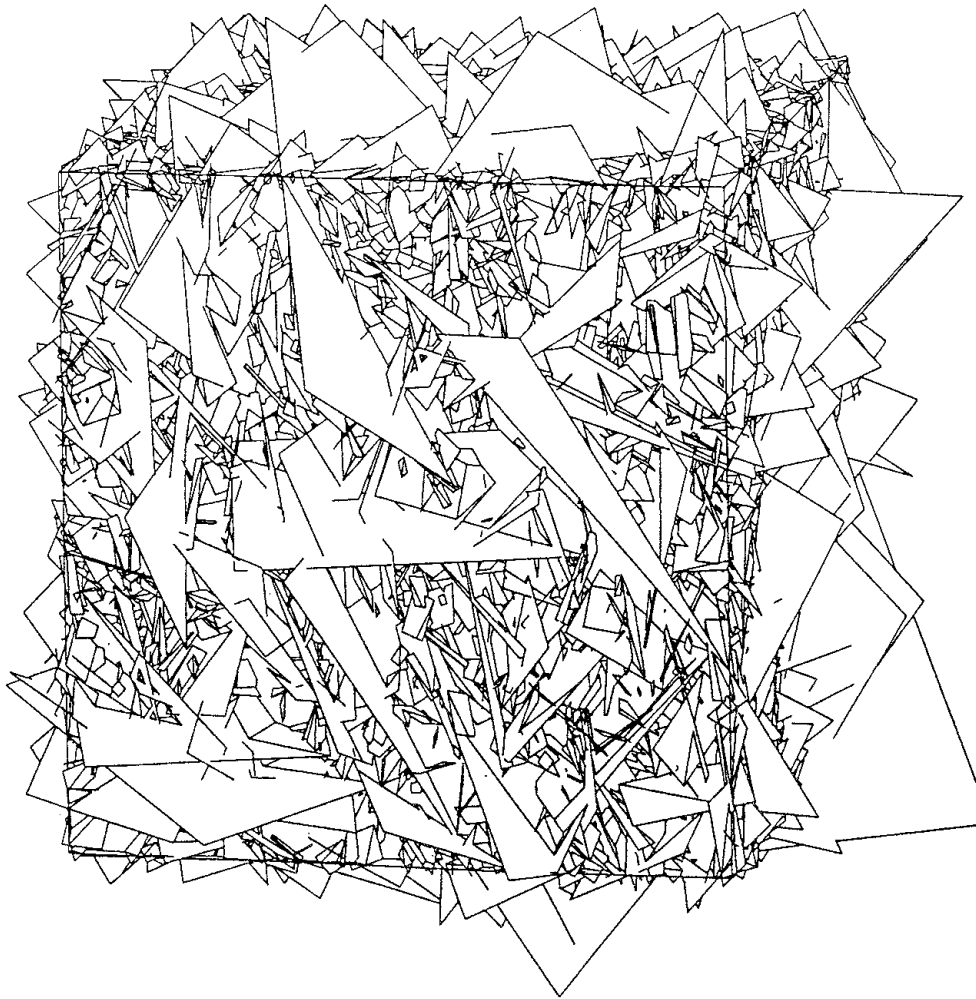


Figure 4-4 Typical realization of a cube of averagely-fractured rock with 12.5 m sides (Herbert et al, 1991).

additional evaluation of the effect of truncating the length scale determined that small fractures with areas less than 0.1 m^2 to 0.15 m^2 could be ignored. Thus, by setting a minimum aperture of $5 \mu\text{m}$ and a minimum area of 0.15 m^2 , 70% of the fractures could be removed from the network, resulting in a permeability reduction to about 70% of the full network.

The Influence of Rock Stress

The *in situ* stress field in the SCV site was anisotropic, as determined from borehole measurements. The axis of the Validation Drift was aligned with the largest principal stress. By use of the computer code BEFE, the stress field in the rock surrounding the Validation Drift was computed, using elastic moduli derived from laboratory measurements. The rock mass was assumed to be an elastic continuum and, because there existed no data, the elastic properties of the fracture zones were assumed to be the same as for the average rock. The stress distributions on the boundaries of the model were based on the *in situ* stress measurements.

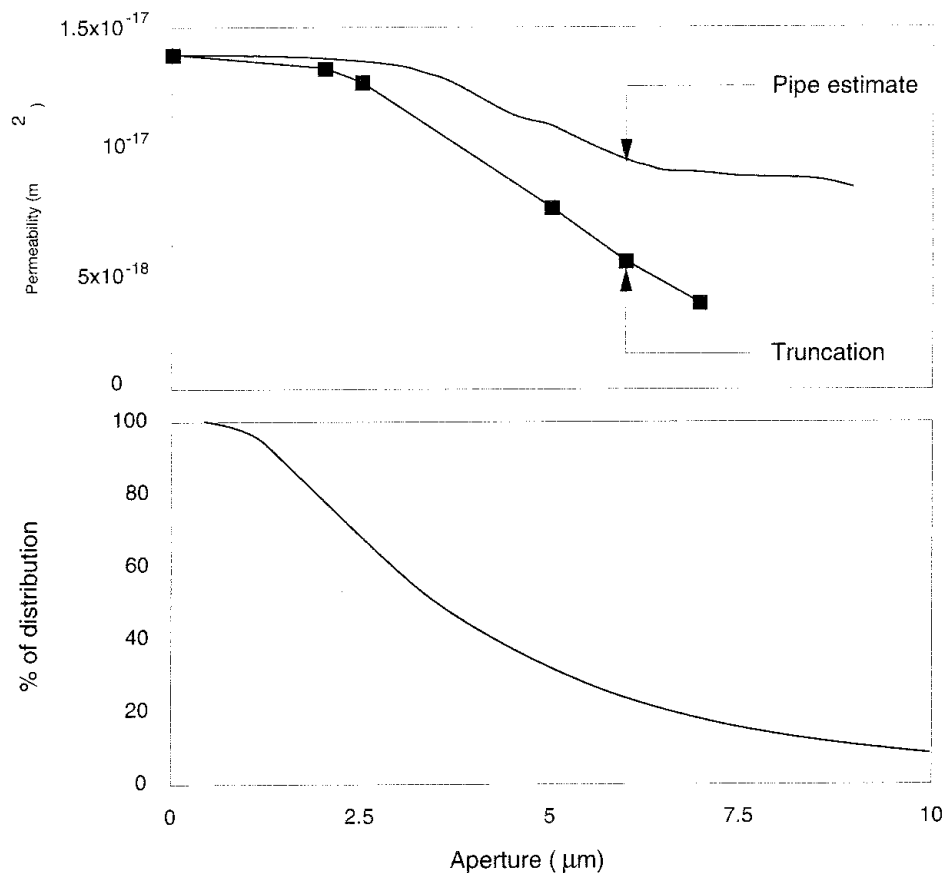


Figure 4-5 Permeability of a fracture network and proportion of network truncated as functions of the threshold for aperture truncation (Herbert et al, 1991).

The principal stresses and their orientations were converted into six components of the tensor. The tensor was rotated from the mine coordinates into the coordinates of the fracture network model for the Validation Drift. The normal stress acting on each fracture plane in the network model was calculated, and, by means of a power law that related transmissivity to normal stress, the fracture transmissivity was altered to correspond to the change in normal stress because of the excavation. The maximum change in aperture due to change in normal stress was limited to a maximum of 100% of the undisturbed aperture. For example, a fracture with an undisturbed aperture of $10 \mu\text{m}$ could only open to a maximum aperture of 1 mm. This abrupt change in aperture took place only in the fracture elements situated close to the drift and with normals to the fracture planes oriented radially to the drift.

Fracture Network Models for the SCV Site

The geometry of the fracture network for the average rock for a section of the SCV site containing the Validation Drift is shown in Figure 4-6. The model can be thought of as a hollow cylinder with an inner diameter of 2.5 m and an outer diameter of 10 m. The length of the hollow cylinder was 10 m. The fracture network model with only the D boreholes was similar to that for the Validation Drift, except for the volume of fractured

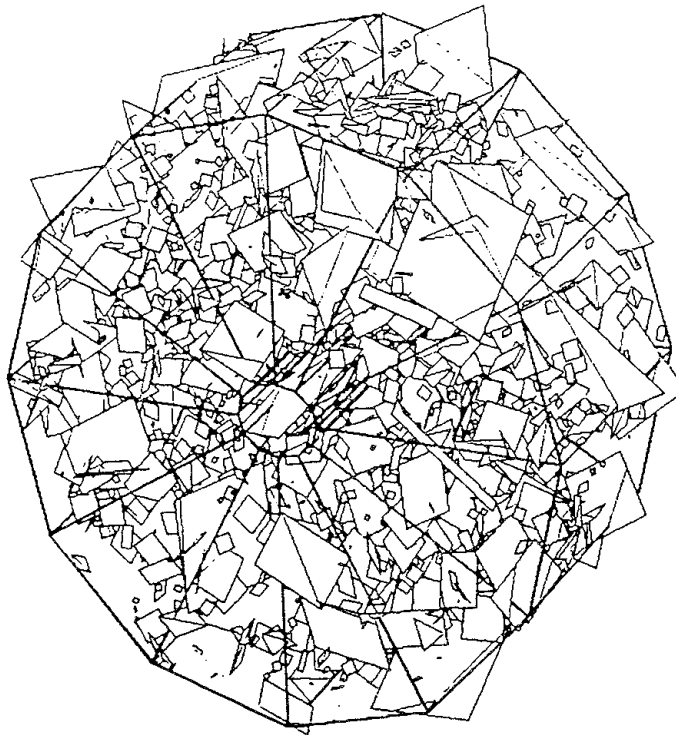


Figure 4-6 Network geometry of the averagely-fractured rock around the Validation Drift (Herbert et al, 1991).

The network geometry of the averagely fractured rock for the region of the SCV site containing the D boreholes is essentially the same. These models were used to predict the groundwater inflow into the D boreholes and the Validation Drift by means of the fracture-flow model encompassed in the computer code NAPSAC.

rock contained within the ring of boreholes. That model contained approximately 40 000 fractures and more than 100 000 intersections. The groundwater pressure distributions on the outer boundaries of the models were based on estimates provided by the EPM modelling. The fracture network model for the H zone was geometrically similar to that for the average rock, except the length of the hollow cylinder was only 5 m.

4.2.3 Golder Fracture-Flow Model

The fracture-flow modelling approach developed by the Golder group involved the creation of a semi-stochastic discrete fracture system that combined deterministic information on the position of fracture zones with statistical information on the properties of hydrologically conductive fractures. Fracture locations were assumed to be distributed randomly throughout a region, with an elevated intensity, in terms of fracture area per unit volume of rock, in the fracture zones that were identified by geophysical methods.

The components of the model are embodied in a computer code known as the FRACMAN discrete fracture simulator (Dershowitz et al, 1991a,b; Dershowitz and Wallman, 1992; Geier et al, 1990a). As shown in

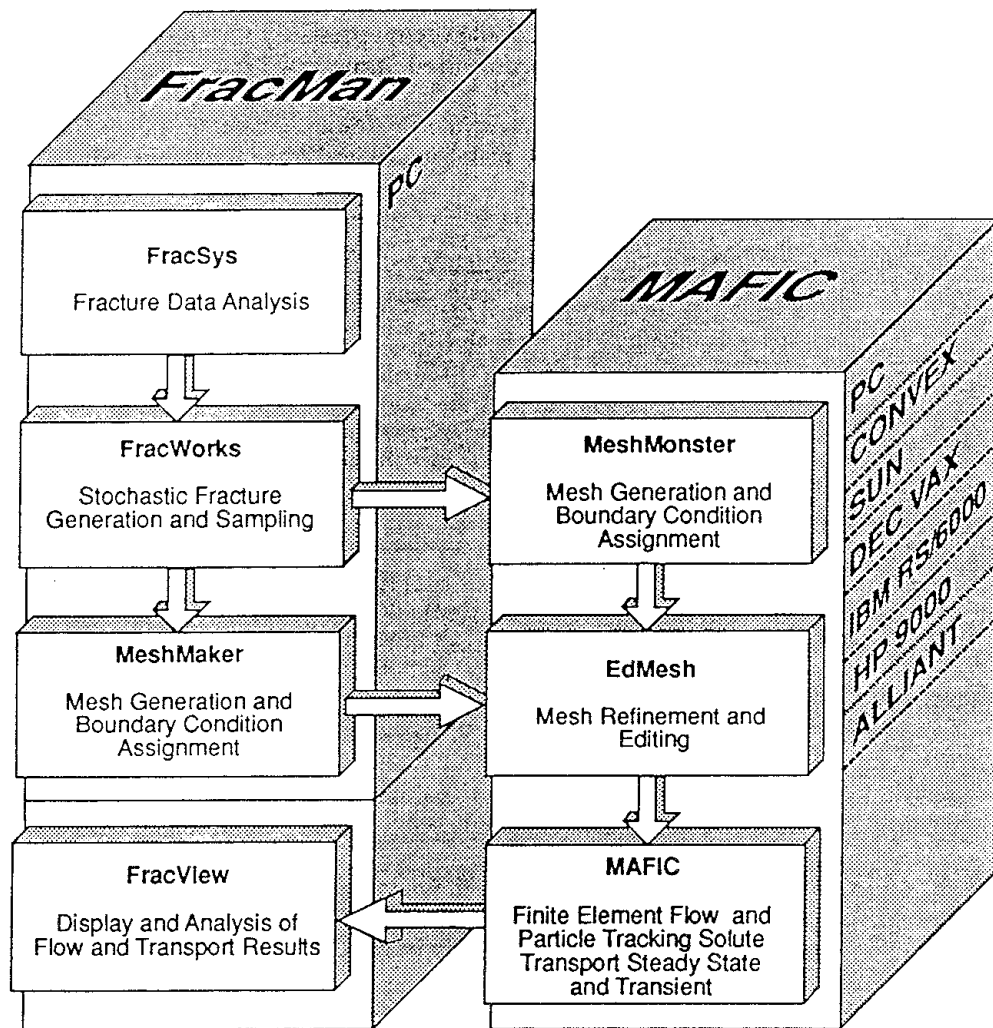


Figure 4-7 Components of the FRACMAN discrete fracture simulator (Dershowitz et al, 1991b).

Figure 4-7, this simulator consists of a component, known as FRACMAN, used to generate the discrete fracture networks and a second component, known as MAFIC, used to solve the flow equations for the finite-element meshes. The procedural steps for modelling fracture flow are shown in Figure 4-8. The data collected at the site for fracture trace length and orientation and hydraulic transmissivity of the rock mass were treated statistically to obtain probability density functions for the distributions of fracture radius, conductive fracture intensity, and fracture transmissivity, together with the distribution of fracture orientations within the site. The conceptual model of the site region was created by use of deterministic information on the location and orientation of major fracture zones. The hydrologic boundary conditions were prescribed on the basis of extrapolations from field data. A typical realization involved selection of fracture properties and transmissivities of the average rock and the fracture zones by means of a Monte Carlo simulation, followed by numerical solution of the groundwater flow and transport equations.

In this modelling approach, alternative probabilistic descriptions of fracture parameters were developed by comparing simulated samples of data taken

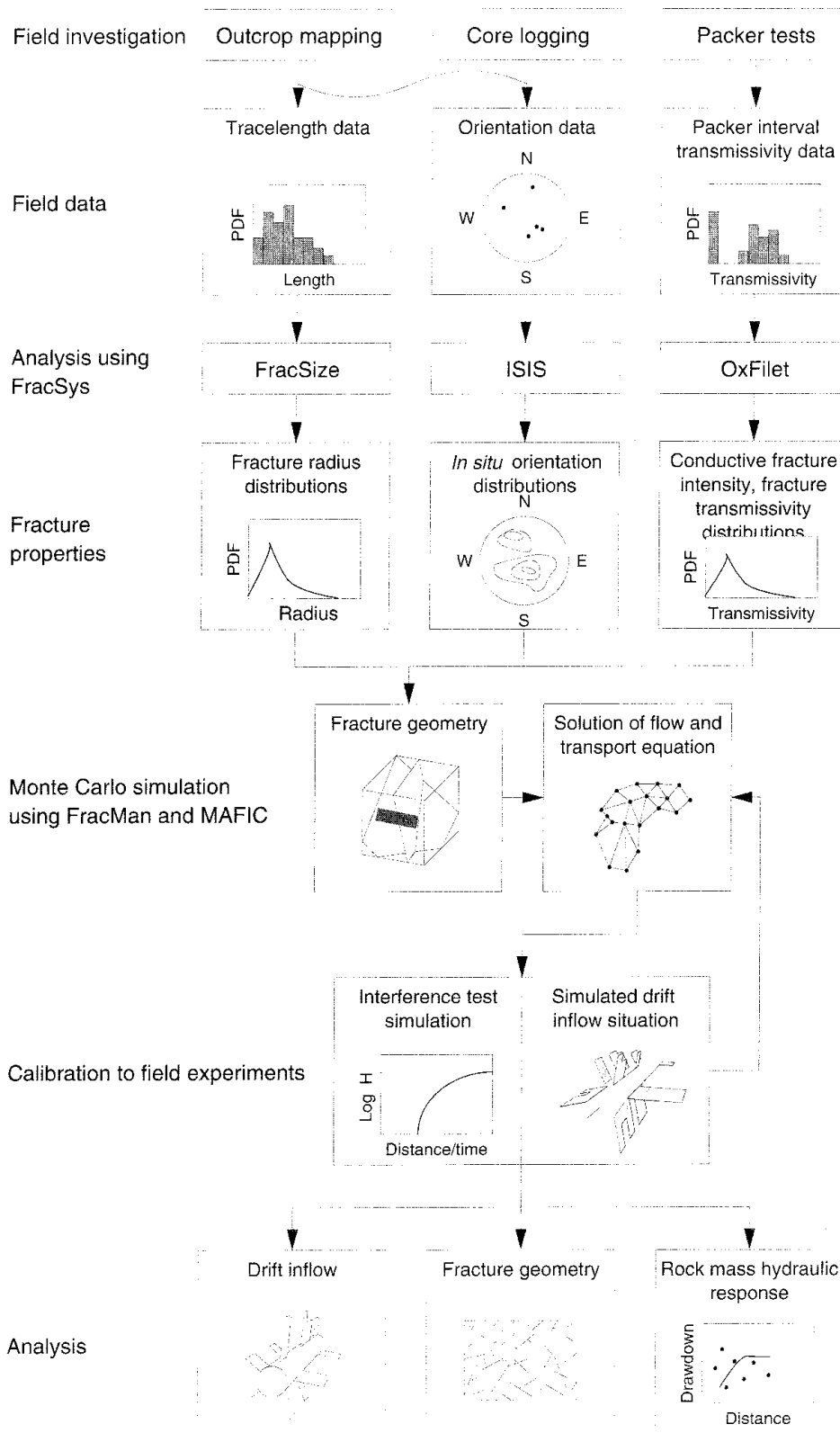


Figure 4-8 Procedure for modelling fracture flow with the FRACMAN discrete fracture simulator (Dershowitz et al, 1991b).

from realisations using possible parameter values for the experimental measurements. The basic steps in this "forward modelling" approach are shown in Figure 4-9. This technique was thought to have several advantages over conventional "inverse modelling" in which an attempt is made to fit a single "optimal" value for the parameters. By deriving the simulated field measurements from assumed parameters, rather than deriving "best fit" parameters from observed field measurements, forward modelling can fully account for error, biases, and uncertainties resulting from data collection procedures. To the extent possible, simulated field measurements were designed to incorporate the same types of errors and biases as occurred with actual field procedures. Forward modelling accepts the concept that several different sets of parameter values and assumptions could account for field observations. This makes it possible to evaluate the implications of different conceptual models, involving various geometric and hydrologic properties, to determine the consistency of these properties with those obtained by field measurements. Forward modelling is well adapted for derivation of probabilistic descriptions of parameters, since simulated field measurements are based upon realizations from assumed parameter distributions.

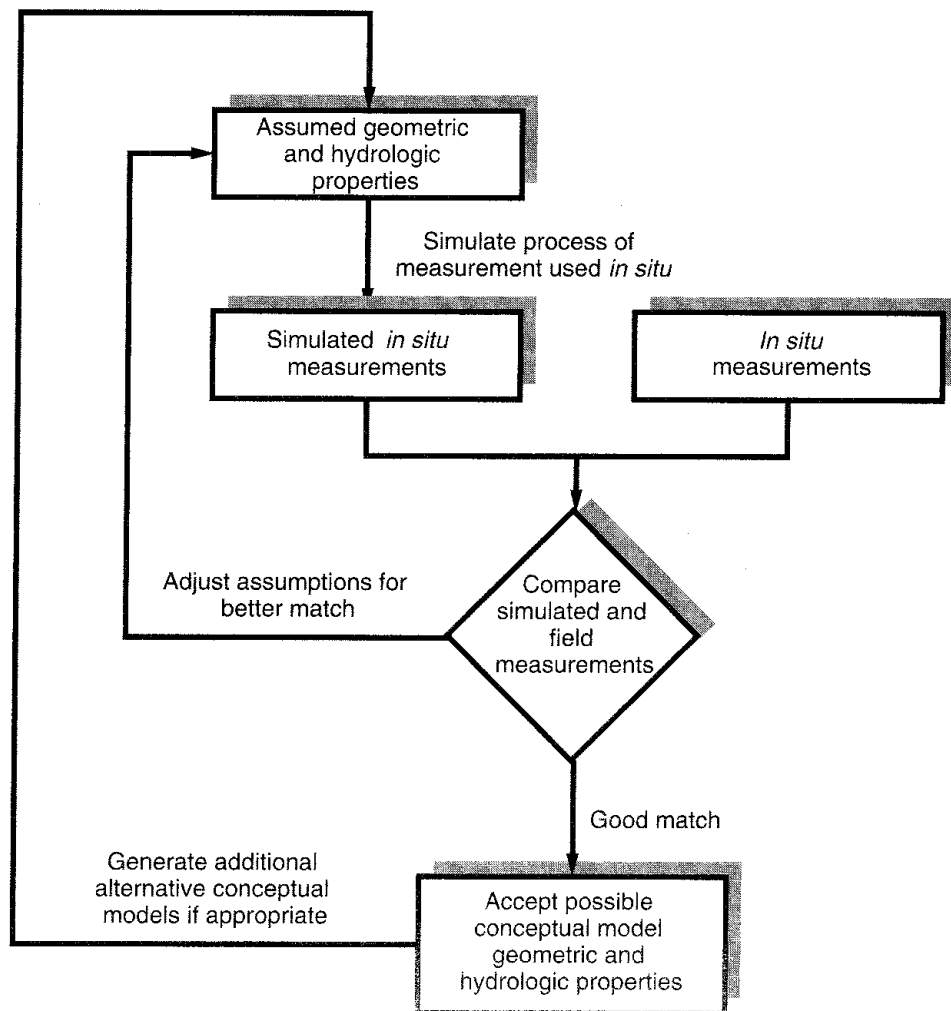


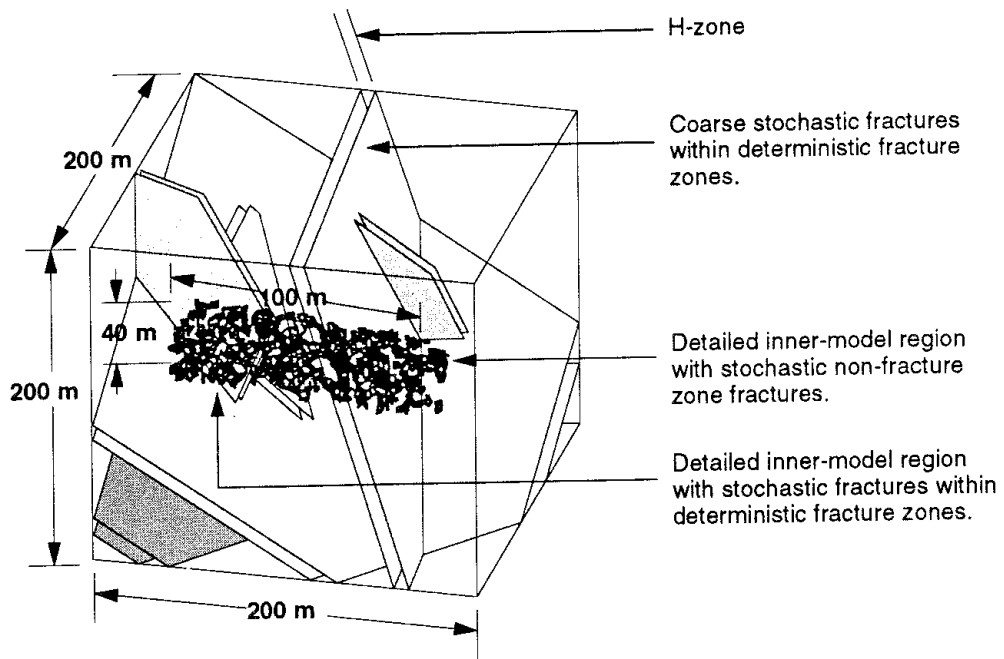
Figure 4-9 Basic steps in the forward modelling approach for creating a conceptualization of the geometric and hydrologic properties of a rock mass (Dershowitz et al, 1991b).

Conceptual Geologic Model of the SCV Site

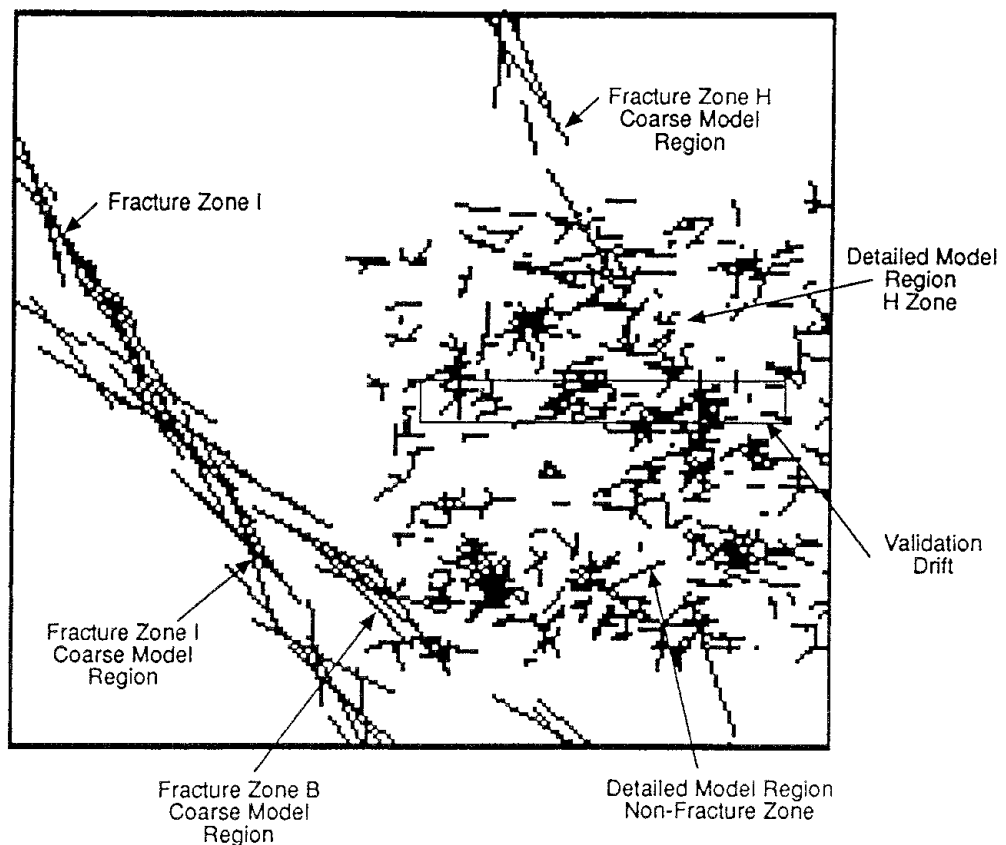
The conceptual geologic model developed by Golder for purposes of discrete fracture modelling recognized that all significant flow within the SCV site took place in interconnected systems of discrete fractures. Since it was impossible to incorporate some one billion fractures within the site into a model, a conceptual model was developed which attempted to decrease the number of fractures that had to be considered without significantly diminishing the heterogeneity and heterogeneous connections of the fractured rock mass. As shown in Figure 4-10, the model encompassed a cube, 200 m on a side, of the rock mass containing the SCV site. In the region containing the Validation Drift, 100 m in length and 40 m in diameter, conductive fractures were included, where the properties of these fractures were derived by direct evaluation of fracture geometric and hydrologic data. This region contained a portion of the H zone with properties that were different from those of the average rock. Outside the detailed region, only a very small subset of fractures were included, with the properties defined to match observed crosshole hydrologic behavior. No fractures were included in the remainder of the cube containing average rock.

Because of drawdown of water from the rock mass around the mine, significant gradients in total head existed within region containing the SCV site. This condition was represented in the model by imposing temporarily fixed, spatially varying heads on each face of the cube. The spatial variation in head was assumed to be linear with respect to an orthogonal coordinate system. Coefficients within the relationship were estimated from measurements of head by Carlsten et al (1988) by taking linear approximations to the head values along each side of the modelling region. The coefficient in the vertical direction was based on an assumption of a hydrostatic gradient. All drifts within the SCV site were assigned zero head boundaries. Boreholes within the site were modelled as "group flux" boundary conditions with a fixed flux of zero. This condition corresponded to shut-in boreholes that acted as linear flow paths, with flow out of some fractures and into others such that the net flux into each borehole was zero.

Observation of the fractures in the walls of the drifts in the Stripa mine indicated clearly that fractures were not distributed uniformly in space. The fractures were more connected than would be indicated by random fracture location, primarily because of a high proportion of fracture terminations found at intersections with other fractures. The "war zone" empirical model was used to simulate large scale heterogeneity in fracture intensity, and the BART (Baecher Algorithm with Revised Termination) model was used to determine fracture termination and small-scale heterogeneity. In the war-zone model, the locations of fractures were based upon a population of fracture centers with higher intensity inside the regions identified as "war zones" because of the degree of overlap, parallelness, and closeness of major fractures that defined the zones. In the conceptual geologic model for the SCV site, the "war zones" were defined deterministically on the basis of the fracture zones identified by geophysical techniques. Within the coarse model region surrounding the location of the Validation Drift, fractures were located uniformly in space within the "war zones". The fracture intensity was 10 000 times greater than that for the coarse model region outside the fracture zones, resulting in a small probability for fractures located outside the fracture zones. Within the region of detailed fractures, the BART model



(a) Schematic view of the conceptualization



(b) Cross section along the Validation Drift

Figure 4-10 Conceptual geologic model of the SCV site for purposes of the FRACMAN discrete fracture modelling (Dershowitz et al, 1991a,b; Dershowitz and Wallmann, 1992).

assumed that a given percentage of fractures were located uniformly in space, with the remaining percentage of fractures located at their terminations on previously generated fractures. This procedure produced a strongly heterogeneous fracture pattern, with a high degree of fracture interconnection.

Fracture termination at intersections was not specified in the coarse region of the conceptual geologic model, because the large fractures modelled in that region were intended in part to represent the effect of networks of interconnected smaller fractures. In the region of detailed fractures, for both the fracture zone and the average rock, the BART model termination percentage was fixed at 30%, which implied that 30% of all fractures terminate at existing fractures. This percentage might have been low relative to observed termination statistics for the SCV site.

Fracture Orientation

Data for the orientation of fractures for the conceptual geologic model were available from borehole and core observations and from trace map surveys of the walls of the drifts (Gale et al, 1990b). Because parametric statistical approaches for dividing the fractures into sets could not be applied successfully, a non-parametric approach was implemented by use of a modified "Bootstrap" statistical technique (Efron, 1972). In the Bootstrap approach, simulated orientations were obtained directly from the set of orientation measurements. The orientation measurements were first corrected for sampling orientation bias using the modified Terzaghi technique (Dershowitz et al, 1991b). Secondly, for each fracture within the fracture model, a single orientation was selected from the set of corrected measurements. A small dispersion was then added by using a Fisher orientation with a specified dispersion parameter centered around the selected orientation. The fracture orientation was then selected from the resulting Fisher distribution. This process was repeated for each fracture that was generated. The stereographic plots in Figure 4-11 illustrate the comparison between fracture orientations measured at the SCV site and fracture orientations computed by the Bootstrap approach.

Effective Fracture Radius

In the FRACMAN discrete-fracture modelling procedure, the size of a fracture is described by an "effective fracture radius". The effective fracture radius is the radius of a circular disc fracture with an area identical to that of the polygonal fracture used by the simulator. Attempts were made unsuccessfully to fit log-normal, normal, parallel, and exponential radius distributions to trace-length data using visual matches of probability density functions and cumulative density functions. As none of the fits were found to be statistically acceptable, a visual fit was made to fracture trace-length data using coarse histograms of fracture radius. This approach introduced error in fitting, because measured traces were divided and compared in batches in the range of 0.2 m to 1 m. However, the fracture-length distributions obtained were consistent with the empirical distributions of Uchida (1990). Comparisons of the measured and fitted histogram trace-length distributions are shown in Figure 4-12.

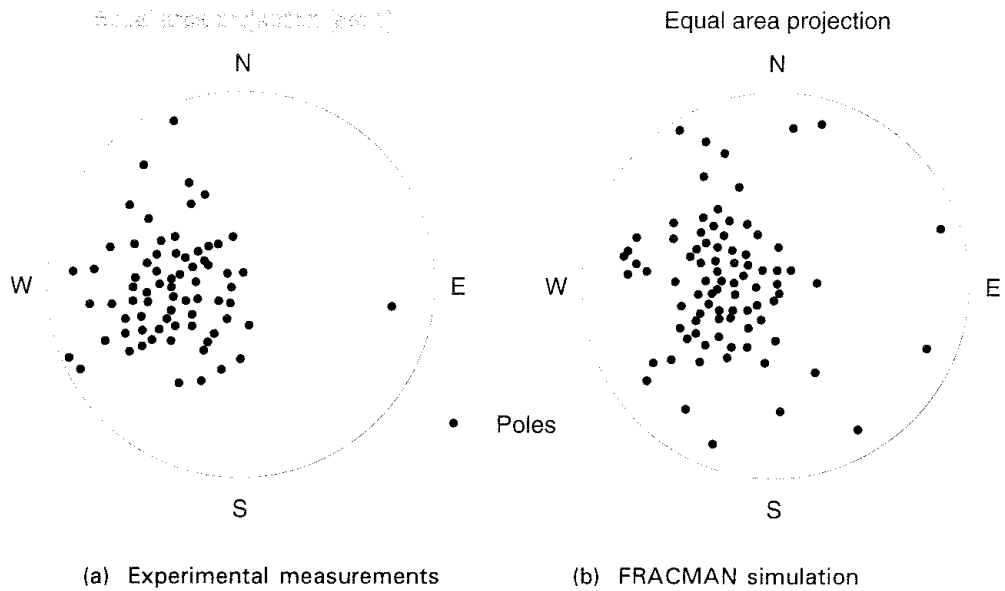
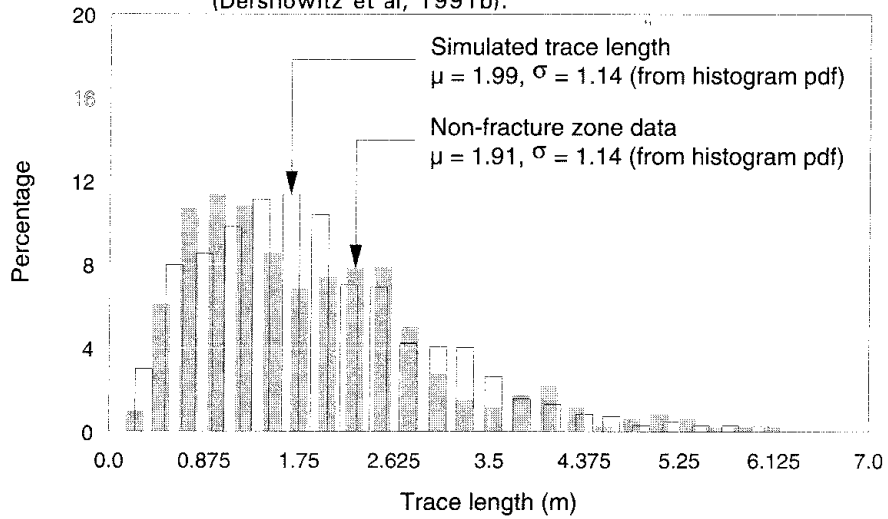
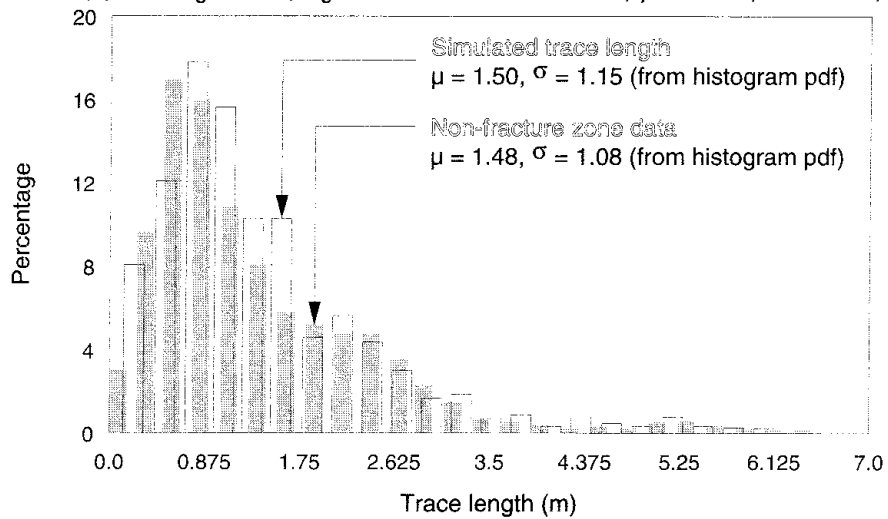


Figure 4-11 Comparison of 100 measured fracture orientations with those generated by the Bootstrap technique for the average rock (Dershowitz et al, 1991b).



(a) Average rock (Log normal radius distribution, $\mu = 1.03, \sigma = 0.49$)



(b) Fracture zone (Log normal radius distribution, $\mu = 0.63, \sigma = 0.44$)

Figure 4-12 Comparison of measured and simulated trace lengths for the average rock and the H zone (Dershowitz et al, 1991b).

Transmissivity and Intensity of Conductive Fractures

Although the intensity of mapped and logged fractures at the SCV site exceeded $7 \text{ m}^2/\text{m}^3$, the observed heterogeneity and heterogeneous hydraulic connection indicated a much lower intensity of conductive fractures. The Golder modelling approach was based on conductive intensity rather than on mapped and logged intensity. Conductive fracture intensity was defined as the sum of the areas of the conductive fractures divided by the volume in which the fractures resided. Fracture transmissivity distributions and conductive fracture frequency were derived simultaneously using the Oxfilet fixed-interval packer test analysis technique (Dershowitz et al, 1991b). Conductive fracture frequency was defined as the expected mean value of the number of conductive fractures that contributed to the packer-interval transmissivity distribution divided by the packer-interval length. Based on the measured fracture intensity in the SCV site and a mean fracture area of 4 m^2 , approximately ten million fractures would be contained within a cube of rock encompassed by the conceptual geologic model. The use of conductive fracture frequency reduced the number of conductive fractures to about ten thousand, which allowed the observed hydraulic response in the site to be reproduced adequately.

The Oxfilet (Osnes Extraction from Fixed-Interval-Length Effective Transmissivities) approach to the derivation of conductive fracture frequency and transmissivity is illustrated in Figure 4-13 (Osnes et al, 1988). The method assumes that the net transmissivity of a test zone is equal to the sum of the transmissivities of the conductive fractures that intersect the test zone as seen at the borehole. Within any given interval, the number of conductive fractures is assumed to be a random number defined by a Poisson distribution (Benjamin and Cornell, 1970). For any given set of parameters that describe the distributions of fracture transmissivity and conductive fracture frequency, the distribution of packer-interval transmissivities were determined by Monte Carlo simulation, with the best fit value selected by a simulated annealing search routine. The intensity and transmissivity distributions for the conductive fractures were then estimated by finding the best match between the observed distribution of packer interval transmissivities and the distribution of test zone transmissivities determined by simulation for given distributions of fracture frequency and single-fracture transmissivity.

Simulations that used the MAFIC component of the FRACMAN fracture-network simulator required that the fracture transmissivity be the effective transmissivity through a fracture between the fractures that intersect a fracture, that is the cross-fracture transmissivity. The hydraulic-packer test is strongly influenced by the local fracture aperture near the borehole. The transmissivity seen by the packer test is a small scale, or "at-borehole", transmissivity, and the cross-fracture transmissivity must be determined as a proportion of transmissivity of the conductive fracture within the interval. In the Oxfilet technique, the proportionality constant was described as a normally distributed random variable with mean and standard deviation provided by the user. In the Golder modelling effort, the values of the mean and standard deviation were based roughly upon the results of numerical experiments by Kenrick and Dershowitz (1991), and included a reduction in standard deviation to account for the removal of fractures with low cross-fracture transmissivity from the data set. Single-fracture transmissivity

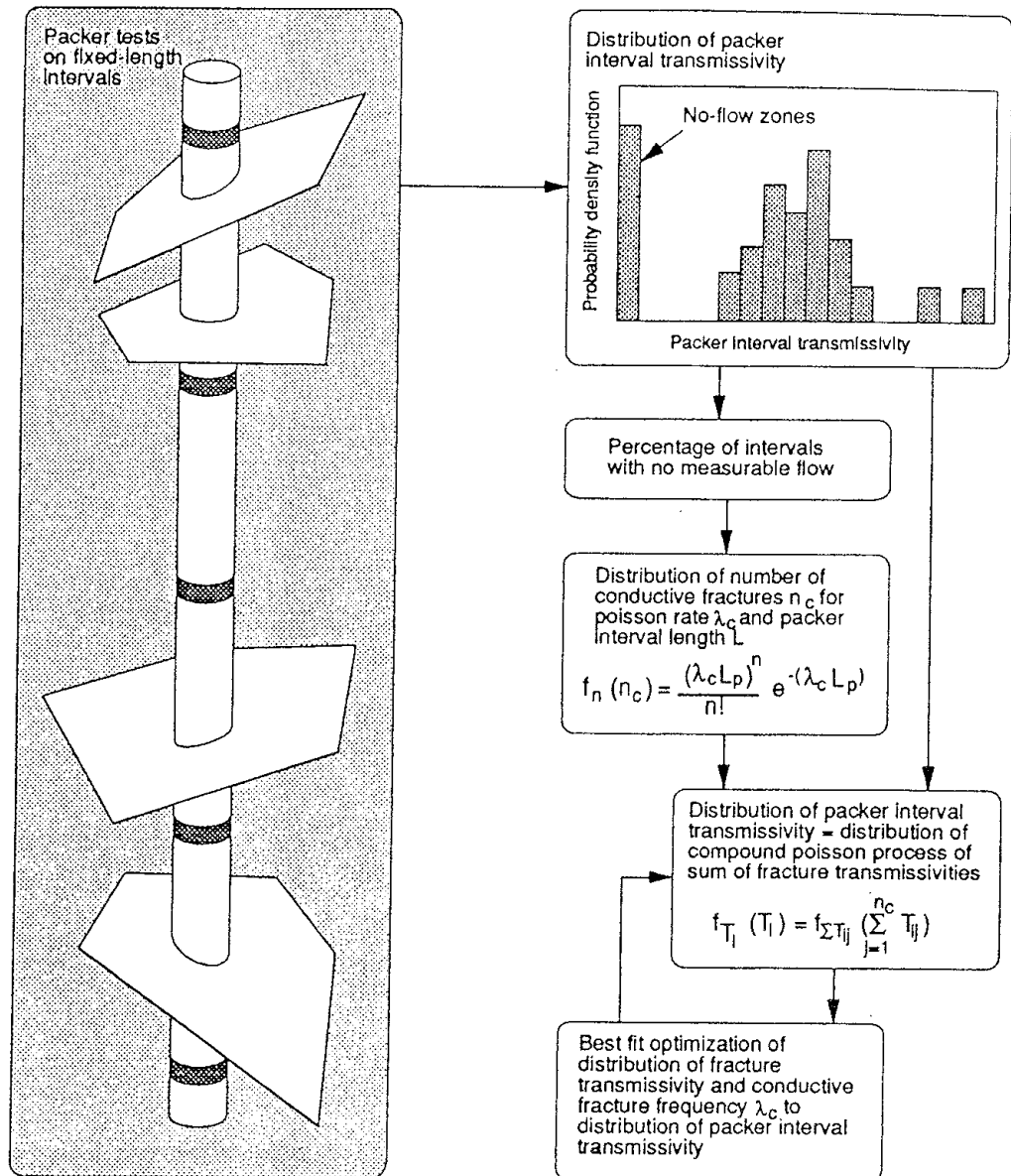


Figure 4-13 The process for derivation of conductive fracture intensity and transmissivity by the Oxfilet technique (Dershowitz et al, 1991b).

results obtained by the Oxfilet technique are shown in Figure 4-14 for data from the N, W, and C boreholes.

Studies by Doe and Geier (1990) indicated that the dimension of flow in fracture zones was generally between 2.7 and 3. This indicates that it was more likely that flow occurred in well interconnected systems of plate-like fractures rather than in linear pipe-like channels. As a consequence, it was deemed more appropriate to make the assumption that the fracture transmissivity seen at the borehole was the effective transmissivity of a fracture network, rather than being a result of channel-like flow due to the spatial structure of fracture roughness. Statistical results obtained by this method indicated that the values of cross-fracture transmissivity were also reasonable in the fracture zones.

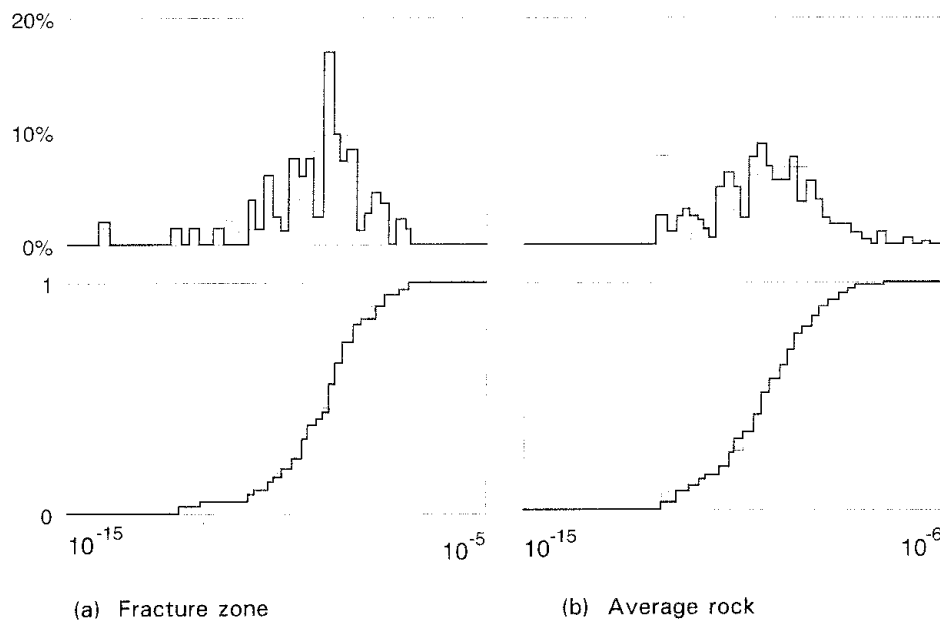


Figure 4-14 Single-fracture transmissivity results obtained by the Oxfilet technique when assuming no channelling (Dershowitz et al, 1991).

A measure of fracture intensity was specific to the orientations of boreholes and fractures that were used in its determination. Because simulations with FRACMAN used a conductive fracture intensity that was independent of the sampling schemes, it was necessary to obtain a transformation from borehole-orientation specific data to the conductive fracture intensity. Because of computer limitations, the practical limit for the number of fractures considered in the Monte Carlo simulations was approximately twenty thousand for the fracture geometry and boundary conditions of the conceptual geologic model. To meet this constraint, it was necessary to decrease the conductive fracture intensities by using truncated distributions for fracture radius, thus eliminating the smallest and least conductive fractures. Sensitivity studies indicated that the errors induced by eliminating such fractures were within approximately 10%.

Drift Excavation Effects

The change in the state of stress in the SCV site because of construction of the Validation Drift was computed on the basis of the Kirsch stress solution (Jaeger and Cook, 1984). The solution assumed that the major principal stress was parallel to the axis of the drift, which was reasonable based on pre-drift construction measurements of the *in situ* stresses, and that the rock in a plane perpendicular to the axis of the drift was in a state of plane strain. Based on experimental evidence, the change in transmissivity of a fracture is proportional to the inverse of the normal stress to the fracture plane. The coefficient in the relationship was selected on the basis of experiments specific to the rock in the SCV site.

In addition to stress effects, attempts were made to model the opening of fractures above the crown of the drift due to kinematic rock block movement into the Validation Drift. The conceptual model of "crown fractures" added

a set of fractures oriented parallel to the roof of the drift, which approximated the additional flow conduit formed by block movement.

To account for the assemblage of effects that could influence the transmissivity of the rock surrounding the Validation Drift, an order of magnitude reduction in transmissivity was assumed for some of the simulations. This reduction, based on judgement, was supposed to include collectively the effects of stress redistribution, rock block movements, blast damage, and desaturation of the free rock surface in the walls of the drift due to evaporation.

4.2.4 LBL Fracture-Flow Model

The fracture-flow modelling procedure developed by the group at Lawrence Berkeley Laboratory (LBL) focussed on the use of "equivalent discontinuum" models (Long et al, 1990, 1992; Long and Karasaki, 1992). An equivalent discontinuum model is one in which a partially filled lattice of one-dimensional conductors is used to represent equivalent fracture flow paths. This style of representation for the discontinuous nature of fracture flow assumes that all partially connected systems have universal properties described by percolation theory, and, as a consequence, it is reasonable to represent the real, complex system by a simpler lattice. That is, fractures or fracture clusters can be represented by some average equivalent conductor and the flow of water through the rock can be modelled with a partially filled lattice of such conductors.

Template Conceptualization

The development of an equivalent discontinuum model begins with the specification of a lattice or "template". An inverse analysis is performed on the template to determine the configuration, or pattern, of lattice elements which can reproduce the hydrologic data obtained by field measurements. The template is in effect a conceptual model for the system of fractures in the rock mass. In granitic rock masses, the groundwater flow is commonly concentrated in zones containing highly fractured rock. These fracture zones are usually quite heterogeneous, with portions of the zones being highly impermeable and unconnected to the rest of the system. For such circumstances, it would appear reasonable to construct templates only along the planes of the fracture zones. This approach inherently assumes that the groundwater flow system is restricted to the fracture zones, and that the average rock is effectively impermeable.

In field situations where the groundwater flow might be substantially restricted to a single structural feature, such as the H zone and its intersection with the Validation Drift, a two-dimensional flow analysis was thought to be reasonably adequate. A two-dimensional template representing the plane of the H zone is shown in Figure 4-15. The template was constructed to provide considerable detail in the vicinity of the Validation Drift, but incorporated a number of elements that kept the bandwidth small to minimize the time required to establish the lattice configuration by inversion. Finally, the mesh had to be large enough to prevent early arrivals of pressure transients at the boundaries. The mesh shown in

Figure 4-15 has five nested grid regions, each having twice the grid spacing of its inner neighbor. In addition, the nodes positioned on the outer edge of the outer grid region are connected to the applied boundaries by 200 m long elements. The total number of elements is 4 687, with 1.5 m grid spacing in the vicinity of the D boreholes and boundaries situated approximately 400 m from the pumping wells. The element conductance and storativity were scaled in such a way that the entire region had the same transmissivity and average storage. Each of the well intervals was included as a node in the mesh.

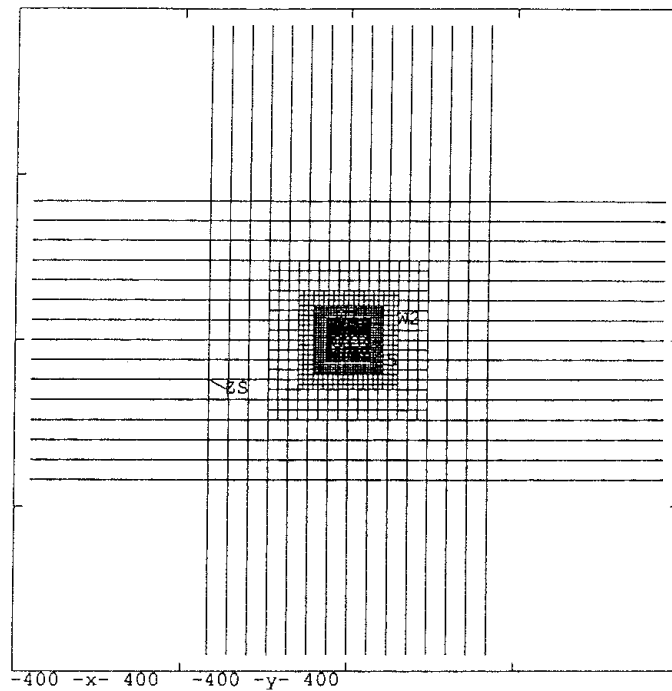


Figure 4-15 The full mesh used for annealing the two-dimensional conceptual model of the H zone (Long et al, 1992).

The template for the three-dimensional conceptual model of the SCV site is shown in Figure 4-16. This model contained the seven fracture zones that were identified within the site. Each zone was represented by a disc, but conductive channels were located only in those portions of the discs within the hypothetical site boundaries. Although not shown in the figure, 200 m long "fin" elements connected the nodes located on the hypothetical site boundaries to the constant-head hydraulic boundaries. Wellbore test intervals were assigned to a node if the center of the interval was close to an existing node in the grid. When this was not the circumstance, the interval was "snapped" into the grid by connecting it to the three closest nodes with new grid elements. The grid spacing in the discs for the H_a and H_b zones was 6 m.

Simulated Annealing

The inversion technique for obtaining the configuration or pattern of lattice elements that can reproduce hydrologic measurements is known as

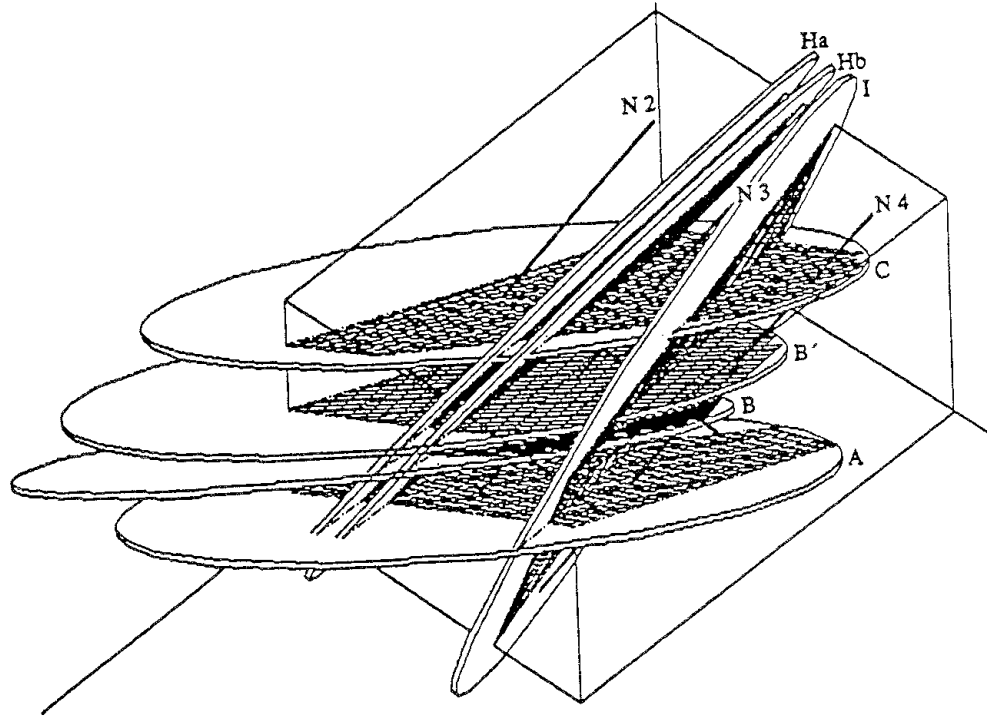


Figure 4-16 Three-dimensional conceptual model of the principal fracture zones at the SCV site (Long et al, 1990).

"simulated annealing" (Davey et al, 1989). This technique can be viewed as a process of minimizing an energy function over a set of possible configurations of elements in the lattice. The elements within the lattice can be thought of as being pipes or channels. The pipes have only two possible states, either off or on. At the outset of an iteration, a configuration of on and off channels is chosen by random selection, and that configuration is used to calculate the response of the template to an *in situ* test, such as an interference test. The calculated response is compared to the measured response and the "energy" is computed. The energy is a term that expresses the difference between the measured responses and the calculated responses. Then, by use of a probability function, a pipe is selected at random in the lattice. If the element is "on", then it is turned "off", or *visa versa*. The new energy is computed and compared to the old energy. If the energy is decreased, the change in the configuration is retained. If the energy is increased by the change, the choice of whether or not to retain the new configuration is based on a probability proportional to the amount of energy increase modified by a factor known as the temperature. This procedure allows the algorithm to bypass local minima and seek a more global solution.

This process is repeated through successive iterations until the energy level has decreased to an acceptable minimum. The process does not, however, guarantee a unique solution for the flow system within the grid of pipes, even though the calculated response of the template may compare quite well with the measured response. In actuality, several or more configurations could yield identical energy levels. An energy level that remains at or near zero over many iterations probably indicates a unique or near-unique solution to the flow system.

Hydraulic Test Data

Measurements of the steady-state head distribution resulting from a pumping test can be used rather conveniently for simulated annealing of a template. The energy function is constructed as a function of the differences between calculated and measured heads or drawdowns. Drawdowns induced by this type of test are conceptually simple to measure, and many annealing iterations are practical because steady flow is relatively easy to model. However, for steady flow, the pattern of drawdowns is independent of the conductance of the medium. Thus, when using the results from a single steady-state flow test, annealing will give only a pattern of conductors that matches the head distribution. The conductance of the elements is simply scaled up or down until the observed or applied flow conditions are matched. This means that the models resulting from the use of such data tend to be more sensitive predictors of head than of flow.

A model can gain greater sensitivity for purposes of predicting flow when measurements from a series of steady-state flow tests are combined. For such circumstances, each of the separate tests would be modelled at each iteration and the element conductance would be chosen to best fit all the flow data. If constant-head boundary conditions are used at the pumping well, the energy function can be constructed as an appropriately scaled combination of squared-head differences and squared-flow differences. If constant flow is applied at the pumping well, the energy function can include the head at the pumping well treated as any other observed head. The use of such multiple data sets may be most suitable because there is no dependence on the storage coefficient and the time required for steady-state flow calculations is very small.

Transient interference data from a constant flow test can also be used to determine an appropriate configuration of lattice elements in a template. The flow rate that was used in the field can be specified in the model to predict the transient drawdown response. At each iteration of annealing, the model predicts curves of drawdown as a function of time. These curves can then be matched to the curves representing the field data. This matching process involves, in essence, picking the best-fit conductance and storage coefficients for the lattice elements in the model. The energy at each iteration is the sum of the differences in the logarithm of head for each observation point at selected times. Imperatively, transient data reflect the distribution of heterogeneities in the fracture zone, while steady-state data are more likely to reflect the most pronounced region of restricted flow.

Conceptual Models

The two-dimensional and three-dimensional conceptual models of the H zone and the SCV site are shown in Figures 4-15 and 4-16, respectively, in terms of the templates that represent the fracture zones. The two-dimensional model was annealed against the data obtained during a constant-flow interference test in which the source was located in the second interval from the bottom of borehole C1. The lattice configuration that was obtained is shown in Figure 4-17, and the corresponding energy level as a function of the number of iterations is shown in Figure 4-18. The temperature schedule

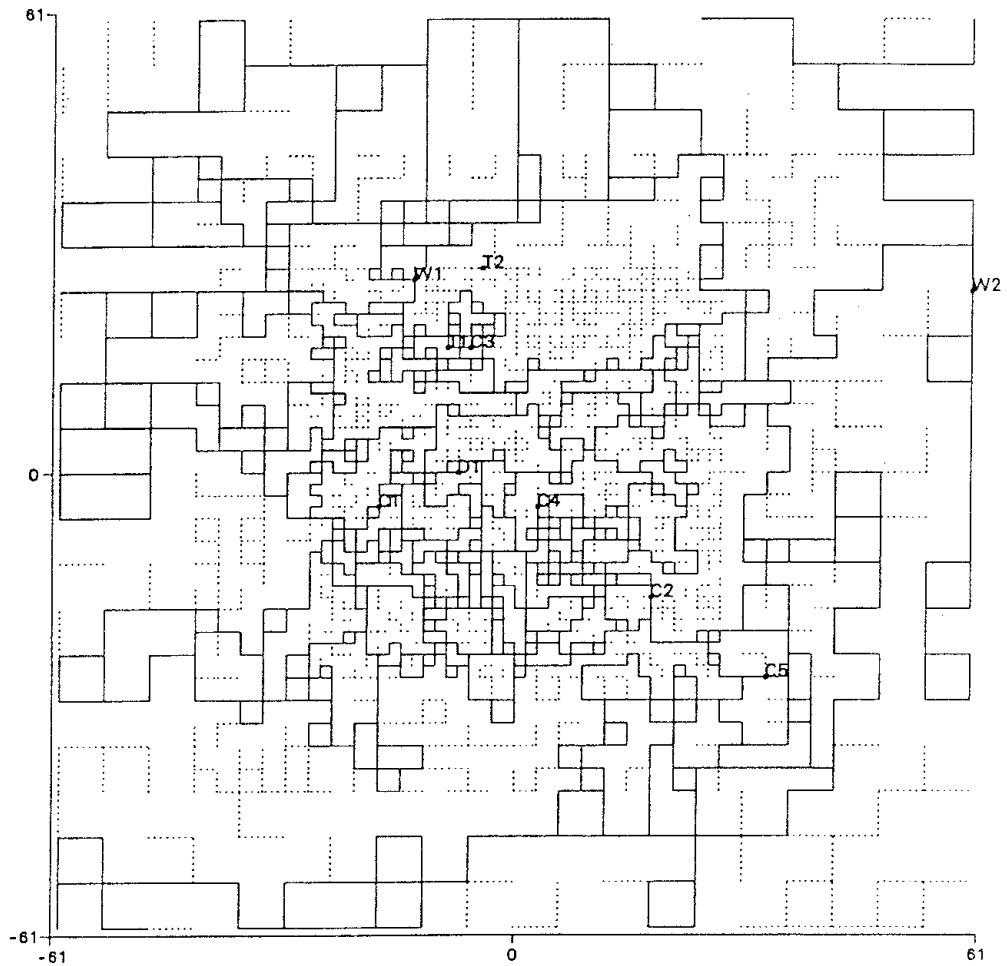


Figure 4-17 The lattice configuration obtained by annealing the two-dimensional conceptual model of the H zone against the C1-2 pump test data (Long et al, 1992).

The dead-end elements are denoted by the dots.

the algorithm will accept an unfavorable change in the lattice configuration. Conversely, if the algorithm accepts every change, the temperature is probably too high and should be adjusted. Such adjustments account for the decreases in the temperature schedule. A comparison of the drawdown curves calculated with the model and measured in the C1-2 pump test is shown in Figure 4-19.

The data used to anneal the three-dimensional conceptual model of the SCV site were taken from the estimated steady-state heads at the end of the third stage of the Simulated Drift Experiment. Because a constant flow condition was applied at the D boreholes during the test, steady-state annealing was used to match the pattern of estimated steady-state heads. The configuration of lattice elements in the H zone obtained by the annealing process is shown in Figure 4-20, and the corresponding energy level curve is shown in Figure 4-21. The energy level never attained a minimum of zero because the measurement error was significant. Generally speaking, the calculated drawdowns in the N and W boreholes were greater, ranging from a few percent to several hundred percent, than the drawdown estimated from the measurements.

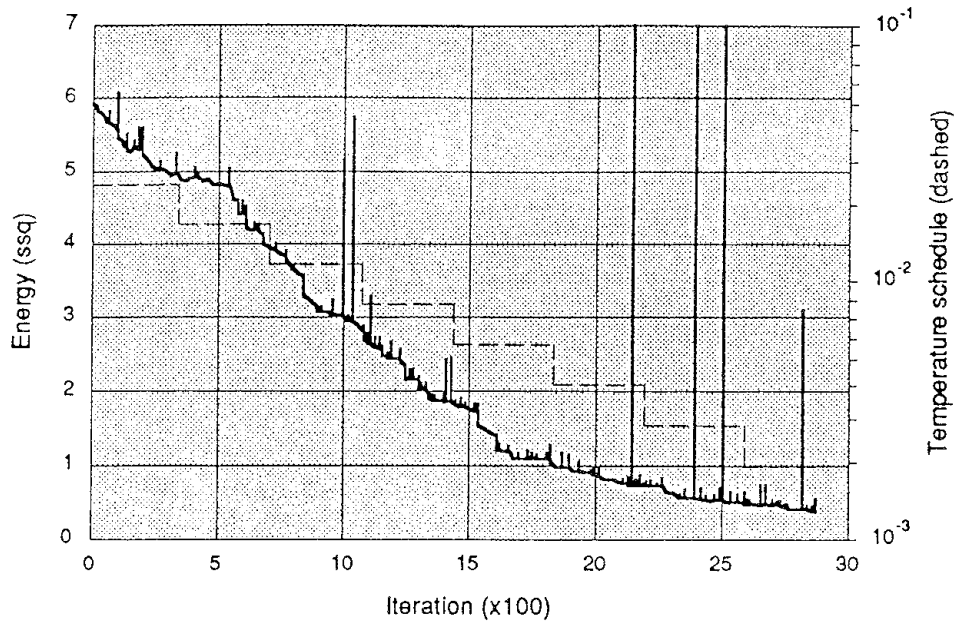


Figure 4-18 The energy level curve obtained by annealing the two-dimensional conceptual model of the H zone against the C1-2 pump test data (Long et al, 1992).

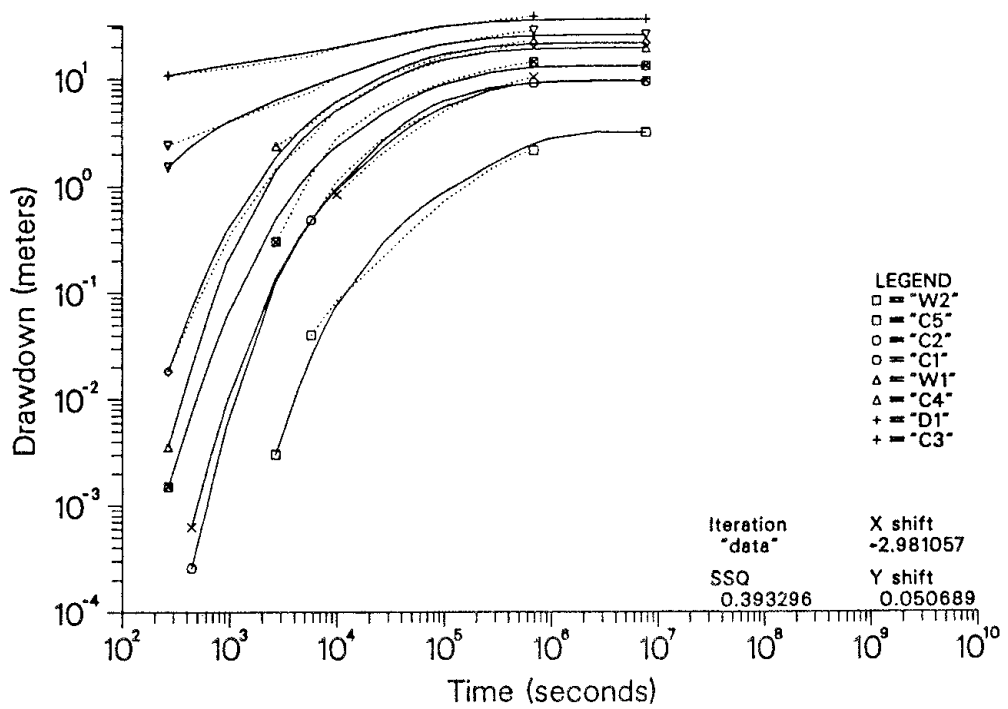


Figure 4-19 Comparison of the drawdown curves obtained from calculations with the two-dimensional conceptual model of the H zone and the C1-2 pump test measurements (Long et al, 1992).

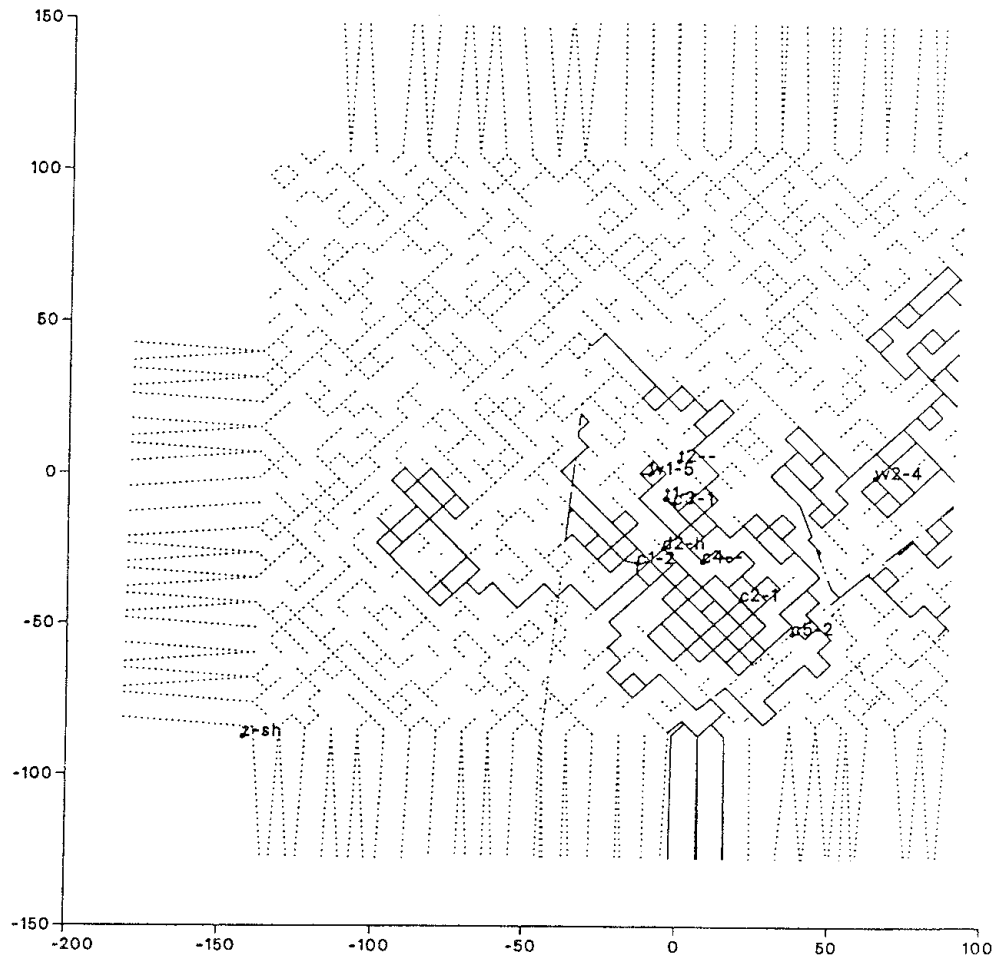


Figure 4-20 The configuration of lattice elements in the H zone of the conceptual model for the SCV site (Long et al, 1992).

The dead-end elements are denoted by the dots.

Drift Excavation Effects

The change in stress in the rock mass due to excavation of the Validation Drift was calculated by application of the Kirsch solution, assuming a condition of plane strain in the plane situated perpendicular to the axis of the drift. Using the laboratory-derived relationship between change in fracture conductivity as a function of change in normal stress on the plane of a fracture, it was estimated that the hydraulic conductivity along fractures oriented radially to the drift should decrease by no more than 50% over the drift perimeter and by no more than 17% when averaged over a 5 m distance from the drift. The absolute magnitudes of the normal stress changes parallel to the drift were small, less than 15%, and averaged to zero around the perimeter of the drift. As a consequence, the fractures oriented perpendicular to the drift, i.e. the longest H zone fractures, should have little direct effect on the inflow. It was estimated that the net effect of the elastic stress perturbations due to drift excavation were unlikely to decrease the permeability around the drift by a factor of more than two.

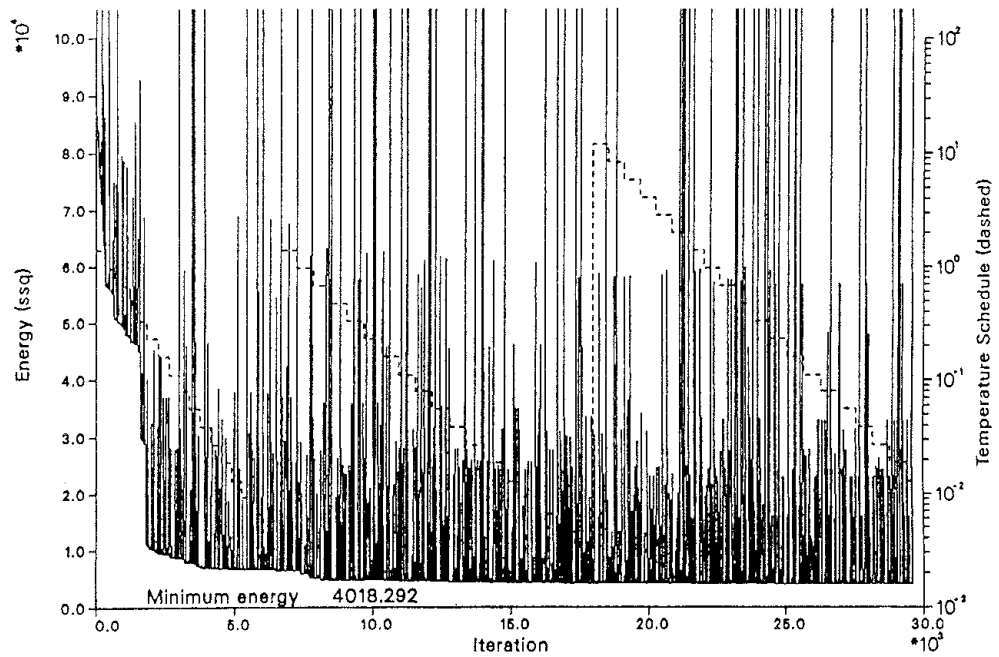


Figure 4-21 The energy level curve obtained by annealing the three-dimensional conceptual model of the SCV site against the hydraulic test data from the Simulated Drift Experiment (Long et al, 1992).

Measurements at the SCV site indicated that there was a very large amount of gas continuously coming out of solution under the environmental conditions of the Validation Drift. It was hypothesized that this gas was responsible for creating a significant decrease in the permeability of the rock in the skin of the Validation Drift, resulting in a decrease in permeability of as much as forty-fold due to the effects of two-phase flow.

Computational Features

The channel network generator CHANGE was used to construct a finite-element mesh for the conceptual model (Billaux et al, 1988). This code can generate a stochastic network of conductors or an irregular grid of conductors. In the finite element analysis, each element is assumed to represent a one-dimensional conductor, i.e. a pipe or a channel. For the purpose of calculating flow, only the location of the end points of the pipe and the conductance of the pipe must be specified.

TRINET was used to calculate the hydrologic response of the zone model to the simulated well test. This finite element code can simulate fluid flow and advective and dispersive solute transport in three-dimensional networks of one-dimensional conductors. The code incorporates a mixed Lagrangian and Eulerian scheme with adaptive gridding for transport calculations. The computational scheme avoids numerical dispersion by creating new Eulerian grid points instead of interpolating the advected profile back to the fixed Eulerian grid.

TRINET first solves the flow field, either steady state or transient, using a simple Galerkin finite-element method, where the timed derivative is treated in a usual finite difference manner. From the pressure distribution at a given time, the velocity distribution in the fracture network is calculated. Since linear shape functions are used to solve the flow field, the velocity is uniform within a given element. The advection-dispersion equation for mass concentration is then solved by decoupling the equation into two stages. In this manner, it is possible to solve the advection term independently of the diffusion term and thereby minimize the numerical dispersion. The advection equation is solved by using the method of characteristics. The concentration values at fixed nodal points are obtained by the technique of single-step backward particle tracking or reverse streak lines. The new concentration profile at the end of the advection stage is now the initial-value for the dispersion calculation in the second stage. The dispersion is treated in the usual finite-element manner.

4.2.5 Verification of Groundwater Flow and Transport Codes

A plan was developed in 1989 for the cross-verification of the discrete fracture codes developed by Harwell, LBL and Golder (Dershowitz et al, 1989). The principal purpose of this study was to demonstrate that the codes would accurately perform the calculations for which they were designed within the context of what was required for their use in Phase 3 of the Stripa Project. A secondary goal was to provide benchmarks for the comparison of the capabilities and performance of the codes, and to verify the numerical accuracy of the codes insofar as it would be possible given the differences between and among the codes.

The study involved the verification of (1) deterministic generators for fracture geometry, (2) solutions to the groundwater flow equation in a discrete, deterministic network of planar fractures and channels, and (3) simple solutions for mass transport in fracture networks as determined by particle or front tracking (Schwartz and Lee, 1991). The NAPSAC version 2C code from Harwell, the set of FRACMAN/MAFIC codes from Golder, and the FMG package of codes from LBL were involved in the computational exercises.

Generation of Fracture Geometry

The verification problem for the deterministic generation of fracture geometry was based on a simple statistical summary that compared the difference in the number of fractures intersecting a given plane. A perfect result for a pair of results from any two computer codes would be a zero difference for a population of 1 000 fractures. For all practical purposes, the discrete fracture networks generated by the three codes were close to being identical. The total fracture planes differing in the number of calculated intersections varied from a low of ten for the comparison between NAPSAC and FRACMAN, to twenty-five for the comparison between NAPSAC and FMG/CHANGE.

A second part of the verification problem compared the cumulative length of fracture traces. For the results obtained with each code, the lengths of

fracture traces found to intersect each of the 1 000 fractures were summed. If the networks generated by the three codes were identical, the sums of the cumulative lengths would also be the same. For the ten fractures that differed in the number of calculated intersections between the NAPSAC and FRACMAN codes, a detailed comparison of the trace lengths showed a maximum difference of about 11% for one of the fracture traces, and differences of less than about 1% for the remaining nine fracture traces. Generally, when the numbers of intersections did not match, the differences in fracture length were small. It was concluded that the codes were capable of generating virtually identical representations of complex fracture networks that were deterministic in character.

Groundwater Flow

The first verification problem for groundwater flow was designed to compare the ability of the codes to solve a steady-state form of the groundwater flow equation in a simple orthogonal fracture network with constant apertures. The network, as illustrated in Figure 4-22, consisted of six fracture planes, all of which were assumed to have a constant transmissivity. The boundary conditions were such that fixed heads of 0 m and 10 m were applied in the x-z plane at the origin and 40 m on the y axis, and conditions of no flow were prescribed on the x-y and y-z planes at the origin and at 40 m on the x and y axis. The analytical solution to this problem showed that the head was directly proportional to distance on the x axis, and the flux was directly proportional to the hydraulic conductivity.

In terms of the predicted values of hydraulic head, the results from the FRACMAN/MAFIC and FMG codes reproduced the analytical solutions exactly to three decimal places. The results obtained with the NAPSAC code deviated from the analytical results because of the approximation that was required within the code to handle the intersections involving three fracture planes. In practice, however, these kinds of triple intersections do not cause computational difficulties with the NAPSAC code because the numerical effects of the approximation are small overall and do not accumulate. In terms of flow into and out of the cube, all three codes predicted results that were identical with those obtained from the analytical solution.

The second verification problem for groundwater flow was designed to verify the capabilities of the codes to model flow in a network that featured irregular fracture geometry and significant variability in fracture aperture. As shown in Figure 4-23, the network was comprised of eight fracture planes. The head conditions were fixed at different values in the x-z planes at the origin and 260 m on the y axis, and conditions of no flow were prescribed on the x-y and y-z planes at the origin and 200 m on the x axis and at 20 m and 135 m on the z axis. The values of transmissivity assigned to the seven fractures varied over nine orders of magnitude.

Since there was no available analytical solution to the problem, the results produced by the three codes were compared on the basis of the calculated heads at prescribed nodes and the total flow rates into and out of model. Because of the particular geometry of the model and the relatively high values of transmissivity assigned to fracture planes 2, 3, and 6, these

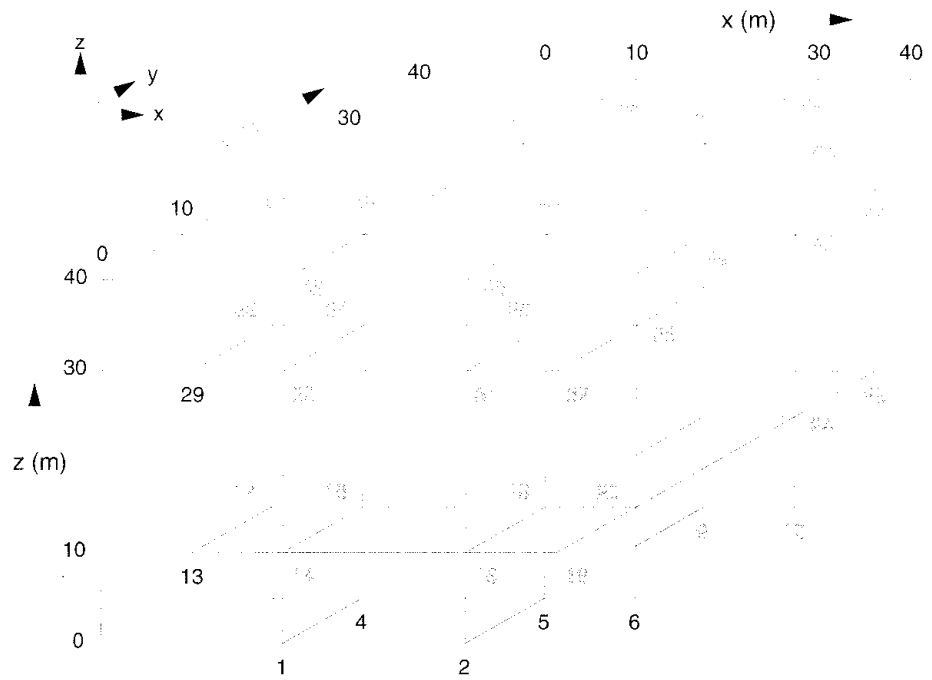


Figure 4-22 Fracture network for the first verification problem for groundwater flow (Schwartz and Lee, 1991).

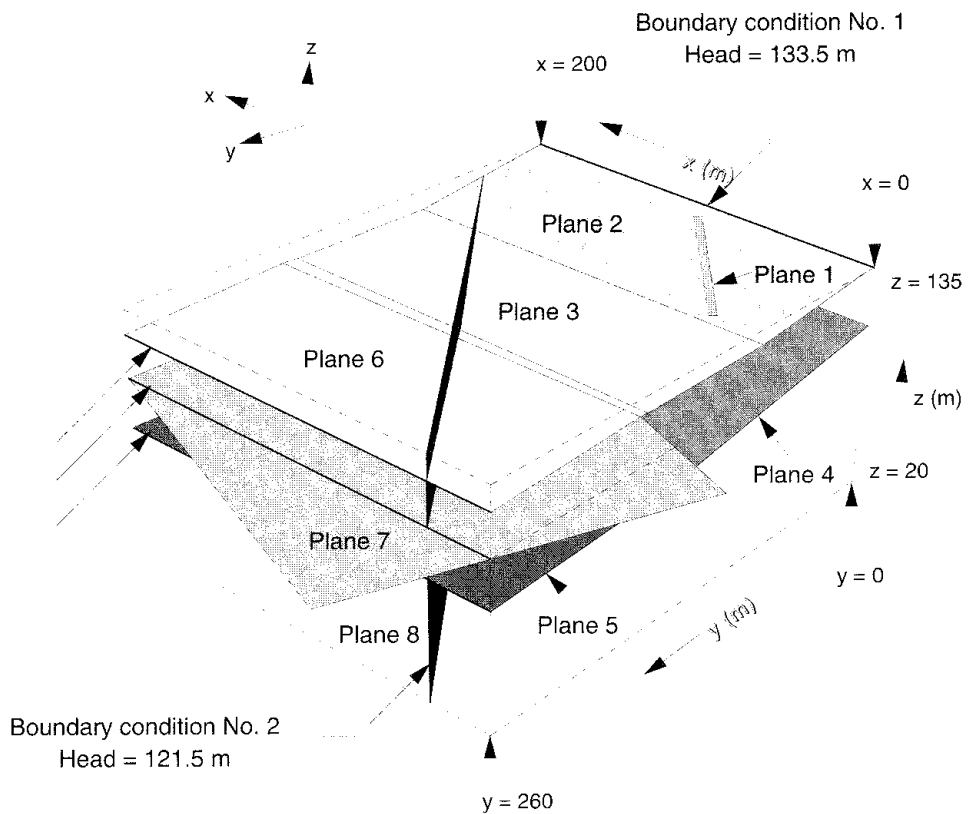


Figure 4-23 Conceptual model of the fracture system for the second verification problems for groundwater flow and transport (Schwartz and Lee, 1991).

fracture planes formed a highly transmissive pathway through the system. Along this pathway, all three codes calculated nearly identical values of hydraulic head, appearing to differ only because of round off in the third decimal place. The principal differences in the calculations for head appeared to occur in fractures with low flow rates, specifically at interior nodes where fractures possessing relatively low transmissivities intersected. This implied that, in networks with large variations in fracture aperture, some numerical difficulty could be encountered in calculating heads for fracture planes carrying small quantities of flow. However, this difficulty did not appear to influence estimates of hydraulic heads and flow rates through the most transmissive parts of a network. In particular, the agreement between values of flow rate calculated by the three codes was quite good.

The purpose of the third problem for groundwater flow was to determine the ability of the codes to simulate flow in a network of fractures comparable to those that would have to be considered in the validation experiments in the SCV programme. Although perhaps not as complicated as originally intended, the geometry of the fracture network for the verification problem for fracture geometry was selected for the purposes of this exercise. Thus, this fracture geometry was embodied in a cube with 200 m side lengths. Only the NAPSAC and the FRACMAN/MAFIC codes took part in this exercise. The channelisation features of the FMG code made it unsuitable for application to this particular style of problem. Assumptions concerning the interconnection of the channels at fracture intersections are made within the FMG code, but these are not critical for situations in which the fracture density is low. However, in the current problem, where the fracture intersections themselves intersected, the treatment of the intersections dominated the calculation.

The initial computations produced a total flow rate into the simulated validation drift from the NAPSAC code that was approximately 24% less than that obtained from the FRACMAN/MAFIC code. However, each code preserved a mass balance with essentially no difference in the calculated discharge through the outer boundary of the cube. As a consequence, the problem was revised in terms of location and size of the Validation Drift so as to provide larger inflows. The same fracture geometry was used, but a square drift, with side lengths of 10 m, was inserted into the model. As in the first computation, the six external boundaries of the cube were assigned fixed heads of 10 m, and all nodes defined on the wall of the simulated drift were assigned a fixed head of 0 m. In the second computation, the flow rate into the Validation Drift obtained with the NAPSAC code was approximately 39% less than that predicted by the FRACMAN/MAFIC code. Based on a sensitivity analysis undertaken with both codes, it appeared that, for such large fracture networks, the flow calculations were sensitive to the extent to which individual fracture planes were discretized with finite elements. The discretization had to be unexpectedly fine in order for the flow solutions to become independent of the grid size, i.e. before grid convergence of the solution was achieved. Because the NAPSAC code inherently accommodates a finer discretization of fracture planes in large networks than does the FRACMAN/MAFIC code, the computations with the NAPSAC code produced flux estimates close to the grid-converged value. In a series of additional computations, a continuously finer discretization of the fractures with the FRACMAN/MAFIC code progressively reduced the differences in

the flux estimates. The network was originally constructed with 150 square fractures distributed in four sets. In a series of nine computations with the NAPSAC code, the mesh on a single fracture was refined by progressively increasing the number of elements from 1 024 to 40 000. The flux values did not converge until the number of individual fractures exceeded 16 384. In these trials, the maximum deviation in flux estimates due to the scale of discretization was about 5%. It was finally concluded that cross verification of the two codes had been demonstrated, provided the fine discretization of the network was used.

Solute Transport

The first verification problem for solute transport by groundwater examined the ability of the three codes to simulate transport along fracture planes and to properly mix mass at fracture intersections. The simple network, shown in Figure 4-24, consisted of four orthogonal fractures, each with a constant aperture of 100 μm which gave a fracture transmissivity of slightly less than $10^{-6} \text{ m}^2/\text{s}$. The fluid viscosity and density were fixed at 10^3 Pa/s and $1\,000 \text{ kg/m}^3$. The heads on the two y-z planes were fixed at different values, and conditions of no flow were prescribed on the remaining four faces of the cube. At zero time, tracer was introduced uniformly along the intersection at $x=0$. With particle tracking, this injection was simulated by adding 1 000 particles on the y axis between 0 m and 40 m. Mathematically speaking, this pulse loading corresponded to a delta function. Because of the regular geometry, uniform fracture aperture, and simplistic boundary conditions, the flow was unidirectional on the fracture planes. That is, the flow on the horizontal fractures was in the x-direction and the flow on the vertical fractures was in the z-direction.

The analytical solution to the transport problem showed that the flux and velocity of flow were proportional to the cube and square, respectively, of the fracture aperture. Because all of the tracer particles were injected into the system both instantaneously and simultaneously, the breakthrough should be a step function, as shown in Figure 4-25, that arrives at 1 200 s. The NAPSAC, FRACMAN/MAFIC, and FMG/TRINET codes predicted exactly the step breakthrough of the mass at the proper time interval.

The third verification problem for groundwater transport was designed to explore the ability of the codes to simulate more complex patterns of transport on individual fracture planes and mixing at the fracture intersections. The network of irregularly orientated fractures with a broad range in aperture variability, as defined previously for the second verification problem for groundwater flow, formed the basis for this problem. With reference to Figure 4-23, mass was injected uniformly into the fracture denoted as 2 along the inflow boundary defined by the intersection of the fracture with the x-z plane.

Although the problem appeared to be complex, an analytical solution could be obtained to provide a good independent estimate of the flow and, consequently, the transport. As discussed previously, almost all of the groundwater flow followed a single, direct pathway through the model along fractures 2, 3, and 6. Leakage downward into the other planes was small because of the small apertures of these fractures. By assuming that all the

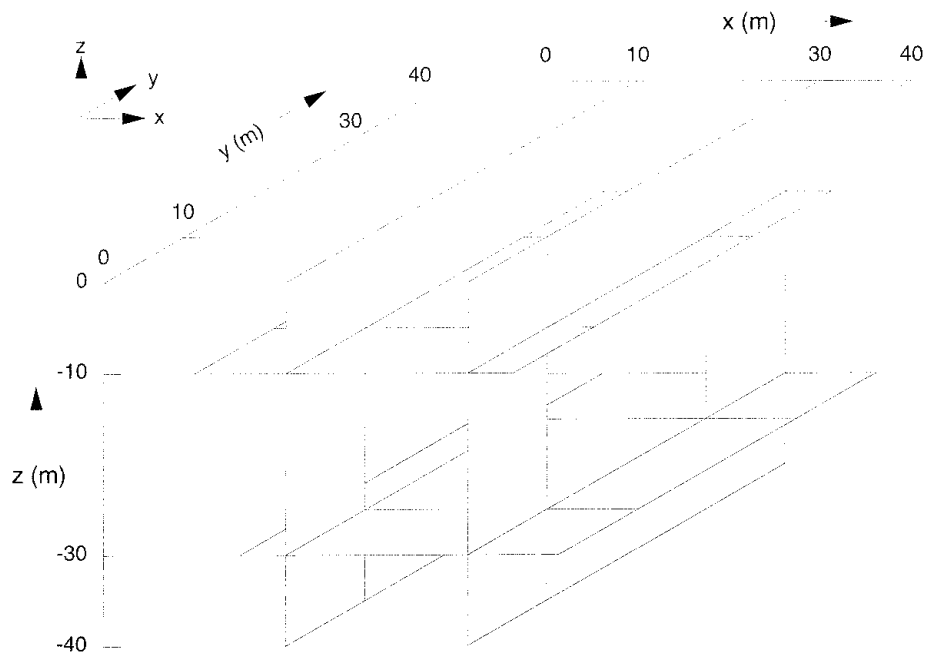


Figure 4-24 Fracture network for the first verification problem for solute transport (Schwartz and Lee, 1991).

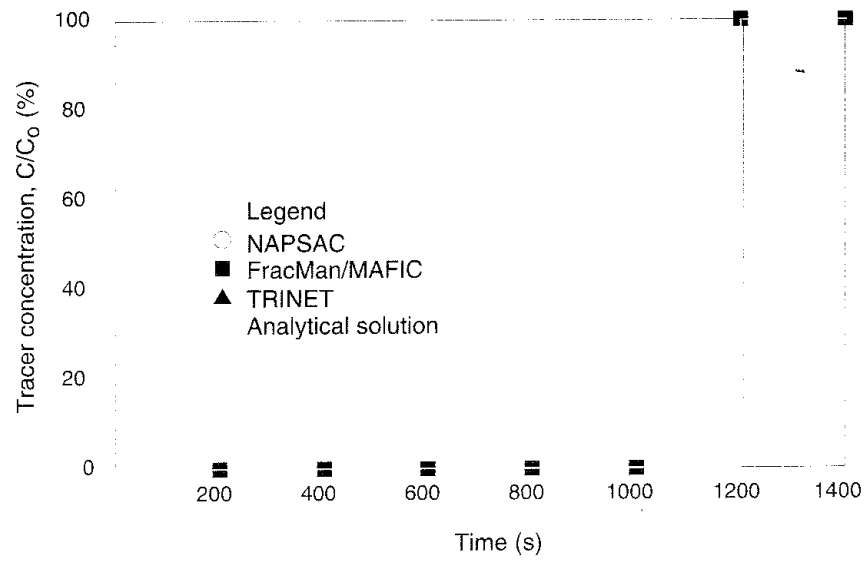


Figure 4-25 Comparison of analytical and numerical results for tracer breakthrough in the first verification problem for groundwater transport (Schwartz and Lee, 1991).

flow moves through one connected pathway, simple equations can be used to estimate the flow velocities and, with the path length, the residence time in each fracture. As shown in Figure 4-26, the breakthrough curve, with the first tracer arrival occurring about twenty days after injection, was a close approximation to a step function. Computations were obtained only with the NAPSAC and FRACMAN/MAFIC codes. It was felt that results from the FMG/TRINET code would be incompatible for comparative purposes because of the manner in which the FMG/TRINET code partitioned mass at the intersection of fracture planes. The computations from the FRACMAN/MAFIC code matched exactly those obtained from the analytical solution. The computations with the NAPSAC code also matched the analytical solution reasonably well, although a small amount of numerical dispersion and a slightly earlier breakthrough time were observed. This inherent dispersion, which is a consequence of the particle tracking algorithm in the NAPSAC code, occurred when particles departing a fracture segment were moved slightly along the line of intersection to adjacent nodes to begin their journey through the next fracture. Particle pathways along individual fracture planes can be rather complicated and several parameters were included in the code to assure "robust" particle tracking under a variety of conditions. Generally, large values for these parameters led to the most robust particle motion, but, unfortunately, the most numerical dispersion. In most applications, the tendency would be to assure robust motion at the expense of numerical dispersion.

The third verification problem for solute transport was designed to evaluate the capabilities of the codes to simulate transport in a network that was more realistic in terms of the number of fractures, as well as their hydraulic properties and pattern of interconnections. The network, generated stochastically and based on four separate fracture sets with statistical properties, consisted of 150 square fractures and 336 intersections within a cube with a 5 m side length. All of the fracture planes were truncated against the sides of this cube. The heads were fixed at different values on the y-z planes that formed two faces of the cube, while no flow conditions were prescribed on the other four faces of the cube. The simulated injection of tracer particles took place at fractures that intersected the inflow

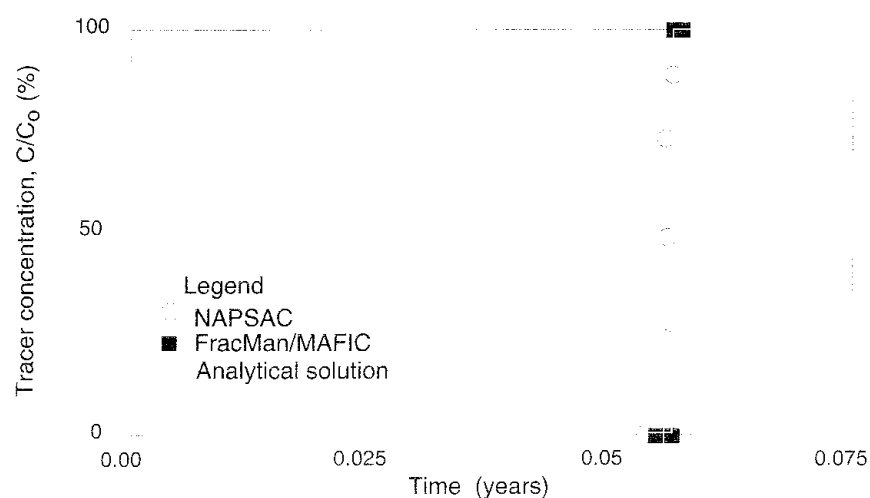


Figure 4-26 Comparison of analytical and numerical results for tracer breakthrough in the second verification problem for groundwater transport (Schwartz and Lee, 1991).

boundary on the y-z plane at 0 m on the x axis. As for the previous problem, the FMG/TRINET code was not a participant in this computational exercise. As shown in Figure 4-27, the NAPSAC and FRACMAN/MAFIC codes predicted initial breakthroughs of the tracer mass in about 0.05 years, with very long tails on the breakthrough curve. Obviously there existed a variety of flow paths throughout the network, some of which were much slower than others. A sensitivity analysis was conducted with the NAPSAC code to evaluate the influence of grid and intersection discretizations, the number of reference particles, and the "tuning" parameters contained in the algorithm. In general, the breakthrough data converged more slowly when the number of elements on a plane was increased. The results were not definite in demonstrating full grid convergence at later times when an individual fracture contained 40 000 elements and there existed 100 000 moving reference particles of the tracer.

The recovery rate of tracer particles in this particular computational exercise with the NAPSAC code was 99.8%. On the other hand, computational results from the FRACMAN/MAFIC code for 1 000 moving particles yielded a 72% particle recovery rate at the time the simulation was discontinued. It was concluded that the agreement between the predictions by both codes was acceptable, and that most of the differences in the breakthrough curves were probably related to the inability to exactly match the different model-based parameters contained in the two codes.

Summary Remarks

In general, the difficulties encountered in the cross-verification exercises did not result from undetected programming errors, but rather from difficulties of maintaining comparability in results between the various codes when given parameters that were unique to the individual simulation approaches. This difficulty was particularly apparent with the larger fracture networks, wherein, it would seem, that a relatively large number of elements was

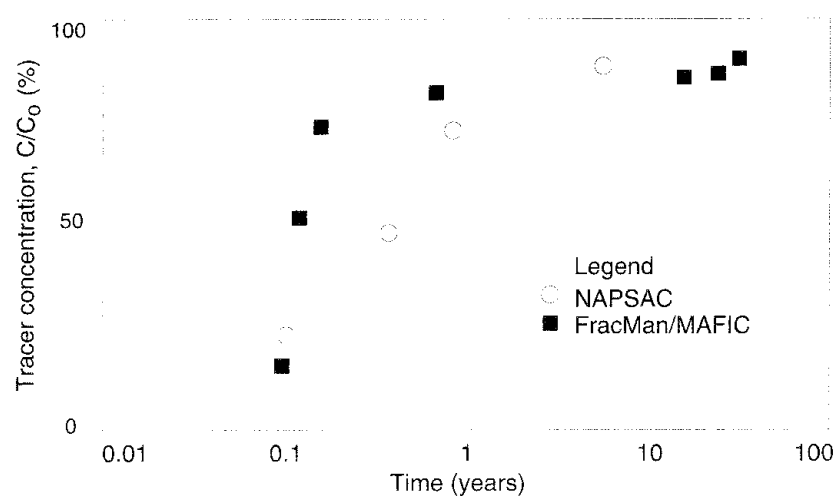


Figure 4-27 Comparison of the numerical results obtained for the third verification problem for groundwater transport without dispersion (Schwartz and Lee, 1991).

required to insure a fully converged flow solution. The codes were able to generate virtually identical representations of a complex fracture network, and, for simple cases of groundwater flow, to accurately predict flow rates. The computational accuracy of the calculations of hydraulic heads was generally acceptable, but appeared to deteriorate when there existed extreme contrasts in fracture apertures. The source of discrepancies in flux predictions for complex fracture networks was determined to be a mismatch in the scale of discretization, which resulted in a lack of grid convergence to the correct flux calculations. Enhancement of the discretization of the finite elements on the fracture planes yielded flux estimates that differed by only 1.7% between the NAPSAC and FRACMAN/MAFIC codes.

The cross verification of the transport segments of the codes was reasonably successful. Sensitivity analyses suggested that the differences in computational results were caused by differences in the particle recovery rates and the numbers of moving reference particles used in the simulations. In summary, the NAPSAC and FRACMAN/MAFIC codes produced nearly identical flow and transport results for all of the verification problems. Similarly for those problems in which it participated, the FMG family of codes produced results that compared favorably with those obtained from the other two codes.

4.3 VALIDITY OF THE GROUNDWATER FLOW MODELS

As mentioned previously, one of the objectives of Phase 3 of the Stripa Project was to develop and evaluate approaches for predicting groundwater flow in a specific, previously unexplored, volume of the Stripa granite, and to compare those predictions with data obtained from field measurements. As described in Section 3.3, extensive characterization of the SCV site was conducted, including single-borehole geophysical logging, hydraulic testing, radar and seismic tomography, together with head monitoring and radar and seismic testing in the single-borehole and crosshole reflection modes. The information obtained in Stage I was used to develop a preliminary conceptual model of the SCV site in Stage II. This model was used to develop predictions of groundwater flow into the D boreholes, in what was known as the Simulated Drift Experiment (SDE). Subsequently, in Stage III, additional characterization of the SCV site was conducted, which led to refinements in the conceptualization of the geology and hydrology of the SCV site. This refined model was used as the basis for predictions of groundwater flow into the Validation Drift excavated in Stage IV, in what was known as the Validation Drift Experiment (VDE).

As explained in Section 4.1, the process for evaluating the validity of the groundwater flow models began with a training exercise, which focussed on the SDE (Hodgkinson, 1991). This exercise provided a framework for gaining experience in using the groundwater flow models, and for evaluating the capabilities of the models in light of the particular geologic features and hydrologic conditions of the SCV site. A principal achievement of the SDE modelling activity was the demonstration that it was feasible to undertake the complex and multidisciplinary tasks associated with the gathering and interpretation of characterization data, the development and application of

complex models, and the process for comparison of predictions with the measurements. The validation exercise focussed on predictions of groundwater inflow into the Validation Drift, as well as on predictions of changes in head distribution in the site because of the drift excavation and of the characteristics of the fractures that were observed within the Validation Drift (Hodgkinson and Cooper, 1992a).

A particular strength of the modelling and validation process was the participation of the four independent modelling groups from AEA Harwell, Golder Associates, Lawrence Berkeley Laboratory, and Fracflow Consultants, along with the Task Force on Fracture Flow Modelling which provided review and direction. All four modelling groups had access to the same site characterization data and conceptual model of the SCV site as provided by the principal investigators for the characterization activities. Using these data, each group formulated a conceptual model to fit within the constraints of their modelling process, developed the necessary parameters on the basis of their interpretations of the data, and conducted the numerical evaluations independently. There was a certain amount of necessary cooperation between AEA Harwell and Fracflow Consultants for purposes of establishing the hydrologic boundary conditions for the NAPSAC model. It must be mentioned that each group made predictions for purposes of the SDE and the VDE without *a priori* knowledge of the results of the field measurements.

4.3.1 Simulated Drift Experiment

The Simulated Drift Experiment, as described in Section 3.3.4, involved the measurement of groundwater flow into six 100 m long boreholes, known as the D boreholes, that were drilled sub-horizontally into the SCV site. The borehole array consisted of a central borehole surrounded by five parallel boreholes on a radial separation of 1.2 m. The pattern of the five boreholes simulated a tunnel with a diameter of 2.4 m. The experiment was designed so that the groundwater inflows could be measured in small isolated sections of each borehole by means of a system of straddle packers, at selected pressure steps to investigate the linearity of flow rates against pressure. The pressures in all six boreholes had to be approximately equal in order to simulate the wall of the tunnel. The modelling groups were asked to predict quantitatively the total rate of groundwater inflow into the six boreholes, as well as to predict qualitatively the distribution of inflows along the boreholes.

Rate of Groundwater Inflow into the D boreholes

A comparison of the measured and predicted total inflow rates of groundwater into the D borehole array in the SCV site is shown in Table 4-1. The measurements were obtained at a hydraulic head of 17 m in the D boreholes rather than for zero head as assumed in the model calculations. Furthermore, the measurements had not fully stabilized to a condition of steady state, as was assumed in the model calculations. As shown in Table 4-1, the range of predictions by the three modelling groups, apart from Golder-1, encompassed the field measurements. The Golder-1 prediction, made prior to publication of the measurements, experienced

calibration difficulties. The Golder-2 calculation, made after publication of the measurements, predicted a mean inflow rate of 1.5 ℓ/min , with a range of 0.5 ℓ/min to 95 ℓ/min in the 90% confidence interval. The field data indicated that about 79% of the groundwater inflow originated from the fracture zones. In comparison to this inflow percentage, the Harwell model predicted a mean value of 94% with the range of 79% to 98%. The Golder-2 calculations predicted that 75% of the inflow occurred where the major features intersected the simulated drift. The LBL model did not consider flow outside the fracture zones and, therefore, predicted that all of the groundwater inflow originated from the fracture zones.

Table 4-1 Comparison of measured and predicted groundwater-inflow rates to the D borehole array in the SCV site (Hodgkinson, 1991).

| Measurement/Model | Mean Inflow (ℓ/min) | Range (ℓ/min) |
|--------------------------|--------------------------------------|--------------------------------|
| Experimental Measurement | 1.71 | 1.67 - 1.75 |
| Harwell/Fracflow model | 1.45 | 0.36 - 5.80 |
| Golder-1 model | 0.055 | 0.001 - 0.156 |
| Golder-2 model | 1.5 | 0.5 - 95 |
| LBL model | 3.1 | 0.0 - 7.7 |

Distribution of Inflow Along the D boreholes

The comparison between the measurements of groundwater influx along the D borehole array and the predictions is shown in Figure 4-28. The distributions obtained with the Harwell and Golder-2 fracture-flow models are shown in more detail in Figures 4-29 and 4-30, respectively. All of the predictions show the same qualitative behavior. That is, regions of high inflow were generally associated with the fracture zones, with regions of relatively small inflow between the zones. The less than perfect agreement between the predictions and measurements for locations of major inflows was due to the lack of precision in the conceptualizations of the location and extent of the various fracture zones, as well as to poorly characterized inhomogeneities within the fracture zones. The Harwell results, shown in Figure 4-29, provided the distribution of fluxes from the average rock over 0.5 m intervals of a typical borehole. However, only one of the 180 intervals exhibited a flow which was above the measurement limit of the testing equipment. The general pattern of inflows into 1 m sections of the D boreholes from the Golder-2 calculations, shown in Figure 4-30, was qualitatively different from that of the Harwell predictions. The inflows were more sparse, which reflected the lower intensity of fracturing assumed in the model.

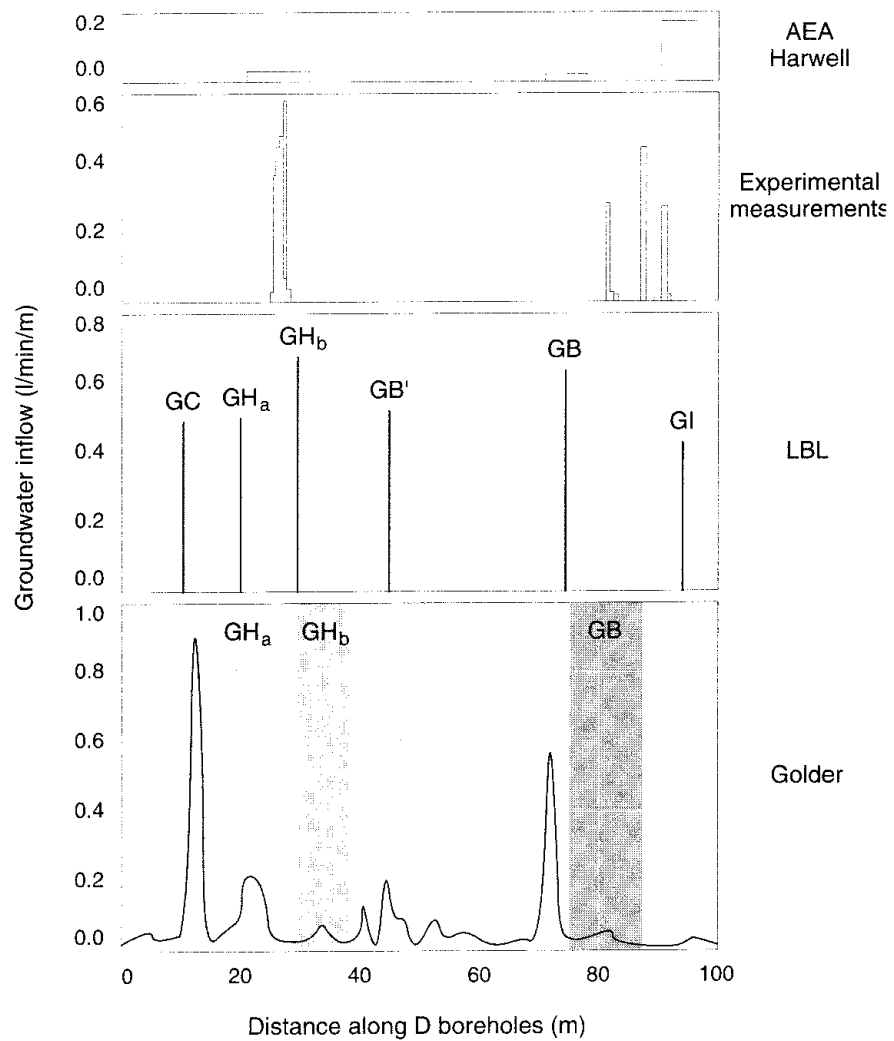


Figure 4-28 Comparison of predictions and measurements of groundwater inflow in the D borehole array for the SDE (Hodgkinson, 1991).

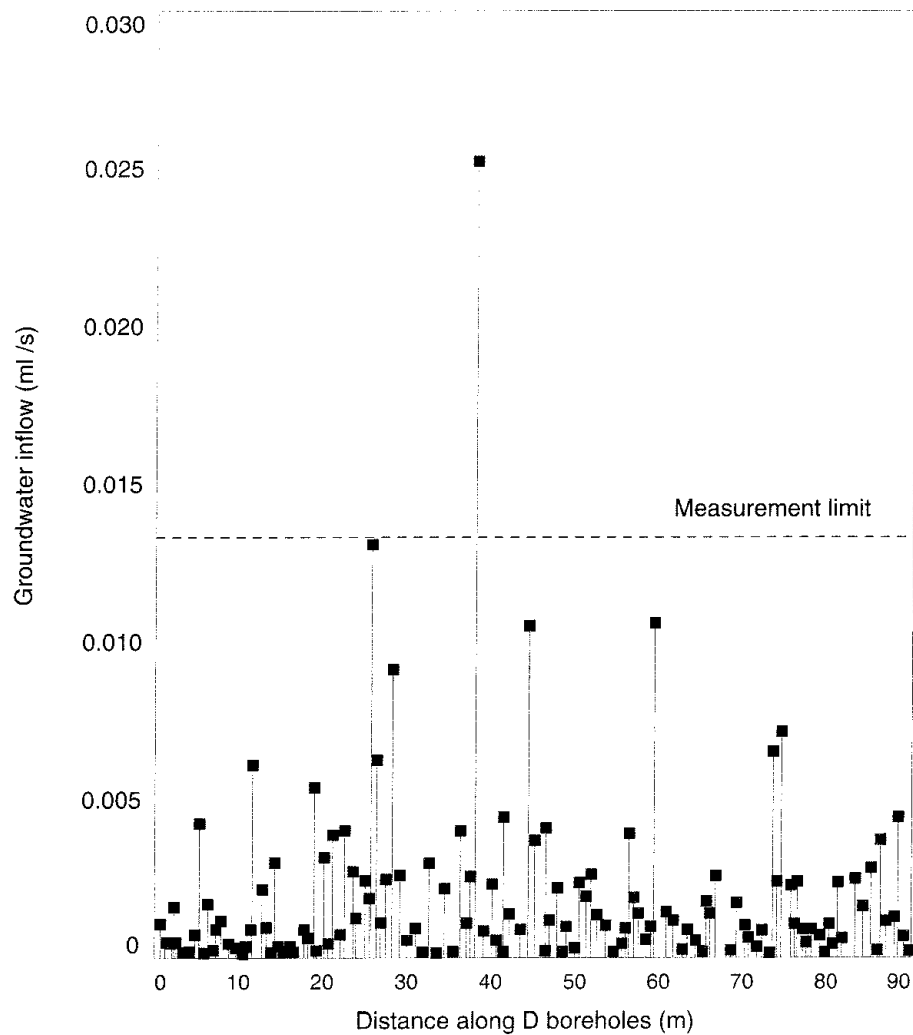


Figure 4-29 Distribution of groundwater fluxes for individual 0.5 m sections of a typical D borehole in averagely fractured rock in the SDE as predicted by the Harwell model (Herbert and Splawski, 1990).

General Discussion

All of the models, with the exception of the original Golder-1 calculation, gave reasonable predictions of total flow into the D boreholes and spatial distribution of inflows. The boundary conditions for head in the region of the SCV site being modelled controlled the large-scale pressure gradient between the D boreholes and the outlying regions. Because of this gradient and the reasonable predictions of total flow into the D boreholes, it can be concluded that the models correctly approximated the gross average permeability of the rock. However, the spatial distribution of permeability was less accurately modelled as indicated by the details of inflow along the borehole array. By using a simple radial flow model and estimated permeabilities of the fracture zones, a total inflow of 2.3 ℓ/min was calculated, which was in reasonable agreement with the measurement (Hodgkinson, 1992).

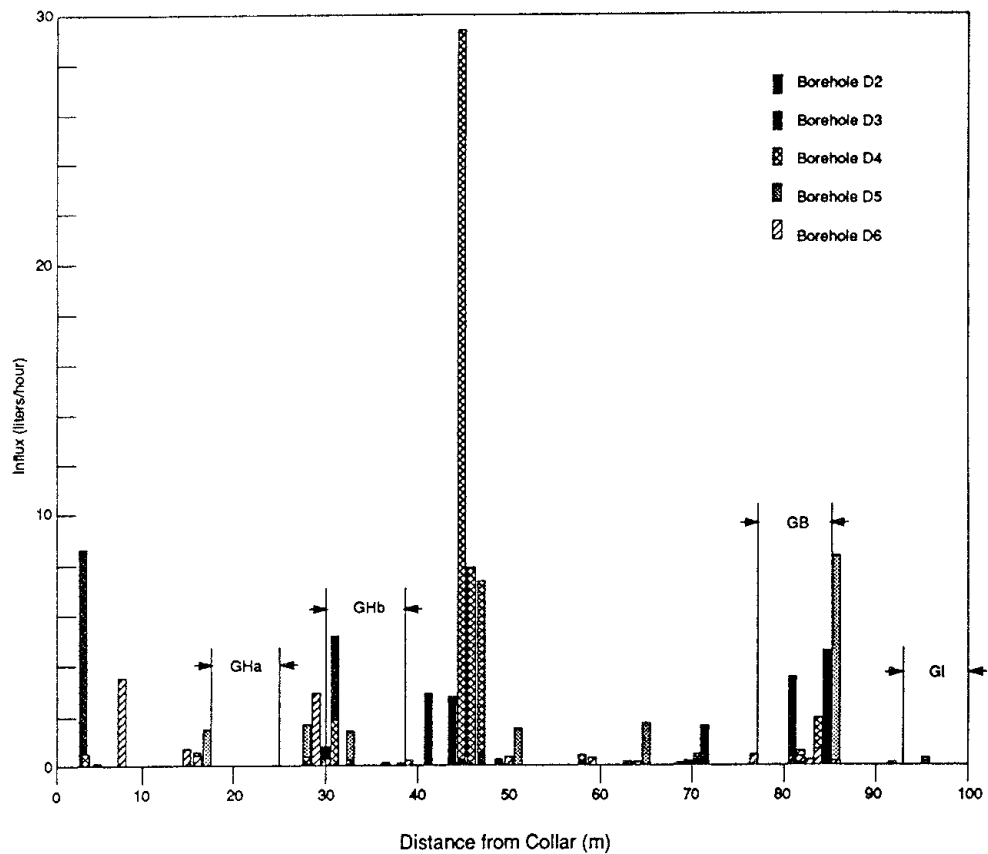


Figure 4-30 Distribution of groundwater fluxes for 1 m sections of the D boreholes in the SDE as obtained by a single realization of the fracture system with the Golder model (Geier et al, 1990).

4.3.2 Validation Drift Inflow Experiment

The second and principal exercise for evaluation of the validity of the groundwater flow models involved the Validation Drift Experiment (VDE). The Validation Drift was constructed over a distance of 50 m within the confines of the ring of five D boreholes. On the basis of discussions with the principal investigators for the modelling and characterization activities, the Task Force established the following seven performance measures. These measures were used to evaluate the validity of each modelling approach in accordance with the criteria given in Section 4.1.3.

- Total rate of groundwater flow to the Validation Drift (quantitative)
- Rate of groundwater flow from the H zone (quantitative) and spatial distribution of such flow (qualitative)
- Rate of groundwater flow from the average rock (quantitative) and spatial distribution of such flow along the Validation Drift (qualitative)
- Characteristics of fractures in the drift (qualitative)
- Magnitude (quantitative) and spatial distribution (qualitative) of head changes due to drift excavation
- Magnitude (quantitative) and spatial distribution (qualitative) of head response due to opening borehole T-1
- Distribution of groundwater inflow to remaining sections of D boreholes (qualitative).

The modelling groups were allowed to use the refined conceptual geohydrologic model of the SCV site, along with any data that had been collected by borehole testing within and around the site before construction of the Validation Drift. The predictions were made without quantitative knowledge of the measurements of groundwater flow and head within and around the Validation Drift, respectively, but with a qualitative understanding that the inflow to the drift was probably perturbed by excavation effects.

Groundwater Flow into the Validation Drift

At the outset of the exercise, the modelling groups made a calculation of the groundwater inflow to the first 50 m of the D borehole array, as shown in Figure 4-31. This calculation, using the refined conceptual geohydrologic model of the SCV site, simulated a situation in which the drift-excavation effects were nonexistent. Clearly, all of the model calculations were of the correct order of magnitude as compared to the measurements, and, for all practical purposes, the range of the measurements was encompassed by the ranges of the calculations. The values provided by the Harwell model were low, by about a factor of two, partially due to an error in applying the pressure boundary condition obtained from the EPM model. These calculations were not appreciably different from those obtained previously in the modelling exercise for the SDE, in spite of the refinements in the conceptual geohydrologic model and improvements in the modelling techniques.

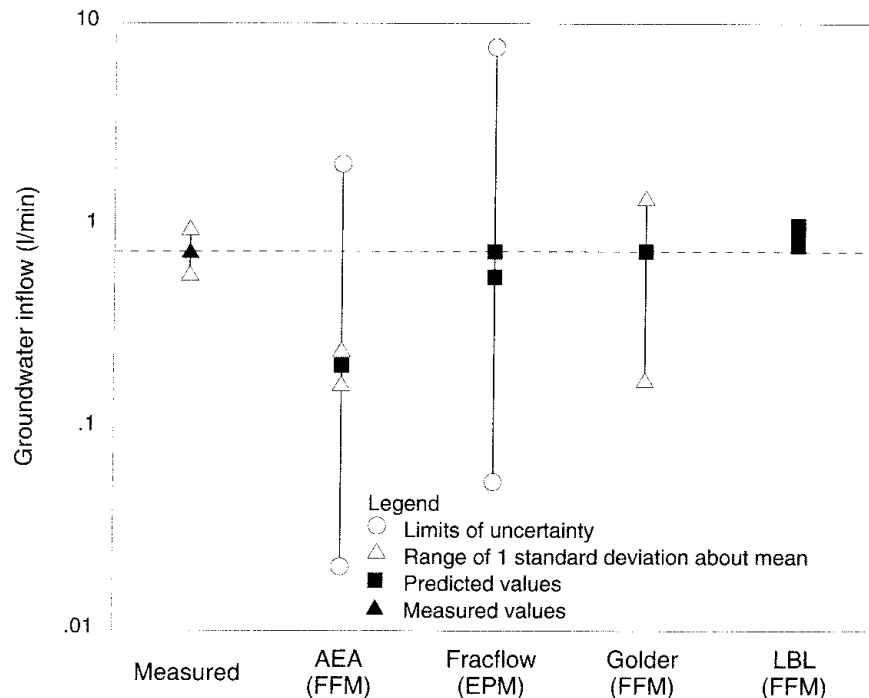


Figure 4-31 Comparison of the predicted and measured inflows into the simulated drift, as outlined by the D borehole array, ignoring excavation effects (Hodgkinson and Cooper, 1992a).

The comparison of predicted and measured groundwater inflows to the Validation Drift are shown in Figure 4-32. Although the predicted mean values of inflow were always greater than those measured, they were nevertheless of the correct order of magnitude. More importantly, however, was the observation that the flow into the Validation Drift was only about 13% of that into the first 50 m of the D borehole array in the SDE. Consideration of the effect of stress redistribution in the rock mass due to drift excavation, by both Harwell and Golder, indicated that any effect of stress was very small. To simulate the change required to produce the decrease in inflow after drift construction, both Golder and LBL used a reduction in permeability in the region of the drift. When the transmissivities of all fractures within 3 m of the drift were reduced by an order of magnitude, the flow prediction by the Golder model was reduced between 60% and 95%. Similarly, LBL introduced a skin factor which effectively reduced the permeability in elements within 5 m of the drift. The inflow was reduced by about 35% when the permeability was reduced by a factor of four, as compared to a reduction in inflow by almost 80% when the permeability was reduced by a factor of twenty.

The comparison of the predicted and measured inflows from the H zone in the Validation Drift, as a percentage of the total inflow, is shown in Figure 4-33. The field measurements indicated that about 97% of the inflow of groundwater to the Validation Drift originated from the H zone, with about 75% of the H zone flow coming from a single fracture. All of the models predicted that the majority of the flow would originate from the H zone. In this respect, the LBL model assumed that all flow originated from the fracture zone. The Harwell model underestimated the relative importance of the H zone, probably due to an underestimation of the transmissivity of this zone. The Golder model correctly predicted the dominance of a single fracture on the inflow to the Validation Drift, while the Harwell model predicted that the inflow originated from a few fractures in the H zone.

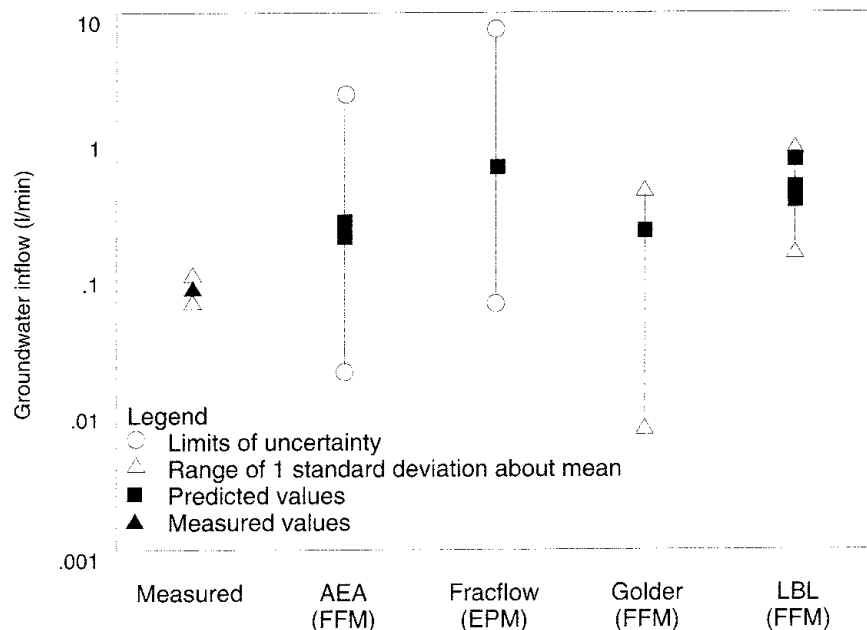


Figure 4-32 Comparison of the predicted and measured inflows of groundwater into the Validation Drift (Hodgkinson and Cooper, 1992a).

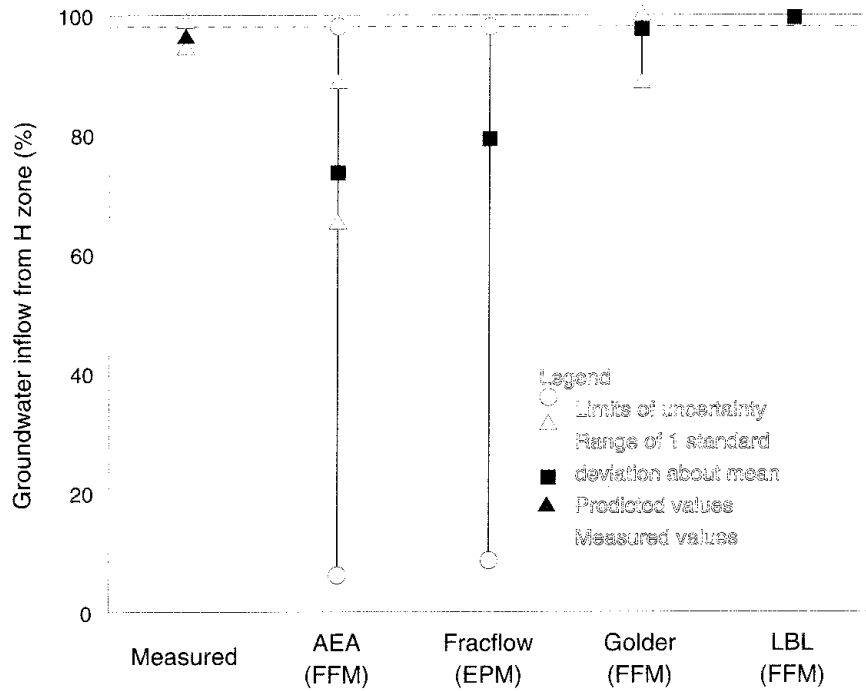


Figure 4-33 Comparison of the predicted and measured inflows of groundwater from the H zone as a percentage of the total inflow into the Validation Drift (Hodgkinson and Cooper, 1992a).

The comparison of the predicted and measured inflows into the Validation Drift from the average rock is shown in Figure 4-34. These flows were significantly lower than those from the fracture zone, and, correspondingly, more difficult to model accurately. The excavation of the Validation Drift appeared to have the greatest impact on inflow from the average rock, in that the measured inflow was about a factor of forty less than that measured in the equivalent section of the D borehole array in the SDE. The predictions varied considerably among the modelling approaches, with only the Golder prediction being of the correct order of magnitude. This is probably due to the fact that the Golder model assumed an order of magnitude reduction in transmissivity near the Validation Drift, while the Harwell and Fracflow models considered only the direct effect of stress changes on the transmissivity of fractures.

The distributions of measured and predicted groundwater inflows into the Validation Drift are shown in Figure 4-35. As mentioned previously, the Golder model predicted that a majority of the inflow originated from a single fracture, as represented by a single panel with an area of 1 m², while the Harwell model predicted flow from a few fractures. Generally speaking, the qualitative agreement between measurements and predictions is reasonably good.

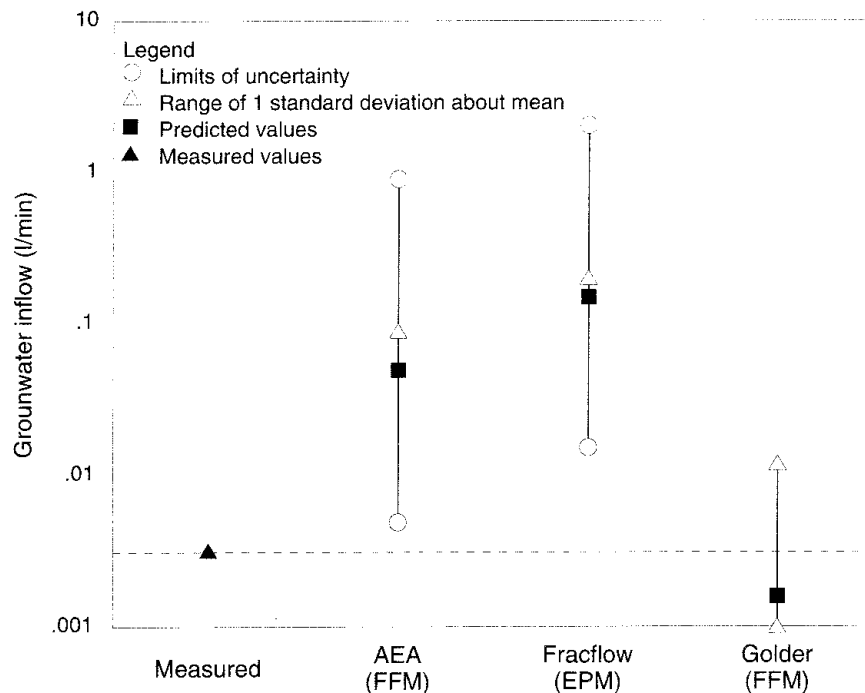


Figure 4-34 Comparison of the predicted and measured inflows of groundwater into the Validation Drift from the average rock (Hodgkinson and Cooper, 1992a).

Characteristics of Fractures in the Drift

A comparison of the predicted and observed fracture patterns in the Validation Drift is shown in Figure 4-36. The Harwell model predicted a greater density of fractures than those observed, whereas the Golder model predicted a density that was much less than observed. Most of the observed fractures were contained within the Harwell model, with their sizes assumed to be log-normally distributed, but no large-scale structure was included. Thus, for these fracture parameters, the rock could be treated as being homogeneous in regions larger than about a 12 m cube. The Harwell model tended to overpredict the fracture frequency because the frequency observed in the boreholes was greater than actually observed in the Validation Drift. Conversely, the Golder model focussed on the hydraulically significant fractures, such as the H zone, with the remaining rock mass around the Validation Drift containing fewer fractures. Generally speaking, however, both models predicted a higher density of fractures in the region defined by the H zone, consistent with field observations.

Magnitude and Spatial Distribution of Head Changes

The predictions of the magnitudes of head changes within the SCV site due to drift excavation, by the Fracflow, Golder, and LBL models, were generally of the correct order of magnitude. However, the LBL model tended to overestimate drawdown, while the Fracflow and Golder models slightly underestimated it. Both the Golder and LBL models tended to overpredict, by a factor of five to twenty, the drawdown in the SCV site when borehole T-1 was opened.

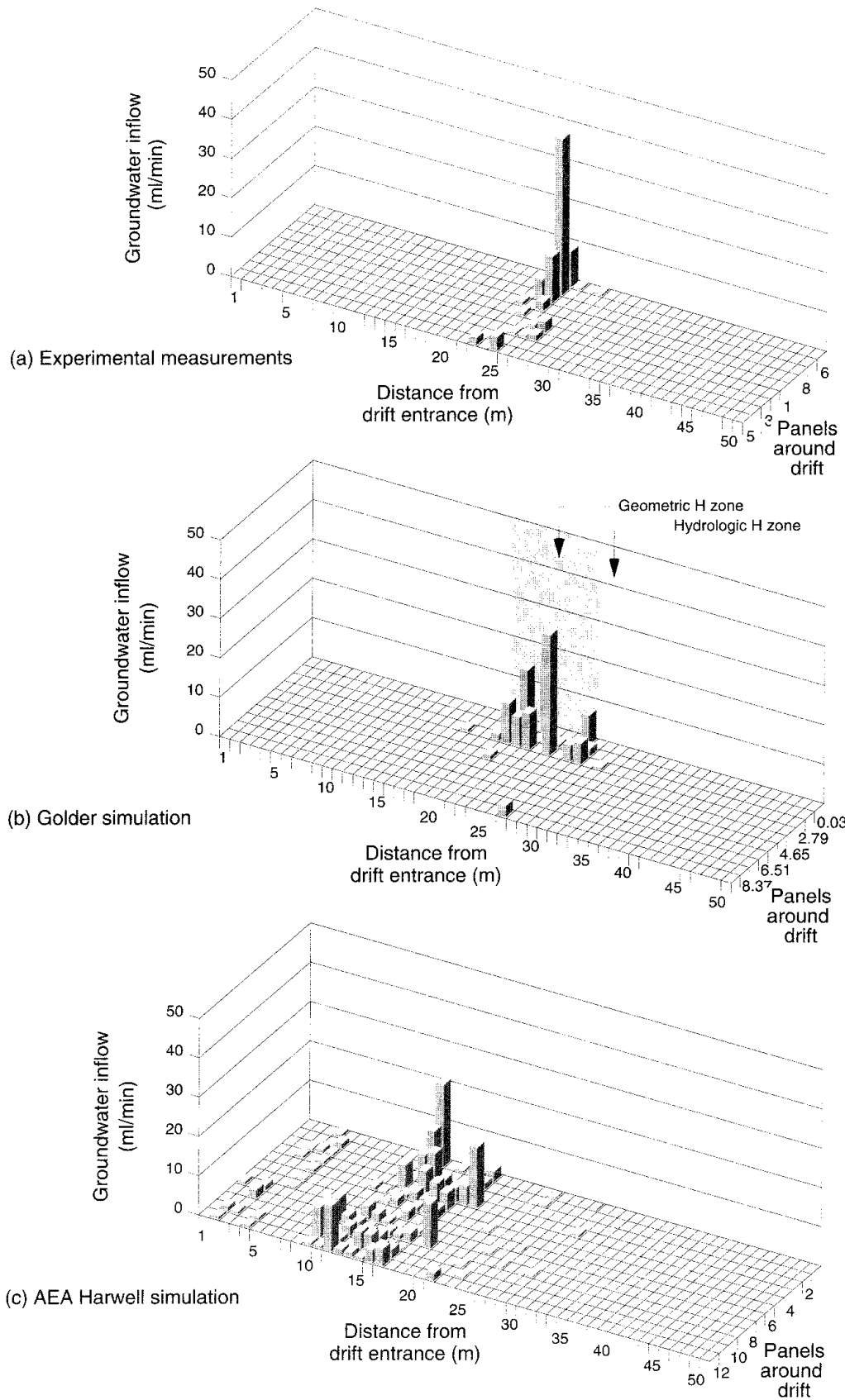
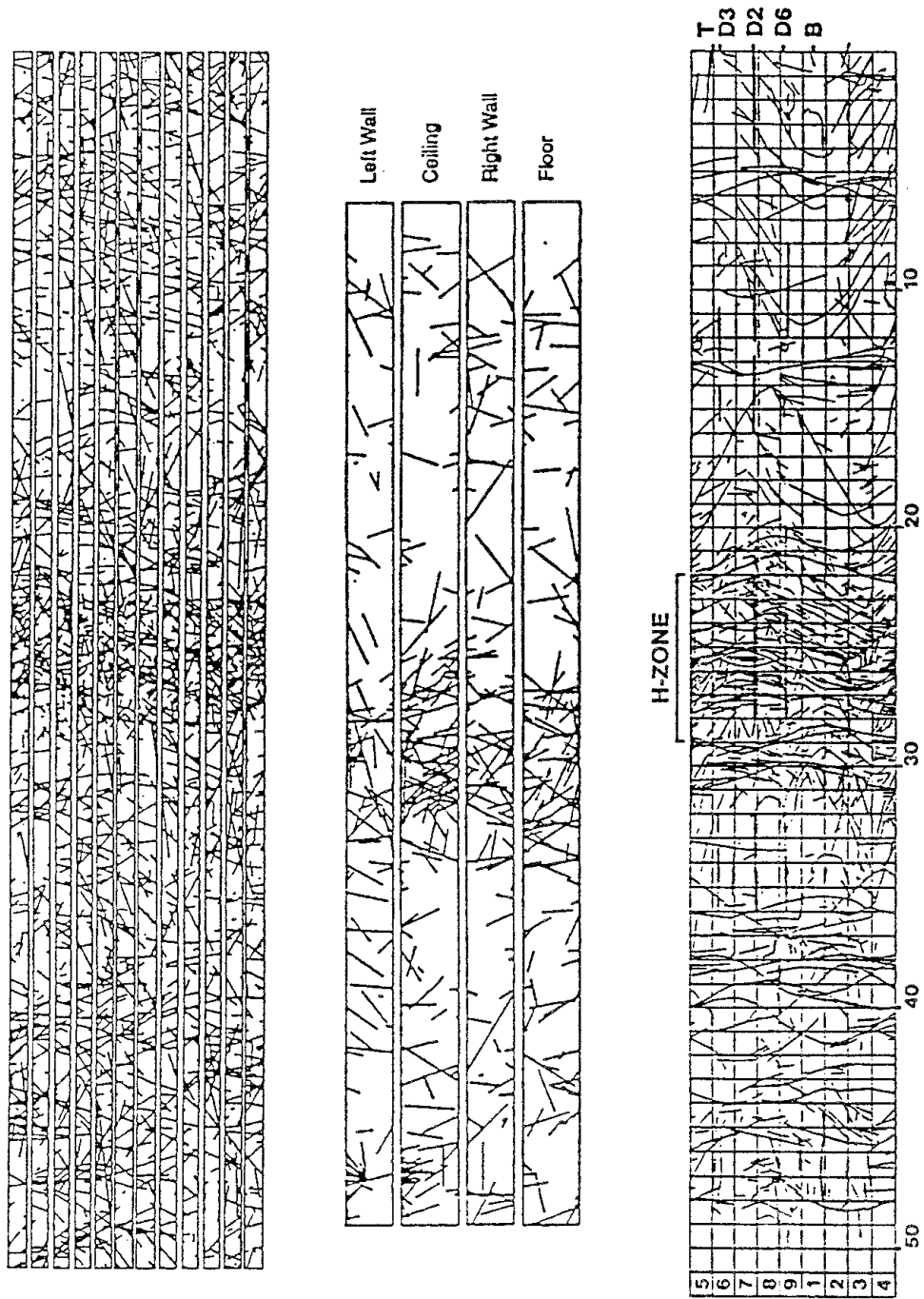


Figure 4-35 Comparison of the distributions of measured and predicted groundwater flows into the Validation Drift (Hodgkinson and Cooper, 1992a).



(a) Harwell/Fracflow Simulation (b) Golder Simulation (c) Experimental Measurement

Figure 4-36 Comparison of the predicted and measured fracture patterns in the Validation Drift (Hodgkinson and Cooper, 1992a).

Groundwater Inflow to the D boreholes

The measurement of inflow to the D borehole array in the SDE was found to be dominated by flows that originated from the H and B zones. Because the inflows from the "average" rock were found to be below the measurement limits, the inflow to the sections of the D boreholes that remained after excavation of the Validation Drift were remeasured with a lower measurement limit. The comparison of the predicted and measured inflows are shown in Figure 4-37. As compared to the SDE, the decrease in inflow to these boreholes after drift excavation was about two orders of magnitude. Generally speaking, all of the model predictions were an order of magnitude or more greater than the measured value. Two of the six boreholes in the array were observed to receive the bulk of the inflow. A similar result was produced by the Golder model in that most of the inflow did originate from one or two of the D boreholes, where the actual boreholes depended upon the realization of fractures.

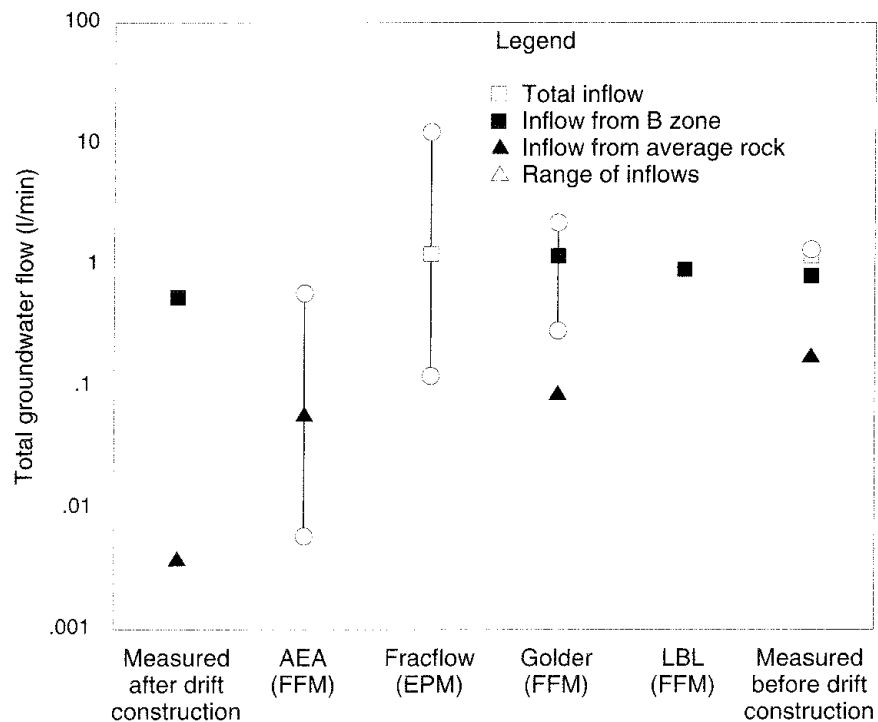


Figure 4-37 Comparison of the predicted and measured inflows of groundwater into the remaining sections of the D boreholes (Hodgkinson and Cooper, 1992a).

General Discussion

The most significant difference between the three fracture-flow modelling approaches was the treatment of the averagely fractured rock, in particular the intensity of fracturing. The Harwell model included many more fractures than the Golder model, while the LBL model did not allow for the existence of fractures in the average rock between the fracture zones. The Harwell model made use of fracture statistics to define a network model. This network was then used to determine the permeability of an equivalent

homogeneous medium, which in turn provided the boundary conditions for detailed models of inflow. In contrast, the Golder model considered the fractures explicitly, in particular focussing on the most transmissive fractures, with an inferred frequency in the H zone and no fractures in the average rock located away from the drift. The Harwell and Golder models used fracture observations to define fracture sets, while the LBL model was configured to use only groundwater flow data.

The calculations with the Harwell model were affected by an error in converting the pressures calculated by the EPM model to boundary conditions for the near-drift network models. Thus, while the EPM approach gave values of inflow comparable to those found during the SDE, the network model gave lower inflows. The Harwell model had difficulty in predicting the very low flows through the average rock, possibly due to disturbed zone effects that were not modelled. The Golder model, calibrated to the SDE observations, gave good predictions for the inflow to the Validation Drift, where a zone of reduced transmissivity was used to compensate for excavation effects in the skin of the drift. The LBL model considered only flow in the fractures, but this assumption was reasonably appropriate at the SCV site. Details of the fracture zone properties were determined by the use of head and flow data, rather than from fracture characterization data. Generally speaking, the predictions made with the EPM model by Fracflow were reasonably good, considering the relative coarseness of the discretization in the SCV model and the relatively large volume of rock that was modelled. None of the modelling groups could explain the decrease in inflow to the Validation Drift on the basis their analyses of changes in the rock stresses due to excavation.

4.3.3 Assessment of Model Validity

On the basis of the comparisons between predictions and measurements, and considering the criteria defined in Section 4.1.3, the Task Force made judgements about the validity of the models for application to the SCV site. These judgements were (Hodgkinson and Cooper, 1992a; Hodgkinson, 1992):

- All of the modelling approaches satisfied the quantitative criteria, insofar as the predictions were, for the most part, of the correct order of magnitude as compared to the measurements.
- The predictions of patterns of groundwater flow, in particular the dominance of the flow in the H zone, were reasonable; because of the lack of steady-state data, it was difficult to confirm the accuracy of the predicted heads.
- From the viewpoint of usefulness, the fracture-flow models were unnecessarily complicated for predicting the average flux of water through the rock; however, for the more detailed calculations of a groundwater flow system, when considering spatial variability of fractures and properties, the Harwell and Golder models were quite relevant.

- The SCV programme demonstrated the feasibility of gathering data, modelling groundwater flow, and making judgements of model validity within a generally reasonable time period of several years.

4.4 VALIDITY OF THE GROUNDWATER TRANSPORT MODELS

One of the principal objectives of Phase 2 was to assess the validity of groundwater transport models at the SCV site in the Stripa mine. This evaluation involved two separate sets of calculations. The first set, known as the training exercise, focussed on the second Radar/Saline Tracer Experiment (RSTE-2), using data from the first Radar/Saline Tracer Experiment (RSTE-1) for calibration of the models. In these experiments, saline tracer was injected into the H zone from borehole C2 and recovered in the D boreholes (RSTE-1) and in the Validation Drift (RSTE-2). Radar tomography was used to track the spread of the tracer from the injection point to the collection points. Following this training exercise, the models were used to predict the migration of tracers injected in boreholes in the rock mass surrounding the Validation Drift and collected in the Validation Drift and in other boreholes in the SCV site, in what was known as the Tracer Migration Experiment (TME).

An important component of the strategy for assessing the validity of models was that the predictions were made "blind". That is, modelling groups developed their predictions before knowing the results of the experiments. The SDE provided the modellers an opportunity to assess their abilities to represent rock fractures in an appropriate and realistic manner in order to predict groundwater inflow to the D boreholes. In the VDE, considerable attention was given to the representation and impact of the drift excavation effects when simulating groundwater flow into the Validation Drift from the H zone and the average rock. The Radar/Saline Tracer Experiments and the Tracer Migration Experiment provided an opportunity to evaluate the capabilities of the modelling procedures to represent the transport of tracers within principally the H zone.

4.4.1 Radar/Saline Tracer Experiment

The Radar/Saline Tracer Experiments were designed to provide characterization data, including transport aperture and dispersivity (for purposes of the transport modelling), and to provide the framework for a "training" exercise before embarking on the validation exercise that involved simulation of the Tracer Migration Experiment. In both Radar/Saline Tracer Experiments, tracer was injected into the H zone at the point where it intersected borehole C2 (Olsson et al, 1991a,b). The high rate of injection, of the order of 200 ml/min, meant that the existing groundwater flow was significantly altered, resembling a dipole structure. In RSTE-1, the tracer concentration was monitored in each of the D boreholes at their intersection with the H zone. In RSTE-2, the concentrations were measured separately in panels in the roof and walls of the Validation Drift. Very little tracer was observed in panels outside the H zone. Radar tomography was undertaken

in three borehole sections surrounding the injection borehole. The three tomographic planes outlined the sides of a tilted pyramid, as shown in Figure 4-38, with the sides being almost perpendicular to the plane of the H zone. As a consequence, the tomograms were able to show the spread of the tracer within, and outside, the H zone.

For RSTE-2, the modelling groups were asked to predict the breakthrough of the saline tracer to the Validation Drift, to the T-1 and T-2 boreholes, and to the 1 m² square sheets lining the Validation Drift, and to provide the histogram of the breakthrough to such sheets. In addition, they were asked to develop the simulated tomogram for the spread of the tracer in the H zone during the injection process. While all the modelling groups made use of the data from RSTE-1 for calibration of their transport models, and later with the data from RSTE-2, only the Golder group was successful in making the predictions for RSTE-2 before the observations were made public.

In the calibration exercise with the data from RSTE-1, the Golder group calibrated the storativity by simulation of the crosshole interference tests, and thereby parameterized the relationship between flux and velocity in the fractures. This relationship was confirmed for the SCV site by comparing observed and predicted drawdown curves. The breakthrough curves and the tomograms from RSTE-1 were used for calibration of the dispersivity parameters. By fitting a one-dimensional model for transport to the data

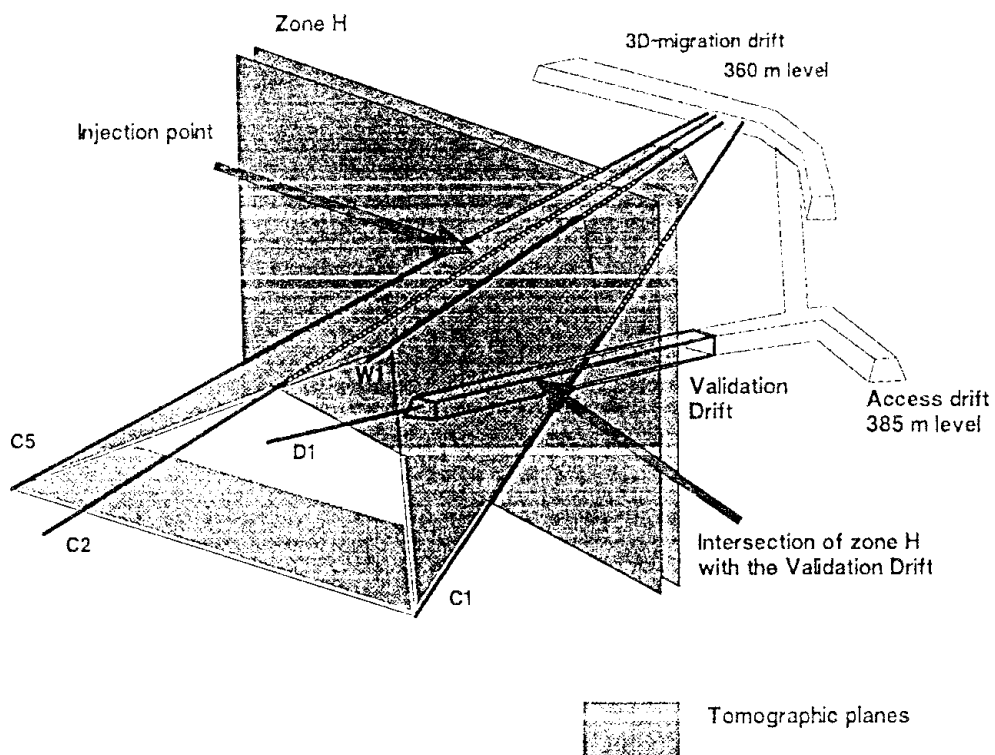


Figure 4-38 Schematic diagram of the second radar/saline experiment at the SCV site (Olsson et al, 1991b).

Saline tracer was injected in borehole C2 where it intersects the H zone. Radar tomography was made in the plane sections between boreholes W1 and C5, C5 and C1, and W1 and C1.

(Maloszewski and Zuber, 1989), a longitudinal dispersion length of about 0.3 m was obtained. An initial guess for the transverse dispersivity was taken to be one-third of the longitudinal dispersivity. When these values were used in the FRACMAN/MAFIC computer code to model RSTE-1, the calculated breakthroughs to the D boreholes agreed reasonably well with field measurements. Similarly, the predicted tomograms were qualitatively in agreement with those obtained by radar testing. After the completion of this calibration exercise, predictions of saline breakthrough into the Validation Drift and the T1 and T2 boreholes were made, together with the radar tomograms of the spreading of the saline solution in the H zone.

Breakthrough of the Saline Tracer

The comparison between the predictions with the Golder model and the field measurements of saline breakthrough in RSTE-2 are summarized in Table 4-2, and illustrated in Figures 4-39 and 4-40. The predicted arrival times and concentration levels of the tracer in the drift agreed remarkably well with the measurements. The irregularities in the predicted breakthrough curve, shown in Figure 4-39, were a consequence of the limited number of particles injected into the H zone during the simulation. Nevertheless, curve-smoothing by interpolation yielded a good match to the observed breakthrough curve. The wide range in the predicted values of the arrival times was due to the effects of variations in transport aperture among the different realizations. The field measurements indicated that the tracer took a long time, 100 h to more than 1 000 h, to migrate to the T1 and T2 boreholes, with reasonably low steady-state concentrations. Although these predicted results were less satisfying from a quantitative viewpoint as compared to those for the drift, long arrival times and low concentrations were nevertheless indicated. The comparison between the predicted locations and concentrations of tracer arrivals in the Validation Drift with

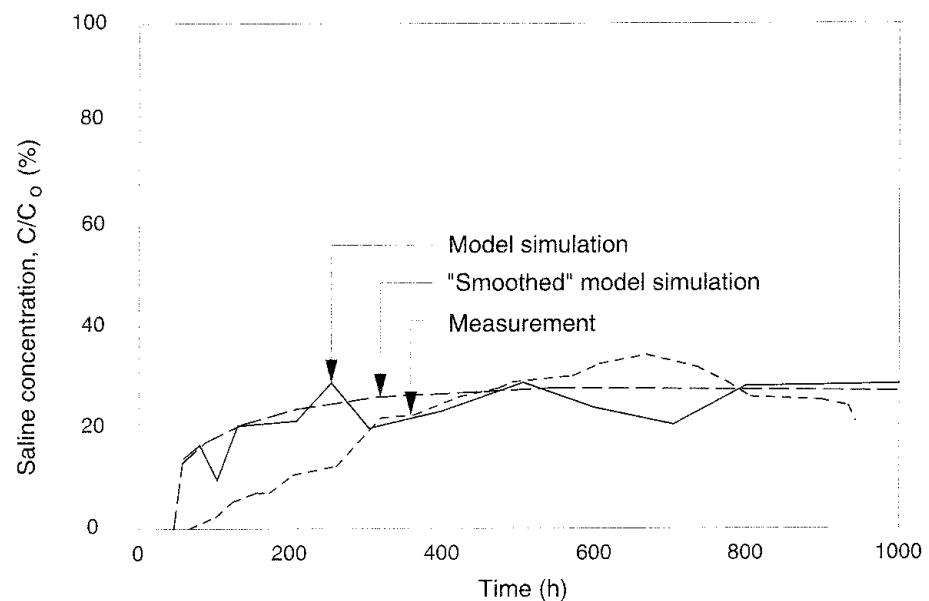
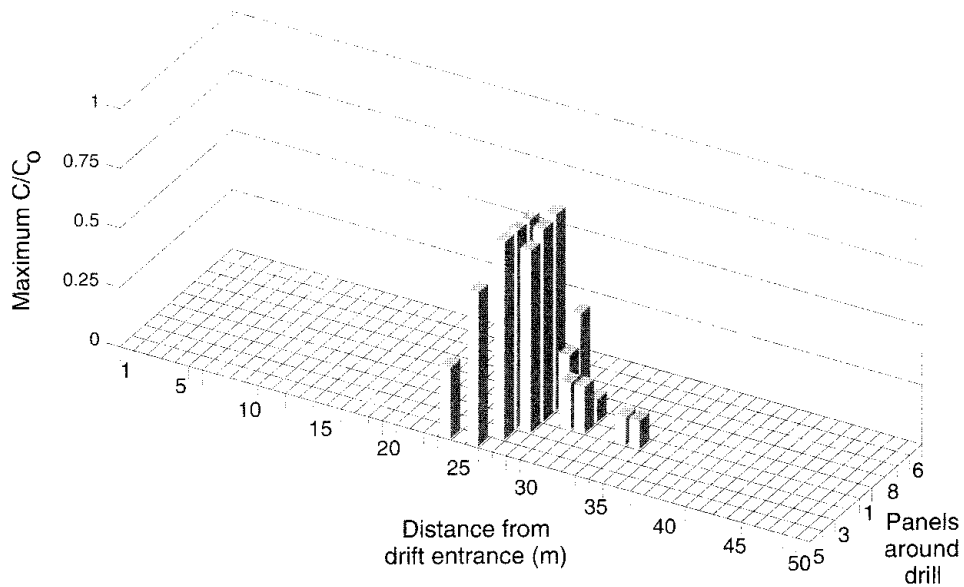
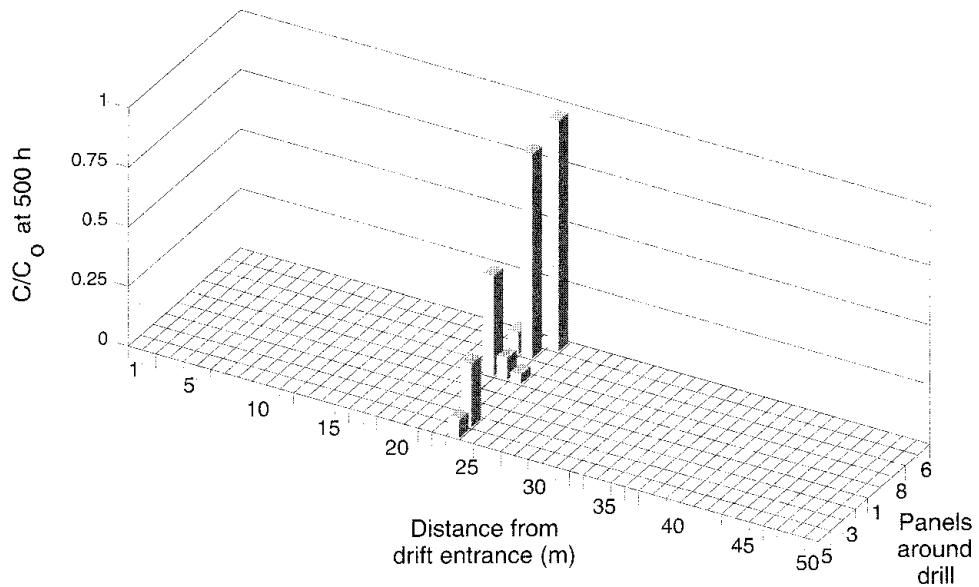


Figure 4-39 Comparison of predicted and measured saline concentration breakthroughs in the Validation Drift (Hodgkinson and Cooper, 1992b).



(a) Experimental measurements of maximum C/C_0



(b) FRACMAN simulation results for C/C_0 at 500 h.

Figure 4-40 Comparison of the predicted and measured distributions of saline tracer collected in the Validation Drift (Hodgkinson and Cooper, 1992b).

those measured in RSTE-2 are shown in Figure 4-40. In the field measurements, most of the saline tracer was collected in sheets that covered the H zone in the Validation Drift, with a few arrivals in the average rock near the contact. The predictions by the Golder group indicated that the tracer migrated entirely to the H zone intersection with the Validation Drift, and was concentrated in a more localized section of the drift on one wall.

Table 4-2 Comparison of predicted and measured breakthrough times and concentrations for the second Radar/Saline Tracer Experiment (Dershowitz et al, 1991; Hodgkinson and Cooper, 1991).

| Prediction | Parameter | Prediction | Measurement |
|---|-------------|--|--|
| T-1 Breakthrough to Drift | t_5 | 30 to 150 hours | 60 to 70 hours |
| | t_{50} | 100 to 150 hours | 125 to 150 hours |
| | C/C_0 | 0.3 to 0.4 | .36 to 0.40 |
| T-2 Breakthrough to T1 and T2 boreholes | T1 Borehole | t_5 =100 to over 1000 hours t_{50} =over 1000 hours C/C_0 =0 to 0.03 | t_5 =200 hours t_{50} =over 600 C/C_0 = 0.07 |
| | T2 Borehole | t_5 =100 to over 1000 hours t_{50} =over 1000 hours C/C_0 =0 to 0.03 | t_5 =450 hours t_{50} =over 1000 C/C_0 = 0.01 |
| T-3, T-4, T-5 Breakthrough to Grid Elements | | t_5 = 20 to 550 hours where measurable t_{50} = 200 to 500 hours where measurable C/C_0 = 0.01 to 1 where measurable | t_5 =50 to 500 hours t_{50} =96 to 800 hours C/C_0 =0.13 to 0.84 |

Simulated Tomograms

Simulated tomograms were developed for sections of rock lying in the planes defined by boreholes W1, C1, and C5. A comparison of the simulated tomogram for the C1-C5 plane with that obtained by borehole-radar testing is shown in Figure 4-41. The measured tomograms were based upon the difference in resistivity in the rock before and after saline injection. The simulated tomograms of saline concentration were approximated by particle locations in 2 m thick slabs around the tomographic planes. The prediction accurately portrayed the plume dimension within the H zone, approximately 40 m in width, and compared well with the responses that were observed in the other two planes.

General Remarks

Overall, the predictions by the Golder group for RSTE-2 compared quite well with the field measurements. This was also the case for the other modelling groups. Although the number of simulations was limited, the predictions were correct within the "order of magnitude" accuracy of the quantitative criteria for validation discussed in Section 4.1.3. The exercise demonstrated that the discrete-fracture approach was a workable method for predicting flow and transport on a scale of tens of metres in fractured rock similar to that of the SCV site, provided that errors in predicted concentrations of the order of 10% could be tolerated.

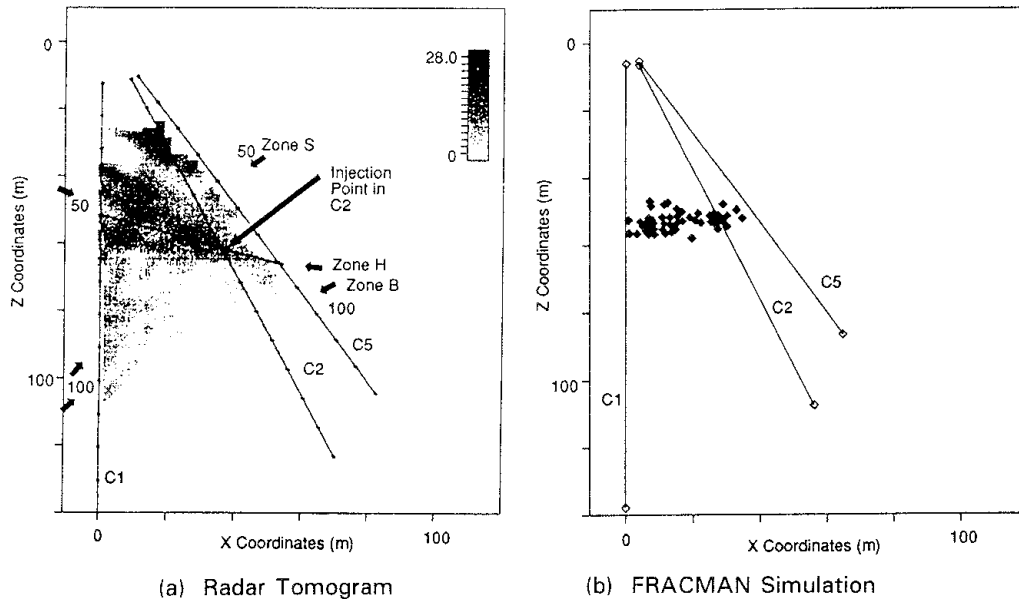


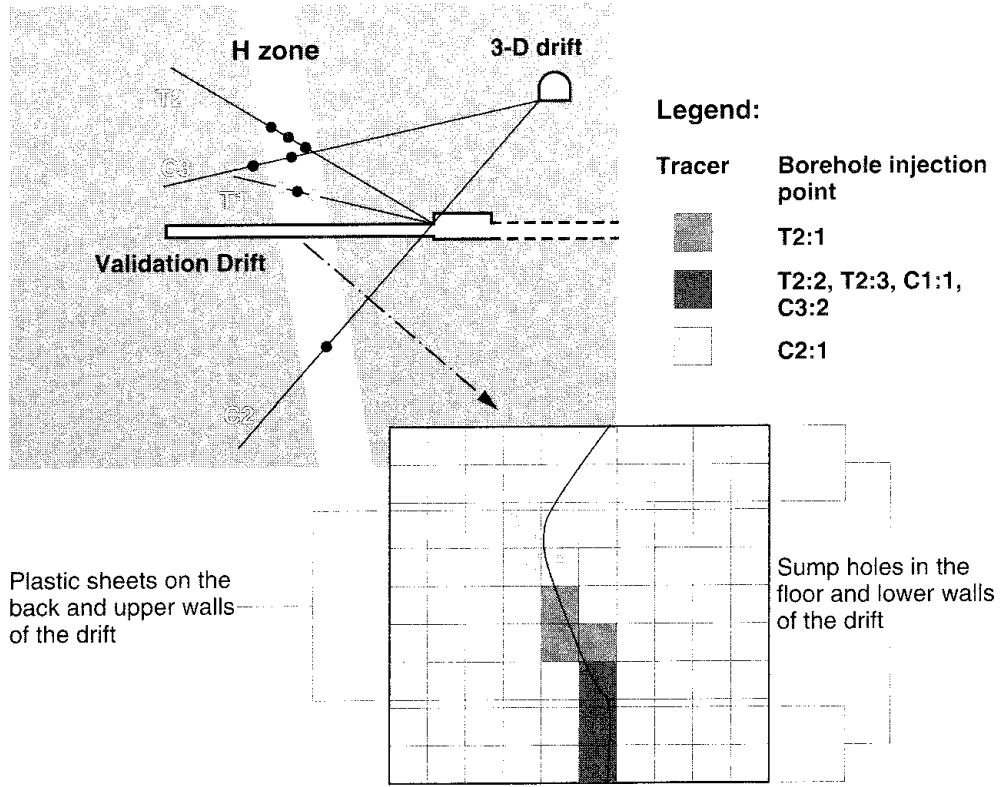
Figure 4-41 Comparison of the simulated and measured tomogram of the spreading of saline tracer in the plane between the C1 and C5 boreholes in the SCV site (Dershowitz et al, 1991a).

4.4.2 Tracer Migration Experiment

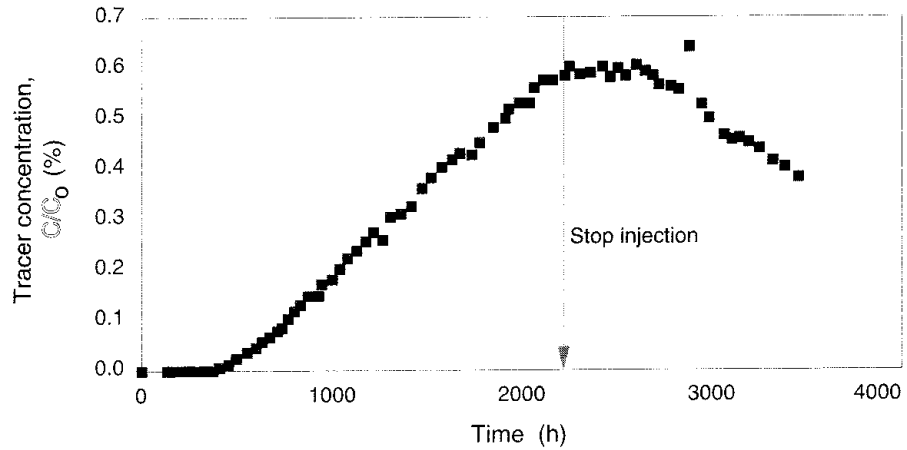
Following the completion of the Radar/Saline Tracer Experiments and the associated modelling exercise, the principal validation exercise for the transport models was initiated in conjunction with the Tracer Migration Experiment (TME). In the experiment, tracers were injected into the rock mass from sealed-off sections of the T1, T2, C2, and C3 boreholes, and collected principally in the Validation Drift and in the T1 borehole. As shown in Figure 4-42, eight of the nine injection intervals were located within the H zone, and one was located in the "average" rock. The distances from the injection intervals to the drift varied between 10 and 25 m. A mixture of two nonsorbing tracers, a metal complex and a dye, were injected at each interval at very low flow rates.

For purposes of assessing the validity of the transport models at the SCV site, the Task Force established the following performance measures for the TME and associated modelling exercise:

- Breakthrough curves for the arrivals of the different tracers in the Validation Drift from the injection intervals in boreholes T1, T2, C2, and C3 (quantitative)
- Breakthrough curves for tracer arrivals in borehole T1 from the injection interval in borehole T2 (quantitative)
- Breakthrough curves for tracer arrivals in interesting grid elements in the Validation Drift (quantitative/qualitative)



(a) Location of major tracer recovery in the Validation Drift



(b) Breakthrough curve for tracer injected in borehole T2

Figure 4-42 Schematic layout and typical results for the tracer migration test at the SCV site (Birgersson et al, 1992a,b).

- Box plots and histograms of the steady-state concentrations of the tracer arrivals (qualitative)
- Tomograms for the second radar/saline tracer experiment (optional).

Because of difficulties in deriving the observed steady-state concentrations, the box plots and histograms of the steady-state concentrations of the different tracer arrivals were not as useful as originally anticipated.

Breakthrough Curves

An example set of observed and predicted breakthrough curves is shown in Figure 4-43 for tracer injection in the first interval of borehole C2 and recovery in the Validation Drift. The experiment approached, but never achieved, a condition of steady state. The most striking feature of these

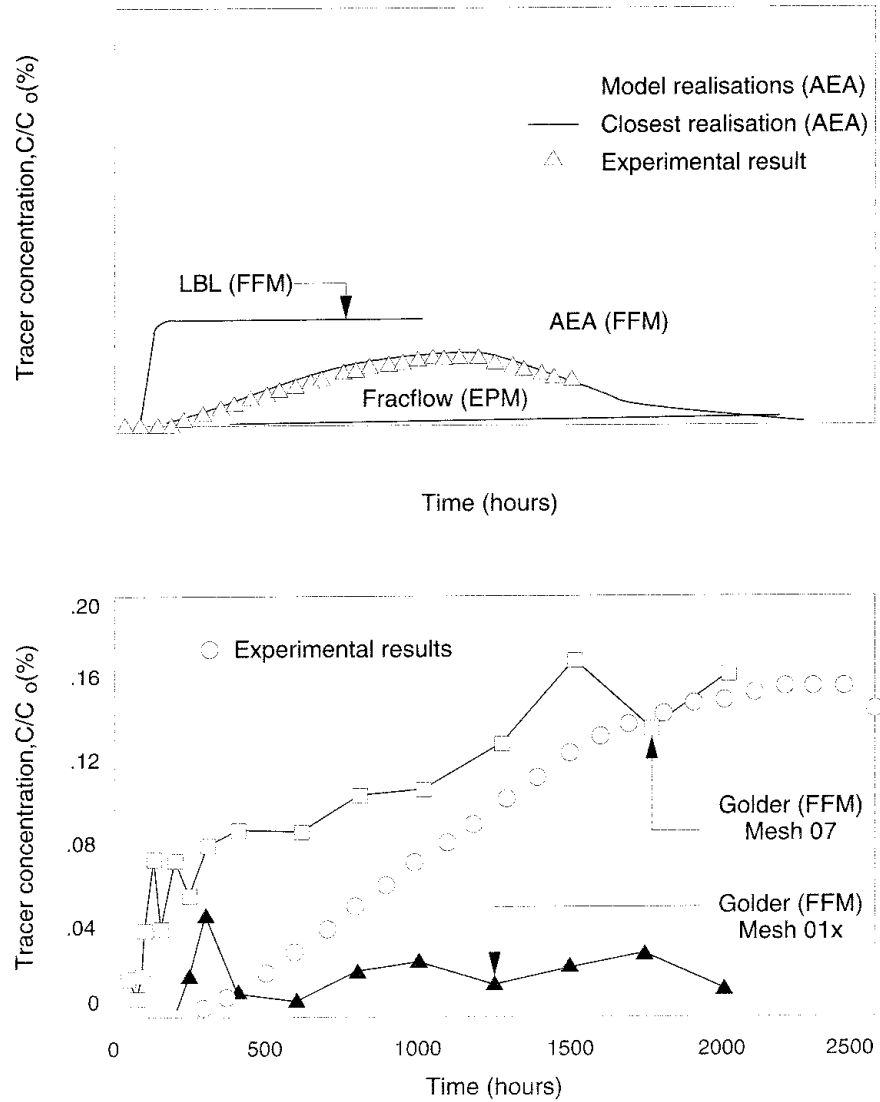


Figure 4-43 A comparison of the observed and predicted steady-state concentration ratios and breakthrough times for Dy tracer injected in the first interval of borehole C2 and recovered in the Validation Drift (Hodgkinson and Cooper, 1992b).

comparisons is the contrast in the shapes of the measured and predicted curves. In general, the measured curve exhibited a rather gentle slope that decreased as a condition of steady state was approached. On the other hand, the models commonly predicted much earlier arrivals of the tracers at a collection point, followed by a steep slope in the breakthrough curve that eventually leveled off to a condition of steady state. Some of the modelling groups used more than one conceptualization of the geohydrologic conditions in the experimental site. The LBL group used two two-dimensional configurations containing the H zone, where one of the configurations was annealed to the data from the C1-2 crosshole test and the other was co-annealed to data from both the C1-2 crosshole test and the SDE. The original Golder model assumed a boundary condition of zero head in the access drift on the 360 m level of the SCV site. In the conceptual model designated as Golder-X, the boundary condition of zero net flow was specified along this drift.

The observed and predicted values of the steady state tracer concentration, as well as the t_5 and t_{50} arrivals, are shown in Figure 4-44 for tracer injection in the first interval of borehole C2 and recovery in the Validation Drift. The t_5 and t_{50} arrivals correspond to the times at which the tracer breakthrough attains 5% and 50%, respectively, of steady-state conditions. Visual inspection of these comparisons indicate that there exists reasonable agreement between the measured and predicted steady-state concentrations of tracer, while the predicted tracer arrivals range from being quite early to approximately the same as measured.

Semi-quantitative comparisons of the predicted and measured steady-state tracer concentration ratios and the t_5 and t_{50} tracer arrival times are given in Tables 4-3, 4-4, and 4-5, respectively, for the suite of tracer migration experiments. The ranges of concentration ratios given in Table 4-3 represent lower-bound and upper-bound values. The maximum observed concentration provides a lower bound for the steady-state concentration ratio, based on the assumption that the breakthrough curve should have been monotonically increasing if the injection had been continuous. The upper bound for the total breakthrough was determined by first calculating the concentration if all the tracer had appeared in the drift, and, secondly, subtracting from this value all the observed (lower bound) mass flux at every other sampling area. For the six borehole-to-drift tracer experiments, the ratio of the upper bound to the lower bound was less than five, indicating that the instantaneous recovery in all experiments reached at least 20% of the injection rate. In the three tables, the first five sets of data represent experiments in which tracer was injected into the H zone from an intersecting borehole and recovered in the drift. The sixth set of data represents the experiment in which tracer was injected into the "average" rock from a borehole and recovered in the drift. The last set of data were obtained from the crosshole test in which different tracers were injected into the H zone from three different intervals in the T2 borehole and recovered in the T1 borehole.

As shown in Table 4-3, the measured steady-state tracer-concentration ratios for the H zone-to-drift experiments ranged from about 10^{-4} to slightly more than 10^{-3} . For this set of experiments, the predictions with the Harwell transport model fell within the ranges of the measurements. The agreement between measurements and predictions for the other three transport models,

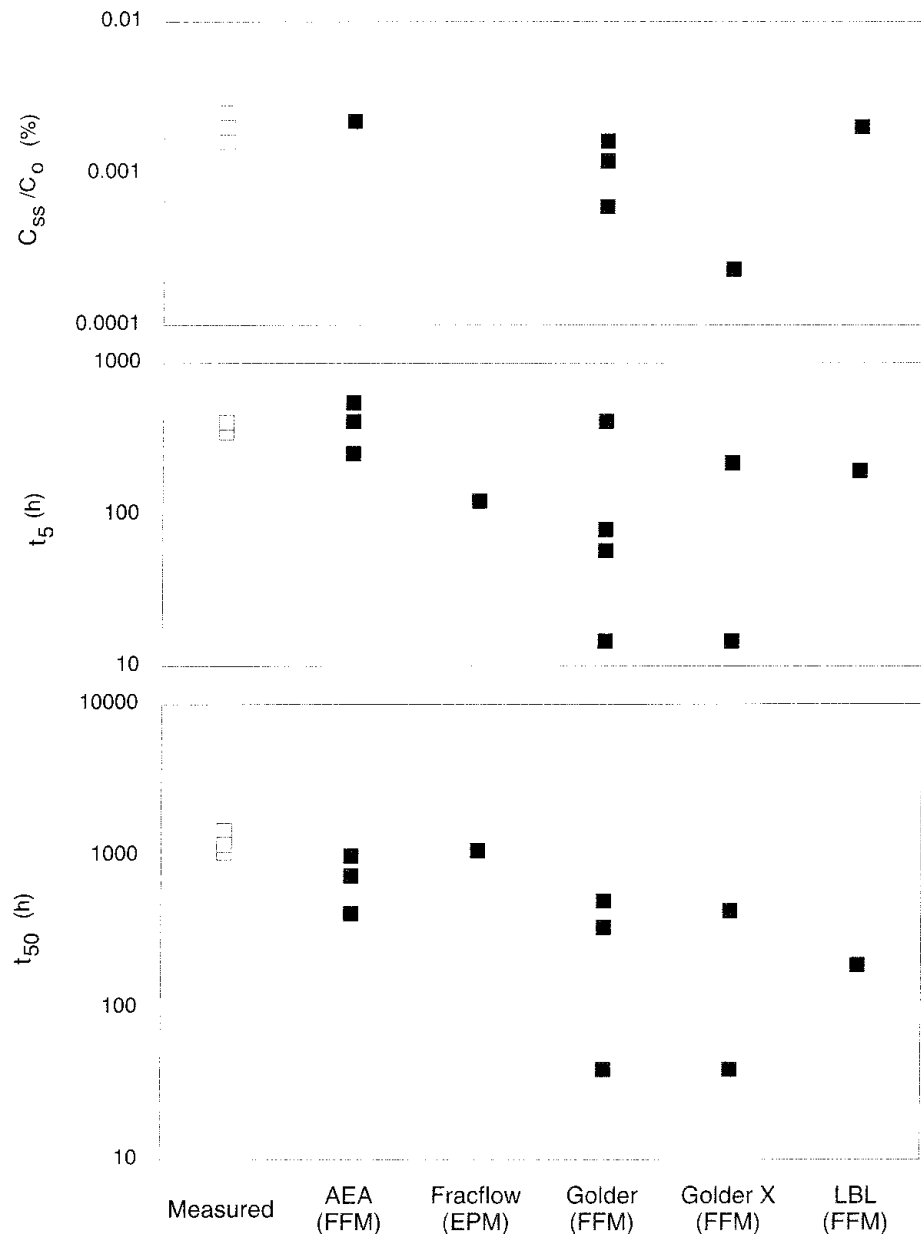


Figure 4-44 A comparison of observed and predicted breakthrough curves for Dy tracer injected in the first interval of borehole C2 and recovered in the Validation Drift (Hodgkinson and Cooper, 1992b).

however, was not comparatively as good. Some of the predictions fell within the range of measurements, while others yielded steady-state concentration ratios that were within an order of magnitude to greater than an order of magnitude less than those measured. For the average rock-to-drift experiment, the predictions with the Fracflow and Golder models fell within the range of the measurements, while the LBL model computation did not achieve a breakthrough of the tracer in the drift. The predictions by the Harwell and LBL models for the crosshole experiment gave values that were within the range of the measurements, while the Golder model underestimated the steady-state concentration ratio by an order of magnitude or more.

Table 4.3 Semi-quantitative comparison of predicted and measured steady-state tracer concentrations for the Tracer Migration Experiment.

"Within range" implies predictions were within the range of the measurements; "low" implies within an order of magnitude; "very low" implies greater than an order of magnitude (based on graphical comparisons from Hodgkinson and Cooper, 1992b).

| Borehole/Injection Interval to Recovery Point | Measurements (10^{-3}) | Transport Model Predictions | | | | |
|---|----------------------------|-----------------------------|--------------|---------------------|--------------------------|---------------------|
| | | Harwell | Fracflow | Golder | Golder-X | LBL |
| T1:2 to Drift | 0.38 - 0.667 | within range | low | within range to low | within range to low | within range to low |
| T2:1 to Drift | 1.43 - 2.92 | within range | within range | -- | -- | low to very low |
| T2:3 to Drift | 1.64 - 5.0 | within range | low | low to very low | within range to very low | -- |
| C2:1 to Drift | 1.6 - 2.5 | within range | -- | low to very low | low | within range |
| C3:1 to Drift | 0.16 - 0.667 | within range | within range | -- | -- | no breakthrough |
| C3:2 to Drift | 0.09 - 0.333 | -- | within range | within range to low | within range | no breakthrough |
| T2 to Borehole T1 (three injection intervals) | 2.1 - 26 | within range | -- | low to very low | very low | within range |

As indicated in Tables 4-4 and 4-5, the predictions of the tracer arrivals at the recovery points were generally faster than observed by about an order of magnitude. The Golder model consistently predicted early to very early arrivals, by as much as an order of magnitude or more. This was also the case for the Fracflow EPM model, except for the borehole C2-to-drift experiment in which the straight-line pathway distance was the greatest as compared to the other experiments. The predicted arrival times from the Harwell model agreed with the measurements in about 30% of the cases, with the remainder being commonly early within an order of magnitude of that observed. The predictions of tracer arrival times with the LBL model varied from early, to on time, to late, to no breakthrough. Generally speaking, the Harwell, Fracflow, and Golder models predicted that the transport was faster than observed. These models also underpredicted the dispersion, whereby predictions of the arrival times t_{50} were greater underestimates, by at least an order of magnitude, than observed. On the other hand, the LBL model tended to overpredict the early breakthrough, but, because of the lack of dispersion in the model, tended to give reasonably accurate predictions of the later t_{50} breakthrough time.

Table 4-4 Semi-quantitative comparison of predicted and measured tracer t_s arrivals for the Tracer Migration Experiment.

"On time" implies that the prediction was within range of the measurements; "early" and "late" imply within an order of magnitude; "very early" implies greater than an order of magnitude (based on graphical comparisons from Hodgkinson and Cooper, 1992b).

| Borehole/Injection-Interval to Recovery Point | Measurements (hr) | Transport Model Predictions | | | | |
|---|-------------------|-----------------------------|------------|-----------------------|---------------------|-----------------|
| | | Harwell | Fracflow | Golder | Golder-X | LBL |
| T1:2 to Drift | 500 - 600 | early | early | early | early | on time to late |
| T2:1 to Drift | 250 - 350 | on time to early | early | -- | -- | early to late |
| T2:3 to Drift | 700 - 950 | early | early | early | early | -- |
| C2:1 to Drift | 350 - 400 | on time | early | on time to very early | early to very early | early |
| C3:1 to Drift | 350 - 500 | early | early | -- | -- | no breakthrough |
| C3:2 to Drift | 1,200 - 1,750 | -- | very early | early | very early | no breakthrough |
| T2 to Borehole T1 (three injection intervals) | 110 - 280 | on time | | early to very early | early to very early | on time |

Table 4-5 Semi-quantitative comparison of predicted and measured tracer t_{50} arrivals for the Tracer Migration Experiment.

"On time" implies that the prediction was within range of the measurements; "early" and "late" imply within an order of magnitude; "very early" implies greater than an order of magnitude (based on graphical comparisons from Hodgkinson and Cooper, 1992b).

| Borehole/Injection-Interval to Recovery Point | Measurements (hr) | Transport Model Predictions | | | | |
|---|-------------------|-----------------------------|------------|---------------------|---------------------|------------------|
| | | Harwell | Fracflow | Golder | Golder-X | LBL |
| T1:2 to Drift | 1,950 - 3,150 | very early | very early | very early | very early | on time to early |
| T2:1 to Drift | 1,000 - 2,150 | early | early | -- | -- | on time to early |
| T2:3 to Drift | 1,700 - 2,150 | early | very early | early to very early | early to very early | -- |
| C2:1 to Drift | 1,050 - 1,500 | on time to early | on time | early to very early | early to very early | early |
| C3:1 to Drift | 750 - 900 | early | early | -- | -- | no breakthrough |
| C3:2 to Drift | 2,800 - 4,300 | -- | very early | early to very early | early to very early | no breakthrough |
| T2 to Borehole T1 (three injection intervals) | 230 - 400+ | on time | -- | early to very early | early | early |

Distribution of Recovered Tracers

A comparison of the measured and predicted histograms of the t_{50} breakthrough of Dy tracer in the Validation Drift for injection in borehole C2 is shown in Figure 4-45. The predicted histograms by the Harwell and Golder models show that the tracer was collected at the intersection of the H zone with the Validation Drift, but the number and distribution of panels in which the tracer was collected varies between model predictions and observations. This variance suggests that the pathways simulated by the models did not correspond directly with those that existed in the H zone. This premise is supported further by the histograms shown in Figure 4-46, in which the breakthrough times to individual sheets predicted by the Golder model are displayed as histograms in terms of a probability density. Although the histogram patterns tended to be similar to those observed, the number of panels, in which tracer was recovered, was less, typically twelve as compared to about thirty.

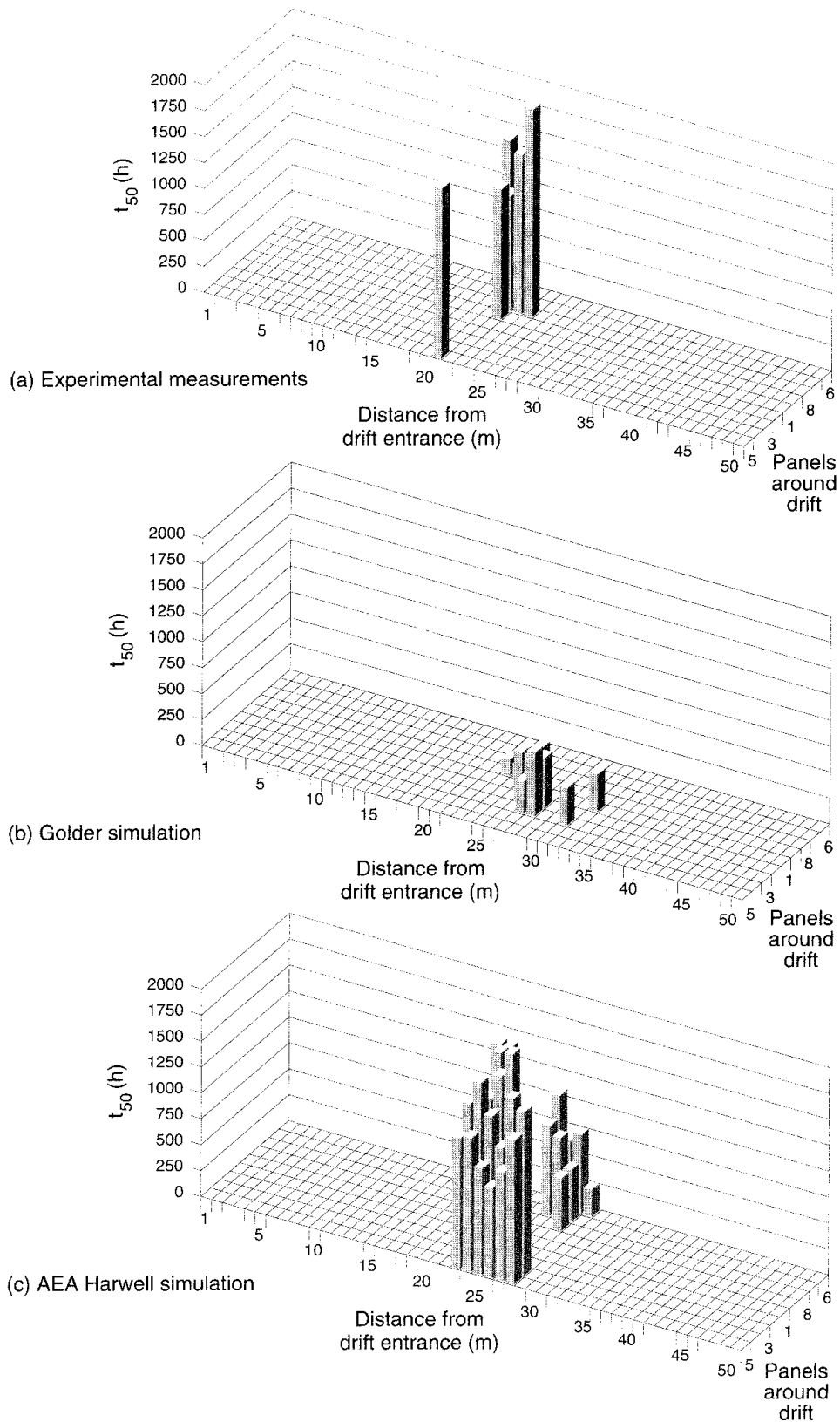


Figure 4-45 Comparison of the measured and predicted histograms of the t_{50} breakthrough for the Dy tracer injected in the first interval of borehole C2 and recovered in the Validation Drift (Dershowitz and Wallman, 1992; Herbert and Lanyon, 1992).

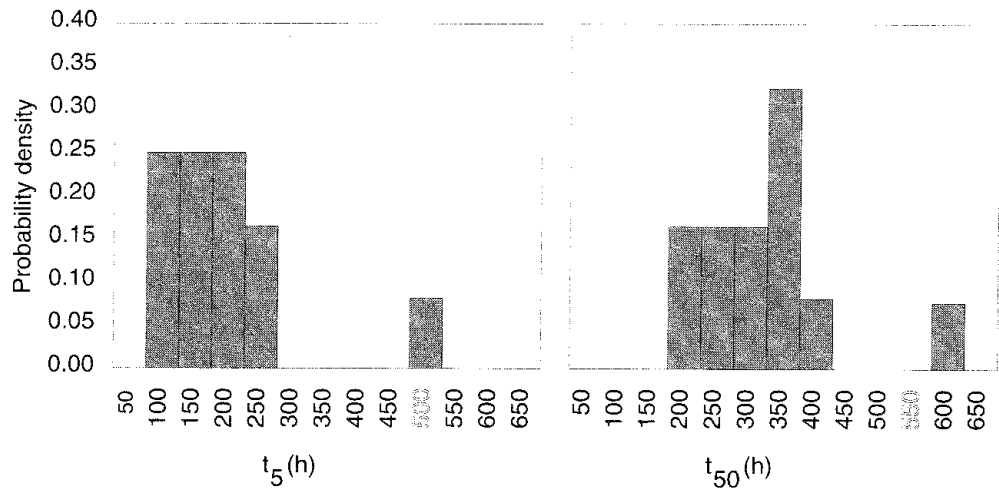


Figure 4-46 Histogram of the predicted breakthrough times by the Golder model for individual sheets in the Validation Drift for tracer injection in borehole C2 (Dershowitz and Wallman, 1992).

Simulated Tomograms for the Radar/Saline Tracer Experiment

Tomograms for the second radar/saline tracer experiment were developed by the modelling groups at Golder and LBL. As discussed previously and shown in Figure 4-41, the prediction with the Golder model accurately portrayed the dimension of the saline plume within the H zone, and gave a strong, clear response in the plane defined by the W1 and C5 boreholes and a weak response in the plane defined by the W1 and C1 boreholes. The prediction with the LBL model was restricted to a tomogram of only the H zone, and gave good agreement with the radar measurements on the spread of tracer throughout the zone from the injection point in borehole C2.

General Discussion

The groundwater flow field used by the Harwell transport model was such that all the tracer migrated to the drift. Thus, as expected, the predicted tracer concentrations agreed well with those observed, except when the recovery was low. The simulation of the transport of tracer from borehole C2 to the drift was particularly accurate, probably due in part to the fact that this was the injection interval in the second Radar/Saline Tracer Experiment used for calibration. For the crosshole experiment, the predicted tracer breakthrough times agreed well with those observed, and the concentrations were within the range of those measured. However, in this computation, the Harwell group had the advantage of prior information on the rate of groundwater inflow to borehole T1. In those instances where the predictions fell outside the range of the observations, they, nevertheless, were within an order of magnitude of the observations. The pattern of recovery in the Validation Drift as predicted exhibited a slightly higher density of panels receiving flow than was observed, but the agreement still was generally good.

Overall, the predictions of the steady-state tracer concentration ratios predicted by the Fracflow EPM model were in good agreement with those observed or, at most, within an order of magnitude. However, this model consistently underestimated the first arrival of a tracer, within an order of magnitude, and, in some instances, subsequent arrival times on the breakthrough curves by more than an order of magnitude. It must be kept in mind, however, that the degree of discretization of the H zone and the surrounding rock mass was considerably less with the EPM model than with the fracture flow models. Considering this caveat, the agreement between the predictions with the EPM model and the observations was reasonably good.

The predictions with the Golder model generally exhibited a wider spread in the predicted ranges of steady-state tracer concentration ratios and tracer breakthrough times than observed in the experiments. This leads to the conclusion that the model contained more heterogeneity in the H zone than was observed. However, the average predictions were, for the most part, within an order of magnitude of the measurements. The tendency for the model to underestimate travel time may be a consequence of the choice of the transport aperture. However, a change in this parameter would probably impact the goodness of the match between the predictions and observations for the second Radar/Saline Tracer Experiment. Furthermore, an increase in the value of dispersivity would probably decrease the steep slopes of the breakthrough curves.

The range of predictions for a given experiment by the LBL modelling approach was commonly large, often encompassing the observations. The use of two configurations of the conceptual model, based on annealing with two separate data sets, often both overestimated and underestimated the steady-state tracer concentration arrivals and travel times. The coarse discretization, along with the assumption of zero dispersivity, yielded breakthrough curves with steep slopes.

The tracer breakthrough curves obtained from experimental measurements in the Validation Drift represented the actuality of the transport features of the rock mass. On the other hand, the predicted curves were based on different realizations using the stochastic fracture parameters developed on the basis of characterization data obtained at the SCV site. The fracture-network models predicted a range of breakthrough curves, reflecting the stochastic nature of the fracture network and the meta stability of the groundwater flow. The field measurements showed that the instantaneous recovery in the drift for each of six injections, after an elapsed ejection time of 2 000 hours, ranged from 8% for injection in the "average" rock to 61% for injection in the H zone. The predictions of tracer breakthrough by the Golder model, as for example shown in Figure 4-43, for an individual injection location indicated a similar spread in instantaneous recovery. Likewise, the Harwell model gave a range in instantaneous recoveries that varied from realization to realization. The point of this discussion is to emphasize that predictions made stochastically will yield ranges of values for the deterministic measurement that was made in the experiment. If the data set for the characteristics of the rock mass was adequately robust, then there should exist some quantifiable probability that the model simulation would reproduce the major features of the field measurement.

4.5 EVALUATION OF MODEL VALIDITY

After the modelling predictions had been completed and evaluated against the experimental measurements, the Task Force arrived at a consensus judgement on the validity of each modelling approach (Hodgkinson, 1992). The criteria for these judgmental assessments were discussed in Section 4.1.3. It must be clearly emphasized that, for such assessments, the Task Force addressed the validity of the models as applied specifically to the simulation of groundwater flow and solute transport at the SCV site in the Stripa mine. The questions of usefulness and feasibility of the models were viewed from the context of potential applications to other sites and rock types. However, the answers to these questions must be viewed as pertaining to sites and rock types that are generally similar to those investigated at Stripa.

The judgments of model validity made by the Task Force are given in Figure 4-47. For purposes of application to the SCV site, all of the modelling approaches were judged to provide predictions that were of the correct order of magnitude as compared to the experimental measurements. However, it must be noted that the treatment of excavation effects on groundwater inflow to a drift was not entirely satisfying, and there existed a tendency to underestimate the time required for a tracer to migrate from the point of injection to the point of recovery. In all fairness, an adequate treatment of excavation effects must be based on the outcome of experiments that specifically address such factors as stress redistribution in a fractured rock mass, the development of partially saturated or nonsaturated zones in the walls of the excavation, and the degasification of water because of the abrupt pressure drop in the near-field zone around the excavation. The underestimation of travel time during transport may be corrected by further consideration of more appropriate values for dispersivity.

The qualitative criterion for model validity requires a judgement of the reasonableness of the predictions of the distribution patterns of phenomena when compared to the observations. The Task Force framed their judgements according to the near-field and far-field geometric zones of application of the models. The near-field was taken to be that mass of rock situated between the drift wall and some imaginary boundary located several excavation diameters into the rock mass. The far-field was taken to be rock located on the other side of the imaginary boundary. The Fracflow EPM model was judged to provide reasonably correct patterns of phenomena in the far-field, but was lacking in that capability in the near-field. The accuracy of the patterns of phenomena in the near-field was probably related closely to the degree of discretisation of the rock mass into finite elements. That is, the reasonableness would be expected to improve in direct proportion to an increasing degree of finer discretisation. On the other hand, the Harwell fracture-flow model was judged to have the capability to predict reasonably accurate patterns of phenomena in the near-field, but lacking in such capability in the far-field. The principal difficulty with the far-field aspect of this modelling approach lies with the requirement for a tremendous amount of computer storage. This requirement is necessitated by the very detailed modelling stochastically of the fracture network within a rock mass. With the computer capability that exists today, it would be impractical to attempt to model a fractured rock mass with the geometric

| Validation criteria | Modelling group | | | |
|--|--|-----------------------------------|-------------------------------------|--------------------------------|
| | Fracflow Consultants (equiv. porous media model) | AEA Harwell (fracture flow model) | Golder Assoc. (fracture flow model) | LBL (fracture flow model) |
| Quantitative (correct order of magnitude?) | Yes | Yes | Yes | Yes |
| Qualitative (reasonable patterns of phenomena?) | Near field: No (by definition) | Near field: Yes | Near field: Yes | Near field: No (by definition) |
| | Far field: Yes | Far field: No (by definition) | Far field: Yes | Far field: Perhaps |
| Usefulness (modelling approach useful elsewhere?) | Near field: ? | Near field: Yes | Yes | Potentially |
| | Far field: Yes | | | |
| Feasibility (Feasible to collect input data?) | | Near field: Yes | Near field: Yes | |
| | Far field: Yes | Far field: Possibly | Far field: Yes | Far field: Yes |

Figure 4-47 Final assessment of model validity by the Task Force on Fracture Flow Modelling (Hodgkinson, 1992).

When the AEA Harwell fracture-flow model is used together with the Fracflow EPM model, the answer is Yes to all criteria. It should be noted that the LBL fracture-flow model requires groundwater flow data, while the other models use principally data for the hydraulic properties and fracture characteristics.

dimensions of the SCV site. However, when the Harwell fracture-flow modelling approach was used in concert with the Fracflow EPM modelling approach, the combination of approaches provided predictions of distribution patterns of phenomena throughout the SCV site that were reasonably accurate when compared to observations.

The Golder approach to modelling groundwater flow and transport in a saturated, fractured rock mass was judged to provide reasonably accurate predictions of phenomena in the near-field and far-field regions of the SCV site. This approach allows deterministic features to be incorporated into the model, along with stochastically generated fracture networks in regions of principal interest. In fact, because of the rather robust geometric

dimensions of the conceptualization, careful attention must be paid to the selection of hydraulic boundary conditions in drifts and boreholes on the outer fringes of the model. This was indeed the situation in the application of this model to the Tracer Migration Test, where the choice of the boundary condition in the 3-D migration drift had a significant influence on the predictions of tracer concentrations and arrivals in the Validation Drift. The approach used by the LBL group for modelling fracture flow in the SCV site was judged to be inappropriate for predicting patterns of phenomena in the near-field, and to be somewhat questionable for predicting such patterns in the far-field. By design, this modelling approach considered only groundwater flow and transport through deterministic fracture zones, and assumed that the rock mass between fracture zones was impermeable. As a consequence, this approach was never intended to provide distribution patterns of phenomena in the near-field for the SCV site, and was never advertised as such. While the Task Force felt that the modelling approach had the potential to reproduce global patterns of heterogeneity within fracture zones in the SCV site, the number of realizations for the experiments was insufficient to demonstrate that the approach was capable of producing consistent patterns.

From the viewpoint of the usefulness of a modelling procedure for representing groundwater flow and solute transport in a geohydrologic environment similar to that at the SCV site, the Task Force concluded that the EPM approach used by the Fracflow group was useful in the far-field and the approach used by the Harwell group was useful in the near-field. Conversely, use of the Fracflow approach in the near-field and the Harwell approach in the far-field was considered to be questionable, for essentially the same reasons as given above when discussing the capabilities of the models for predicting reasonably accurate patterns of phenomena. However, the combination of the two modelling approaches, when applied in an integrated manner, was considered to be useful. The Golder approach to fracture-flow modelling was judged to be useful, particularly because it effectively links together the local and global features of a saturated, fractured rock mass. The Task Force judged the fracture-flow modelling approach used by the LBL group to be potentially useful. Once again, this judgement was necessitated by the lack of a demonstration of usefulness at the SCV site because of an inadequate number of realizations when making the predictions.

The last criterion dealt with the question of whether the characterization data required to fully support a modelling approach could be collected in a feasible and timely manner. It was the consensus judgement of the Task Force that the necessary data could indeed be collected in a feasible and timely manner for each of the modelling approaches. This facet was indeed demonstrated in the SCV programme over its five-year duration. However, it must be kept in mind that the data required to support the LBL model are principally the products of hydraulic head testing in a groundwater system, while the data necessary to support the other three modelling approaches are derived from fracture mappings and hydraulic packer tests. Finally, the answer to feasibility is convincingly more positive when the Fracflow EPM model and the Harwell fracture-flow model are used in a complimentary manner, than when used separately.

4.6 SUMMARY OF ACHIEVEMENTS

The evaluation of the validity of models for groundwater flow and transport in a saturated, fractured rock mass was an integral part of the SCV programme. To this end, the Task Force on Fracture Flow Modelling, in concert with the principal investigators for the characterization and modelling activities, developed and implemented a formalized process for evaluating the validity of models that were applied at the SCV site. The process involved definition of the appropriate measures for evaluation, including the scope of the evaluation, and criteria against which the validity of the various models and modelling approaches could be judged by a group of knowledgeable experts. As demonstrated, the process required close cooperation and coordination among the experimentalists, modellers, and experts. At the close of the SCV programme, the experts made documented judgements of the validity of the various approaches for modelling groundwater flow and solute transport in the SCV site, and the usefulness of applying those models to other sites and rock types, together with the feasibility of obtaining the required information to support the modelling approaches. In terms of significance, this effort over a period of about five years constitutes a case-history example of a formalized and deliberate approach for evaluating the validity of numerical models for a very specific application.

5 CONCLUDING REMARKS

Over a period of some thirteen years, the development of tools and techniques to characterize the natural barriers at Stripa evolved through successive stages of learning, development, and application. Although this evolution of activities was not perceived as such at the outset of the Stripa Project in 1980, it did take place through the collective thinking and efforts of the group of geoscientists from seven to nine countries who were responsible for the planning, review, investigation, and management facets of the project. Many of the significant achievements from the many investigations throughout the years did not become apparent until the last years of the project when the various aspects of the SCV programme were drawn together into the final reports. These achievements can be summarized according to their contribution to site characterization in general and to characterization of saturated, fractured granitic rock in particular. Finally, some comments on the potential transfer of technology from the Stripa work to other rock types and conditions are provided.

5.1 SUMMARY OF SIGNIFICANT ACHIEVEMENTS

From the particular viewpoint of the characterization of a saturated, fractured granitic rock mass, the significant achievements of the Stripa Project were:

- **Development of a suite of tools and a focussed strategy for geohydrologic characterization.** This suite of tools included the radar, seismic, and hydraulic methods for both single-borehole and crosshole testing, as well as borehole photography and drill-core observations. For site conditions similar to those encountered at Stripa, tests in boreholes spaced as much as 200 m apart can be expected to provide data to identify the principal structural features and hydraulic anomalies. The characterization strategy would involve first identifying the distribution of major features within the rock mass from a combination of data obtained by single-borehole radar reflection testing and tomographic inversion of crosshole radar and/or seismic data. This would be followed by a combination of single-borehole and crosshole hydraulic tests for the purpose of describing the distribution of the hydraulic properties of the structural features and the "average" rock. In particular, much of the hydraulic testing would be focussed on structural features that are expected to be the principal conduits for the transport of groundwater.
- **Development of methods and techniques for geochemical characterization.** This work involved the development and implementation of methods and techniques to determine the age, or residence time, and origin of the groundwaters in the granitic rock mass at Stripa. A principal technique involved the identification of concentrations of key radionuclides and a reliable computation of the

background concentrations of these radionuclides due to subsurface equilibrium production.

- **Demonstration of the applicability of the equivalent porous media (EPM) approach for simulating groundwater flow and transport.** The EPM modelling approach was used to simulate groundwater flow and transport in the Stripa area, the Stripa mine, and a portion of the mine containing the SCV site. These models represented volumes of rock ranging from about 300 billion cubic metres to some five million cubic metres. The calculations of groundwater flow into the mine agreed quite well with the measured pumping rate when the models for the Stripa area and the Stripa mine were used. This agreement is a significant achievement, considering the dimensions of the areas modelled and the relative sparseness of the geologic information and hydraulic data. The predictions of groundwater flow and solute transport within the SCV site for the validation experiments also were reasonably good, considering the relatively coarse discretisation of the rock mass as compared to the dimensions of the Validation Drift.
- **Demonstration of the applicability of the fracture flow modelling for simulating groundwater flow and transport.** Three fracture flow modelling approaches were used with reasonable success to simulate groundwater flow and solute transport within the SCV site. The approaches differed in the manner in which the fracture networks were constructed, in the extent of the regions modelled within the site, and in the types of input data required from the characterization activities. The combination of approaches and the differences among them provided a rather robust demonstration of modelling capability and usefulness.
- **Specification of requirements for design of a tracer test to identify groundwater flow paths.** The tracer tests at Stripa have demonstrated the importance of understanding the groundwater flow field and the potential pathways in a rock mass prior to conducting a tracer test. There is little hope for quantifying the migration characteristics of a pathway unless the geometric aspects of the pathway and the generalized groundwater flow field within the pathway are defined before the tracers are injected into the pathway. These types of information can be obtained through the integrated use of the radar, seismic, and hydraulic borehole-testing methods. In addition, the sorbing characteristics of the tracer substances must be determined *a priori* in the laboratory.
- **Demonstration of the influence of the "disturbed" zone around an underground drift on groundwater inflow.** The groundwater inflow to the Validation Drift at the SCV site was almost an order of magnitude smaller than that measured previously in the D boreholes which outlined the drift periphery before excavation. However, the circumstances that caused the reduced inflow could not be identified, even when the stress redistribution, gas bubbles in the water, desaturation, etc., were considered. This unexplained effect was also observed at the site of the 3-D Migration Drift in the Phase 2 investigations. These observations will form a basis for designing experiments in the future to obtain a quantitative understanding of the

influence of the disturbed zone on groundwater flow into and around an underground excavation.

From the viewpoint of the characterization of other rock types at other sites, the significant achievements from the Stripa Project can be summarized as follows:

- **Demonstration of a programme of progressive site characterization.**
The SCV site encompassed some one million cubic metres of rock and was characterized in progressive stages over a period of about five years. Based on remote-sensing data from only five boreholes in the site during the first stage of characterization, it was possible to identify the locations of the principal structural features and hydraulic anomalies. This information provided a basis for deciding upon the orientation and length of boreholes to be drilled for the specific purpose of more detailed characterization of these features and anomalies. The test data from these additional boreholes subsequently provided the basis for determining the dimensions of the Validation Drift that was constructed in the SCV site and for the designing the groundwater flow and tracer tests in the rock mass surrounding the drift. At the outset of the SCV programme, it had already been decided that these tests would be conducted in the last stage of the programme. However, the specific details of the tests could not be determined until the principal structural features and hydraulic anomalies within the site area had been identified and initially characterized.
- **Procedure for development of a conceptual geohydrologic model.**
During the mid-years of the Stripa Project, the principal investigators developed conceptualizations of the geohydrology of the Stripa area and the Crosshole site in the Stripa mine. The conceptual model of the Crosshole site was developed principally to illustrate the integrated use of core logs, borehole photography, and single-borehole and crosshole testing with radar, seismic, and hydraulic techniques. The conceptualization of the Stripa area was developed principally to complement the characterization work that was being initiated at the SCV site, as well as to illustrate how the large collection of geologic, hydrologic, and geochemical data for the general area and the mine could be assembled together in a consistent and realistic fashion. During the early stages of the SCV programme, a conceptualization of the geohydrology of the SCV site was developed on the basis of core logs, drift mappings, borehole test data, and the information provided by the conceptual model of the Stripa area. In the later stages of the SCV programme, as more data was obtained from additional boreholes, the conceptualization of the geohydrologic characteristics of the SCV site was refined. As a consequence of these efforts, a procedure for the rational and consistent development of a conceptual geohydrologic model of a rock mass evolved. This procedure incorporated testing techniques and methods, consistency checks, and decision points concerning the need for more data. Although the intended use of a conceptual model will differ from site to site, and necessarily the amount of data required for details and consistency checks, this case history does serve as an example of a rational and systematic process for the development of a conceptual geohydrologic model.

- **Demonstration of a process for evaluating the validity of numerical models.** An evaluation of the validity of numerical models of groundwater flow and solute transport at the SCV site was an integral part of the SCV programme. To this end, the JTC established the Task Force on Fracture Flow Modelling, consisting of recognized experts from the member countries. The Task Force, in concert with the principal investigators for the characterization and modelling activities, developed a formalized process for evaluating the validity of the models that were applied at the SCV site. The process involved definition of the appropriate measures for the evaluation, including the scope of the evaluation, and criteria against which the validity of the various models and modelling approaches could be judged by the Task Force. The process required close cooperation and coordination among the experimentalists, modellers, and experts. At the close of the SCV programme, the Task Force made documented judgments of the validity of various approaches for modelling groundwater flow and solute transport in the saturated, fractured granite at the SCV site. This effort constituted a case-history example of a formalized and deliberate approach for evaluating the validity of numerical models for a very specific application.

5.2 TRANSFER OF TECHNOLOGY

The original goals of the Stripa Project in 1980 involved the development of techniques to characterize crystalline rock masses that were potentially suitable for development as geologic repositories for the disposal of high-level radioactive wastes. The Stripa mine was considered to be the test site for the development of such characterization techniques. Technique development began as a "learning exercise" in 1980, and evolved, initially in 1983, into technique improvements at the Crosshole site and the 3-D tracer-migration site, and, finally in 1985, into technique applications at the SCV site. The emphasis on "data gathering to understand conditions and processes" in the early 80's evolved during the late 80's into an emphasis on "data gathering to support model development and evaluations of model validity". During the thirteen years of investigative effort, the focus on technique development for crystalline rock, in particular saturated, fractured granite, gradually expanded to include the question of "how can the Stripa technology be applied to other rock types in other site areas?"

The application of the characterization tools and techniques to other rock types and conditions in other site areas is related to the particular characteristics of the rock mass under consideration. The success of the borehole-radar testing technique depends on the dielectric constant of the rock, and, likewise, the success of the borehole-seismic testing technique depends on contrasts in sonic velocity within the rock mass. A programme of hydraulic testing has to be adapted to conditions of saturation or non-saturation within the rock mass, as well as to the existence, or lack thereof, of structural features like zones of intense fracturing. The continuity of the fracture zones, as well as the characteristics of the fractures, depends on the ductility of the rock and the past tectonic history of the area. The success of a hydrogeochemical investigation in other site areas will depend, of course, on the water content in the rock mass, and, from the viewpoint of the work at Stripa, on the uranium content of the rock.

For purposes of design reference, the tracer tests at Stripa involved three scales of dimension. The single-fracture tests were conducted over a scale of a few metres, while the 3-D migration test involved a scale that ranged from principally from tens of metres and to more than 100 m. At the SCV site, where the fracture zone of interest was well characterized and the test conditions were well controlled, the scale of the tracer tests was on the order of tens of metres. Clearly, channelling may not be present in some rock types, such as evaporites. Also, retardation mechanisms can vary, in that some rock types will possess little or no capability for matrix diffusion.

For the purpose of modelling groundwater flow and solute transport at Stripa, the equivalent-porous-media model was shown to be applicable for modelling large-scale regions, where fracture dimensions were small as compared to the dimensions of the region. This modelling approach was also useful for providing boundary conditions for the more localized fracture-flow models. In general, it would appear that the fracture-flow models would be practical to apply when the number of fractures carrying water is small as compared to the total number of fractures existing within the site. Because of the relatively large computer-storage requirements required by these models, particularly when the fracture density of a rock mass is high, the integrated use of an equivalent-porous-media model in the far-field and a fracture-flow model in the near-field appears to be the most practicable.

REFERENCES

- Abelin, H. and Birgersson, L. (1987). 3-D migration experiment - report 1: site preparation and documentation. Stripa Project TR 87-19, SKB, Stockholm, Sweden.
- Abelin, H. and Gidlund, J. (1985). Migration in a single fracture - instrumentation and site description. Stripa Project IR 85-02, SKB, Stockholm, Sweden.
- Abelin, H. and Neretnieks, I. (1981). Migration in a single fracture - preliminary experiments in Stripa. Stripa Project IR 81-03. Swedish Nuclear Fuel Supply Co./Division KBS, Stockholm, Sweden.
- Abelin, H., Birgersson, L., and Ågren, T. (1990a). The channeling experiment - instrumentation and site preparation. Stripa Project TR 90-12, SKB, Stockholm, Sweden.
- Abelin, H., Birgersson, L., Ågren, T. and Neretnieks, I. (1990b). A channelling experiment to study flow and transport in natural fractures. Proc. 3rd NEA/SKB Symp. of the International Stripa Project, Stockholm, pp. 135-146.
- Agarwal, R., Al-Hussainy, R., and Ramey, H. (1970). An investigation of wellbore storage and skin effect in unsteady liquid flow: I. Analytical treatment. Journal of the Society of Petroleum Engineers (Sept. 1970), pp. 84-95.
- Abelin, H., Birgersson, L., and Gidlund, J. (1987a). 3-D migration experiment - Report 2: instrumentation and tracers. Stripa Project TR 87-20, SKB, Stockholm, Sweden.
- Abelin, H., Birgersson, L., Gidlund, J., Moreno, L., Neretnieks, I., Widén, H. and Ågren, T. (1987b). Part I: 3-D migration experiment - Report 3: performed experiments, results and evaluation. Stripa Project TR 87-21(a), SKB, Stockholm, Sweden.
- Abelin, H., Birgersson, L., Gidlund, J., Moreno, L., Neretnieks, I., Widén, H. and Ågren, T. (1987c). Part II: 3-D migration experiment - Report 3: performed experiments, results and evaluations. Appendices 15, 16 and 17. Stripa Project TR 87-21(b), SKB, Stockholm, Sweden.
- Abelin, H., Birgersson, L., Widén, H., Ågren, T., Moreno, L., and Neretnieks, I. (1990c). Channeling experiment. Stripa Project TR 90-13, SKB, Stockholm, Sweden.

- Abelin, H., Neretnieks, I., Tunbrant, S., and Moreno, L. (1985). Final report of the migration in a single fracture - experimental results and evaluation. Stripa Project TR 85-03, SKB, Stockholm, Sweden.
- Allard, B., Kipatsi, H., and Torstenfelt, B. (1978). Absorption of long lived radionuclides in clay and rock. KBS TR 98, Stockholm, Sweden.
- Andersson, J. and Dverstorp., B. (1987). 3-D migration experiment - Report 4: fracture network modeling of the Stripa 3-D site. Stripa Project TR 87-22, SKB, Stockholm, Sweden.
- Andersson, P. (1989). Site characterization and validation - geophysical single hole logging, Stage 3. Stripa Project IR 89-07, SKB, Stockholm, Sweden.
- Andrews, J., Fontes, J.-C., Fritz, P. and Nordstrom, K. (1988). Hydrogeochemical assessment of crystalline rock for radioactive waste disposal - the Stripa experience. Stripa Project TR 88-05, SKB, Stockholm, Sweden.
- Andrews, J., Fontes, J.-C., Michelot, J.-L., and Elmore, D. (1986). *In situ* neutron flux, ³⁶Cl production and groundwater evolution in crystalline rocks at Stripa, Sweden. Earth and Planetary Science Letters, Vol. 77, pp. 49-58.
- Ball, J.K., Black, J.H., Brightman, M. and Doe, T. (1991). Large scale cross hole testing. Stripa Project TR 91-17, SKB, Stockholm, Sweden.
- Barker, J. and Black, J. (1983). Slug tests in fissured aquifers. Water Resources Research, Vol. 19, pp. 1558-1564.
- Barton, N., Makurat, A., Monson, K., Vik, G. and Tunbridge, L. (1992). Rock mechanics characterization and modelling of the disturbed zone phenomena at Stripa. Stripa Project TR 92-12, SKB, Stockholm, Sweden.
- Benjamin, J. and Cornell, C. (1970). Probability, statistics, and decision for civil engineers. McGraw-Hill Book Company, New York.
- Billaux, D., Chiles, J.P., Hestir, K. and Long, J. (1989). Three-dimensional statistical modelling of a fractured rock mass: an example for the Fanay-Augeres Mine. International Journal of Rock Mechanics and Mining Science (Special Issue on Forced Fluid Flow Through Fractured Rock Masses), in press.
- Birgersson, L. and Ågren, T. (1992). Site characterization and validation - tracer migration experiment in the Validation Drift, Report 1: Instrumentation, site preparation and tracers. Stripa Project TR 92-02, SKB, Stockholm, Sweden.
- Birgersson, L. and Neretnieks, I. (1982). Diffusion in the matrix of granitic rock -- Field test in the Stripa mine: Part 1. SKBF/KBS TR 82-08, Stockholm, Sweden.

- Birgersson, L. and Neretnieks, I. (1983). Diffusion in the matrix of granitic rock -- Field test in the Stripa mine: Part 2. SKBF/KBS TR 83-39, Stockholm, Sweden.
- Birgersson, L., Widén, H., Ågren, T. and Neretnieks, I. (1992a). Tracer migration experiments in the Stripa mine: 1980-1991. Stripa Project TR 92-25, SKB, Stockholm, Sweden.
- Birgersson, L., Widén, H., Ågren, T., Neretnieks, I. and Moreno, L. (1992b). Site characterization and validation - tracer migration experiment in the Validation Drift, Report 2, Part 1: performed experiments, results and evaluation. Stripa Project TR 92-03, SKB, Stockholm, Sweden.
- Birgersson, L., Widén, H., Ågren, T., Neretnieks, I. and Moreno, L. (1992c). Site characterization and validation - tracer migration experiment in the Validation Drift, Report 2, Part 2: breakthrough curves in the Validation Drift. Appendices 5-9. Stripa Project TR 92-03, SKB, Stockholm, Sweden.
- Bjarnason, B. and Raillard, G. (1987). Rock stress measurements in borehole V3. Stripa Project IR 87-13, SKB, Stockholm, Sweden.
- Black, J.H. and Holmes, D.C. (1990). Hydraulic characterization techniques used within the Stripa Project (1985-9). Proc. 3rd NEA/SKB Symp. of the International Stripa Project, Stockholm, pp. 96-108.
- Black, J.H. and Olsson, O. (1990). An integrated approach to site characterization: experience from the Crosshole Project. Proc. 3rd NEA/SKB Symp. of the International Stripa Project, Stockholm, pp. 109-120.
- Black, J., Barker, J. and Noy, D. (1986). Crosshole investigations - the method, theory and analysis of crosshole sinusoidal pressure tests in fissured rock. Stripa Project IR 86-03, SKB, Stockholm, Sweden.
- Black, J., Holmes, D. and Brightman, M. (1987). Crosshole investigations - hydrogeological results and interpretations. Stripa Project TR 87-18, SKB, Stockholm, Sweden.
- Black, J., Olsson, O., Gale, J. and Holmes, D. (1991). Site characterization and validation - Stage 4: preliminary assessment and detail predictions. Stripa Project TR 91-08, SKB, Stockholm, Sweden.
- Burse, G., Gale, J., MacLead, R., Strähle, A. and Tiren, S. (1991). Site characterization and validation - Validation Drift fracture data, Stage IV. Stripa Project TR 91-19, SKB, Stockholm, Sweden.
- Carlsson, H., Stillborg, B., Beck, R. and Gnirk, P. (1987). Program for the Stripa Project Phase 3, 1986-1991. Stripa Project TR 87-09, SKB, Stockholm, Sweden.
- Carlsson, L. and Olsson, T. (1985a). Hydrogeological and hydrogeochemical investigations in boreholes - shut-in tests. Stripa Project IR 85-08, SKB, Stockholm, Sweden.

- Carlsson, L. and Olsson, T. (1985b). Hydrogeological and hydrogeochemical investigations in boreholes - injection-recovery tests and interference tests. Stripa Project IR 85-09, SKB, Stockholm, Sweden.
- Carlsson, L. and Olsson, T. (1985c). Hydrogeological and hydrogeochemical investigations in boreholes - final report. Stripa Project IR 85-10, SKB, Stockholm, Sweden.
- Carlsson, L., Eggert, T., Westlund, B. and Olsson, T. (1982a). Core-logs of the vertical borehole V2. Stripa Project IR 82-05. Swedish Nuclear Fuel Supply Co./Division KBS, Stockholm, Sweden.
- Carlsson, L., Olsson, T., Andrews, J., Fontes, J., Michelot, J. and Nordstrom, K. (1983). Geochemical and isotope characterization of the Stripa ground waters - progress report. Stripa Project IR 83-01. Swedish Nuclear Fuel Supply Co./Division KBS, Stockholm, Sweden.
- Carlsson, L., Olsson, T., Neretnieks, I. and Pusch, R. (1980). Summary of defined programs. Stripa Project TR 81-01. Swedish Nuclear Fuel Supply Co./Division KBS, Stockholm, Sweden.
- Carlsson, L., Stejskal, V. and Olsson, T. (1981). Part I: Core-logs of borehole VI down to 505 m. Stripa Project IR 81-05. Swedish Nuclear Fuel Supply Co./Division KBS, Stockholm, Sweden.
- Carlsson, L., Stejskal, V. and Olsson, T. (1982b). Core-logs of the Subhorizontal boreholes N1 and E1. Stripa Project IR 82-04. Swedish Nuclear Fuel Supply Co./Division KBS, Stockholm, Sweden.
- Carlsten, S. (1985). Hydrogeological and hydrogeochemical investigations in boreholes - compilation of geological data. Stripa Project IR 85-04, SKB, Stockholm, Sweden.
- Carlsten, S. and Stråhle, A. (1985). Crosshole investigations - compilation of core log data from F1-F6. Stripa Project IR 85-13, SKB, Stockholm, Sweden.
- Carlsten, S., Magnusson, K. and Olsson, O. (1985). Crosshole investigations - description of the small scale site. Stripa Project IR 85-05, SKB, Stockholm, Sweden.
- Carlsten, S., Nyberg, G., Olsson, O., Sehlstedt, M. and Tammela, P-T. (1990). Site characterization and validation - monitoring of head in the Stripa mine during 1989. Stripa Project IR 91-02, SKB, Stockholm, Sweden.
- Carlsten, S., Nyberg, G., Olsson, O. and Tammela, P-T. (1991a). Site characterization and validation - monitoring of head in the Stripa mine during 1991. Stripa Project IR 91-32, SKB, Stockholm, Sweden.
- Carlsten, S., Nyberg, G., Tammela, P. and Olsson, O. (1991b). Site characterization and validation - monitoring of head in the Stripa mine during 1990. Stripa Project IR 91-12, SKB, Stockholm, Sweden.

- Carlsten, S., Olsson, O., Persson, O. and Sehlstedt, M. (1988). Site characterization and validation - monitoring of head in the Stripa mine during 1987. Stripa Project IR 88-02, SKB, Stockholm, Sweden.
- Cooper, H. Jr., Bredehoeft, J., and Papadopoulos, I. (1967). Response of a finite diameter well to an instantaneous charge of water. *Water Resources Research*, 3(1), pp. 263-269.
- Cosma, C. (1987). Crosshole investigations - short and medium range seismic tomography. Stripa Project TR 87-08, SKB, Stockholm, Sweden.
- Cosma, C. (1990). Fracture characterization by seismic and sonic methods. Techniques applied during Phase III of the Stripa Project. Proc. 3rd NEA/SKB Symp. of the International Stripa Project, Stockholm, pp. 85-95.
- Cosma, C., Bähler, S., Hammarström, M. and Pihl, J. (1986). Reflection and tubewave analysis of the seismic data from the Stripa Crosshole site. Stripa Project TR 87-07, SKB, Stockholm, Sweden.
- Cosma, C., Heikkinen, P., Keskinen, J. and Korhonen, R. (1991a). Site characterization and validation - results from seismic crosshole and reflection measurements - Stage 3. Stripa Project TR 91-07, SKB, Stockholm, Sweden.
- Cosma, C., Heikkinen, P. and Pekonen, S. (1991b). Improvement of high resolution borehole seismics: Part I--development of processing methods for VSP surveys; Part II--piezoelectric signal transmitter for seismic measurements. Stripa Project TR 91-13, SKB, Stockholm, Sweden.
- Cosma, C., Korhonen, R., Hammarström, M., Morén, P. and Pihl, J. (1988). Site characterization and validation - results from seismic crosshole and reflection measurements, Stage I. Stripa Project IR 88-07, SKB, Stockholm, Sweden.
- Dagan, G. (1979). Model of groundwater flow in statistically homogeneous formation. *Water Resources Research* 15(1), pp. 47-63.
- Danielson, J., Ekman, L. and Jönsson, S. (1991). Inflow measurements in the D-Holes at the Stripa mine. Stripa Project IR 91-15, SKB, Stockholm, Sweden.
- Davey, A., Karasaki, K., Long, J.C.S., Landsfeld, M., Mensch, A. and Martel, S. (1989). Analysis of the hydraulic data of the MI Experiment. Report No. LBL-27864, Lawrence Berkeley Laboratory, Berkeley, CA/USA.
- Davis, S. and Nordstrom D. (Editors) (1992). Hydrogeochemical investigations in boreholes at the Stripa mine. The Hydrochemical Advisory Group and their associates. Stripa Project TR 92-19, SKB, Stockholm, Sweden.

- Dershowitz, W. and Wallmann, P. (1992). Discrete fracture modelling for the Stripa tracer validation experiment predictions. Stripa Project TR 92-15, SKB, Stockholm, Sweden.
- Dershowitz, W., Herbert, A. and Long, J. (1989). Fracture Flow Code Cross - Verification Plan. Stripa Project TR 89-02, SKB, Stockholm, Sweden.
- Dershowitz, W.S., Wallmann, P., Geier, J.E. and Lee, G. (1991a). Preliminary - discrete fracture network modelling of tracer migration experiment at the SCV site. Stripa Project TR 91-23, SKB, Stockholm, Sweden.
- Dershowitz, W., Wallmann, P. and Kindred, S. (1991b). Discrete fracture modelling for the Stripa site characterization and Validation Drift inflow predictions. Stripa Project TR 91-16, SKB, Stockholm, Sweden.
- Doe, T. and Geier, J. (1990). Interpretation of fracture system geometry using well test data. Stripa Project TR 91-03, SKB, Stockholm, Sweden.
- Doe, T., Geier, J. and Dershowitz, W. (1990a). Analysis of hydraulic connections between BMT and SCV areas. Stripa Project TR 90-15, SKB, Stockholm, Sweden.
- Doe, T.W., Geier, J.E. and Osnes, J.D. (1990b). Estimation of fracture lengths and conductivities using closely-spaced well tests. Proc. 3rd NEA/SKB Symp. of the International Stripa Project, Stockholm, pp. 200-217.
- Efron, B. (1982). The Jackknife, the Bootstrap, and other resampling plans. SIAM Monograph No. 38, Society of Industrial and Applied Mathematics.
- Executive Summary of Phase 1. Stripa Project TR 86-04, SKB, Stockholm, Sweden (1986).
- Executive Summary of Phase 2. Stripa Project TR 89-01, SKB, Stockholm, Sweden (1989).
- Falk, L. (1992). Directional borehole antenna – theory. Stripa Project TR 92-16, SKB, Stockholm, Sweden.
- Falk, L., Olsson, O., Sandberg, E., Forslund, O. and Lundmark, L. (1990). A directional antenna for borehole radar. Proc. 3rd NEA/SKB Symp. of the International Stripa Project, Stockholm, pp. 61-72.
- Fontes, J.-Ch., Fritz, P., Louvat, D., and Michelot, J.-L. (1989). Aqueous sulphites from Stripa groundwater systems. *Geochim. et Cosmochim. Acta*, Vol. 53, No. 8, pp. 1783-1789.
- Fridh, B. (1987). Site characterization and validation - geophysical single hole logging. Stripa Project TR 87-17, SKB, Stockholm, Sweden.
- Fritz, P., Barker, J., and Gale, J. (1979). Geochemistry and isotope hydrology of groundwaters in the Stripa granite -- results and preliminary

interpretation. Lawrence Berkeley Laboratory Report, LBL-8285/SAC-12.

- Fritz, P., Frape, S., and Miles, M. (1987). Methane in crystalline rocks of the Canadian shield. Geol. Assoc. of Canada, Special Paper 33 (In Saline Water and Gasses in Crystalline Rocks), pp. 211-223.
- Gale, J. (1981). Fracture and hydrology data from field studies at Stripa, Sweden. Lawrence Berkeley Laboratory Report LBL-13101, SAC-46.
- Gale, J. and Rouleau, A. (1986). Hydrogeological characterization of the Ventilation Drift (Buffer Mass Test) area, Stripa, Sweden. Stripa Project IR 86-02, SKB, Stockholm, Sweden.
- Gale, J. and Stråhle, A. (1988). Site characterization and validation - drift and borehole fracture data, Stage I. Stripa Project IR 88-10. SKB, Stockholm, Sweden.
- Gale, J., MacLeod, R., Bursey, G., Stråhle, A. and Tirén, S. (1991). Characterization of the structure and geometry of the H fracture zone at the SCV site. Stripa Project TR 91-37, SKB, Stockholm, Sweden.
- Gale, J., MacLeod, R. and LeMessurier, P. (1990a). Site characterization and validation - measurement of flowrate, solute velocities and aperture variation in natural fractures as a function of normal and shear stress, Stage 3. Stripa Project TR 90-11, SKB, Stockholm, Sweden.
- Gale, J., MacLeod, R., Stråhle, A. and Carlsten, S. (1990b). Site characterization and validation - Drift and borehole fracture data, Stage 3. Stripa Project IR 90-02, SKB, Stockholm, Sweden.
- Gale, J., MacLeod, R., Welhan, J., Cole, C. and Vail, L. (1987). Hydrogeological characterization of the Stripa site. Stripa Project TR 87-15, SKB, Stockholm, Sweden.
- Gale, J., Welhan, J., MacLeod, R., Cole, C. and Vail, L. (1990c). A Comparison of measured porosity with that inferred from isotopic data and three-dimensional flow models. Proc. 3rd NEA/SKB Symp. of the International Stripa Project, Stockholm, pp. 161-174.
- Geier, J., Dershowitz, W. and Sharp, G. (1990). Prediction of inflow into the D-holes at the Stripa mine. Stripa Project TR 90-06, SKB, Stockholm, Sweden.
- Geijer, P. (1938). Stripa Odalfalts Geologi (Geology of the Stripa mining field). SGU Report No. 28, Stockholm, Sweden.
- Gnirk, P. (1991). Process and criteria for validation of the groundwater flow models in the OECD/NEA International Stripa Project. Proc. Second Annual International Conf. on High Level Radioactive Waste Management, Las Vegas, NV, pp. 895-901.

- Gnirk, P. (1992). The process for validation of the groundwater flow and transport models in the SCV program. Stripa Project TR 92-28, SKB, Stockholm, Sweden.
- Grindrod, P., Herbert, A., Roberts, D. and Robinson, P. (1991). NAPSAC technical document. Stripa Project TR 91-31, SKB, Stockholm, Sweden.
- Gupta, S., Cole, C., Kincaid, C., and Monti, A. (1986). Coupled fluid, energy and solute transport (CFEST) model: formulation, computer source listings, and user's manual. Battelle Memorial Institute/ONWI (in press).
- Gupta, S.K., Kincaid, C.T., Meyer, P.R., Newbill, C.A. and Cole, C.R. (1982). CFEST-Multi-Dimensional Finite-Element Code for the Analysis of Coupled Fluid, Energy, and Solute Transport. PNL-4260, Pacific Northwest Laboratory, Richland, Washington/USA.
- Haigh, D., Brightman, M., Black, J. and Parry, S. (1992). Site characterization and validation – head variations during the entire experimental period. Stripa Project TR 92-13, SKB, Stockholm, Sweden.
- Harding, W. and Black, J. (1992). Site characterization and validation – inflow to the Validation Drift. Stripa Project TR92-14, SKB, Stockholm, Sweden.
- Herbert, A. and Lanyon, G. (1992). Modelling tracer transport in fractured rock at Stripa. Stripa Project TR 92-01, SKB, Stockholm, Sweden.
- Herbert, A. and Splawski, B. (1990). Prediction of inflow into the D-holes at the Stripa mine. Stripa Project TR 90-14, SKB, Stockholm, Sweden.
- Herbert, A., Gale, J., Lanyon, G. and MacLeod, R. (1991). Modelling for the Stripa site characterization and Validation Drift inflow: Prediction of flow through fractured rock. Stripa Project TR 91-35, SKB, Stockholm, Sweden.
- Hodgkinson, D. (1991). A comparison of predictions and measurements for the Stripa simulated drift experiment. Stripa Project TR 91-10, SKB, Stockholm, Sweden.
- Hodgkinson, D. (1992). A compilation of minutes for the Stripa Task Force on Fracture Flow Modelling. Stripa Project TR 92-09, SKB, Stockholm, Sweden.
- Hodgkinson, D. and Cooper, N. (1992a). A comparison of measurements and calculations for the Stripa Validation Drift inflow experiment. Stripa Project TR 92-07, SKB, Stockholm, Sweden.
- Hodgkinson, D. and Cooper, N. (1992b). A comparison of measurements and calculations for the Stripa tracer experiments. Stripa Project TR 92-20, SKB, Stockholm, Sweden.

- Holmes, D. (1984). Crosshole investigations - equipment design considerations for sinusoidal pressure tests. Stripa Project IR 84-05. Swedish Nuclear Fuel Supply Co./Division KBS, Stockholm, Sweden.
- Holmes, D. (1989). Site characterization and validation - single borehole hydraulic testing. Stripa Project IR 89-04, SKB, Stockholm, Sweden.
- Holmes, D. and Sehlstedt, M. (1986). Crosshole investigations - details of the construction and operation of the hydraulic testing system. Stripa Project TR 87-04, SKB, Stockholm, Sweden.
- Holmes, D.C. and Sehlstedt, M. (1991). Site characterization and validation - equipment design and techniques used in single borehole hydraulic testing, simulated drift experiment and crosshole testing. Stripa Project TR 91-25, SKB, Stockholm, Sweden.
- Holmes, D., Abbott, M. and Brightman, M. (1990). Site characterization and validation - single borehole hydraulic testing of 'C' boreholes, simulated drift and small scale hydraulic testing, Stage 3. Stripa Project TR 90-10, SKB, Stockholm, Sweden.
- International Atomic Energy Agency, 1982. Radioactive Waste Management Glossary. IAEA-TECDOC-264, Vienna.
- Ivansson, S. (1984). Crosshole investigations - tomography and its application to crosshole seismic measurements. Stripa Project IR 84-08. Swedish Nuclear Fuel Supply Co./Division KBS, Stockholm, Sweden.
- Jacobsson, L. and Norlander, H. (1981). Equipment for hydraulic testing. Stripa Project IR 81-04. Swedish Nuclear Fuel Supply Co./Division KBS, Stockholm, Sweden.
- Jaeger, J.C. and Cook, N.G. (1984). Fundamentals of Rock Mechanics. 3rd Edition, Chapman and Hall, New York.
- Kenrick, M. and Dershowitz, W. (1991). Hydrological Testing of Channelized Rock Fractures: A Numerical Simulation. Submitted to Journal of Water Resources Research.
- Koark, A. and Lundstrom, I. (1979). Berggrundskartan (Underground mine map). Lindsberg SV. SGU ser. Af. 126.
- Laaksoharju, M. (1990). Site characterization and validation - hydrochemical investigations, Stage 3. Stripa Project TR 90-08, SKB, Stockholm, Sweden.
- Long, J. and Karasaki, K. (1992). Simulation of tracer transport for the site characterization and validation site in the Stripa mine. Stripa Project TR 92-06, SKB, Stockholm, Sweden.
- Long, J., Karasaki, K., Davey, A., Peterson, J., Landsfeld, M., Kemeny, J. and Martel, S. (1990). Preliminary prediction of inflow into the D-holes at the Stripa mine. Stripa Project TR 90-04, SKB, Stockholm, Sweden.

- Long, J., Mauldon, A., Nelson, K., Martel, S., Fuller, P. and Karasaki, K. (1992). Prediction of flow and drawdown for the site characterization and validation site in the Stripa mine. Stripa Project TR 92-05, SKB, Stockholm, Sweden.
- Lundstrom, I. (1983). Beskrivning till berggrundskartan Lindesberg SV. SGU Af 126.
- MacLeod, R., Gale, J. and Bursey, G. (1992). Site characterization and validation – porous media modelling of validation tracer experiments. Stripa Project TR 92-10, SKB, Stockholm, Sweden.
- Magnusson, K-Å., Carlsten, S., and Olsson, O., 1987. Crosshole investigations - physical properties of core samples from boreholes F1 and F2. Stripa Project TR 87-10, SKB, Stockholm, Sweden.
- Makurat, A., Barton, N., Vik, G. and Tunbridge, L. (1990a). Site characterization and validation - coupled stress-flow testing of mineralized joints of 200 mm and 1400 mm length in the laboratory and in situ, Stage 3. Stripa Project TR 90-07, SKB, Stockholm, Sweden.
- Makurat, A., Barton, N., Tunbridge, L. and Vick, G. (1990b). Mechanical and hydraulic properties of joints at different scales. Proc. 3rd NEA/SKB Symp. of the International Stripa Project, Stockholm, pp. 187-199.
- Maloszewski, P. and Zuber, A. (1989). Mathematical models for interpreting tracer experiments in fissured aquifers. The Application of Isotope Techniques in the Study of the Hydrogeology of Fractured and Fissured Rocks, IAEA, Vienna, pp. 287-301.
- McKinnon, S. and Carr, P. (1990). Site characterization and validation - stress field in the SCV block and around the Validation Drift, Stage 3. Stripa Project TR 90-09, SKB, Stockholm, Sweden.
- Milton, G. (1987). Paleohydrological inferences from fracture calcite analyses. Applied Geochemistry, Vol. 2, pp. 33-36.
- Monsen, K., Barton, N. and Makurat, A. (1992). Fully-coupled hydro-mechanical modelling of the D-holes and validation drift inflow. Stripa Project TR 92-11, SKB, Stockholm, Sweden.
- Monsen, K., Makurat, A. and Barton, N. (1991). Disturbed zone modeling of SVC Validation Drift using UDEC - BB, Models 1 to 8 - Stripa Phase 3. Stripa Project TR 91-05, SKB, Stockholm, Sweden.
- Moser, H., Wolf, M., Fritz, P., Fontes, J.-Ch., Florkowski, T., and Payne, B. (1989). Deuterium, oxygen-18, and tritium in Stripa groundwater. Geochim. et Cosmochim. Acta, Vol. 53, No. 8, pp. 1757-1763.
- Neretnieks, I. (1985). Transport in fractured rocks. Proceedings IAH 17th Congress, Memoires Vol. XVII, part 2, pp. 301-318.

- Neretnieks, I., Abelin, H., Birgersson, L., Moreno, L., Widén, H. and Ågren, T. (1990). A large scale flow and tracer experiment in granite. Proc. 3rd NEA/SKB Symp. of the International Stripa Project, Stockholm, pp. 123-134.
- Neretnieks, I., Eriksen, T., and Tähtinen, P. (1982). Tracer movement in a single fissure in granitic rock: Some experimental results and their interpretation. Water Resources Research, Vol. 18, p. 849.
- Nordstrom, D., Andrews, J., Carlsson, L., Fontes, J-C., Fritz, P., Moser, H. and Olsson, T. (1985). Hydrogeological and hydrogeochemical investigations in boreholes - final report of the phase I geochemical investigations of the Stripa ground waters. Stripa Project TR 85-06, SKB, Stockholm, Sweden.
- Noy, D., Barker, J., Black, J. and Holmes, D. (1988). Crosshole investigations - implementation and fractional dimension interpretation of sinusoidal tests. Stripa Project TR 88-01, SKB, Stockholm, Sweden.
- Olkiewicz, A., Gale, J.E., Thorpe, R. and Paulsson, B. (1979). Geology and fracture system at Stripa. Lawrence Berkeley Laboratory Report No. LBL-8907, SAC-21.
- Olkiewicz, A., Hanson, K., Almén, K.-E. and Gidlund, G. (1978). Geological and hydrological documentation at the Stripa Research Station. KBS Report No. 63, Stockholm, Sweden, p. 16.
- Olsson, O. (Editor) (1992). Site characterization and validation report – final report. Stripa Project TR 92-22, SKB, Stockholm, Sweden.
- Olsson, O. and Jämtlid, A. (1984). Hydrogeological and hydrogeochemical investigations - geophysical borehole measurements. Stripa Project IR 84-03. Swedish Nuclear Fuel Supply Co./Division KBS, Stockholm, Sweden.
- Olsson, O. and Sandberg, E. (1984). Crosshole investigations - preliminary design of a new borehole radar system. Stripa Project IR 84-04. Swedish Nuclear Fuel Supply Co./Division KBS, Stockholm, Sweden.
- Olsson, O., Andersson, P. and Gustafsson, E. (1991a). Site haracterization and validation - monitoring of saline tracer transport by borehole radar measurements - Phase 1. Stripa Project TR 91-09, SKB, Stockholm, Sweden.
- Olsson, O., Andersson, R. and Gustafsson, E. (1991b). Site characterization and validation - monitoring of saline tracer transport by borehole radar measurements, final report. Stripa Project TR 91-18, SKB, Stockholm, Sweden.
- Olsson, O., Black, J., Cosma, C. and Phil, J. (1987a). Crosshole investigations - final report. Stripa Project TR 87-16, SKB, Stockholm, Sweden.

- Olsson, O., Black, J., Gale, J. and Holmes, D. (1989). Site characterization and validation Stage 2 - preliminary predictions. Stripa Project TR 89-03, SKB, Stockholm, Sweden.
- Olsson, O., Black, J.H., Holmes, D.C. and Gale, J.E. (1990a). Site characterization and validation - preliminary characterization and prediction. Proc. 3rd NEA/SKB Symp. of the International Stripa Project, Stockholm, pp. 175-186.
- Olsson, O., Eriksson, J., Falk, L. and Sandberg, E. (1988). Site characterization and validation - borehole radar investigations, Stage I. Stripa Project TR 88-03, SKB, Stockholm, Sweden.
- Olsson, O., Falk, L., Forslund, O., Lundmark, L. and Sandberg, E. (1987b). Crosshole investigations - results from borehole radar investigations. Stripa Project TR 87-11, SKB, Stockholm, Sweden.
- Olsson, O., Falk, L., Forslund, O., Lundmark, L., and Sandberg, E. (1992). Borehole radar applied to the characterization of hydraulically conductive fracture zones in crystalline rock. Geophysical Testing, Vol. 40, pp. 109-142.
- Olsson, O., Sandberg, E. and Nilsson, B. (1983). Crosshole investigations - the use of borehole radar for the detection of fracture zones in crystalline rock. Stripa Project IR 83-06. Swedish Nuclear Fuel Supply Co./Division KBS, Stockholm, Sweden.
- Osnes, J.D., Winberg, A. and Andersson, J. (1988). Analysis of well test data: application of probabilistic models to infer hydraulic properties of fractures. Topical Report RSI-0338, RE/SPEC Inc., Rapid City, SD/USA.
- Persson, O., Olsson, O. and Sehlstedt, M. (1989). Site characterization and validation - monitoring of head in the Stripa mine during 1988. Stripa Project IR 89-06, SKB, Stockholm, Sweden.
- Pihl, J., Hammarström, M., Ivansson, S. and Morén, P. (1986). Crosshole investigations - results from seismic borehole tomography. Stripa Project TR 87-06, SKB, Stockholm, Sweden.
- Pihl, J., Hammarström, M., Ivansson, S. and Morén, P. (1990). Development of large and small scale seismic crosshole techniques. Proc. 3rd NEA/SKB Symp. of the International Stripa Project, Stockholm, pp. 73-84.
- Raghavan, R. (1980). The effect of producing time on type curve analysis. Journal Petroleum Technology (June 1980), pp. 1053-1064.
- Sandberg, E., Olsson, O. and Falk, L. (1989). Site characterization and validation - borehole radar investigations, Stage 3. Stripa Project TR 90-01, SKB, Stockholm, Sweden.

- Schwartz, F. and Lee, G. (1991). Cross-verification testing of fracture flow and mass transport codes. Stripa Project TR 91-29, SKB, Stockholm, Sweden.
- Skagius, K. and Neretnieks, I. (1986a). Porosities and diffusivities of some nonsorbing species in crystalline rocks. *Water Resources Research*, Vol. 22, p. 389.
- Skagius, K. and Neretnieks, I. (1986b). Diffusivity measurements and electrical resistivity measurements in rock samples under mechanical stress. *Water Resources Research*, Vol. 22, p. 570.
- Stratford, R., Herbert, A. and Jackson, C. (1990). A parameter study of the influence of aperture variation on fracture flow and the consequences in a fracture network. *Proc. International Symposium on Rock Joints*, Loen, Norway.
- Strelsova, T. (1983). Well pressure behavior of a naturally fractured aquifer. *Journal of the Society of Petroleum Engineers* (Oct. 1983), pp. 769-780.
- Strindell, L. and Andersson, M. (1981). Part II: Measurement of triaxial rock stresses in borehole VI. Stripa Project IR 81-05. Swedish Nuclear Fuel Supply Co./Division KBS, Stockholm, Sweden.
- Tinucci, J.P. and Israelsson, J. (1991). Site characterization and validation - excavation stress effects around the validation drift. Stripa Project TR 91-20, SKB, Stockholm, Sweden.
- Uchida, M. (1990). Geologic mapping and analysis of the Stripa mine. Golder Assoc. Inc. Internal Report.
- Vik, G. and Barton, N. (1988). Stage I joint characterization and Stage II preliminary prediction using small core samples. Stripa Project IR 88-08, SKB, Stockholm, Sweden.
- Watanabe, K. (1991a). Evaporation measurement in the Validation Drift - Part 1. Stripa Project TR 91-06, SKB, Stockholm, Sweden.
- Watanabe, K. (1991b). Evaporation measurement in the Validation Drift - Part 3: comparison between the first and second set of measurement results. Stripa Project TR 91-36, SKB, Stockholm, Sweden.
- Watanabe, K. and Osada, M. (1991). Evaporation measurement in the Validation Drift - Part 2. Stripa Project TR 91-27, SKB, Stockholm, Sweden.
- Wikberg, P., Laaksoharju, M., Bruno, J. and Sandino, A. (1988). Site characterization and validation - hydrochemical investigations in Stage I. Stripa Project IR 88-09, SKB, Stockholm, Sweden.
- Witherspoon, P., Wilson, C., Long, J., Galbraith, R., DuBois, A., Gale, J. and McPherson, M. (1980). Mesures de Permeabilite en Grand Dans Les Roches Cristallines Fracturees (Large-scale measurements of

permeability in fractures in crystalline rock). Bull. B.R.G.M. III(1), pp. 53-61.

Wollenberg, H., Andersson, L. and Flexser, S. (1982). Petrology and radiogeology of the Stripa pluton. Lawrence Berkeley Laboratory Report No. LBL-11654, SAC-36.

BIBLIOGRAPHY

Annual Report 1980. Stripa Project TR 81-02. Swedish Nuclear Fuel Supply Co./Division KBS, Stockholm, Sweden (1981).

Annual Report 1981. Stripa Project TR 82-01. Swedish Nuclear Fuel Supply Co./Division KBS, Stockholm, Sweden (1982).

Annual Report 1982. Stripa Project TR 83-02. Swedish Nuclear Fuel Supply Co./Division KBS, Stockholm, Sweden (1983).

Annual Report 1983. Stripa Project TR 84-01. Swedish Nuclear Fuel Supply Co./Division KBS, Stockholm, Sweden (1984).

Annual Report 1984. Stripa Project TR 85-07, SKB, Stockholm, Sweden (1985).

Annual Report 1985. Stripa Project TR 86-05, SKB, Stockholm, Sweden (1986).

Annual Report 1986. Stripa Project TR 87-14, SKB, Stockholm, Sweden (1987).

Annual Report 1987. Stripa Project TR 88-06, SKB, Stockholm, Sweden (1988).

Annual Report 1988. Stripa Project TR 89-05, SKB, Stockholm, Sweden (1989).

Annual Report 1989. Stripa Project TR 90-16, SKB, Stockholm, Sweden (1990).

Annual Report 1990. Stripa Project TR 91-11, SKB, Stockholm, Sweden (1991).

Annual Report 1991. Stripa Project TR 92-26, SKB, Stockholm, Sweden (1992).

Davis, S. and Andrews, J. (1990). Results of Phase II geochemical studies at Stripa. Proc. 3rd NEA/SKB Symp. of the International Stripa Project, Stockholm, pp. 147-160.

Geier, J., Dershowitz, W. and Sharp, G. (1990). Three-dimensional Discrete-fracture modelling of the Stripa simulated drift experiment. Proc. 3rd NEA/SKB Symp. of the International Stripa Project, Stockholm, pp. 235-247.

- GEOCHIMICA ET COSMOCHIMICA ACTA (Reprint), Vol. 53, No. 8 (1989). Hydrogeochemical investigations within the Stripa Project. Stripa Project TR 90-05, SKB, Stockholm, Sweden.
- Gnirk, P. (1990). Executive summary. Proc. 3rd NEA/SKB Symp. on the International Stripa Project, Stockholm, pp. 11-18.
- Gnirk, P. and Stillborg, B. (1990). The status of the site characterization and validation program in Phase III of the OECD/NEA Stripa project. Proc. International Topical Meeting on High-Level Radioactive Waste Management, 2, Las Vegas, pp. 855-862.
- Gustafson, G. (1990). Identification and nomenclature of fracture zones. Proc. 3rd NEA/SKB Symp. of the International Stripa Project, Stockholm, pp. 218-222.
- Hakami, E. (1989). Water flow in single rock joints. Stripa Project TR 89-08, SKB, Stockholm, Sweden.
- Herbert, A., Dershowitz, W., Long, J. and Hodgkinson, D. (1990). Validation of fracture flow models in the Stripa Project. Proc. GEOVAL-90 Symp., Stockholm.
- Herbert, A.W. and Gale, J.E. (1990). Fracture flow modelling of the site characterization and validation area in the Stripa mine. Proc. 3rd NEA/SKB Symp. of the International Stripa Project, Stockholm, pp. 223-234.
- Hökmark, H. (1990). Distinct element method modeling of fracture behavior in near field rock. Stripa Project TR 91-01, SKB, Stockholm, Sweden.
- Hökmark, H. and Israelsson, J. (1991). Distinct element modelling of joint behavior in nearfield rock. Stripa Project TR 91-22, SKB, Stockholm, Sweden.
- Karasaki, K. (1987). A new advection-dispersion code for calculating transport in fracture networks. Report No. LBL-22090, Lawrence Berkeley Laboratory, Berkeley, CA/USA.
- Lindblom, S. (1984). Hydrogeological and hydrogeochemical investigations in boreholes - fluid inclusion studies in the Stripa granite. Stripa Project IR 84-07. Swedish Nuclear Fuel Supply Co./Division KBS, Stockholm, Sweden.
- Long, J., Karasaki, K., Davey, A., Peterson, J., Landsfeld, M., Kemeny, J. and Martel, S. (1990). Preliminary calculations of inflow to the D-holes at the Stripa mine. Proc. 3rd NEA/SKB Symp. of the International Stripa Project, Stockholm, pp. 248-259.
- Moreno, L., Neretnieks, I., and Klackers, C-E. (1983). Evaluation of some tracer tests in the granitic rock at Finnsjön. KBS TR 83-38, Stockholm, Sweden.

- Moreno, L., Neretnieks, I., and Landström, O. (1989). An Evaluation of some tracer tests performed at Studsvik. SKB TR 89-09, Stockholm, Sweden.
- Neretnieks, I. (1988). The Swedish repository for low and intermediate level reactor waste -- SFR: Radioactivity release and transport calculations. Symposium on Scientific Basis for a nuclear waste management, Berlin, Germany.
- Nilsson, G. and Olsson, O. (1986). Crosshole investigations - description of the large scale site. Stripa Project IR 86-01, SKB, Stockholm, Sweden.
- Olsson, O., Falk, L., Forslund, O., Lundmark, L. and Sandberg, E. (1990b). Borehole radar applied to site characterization in crystalline rock. Proc. 3rd NEA/SKB Symp. of the International Stripa Project, Stockholm, pp. 47-60.
- Press, D., Halliday, S. and Gale, J. (1990). Application of computer aided design (CADD) in data display and integration of numerical and field results - Stripa Phase 3. Stripa Project TR 91-04, SKB, Stockholm, Sweden.
- Rouleau, A., Gale, J. and Baleshta, J. (1981). Results of fracture mapping in the ventilation drift at Stripa. Lawrence Berkeley Laboratory Report LBL-13071, SAC-42.
- Schunnesson, H. and Lundholm, I. (1992). Economical and technical optimization of site investigations - a multivariate approach based on Stripa F1 and F2 borehole information. Stripa Project TR 92-04, SKB, Stockholm, Sweden.
- Toth, J. (1963). A theoretical analysis of groundwater flow in small drainage basins. *J. Geophys Res.*, V. 68, pp. 4795-4812.
- Triumpf, C-A. (1992). Classification of lithological units based on geophysical borehole logging – data from the Stripa mine. Stripa Project TR 92-18, SKB, Stockholm, Sweden.
- Tsang., O., Tsang, Y. and Hale, F. (1991). Tracer transport in fractures: analysis of field data based on a variable - aperture channel model. Stripa Project TR 91-14, SKB, Stockholm, Sweden.
- U.S. Nuclear Regulatory Commission: Disposal of High-Level Radioactive Wastes in Geologic Repositories. Part 60 of Title 10 of the Code of Federal Regulations [CFR Part 60].
- U.S. Nuclear Regulatory Commission (1983). Final Technical Position on Documentation of Computer Codes for the High-Level Waste Management. NUREG-0856.
- Voss, C. (1990). A proposed methodology for validating performance assessment models for the DOE Office of Civilian Radioactive Waste Management Program. Proc. International Topical Meeting on High-Level Radioactive Waste Management, 1, Las Vegas, 359-363.

Winberg, A. (1991). Analysis of spatial correlation of hydraulic conductivity data from the Stripa mine. Stripa Project TR 91-28, SKB, Stockholm, Sweden.

BIOGRAPHY: Dr. Paul Gnirk

Paul Gnirk was born in Burke, SD/USA in 1937 and lived on his parents' cattle ranch until he graduated from Burke High School in 1955. He graduated from the South Dakota School of Mines and Technology in 1959 with a B.S. degree (with honors) in Mining Engineering, and from the University of Minnesota in 1966 with a Ph.D. in Rock Mechanics with minors in Applied Mathematics and Mechanical Engineering. Between 1963 and 1973, he taught at the South Dakota School of Mines and Technology, first in the Department of Mining Engineering as an Assistant Professor and later in the Department of Mechanical Engineering with the rank of Professor. As one of the founders of RE/SPEC Inc., Dr. Gnirk became its President in 1972 and continued in that capacity until 1988, and as a Principal Consultant for the company until 1991. In 1992, he organized Table Top Consultants Inc. and founded Table Top Ranch Inc., with offices in Rapid City, SD/USA. He is a registered Professional Engineer in the States of South Dakota and Texas.

Dr. Gnirk has more than 30 years of experience in rock mechanics, geotechnical engineering, and many areas of geologic disposal, including numerical modeling, *in situ* testing, repository design analysis, and performance assessment, and, in more recent years, applied decision analysis. Between 1961 and 1967, he worked for Shell Development Company as a Mechanical Engineer in the summers and as a Consultant. From 1968 until 1975, he was a Consultant to the South Dakota Department of Transportation. In 1969, he was the recipient of the first Standard Oil (Indiana) Foundation Good Teaching Award given in the engineering division of the South Dakota School of Mines and Technology, and, in 1970, was selected as an Outstanding Educator of America. Between 1978 and 1992, Dr. Gnirk was involved with many activities conducted by the U.S. Department of Energy (DOE) for the purpose of siting and developing a geologic repository for the disposal of radioactive wastes from nuclear reactors. From 1978 until 1983, he either chaired or participated in Working Groups for the development of DOE's Earth Science Technical Plan, the development of performance constraints for geologic repository designs in basalt, granite, salt, and tuff, and the preparation of DOE's confidence rule-making testimony before the Nuclear Regulatory Commission. Between 1983 and 1989, under the auspices of DOE's Office of Civilian Radioactive Waste Management, he was a member of the Task Force for the preparation of the Siting Guidelines for geologic repositories (10 CFR Part 960), the Methodology Lead Group for the comparative evaluation of five geologic repository sites nominated as suitable for characterisation, the Site-Characterisation-Plan Overview Consultants, and the Technical Integration Group for performance assessment of the repository site at Yucca Mountain. In 1990 and 1991, he was the co-leader of Sandia's Decision Methodology Lead Group for the comparative evaluation of 34 exploratory-study-facility design alternatives for characterisation of the Yucca Mountain site. Dr. Gnirk was one of DOE's representatives to the Technical Subgroups of the Stripa Project from 1980 until 1992 and a member with observer status to the Joint Technical Committee. He served as Chairman of the Technical Subgroup on Engineered Barriers and Rock Mechanics in Phases 1 and 2, co-Chairman of the Technical Subgroup in Phase 3, and Chairman of the Task Forces on Fracture Flow Modelling and Repository Sealing Materials and Techniques in Phase 3.